GISERA | Gas Industry Social and Environmental Research Alliance

Integration of airborne electromagnetic surveys, environmental tracers and geochemical modelling to refine the understanding of connectivity between coal seams and overlying aquifers in the Gunnedah and Surat basins, NSW

30/06/2025

Citation

Raiber, M., Davis, A., Dupuy, M., Prommer, H., Wu, G., Suckow, A., Cunningham, P., Deslandes, A. and Cendón, D. (2025) Integration of airborne electromagnetic surveys, environmental tracers and geochemical modelling to refine the understanding of connectivity between coal seams and overlying aquifers in the Gunnedah and Surat basins. CSIRO, Australia. EP2025-2463.

Copyright

Important disclaimer

Cover image: The magnificent Sawn Rocks in Mount Kaputar National Park in New South Wales are one of Australia's best examples of a rare volcanic rock formation called 'organ-piping'. Sawn Rocks provides a fascinating glimpse of the complex volcanic forces that have shaped the Narrabri region landscape, from the mountains to deep below the surface. While mountains may be easy to see, we need the latest science to understand what's happening below the earth's surface. The CSIRO, Australia's national science agency, is looking deeper into the Narrabri region, seeking to improve our knowledge of groundwater systems in the Gunnedah and Surat Basins. CSIRO's previous research in this area has generated important knowledge on the nature of these groundwater systems, and potential for connectivity between primary target seams for coal seam gas (CSG) development and agricultural aquifers. This research project, funded through CSIRO's Gas Industry Social and Environmental Research Alliance, adopts a multi-disciplinary approach that combines existing data with targeted acquisition of new hydrochemistry, geochemistry, and geophysical survey data. This information will support future water resource management and decision-making in the region. Find out more about this project on the GISERA web site. Credit: Paul Cunningham.

Contents

Summary 17

1 Introduction 29

1.1 Aims of this report 29

1.2 Geological and hydrogeological background 31

1.3 The role of geological structures as potential connectivity pathways 36

1.4 Evolution of conceptual models of potential hydrogeological connectivity pathways in the Narrabri region (2013 to 2022) 40

2 Methodology 44

2.1 Integrated multi-disciplinary geoscientific approaches 44

2.2 Compilation of existing geological and hydrogeological data 45

2.3 Airborne electromagnetic survey 51

2.4 Geochemical analysis of rocks 76

2.5 Groundwater hydrochemistry and tracer analyses 86

2.6 Multivariate statistical analysis 94

2.7 Integration of geological, geophysical, hydraulic and tracer data through numerical modelling 95

3 Results 100

3.1 Stratigraphic data 100

3.2 Hydraulic data 107

3.3 Geochemical analysis of rocks 110

3.4 K-Ar age dating 128

3.5 Airborne geophysical survey 131

3.6 Geological cross-sections 158

3.7 Groundwater hydrochemistry 162

3.8 Insights from new measurements of noble gases and ‘age’ tracers 203

3.9 Numerical modelling of groundwater flow and age patterns 240

3.10 Inverse geochemical modelling 243

4 Discussions 254

4.1 Hydrogeological connectivity pathways in the Narrabri region 254

4.2 Revised stratigraphic table 262

4.3 Revised conceptual model of potential hydrogeological connectivity pathways in the Narrabri region 263
4.4 Data worth analysis 266
4.5 Limitations and opportunities for future work 272
5 Conclusions 274
6 References 277

Figures

Figure 1-1 – Stratigraphy of the Surat and Gunnedah basins in NSW (compiled from Tadros (1993, 1995), Carty and Smith (2003), Korsch and Totterdell (2009), Totterdell et al. (2009), Geoscience Australia (2013), Ransley et al. (2015), Ruming (2015) and Raiber et. al (2022a). Q and P/N in the Cenozoic era correspond to Quaternary and Palaeogene/Neogene. 32

Figure 1-2 – Stratigraphy of the Surat and Gunnedah basins at Plumb Road nested bore sites and Bohena 4 stratigraphic well (modified from Raiber et al., 2022a). Detailed stratigraphy of the Purlawaugh Formation at Plumb Road is also shown. 33

Figure 1-3 – Simplified geological map of the Surat Basin in northern NSW showing the proposed Narrabri Gas Project area, extent of Gunnedah Basin, Great Artesian Basin extent and inferred groundwater flow directions and extent of previous groundwater studies (Raiber et al., 2022a). 35

Figure 1-4 – Conceptual model of geological and hydraulic impact of dolerite dyke intrusions on sedimentary host rock (Senger et al., 2015). 38

Figure 1-5 – Previous conceptual hydrogeological model of potential structural and hydrogeological connectivity pathways between coal seams and major aquifers of Great Artesian Basin in the Narrabri Gas Project area (Raiber et al., 2019). 41

Figure 1-6 – Potential structural and hydrogeological connectivity pathways between coal seams and major aquifers of Great Artesian Basin in the Narrabri Gas Project area (Raiber et al., 2022a). 43

Figure 2-1 – Systematic and iterative approach to integrate multiple lines of evidence applied in this study 45

Figure 2-2 – Overview on AgTEM survey lines (modified from Raiber et al., 2022a). The proposed Narrabri Gas Project area is shown by the white outline (image supplied by Dr. David Allen, Groundwater Imaging). 47

Figure 2-3 – Selected major seismic lines in the Pilliga Forest and Narrabri region considered by Raiber et al. (2022a). 48

Figure 2-4 – Blend of DMOMIG algorithm and spectral decomposition attribute with annotation of horizon interpretations and major structural features along seismic line FSG98-AAC. Stratigraphic horizon interpretations are based on Raiber et al. (2022a) (including interpretation from HiSeis) and seismic interpretations provided by Santos. For orientation of seismic line, see Figure 2-3. 48

Figure 2-5 – Total magnetic intensity (TMI) grid (40 m resolution) – first vertical derivative (Poudjom Djomani, 2019, modified from Raiber et al., 2022a). 51

Figure 2-6 – Schematic of expected conductivity or resistivity of common earth materials. Overlapping values of conductivity show that the inverted conductivity values of the subsurface may not allow for unique determination of material (after Palacky 1983)................................ 52

Figure 2-7 - Operating principles of a helicopter airborne electromagnetic (AEM) system such as the SkyTEM system. 53

Figure 2-8 – SkyTEM airborne electromagnetic survey (AEM) flight path lines (with more than 60 east-west lines in a 1200 m spacing) overlain on simplified surface geology. Non-straight lines indicate areas where the survey path was amended to avoid cultural features (e.g. infrastructure). Selected exploration wells are also shown. 55

Figure 2-9 – SkyTEM helicopter AEM array (image courtesy of SkyTEM). 56

Figure 2-10 – Narrabri Courier (2023) 57

Figure 2-11 - Schematic representation of helicopter time domain EM data acquisition and inversion. A) Data are acquired along parallel flight lines along each flight line; B) The EM receiver measures the secondary high and low moment responses; C) The measured response is used to determine the conductivity-depth function by inversion; D) The modelled conductivity structure for each sounding is gridded into conductivity-depth intervals to provide a spatial representation of the subsurface conductivity structure at different depths below the ground surface; E) Individual soundings from a flight line are stitched together into conductivity-depth sections to provide a representation of the variation of conductivity. 60

Figure 2-12 - An example of high-moment SkyTEM data from the Narrabri AEM survey badly affected by noise from a nearby coal mine. Signal from 1500 m to 3000 m is significantly affected by electrical machinery causing typical ringing effects in the data that must be removed prior to inversion. There are minor noise artefacts at 250 m and 750 m.................. 61

Figure 2-13 - Plan view of the Narrabri survey with total number of time gates, or channels, used in the inversion calculations after processing for anthropogenic and geological noise...... 62

Figure 2-14 - Noise estimates from an AEM system. Solid black lines show the high-altitude measurements, while the dashed lines show the estimates from a Green and Lane (2003) analysis of repeat lines.. 65

Figure 2-15 - An example of a posterior mean conductivity section resulting from the RJMCMC process on the repeat lines used in the Narrabri AEM survey. Blanked areas are due to a wide spread of accepted models relative to the prior conductivity. 66

Figure 2-16 - Estimates of total noise for each delay time of both low-moment and high-moment systems. The shading variations show the distributions of the noise estimates from the RJMCMC simulations. The solid fuchsia line shows the peak of the distributions and is taken as the average measurement noise for the entire survey. The solid black line is from high-altitude tests, and the dashed black line is the Green and Lane (2003) estimate. 67

Figure 2-17 - Inversions showing the effect of model regularisation for a wide range of regularisation weighting values (α). All inversion runs were initialised with the same starting model. The model regularisation structure for each is the same. A depth of investigation (DOI) line is shown in white. There is very little variation in models above the DOI when regularisation parameter α is below 1... 70

Figure 2-18 - Plots of the differences in the inversion models from the comparison model at regularisation value 0.215. differences are in the log base 10 of conductivity. We can see that each model agrees with the comparison model, within a factor of 10, above the depth of investigation.. 71

Figure 2-19 - Plot of data misfit versus model misfit (L-Curve) for the inversion products shown in Figure 2-18 with varying (α). The parameter of 0.316, which is near the maximum curvature of the L-Curve is chosen for all inversions. 72

Figure 2-20 Comparison of (a) deterministic inversion with a regularisation parameter of 0.316 to (b) the RJMCMC simulation models for the repeat line considered. 73

Figure 2-21 Comparisons of inversion results for repeat line 1 with different prior conductivities. (a) Inversion with a 10000 Ωm half-space prior model. (b) Inversion with a 1 Ωm prior model. (c) Compiled model taken from the geometric mean of the 10000 Ωm and 1 Ω models. (d) Data misfit for each of the 3 models in (a) – (c). 75

Figure 2-22 Comparison of (a) the combined deterministic inversion with a regularisation parameter of 0.316 and parameter shading based on 2 different prior models to (b) the RJMCMC simulation models for the repeat line. 76

Figure 2-23 – a) NSW WB Clark Geoscience Centre - Londonderry Drillcore Library and b) example of cores with intrusive rocks in the Narrabri region (exploration well DME Narrabri 38). 77

Figure 2-24 – Core of dolerite intrusion at Rosevale 1 exploration well in the NSW WB Clark Geoscience Centre - Londonderry Drillcore Library. 78

Figure 2-25 – Core of Digby Formation conglomerate at Tintsfield 1 exploration well in the NSW WB Clark Geoscience Centre - Londonderry Drillcore Library. 79

Figure 2-26 – Core sampling locations of igneous (intrusive) and sedimentary rocks in the Narrabri region overlain on simplified surface geology. 80

Figure 2-27 – Schematic example highlighting the timing of intrusive activities in the Narrabri region. 83

Figure 2-28 – Selected examples of igneous rock samples collected for K-Ar geochronological analysis. 85

Figure 2-29 – Groundwater sampling locations of the current study and previous groundwater investigations in the Narrabri region (updated from Raiber et al. (2022a) overlain on simplified surface geology. 87

Figure 2-30 – Exsolution of gas during sampling of groundwater bore Plumb Road 2 (GW971623-2) (Suckow et al., 2019). 88

Figure 2-31 – a) Conceptual model of GAB aquifers and aquitards and spatial relationships with volcanic and alluvial aquifers and geological structures (modified from Raiber et al., 2022b) and b) examples of approximate age scales and tracer concentrations (Suckow, 2014) expected at different flow path intervals in a). 91

Figure 2-32 – Simplified explanation of the inverse geochemical modelling calculation. 99

Figure 3-1 – Three-dimensional view of stratigraphic logs and intrusions (dark blue intervals) recorded within sedimentary bedrock (beige intervals) sequences along exploration well paths in the Narrabri Gas Project area. 101

Figure 3-2 - Observed occurrences of intrusive igneous rocks and corresponding stratigraphic units intersected in stratigraphic and exploration wells and groundwater monitoring bores. . 102

Figure 3-3 – Igneous intrusions at Bohena anticline, showing variability of thickness observed at different exploration wells and groundwater observation bores (Plumb Road – GW971623) (stratigraphic logs are sourced from NSW DIGS). 103

Figure 3-4 – Lithological variability within Surat Basin and Gunnedah Basin formations in NSW along selected exploration wells (modified from Norton and Rollet, 2023). The locations of wells are shown in Figure 2-8 and Figure 3-1. 104

Figure 3-5 – Sedimentary environment at the time of the deposition of the a) upper and b) lower part of the Purlawaugh Formation (deposited between 190 to 165 million years ago; Australian Stratigraphic Unit Database) (Geoscience Australia, 2025a). 105

Figure 3-6 – Sedimentary environment at the time of the deposition of the Orallo Formation (deposited during the Cretaceous between 140 to 149 million years ago; Australian Stratigraphic Unit Database) (Geoscience Australia, 2025a). 106

Figure 3-7 – Hydrographs for selected bores used in our cross-section groundwater flow models. Note that both GW971623-1 and GW971623.2 are artesian and measured in pressure. 109

Figure 3-8 – XRD results from various intervals in the Coonarah 2 and Tunamallalee 1 exploration wells in the Narrabri Gas Project area. It shows that the mineralogy of most intervals is dominated by quartz and feldspar. 112

Figure 3-9 – XRD results of core samples from borehole Tintsfield 1 at various depth intervals, which are rounded to the nearest 0.1 m for annotation purposes. 113

Figure 3-10 – XRD results of core samples of igneous intrusions from exploration wells in the Narrabrah Gas Project region, which show a dominant quartz, plagioclase and pyroxene compositions. 115

Figure 3-11 – X-ray diffraction (XRD) showing mineralogical composition of Surat Basin and shallow Gunnedah Basin formations. Where multiple measurements were available for a formation, the median composition is presented. 116

Figure 3-12 – X-ray diffraction (XRD) showing mineralogical composition of deeper Gunnedah Basin formations. Where multiple measurements were available for a formation, the median composition is presented. 117

Figure 3-13 - Strontium isotope ($^{87}Sr/^{86}Sr$) signature in rock (core) samples. 120

Figure 3-14 – Thin section of Parkes 3 (PPL) 122

Figure 3-15 – Thin section of Parkes 3 (200.38-200.40 m depth) 122

Figure 3-16 – Thin section of Parkes 3 (200.38-200.40 m depth) 123

Figure 3-17 – Thin section of Dewhurst DDH1 (PPL) (293.80-293.87m). 124

Figure 3-18 – Thin section of Turrawan 1 Set 3 PPL 125

Figure 3-19 – Thin section of Narrabri 6 at 10x exaggeration. 125

Figure 3-20 – Selected part of thin section of Narrabri 6 Set 1 XPL 126

Figure 3-21 – Selected part of thin section of Narrabri 6 Set 1 XPL 126

Figure 3-22 – Selected part of thin section of Narrabri 6 Set 5 XPL 127

Figure 3-23 - Historic and new igneous (intrusive and extrusive) rock age analysis data and airborne magnetic survey overlain on simplified surface geology and total magnetic intensity. The scale for the total magnetic intensity survey data is shown in Figure 3-24. 130

Figure 3-24 – Total Magnetic Intensity map in the Narrabri Gas Project area derived from SkyTEM airborne electromagnetic survey overlain on simplified surface geology. 132

Figure 3-25 – First derivative of Total Magnetic Intensity map in the Narrabri Gas Project area derived from SkyTEM airborne electromagnetic survey overlain on simplified surface geology. 133

Figure 3-26 – Comparison of a) intersection of igneous rocks in stratigraphic wells with b) Total Magnetic Intensity map in the Narrabri Gas Project area derived from SkyTEM airborne electromagnetic survey. 134

Figure 3-27 – Composite seismic section through the Brigalow Park and Coonarah anticlines (for locations, see Figure 3-25) with mapped horizons (Eastern Star Gas, 2004), modified by Raiber et al. (2022a). 135

Figure 3-28 – Narrabri airborne electromagnetic (AEM) inversions, showing >60 AEM sections, major surface water courses and outcrop areas of the Pilliga Sandstone. Red colours correspond to conductive material (e.g. clay) and blue colours correspond to resistive material such as sand. 136

Figure 3-29 – Narrabri airborne electromagnetic (AEM) inversions, showing >60 AEM sections, surface water courses and selected geological features. The figure also shows the location of the Hunter-Mooki Thrust Fault. 137

Figure 3-30 – Three-dimensional model of Narrabri airborne electromagnetic (AEM) inverted conductivity, surface water and selected geological features. Red colours correspond to conductive material (e.g. clay) and blue colours correspond to resistive material such as sand. 138

Figure 3-31 – Selected representative AEM depth conductivity sections discussed further in this report. The orange line represents the minimum inferred extent of the Cenozoic Nandewar Volcanic Centre. The approximate locations of selected exploration wells are shown in italic letters. 139

Figure 3-32 – Comparison of AEM patterns with stratigraphic well data. The dashed black line represents the inferred interface between the Pilliga Sandstone and the Purlawaugh Formation. Green labels on cross-section show where the formation top of the Purlawaugh Formation has been identified in stratigraphic logs. 145

Figure 3-33 – Conductivity-depth structure along AEM line 100100. The orientation of the line is shown in the inset map. 146

Figure 3-34 – Conductivity-depth structure along AEM line 100700. The orientation of the line is shown in the inset map. 147

Figure 3-35 – Selected AEM lines and base of Cenozoic elevation showing increase of thickness of Cenozoic from south to north and east to west. 148

Figure 3-36 – Selected AEM lines, elevation of the base of Pilliga Sandstone and representative XRD patterns of the Pilliga Sandstone within the recharge beds and in deeper parts of the Surat Basin. 149

Figure 3-37 – Conductivity-depth structure along AEM line 102000. The orientation of the line is shown in the inset map. The question mark indicates the possible extent of a Jurassic intrusion at Nyora where the stratigraphic log at Nyora 1 exploration well suggests that both Purlawaugh Formation and Napperby Formations are absent. 150

Figure 3-38 – Conductivity-depth structure along AEM line 102800. The orientation of the line is shown in the inset map. The question mark indicates an area where the interface between the Orallo Formation and Pilliga Sandstone cannot be differentiated with high confidence based on the electromagnetic signal. 151

Figure 3-39 – Conductivity-depth structure along AEM line 103400. The orientation of the line is shown in the inset map. 152

Figure 3-40 – Conductivity-depth structure along AEM line 103900. The orientation of the line is shown in the inset map. The question mark indicates an area where a miss-match between AEM interpretations and well log stratigraphic picks has been observed, likely due to an incorrect well location or stratigraphic records. 153

Figure 3-41 – Conductivity-depth structure along AEM line 104300. The orientation of the line is shown in the inset map. The question mark in the west indicates an area where a miss-match between AEM interpretations and well log stratigraphic picks has been observed, possibly due to an incorrect well location or stratigraphic records. Question marks in the east indicate uncertain formation attributions, which will be further explored in updated inversions. 154

Figure 3-42 – Conductivity-depth structure along AEM line 105000. The orientation of the line is shown in the inset map. Question marks in the east indicate uncertain formation attributions and boundaries, which will be refined further in updated inversions. 155

Figure 3-43 – Conductivity-depth structure along AEM line 105700. The orientation of the line is shown in the inset map. 156

Figure 3-44 – a) Seismic line FSG98-AAC (see also Figure 2) and stratigraphic logs along transect for geochemical modelling (see also Figure 2-4) and b) AEM, stratigraphic logs and inferred shallow formation interfaces along transect CS1. For orientation, see Figure 3-25. The vertical exaggeration is approximately 25. 159

Figure 3-45 – Representative east-west oriented geological cross-section CS1 through the Narrabri Gas Project area (for orientation of cross-section, see Figure 3-25). The vertical exaggeration is approximately 25. 160

Figure 3-46 – Representative east-northwest oriented geological cross-section CS2 with stratigraphic logs, AEM and inferred layer boundaries through the Narrabri Gas Project area (for orientation, see Figure 3-25). The vertical exaggeration is approximately 30. 161

Figure 3-47 – Representative east-northwest oriented geological cross-section CS2 through the Narrabri Gas Project area (for orientation, see Figure 3-25). The vertical exaggeration is approximately 30. 161

Figure 3-48 – Spatial distribution of groundwater salinity for Pilliga Sandstone in the Narrabri Gas Project area overlain on simplified surface geology (from Raiber et al., 2022a). 163

Figure 3-49 – Groundwater salinity for Surat and Gunnedah basins formation and electromagnetic depth-conductivity structure for the Orallo Formation and Pilliga Sandstone along east-west oriented geological cross-section CS1 through the Narrabri Gas Project area (for orientation, see Figure 3-25). 164

Figure 3-50 – Groundwater salinity for Surat and Gunnedah basins formation and Pilliga Sandstone along east-northwest oriented geological cross-section CS2 through the Narrabri Gas Project area (for orientation, see Figure 3-25). 165

Figure 3-51 - Piper diagram that represent relative proportion of major ions in all groundwaters within the Narrabri Gas Project area. The data displayed in this figure present an ionic balance below 20%. 166

Figure 3-52 – Cluster-membership for groundwaters in the Pilliga region based on all available data (Cresswell (2014), WaterNSW (2024), Iverach et al. (2017, 2020a), Raiber and Suckow (2018), Suckow et al. (2019), NSW DPIE (2021), Raiber et al. (2022a) and the current study).. 167

Figure 3-53 – Groundwater chemistry cluster membership for Surat and Gunnedah basins formation along east-northwest oriented geological cross-section through the Narrabri Gas Project area (for orientation, see Figure 3-25). 169

Figure 3-54 - Water stable isotopes (δ^2H vs $\delta^{18}O$) in groundwaters displayed by aquifer......... 172

Figure 3-55 – Concentrations of methane versus a) electrical conductivity (EC); and b) bore depth. 175

Figure 3-56 – Spatial distribution of dissolved methane concentrations without differentiation of hydrostratigraphic formations overlain on simplified surface geology. Methane concentrations are based on Cresswell (2014), Iverach et al. (2020a), Suckow et al. (2019), Raiber et al. (2022a) and the current study. 177

Figure 3-57 – Spatial distribution of methane concentrations in formations below the Pilliga Sandstone (i.e. Purlawaugh Formation and Gunnedah Basin strata) overlain on simplified surface geology. 178

Figure 3-58 – Ternary diagram showing dissolved methane based on measurements at three different analytical laboratories. The mid-point indicates where a sample would be located if concentrations in all laboratories were equal. 179

Figure 3-59 – Spatial distribution of methane (CH_4) concentrations within Pilliga Sandstone and Orallo Formation overlain on simplified surface geology and total magnetic intensity. For scale bar of total magnetic intensity, see Figure 3-24 182

Figure 3-60 – Dissolved methane concentrations for Surat and Gunnedah basins formation along east-northwest oriented geological cross-section through the Narrabri Gas Project area (for orientation, see Figure 3-25)........ 183

Figure 3-61 – Histogram of methane concentrations displayed by aquifers. The number of samples assigned to each interval are shown in table below the histogram. This includes multiple measurements at some sites. The *relates to measurements of dissolved methane at groundwater bore GW099038, the only groundwater bore screened within the Pilliga Sandstone where dissolved methane of >5000 µg/L was measured........ 184

Figure 3-62 – Methane concentration versus redox potential of Pilliga Sandstone groundwater samples. Methane concentrations are based on Cresswell (2014), Iverach et al. (2020a), Suckow et al. (2019), Raiber et al. (2022a) and the current study. 185

Figure 3-63 – Spatial distribution of CH_4 concentrations within alluvium/colluvium overlain on simplified surface geology (Cresswell (2014), Iverach et al. (2020a), Raiber et al., (2022a) and the current study). 188

Figure 3-64 – Isotopes of a) $\delta^{13}C$ of CH_4 versus $\delta^{13}C$ of CO_2; and b) $\delta^{2}H$ of CH_4 versus $\delta^{13}C$ of CH_4. 190

Figure 3-65 Comparison of δ13C of CH4 versus bore depth. Alluvial data are from Iverach et al. (2020a) and other data are from Eastern Star Gas (2008-2011), Suckow et al. (2019), Raiber et al. (2022a) and the current study. 191

Figure 3-66 – Strontium isotope ratios versus a) electrical conductivity (EC); and b) depth in groundwaters collected from the Pilliga Sandstone and other formations within the Surat and Gunnedah basins........ 193

Figure 3-67 – Spatial distribution of $^{87}Sr/^{86}Sr$ ratios in Pilliga Sandstone groundwater overlain on simplified surface geology. 195

Figure 3-68 – Spatial distribution of $^{87}Sr/^{86}Sr$ ratios in groundwater (other than Pilliga Sandstone) in the Narrabri region overlain on simplified surface geology. Where only one circle is shown at nested bore sites, this means that the values of different formations are in the same $^{87}Sr/^{86}Sr$ interval. 196

Figure 3-69 – Spatial distribution of $^{87}Sr/^{86}Sr$ ratios in groundwater along transect through central part of Narrabri Gas Project area (for orientation, see Figure 3-25)........ 197

Figure 3-70 Geochemical evidence of similarity in hydrochemical composition of the Pilliga Sandstone and Orallo Formation at Nyora in the north-western part of the Narrabri Gas Project area 198

Figure 3-71 – Strontium isotope ratios versus a) Sr concentrations; and b) $\delta^{13}C$-DIC in groundwaters collected from the Pilliga Sandstone and other formations within the Surat Basin in NSW........ 200

Figure 3-72 Saturation indexes displayed by aquifer for all bores sampled in the survey area. 202

Figure 3-73 Saturation indexes displayed by aquifer for selected bores along the geochemical cross-section 203

Figure 3-74 Comparison of ^{3}H and ^{14}C in groundwaters of the alluvium, Surat Basin, Gunnedah Basin and Garrawilla Volcanics. ... 205

Figure 3-75 – Spatial distribution of radiocarbon activities of groundwater in the Pilliga Sandstone overlain on simplified surface geology. ... 206

Figure 3-76 – Distribution of radiocarbon (^{14}C) in bores along cross-section 1 (for orientation of this cross-section, see Figure 3-25). ... 208

Figure 3-77 – Chlorine-36 in groundwaters of formations below the Pilliga Sandstone (Gunnedah Basin strata, Garrawilla Volcanics and Purlawaugh Formation) in the Narrabri Gas Project area)(some measurements are still pending) overlain on simplified surface geology. 210

Figure 3-78 – Vertical distribution of ^{36}Cl in bores along cross-section 2 (for orientation of this cross-section, see Figure 3-25) and electromagnetic depth-conductivity structure for the Orallo Formation and Pilliga Sandstone. ... 211

Figure 3-79 – Spatial distribution of $^{36}Cl/Cl$ of groundwater in the Pilliga Sandstone overlain on simplified surface geology. ... 213

Figure 3-80 – Spatial distribution of $^{36}Cl/Cl$ of groundwater in the Pilliga Sandstone, Orallo Formation and a Cenozoic groundwater bore (IR1) in the Narrabri Gas Project area overlain on simplified surface geology. ... 214

Figure 3-81 – Vertical distribution of chlorine-36 (^{36}Cl) in bores along cross-section 1 (for orientation of this cross-section, see Figure 3-25) and electromagnetic depth-conductivity structure for the Orallo Formation and Pilliga Sandstone. ... 215

Figure 3-82 – Spatial distribution of ^{4}He in groundwaters below the Pilliga Sandstone (Gunnedah Basin strata and Purlawaugh Formation) in the Narrabri Gas Project area overlain on simplified surface geology. ... 217

Figure 3-83 – Spatial distribution of ^{4}He in Pilliga Sandstone the wider Coonamble Embayment (a sub-basin of the Surat Basin) overlain on simplified surface geology. ... 218

Figure 3-84 – Spatial distribution of ^{4}He in the Pilliga Sandstone, Orallo Formation and Bohena Creek alluvium (Inland Rail bore) in the Narrabri Gas Project area overlain on simplified surface geology. Selected exploration wells are shown for geological context. ... 220

Figure 3-85 – ^{4}He distribution in bores along cross-section 1 (for orientation of this cross-section, see Figure 3-25). ... 221

Figure 3-86 – ^{4}He distribution in bores along cross-section 2 (for orientation of this cross-section, see Figure 3-25). ... 222

Figure 3-87 – Helium isotope ($^{3}He/^{4}He$) ratios versus the Ne/He elemental ratio in Surat Basin and Gunnedah Basin groundwaters and other selected samples. ... 223

Figure 3-88 – Spatial distribution of estimated mantle (primordial) helium in the sedimentary bedrock below the Pilliga Sandstone in the wider Narrabri Gas Project area overlain on simplified surface geology and total magnetic intensity map. ... 224

Figure 3-89 – Vertical distribution of mantle helium in bores along cross-section 1 (for orientation of this cross-section, see Figure 3-25). ... 226

Figure 3-90 – Vertical distribution of mantle helium in groundwater and electromagnetic depth-conductivity structure for the Orallo Formation and Pilliga Sandstone along cross-section 2 (for orientation of this cross-section, see Figure 3-25). 227

Figure 3-91 – Spatial distribution of $^{3}He/^{4}He$ ratios in the Pilliga Sandstone within the Coonamble Embayment area overlain on simplified surface geology. 231

Figure 3-92 – Spatial distribution of estimated mantle (primordial) helium in the Pilliga Sandstone, Orallo Formation and alluvium (Inland Rail bore) in the wider Narrabri Gas Project area overlain on simplified surface geology and total magnetic intensity map. 232

Figure 3-93 – Three-isotope plot of argon (based on data from Suckow et al., 2019, Raiber et al., 2022a and the current study). 233

Figure 3-94 – A) $^{3}He/^{4}He$ versus $^{40}Ar/^{36}Ar$; and B) $^{40}Ar/^{36}Ar$ versus helium concentration. 236

Figure 3-95 – Comparison of ^{36}Cl and ^{81}Kr in Great Artesian Basin groundwaters. 237

Figure 3-96 – Simulated and observed hydraulic heads in the investigated transect. Circles indicate observed heads at monitoring locations. The primary target coal seams are hosted within the Maules Creek Formation. 241

Figure 3-97 – Simulated and observed groundwater ages in the investigated transect. Circles indicate observed age estimates at monitoring locations. The primary target coal seams are hosted within the Maules Creek Formation. 241

Figure 3-98 - Geochemical evolution along inferred flow path in the Pilliga Sandstone at selected groundwater monitoring bores along the CS2 246

Figure 3-99 - Inverse model results represented with conceptual flows in cross-section 1 (CS1) (Part A) 249

Figure 3-100 - Inverse model results represented with conceptual flows in cross-sections 2 (CS2) and cross-section 1 (CS1) (Part B) 250

Figure 4-1 – Stratigraphy of the Surat and Gunnedah basins in NSW (compiled from Tadros (1993, 1995), Carty and Smith (2003), Korsch and Totterdell (2009), Totterdell et al. (2009), Geoscience Australia (2013), Ransley et al. (2015), Ruming (2015), Raiber et. al (2022a), Norton and Rollet (2023)) and the current study. Q and P/N in the Cenozoic era correspond to Quaternary and Palaeogene/Neogene. 263

Figure 4-2 – Refined conceptual hydrogeological model and potential connectivity pathways in the wider Narrabri region. 265

Figure 4-3 – Spatial data gaps within the Narrabri Gas Project area overlain on simplified surface geology. 274

Tables

Table 1 Secular equilibrium ^{36}Cl values used for calculation (Bentley et al., 1986). 93

Table 2 Petrophysical properties used in the groundwater flow modelling. 107

Table 3 Hydraulic head median measurements used as history matching constraints for the groundwater flow and solute transport model. See Figure 3-45 for the location of the bores on the cross-section. 109

Table 4 Quantitative XRD analysis results (weight %) of the bulk, micronized and calcium saturated samples. 115

Table 5 Strontium isotope signatures of rocks (min, max and samples count (N)) displayed by stratigraphic unit and according to analytical method (i.e. whole rock or partial digestion by weaker acid) 118

Table 6 K-Ar dating results of core samples from various intrusions within the Narrabri Gas Project region. 129

Table 7 – Median concentrations of hydrochemical parameters for the five groundwater chemistry clusters of data in the Narrabri region based on all data available for this study (Cresswell (2014), Raiber et al. (2018), Suckow et al. (2019), Raiber et al. (2022a), data provided by WaterNSW and the current study. The ratios are by mass. Median depths of each cluster are also shown. 168

Table 8 - Water stable isotope signature by aquifer. GB : Gunnedah Basin, SB : Surat Basin. Alluvial groundwater samples are mostly sourced from Iverach et al. (2017). 173

Table 9 Apparent groundwater age estimates based on ^{14}C and ^{36}Cl and complemented by evidence from ^{3}H, $^{3}He/^{4}He$, ^{4}He, ^{40}Ar, ^{81}Kr and ^{85}Kr used as history matching constraints for the groundwater flow and solute transport model. See Figure 3-96 for the locations of the bores on the cross-section. 239

Table 10 Groundwater bores along cross-sections 1 and 2 used for geochemical mixing calculations 247

Table 11 Interrogated inverse modelling variants (WQ: Water quality) 248

Table 12 Data worth analysis 270

Acknowledgement

This research has been funded through CSIRO's Gas Industry Social and Environmental Research Alliance (GISERA) with contributions from the Australian Government's Department of Industry, Science and Resources. GISERA is a collaboration between CSIRO, Commonwealth, state and territory governments and industry established to undertake research on the impacts of onshore gas exploration and development on the environment, and the socio-economic costs and benefits. For information about GISERA's governance structure, projects and research findings visit https://gisera.csiro.au.

The authors would like to thank Santos for providing access to their groundwater monitoring wells for sampling of environmental tracers.

Water NSW are also thanked for their on-going support of the project, for data provision, for providing access to groundwater monitoring bores and for field sampling support.

We would like to thank the NSW Department of Climate Change, Energy, the Environment and Water (DCCEEW) for discussions, feedback and their on-going support of this project.

We further would like to thank Associate Professor Bryce Kelly from the University of New South Wales and Dr. Dioni Cendón from the Australian Nuclear Science and Technology Organisation for sharing their insights into the hydrogeology of the Namoi region.

Richard Cresswell (Eco Logical) and Titus Murray (Southern Highlands Geoscience) are thanked for feedback on design of airborne electromagnetic survey. Keith Phillipson (AGE Consulting) is thanked for providing data on groundwater hydraulics.

The authors would also like to acknowledge the Australian Nuclear Science and Technology Organisation for providing a grant for the analysis of groundwater age tracers and for providing analyses of tritium, radiocarbon and ^{36}Cl.

Stewart Fallon and Keith Fifield (both Australian National University) are thanked for providing analyses of radiocarbon and ^{36}Cl.

We would like to thank Andrew McPherson, Nadege Rollet and John Vizy from Geoscience Australia for sharing data and providing valuable insights and feedback that helped to significantly improve the interpretations of the geological framework and airborne electromagnetic data.

Michael Silburn and colleagues from the Geological Survey of New South Wales and the Clarke Geoscience Centre are thanked for facilitating access to the core library and logistical support during the collection of core samples for mineralogical and geochronological analysis.

The authors would also like to thank Astrid Carlton and John Davidson from the NSW Geological Survey for feedback on the design of the AEM survey.

David Midgley (CSIRO Energy) and his team are thanked for providing groundwater samples for hydrochemical and isotope analysis in the Narrabri region.

Chris Turnadge, Sreekanth Janardhanan and Adam Siade, all CSIRO and working on the parallel GISERA project "Groundwater modelling and predictive analysis to inform CSG impact assessment, monitoring and management", are thanked for on-going discussions on groundwater age simulations.

Harald Hofmann and Adam Siade (both CSIRO Environment) are thanked for discussions during geochemical modelling workshops.

Andrew Todd (CSIRO Energy) is thanked for conducting K-Ar geochronological analysis of igneous rocks.

SkyTEM Australia are thanked for conducting the airborne electromagnetic survey in November 2023.

Julie Pearce from the University of Queensland is thanked for on-going discussions on sampling techniques of methane concentrations and isotopes.

Thin Section Australia are thanked for generating thin sections of igneous rocks.

Mathew Beddard from SLR Consulting is thanked for generating images of thin sections and for providing petrographic descriptions of thin sections of igneous rocks.

The Central Analytical Research Facility at Qld University of Technology is thanked for developing thin sections and conducting XRD and XRF analyses.

The authors also wish to thank GISERA Director Damian Barrett, Jizelle Khoury, Paul Cunningham, Melina Gillespie, Francoise van Es, David Midgley and Cameron Huddlestone-Holmes (GISERA) for their continuous support in planning and conducting this study and reporting and communicating the results.

The authors would also like to thank Andrew Taylor and Russell Crosbie (CSIRO Environment) for their very useful internal review comments.

Summary

Background

This project "Geochemical modelling and geophysical surveys to refine understanding of connectivity between coal seams and aquifers" originated in response to (i) on-going uncertainties and community concerns related to the role of geological structures (e.g. faulting and igneous intrusions) as potential pathways for aquifer inter-connectivity, (ii) on-going knowledge gaps highlighted by previous GISERA projects in the Narrabri region ('Impacts of CSG depressurisation on the Great Artesian Basin (GAB) flux' and 'Assessment of faults as potential hydraulic seal bypasses in the Pilliga Forest area, NSW'), and (iii) to advice on the Narrabri Gas Project by the Independent Expert Scientific Committee on Coal Seam Gas and Large Coal Mining Development (IESC, 2017).

Understanding the impacts of coal seam gas (CSG)-driven depressurisation on aquifers and surface water features requires identifying geological structures, assessing their role as potential connectivity pathways or barriers in inter-aquifer-aquitard connectivity, and assessing hydraulic head observations and hydrochemical and environmental tracer patterns that can indicate presence or absence of hydrogeological connectivity pathways. Developing this knowledge involves studying fluid movement mechanisms through sedimentary sequences from hydrocarbon resources to groundwater resources, using multiple lines of evidence.

In the previous GISERA project 'Assessment of faults as potential hydraulic seal bypasses in the Pilliga Forest area, NSW', Raiber et al. (2022a) identified on-going uncertainties and knowledge gaps relating to the role of faults and in particular the geometry and timing of igneous intrusions as key knowledge gaps. Although ground-based electromagnetic surveys provided valuable results in previous hydrogeological investigations, Raiber et al. (2022a) suggested that conducting an airborne electromagnetic (AEM) survey could help to obtain a more spatially continuous picture of the subsurface structure. Based on lessons learned from ground-based surveys, the authors also suggested that insightful imagery to great depths (>400 m below ground surface) could be obtained.

This project addressed knowledge gaps identified in the previous GISERA project 'Assessment of faults as potential hydraulic seal bypasses in the Pilliga Forest area, NSW' through the application of a comprehensive and integrated multi-disciplinary approach consisting of six major components:

1) Geochronological (K-Ar) analysis of igneous rocks to determine the timing of intrusive activity in the Narrabri region.
2) Mineralogical and lithological assessment of key aquifers, partial aquifers, aquitards and coal seams in Surat and Gunnedah basins and of intrusive rocks.
3) Assessment of aquifer geometry and identification of potential hydrogeological connectivity pathways using an AEM survey to complement geophysical surveys conducted in previous hydrogeological and hydrocarbon investigations and obtain a more spatially continuous picture of the subsurface structure.

4) Collection of additional hydrochemistry and environmental tracer data with a focus on Gunnedah Basin aquitards and coal seams to improve the availability of baseline data in these formations and refine the understanding of potential hydrogeological connectivity pathways between the Gunnedah and Surat basins. This involved integration of new findings from newly acquired data with the knowledge from previous hydrogeological investigations in the region.

5) Integration of all geological, hydraulic, hydrogeological, hydrochemical and geophysical information through numerical modelling and development of a suite of flow, solute transport and geochemical mixing models to test conceptual models of hydrogeological connectivity pathways

6) Refinement of conceptual hydrogeological models and data worth analysis to assess the efficiency of different techniques to resolve key questions and identification of critical knowledge gaps and opportunities for future work.

Key results

Geochronological (K-Ar) analyses to determine the timing of intrusive activity in the Narrabri region.

The geochronological assessment of intrusive rocks based on K/Ar analyses in the Narrabri region aimed to understand the timing of intrusive activity within the wider Narrabri Gas Project area and to provide insights on whether intrusions can form potential connectivity pathways between coal seams and the Pilliga Sandstone, the major GAB aquifer in this region. This investigation revealed that there were likely more phases of intrusive activity during the Mesozoic and Cenozoic eras than previously identified in this area, with main phases occurring during the Late Triassic (approximately 237 to 200 million years ago), Early and Middle Jurassic (approximately 200 to 160 million years ago) and Cretaceous (approximately 145 to 66 million years ago) periods. A core sample from the Coonarah 2 exploration well in the north-west of the Narrabri Gas Project area indicated a more recent Eocene intrusion (~50 million years ago), but all 17 intrusions analysed in this study yielded ages older than the Cenozoic igneous rocks that erupted from the Nandewar and Warrumbungle volcanic centres approximately 13-20 million years ago north and south of the Narrabri Gas Project area.

The wide range of ages of intrusive rocks is likely related to large-scale tectonic processes in Eastern Australia, controlled by the subduction of the Pacific plate beneath the Australian plate. Mesozoic intrusions are linked to collisional events, while those after ~90 Ma are associated with rifting and seafloor spreading. Recent Cenozoic igneous activity generated extrusive magmas in the Nandewar and Warrumbungle volcanic complexes. The implications of this for the role of intrusions as potential connectivity pathways are discussed further below.

Mineralogical and lithological assessment of Surat Basin, Gunnedah Basin and intrusive rocks

The mineralogical, lithological and stratigraphic assessment aimed to refine the existing understanding of the architecture of the Gunnedah and Surat basins formations, including their spatial arrangement, geometry, distribution, and likely connectivity of aquifer materials (such as sand, gravel, or fractured rock) and aquitards (layers of low permeability that restrict water flow).

It also assessed the spatial and geometric relationships between sedimentary host-rock (the rock into which the intrusions were emplaced) and igneous intrusions.

This assessment provided valuable new insights into the composition of the Pilliga Sandstone. The Pilliga Sandstone aquifer was previously often described as a quartzose sandstone with only minor clay and feldspar content, whereas the mineralogical assessment in this study demonstrated that its composition is likely more complex. Within the recharge areas, the Pilliga Sandstone is chemically mature with very high quartz contents (ranging from 75 to 97%, with no or only very minor plagioclase and k-feldspar and the fine component almost entirely consisting of kaolinite). Well-sorted, coarse-grained quartz sandstones typically have higher hydraulic conductivity because the grains are more uniform, creating larger and more connected pore spaces. Further down along the hydraulic gradient at the Coonarah 2 exploration well in the north-western part of the Narrabri Gas Project area, the Pilliga Sandstone has a much more heterogeneous and immature mineralogy with significantly less quartz (60-70%) and higher content of detrital micas, feldspars (plagioclase and k-feldspar), kaolinite, smectite, and Ca–Mg-Fe carbonates. The assessment also further underpinned the differentiation of the Purlawaugh Formation into an upper aquitard (composed of claystone and other low permeability strata) and a basal aquifer (composed of coarser sediments such as sand).

The assessment of the spatial and geometric relationships of intrusions and their host-rock (the rock into which the intrusions were emplaced) provided valuable information. The geochronological assessment of intrusive rocks demonstrated that some intrusions were emplaced after the deposition of the Pilliga Sandstone, which occurred approximately 150 million years ago. Although these could therefore have intruded into the Pilliga Sandstone, no intrusive rocks were identified in stratigraphic logs within the Pilliga Sandstone and other Surat Basin strata. However, some igneous rocks were identified at the base of the Purlawaugh Formation (the deepest formation of the Surat Basin) in the centre of the Narrabri Gas Project area at the Bohena anticline. A possible reason for the lack of intrusions observed within the Surat Basin strata includes the proposed absence of significant basement faults with major displacements that continued from the Gunnedah Basin into the Surat Basin (as intrusions often follow zones of structural weakness). Another possible reason for the inferred absence is the thermal conductivity and higher convective heat loss of siliciclastic sandstones, which means that the heat associated with intruding lava would have likely dissipated through the pores and fractures and rapid heat loss would have occurred as lava hit groundwater before it could form a significant intrusion. Relatively-widely spaced exploration wells in the eastern part of the Narrabri Gas Project area mean that it cannot be ruled out that some small intrusions were not identified here.

Assessment of aquifer geometry and identification of potential hydrogeological connectivity pathways using an Airborne Electromagnetic (AEM) survey

The AEM survey conducted by SkyTEM with a helicopter on behalf of CSIRO in November 2023 generated 2,765 line km of electromagnetic data. The processed data formed the basis for 60 east-west-oriented conductivity-depth sections with lengths of up to 80 km. The patterns of the conductivity-depth structure were assessed throughout different geographic zones within the Narrabri Gas Project area from north to south and towards the east to identify notable structural patterns related to the geometry and architecture of the subsurface within depths to approximately 400 m below the ground surface.

In the northern part of the AEM survey area (corresponding to the area north of the Narrabri Gas Project area), the results showed that there is a thick (>100 m), conductive cover comprised of low permeability sediments, limiting the resolution of the conductivity-depth structure of underlying formations and making it difficult to identify formation boundaries accurately in this area. Additional re-processing and inversions of the AEM data may help to further increase the depth resolution here. Two survey lines extended east to include the outcrop of the Pilliga Sandstone and remnants of Cenozoic volcanism. In this north-eastern area, the conductive cover thins, and bedrock formations are exposed at the surface or underneath thin cover. Furthermore, the survey indicated the presence of subsurface structures near the Nandewar Volcanic Centre in this north-eastern part of the AEM survey area. These are at approximately 20-30 km north of the Narrabri Gas Project area and possibly linked to faults or intrusions associated with Cenozoic volcanism. The Namoi River alluvium is distinguishable in the AEM conductivity-depth sections from surrounding lower permeability strata by its lower conductivity.

In the central part of the AEM survey area, the conductive cover thins significantly compared to the northern region but remains relatively thick. The Pilliga Sandstone shows a more resistive electromagnetic response here, influenced by the thinning cover. An east-west evolution of the geo-electrical response within the Pilliga Sandstone is observed, confirming the results of the mineralogical analyses, with cleaner, sandier and resistive facies in the east and more conductive, finer-grained material including clay minerals, feldspar and carbonates in the west. Conductivity-depth sections show that there is no distinct and mappable boundary between the Pilliga Sandstone and Orallo Formation throughout this area. There is no evidence for deep-seated faults in this area extending into the Surat Basin, but as also suggested by seismic surveys and hydrocarbon investigations in previous investigations, the AEM survey indicates that low amplitude or forced folds possibly linked to intrusions are likely present in the northern part of the Narrabri Gas Project area. These are characterised by gently undulating geometry of more conductive layers such as the Purlawaugh Formation. Some of the intrusions near these features were dated with the K-Ar technique as Cretaceous (and thus have occurred after the deposition of the Pilliga Sandstone). These areas were identified in previous investigations as anticlines and as potential hydrocarbon traps (suggesting that they are likely sealed off by aquitards at all four sites as hydrocarbons such as methane would otherwise escape). Although the depth resolution is limited by the relatively thick conductive cover, the AEM sections do not show any obvious significant vertical displacements of conductive layers here. However, previous seismic imagery suggested displacements of Gunnedah Basin formations and a possible minor displacement of the base of the Purlawaugh Formation.

In the southern and south-eastern part of the Narrabri Gas Project area, the thickness of the conductive cover is very small. The base of the Pilliga Sandstone and its interface with the Purlawaugh Formation are characterised by a well-defined contrast in the conductivity-depth sections. The Pilliga Sandstone shows a resistive electro-magnetic response in the south and south-east, indicating a clean, sandy facies, while the top of the Purlawaugh Formation is more conductive as it contains more clays and other fine-grained material. The uniform response of the Pilliga Sandstone here is due to the proximity to the sediment source area and the maturity of the Pilliga Sandstone facies described above. The interface between the Pilliga Sandstone and

Purlawaugh Formation is smooth and the thickness of the first conductive layer (corresponding to the upper part of the Purlawaugh Formation) is maintained from east to west, with no obvious vertical juxtaposition. However, low-amplitude folds can be observed in the conductivity-depth sections, coinciding with magnetic anomalies and thus indicating possible igneous intrusions. An intrusion at the Dewhurst DDH1 exploration well in the south of the Narrabri Gas Project area was dated as Mid-Jurassic during this project, suggesting that it occurred after the deposition of the Purlawaugh Formation but likely before or at a similar time to the deposition of the Pilliga Sandstone.

In the eastern part of the AEM survey area to the east of the Narrabri Gas Project area, multiple elongated lines were selected to extend over the Hunter-Mooki Thrust fault. The Hunter-Mooki Thrust fault, located approximately 50 km to the east of the Narrabri Gas Project area, is one of the major tectonic boundaries in Eastern Australia and defines the eastern edge of the Gunnedah Basin and the western front of the New England Orogen in this area. Compared to other areas within the Narrabri Gas Project area where minor deformation is likely to have occurred via low amplitude folds, the eastern extension of the AEM depth-conductivity lines suggests that there was higher amplitude folding in closer proximity of Hunter-Mooki Thrust fault, indicating more significant deformation of the Gunnedah Basin formations. However, on the AEM imagery, the deformation does not visibly extend very far into the west.

Hydrochemical evidence of connection or separation between Gunnedah Basin and Surat Basin formations

Building up on hydrochemical and environmental tracer data collected by previous GISERA projects and other hydrogeological investigations, this study significantly enhanced the understanding of inter-basin and inter-aquifer connectivity in the Narrabri Gas Project area through the integration of existing and newly acquired data. In particular, the collection of additional baseline hydrochemistry and environmental tracer data from the Gunnedah Basin formations in the eastern part of the wider Narrabri Gas Project area provided valuable new insights. The assessment showed that generally, there is a very distinct contrast in measurements for all major connectivity indicators between the Gunnedah and Surat basins. Connectivity indicators used in this study included salinity, major and trace element chemistry, methane concentrations and isotopes, strontium isotopes, groundwater age tracers (e.g. ^{14}C and ^{36}Cl) and stable noble gas concentrations and isotopes. The salinity and concentrations of major and trace elements and dissolved methane are generally low within the Pilliga Sandstone within the eastern, southern and central part of the Narrabri Gas Project area, whereas significantly higher values were observed within the Gunnedah Basin formations. Groundwater age tracers suggest that groundwater in the Pilliga Sandstone is generally relatively young in the south, centre and east of the Narrabri Gas Project area, whereas apparent groundwater ages in some parts of the Purlawaugh Formation and within the Gunnedah Basin formations are much higher (hundreds of thousands of years to > 1 million years). This agrees with the mineralogical assessment, which confirmed that most Gunnedah Basin formations and the upper part of the Purlawaugh Formation are composed of low permeability strata, which limit the rate at which groundwater flows through the rocks, whereas the Pilliga Sandstone is comprised of a sandier and more permeable facies.

Stable noble gases results were very insightful due to their ability to detect interaction of groundwater with igneous intrusions. They demonstrated that high percentages of mantle helium (characterised by elevated $^{3}He/^{4}He$ relative to the Ne/He ratio) and ^{40}Ar are present in all groundwater samples from all Gunnedah Basin formations, including the highest $^{40}Ar/^{36}Ar$ ratios measured in Australia to date (to our knowledge). This is due to the widespread presence of intrusions within the Gunnedah Basin formations. In contrast, most Pilliga Sandstone groundwater samples within the Narrabri Gas Project area have low or very low values for these stable noble gas isotopes. This likely reflects the inferred absence or scarcity of intrusions within the Pilliga Sandstone, and the strong vertical contrast observed between the Pilliga Sandstone and underlying formations suggests a high degree of hydrogeological separation. It also confirms that the Pilliga Sandstone is a transmissive and productive aquifer. Close to the Nandewar Volcanic Centre approximately 10 to 30 km north of the Narrabri Gas Project area, high values of mantle helium (including the highest values measured within the extent of the Great Artesian Basin to date) are observed in some groundwater samples, likely indicating the presence of dyke swarms and tectonic activity associated with the eruption of the lavas approximately 15-20 million years ago in this area.

Some areas of potential connectivity between the Pilliga Sandstone and underlying formations and between the Purlawaugh Formation and Gunnedah Basin formations were identified in previous investigations in the central part of the Narrabri Gas Project area at Plumb Road within the area previously described as Bohena anticline and in the north-western part of the Narrabri Gas Project area. The hydrochemical and environmental tracer patterns are discussed in the next section.

Integration of all geological, hydraulic, hydrogeological, hydrochemical and geophysical information through numerical modelling and geochemical mixing models

As described above, hydrochemistry and environmental tracers suggest that there is a high degree of separation between the Pilliga Sandstone and underlying formations in the south and east of the Narrabri Gas Project area. In contrast, some potential connectivity between the Pilliga Sandstone and underlying formations and between the Purlawaugh Formation and Gunnedah Basin formations was hypothesised in previous studies at Plumb Road (in the centre of the Narrabri Gas Project area) and in the north-western part of the Narrabri Gas Project area. This was based on the observed east-west evolution of hydrochemistry and environmental tracers.

These two areas of potential hydrogeological connectivity were investigated further in this study through the integration of all geological, hydraulic, hydrogeological, hydrochemical and geophysical information through numerical modelling and geochemical mixing models along two representative geological cross-sections CS1 and CS2.

Geological cross-section CS1

At the Bohena anticline in the centre of geological cross-section CS1, a thick (up to approximately 100 m) and spatially extensive sill (a horizontal igneous intrusion) has intruded into the shallow Gunnedah Basin (Napperby and Digby formations) and to the base of the Purlawaugh Formation. Purlawaugh Formation groundwater has high concentrations of methane and high values of mantle helium and ^{40}Ar and low values of ^{36}Cl and ^{81}Kr at this location, indicating that groundwater at this location is very old (likely> 600.000 years) and has experienced some influence of igneous intrusive activity. This indicates that there may be some connectivity between the uppermost Gunnedah Basin formations and the Purlawaugh Formation facilitated by the significant intrusion here. However, the observed presence of coal in the Purlawaugh Formation and the observed sill at the base of the Purlawaugh Formation (which possibly resulted in heating or contact metamorphism of the lower part of the Purlawaugh Formation) suggest that some of the hydrochemical patterns may also be linked to processes occurring within the Purlawaugh Formation. Furthermore, interaction via diffusion between the thin lower aquifer of the Purlawaugh Formation with thicker over- or underlying aquitards (corresponding to the upper part of Purlawaugh Formation and underlying Napperby or Digby formations) may also have occurred and could explain some of the observed patterns such as the changes in ^{36}Cl. In contrast to the Purlawaugh Formation, the Pilliga Sandstone groundwater at this location has a low salinity and shows only a small (but measurable) concentration of methane, has some mantle helium but no elevated ^{40}Ar and the apparent groundwater age is young.

To further investigate whether there is any hydrogeological connection between the different formations along transect CS1, a suite of numerical modelling tools was employed to integrate and interpret the multitude of characterisation and monitoring data that were collected along a representative vertical transect. Groundwater flow was simulated with the widely used numerical modelling tools MODFLOW and MT3DMS. A joint inversion of groundwater heads and apparent groundwater ages (simulated as direct groundwater age) was performed to reduce model uncertainties associated with the non-uniqueness of a head-only model calibration. The results of the modelling suggested that the upper section of the Purlawaugh Formation acts as an effective seal that causes significant head drops of >25 m over short vertical distances. This section of the Purlawaugh Formation likely acts as major groundwater barrier over the entire transect due to the dominance of claystone in the upper part of the Purlawaugh Formation, with the continuity of this low permeability layer also indicated by the AEM survey. In contrast to the upper Purlawaugh Formation, the thinner, lower section of the Purlawaugh Formation appears to have a significantly higher hydraulic conductivity, therefore acting as an effective lateral flowpath from the Purlawaugh Formation outcrop area towards the west.

This assessment was further complemented by geochemical mixing models using hydrochemical and mineralogical data, designed to represent different scenarios of mixing along potential hydrogeological connectivity pathways. The models suggested plausible connectivity between the uppermost Gunnedah Basin (e.g. Digby Formation) and the Purlawaugh Formation, based on hydrochemical patterns. However, some geochemical mixing models were also able to explain observed patterns without a contribution from the Digby Formation. Furthermore, as explained above, lithological heterogeneity within the Purlawaugh Formation, the presence of coal and the localised upwards continuation of sills to the Purlawaugh Formation mean that processes occurring within the Purlawaugh Formation may also contribute to the observed changes in water chemistry.

Geochemical mixing models suggested that based on the mineralogy and water chemistry, it is plausible that there may be a very small admixture of groundwater from the Purlawaugh Formation to the Pilliga Sandstone. In contrast, the mixing models suggested that the hydrochemical evolution cannot be explained by an admixture of groundwater from the Maules Creek Formation (the primary CSG target unit). This could be further refined through the collection of environmental tracer data from a bore screened within the Digby Formation at Plumb Road, which was not operational throughout the course of this study.

Geological cross-section CS2

In the north-western part of the Narrabri Gas Project area, previous GISERA studies suggested that the thinning and pinching out of the Purlawaugh and Napperby formations close to an intrusion observed at Nyora may have resulted in a small admixture of upwards discharging groundwater from the Purlawaugh Formation or uppermost Gunnedah Basin (Napperby or Digby formations) into the Pilliga Sandstone. This was inferred based on (i) the observed change of hydrochemical and environmental parameters including increasing groundwater ages from east towards the north-west and (ii) the assumption that the inferred homogeneity and proposed quartzose nature of the Pilliga Sandstone mean that the changes are unlikely to be a result of a step change in distance velocity associated with changes in hydraulic properties of the Pilliga Sandstone aquifer.

However, as described above, new insights provided by the mineralogical analysis and AEM survey indicate that there is likely a significant change of mineralogical and lithological properties in the Pilliga Sandstone from the eastern recharge beds towards the north-west of the Narrabri Gas Project area. Furthermore, the AEM survey results also indicate that there is no visible aquitard separating the Pilliga Sandstone and the overlying Orallo Formation.

To investigate further if there is a likely hydrogeological connection between the Pilliga Sandstone and the underlying formations along cross-section CS2, a series of geochemical mixing models were developed. The models suggested that the observed evolution of water chemistry from the eastern part of the Narrabri Gas Project area to Nyora could be explained by an admixture from the Purlawaugh Formation and a small contribution from the Digby Formation. It could also be explained by a very small contribution from the Digby Formation if the Purlawaugh Formation is excluded from the mixing models, representing the areas where both Purlawaugh Formation and Napperby Formation are absent. However, none of the mixing models in this area included the Orallo Formation, which overlies the Pilliga Sandstone, as no reliable mid-gradient hydrochemical record was available for the Orallo Formation.

Although multiple hydrochemical parameters and the geochemical mixing models suggest that the observed changes could be explained by mixing with underlying formations, other parameters such as the estimates of mantle helium and ^{40}Ar indicate that it is unlikely that there is any significant mixing between these formations and the Pilliga Sandstone in this area; however, a small admixture (<1-3%) from the deeper formations cannot be ruled out. As an alternative hypothesis, based on the integration of the results from the AEM survey, mineralogical analysis and environmental tracers, this study suggest that the east-west evolution of hydrochemistry and environmental tracers is likely primarily controlled by processes occurring within the Pilliga Sandstone and/or potential connectivity with the Orallo Formation.

Refinement of conceptual hydrogeological models

Based on the multiple lines of evidence presented above, the conceptual hydrogeological model of potential connectivity pathways was further refined. This comprehensive assessment largely confirmed the findings by Raiber et al. (2022a) who suggested that more structural activity is likely to be found in the north and north-west than in the south and east of the Narrabri Gas Project area. The geochronological analyses (rock dating) together with an assessment of the stratigraphic intervals into which intrusions have been emplaced demonstrated that although the intrusions occurred from the Late Triassic to the Cenozoic, they are mostly limited to the uppermost Gunnedah Basin and up to the base of the Purlawaugh Formation. Seismic images and AEM conductivity-depth sections did not reveal a presence of faults with significant displacements in the Surat Basin strata within the Narrabri Gas Project area, although geological structures (faults or dykes) extending into the Surat Basin can be observed in conductivity-depth sections to the north of the Narrabri Gas Project area. This indicates that intrusions are probably the major potential connectivity pathway. However, they are unlikely to form direct connectivity pathways from the coal seams and CSG targets of the Gunnedah Basin to the Pilliga Sandstone in the Narrabri Gas Project area as their occurrence is mostly limited to below the Pilliga Sandstone.

The AEM survey together with the mineralogical assessment provided new insights into the spatial variability of the composition of the Pilliga Sandstone. Previous GISERA studies and geochemical mixing models conducted in the present study proposed that there may be some upwards discharge from the Gunnedah Basin and/or Purlawaugh Formation into the Pilliga Sandstone in the north-western part of the Narrabri Gas Project area. However, the comprehensive data set of stable noble gas ($^{3}He/^{4}He$ and ^{40}Ar) compiled in previous investigations and the current study suggests that within Pilliga-Sandstone processes and connectivity with the Orallo Formation may be the major control of the hydrochemical evolution observed in this area. The integration of all geological, hydraulic, hydrogeological, hydrochemical and geophysical information through numerical modelling supported the hypothesis that the upper part of the Purlawaugh Formation forms an effective seal separating the Pilliga Sandstone from the underlying formations.

Conclusions

The integration of results from the newly acquired AEM survey, mineralogical, hydrochemical and environmental tracer analyses integrated through conceptual, numerical and geochemical mixing models largely confirmed findings by Raiber et al. (2022a). However, the acquisition of these additional geophysical, mineralogical and environmental tracer data from the Gunnedah Basin formations in this project resulted in a higher confidence and less uncertainties.

Some key conclusions are:

- The Narrabri region is characterized by a complex pattern of intrusive igneous activity, which included multiple phases commencing during the late Triassic (approximately 229 million years ago) to the most recent activity during the Cenozoic (approximately 13-20 million years ago). Although some intrusions occurred after the deposition of the Pilliga Sandstone (~150 million years ago), there is no evidence from stratigraphic records within the Narrabri Gas Project area that intrusions have intruded into the Pilliga Sandstone. However, the presence of mantle helium in some Pilliga Sandstone groundwater samples suggested that some water-rock interaction with some intrusive rocks may have occurred.
- The Airborne Electromagnetic (AEM) survey yielded valuable insights to depths of up to approximately 400 m below ground surface. The penetration depth of the AEM survey varied spatially throughout the survey area depending on the thickness of the conductive cover, which significantly decreased from north to south and west to east. The AEM survey

demonstrated that the lithology of the Pilliga Sandstone is much more heterogeneous than what was previously assumed. In the AEM survey, this was marked by a change from a resistive conductivity structure to a more conductive conductivity structure from the eastern outcrop beds to the western part of the Narrabri Gas Project area. The AEM survey also suggested that the Pilliga Sandstone may be connected to the Orallo Formation, as there is no obvious spatially continuous aquitard separating them visibly in conductivity-depth sections.

- The AEM survey confirmed previous assumptions from seismic survey data that faults with significant displacements are unlikely to extend from the Gunnedah Basin into the Pilliga Sandstone, whereas more significant deformation of Gunnedah Basin formations appears to occur east of the Narrabri Gas Project area in proximity of the Hunter-Mooki Thrust Fault. Some geological structures extending closer to the surface (into the Surat Basin strata) can also be observed north of the Narrabri Gas Project area.
- The strong contrast in measurements of connectivity indicators such as stable noble gas isotopes ($^{3}He/^{4}He$) and other environmental tracers and hydrochemical parameters suggest that inferred aquitards (e.g. Porcupine Formation, Watermark Formation and Napperby Formation in the Gunnedah Basin and the upper part of the Purlawaugh Formation in the Surat Basin) are likely continuous and limit hydrogeological connectivity between the Pilliga Sandstone and underlying Gunnedah Basin formations in the eastern and southern part of the Narrabri Gas Project area. High estimates of mantle helium and high ^{40}Ar values, which both indicate some interaction with intrusive rocks, are largely absent or relatively low in most Pilliga Sandstone groundwaters within the Narrabri Gas Project area. In contrast, very high mantle helium percentages are estimated for Pilliga Sandstone groundwaters north of the Narrabri Gas Project area due to the proximity to the Nandewar Volcanic Centre.
- As proposed in previous studies, some local hydrogeological connectivity between the uppermost Gunnedah Basin formations and the Purlawaugh Formation is likely to exist near the Plumb Road groundwater monitoring site. In this area, fracturing associated with a spatially extensive igneous intrusion emplaced into the uppermost Gunnedah Basin (Digby and Napperby formations) and to the base of the Purlawaugh Formation may facilitate some connection between these formations.
- Previous studies assumed that the increase in chloride concentrations, methane concentrations and groundwater ages within the Pilliga Sandstone from the eastern towards the north-western part of the Narrabri Gas Project area near Nyora may be due to potential hydrogeological connectivity between the Pilliga Sandstone and deeper formations. Based on the evidence from additional stable noble gas isotope analyses (particularly of Gunnedah Basin formation groundwater samples) and strontium isotopes, the current study suggests that the observed evolution of hydrochemistry and environmental tracers is likely primarily controlled by within-Pilliga Sandstone processes associated with a change in lithological and hydraulic properties from east to west, and a possible connection with the overlying Orallo Formation.

Knowledge gaps and opportunities for future work

Although this research has resolved multiple knowledge gaps identified by previous GISERA projects and other hydrogeological investigations and has significantly improved our understanding of the groundwater dynamics of the Pilliga Sandstone and adjacent formations, some knowledge gaps remain.

A suite of potential options for future work to further reduce uncertainties in the understanding of hydrogeological connectivity pathways include:

- Conducting a baseline hydrochemistry assessment: at present, all baseline hydrochemistry and environmental tracer data from uppermost Gunnedah Basin formations are from the eastern part of the Narrabri Gas Project area. The collection of additional samples for a comprehensive hydrochemistry and environmental tracer suite from Water NSW Gunnedah Basin bores (e.g. Digby Formation at Plumb Road) that could not be sampled in this project due to issues with permanently installed pumps would help to further reduce uncertainties of geochemical mixing models and the conceptual hydrogeological models of connectivity pathways.
- Sampling new Santos bores (Napperby and Digby formations) in the central part of the Narrabri Gas Project area and analyse for comprehensive suite of hydrochemistry and environmental tracers. This would provide valuable baseline data that could reduce the uncertainty of mixing models.
- Refining AEM survey interpretations through additional processing and inversions: this will likely allow improved resolution of layer boundaries especially in areas where a thick and conductive cover is present.
- Expanding on integration of seismic data with AEM survey data.
- Analysing additional Pilliga Sandstone samples for mineralogy (XRD) to confirm the findings from this study.
- Refining existing 3D geological model: the existing 3D geological model used can be updated with new data to more accurately represent the subsurface structure in the Narrabri Gas Project area.
- Refining the lithological characterisation of the Purlawaugh Formation: the upper part of the Purlawaugh Formation is assumed to be an aquitard that limits connection between the Purlawaugh and shallow Gunnedah formations with the Pilliga Sandstone based on hydraulic and environmental tracer and numerical modelling. Development of a regional sedimentary facies model of the Purlawaugh Formation could help to further confirm the characterisation of the Purlawaugh Formation as an aquifer (lower part) and aquitard (upper part).
- Closing spatial data gaps: the study confirmed previous assessments that there is no evidence for significant connectivity in the south and east of the Narrabri Gas Project area based on baseline data from a relatively large number of groundwater observation bores. However, no groundwater observation bores are available in the central-western and northern part of the Narrabri Gas Project area. Additional nested groundwater monitoring

bore sites and data collection could help to further reduce uncertainties of conceptual hydrogeological models in this area.

1 Introduction

Section 1 of this report provides an overview on previous work and the geological and hydrogeological framework of the wider Narrabri Gas Project area, including a description of the major aquifers and aquitards of the Surat and Gunnedah basins and the understanding of igneous intrusive activity in this region prior to this study. This section explains how faults and igneous intrusions can form potential connectivity pathways and demonstrates how the understanding and conceptual models of potential hydrogeological connectivity pathways in the Narrabri region has evolved over time.

1.1 Aims of this report

This report forms the major delivery task of the GISERA project 'Geochemical modelling and airborne geophysical surveys to refine the understanding of connectivity between coal seams and overlying aquifers' (https://gisera.csiro.au/research/surface-and-groundwater/understanding-connectivity-between-coal-seams-and-aquifers/) and builds on work from previous hydrogeological and geological investigations, including Tadros, 1995; Cresswell (2014), Iverach et al. (2017, 2020a), Santos (2017a and b); Raiber and Suckow (2018), Suckow et al. (2019) and Raiber et al. (2022a, b).

In the Narrabri region (NSW), there have been conflicting views on whether faults extend to the surface in the Jurassic formations of the Surat Basin, and whether they have the potential to form seal-bypass structures that may compromise the integrity of aquitards. There are also significant regional-scale volcanic intrusions (a body of rock that has crystallized from molten magma and which has penetrated existing rock layers) associated with regional-scale tectonism, and their role as potential connectivity pathways has not yet been fully understood. Seismic images confirm that some of these likely penetrate strata of both the Gunnedah and Surat basins in some areas within the broader Narrabri region (Totterdell et al., 2009). Such intrusive features are often associated with regional structural weaknesses such as fault zones, where potential pathways for the upward migration of fluids or gas can exist (Drymoni et al., 2021).

Faults, igneous intrusions, and their associated hydraulic properties have not been considered in the initial groundwater models developed to predict potential impacts from the proposed Narrabri Gas Project or subsequent groundwater models (as discussed by Turnadge et al., 2018; NSW DPIE, 2020). However, where present, fault zones and other seal-bypass structures may form, under certain conditions, preferential pathways to gas and water migration from coal seams to shallow aquifers and surface.

In a previous GISERA project, Raiber et al. (2022a) investigated the role of faults and igneous intrusions as potential hydrogeological connectivity pathways linking Gunnedah Basin strata and shallower productive aquifers such as the Pilliga Sandstone, the most important Great Artesian Basin (GAB) aquifer in this region. Findings from this project based on the combined evidence from geophysics (selected seismic and ground-based electromagnetic data), geology, hydrogeology, hydrochemistry and tracers and hydrochemical mixing models indicated that there may be some hydrogeological connection between the Pilliga Sandstone and the underlying Purlawaugh

Formation and/or the late Gunnedah Basin strata (Napperby or Digby formations) in the northern and north-western parts of the Narrabri Gas Project area, starting near the Plumb Road groundwater monitoring site at the Bohena anticline where a spatially extensive sill (a horizontal intrusion) was identified. In contrast, Raiber et al. (2022a) proposed that it is less likely that there is a hydraulic connection between the Pilliga Sandstone and the deep Gunnedah Basin strata (e.g. the primary CSG target unit Maules Creek Formation) here. In the south and east, the available evidence presented by Raiber et al (2022a) suggested that there is a high degree of separation between the Gunnedah Basin and the Pilliga Sandstone, indicating that the inferred aquitards that separate the CSG target units from the Pilliga Sandstone in the stratigraphic column (e.g. Gunnedah Basin aquitards Porcupine Formation, Watermark Formation and Napperby Formation and the upper low-permeability sequences of the Purlawaugh Formation) are likely continuous with relatively minor structural disruption.

Raiber et al. (2022a) identified multiple on-going knowledge and data gaps resulting in uncertainties on the interpretation of potential hydrogeological connectivity pathways. These included:

- A lack of geophysical data focussing on the characterisation of the upper 400 m of the subsurface (with seismic data acquired in hydrocarbon studies generally focussing on characterisation of the subsurface below depths of approximately 400 m);
- On-going uncertainties on the role (e.g. spatial distribution and timing) of igneous intrusions as potential hydrogeological connectivity pathways in the Narrabri Gas Project area;
- A lack of baseline hydrochemistry and environmental tracer data from Gunnedah Basin strata within the extended Narrabri Gas Project area, resulting in uncertainties in geochemical mixing calculations;

The aims of this report are to close these knowledge and data gaps and:

- continue to provide an independent assessment of community concerns on the role of geological structures in aquifer connectivity in the Pilliga Forest area.
- address knowledge gaps related to the presence or absence and role of geological structures identified in a previous GISERA research project (‘Assessment of the influence of geological structures on aquifer connectivity in the Pilliga Forest area, NSW – an integrated hydrogeological, geophysical, hydrochemical and environmental tracer approach’) (Raiber et al., 2022a).
- assess publicly available stratigraphic data to determine which formations were intersected by igneous intrusions and conduct age dating of intrusive rocks to better understand intrusive history of Narrabri region.
- conduct an airborne electromagnetic (AEM) survey to confirm if deep-seated faults mapped by legacy seismic surveys and dykes (near-vertical igneous intrusions) extend to the shallower subsurface (top 400 m) and determine if they are likely to act as potential fluid migration pathways based on integration with other independent lines of evidence.
- conduct a targeted hydrochemistry and environmental tracer sampling campaign with a focus on the collection and analysis of hydrochemistry and a comprehensive suite of environmental tracers from NSW coal basin groundwater bores (NSW DPIE, 2019) screened in the Gunnedah

Basin formations and in the Purlawaugh Formation. This provides valuable baseline data and allows to detect groundwater contribution from deeper aquifers in shallow aquifers to assess the degree of connectivity and/or separation between deep and shallow systems.

- integrate all geological, hydraulic, hydrogeological, hydrochemical and geophysical information through numerical modelling and development of a suite of flow, solute transport and geochemical mixing models to test hypotheses on the likely presence or absence of different hydrogelogical connectivity pathways between coal seams and shallower groundwater resources in the Narrabri region in NSW.
- identify on-going knowledge gaps that can support future research efforts to further reduce uncertainties and provide best-available information to the public, industry, and groundwater managers.

1.2 Geological and hydrogeological background

The Pilliga Forest and Narrabri region are located within a complex geological and hydrogeological area where the Surat and Gunnedah (sedimentary) basins (Figure 1-1) overlap and where important alluvial and surface water resources of the Murray–Darling Basin occur. A comprehensive overview on the geology and hydrogeology of this region has been provided by Raiber et al. (2022a). A shortened version of that description is provided here as geological and hydrogeological context.

The primary Great Artesian Basin (GAB) aquifer in this region and more broadly within the Coonamble Embayment, a sub-basin of the Surat Basin and GAB in New South Wales (NSW) (Figure 1-3), is the Pilliga Sandstone, which outcrops along the south-eastern margin of the GAB. The thickness of the Pilliga Sandstone in the Surat Basin in NSW ranges from less than 100 m near the basin margin to approximately 390 m, with a median thickness of 221 m based on the assessment of exploration and stratigraphic wells that fully intersect the Pilliga Sandstone (Raiber et al., 2022a). It is composed of well-sorted medium to coarse-grained (mostly quartzose) sandstone and conglomerate with minor interbedded mudstone, siltstone, shale, fine sandstone and coal, and it is considered a high-yielding aquifer containing good quality groundwater (Tadros, 1995; Watkins and Meakin, 1996; Northey et al., 2014; Bull et al., 2021).

Overlying the Pilliga Sandstone in northern NSW are the younger strata of the Surat Basin (Figure 1-1), including the Keelindi beds (an informal unit corresponding to the Orallo Formation, Mooga Sandstone and lowermost Bungil Formation), comprised of sandstone, siltstone, shale and mudstone (Stewart and Alder, 1995) and classified as partial aquifers (Smerdon and Ransley, 2012; Ransley et al., 2015) and the Drildool beds, equivalent to the upper part of the Bungil Formation. These stratigraphic units form part of the Blythesdale Group and are often referred to as the BMO formation (consisting of the Bungil Formation, Mooga Sandstone and the Orallo Formation). In many parts of the eastern Coonamble Embayment, the Surat Basin strata are covered by Cenozoic alluvial sediments (including the Namoi River alluvium).

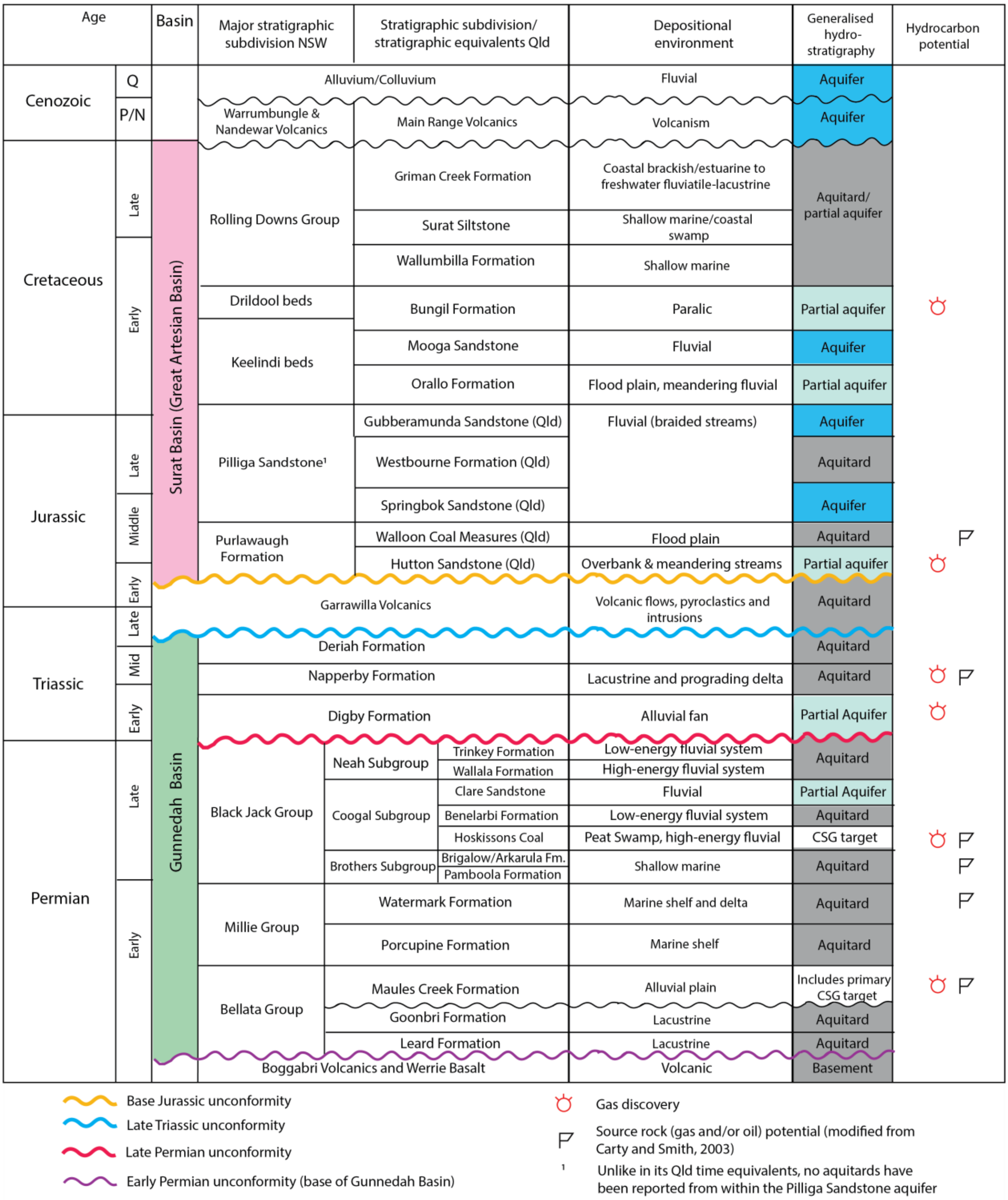

Figure 1-1 – Stratigraphy of the Surat and Gunnedah basins in NSW (compiled from Tadros (1993, 1995), Carty and Smith (2003), Korsch and Totterdell (2009), Totterdell et al. (2009), Geoscience Australia (2013), Ransley et al. (2015), Ruming (2015) and Raiber et. al (2022a). Q and P/N in the Cenozoic era correspond to Quaternary and Palaeogene/Neogene.

Underlying the Pilliga Sandstone is the Purlawaugh Formation, which is sometimes described as the stratigraphic equivalent to the Walloon Coal Measures of the Surat Basin in Queensland (Qld) (Geoscience Australia, 2013), or the equivalent of the Walloon Coal Measures and Hutton Sandstone in Qld (Totterdell et al., 2009). It is sometimes characterised as an aquitard or aquiclude (CDM Smith, 2016); other studies suggest that there is a local development of intra-formational seals especially within the upper part of the Purlawaugh Formation and also good reservoir-quality sandstones (rocks with higher porosity and transmissivity). At a central location within the Narrabri Gas Project area at Plumb Road (Figure 1-3), the lithological logs in the well completion report of a recently drilled groundwater monitoring well (InGauge, 2017) suggest that out of the total thickness of 55 m recorded for the Purlawaugh Formation at this location, the upper 45 m are composed of low permeability formations (claystone and siltstone) with some minor coal and sandstone. This indicates that the upper part of the Purlawaugh Formation at this location is a seal or aquitard (a relatively impermeable geological formation, which does not allow water to flow through it easily). In contrast, the basal 10 m of the formation consist of a massive sandstone composed of fine to very coarse quartz grains with a high porosity.

At this site, high artesian pressure with discharge (if uncapped) of approximately 12,000 L/hour was recorded in the groundwater monitoring bore screened in the basal sandstone of the Purlawaugh Formation (Figure 1-2). High dissolved methane (CH_4) concentrations in this groundwater bore were also observed (Suckow et al., 2019; Raiber et al., 2022a), suggesting that there may be pathways potentially connecting this unit to underlying geological formations, as will be discussed further throughout this document.

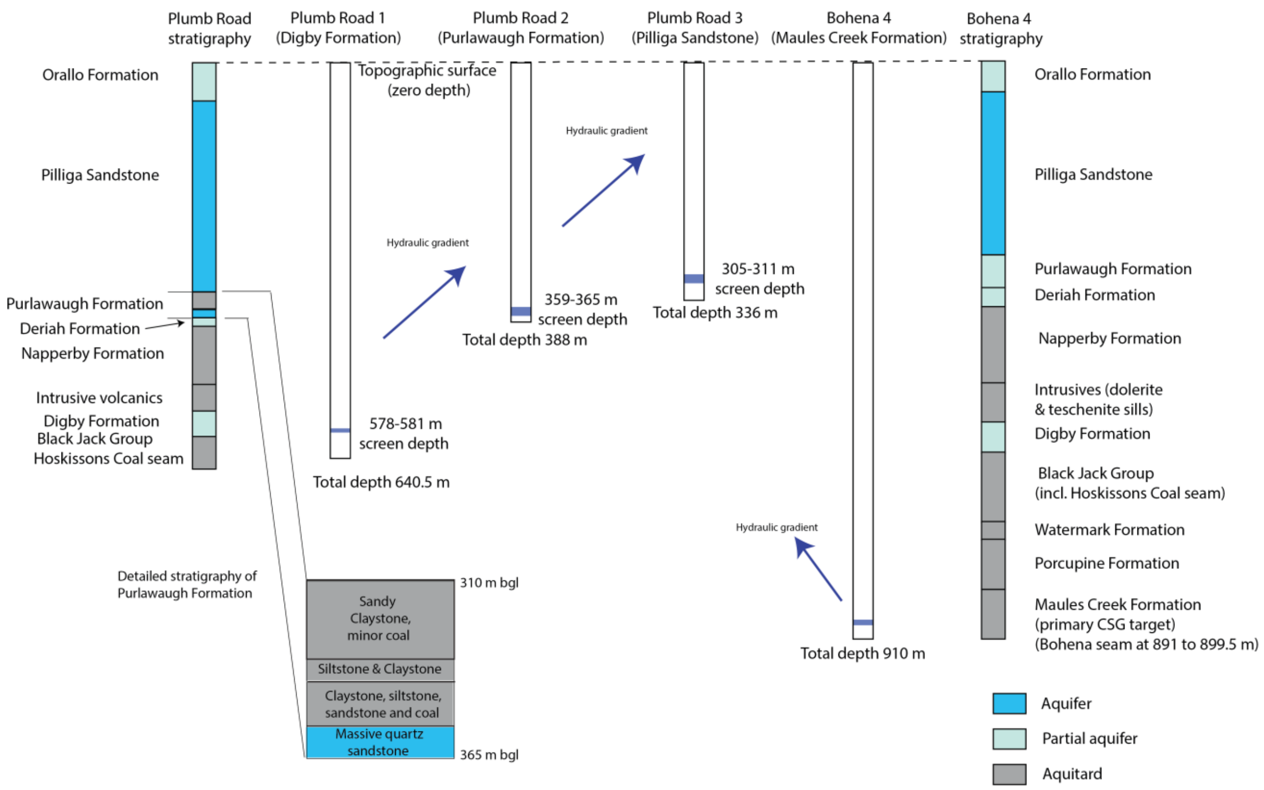

Figure 1-2 – Stratigraphy of the Surat and Gunnedah basins at Plumb Road nested bore sites and Bohena 4 stratigraphic well (modified from Raiber et al., 2022a). Detailed stratigraphy of the Purlawaugh Formation at Plumb Road is also shown.

The basal unit marking an unconformity at the base of the Surat Basin in the eastern part of the Coonamble Embayment is the Garrawilla Volcanics (Figure 1-1), contemporary igneous rocks composed of lavas, pyroclastic deposits and intrusions (Tadros, 1995; Barnes et al., 2002) which are discontinuous throughout the Gunnedah Basin and the Narrabri Gas Project area (Raiber et al., 2022a).

Underlying the Surat Basin and Garrawilla Volcanics strata are the Permian to Triassic formations of the Gunnedah Basin comprising up to 1200 m of marine and non-marine sediments (Figure 1-1). The uppermost units of the Gunnedah Basin are the Napperby and Digby formations. The Napperby Formation is composed of nearshore marine shales and is considered a tight aquitard, whereas the Digby Formation is more variable and includes basal conglomerates and sandstones deposited in a braided fluvial environment. It has therefore been considered a conventional hydrocarbon exploration target (Eastern Star Gas, 2011) and is likely to be a partial aquifer in some areas.

Gunnedah Basin sediments also include the Hoskissons Coal seams hosted within the Black Jack Group, and multiple coal seams within the Maules Creek Formation. In the past, both conventional and unconventional gas exploration has occurred within the Narrabri Gas Project area (and the wider area) on multiple Gunnedah Basin (and to a lesser extent Surat Basin) formations (Figure 1-1). In conventional hydrocarbon reservoirs, gas accumulations within reservoir rocks are targeted, where gas is trapped in the pore space of permeable rocks such as sandstone (Upstream Petroleum Consulting Services, 2000). Such natural gas reservoirs are often formed by structural traps associated with anticlines (or horst–graben systems) (discussed more in Section 1.2 and throughout subsequent sections of this report) or faults. Hydrocarbons migrate through the pore space in rocks under the influence of buoyancy and accumulate in hydrocarbon traps where their further upwards migration is prevented by an impermeable seal (or cap rock or aquitard) (Upstream Petroleum Consulting Services, 2000).

In unconventional gas exploration, coal seam gas (CSG) (or coal bed methane) is trapped in coal and adsorbed onto the coal grain surfaces or micropores and held in place by reservoir (water) hydrostatic pressure. The coal therefore simultaneously acts as a source, reservoir, and seal for the methane (Upstream Petroleum Consulting Services, 2000). In the Narrabri region, sandy facies within the Triassic Digby Formation, Late Permian Porcupine Formation and lower part of the Jurassic Purlawaugh Formation were historic conventional gas exploration targets.

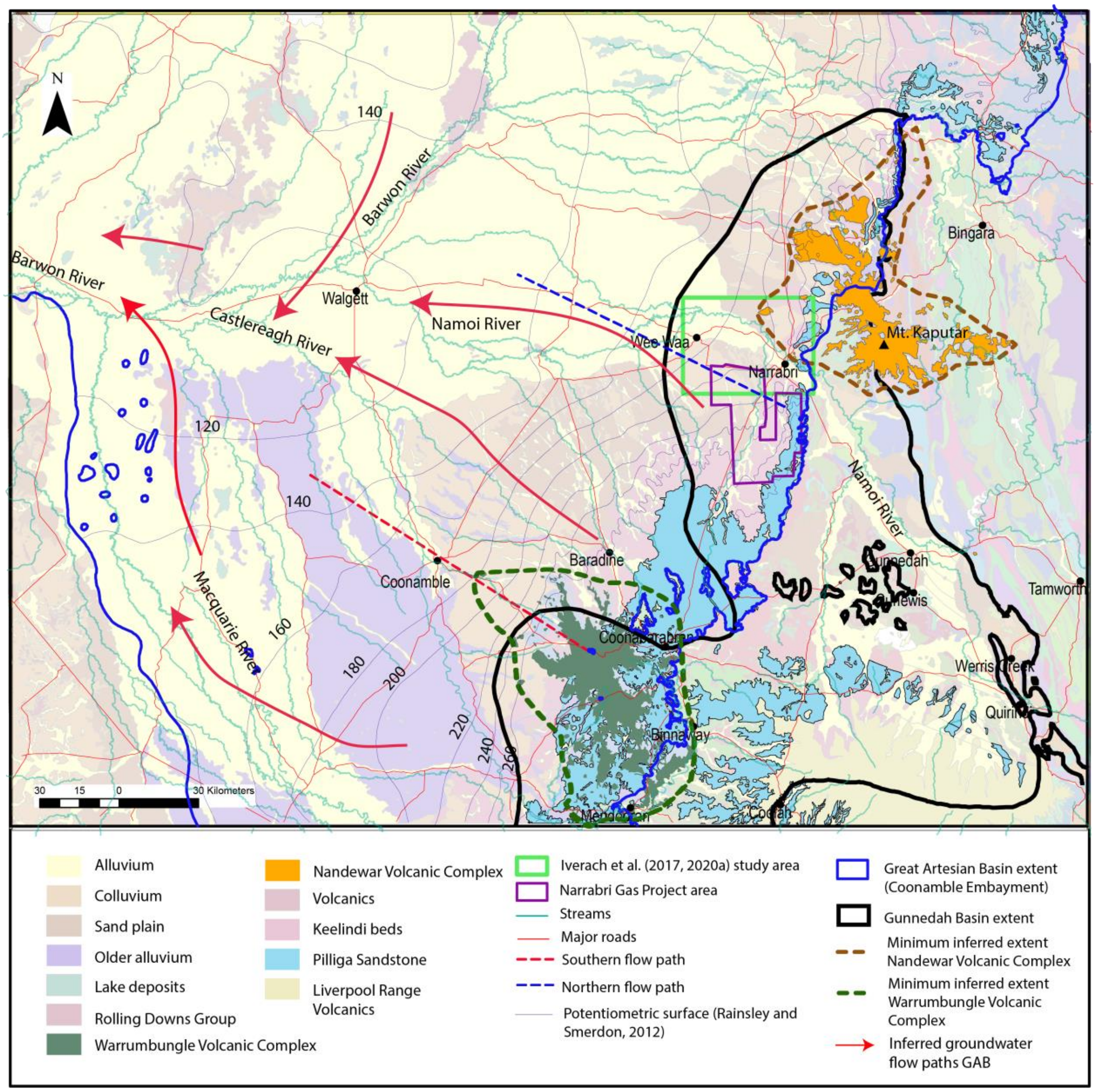

Figure 1-3 – Simplified geological map of the Surat Basin in northern NSW showing the proposed Narrabri Gas Project area, extent of Gunnedah Basin, Great Artesian Basin extent and inferred groundwater flow directions and extent of previous groundwater studies (Raiber et al., 2022a).

The orientation of proposed southern and northern flow paths (and associated block diagrams) within the Pilliga Sandstone (based on Raiber and Suckow (2018) and Suckow et al. (2019)) is also shown.

The primary CSG target unit within the Narrabri Gas Project area is the Maules Creek Formation (overlain by the Watermark and Porcupine formations; Figure 1-1), whereas the shallower Hoskissons Coal seams within the Black Jack Group is a secondary target (CDM Smith, 2016). Phase 1 of the proposed Narrabri Gas Project is expected to focus on the south and centre of the Narrabri Gas Project area (Santos, 2017a) and would include, for example, exploration and appraisal activities and the drilling of production wells.

Locally overlying the Surat Basin and Gunnedah Basin strata are Cenozoic volcanic rocks associated with the Warrumbungle and the Nandewar volcanic complexes (Figure 1-1). These rocks erupted between ~16 and 20 million years ago (Wellman et al., 1969; Wellman and McDougall, 1974; Northey et al., 2014; Bull et al., 2021), infilling an irregular erosional surface of the Surat and Gunnedah basins and basement rocks (Bull et al., 2021). The Warrumbungle Volcanic Complex south of Narrabri (with Mount Exmouth at about 1200 mAHD) and the Nandewar Volcanic Complex north-east of Narrabri (with Mount Lindesay at about 1370 mAHD and Mount Kaputar at about 1500 mAHD) form prominent topographic landmarks within the Coonamble Embayment, towering over the Surat Basin and Namoi alluvium (where topographic elevations are approximately 200 mAHD near Narrabri). The Warrumbungle Volcanic Complex is composed of a variety of volcanic rocks (e.g. basalt, dolerite, trachyte and tuff), whereas the Nandewar Volcanic Complex is composed of alkaly rhyolite, trachyte, tuff, trachyte plugs and comendite (Geoscience Australia, 2021).

In a new study on the evolution of the Warrumbungle Volcanic Complex, Bull et al. (2021) suggested that a complex alkaline shield volcano erupted first along regional-scale basement lineaments, which was subsequently intruded by lava domes, cryptodomes, dykes and a radial dyke swarm.

1.3 The role of geological structures as potential connectivity pathways

Different types of potential hydrogeological connectivity pathways between vertically stacked hydrocarbon reservoirs and aquifer–aquitard sequences have been described in the literature. Understanding the influence of geological structures on groundwater flow is very important because if an aquitard is not continuous or if it is compromised by so-called seal-bypass systems (Cartwright et al., 2007) or by the existence of preferential pathways, then pressure changes may be transmitted faster, with potential impacts on both the water quantity and water quality of the overlying aquifers. They identified faults, intrusions and pipes as the three major types of seal-bypass structures in petroleum systems. The term ‘seal’ is frequently used in petroleum studies to describe formations of very low permeability whereas ‘aquitard’ is commonly used in hydrogeological studies to describe such formations.

1.3.1 Faults

In a recent explanatory draft note on the characterisation and modelling of geological fault zones prepared for the Independent Expert Scientific Committee (IESC) on Coal Seam Gas and Large Coal Mining Development, Murray and Power, 2021a noted that ‘In some cases, faults can have little to no influence on groundwater flow, and in other situations faults can provide a barrier, a flow pathway or both that results in significant changes to water assets and GDEs’. Whether a fault forms a hydraulic barrier or conduit to groundwater (or more broadly fluid) flow depends on many factors, including the juxtaposition (the degree of displacement) of aquifers versus aquitards across faults, the fault zone properties, regional stress regime and the orientation and magnitude of the hydraulic gradient in and around fault zones (e.g. Bense et al., 2013; Underschultz et al., 2018; OGIA, 2020, Murray and Power, 2021 a, b).

Anticlines are formed by the folding of geological formations into an arch-like shape. The rock formations in an anticline were originally deposited horizontally, and post-depositional tectonic or structural activity resulted in uplifting or doming and folding (e.g. Onajite, 2014). Oil and/or gas can migrate from the source rock into the permeable reservoir rocks (e.g. sandstones), with further upwards migration prevented by a low-permeability seal (or cap-rock). Hence, like in groundwater investigations, understanding if competent seals are in place is a critical part of petroleum investigations.

1.3.2 Igneous intrusions

As highlighted by Cartwright et al. (2007), apart from faults and structures such as anticlines or horst–graben systems, another type of seal-bypass system is that associated with igneous intrusions such as dykes, sills and laccoliths.

Dykes are igneous intrusive bodies that are often near-vertical and intrude into horizontal sedimentary formations along pre-existing faults or fractures (Drymoni et al., 2021). Dykes feed volcanoes, although many dykes may not reach the surface and remain trapped in the crust (Menand et al., 2010). Dykes are typically relatively thin, but their lateral dimensions can extend over many kilometres (Donaldson et al., 2003). For example, a study investigating dykes in the Sydney Basin in NSW showed that most mapped dykes in this region range in thickness from <1 m to approximately 16 m but could be traced laterally over up to approximately 16 km (Baxter-Crawford, 2018).

During the intrusive event, igneous intrusions emplaced into siliciclastic sedimentary host rocks can result in the expulsion of pore water fluids and thermal, mechanical and chemical alteration of the host rock (Mark et al., 2024). Intense fracturing and deformation of the sealing sequence can occur, and the increased permeability of the rocks in the contact zone can facilitate fluid flow.

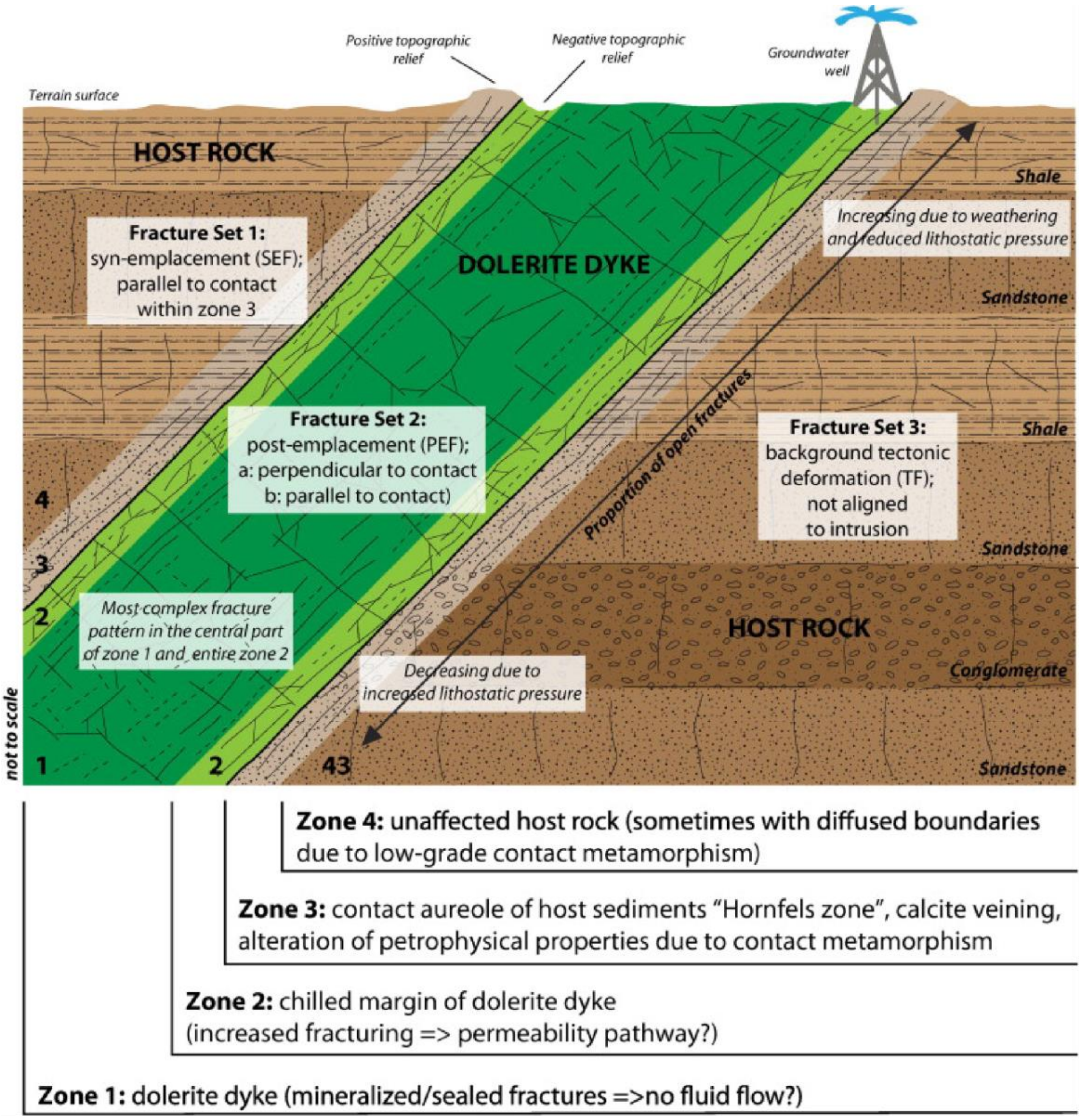

Figure 1-4 – Conceptual model of geological and hydraulic impact of dolerite dyke intrusions on sedimentary host rock (Senger et al., 2015).

Igneous intrusions such as dykes can act as both conduits and barriers to subsurface fluid flow and are therefore expected to significantly influence the distribution and migration of groundwater and hydrocarbons in sedimentary basins where intrusive activity has occurred (Senger et al., 2015). Mark et al. (2024) explained that reservoirs may be compartmentalized by low permeability igneous intrusions, which may inhibit lateral and vertical migration of fluids. In an example from the Karoo Basin of the Eastern Cape province of South Africa, Senger et al. (2015) presented a conceptual model of the geological and hydraulic impact of dolerite intrusions into sedimentary host rock (Figure 1-4). They explained that due to the low matrix permeability of igneous rocks such as dolerites, the effective permeability associated with intrusions is primarily related to the characteristics of their fracture networks. The fracture networks can occur through various processes including the cooling of magma, thermal contraction, magma movement, and mechanical disturbances in the host rock. Senger et al. (2015) explained that this fracturing can be further intensified at points where intrusions intersect the host rock, at the junctions of dykes and sills, or along the base of curving sills. As a result, these features can significantly influence the permeability in their vicinity.

Sills are fed by dykes, but unlike dykes, the sills are horizontal sheet intrusions that intrude between older rock layers of different rock types (e.g. different types of sedimentary or metamorphic rocks); furthermore, they do not typically cut across pre-existing rocks but are often distributed along bedding planes of rock layers. Sills form when their feeder dyke stops propagating mainly vertically and instead intrudes concordantly along a lithological plane of weakness (Menand et al., 2010). However, Bunny and Weber (1996), Gurba and Weber (2001) and Othman et al. (2001) concluded that in contrast to dykes, sills can have a beneficial influence on coal seam gas accumulation as they can act as an impermeable seal, as observed at the Yannergee DDH1 well in the southern part of the Gunnedah Basin.

Laccoliths are a variant of sills and they commonly have acidic or intermediate magma (Bradely, 1989; Australian Museum, 2018). Laccoliths are also fed by dykes (Donaldson et al., 2003). However, unlike the sheet-shaped sills, their geometry is lens-shaped (Bradley, 1989).

1.3.3 Influence of intrusions on the sedimentary host rock

Both sills and laccoliths can cause uplift and bending of the overlying strata, creating forced folds (Magee, 2024). The emplacement of these horizontal magmatic intrusions begins as a sill with a horizontal base with a stable roof. As the magmatic intrusion extends further, space for its emplacement is commonly created by uplift of the overlying rock, resulting in a weakening of the roof (e.g. Segall 2013; Magee, 2024). When pressure yields, the uplift bends the overburden to produce flat-topped or dome-like forced folds (Magee, 2024). Geometrically, forced folds represent four-way dip closures in the subsurface (Magee, 2024), which means that the structural features dip away in all four possible directions, forming potential hydrocarbon traps in the bend of the arch where upwards migration of any hydrocarbons is prevented by a seal (cap rock or aquitard). Such four-way dip closures were previously identified in the north-western part of the Narrabri Gas Project area (Carty and Smith, 2003; Carty and Smith, 2004).

In a recent publication on the impact of igneous intrusions on sedimentary host rocks, Mark et al. (2024) explained that the extent of host rock alteration from igneous intrusions is highly variable and is commonly accompanied by mechanical compaction and fracturing of the host rock within the initial 10 to 20 cm of altered host rock. Based on a detailed assessment of field outcrop data, well log and geophysical log data in multiple studies including at the north-eastern Atlantic Margin and the Bass Basin between Victoria and Tasmania, Mark et al. (2024) suggested that the extent of the alteration zone caused by igneous intrusions in sedimentary host rocks is highly variable and difficult to predict. However, they proposed that some general observations can be made:

- approximately 97% of the intrusions considered by the authors occurred in claystone, with only limited examples in siliciclastic sandstone.
- the minimum extent of alteration observed was 0.15 m for a 1.2 m thick intrusion and the maximum extent of alteration observed was 106 m for a 182 m thick igneous intrusion.
- the greatest lateral extent of alteration is seen within argillaceous claystones, whereas siliciclastic sandstones appear to have thinner alteration zones. This was attributed by the authors to the higher thermal conductivity of siliciclastic sandstone and higher convective heat loss (due to higher permeabilities and presence of more pore fluids).

1.4 Evolution of conceptual models of potential hydrogeological connectivity pathways in the Narrabri region (2013 to 2022)

Conceptual hydrogeological models provide the basic understanding of how hydrogeological system components and processes operate and interact (Bredehoeft, 2005). They describe the understanding of groundwater systems, and they are considered one of the major sources of uncertainty in groundwater flow and transport modelling (Enemark et al., 2019).

Hydrogeological investigations are generally based on the assessment of scarce point information from widely spaced groundwater bores, geophysical surveys or other geoscientific data sets. It is generally acknowledged that knowledge gaps and uncertainties can be reduced over time as more field data are acquired (Mallants et al., 2018).

In this section, we provide an overview on how the conceptual models of potential hydrogeological connectivity pathways have evolved in the Narrabri region in the last 10 years as more data became available with the progression of field-based data acquisition campaigns.

1.4.1 Namoi subregion Bioregional Assessment (2014 to 2018)

The Namoi subregion Bioregional Assessment formed part of the Bioregional Assessment Programme, which provided a baseline assessment to increase the available science for decision making associated with coal seam gas and large coal mines. The basis of the Bioregional Assessment in the Namoi subregion was a comprehensive desktop investigation that examined the existing geoscientific and ecological data and developed causal pathway models. This was followed by the development of groundwater models to predict the cumulative impacts of coal seam gas developments and large coal mines on water assets. The geological model which underpinned the groundwater modelling did not include fault locations and depths (Herr et al., 2018; Janardhanan et al., 2018). The authors suggested that inclusion of faults would likely increase the precision of groundwater modelling but due to the regional scale of this assessment, it would not change the extent of the zone of potential hydrological change. However, the authors suggested that probabilistic groundwater modelling accuracy and precision at the local scale would likely benefit from fault inclusion.

1.4.2 GISERA W7 Impacts of CSG depressurisation on the Great Artesian Basin (GAB) flux (2017 - 2019)

GISERA project “Impacts of CSG depressurisation on the Great Artesian Basin (GAB) flux” consisted of the following components:

- one component with the primary focus to improve the understanding of recharge in the Coonamble embayment (a sub-basin of the Surat Basin) (Raiber and Suckow, 2018 and Suckow et. al., 2019) and
- a second component involving a preliminary numerical groundwater modelling assessment of potential groundwater flux (flow volume) changes in the main GAB aquifer (Pilliga Sandstone) in the Coonamble Embayment (a sub-basin of the Surat Basin in NSW), parts of

which overlies the Gunnedah Basin from which it is proposed to extract water for coal seam gas development (Janardhanan et al., 2018).

Aiming to close knowledge gaps identified by the Namoi subregion Bioregional Assessment, this project involved the collection of a comprehensive environmental tracer suite including novel tracers such as stable and radioactive noble gas isotopes to assess recharge processes to the Pilliga Sandstone and connectivity with the underlying Gunnedah Basin (Figure 1-5). The environmental recharge tracer outcome identified potential faster southern and slower northern flow path within Pilliga Sandstone. Due to the limited number of environmental tracer data from groundwater bores in the GAB and Gunnedah Basin within the Narrabri Gas Project area, only limited insights were gained into subsurface geometry and potential hydrogeological connectivity pathways.

The project identified faults and igneous intrusions and stratigraphic contacts between coal seams and GAB aquifers in the western part of the Narrabri Gas Project area as potential connectivity pathways. Raiber and Suckow (2018) and Suckow et. al. (2019) cited the general lack of environmental tracer data in GAB and Gunnedah Basin formations within the Narrabri Gas Project area and geophysical surveys characterising the shallow subsurface (surface to approximately 400 m below ground surface) as limitations and on-going key knowledge and data gaps.

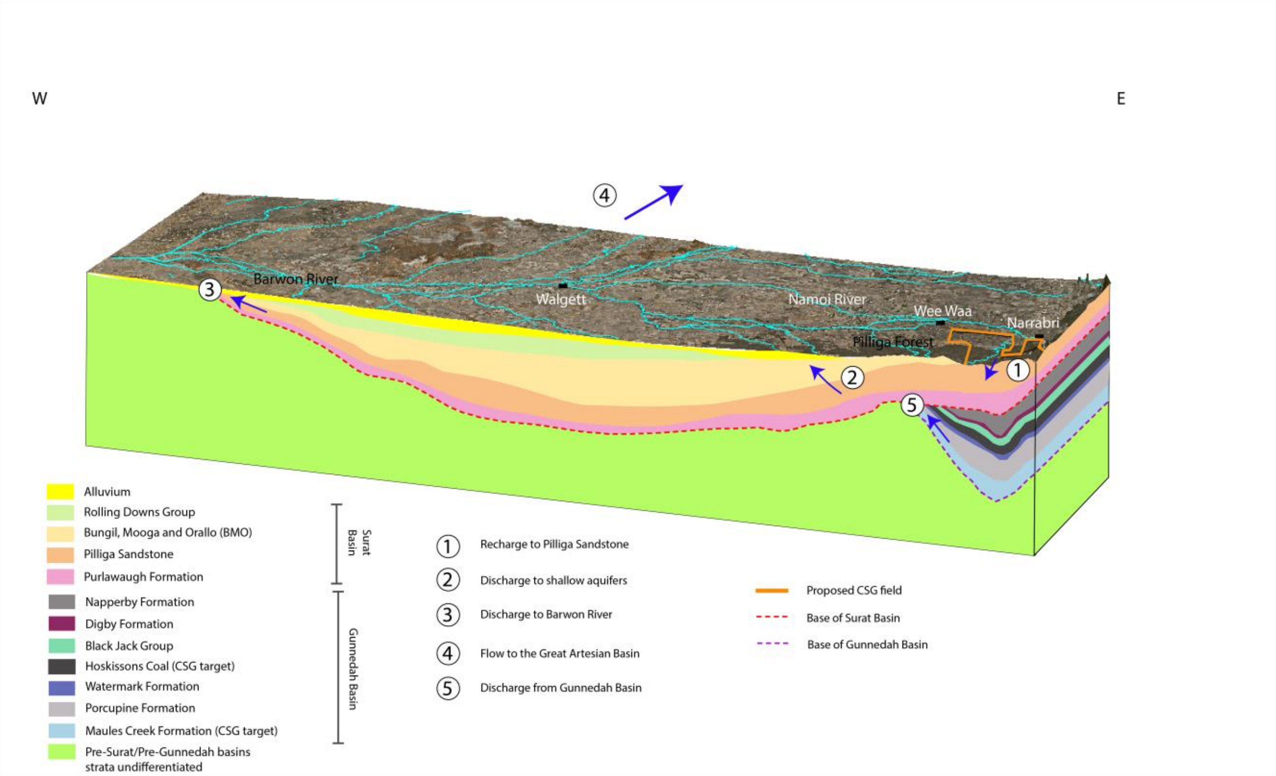

Figure 1-5 – Previous conceptual hydrogeological model of potential structural and hydrogeological connectivity pathways between coal seams and major aquifers of Great Artesian Basin in the Narrabri Gas Project area (Raiber et al., 2019).

1.4.3 GISERA W19 Assessment of faults as potential connectivity pathways (2020 - 2022) – current state of understanding

The GISERA project "Assessment of faults as potential connectivity pathways" (Raiber et al., 2022a) was developed to close on-going knowledge gaps identified in the Namoi subregion Bioregional Assessment and in the GISERA project "Impacts of CSG depressurisation on the Great Artesian Basin (GAB) flux", address public concerns and help to refine the understanding of faulting in the shallow subsurface. The project focussed on specific areas within the Narrabri Gas Project area where faults or igneous intrusions were inferred to be present, and used the combined evidence from existing and newly acquired geophysical data, geology, hydrogeology, hydrochemistry and new tracer data and hydrochemical mixing models to update the conceptual hydrogeological models of potential connectivity pathways (Figure 1-6). Within the Narrabri Gas Project area, Raiber et al. (2022a) identified multiple plausible potential hydrogeological connectivity pathways that could potentially link gas reservoirs of the Gunnedah Basin with aquifers of the Surat Basin (Figure 1-6), including faults, stratigraphic contacts and igneous intrusions such as dykes and sills.

Raiber et al. (2022a) suggested that there is likely some hydrogeological connection between the Pilliga Sandstone and the underlying Purlawaugh Formation and/or the late Gunnedah Basin strata (Digby Formation) in the central and northern and north-western parts of the Narrabri Gas Project area. In contrast, the authors proposed that the available evidence suggests that it is less likely that there is a hydraulic connection between the Pilliga Sandstone and the deep Gunnedah Basin strata (e.g. the primary CSG target unit Maules Creek Formation) here. Raiber et al. (2022a) also hypothesised that the available evidence suggests that there is a high degree of separation between the Gunnedah Basin and the Pilliga Sandstone in the south and south east, indicating that the inferred aquitards that separate the CSG target units from the Pilliga Sandstone in the stratigraphic column (e.g. Gunnedah Basin aquitards Porcupine Formation, Watermark Formation and Napperby Formation and the upper low-permeability sequences of the Purlawaugh Formation (Surat Basin), which is very thick in this area) are more likely continuous with relatively minor structural disruption. Raiber et al. (2022a) revised some of the subsurface geometrical features proposed in GISERAW7 with the help of seismic interpretations; for example, the seismic data confirmed that there are unlikely to be any direct contacts between CSG target units and GAB aquifers at the western margin (as indicated in the previous conceptual model in Figure 1-5 by the connectivity pathway ⑤). Instead, the Maules Creek Formation sub-crops at depth and appears to be continuously separated from the Pilliga Sandstone via multiple aquitards. Raiber et al. (2022a) suggested that additional data acquisition would help reduce the inherent uncertainties involved in this assessment of potential connectivity pathways. This included a suggestion to conduct an AEM survey which could complement seismic data and provide a continuous three-dimensional model of the upper 400 m of the subsurface, the collection of additional hydrochemistry and environmental baseline data from the Purlawaugh Formation and shallow Gunnedah Basin hydrostratigraphic units (e.g. Digby Formation, Napperby Formation and Hoskissons Coal seam) and development of more comprehensive geochemical models to test plausible connectivity pathways.

This led to the development of the integrated multi-disciplinary assessment conducted in this present study.

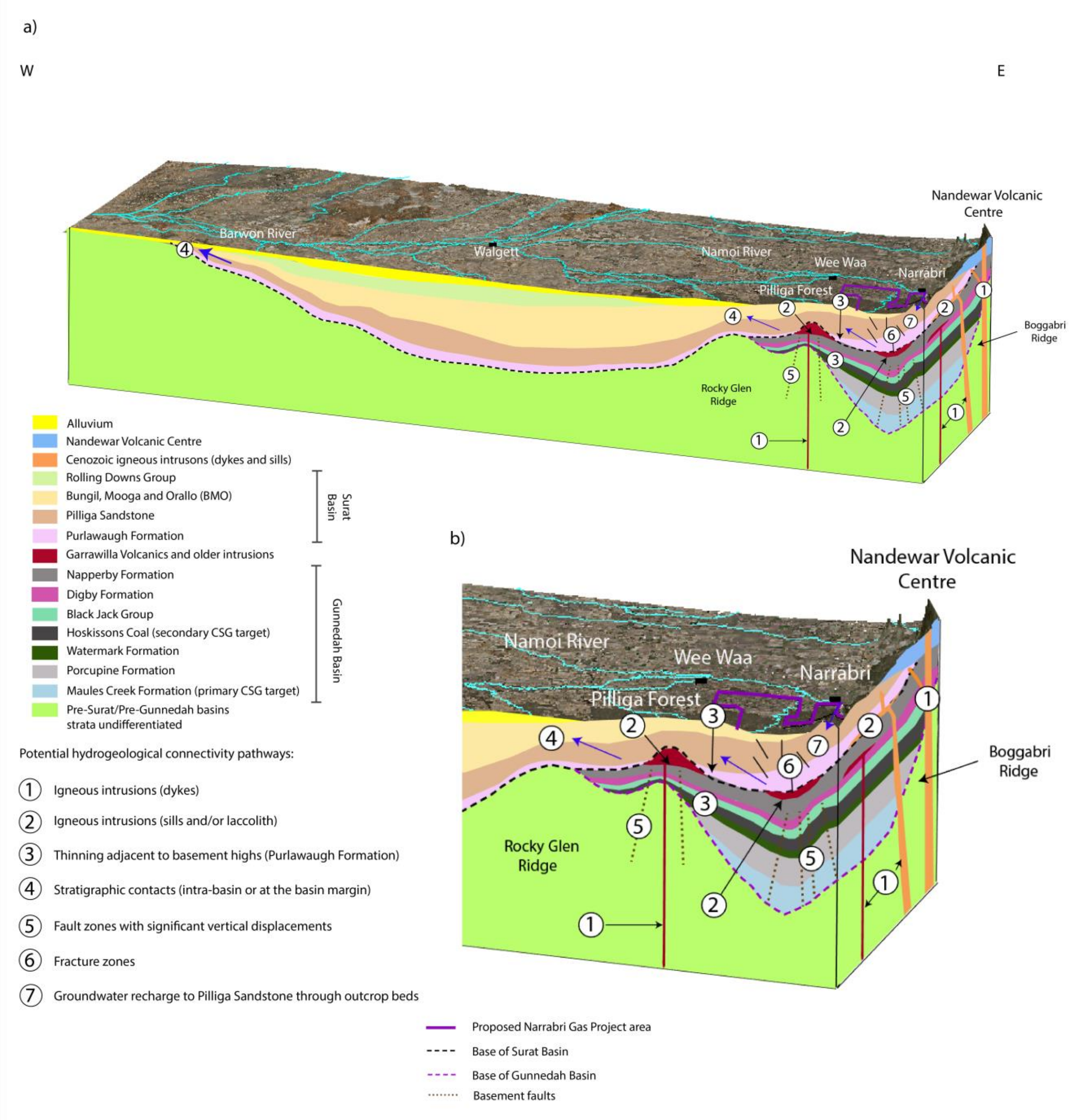

Figure 1-6 – Potential structural and hydrogeological connectivity pathways between coal seams and major aquifers of Great Artesian Basin in the Narrabri Gas Project area (Raiber et al., 2022a).

2 Methodology

Section 2 of this report describes the multi-disciplinary approach applied and provides an overview on the wide array of techniques considered in this study. This includes the compilation of pre-existing and newly acquired data from the mineralogical and geochronological analyses of rocks, geophysical assessments and hydrochemical and environmental tracer analysis.

The methodological descriptions are presented systematically in the order of the iterative workflow steps presented in Section 2.1.

2.1 Integrated multi-disciplinary geoscientific approaches

Building on previous studies, this project integrates multiple lines of geoscientific evidence to assess how geological and hydrogeological components interact in the Narrabri Gas Project area.

The first step in this multi-disciplinary approach was the assessment of geology, hydrogeology and composition of the major hydrostratigraphic formations in the Narrabri Gas Project area. This involved multiple geoscientific lines of evidence including mineralogical analysis, K/Ar geochronological dating of intrusive rocks and construction of thin sections to determine rock properties and characterise the internal architecture of different hydrostratigraphic formations in the Surat and Gunnedah basins. Building up on this, we have conducted an airborne electromagnetic (AEM) survey (Figure 2-1) of the Narrabri Gas Project area to further enhance the fundamental understanding of the subsurface geometry and complement existing seismic survey data and integrated the results with selected seismic sections.

These first two steps together supported the identification of plausible hydrogeological connectivity pathways.

To further validate the identified hydrogeological connectivity pathways and determine if inter-aquifer or inter-basin exchange is likely to occur via potential connectivity pathways, existing hydrochemical and environmental tracer data were supplemented with newly acquired data from a targeted field campaign. Groundwater samples were analysed for a comprehensive suite of hydrochemical parameters, including major and minor ions, dissolved methane concentrations and isotopes, hydrocarbon compounds, tritium (^{3}H), stable isotopes of the water molecule ($\delta^{18}O/\delta^{2}H$), $\delta^{13}C$-DIC, $^{87}Sr/^{86}Sr$, ^{14}C-DIC, ^{36}Cl and all stable noble gases (He, Ne, Ar, Kr and Xe). Building up on research and samples collected by Suckow et al. (2019) and Raiber et al. (2022a), the focus in the current investigation was to increase the availability of baseline data from the shallower formations of the Gunnedah Basin to reduce uncertainties of geochemical mixing models resulting of the lack of Gunnedah Basin groundwater hydrochemistry data identified by Raiber et al. (2022a). These different lines of geoscientific evidence together provided the knowledge to update hydrogeological conceptual models including pathways that could potentially link coal seams and productive aquifers of the Great Artesian Basin (in particular the Pilliga Sandstone).

In the final steps of this multi-disciplinary approach, a suite of numerical modelling tools was developed to integrate and interpret the multitude of characterisation and monitoring data, with inverse geochemical modelling being used as a secondary line of evidence to unravel the dominating groundwater flow and solute transport patterns. This approach enabled us to test conceptual hydrogeological models and define the contributions of different source water.

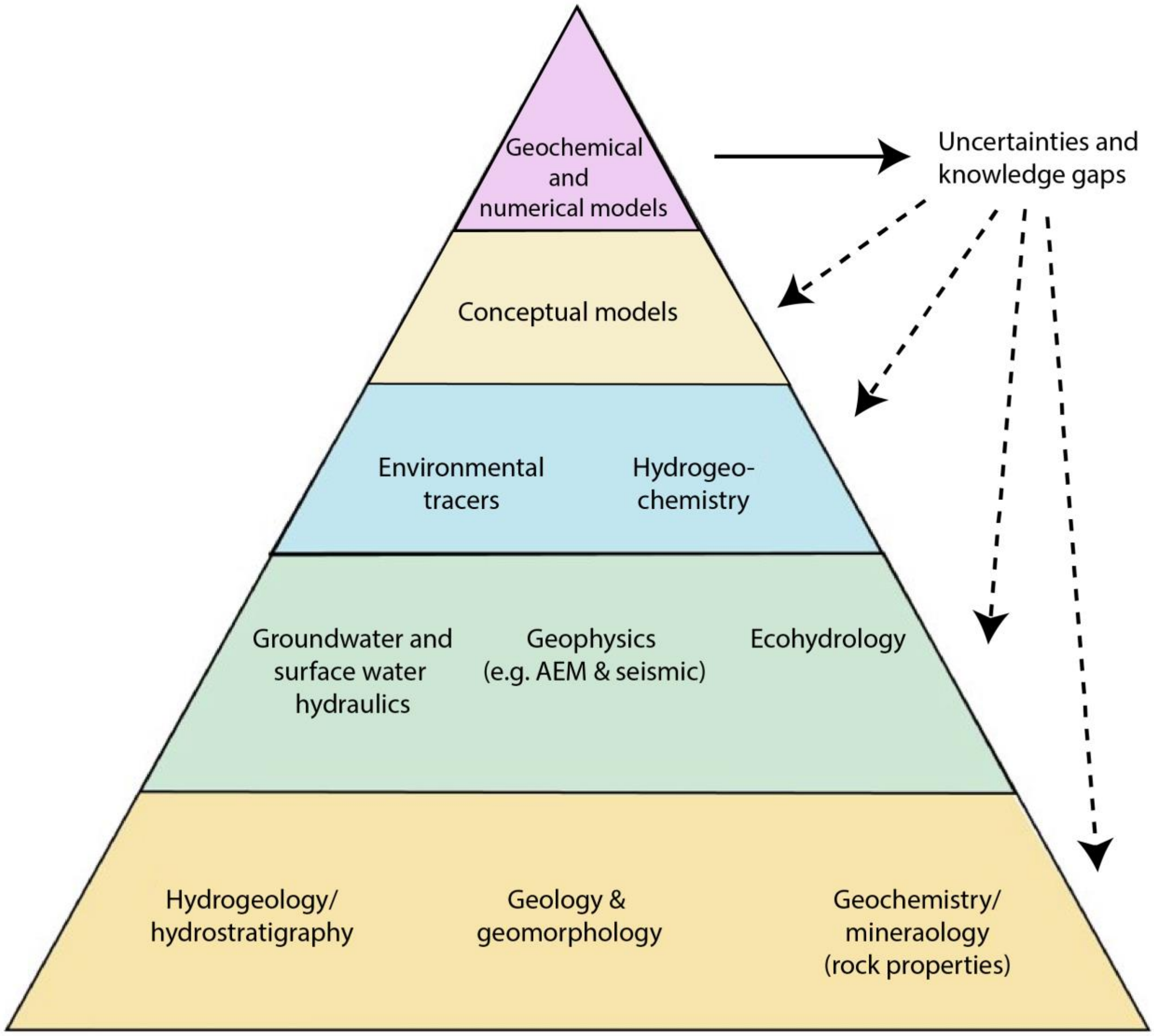

Figure 2-1 – Systematic and iterative approach to integrate multiple lines of evidence applied in this study

2.2 Compilation of existing geological and hydrogeological data

To confirm the present understanding of the subsurface geometry within the Gunnedah and Surat basins or refine this understanding, Raiber et al. (2022a) have reviewed and compiled available contextual geological and hydrogeological and selected geophysical information from published literature and datasets generated in previous projects. These data, where considered useful for the current study, are included in this assessment. A brief description of data types and data sets is provided below.

2.2.1 Geological maps and geological interpretations

Geological maps and geoscientific data sets and interpretations from previous studies were compiled by Raiber et al. (2022a) and used in the current study, complemented with information from additional data sources. This included for example:

- Frogtech SEEBASE product (Frogtech, 2013).
- hydraulic properties of inferred aquitards (Turnadge et al., 2018)
- information presented by Santos (2017a, 2017b, 2020) and CDM Smith (2016) as part of the Narrabri Gas Project environmental impact statement (EIS) process.
- a comprehensive overview on the Gunnedah Basin geology and structure by Tadros (1995)
- a NSW stress field database presented by Rajabi et al. (2016).
- a total magnetic intensity (TMI) map from Geoscience Australia (Minty and Poudjom Djomani, 2019).
- Geological maps (Geoscience Australia, 2012).
- Geoscience Australia Palaeogeographic Atlas (Geoscience Australia, 2025a).

2.2.2 Ground-based transient electromagnetic survey data

Two ground-based transient electromagnetic (TEM) methods have been applied in a previous GISERA study by Raiber et al. (2022a). The aim of implementing TEM in this previous study was to identify and investigate electrical resistivity anomalies in the vertical profile that could potentially indicate the continuation of deep-seated geological structures to near the surface.

The first geophysical data collection method applied by Raiber et al. (2022a) was a TEM technique known as moving loop electromagnetics (MLEM), conducted by Zonge Engineering and Research Organization in collaboration with CSIRO in February 2020. This technique is based on creating a double-turn 100 x 100 m transmitter loop.

Although the results yielded valuable information to a depth of approximately 400 m below ground surface, the density of the Pilliga Forest and flooding meant that only a 4550 m long tomography section with direction predominantly east–west could be completed.

A second TEM data collection campaign was conducted in May 2021 using the AgTEM approach (with the methodology developed by Dr. David Allen (Groundwater Imaging) and the survey conducted by Dr. David Allen in collaboration with CSIRO), following the methodology described by Allen (2019). The images provided valuable insights into the subsurface to a depth of approximately 80 m and the survey covered a total length of approximately 200 km along the survey lines (Figure 2-2).

The results from applying these two TEM techniques demonstrated that there is a general lack of resistive cover throughout the east and south of the Narrabri Gas Project area (likely due to the dominance of sandy over clay-rich soils and corresponding freshness of infiltrating water), which also meant that a very considerable depth could be achieved from the TEM survey. This supported the decision to conduct an AEM survey in the present study to obtain a more spatially continuous and deeper picture of the subsurface structure.

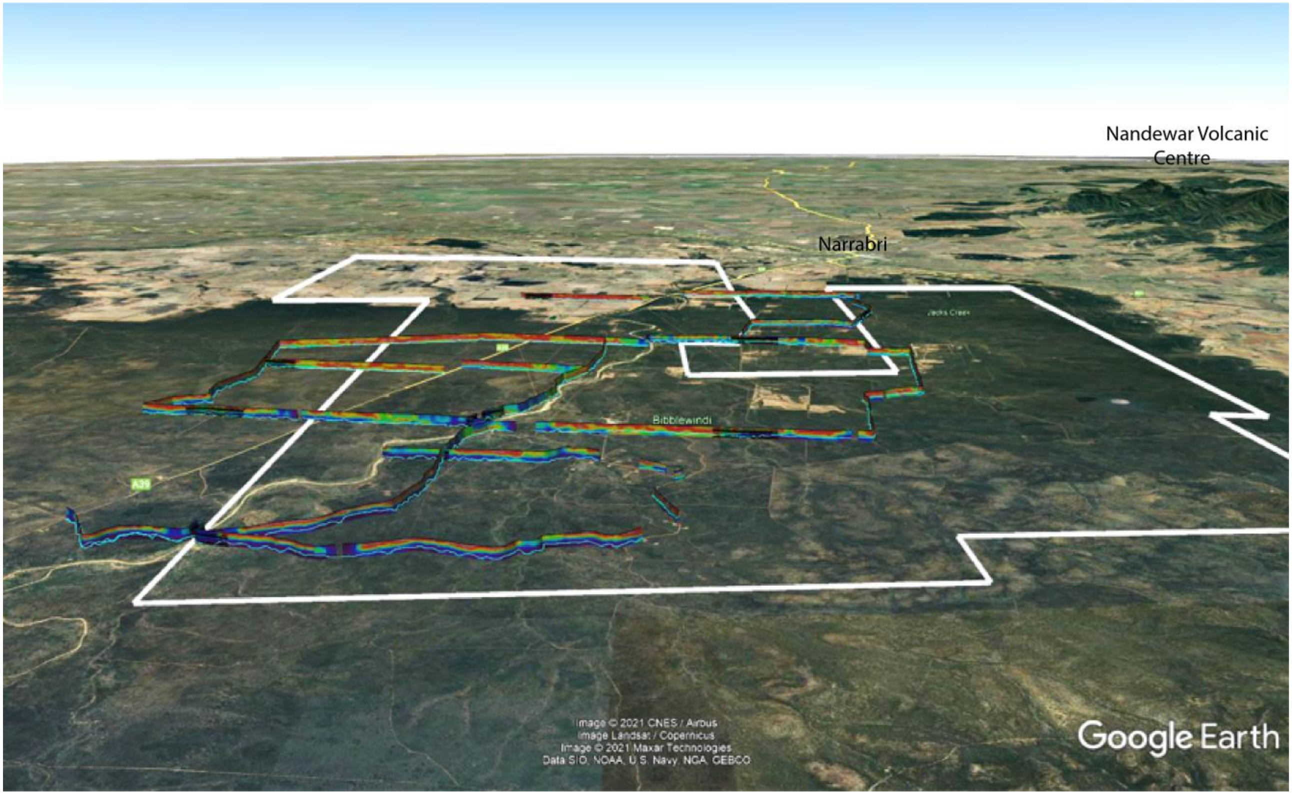

Figure 2-2 – Overview on AgTEM survey lines (modified from Raiber et al., 2022a). The proposed Narrabri Gas Project area is shown by the white outline (image supplied by Dr. David Allen, Groundwater Imaging).

2.2.3 Seismic survey data

As a complementary geophysical technique to the transient electromagnetic (ground-based) surveys, Raiber et al. (2022a) also reviewed >70 seismic publicly available legacy seismic lines sourced from the Geological Survey of New South Wales DIGS® (Digital Imaging Geological System) (Geological Survey of New South Wales, 2019) across the study area and its immediate surrounding. From these lines, Raiber et al. (2022a) identified two suitable lines (FSG98-AAC and EB08-03 in Figure 2-3) for further re-processing. Re-processing was conducted by HiSeis Pty Ltd on behalf of CSIRO, aiming to determine whether more value could be obtained from the shallower subsurface (upper approximately 400 m) of existing seismic lines. Of particular interest was the identification of major fault displacements and breaks in the near surface, as well as recognising deep-seated structures that may be continuous to the surface. The detailed procedure is described in Raiber et al. (2022a), and the re-processed seismic line FSG98-AAC is shown in Figure 2-4.

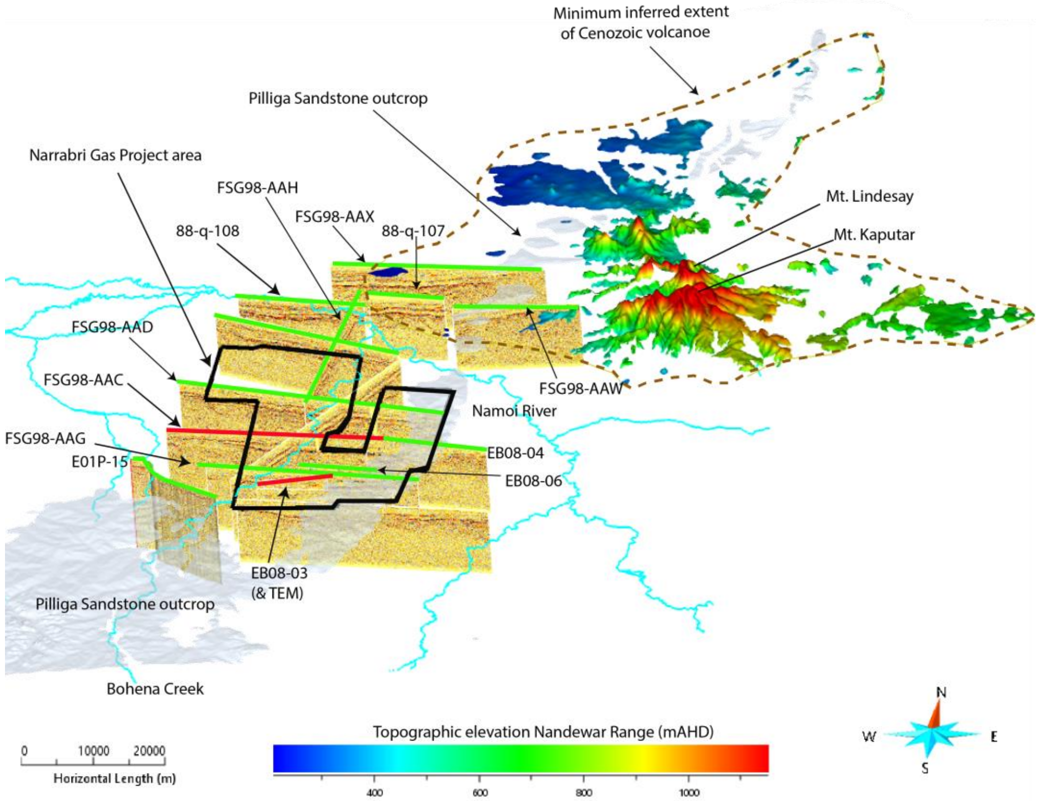

Figure 2-3 – Selected major seismic lines in the Pilliga Forest and Narrabri region considered by Raiber et al. (2022a).

Sections are shown as SEQ-Y (a standard format for storing geophysical data) in relation to the Narrabri Gas Project outline (black line), stratigraphic and exploration wells (shown as red vertical lines), streams (blue lines) and the Nandewar Volcanic Complex displayed in GoCAD/SKUA (Aspentech ™) 3D geological modelling software. The topographic elevation of the Nandewar Range is based on the SRTM DEM (Geoscience Australia, 2011). The names on seismic lines refer to the names of selected seismic lines discussed in the text. Seismic lines FSG98-AAC and EB08-03 were selected for re-processing during this study. Seismic line EB08-03 partly overlaps with the TEM survey line. Most seismic lines are projected into the three-dimensional geological modelling software as straight lines.

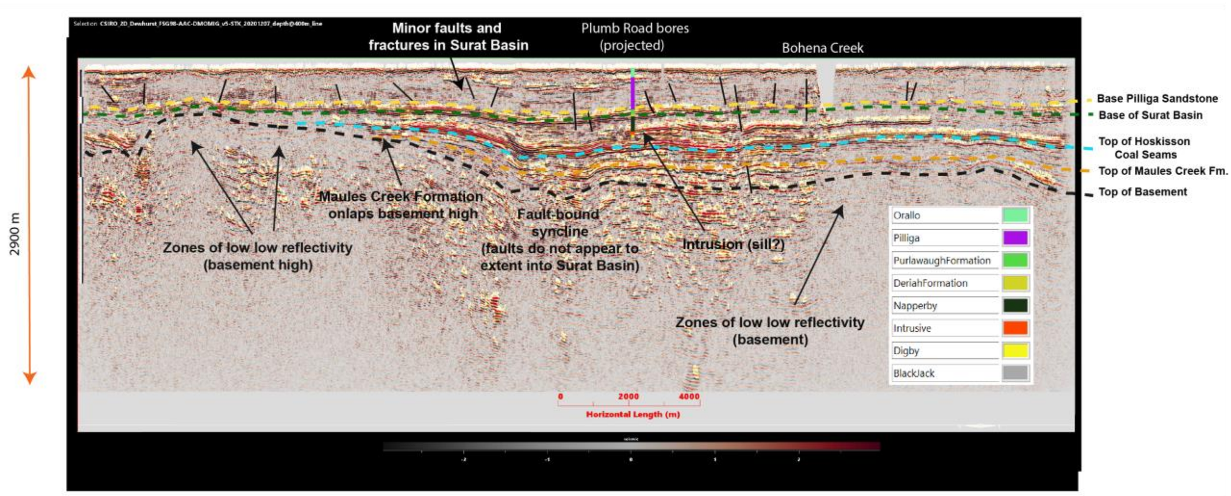

Figure 2-4 – Blend of DMOMIG algorithm and spectral decomposition attribute with annotation of horizon interpretations and major structural features along seismic line FSG98-AAC. Stratigraphic horizon interpretations are based on Raiber et al. (2022a) (including interpretation from HiSeis) and seismic interpretations provided by Santos. For orientation of seismic line, see Figure 2-3.

Selected seismic images were considered in this report to support the interpretations of the airborne electromagnetic survey (Section 2.3), refine the understanding of potential hydrogeological connectivity pathways and underpin the construction of a high-resolution vertical transect model developed to simulate groundwater flow (Section 2.7).

2.2.4 Stratigraphic data

Previous investigation (e.g. Gurba and Weber, 2001; Raiber et al., 2022a) suggested that igneous intrusions (mostly sills) are intersected in many wells. However, south of the Wilga Park anticline (located in the northern part of the Narrabri Gas Project area) these intrusions (mostly sills) do not appear to extend vertically beyond the Napperby or Digby formations. This was considered as an indication by Raiber et al. (2022a) that intrusions observed at anticlines further south (e.g. Bohena anticline) are likely Early Jurassic or older in age (pre-Surat Basin deposition) rather than Cenozoic, possibly associated with the same phase of volcanic activity as the volcanic intrusion dated as Early Jurassic at Nyora 1.

In the present study, a more systematic assessment of the stratigraphic and exploration well log data compiled by Raiber et al. (2022a) from the Geological Survey of NSW DIGS® (Digital Imaging Geological System, Geological Survey of NSW, 2024) system was conducted to determine the spatial distribution of intrusions within the Narrabri Gas Project area by identifying and categorising the stratigraphic units intersected by the intrusions.

Recent stratigraphic interpretations across the Great Artesian Basin and adjacent basins from Geoscience Australia (Norton and Rollet, 2023) were also used to assess the spatial variability of lithological properties within the formations of the Surat and Gunnedah basins in NSW and support the interpretation of airborne electromagnetic survey data, environmental tracers and numerical and geochemical modelling outputs.

2.2.5 Total magnetic intensity maps

In a previous GISERA project, Raiber et al. (2022a) used a total magnetic intensity (TMI) grid from Geoscience Australia (Minty and Poudjom Djomani, 2019) to identify subsurface anomalies related to geological structures (e.g. faults and spatially extensive intrusions) in the Narrabri Gas Project area (Figure 2-5). TMI maps display the intensity of the Earth's magnetic field, which is influenced by the magnetic properties of rocks.

The TMI data ‘measures variations in the intensity of the Earth’s magnetic field caused by the contrasting content of rock-forming minerals in the Earth crust. Magnetic anomalies can be either positive (field stronger than normal) or negative (field weaker) depending on the susceptibility of the rock.’ The first vertical derivative (1VD) grid (Poudjom Djomani, 2019), derived from the 2019 TMI grid of Australia and with a grid cell size of ~3 seconds (approximately 80 m) was also obtained. The 1VD is a high-pass filter for aeromagnetic survey data which is commonly used due to its computational robustness and the reliability and ease of interpretation when assessing magnetic rock bodies (Isles and Rankin, 2013).

Peaks in total magnetic intensity (TMI) maps indicate areas where the magnetic field strength is higher than the surrounding regions. This can correspond to areas with high concentrations of magnetic minerals (e.g. magnetite or hematite), which increase the magnetic susceptibility of the rocks. This can be linked to the presence of igneous intrusions, such as dikes or sills, which are typically rich in magnetic minerals, basement rocks or geological structures (e.g. folds) where magnetic rocks may be closer to the surface.

Troughs in total magnetic intensity maps can represent areas where the magnetic field strength is lower than in the surrounding regions. These troughs can indicate presence of non-magnetic rocks or deeper magnetic rocks with a weaker magnetic signal compared to shallower bodies.

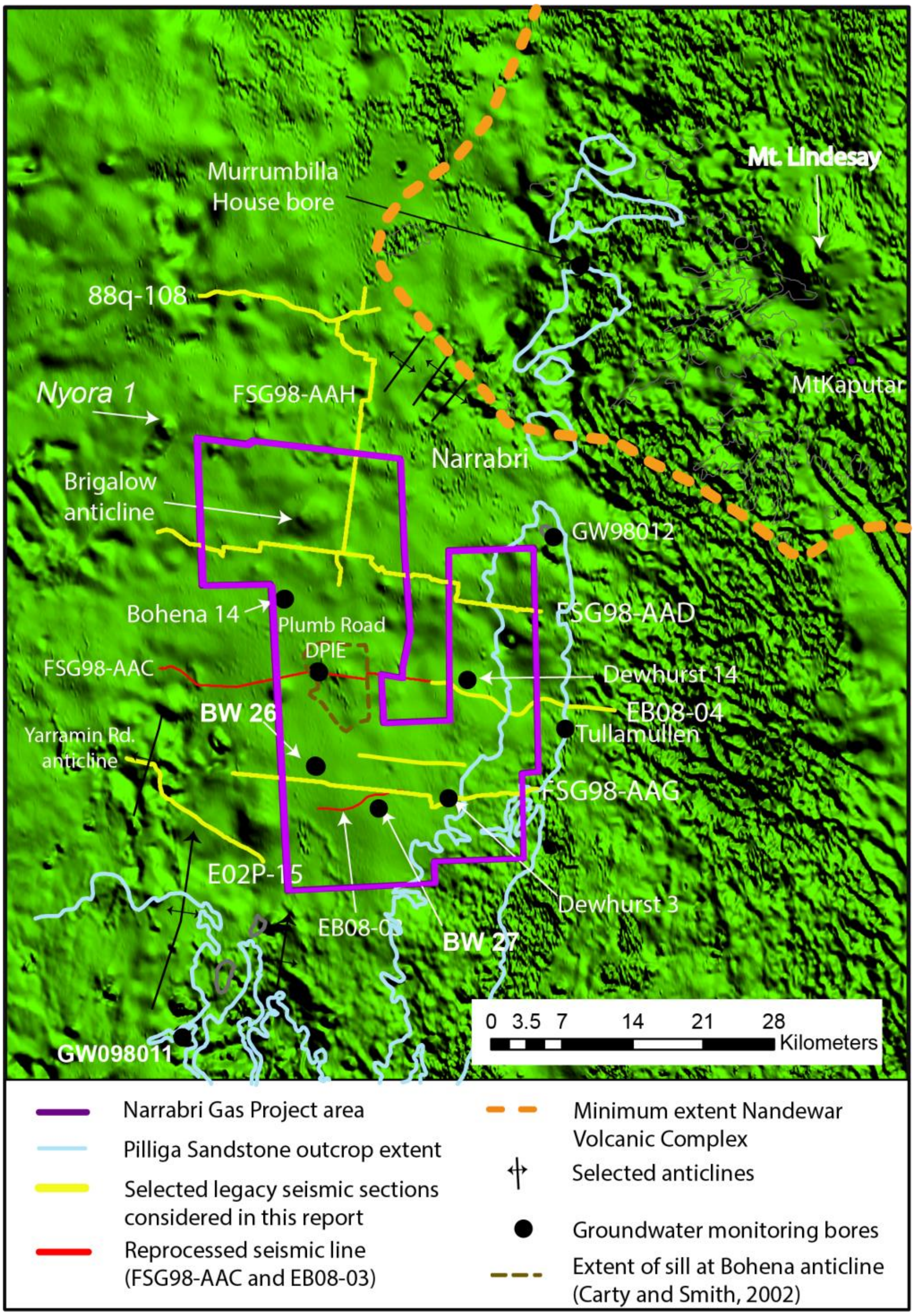

Figure 2-5 – Total magnetic intensity (TMI) grid (40 m resolution) – first vertical derivative (Poudjom Djomani, 2019, modified from Raiber et al., 2022a).

2.2.6 Hydraulic and petrophysical data

Groundwater level data and bore attribute data have been compiled from the Bureau of Meteorology National Groundwater Information System, Santos monitoring bores (from the Santos water portal, 2025), NSW Department of Planning and Environment and Water NSW.

We also compiled hydraulic conductivities and porosity data for each key formation in the broader Narrabri Gas Project area from multiple sources, including CDM Smith (2016), the Bioregional Assessment Program (2016), Turnadge et al. (2018) and OGIA (2019). Hydraulic heads and key statistics for hydraulic conductivities and porosity and hydrographs for selected bores used in the transect groundwater flow models are presented in Section 4.2. The results are used to constrain groundwater flow models and inverse geochemical models and underpin the general understanding of hydrogeology within the Narrabri Gas Project area.

2.3 Airborne electromagnetic survey

In the previous GISERA project "Assessment of faults as potential hydraulic seal bypasses in the Pilliga Forest area", multiple ground-based transient electromagnetic (TEM) surveys were conducted (Raiber et al., 2022a).

The results of the previous ground-based electromagnetic surveys described in Section 2.2.2 and in more detail by Raiber et al. (2022a) indicated that electromagnetic surveys are generally useful for subsurface characterisation in this area. For example, within the south and east of the proposed AEM survey area, the TEM surveys demonstrated that there is a general lack of conductive cover (likely due to the dominance of sandy soils over clay-rich soils and corresponding freshness of infiltrating water), suggesting that a considerable depth (>400 m below ground surface) could be achieved from an AEM survey. For this new project, due to the density of vegetation in the Pilliga Forest, an airborne geophysical survey was considered more appropriate and cost-effective, allowing to cover a larger spatial area than ground-based techniques.

Sedimentary rocks, whether consolidated or unconsolidated, are characterised by a range of conductivities (Figure 2-6), but the influence of contained water salinity and quantity can also be significant (Palacky, 1987). Igneous rocks (e.g. intrusive rocks such as granite and extrusive rocks such as basalts) often show high resistivity (low conductivity) in AEM surveys. This is because they are often composed of minerals such as quartz and feldspar, which are poor conductors of electricity. Furthermore, the presence of magnetic minerals such as magnetite and hematite can also create magnetic anomalies and help in identifying igneous intrusions and their extent.

The observed ground conductivity, whether measured by a ground or airborne system, is caused by various combinations of lithology and salinity. In both consolidated and unconsolidated regolith and sedimentary materials, including alluvial materials and underlying sedimentary rocks, the conductivity will be significantly influenced by the electrolyte (salt) which occurs in moisture-filled pores within an insulating matrix (McNeill, 1980). Although the porosity and connectivity of the pores in sediments and in-situ regolith materials play a part in determining conductivity, particularly in the absence of clays, it is the quantity and the salinity of the contained pore water that is critical. Clay content and type becomes important when the concentration of ionic conductors (e.g., salts in solution) is low. Their significance becomes negligible at high ionic concentrations, particularly for clays of low to moderate cation exchange capacity, such as kaolinite (Emerson and Wang, 1997).

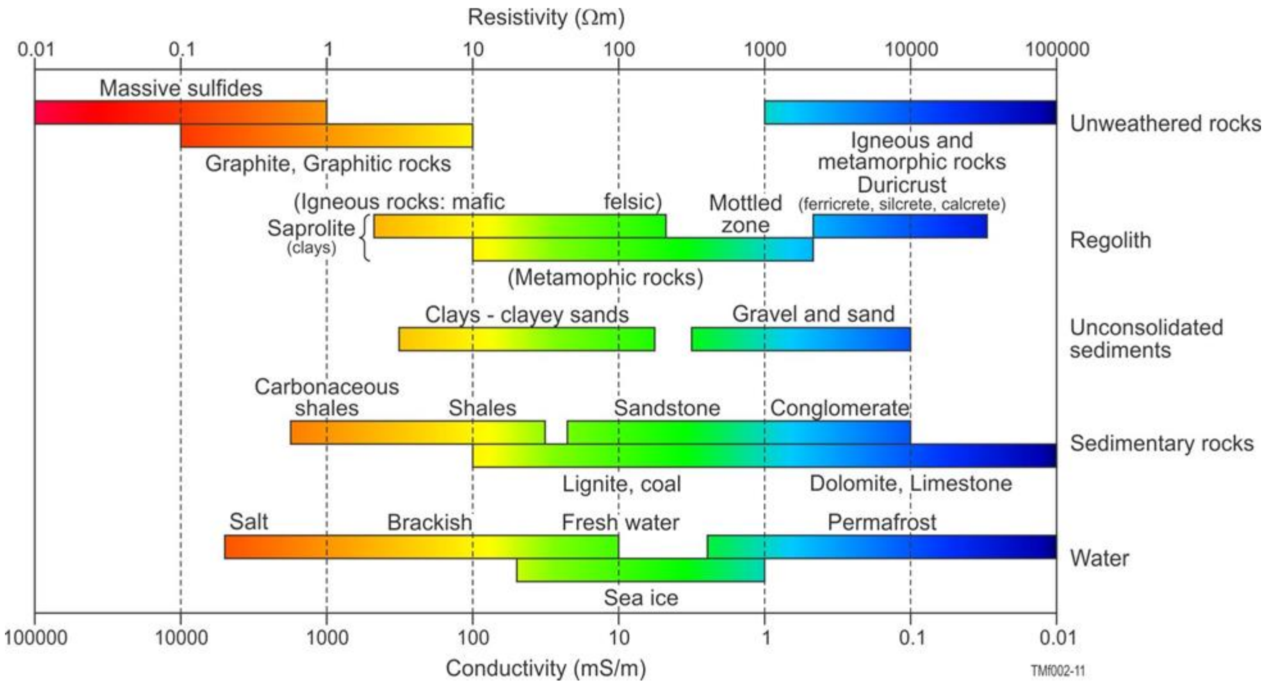

Figure 2-6 – Schematic of expected conductivity or resistivity of common earth materials. Overlapping values of conductivity show that the inverted conductivity values of the subsurface may not allow for unique determination of material (after Palacky 1983).

2.3.1 Principles of AEM data acquisition

Electromagnetic survey techniques involve the measurement of the varying response of the subsurface due to the propagation of electromagnetic fields. Primary fields are generated by passing a current through a loop or coil positioned in the air, referred to as the transmitter loop (Figure 2-7). A secondary field is induced in the subsurface and these secondary fields are detected by the alternating currents that are induced to flow in a receiver coil by a process known as electromagnetic induction.

As the induced current results from the magnetic component of the electromagnetic field there is no need to have physical contact between transmitter or receiver and the ground. Consequently, EM surveys can proceed effectively both on the ground, and in the air.

The primary field travels from the transmitter to the receiver via paths above and below the ground surface (Figure 2-7). In the presence of a conducting body (for example conductive regolith and/or saline groundwater), the magnetic component of the electromagnetic field penetrating the ground induces eddy, or alternating, currents to flow in the conductor. These eddy currents generate the secondary electromagnetic field which is measured by the receiver. In time domain EM systems, such as the SkyTEM AEM system, the receiver coils record the response of a decaying signal in the ground at various times (referred to as gates or time windows) after the transmitter pulse has been switched off.

The difference between the transmitted (primary) and received (secondary) electromagnetic fields will be determined by the geometry and electrical properties of conductors in the ground. Materials that are highly conductive produce strong secondary electromagnetic fields. Sediments (e.g. alluvium), soils or other regolith materials that contain saline pore water can generate such fields. The shape of the decaying signal provides information about the vertical conductivity structure of the ground.

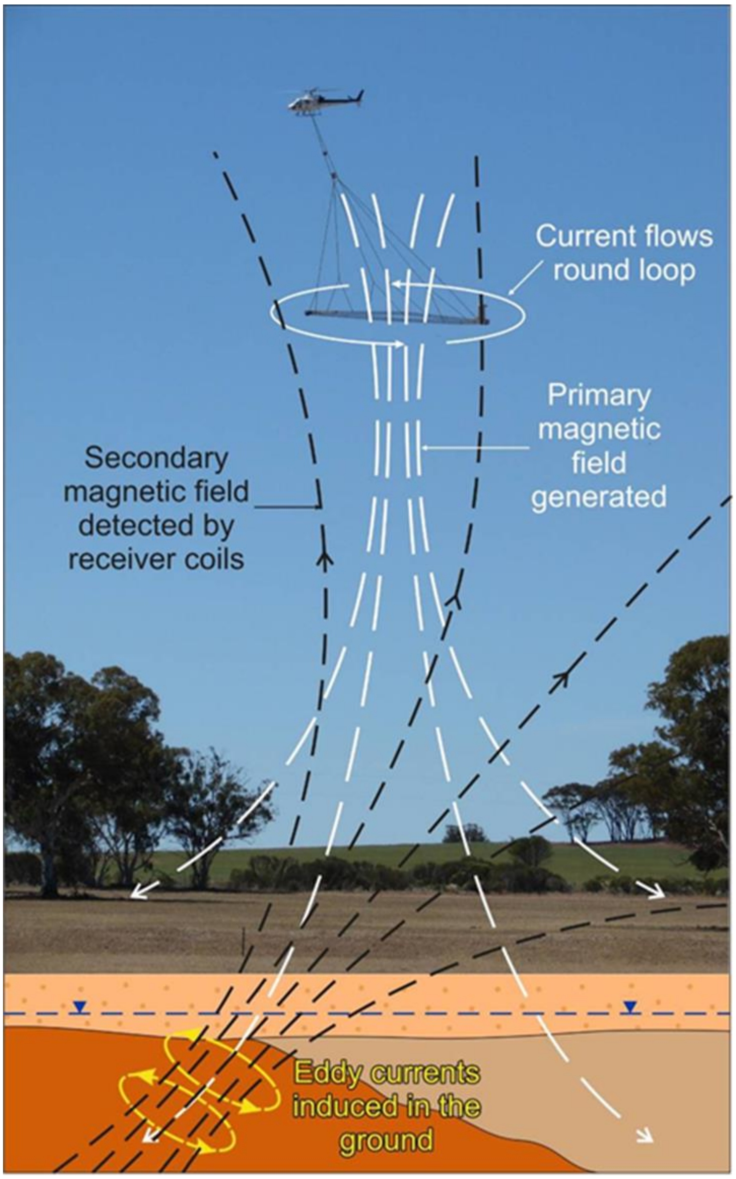

Figure 2-7 - Operating principles of a helicopter airborne electromagnetic (AEM) system such as the SkyTEM system.

Most AEM systems map contrasts in ground conductivity that are then interpreted based on experience and with the support of ancillary data, including surface and bore water EC, downhole conductivity measurements, lithology logs from drilling, surface geophysical investigations and other observations.

2.3.2 Narrabri AEM survey objectives

The design of this AEM survey focussed on closing knowledge gaps related to subsurface geometry identified during a previous GISERA project (GISERA W.19. “Assessment of faults as potential hydraulic seal bypasses in the Pilliga Forest area”). During the design phase, the set-up of the proposed AEM survey has been discussed with various stakeholders, including NSW state agencies (NSW Geological Survey and NSW Department of Primary Industries), academia and industry to maximise the benefit for all stakeholders.

Specific aims included providing information at a detailed to reconnaissance scale, such as:

a) Generating geophysical and geological mapping information from a depth of 10 m to a total depth of at least 400 m (with the depth varying locally, depending on the conductivity of the Cenozoic conductive (clay-rich) cover).

b) Enhancing the understanding of the electrical conductivity between and within different geological units.

c) Refining the understanding of aquifer geometry and geometric relationships between coal seams, Great Artesian Basin, and alluvial aquifers, with a focus on the following interfaces between stratigraphic units:

- Base of alluvium and Cenozoic (surface) cover
- Base of Orallo Formation
- Base of Pilliga Sandstone
- Interface of Purlawaugh Formation and Napperby Formation (corresponding to the base of the Surat Basin and Great Artesian Basin).

d) identifying whether there are any deformations (e.g. vertical displacements) of the stratigraphic unit interfaces, providing insight into local geological structures and in particular mapping of geological features in the Surat and Gunnedah basins to complement seismic surveys and refine mapping of stratigraphy and subsurface geometry, including underlying faults and intrusive igneous structures.

e) defining the geometry of the Gunnedah Basin strata close to the Hunter-Mooki Thrust fault, one of the major tectonic boundaries in eastern Australia.

f) assessing whether there is any systematic internal architecture within the Namoi alluvium.

The AEM survey was designed in an orientation where survey lines traverse along the strike of the Surat Basin and Gunnedah Basin formations from outcrop beds to the deeper part of the basins (Figure 2-8).

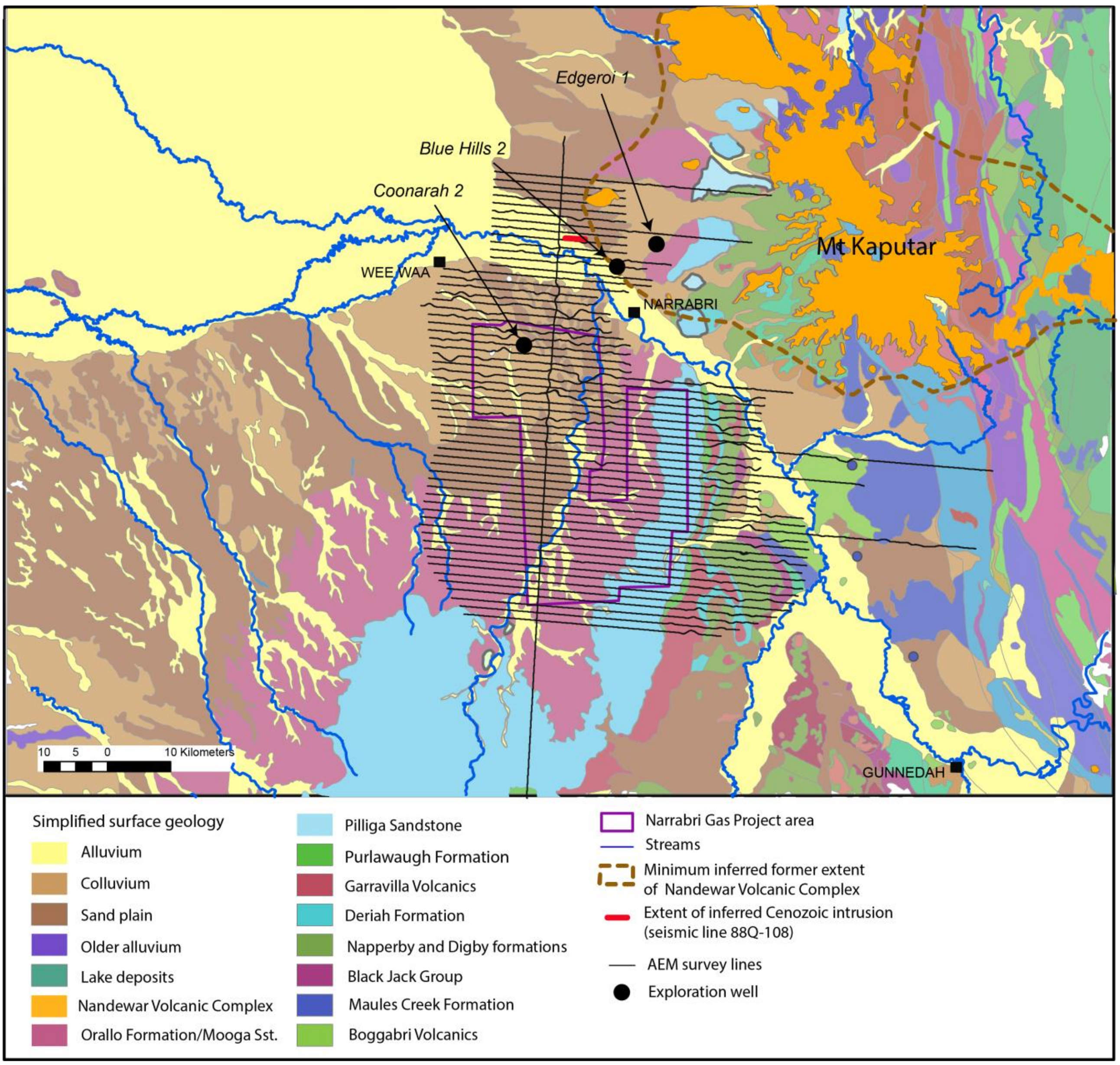

Figure 2-8 – SkyTEM airborne electromagnetic survey (AEM) flight path lines (with more than 60 east-west lines in a 1200 m spacing) overlain on simplified surface geology. Non-straight lines indicate areas where the survey path was amended to avoid cultural features (e.g. infrastructure). Selected exploration wells are also shown.

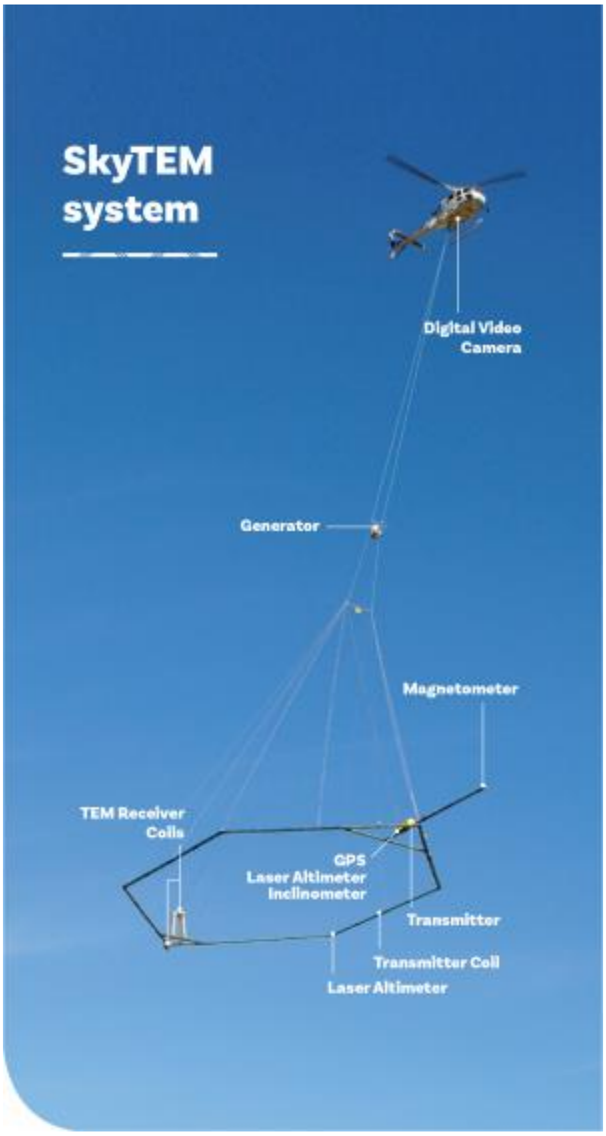

Figure 2-9 – SkyTEM helicopter AEM array (image courtesy of SkyTEM).

2.3.3 AEM survey specifications

The SkyTEM electromagnetic system is carried as a sling load towed beneath a helicopter (Figure 2-9). For the Narrabri survey, the SkyTEM306HP system was used. It has an eight-sided transmitter loop mounted in a lightweight carbon-fibre frame. The survey was flown by SkyTEM Australia Pty Ltd with a AS350 B3 helicopter on behalf of CSIRO in twenty-one production flights between the 21st November and 3rd December 2023. The survey area encompassed the town of Narrabri and the surrounding areas in the North West Region of New South Wales (Figure 2-8). The nominal survey altitude of the transmitter in the Narrabri survey was 45 – 60 m, with the altitude varying depending on the presence of trees, power lines and related anthropogenic features.

This survey area comprised a large block extending approximately 73 kilometres from north to south and 59 kilometres from west to east. The flight lines were spaced approximately 1200 metres apart, although some lines had been angled slightly sub-parallel to avoid infrastructure. Several of the flight lines extend eastward beyond the main block. An additional north-east to south-west line with a length 104 km was also acquired.

The total length of the AEM survey flown in this study was 2,765.7 km. This included three repeat lines, and two test lines flown with repetition frequency of 18.75Hz. The projected grid coordinates were supplied by SkyTEM to CSIRO in GDA94 / MGA Zone 55 projection.

Further technical details are provided in SkyTEM (2024).

2.3.4 AEM survey - community engagement

The helicopter AEM survey required comprehensive engagement with the Narrabri community to ensure widespread understanding of the survey purpose and activities.

The AEM involved a helicopter flying at a height of 60-80 metres and towing a large circular carbon-fibre frame approximately 45-60 metres above ground level, on a daily basis over a two-week period.

The combination of the low altitude flight path and the large electromagnetic frame being towed meant that the activity would be highly visible and quite remarkable to members of the community both in the Narrabri township and surrounding farming areas.

Figure 2-10 – Narrabri Courier (2023)

While the contracted AEM operator (SkyTEM) managed all flight planning communication and compliance activities with aviation authorities, the CSIRO was responsible for informing the local community about the survey activities.

The CSIRO researchers collaborated with communication colleagues to identify key community stakeholders in the region, including locally based CSIRO research organisations (cotton research and astronomy), National Parks, local government, police, hospitals, agricultural organisations, NSW Forestry, NSW fire and rescue, landowners, university students and industry reps.

Development of the stakeholder list was informed by the research team's knowledge of the local community and cross-checked with a "what could go wrong" scenario analysis.

Based on the list of key stakeholders the communication team then identified appropriate communication channels to reach various target audiences, including local media advertising, web-based resources on the CSIRO GISERA web site, leveraging third party social channels, direct contact via phone calls supported by emailed fact sheets/links, and face to face meetings.

CSIRO communication officers developed a comprehensive media plan, which involved regular advertisements in the newspaper, media news articles (Figure 2-10), social media and relationship building with the local paper. It was further supported by emails, development of factsheets, questions and answers, a cold-calling campaign to local businesses, and face to face meetings by the communication team and researchers with key local stakeholders.

During the cold calling campaign and face to face meetings, researchers asked "who else would like to know about this activity" which elicited further valuable local stakeholder details not identified in the first assessment.

Throughout the survey period, the communication team and researchers continuously maintained close communication with the AEM contractor and local stakeholders to minimise disturbance.

Examples of the benefits of this approach included:

- Provision of notice to landholders to ensure livestock are not "spooked" by low flying transits;
- Ability to work with the AEM contractor and CSIRO's Australia Telescope Array in Narrabri to schedule survey flight paths to co-incide with scheduled telescope maintenance shut-downs (ensuring survey electromagnetic signals did not interfere with stellar observation data);
- Liaison with NSW Forestry to share information about a helicopter-based pest animal culling program being run concurrently to the west of Narrabri;
- Establishing a strong relationship with local news outlet (Narrabri Courier) which ensured any community queries about the survey were promptly directed to paid advertising, news articles (Figure 2-10; Narrabri Courier, 2023) and CSIRO's web-based resources.

The collaboration between communication managers, researchers and AEM contractor was instrumental in ensuring successful and incident-free completion of this survey, underpinning the generation of some of the most detailed subsurface visualisations obtained in the Great Artesian Basin.

CSIRO communication resources:

Earned media news article https://narrabricourier.com.au/2023/11/07/csiro-narrabri-airborne-electromagnetic-survey/

Factsheets https://gisera.csiro.au/wp-content/uploads/2023/11/23-00522_GISERA_FACTSHEET_W28-NarrabriAEMSurvey_WEB_231026.pdf

Q&A https://gisera.csiro.au/wp-content/uploads/2023/11/GISERA-Narrabri-AEM-QA-v1-Social.pdf

2.3.5 AEM data inversion and interpretation

Given that one of the objectives of the Narrabri AEM survey is to map and interpret spatial variations in conductivity for geological inference, it is necessary to convert measurements of the electromagnetic response to bulk subsurface conductivity and present the results in a form that allows their ready analysis against existing or new ground data. The conversion is achievable through a modelling process known as inversion.

The inversion of AEM data and their presentation as maps or sections detailing a conductivity distribution in the subsurface is now commonplace. The representation of continuous and gradational conductivity distributions as discrete conductive “units” or bounding layers is an effective way of summarising information from large AEM surveys. It enables users to visualise conductivity variations in the subsurface in three dimensions (Lane 2000, 2002, Lane and Pracilio, 2000). To determine the electrical conductivity variation with depth the airborne electromagnetic data must be modeled. This entails taking data from each measurement point, sounding or fiducial along a flight line and estimating the parameters of a layered-earth, conductivity-depth model, which would produce the observed response (Figure 2-11). Through the application of approximate transforms or layered inversions, conductivity values with depth can be calculated for each observation (sounding) made by the AEM system and then stitched together into sections to provide a representation of the 2D variation of conductivity. Further, the conductivity depth profiles are combined into 3D gridded volumes from which arbitrary sections, horizontal depth slices (or interval conductivity images) and iso-surfaces can be derived. The schematic in Figure 2-11 summarises the process of acquiring AEM data, inverting the resulting data, and presenting the results as conductivity images.

Airborne electromagnetic (AEM) data acquired for exploration or environmental applications are commonly modelled using algorithms such as conductivity depth transforms (CDT’s) or Layered Earth Inversions (LEI’s) that assume a 1D earth (Sattel 1998, 2005). Presently, the application and relevance of full 2 or 3D inversion of AEM data remains undetermined, although more recent case studies (see, for example, Paterson et al. 2016) are providing greater insight into their application. In many respects it may be unrealistic and unnecessary to employ these computationally intensive methods particularly for the investigation of sedimentary sequences in many Australian settings, where it is reasonable to assume that the subsurface, *at the scale of the footprint of an AEM system,* can be represented as a series of horizontal layers. The 1D model assumption, legitimate in sub-horizontal, layered sedimentary areas where it produces results that are only slightly distorted by 2D or 3D effects which may be induced by faults, fractures, or other geological phenomena (Auken et al., 2005; Newman et al., 1987; Sengpiel and Siemon, 2000).

In the following section we explore the processing and inversion methods used to interpret the Narrabri AEM data set.

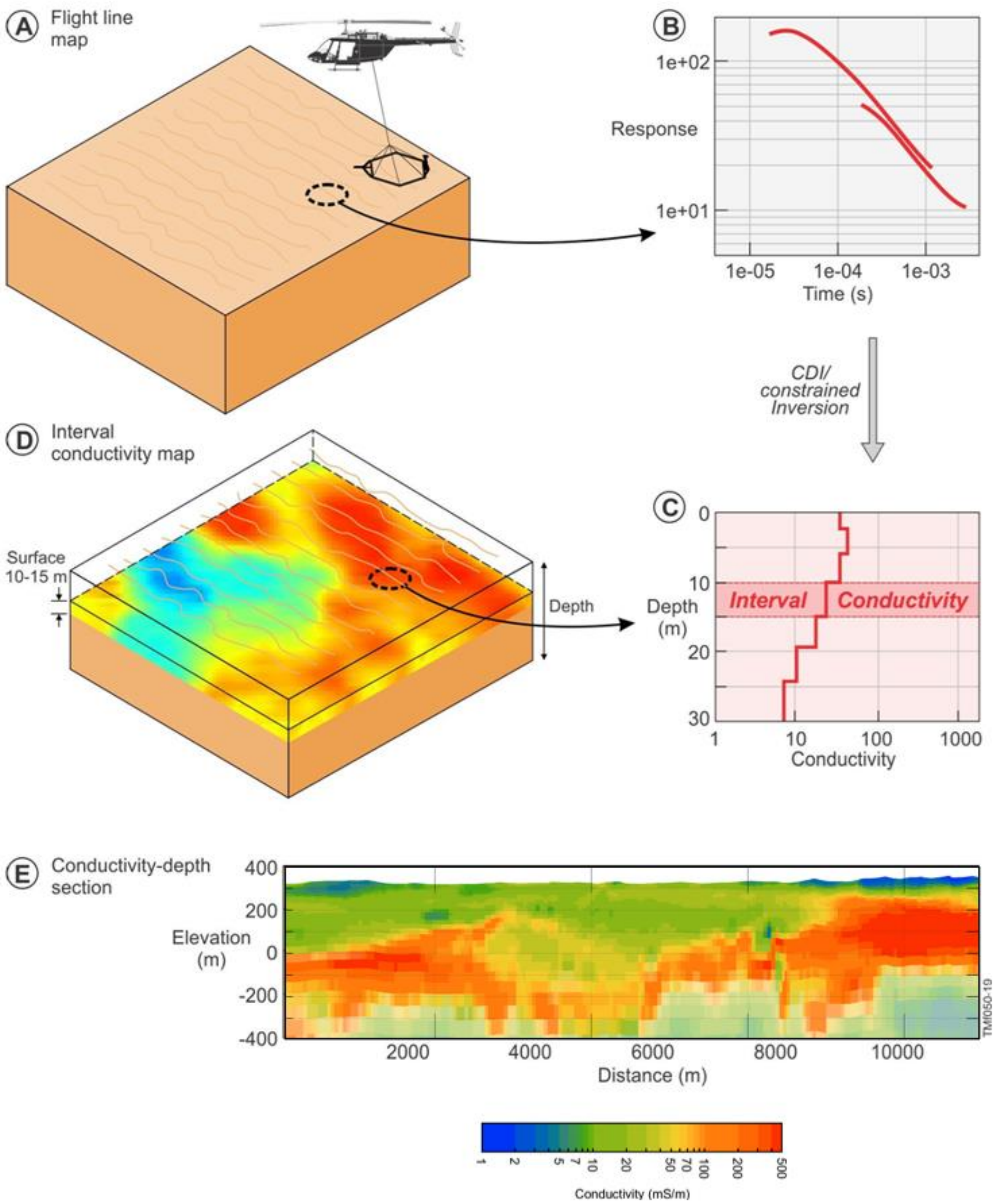

Figure 2-11 - Schematic representation of helicopter time domain EM data acquisition and inversion. A) Data are acquired along parallel flight lines along each flight line; B) The EM receiver measures the secondary high and low moment responses; C) The measured response is used to determine the conductivity-depth function by inversion; D) The modelled conductivity structure for each sounding is gridded into conductivity-depth intervals to provide a spatial representation of the subsurface conductivity structure at different depths below the ground surface; E) Individual soundings from a flight line are stitched together into conductivity-depth sections to provide a representation of the variation of conductivity.

2.3.6 Processing AEM data

Prior to inverting AEM data, the survey data must be processed. This crucial step in our workflow is important because raw AEM data is noisy, incomplete, and not often in a form that inversion algorithms can reliably use. Processing is important because instrument noise, cultural noise (such as power lines, fences and man-made structures) and natural interference such as sferics can distort the measured signal. If these noise sources are not reduced or eliminated from the workflow, noise will propagate through the inversion producing unreliable or implausible electrical conductivity models. An example of high-moment SkyTEM data badly affected by noise due to a nearby coal mine (Narrarbi Coal Mine) is shown in Figure 2-12.

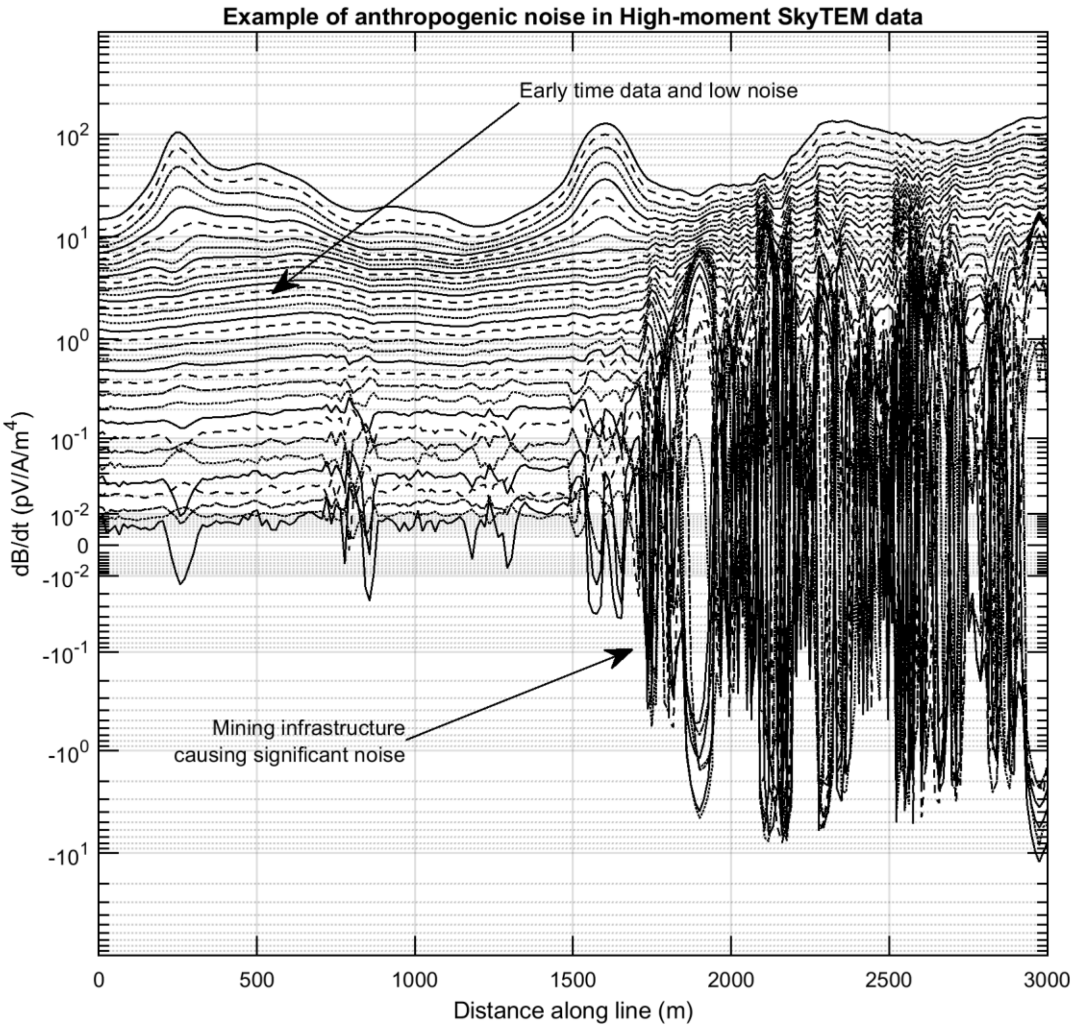

Figure 2-12 - An example of high-moment SkyTEM data from the Narrabri AEM survey badly affected by noise from a nearby coal mine. Signal from 1500 m to 3000 m is significantly affected by electrical machinery causing typical ringing effects in the data that must be removed prior to inversion. There are minor noise artefacts at 250 m and 750 m.

For this report, we manually processed all the SkyTEM survey data and removed or masked out time gates that were noticeably affected by noise. This was completed for both the low- and the high-moment data. Figure 2-13 shows a scatterplot of the processed data where the colour indicates the total number of low-moment and high-moment time gates (or channels) that are permitted to enter the inversion

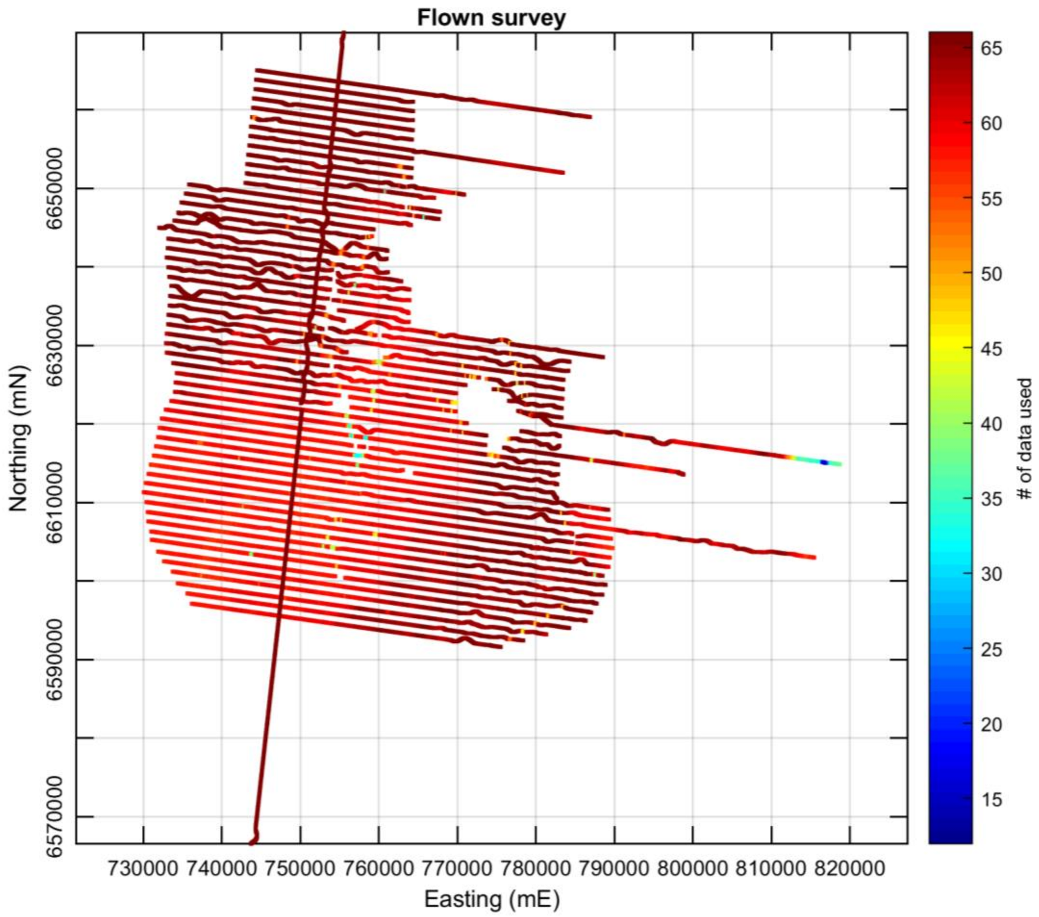

Figure 2-13 - Plan view of the Narrabri survey with total number of time gates, or channels, used in the inversion calculations after processing for anthropogenic and geological noise.

2.3.7 Reversible-jump Markov chain Monte Carlo Estimation of noise in AEM data

Inversion of AEM data for electrical conductivity models involves many factors that need to be addressed. These include: the description of the AEM system to be modelled, discretisation of the model used to estimate conductivity, the choice of inversion algorithm, and the amount of regularisation needed to ensure reasonable convergence. Perhaps one of the most important factors that needs to be mentioned, and one that is closely tied to model regularisation, is estimates of noise in the AEM survey data. Noise is any unwanted signal that interferes with the electromagnetic signal transmitted and received by the AEM sensor. It can be generated by various sources categorised as anthropogenic or natural. The former comprises man-made structures such as buildings, pipelines, fences and power lines, with the latter including sferics (a broadband electromagnetic impulse resulting from natural atmospheric lightning discharge) and other atmospheric disturbances. Other natural noise sources include variations in the earth's natural electromagnetic fields and, one that is rarely discussed, the actual geological variability of the survey area.

Different types of noise can be present in AEM data, but they are generally classified as random and systematic noise. Systematic noise, caused by a specific source that produces a consistent pattern of interference in the AEM data, can often be corrected by identifying the source and applying appropriate correction methods. Random noise is caused by the statistical variation of the electromagnetic signal received by the AEM sensor. This noise is difficult to remove as it is not correlated with any causes.

An accurate estimation of noise levels in AEM survey data is considered necessary since they directly influence the accuracy and reliability of the data and the models of the subsurface conductivity structure, that can be generated from them. This can have a profound impact on our interpretation of the subsurface geology. Despite the importance of obtaining accurate estimates of data noise, there is relatively little in the literature that describes how we obtain them.

Determining noise

It can be difficult to determine the noise characteristics of AEM survey data since there is little opportunity to operate AEM systems at full capacity while on the ground. To address this, many contractors now offer measurements of high-altitude data. With the transmitter operating at full capacity, the AEM system is taken to extreme altitude in the assumption that the signals measured by the receiver coils will be uninterrupted or affected by earth responses. These measurements offer an understanding of the noise floor of the AEM receiver assembly: the measurements of the receivers in the absence of any signal other than the system itself. This is a good first step to understanding the bias of the system. An example of high-altitude noise recordings is shown with the solid lines in Figure 2-14.

Green and Lane (2003) suggest a different strategy for estimating noise in survey data through use of repeat lines. The assumption here is that the system should always measure the same responses over the same survey transect. They recommend characterising noise as either additive or multiplicative in nature, meaning that noise levels for a given delay time are composed of some base level of noise plus some factor multiplied by the signal itself at that delay time. This can be written as

$$\sigma_i = \sqrt{\sigma_{iadd}^2 + (\sigma_{im} \cdot d_i)^2}, \tag{1}$$

where σ_i is the noise at delay time i, d_i is the measured data for that delay time, and σ_{iadd} and σ_{im} are the additive noise term and the multiplicative factor, respectively. It should be noticed that the noise term σ_i enters the data misfit equations as an additive term when used in this manner. An example of an additive noise estimate following this method is shown with dashed lines in in Figure 2-14.

One of the drawbacks of the method of Green and Lane (2003) is that repeat lines are impossible to replicate exactly due to the platforms being airborne. Differences in altitude can have a profound effect on the measured response. Another drawback is that many older surveys do not have repeat lines flown (or are not available as part of the delivered data); so, a compromise must be sought. In the approach taken here, we assume that while repeat lines may not have the same measured responses due to variations in acquisition, they should have the same earth and noise model provided the repeat lines are flown reasonably close together. At each station of the repeat lines, differences between the recorded data and the forward response for each station can therefore be classified as 'noise'. Noise in this sense incorporates variations in measurement at each station but also encompasses the choice of model used to determine the earth response.

To achieve estimates of electrical conductivity distribution and noise for the repeat lines, we employ the Reversible-jump Markov chain Monte Carlo (RJMCMC) method described by Green, (1995) with a few modifications similar to those employed by Minsley et al., (2021).

We begin by ensuring that sampling of the repeat line data is consistent across a regular spacing along the survey line. The simplest way of doing this is by taking stations from each repeat line that are close enough that we can assume they are measuring the same volume of the earth (eg, Reid et al., 2006) or by resampling the data to a regular spacing. For every station, we create a 1D layered-earth model of variable electrical conductivity layers (and thickness) and a common noise estimate for every delay time of the system. Using $\boldsymbol{m_s}$ to describe the model at station s, the model is composed of k layers of resistivity $\boldsymbol{\rho}$ with thickness $\boldsymbol{t}$ to describe the earth, and n values of $\boldsymbol{\sigma}$ to describe the additive error applied to the n delay times for the j measurements at location s. Notice that the variables in bold are vectors.

At every iteration in the chain, a new model $\boldsymbol{m'_s}$ is proposed from the previous model $\boldsymbol{m_s}$. The new model is accepted or rejected based on the Metropolis, Hastings, Green (MHG) algorithm according to the following acceptance criterion α

$$\alpha(\mathbf{m}'_s|\mathbf{m_s}) = \min\left[1, \frac{p(\boldsymbol{m}'_s)}{p(\boldsymbol{m_s})}\frac{p(\mathbf{d}|\boldsymbol{m}'_s)}{p(\mathbf{d}|\boldsymbol{m_s})}\frac{q(\boldsymbol{m_s}|\boldsymbol{m'_s})}{q(\boldsymbol{m'_s}|\boldsymbol{m_s}),}|\mathbf{J}|\right],$$

(2)

where $p(\boldsymbol{m}'_s)/p(\boldsymbol{m_s})$ is the prior ratio of the models, $p(\mathbf{d}|\boldsymbol{m}'_s)/p(\mathbf{d}|\boldsymbol{m_s})$ is the likelihood ratio of the data given the models, $q(\boldsymbol{m_s}|\boldsymbol{m'_s})\backslash q(\boldsymbol{m'_s}|\boldsymbol{m_s})$ is the proposal ratio, and $\boldsymbol{J}$ is the Jacobian governing changes between dimensions. Of special interest is the data likelihood function $p(\mathbf{d}|\boldsymbol{m_s})$ which will change at every iteration due to choices of perturbations in $k, \boldsymbol{\rho}, \boldsymbol{t}$, or $\boldsymbol{\sigma}$. We write the likelihood function as

$$p(\mathbf{d}|\boldsymbol{m_s}) = \sum_{i=1}^{j} \frac{1}{\sqrt{2\pi|\boldsymbol{C_d}(\boldsymbol{\sigma})|}} \exp\left(-\frac{1}{2}\left((\boldsymbol{f}(\boldsymbol{\rho},\boldsymbol{t},k) - \boldsymbol{d_{si}})^T \boldsymbol{C_d}(\boldsymbol{\sigma})(\boldsymbol{f}(\boldsymbol{\rho},\boldsymbol{t},k) - \boldsymbol{d_{si}})\right)\right)$$

(3)

where $\boldsymbol{f}(\boldsymbol{\rho}, \boldsymbol{t}, k)$ is the predicted data given the model parameters, $\boldsymbol{d_{si}}$ is the measured data at station s for measurement i ,and $\boldsymbol{C_d}(\boldsymbol{\sigma})$ the data covariance matrix that models the error in the system responsible for the measurements. In this report, $\boldsymbol{C_d}(\boldsymbol{\sigma})$ is assumed to be diagonal.

Model proposals are based on the usual choices for MHG samplers. At every iteration, we choose to: create a conductivity interface, destroy a conductivity interface, change the structure of the existing model (by creating and destroying random interfaces, or vice versa), or changing one of the n noise parameters in $\boldsymbol{\sigma}$. For each station, several chains (8) are run for many iterations (1×10^5). Several thousand models are excluded from the beginning of each of the chains, and the results are accumulated.

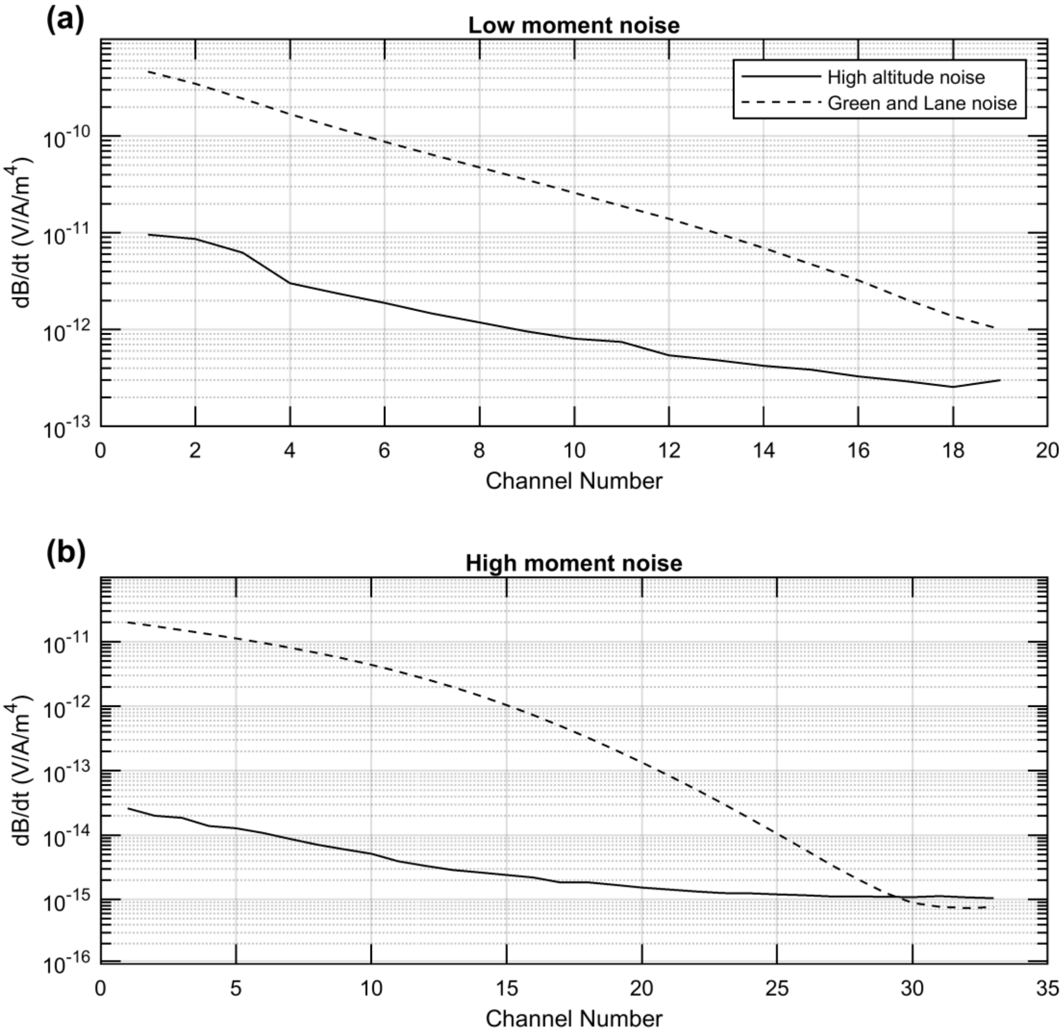

Figure 2-14 - Noise estimates from an AEM system. Solid black lines show the high-altitude measurements, while the dashed lines show the estimates from a Green and Lane (2003) analysis of repeat lines.

Figure 2-15 shows a posterior mean electrical conductivity distribution transect for the example discussed earlier. Areas that are made transparent reveal that the spread in conductivity of the accepted models is almost equivalent to the prior probability range of the conductivity proposals (and, therefore, less informative). The section looks reasonable, and there is clear structure to depths of approximately -400 mAHD. Figure 2-16 shows the mean distributions of the marginalised noise estimates for every model in the reduced RJMCMC chains, and for every station. The distributions are shown in shaded blue, while the mean additive noise value for each delay time is marked by the solid gold line. The mean values from the gold line are chosen to represent the average additive noise values for the entire survey. Also shown are the high-altitude (black), and the Green and Lane (2003) noise estimates (red). The RJMCMC noise estimates are consistently higher than the high-altitude noise estimates, but mostly lower than the Green and Lane (2003) estimates. For the remainder of this report, we use the RJMCMC estimates of noise in the models for estimating electrical conductivity.

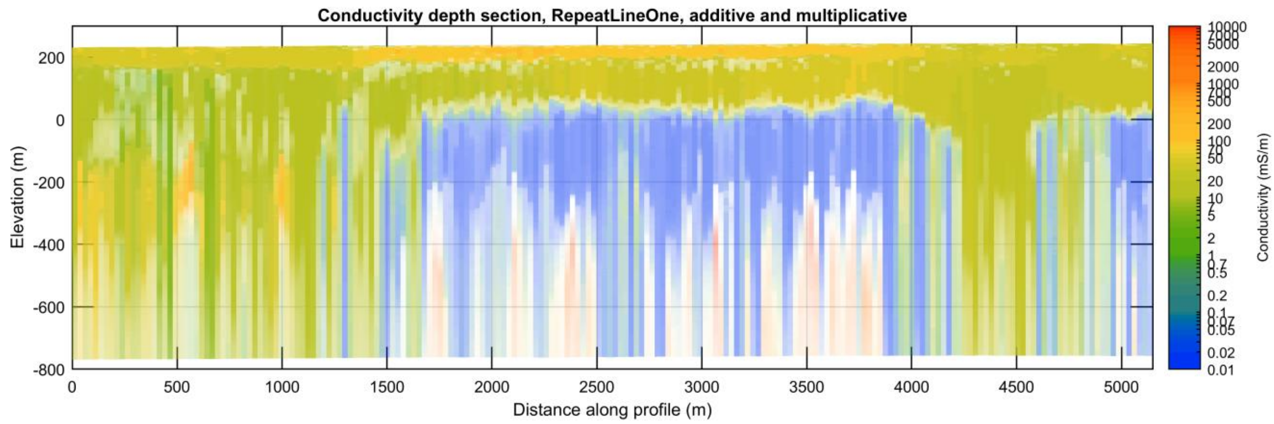

Figure 2-15 - An example of a posterior mean conductivity section resulting from the RJMCMC process on the repeat lines used in the Narrabri AEM survey. Blanked areas are due to a wide spread of accepted models relative to the prior conductivity.

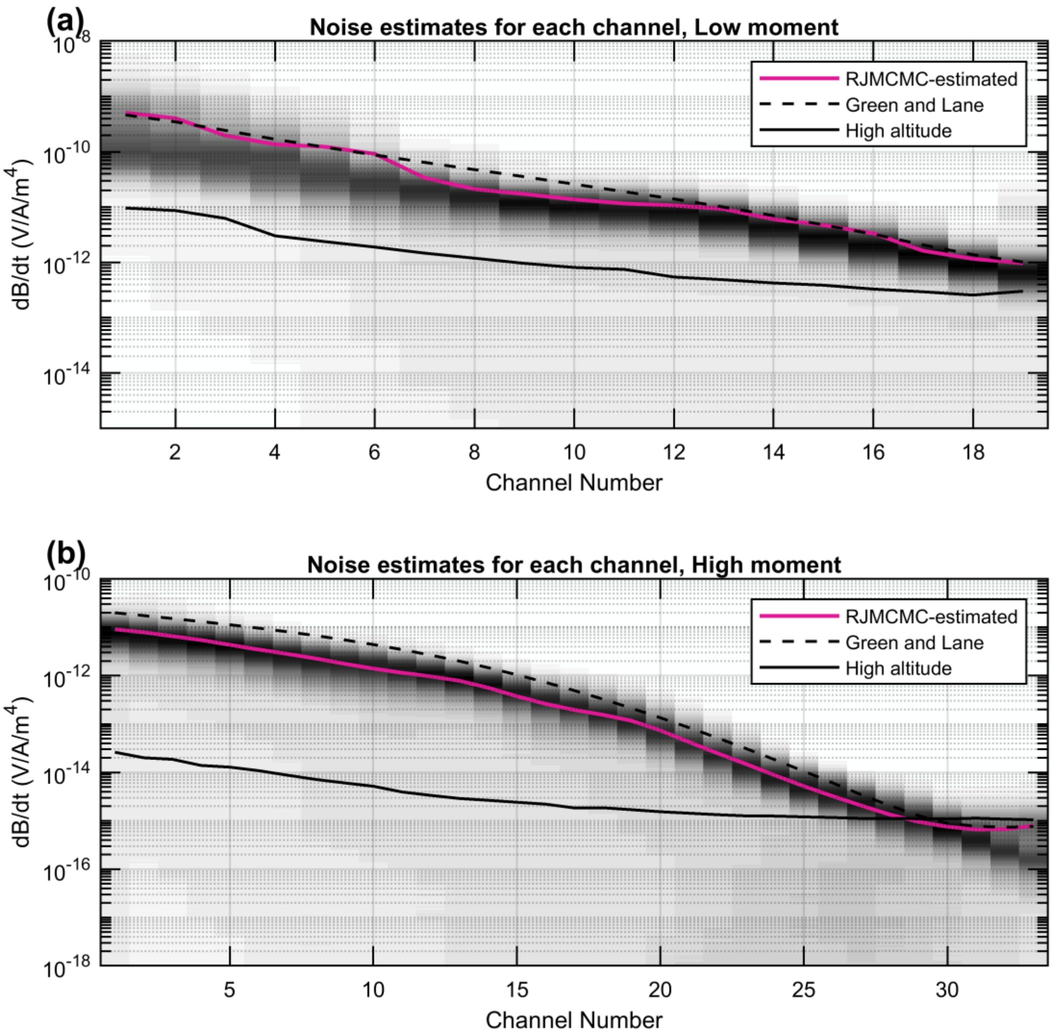

Figure 2-16 - Estimates of total noise for each delay time of both low-moment and high-moment systems. The shading variations show the distributions of the noise estimates from the RJMCMC simulations. The solid fuchsia line shows the peak of the distributions and is taken as the average measurement noise for the entire survey. The solid black line is from high-altitude tests, and the dashed black line is the Green and Lane (2003) estimate.

Description of the inversion algorithm

Having determined an average noise estimate for the entire survey based on several repeat lines, it is useful to see the effect the noise estimates have on deterministic inversion. The deterministic inversion algorithm is run by trying to minimise an objective function that compares the data measured while on survey to the data predicted by the layered earth forward model.

Briefly, the objective measure function ϕ can be written

$$\phi = (\boldsymbol{f}(\boldsymbol{m}) - \boldsymbol{d})^{\boldsymbol{T}} \boldsymbol{C}_{\boldsymbol{d}}^{-1} (\boldsymbol{f}(\boldsymbol{m}) - \boldsymbol{d}) + \alpha (\boldsymbol{m} - \boldsymbol{m}_{\boldsymbol{p}})^{T} \boldsymbol{C}_{\boldsymbol{m}}^{-1} (\boldsymbol{m} - \boldsymbol{m}_{\boldsymbol{p}}), \tag{4}$$

where $\boldsymbol{f}(\boldsymbol{m})$ is the predicted data at a survey location based on a layered earth conductivity model $\boldsymbol{m}$, $\boldsymbol{d}$ is the data measured at the survey locations, $\boldsymbol{C}_{\boldsymbol{d}}$ is the data covariance matrix, $\boldsymbol{m}_{\boldsymbol{p}}$ is the prior layered earth electrical conductivity model, $\boldsymbol{C}_{\boldsymbol{m}}$ is the model covariance matrix that determines the smoothness in the model structure, and α is the model smoothness factor that governs the influence of the smoothness and the prior model in the objective function.

Equation (4) describes the objective function to be minimised in the inversion algorithm that models electrical conductivity of the subsurface resulting from measurements of electromagnetic survey data in the region of interest. The first term is a comparison of the predicted data for a given model to the data measured by the system, weighted by the noise in the data. We call this term the model misfit. Because the difference between measured and predicted data is added together in a squared sense, the model misfit measure can be described as an L_2 norm. The second term, also L_2, is the model misfit. It is a comparison between the updated electrical conductivity model and the prior electrical conductivity model. The factor $(\boldsymbol{m} - \boldsymbol{m_p})$ is weighted by the inverse of the model covariance matrix ($\boldsymbol{C_m^{-1}}$), otherwise known as the precision matrix. The precision matrix imposes restrictions on the model parameters themselves and the relationship between adjacent and nearby model parameters. For example, the second term in Equation (4) penalises large differences between model parameters. It behaves, therefore, as a smoothing operator. The factor α modifies the importance of the model misfit term in the objective function. Our goal is to achieve a model that is smooth enough to satisfy the model misfit term, yet rough enough to satisfy the data misfit term.

The inversion of the survey data to electrical conductivity models is non-linear, ill-posed and often ill-conditioned. This means that the forward model prediction $\boldsymbol{f}(\boldsymbol{m})$ can vary greatly depending on input parameters and that there are infinitely many model parameter combinations that can satisfy the misfit function. We conduct the inversion solution, despite the ill-posedness of the problem and the poor conditioning of the matrices, using iterative methods. Beginning with a starting model of the electrical conductivity of the subsurface, we compute the sensitivity of the predicted data to the model parameters and the data and model misfits. Using the sensitivity matrix and the misfit values, we update the model parameters using a linear approximation to the perturbation of the objective function resulting from varying the model parameters. We stabilise the linear approximation by using the Levenberg-Marquardt (LM) method (Levenberg 1944; Marquardt 1963) to provide model updates. Updates to the LM parameter are based on the work of Zhao and Fan (2016).

2.3.8 Effect of Regularisation

Figure 2-17 shows smooth 1D layered earth inversion models for a wide range of model regularisation values of α on repeat line 1 from this survey. In these inversions, an isotropic exponential model with 25 m correlation length was chosen for the model regularisation and only the weighting was changed. The prior resistivity was chosen to be a 10^4 Ωm half space. A depth of investigation line (DOI) (Christiansen and Auken 2012) for each inversion is shown in white. The figures show little variation in inverted conductivity models above the DOI line, as is more clearly illustrated in Figure 2-18. This indicates that the model regularisation has little effect in determining model structure where the models are informed by the data, which is precisely what is desired in an inversion.

In addition to Figure 2-17 and Figure 2-18, it is useful to visualise the trade-off between data misfit and model misfit for different values of α. One convenient way to demonstrate this is the use of an L-curve (Hansen 1998), as shown in Figure 2-19. This figure shows how data misfit reduces – and model misfit increases – with decreasing regularisation. We generally take the point of maximum curvature in the L-curve for the optimum choice of model regularisation, but this can be an arbitrary choice. In this report, we have chosen an α value of 0.316 for all inversions as it yields models that closely resemble the results from the RJMCMC estimations. A comparison of the inverted model using α = 0.316 and the RJMCMC model for the repeat line is shown in Figure 2-20. We can see that much of the fine structure of the RJMCMC inversion is faithfully recovered in the inverted model at a fraction of the total computational cost.

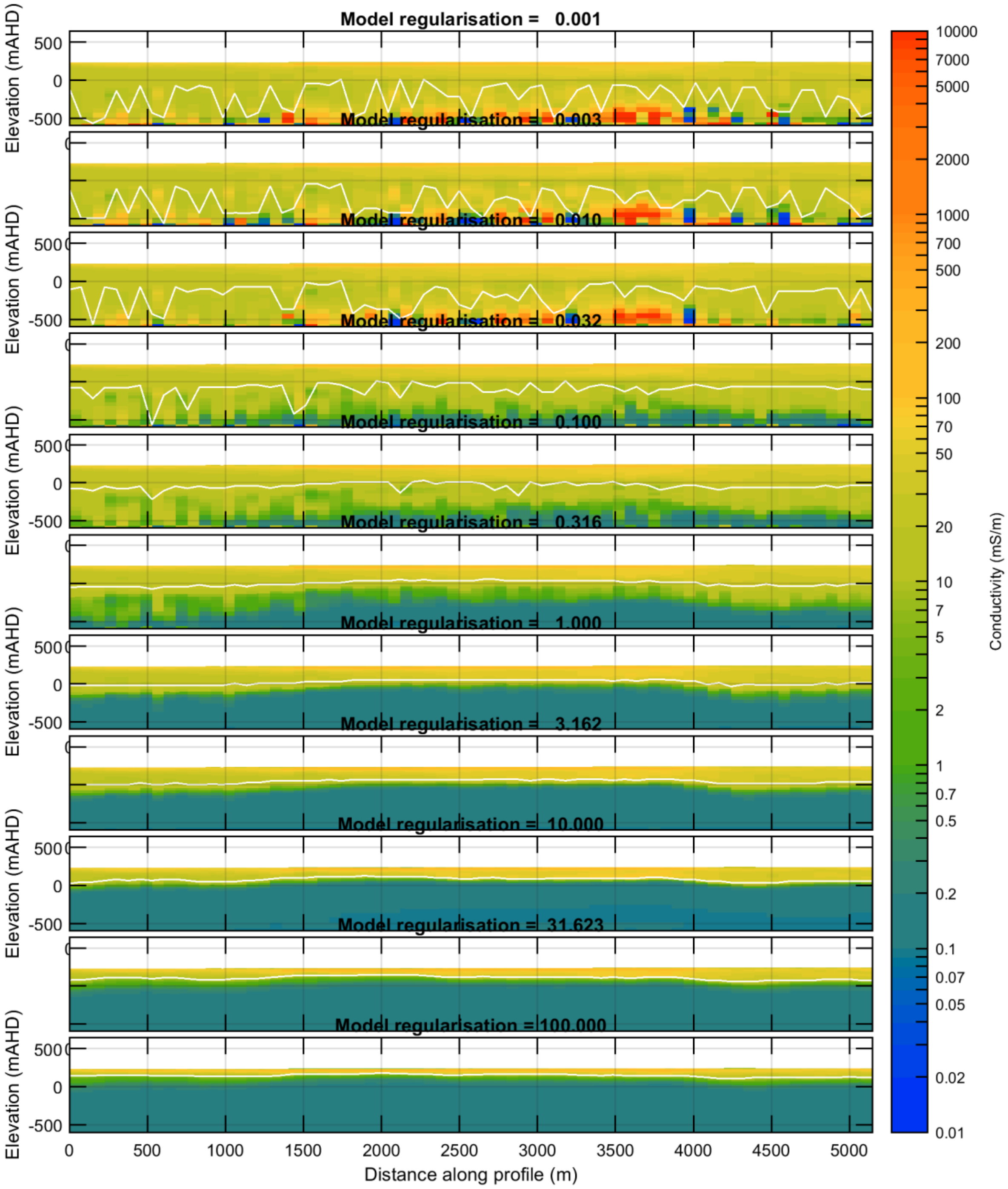

Figure 2-17 - Inversions showing the effect of model regularisation for a wide range of regularisation weighting values (α). All inversion runs were initialised with the same starting model. The model regularisation structure for each is the same. A depth of investigation (DOI) line is shown in white. There is very little variation in models above the DOI when regularisation parameter α is below 1.

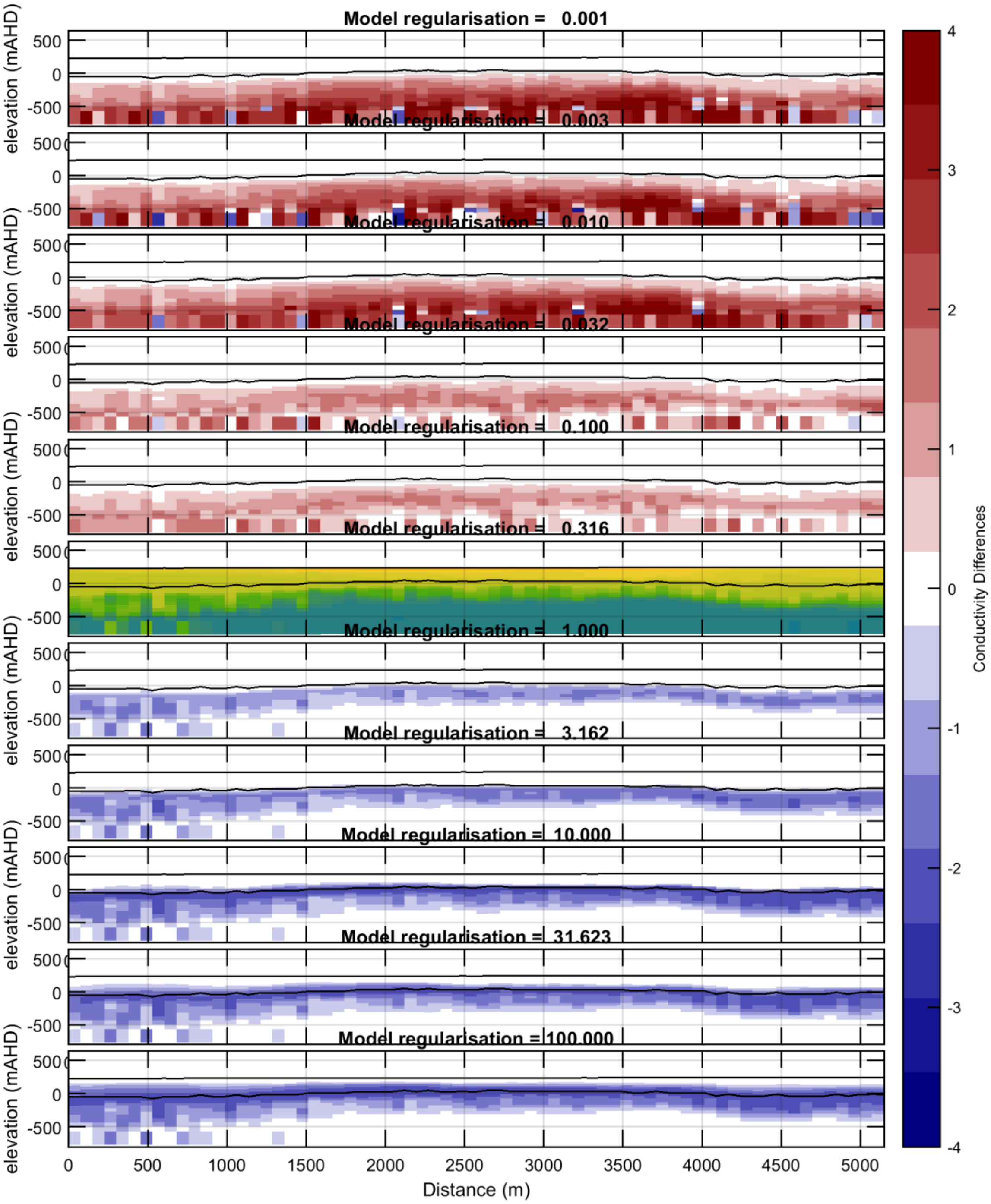

Figure 2-18 - Plots of the differences in the inversion models from the comparison model at regularisation value 0.215. differences are in the log base 10 of conductivity. We can see that each model agrees with the comparison model, within a factor of 10, above the depth of investigation.

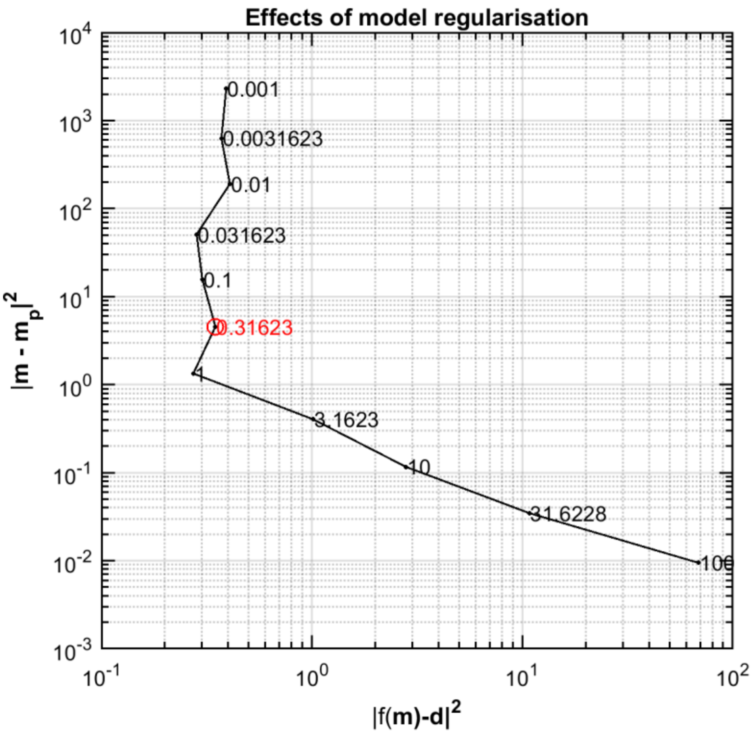

Figure 2-19 - Plot of data misfit versus model misfit (L-Curve) for the inversion products shown in Figure 2-18 with varying (α). The parameter of 0.316, which is near the maximum curvature of the L-Curve is chosen for all inversions.

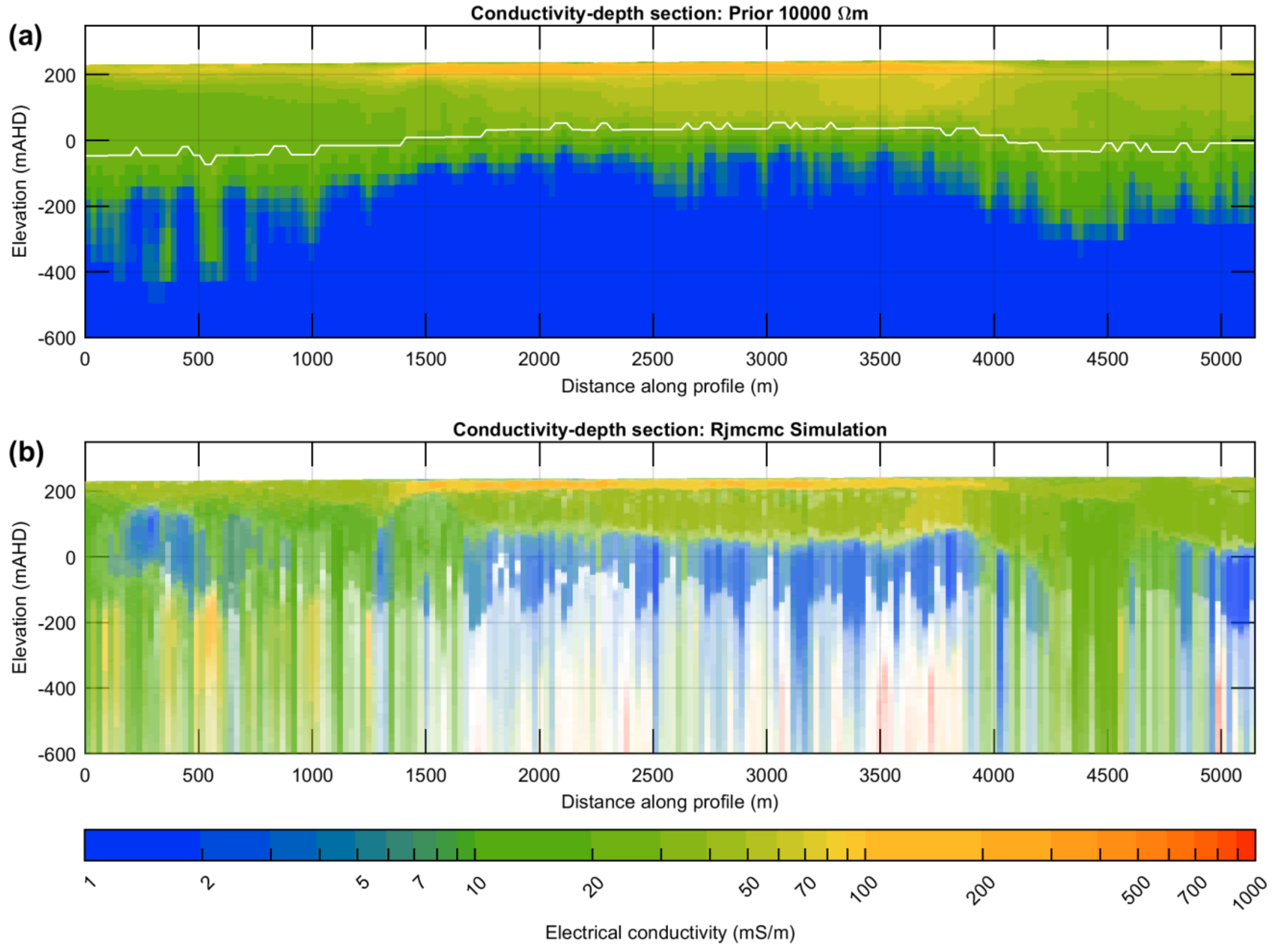

Figure 2-20 Comparison of (a) deterministic inversion with a regularisation parameter of 0.316 to (b) the RJMCMC simulation models for the repeat line considered.

2.3.9 Effects of prior on inversion

Finally, we examine the effect that the prior resistivity model has on the inverted data. The objective function in Equation (4) shows that the model misfit calculation in the second term of the right-hand side encourages the inversion to honour the prior resistivity vector $\boldsymbol{m_p}$. The degree to which the inverted model must reflect the prior resistivity is governed by the model regularisation matrix $\boldsymbol{C_m^{-1}}$ and the regularisation parameter α. Figure 2-21 a shows the inversion results when $\boldsymbol{m_p}$ is set to a homogeneous half space with resistivity equal to 10000 Ωm (0.1 mS/m), and Figure 2-21b shows the inversion model when the prior resistivity is set to a relatively conductive half space of 1 Ωm (1000 mS/m).

Comparison of Figure 2-21a and b show that there is remarkable similarity in the inverted models in the near surface where the data is very informative to the model structure. The differences between the inversion models begin to appear noticeable below the depth of investigation lines in the figures. However, examination of the total misfit for the inversions, shown in Figure 2-21d, reveals very little difference. The obvious implication of these results is that it is only where the inverted models are similar that they have any effect on the measured data. We can immediately extend this analysis by computing a mean model of the two inversion models. Figure 2-21c displays a conductivity depth section that is created from the geometric mean of the models in a and b using the equation

$$\bar{\boldsymbol{m}} = \sqrt{\boldsymbol{m}_{\mathbf{10000}} \cdot \boldsymbol{m}_{\mathbf{1}}} = \exp((\log(\boldsymbol{m}_{\mathbf{10000}}) + \log(\boldsymbol{m}_{\mathbf{1}}))\,/\mathbf{2}) \tag{5}$$

where $\boldsymbol{m}_{\mathbf{10000}}$ is the model resulting from the inversion with the 10000 Ωm prior resistivity, $\boldsymbol{m}_{\mathbf{1}}$ is the model from the inversion with the 1 Ωm prior resistivity, and $\bar{\boldsymbol{m}}$ is the mean model. We can calculate the total misfit for model $\bar{\boldsymbol{m}}$ by adjusting Equation (4) so that the new prior resistivity has a value of 100 Ωm. The misfit for this model, and the $\boldsymbol{m}_{\mathbf{10000}}$ and $\boldsymbol{m}_{\mathbf{1}}$ models are shown in Figure 2-21d.

In addition to calculating the geometric mean of the two inversions, we can also calculate the difference factor to measure the similarity of the $\boldsymbol{m}_{\mathbf{10000}}$ and the $\boldsymbol{m}_{\mathbf{1}}$models. By keeping the inversion products in logarithmic space, the differences between the $\boldsymbol{m}_{\mathbf{10000}}$ and the $\boldsymbol{m}_{\mathbf{1}}$ are equivalent to ratios between resistivity in the linear space. We see, then, that if the resistivity at a given location from the $\boldsymbol{m}_{\mathbf{10000}}$ model is 200 Ωm, and the resistivity at that location in the $\boldsymbol{m}_{\mathbf{1}}$ model is 50 Ωm, then the resistivity in the $\bar{\boldsymbol{m}}$ model is 100 Ωm. The difference ratio between the $\boldsymbol{m}_{\mathbf{10000}}$ and the $\boldsymbol{m}_{\mathbf{1}}$ models is 2. If the difference ratio at that location was 4, then the $\boldsymbol{m}_{\mathbf{10000}}$ value at that location could be 400 Ωm and the $\boldsymbol{m}_{\mathbf{1}}$ could be 25 Ωm. We now add transparency to the geometric mean inversion model based on the resistivity ratios from the $\boldsymbol{m}_{\mathbf{10000}}$ and $\boldsymbol{m}_{\mathbf{1}}$ models. Areas where the resistivity ratio is less than 2 have no transparency. Because the transparency scale indicates regions where the resistivity ratios are less than 2, and they are not continuous from the surface, we have decided to rename the transparency shading as ‘regions of investigation’ rather than ‘depth of investigation’, since they indicate volumes in the model that are insensitive to the prior model and, hence, can be regarded as being relatively well-determined by the data.

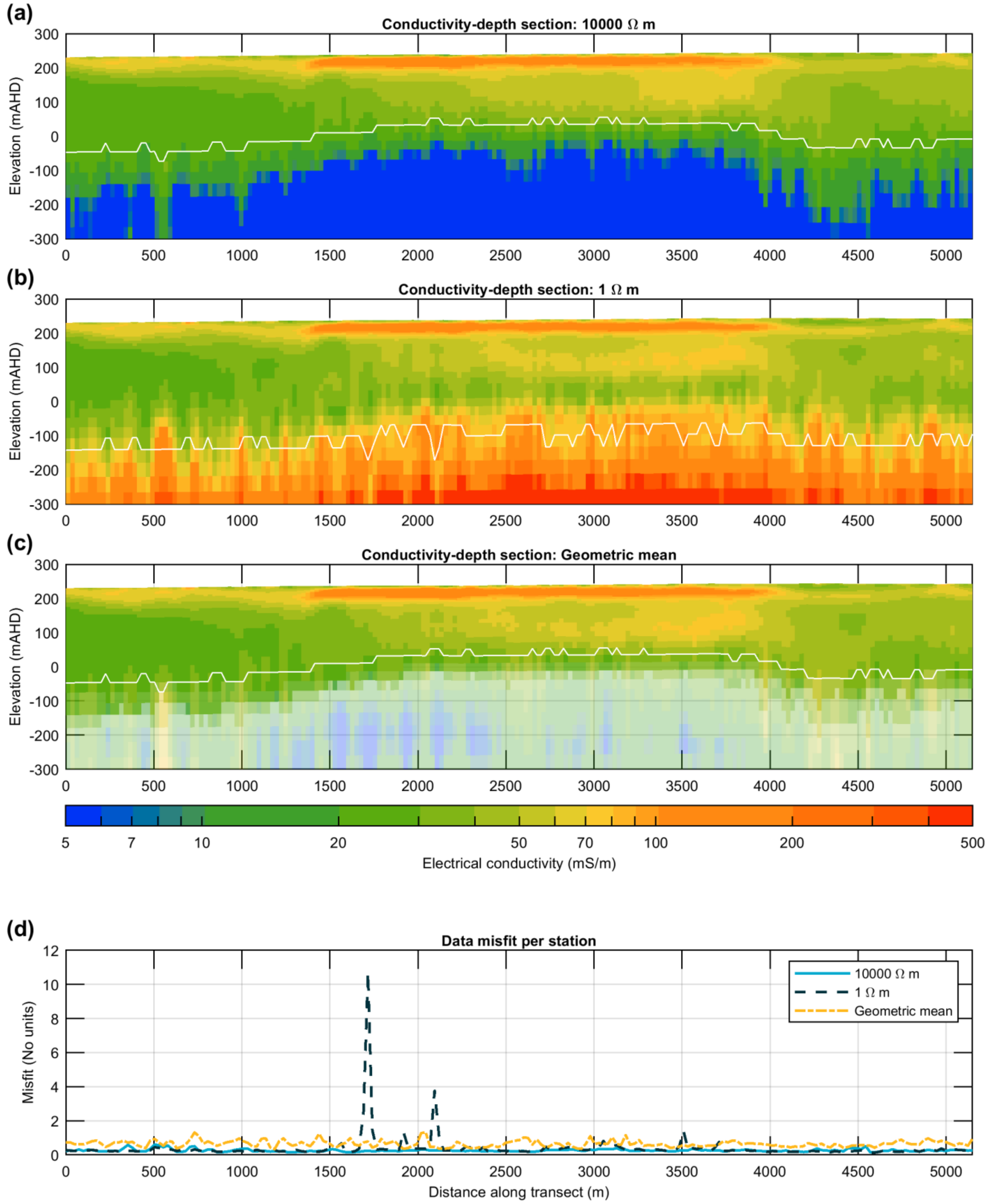

Figure 2-21 Comparisons of inversion results for repeat line 1 with different prior conductivities. (a) Inversion with a 10000 Ωm half-space prior model. (b) Inversion with a 1 Ωm prior model. (c) Compiled model taken from the geometric mean of the 10000 Ωm and 1 Ω models. (d) Data misfit for each of the 3 models in (a) – (c).

2.3.10 Combining regularisation and prior models

We are now in the position to show how the selection of an appropriate regularisation term and the use of prior conductivity values in the inversion. The regularisation parameter adjusts the smoothness of the inversion model, and the prior conductivity values in the inversion algorithm indicate which model parameters are important for the data misfit term in the objective function (Equation (4)). We will do this by reproducing Figure 2-20 but using the geometric model and the model shading resulting from the inversions with differing prior conductivities. The result is shown in Figure 2-22. We can see excellent agreement between the RJMCMC models and the deterministic inversions.

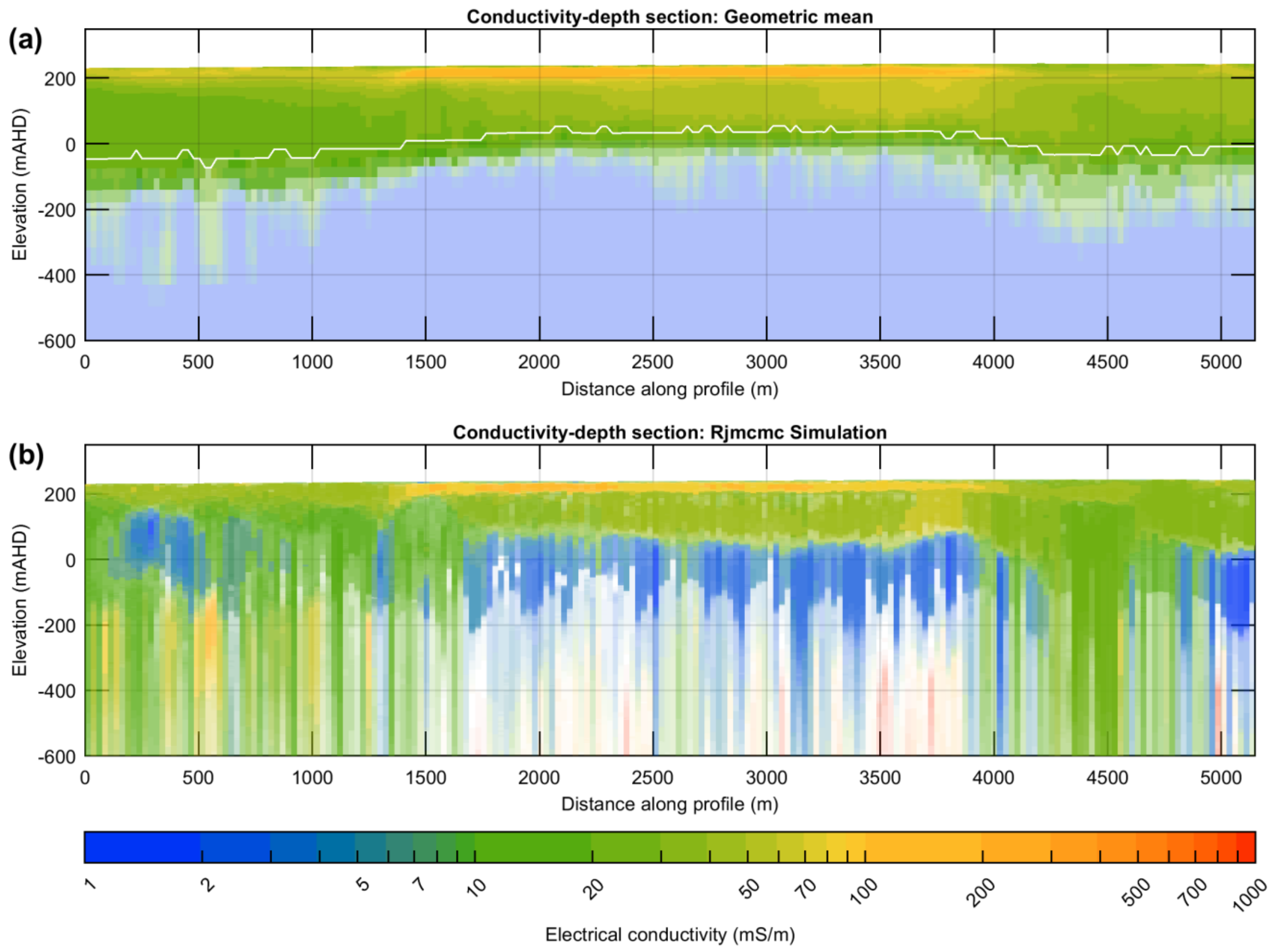

Figure 2-22 Comparison of (a) the combined deterministic inversion with a regularisation parameter of 0.316 and parameter shading based on 2 different prior models to (b) the RJMCMC simulation models for the repeat line.

2.4 Geochemical analysis of rocks

2.4.1 Sample collection from the NSW core library

Stratigraphic logs of exploration wells were reviewed and suitable targets for selection of core were identified. Core samples were collected from 14 exploration wells from the NSW WB Clarke Geoscience Centre - Londonderry core library (Figure 2-23a) for analysis of rock samples (strontium isotope, XRF, XRD, trace element analysis, K-Ar age dating of igneous and development of thin sections). Although most intervals did not show any visual signs of alteration, some intrusive rock samples exhibit a high degree of fracturing and weathering. For example, on Figure 2-23 b, mineral precipitation is visible in fractures in an igneous rock core sample in exploration well DME Narrabri 38.

A visual inspection of the cores was carried out prior to sampling to ensure collection of the most representative intervals of igneous (Figure 2-24) and sedimentary rocks (e.g. Pilliga Sandstone, Purlawaugh Formation, Digby Formation (Figure 2-25) and Early and Late Permian coal seams). This inspection aimed to avoid collection of weathered samples as this could affect analytical results of K-Ar age dating. Samples of several cm size have been removed from the core to be then analysed for $^{87}Sr/^{86}Sr$ and mineral assemblages.

The locations of exploration wells from where core samples were collected are shown on Figure 2-26.

a) b)

Figure 2-23 – a) NSW WB Clark Geoscience Centre - Londonderry Drillcore Library and b) example of cores with intrusive rocks in the Narrabri region (exploration well DME Narrabri 38).

Figure 2-24 – Core of dolerite intrusion at Rosevale 1 exploration well in the NSW WB Clark Geoscience Centre - Londonderry Drillcore Library.

Figure 2-25 – Core of Digby Formation conglomerate at Tintsfield 1 exploration well in the NSW WB Clark Geoscience Centre - Londonderry Drillcore Library.

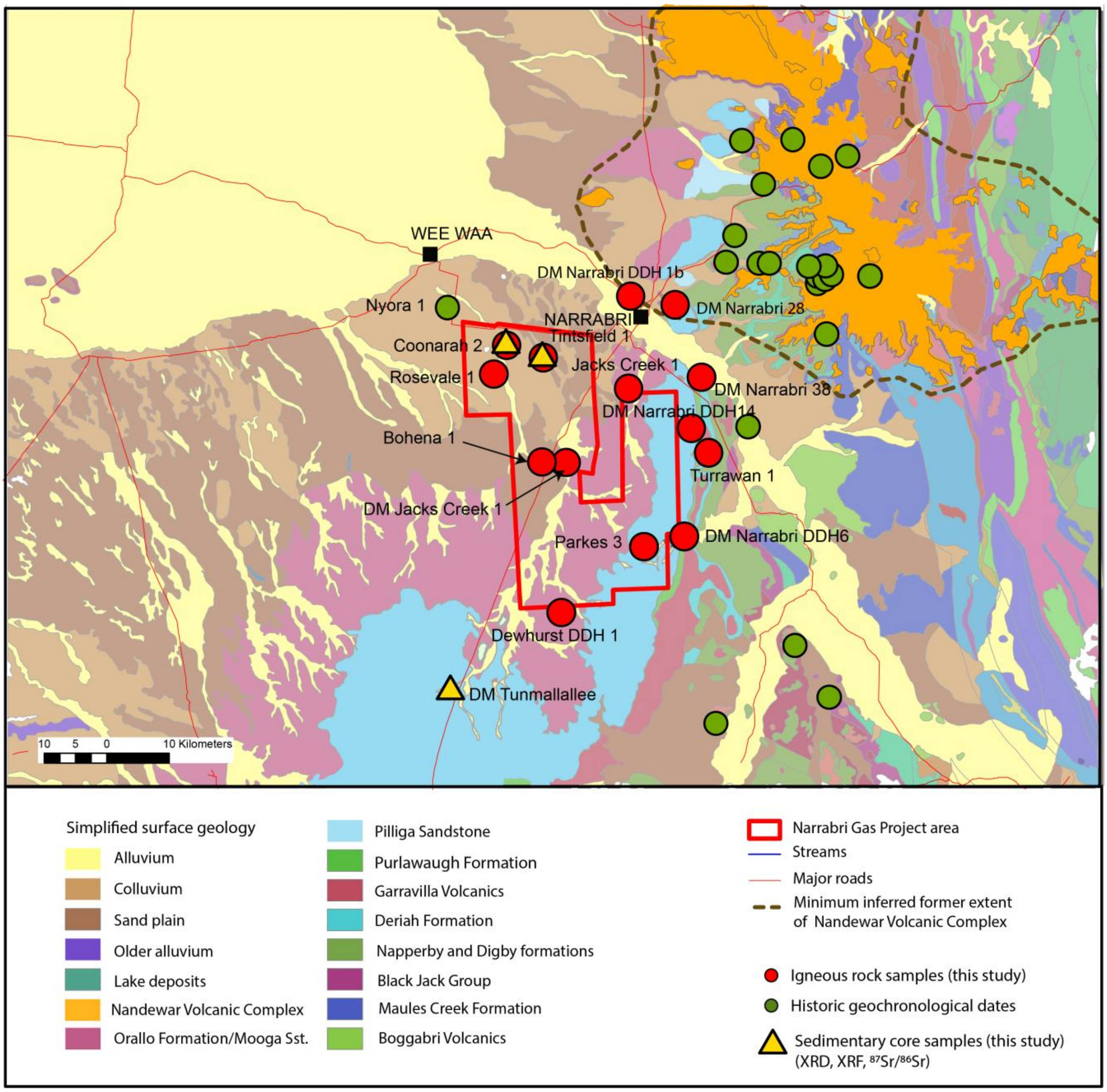

Figure 2-26 – Core sampling locations of igneous (intrusive) and sedimentary rocks in the Narrabri region overlain on simplified surface geology.

2.4.2 XRF and XRD

X-ray diffraction (XRD) is often utilized to identify crystalline and mineral phases in rock samples. It provides more accurate and quantitative mineralogical compositions than that from simple descriptions of rock samples. XRD analysis of igneous intrusions and representative core samples of major sedimentary bedrock formations in Surat Basin strata and the underlying Gunnedah Basin in the Narrabri Gas Project region was carried out at Queensland University of Technology Central Analytical Research Facility. In addition, selected samples of igneous intrusions were analysed at the Diffraction, Mineralogy and Geochemistry laboratory at CSIRO Mineral Resources in Adelaide.

Core samples were analysed for bulk mineralogy by X-ray powder diffraction (XRD) and elemental composition analysis by X-ray fluorescence spectroscopy (XRF).

The description of sample preparation and analysis below is from the Materials Characterisation Report provided by Henry Spratt from the QUT Central Analytical Research Facility.

Sample preparation

Sub-samples at the Queensland University of Technology Central Analytical Research Facility were accurately weighed and specimens prepared for X-ray diffraction analysis by the addition of a corundum (Al_2O_3) internal standard at 20 wt%. The specimens were micronised in a McCrone mill using zirconia beads and ethanol, then dried in an oven overnight at 40 °C. The resultant homogenous powders were back-pressed into sample holders.

A small portion of the crushed samples were dispersed in water. After sonication (5 min) and settling for 5 min, the fine fraction (nominally < 5 µm in suspension) was transferred via pipette to a low background plate and allowed to settle and dry (these samples have the label N in this report). This preparation is used to concentrate the fine (clay dominant) fraction and aids identification of the clays present. This means ratios of the clays and other phases present in this extract may vary from the bulk sample: the fine fraction result is qualitative. The air dried slides were further treated in an ethylene glycol atmosphere (60 °C) for several hours, then immediately re-examined. The ethylene glycol treated samples have the label G in this report.

Sample analysis

Step scanned X-ray diffraction patterns were collected for an hour per sample using a Bruker D8 Advance powder diffractometer and cobalt Kα radiation operating in Bragg-Brentano geometry using the usual conditions. The collected data was analysed using JADE (V2010, Materials Data Inc.), EVA (V5, Bruker) and X'Pert Highscore Plus (V4, PANalytical) with various reference databases (PDF4+, AMCSD, COD) for phase identification. Rietveld refinement was performed using TOPAS (V6, Bruker). The known addition of corundum facilitates reporting of absolute phase abundances for the modelled phases. The sum of the absolute abundances is subtracted from 100 wt% to obtain a residual (called non-diffracting/unidentified, also known as "amorphous"). The residual represents the unexplained portion of the pattern: it may be non-diffracting content but will also contain unidentified phases and the error from poorly modelled phases. It is the least accurate measure as its error is the sum of the errors of the modelled phases. The estimated uncertainties in the reported phase abundances are 20 wt% relative or better for every modelled phase. Due to propagation of errors the uncertainty in the amorphous (non-diffracting/unidentified) content is higher at approximately 30 wt% relative. The detection limit using this method is approximately 0.5 – 1 wt% depending on the phase in question and sample matrix. In general, clay phases (e.g. kaolinite) have higher detection limits and more uncertainty than non-clay phases (e.g. quartz).

Powder X-ray diffraction is a bulk phase analysis, it is not bulk chemical analysis or trace phase analysis. Phase abundances may be mis-estimated if an incorrect chemical formula is assigned to a phase. Therefore, the closest matches in the reference phase identification databases were used in the Rietveld refinement model, but other members of the identified mineral groups may be present.

2.4.3 Petrographic thin sections

Petrographic thin sections of selected igneous rock samples for microscopic examination were prepared at Queensland University of Technology Central Analytical Research Facility and at Thin Section Australia.

A focus was on igneous rock samples where the XRD analysis suggested that high amounts of minerals such as smectite and chlorite or some calcite.

Petrographic descriptions from selected thin sections discussed in Section 3.3.3 were provided by Mathew Beddard from SLR Consulting. By examining thin sections under a petrographic microscope, minerals can be identified based on their optical properties, allowing to determine for example if there are any alterations or pathways that could affect K-Ar ages (Section 2.4.5).

2.4.4 Strontium isotopes

Strontium isotopes are widely used to provide information about water-rocks interactions of groundwater. Comparison between rock and groundwater signatures (strontium isotope ratios - $^{87}Sr/^{86}Sr$) can provide evidence of preferential flow path and groundwater mixing (Raiber et al., 2009; Raiber et al., 2024). To analyse the strontium isotope ratios ($^{87}Sr/^{86}Sr$) in groundwaters, water samples were collected from springs or boreholes within a 60 mL Nalgene bottles and were analysed at the University of Melbourne using multi-collector inductively coupled plasma mass spectrometry (MC-ICP-MS). For detailed methodology please refer to Raiber et al. (2024).

To determine the strontium isotope ratios ($^{87}Sr/^{86}Sr$) in rocks, 41 samples were selected from visually unweathered and representative rocks of the major geological formations in the Narrabri region (Orallo Formation, Pilliga Sandstone, Purlawaugh Formation, Napperby Formation, Digby Formation, Black Jack Group (including Hoskissons Coal seam), Watermark Formation, Maules Creek Formation (including Bohena Coal Seam) and several igneous intrusions). These samples, originating from 11 drill cores and documented with precise location and depth information, were analysed at the University of Melbourne for whole-rock analysis (using hydrofluoric acid) and selected samples were analysed for partial digestion (using 1M acetic acid) following the procedure described by Raiber et al. (2024).

2.4.5 K-Ar age dating

Igneous intrusions such as dykes and sills have been identified as plausible hydrogeological connectivity pathways in previous hydrogeological investigations in the Narrabri region in NSW (Raiber et al., 2022a). Understanding the timing of when intrusive activity has occurred in the Narrabri region is critical to understanding potential connections between different Gunnedah Basin formations and the aquifers of the Surat Basin (especially the Pilliga Sandstone). As shown in hypothetical example on Figure 2-27 a, an intrusion that occurred for example 20 million years ago during the Cenozoic could theoretically vertically extend into the Pilliga Sandstone (which was deposited much earlier during the Mid-Jurassic period approximately 150 million years ago) and could form a potential hydrogeological connectivity pathway with coal seams. Conversely, an intrusion that occurred for example 180 million years ago (Figure 2-27 b) intruded into the host rock prior to the deposition of the Pilliga Sandstone and can therefore not form a connectivity pathway between coal seams and the Pilliga Sandstone.

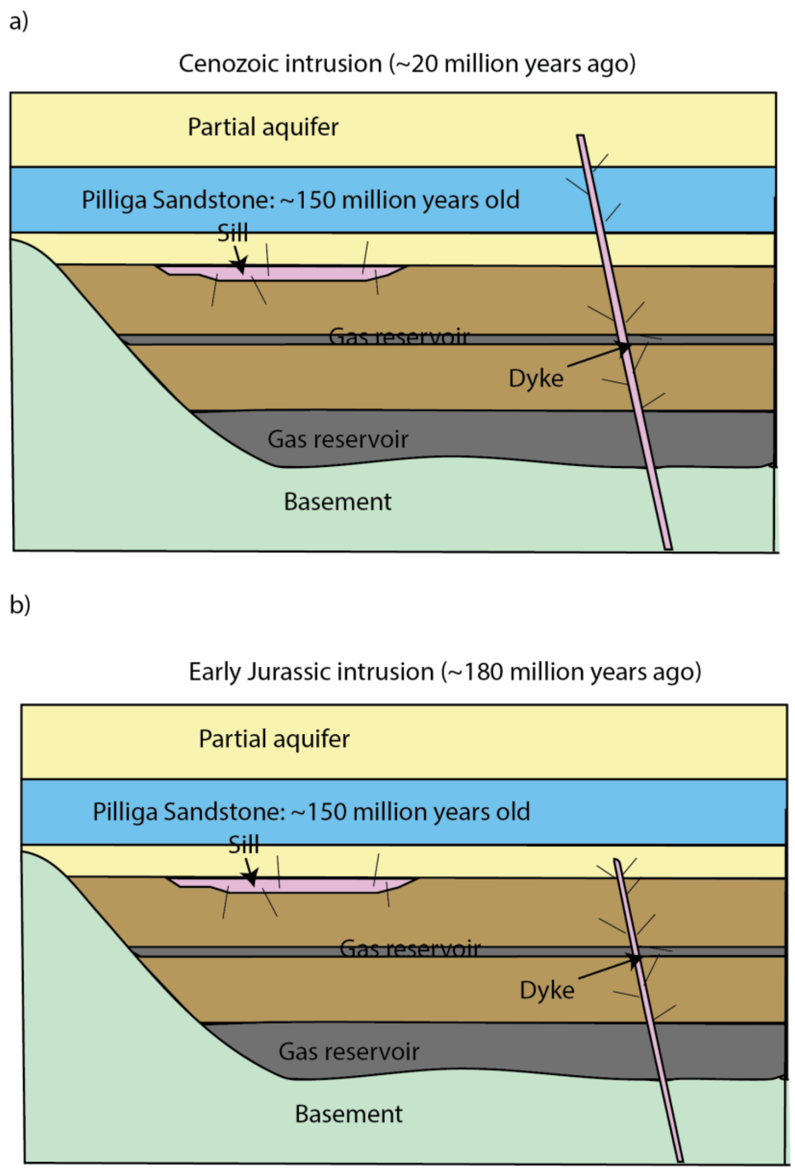

Figure 2-27 – Schematic example highlighting the timing of intrusive activities in the Narrabri region.

In a) a hypothetical Cenozoic intrusion erupted approximately ~20 million years ago could intersect the Pilliga Sandstone (deposited approximately 150 million years ago); in b) a hypothetical Early Jurassic (~180 million years ago) intrusion cannot intersects the Pilliga Sandstone, as the Pilliga Sandstone did not exist at the time of this intrusion.

Geochronological dating of intrusive rocks can help to refine the understanding of timing of intrusive activity and whether intrusions could form potential hydrogeological connectivity pathways between coal seams and Pilliga Sandstone. For this assessment, we have compiled existing geochronology dates of igneous rocks in the wider Narrabri region, and have conducted additional geochronological analyses of intrusive rocks sourced from the NSW core library using the K/Ar dating technique.

2.3.2.2 Compilation of existing data

Historic radiometric age dating results of igneous rocks in the Narrabri region were obtained from NSW MinView (Department of Primary Industries and Regional Development, 2023). A single geochronological result was also obtained from an igneous intrusion in a well completion report at Nyora (Morrison and Harris, 1988; Totterdell et al., 2009). The locations of sites with available historical rock geochronological data in the Narrabri region are shown on Figure 2-26. This map highlights that no rock age dating was conducted within the Narrabri Gas Project area prior to this study.

2.3.2.2 Analysis of new core samples

Seventeen core samples of intrusive rocks from 12 different exploration wells (shown in green in Figure 2-26) were analyzed using the K-Ar dating technique at the CSIRO geochronology laboratory in Perth.

Many intrusive rock samples within the extended Narrabri Gas Project area were described in stratigraphic logs as dolerites and teschenite sills. Dolerites are intrusive rocks that form from molten magma that cools and solidifies beneath the Earth's surface. They are primarily composed of minerals such as plagioclase feldspar, pyroxene, olivine, magnetite and apatite. Teschenites are coarse- to fine-grained, dark-coloured, intrusive igneous that occur in sills and are primarily composed of plagioclase feldspar, analcime, and titaniferous augite.

K-Ar dating is a radiometric technique, which can be used to determine the age of intrusive rocks by measuring the ratio of potassium-40 (^{40}K) to argon-40 (^{40}Ar) isotopes, which are products of the radioactive decay of potassium (McDougall, 1990). The "date" measured by the K-Ar technique represents the time since radiogenic argon produced by decay of ^{40}K became trapped in the mineral or rock. This may be the "age" of the rock or it can represent the most recent cooling event after emplacement of intrusive rocks or after eruption as lava flows (McDougall, 1990), and in some samples may represent an integrated cooling age for a range of sub-grains (Kelley, 2002).

Multiple assumptions must be met for the K-Ar dating to yield a representative age for a geological event. This includes that the sample must have remained a closed system since the event being dated (e.g. an igneous intrusion or a volcanic eruption). Thus, there should have been no loss or gain of ^{40}K or radioactive ^{40}Ar, other than by radioactive decay of ^{40}K (New Mexico Geochronology Research Laboratory, 2025).

Weathering of rocks can significantly affect the accuracy of K-Ar dating of igneous rocks (Dickin, 2005). For example, weathering can lead to the loss of argon-40 from the rock, as chemical alteration and physical breakdown can open the rock's structure, allowing argon to escape. This loss of argon can lead to an underestimation of the rock's age. It can also lead to potassium addition, through the introduction of potassium through the infiltration of groundwater or other fluids. The formation of clay minerals from feldspar during weathering can also affect the rock's argon retention properties (Wilson, 2004).

Weathering commonly refers to alteration processes resulting from environmental conditions when rocks are exposed at the surface. However, most rock samples in this study were igneous (mostly intrusive) rocks collected from significant depths, and they were never exposed at the surface. Although some of the wider core intervals of igneous rocks samples analysed in this study showed some physical signs of alterations (e.g. cracks and fractures in Figure 2-23), samples were mostly chosen from rock intervals with an unaltered macroscopic appearance (with selected igneous rock samples shown in Figure 2-28).

Figure 2-28 – Selected examples of igneous rock samples collected for K-Ar geochronological analysis.

2.5 Groundwater hydrochemistry and tracer analyses

2.5.1 Compilation of existing groundwater chemistry data

Groundwater chemistry data from the NSW groundwater database (WaterNSW, 2017) were compiled by Raiber and Suckow (2018) and included in the current hydrochemical assessment. Data from Cresswell (2014) compiled for Santos were also used (this dataset included data by Radke et al., 2000), and combined with datasets from Iverach et al. (2017, 2020a), Suckow et al. (2019), NSW DPIE (2021), Raiber et al. (2022a) and analytical results from the current study. Data from NSW DPIE (2021) include major ion groundwater chemistry data for multiple new DPIE groundwater monitoring bores (Figure 2-29), including hydrochemistry and methane concentrations from the Pilliga Sandstone, Purlawaugh Formation and Digby Formation at the Plumb Road nested bore site. Samples from most of these bores were collected during the current study for a wider range of parameters, but some groundwater bores from the NSW coal basin groundwater monitoring network (NSW DPIE, 2019) could not be sampled due to technical issues with installed low-flow pumps.

In addition to the historic water chemistry records, additional sample collection activities were conducted between 2023 and 2024 (with previous and new sampling sites shown in Figure 2-29).

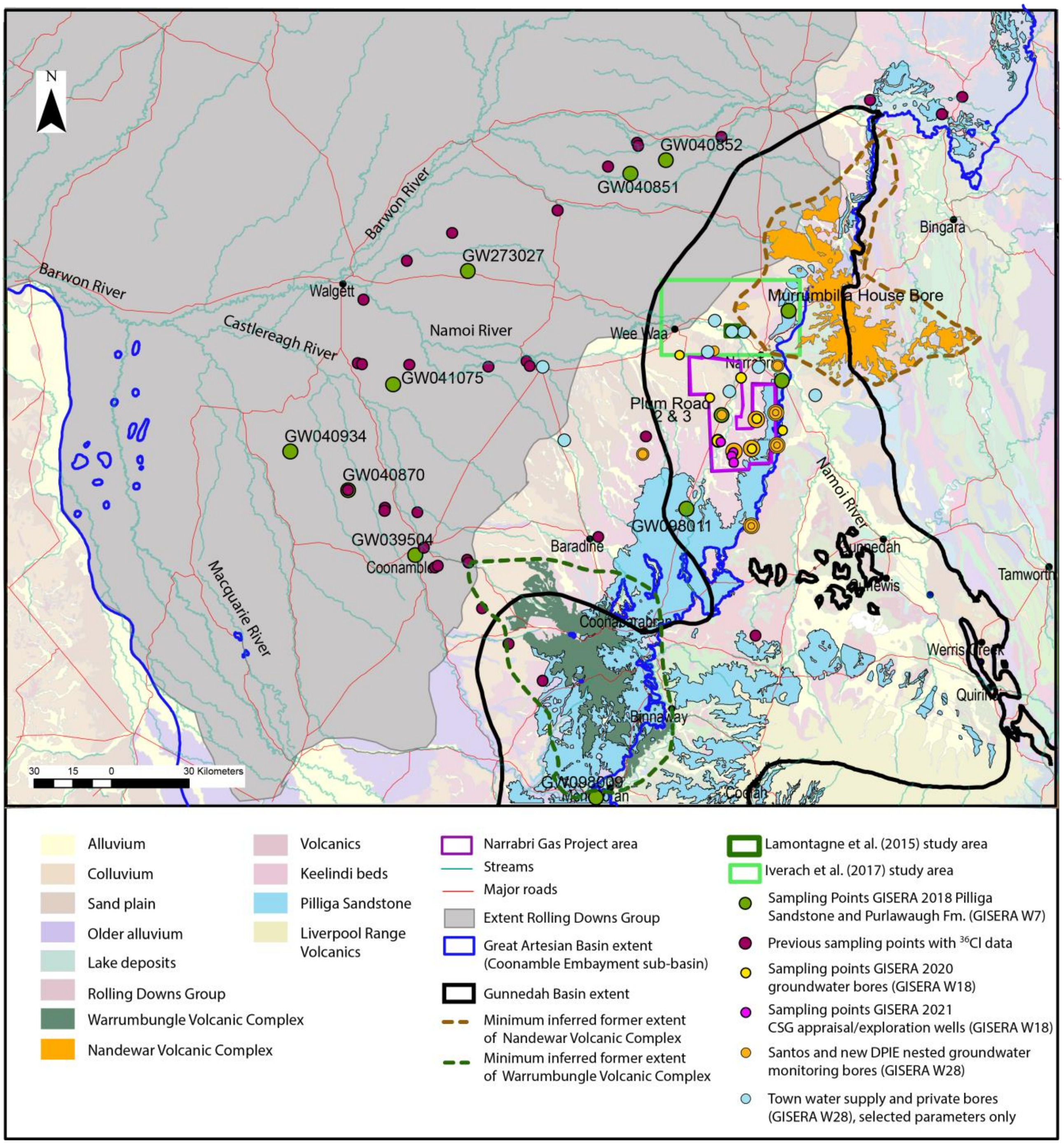

Figure 2-29 – Groundwater sampling locations of the current study and previous groundwater investigations in the Narrabri region (updated from Raiber et al. (2022a) overlain on simplified surface geology.

Sampled groundwater bores include NSW DPIE groundwater monitoring bores, NSW coal basin monitoring bores (NSW DPIE, 2019), CSG appraisal and exploration wells, Santos groundwater monitoring bores and groundwater bores.

2.5.2 Hydrochemical and tracer sample collection and analysis

2.3.2.1 Field parameters

Chemical parameters (including EC, redox potential, dissolved oxygen, pH and temperature) were monitored and recorded during purging and sampling under gently flowing conditions, using a YSI 556 multi-parameter probe (YSI Environmental). The presence of H_2S was noted qualitatively when detected (i.e. by odour) during sampling as was the amount of gas bubbles, and for health, safety and environment purposes, a QRAE II LEL 4 gas monitor for methane (Honeywell RAE Systems) was also used.

2.3.2.2 Groundwater chemistry and environmental tracer sampling and analysis

Groundwater samples were collected and analysed in this project from 11 NSW DPIE and three Santos groundwater monitoring bores for a comprehensive suite of hydrochemical and environmental tracer parameters including major and minor ions, dissolved methane concentrations and isotopes, hydrocarbon compounds, tritium (^{3}H), stable isotopes of the water molecule ($\delta^{18}O/\delta^{2}H$), $\delta^{13}C$-DIC, $^{87}Sr/^{86}Sr$, ^{14}C-DIC, ^{36}Cl and all stable noble gas concentrations (He, Ne, Ar, Kr and Xe) and isotopes. Samples were also collected and analysed from eight private and town water supply bores for a smaller set of hydrochemical and environmental tracer parameters.

Sampling for all tracers was conducted by initially establishing a gas-tight connection to existing headworks and discharge hoses (on sub-artesian bores).

Figure 2-30 – Exsolution of gas during sampling of groundwater bore Plumb Road 2 (GW971623-2) (Suckow et al., 2019).

Groundwater samples were collected for laboratory analysis of general chemistry (pH, EC and alkalinity) as well as major and minor ions. Samples for major and minor ions were filtered with a 0.45 µm Acrodisc syringe filter and placed in 60- and 150-mL polyethylene terephthalate (PET) plastic bottles. Samples for cation analysis were acidified with nitric acid (HNO_3). Samples for analysis of methane concentrations were collected in amber glass volatile organic compound vials and preserved with sulfuric acid. These samples were analysed at the ALS Laboratory. For $\delta^{2}H$ and $\delta^{18}O$, duplicate samples were collected in 28 mL gas-tight glass bottles (McCartney bottle) to prevent evaporation and analysed at the University of Queensland. Strontium isotope samples were collected in 60 mL Nalgene bottles. Samples for isotopes of CH_4 ($\delta^{2}H$-CH_4 and $\delta^{13}C$-CH_4) were filtered, acidified with HCl and collected in 12 mL glass vials, and analysed at the University of California (Davis Campus). Samples from unacidified vials were also analysed for the isotopes of

CO_2 at the University of California. Samples for concentrations and isotopes of CH_4 (δ^2H-CH_4 and $\delta^{13}C$-CH_4) were also collected in IsoFlask™ and analysed at Isotech laboratories (Stratum Reservoir) in Illinois, United States of America. The advantage of collecting samples for concentrations and isotopes of CH_4 (δ^2H-CH_4 and $\delta^{13}C$-CH_4) in isoflasks is that there is an airtight connection between the sampling hose and the isoflask, reducing the degree of exsolution (Figure 2-30) and thus loss of CH_4 during sampling.

Duplicate or triplicate samples for dissolved stable noble gases were collected from 12 bores in copper tubes with custom-designed pinch-off clamps (Weiss, 1968) during the current study. This involved creating a gas-tight connection between the copper tube and the discharge outlet on the bore, gently flushing the tube, and applying a back pressure using a flow regulator before clamping the copper tube at each end without trapping any gas bubbles. For some bores with higher gas concentrations, degassing of sampled water was not always avoidable. In these cases, a fractionation of noble gas values cannot be excluded, although care was taken during sampling to ensure that gas bubbles were not enclosed within the copper tubes. This was achieved by turning the copper tube upside down after closing the first clamp and letting the gas bubbles escape through the connecting tubing.

Noble gas concentrations (He, Ne, Ar, Kr and Xe) were determined at the CSIRO Environmental Tracer Laboratory, Waite Campus, Adelaide. Measurements involved the following steps: (1) separating all dissolved gases from water using an off-line high vacuum extraction system; (2) separating all reactive gases from noble gases by several getter systems; (3) separating the noble gases from each other using cryo techniques down to 10 K; and (4) measuring gas amounts and their isotopic composition using a spinning rotor gauge, quadrupole mass spectrometers and a high-resolution HelixMC Plus (Thermo) noble gas mass spectrometer (Suckow et al., 2019; Frery et al., 2022; Raiber et al., 2022a). Post-processing of all noble gas measurements was conducted using the LabData laboratory information management and database system (Suckow and Dumke, 2001). To ensure reproducibility of the results, duplicate, and in some cases triplicate samples were collected and analysed.

Samples for tritium (^3H), ^{14}C and ^{36}Cl were collected in 1 L Nalgene plastic bottles filled to the top under gently flowing conditions to avoid excessive air contact and capped without a head space to avoid contact with the atmosphere. Samples for tritium were analysed at Australian Nuclear Science and Technology Organisation (ANSTO) by electrolytic enrichment and subsequent liquid scintillation counting. Samples for ^{14}C and ^{36}Cl were analysed at the Australian National University and at ANSTO and at the Australian National University (ANU) (for ^{14}C and ^{36}Cl) using AMS (e.g. Fifield et al., 1987; Fink et al., 2004; Wilcken et al., 2017).

2.5.3 Groundwater age estimation from environmental tracer data

Each environmental tracer has different properties and originates from different sources. Some tracers decay over time; for example, ^3H has a half-life of ~12.4 years, whereas ^{14}C has a half-life of 5700 years and ^{36}Cl of ~301,000 years. Other tracers (e.g. noble gases such as ^4He and ^{40}Ar) accumulate in groundwater over time due to the decay of uranium, thorium and potassium contained in minerals within the aquifer. In studies elsewhere, noble gases have been identified as a very useful tracer to examine the diffusive and advective pathways in sedimentary basins due to their non-reactive nature (they are for example not affected by microbial activity or chemical reactions such as sulfate reduction) and well-characterised isotopic compositions (Darrah et al., 2014; Darrah et al., 2015; Suckow et al., 2019; Raiber et al., 2022a, b). Since it is beyond the scope of the present report to give a detailed introduction into the methodologies of environmental tracers, we refer to Raiber et al. (2022a, b) and Appendix C in Raiber et al. (2022a).

Where environmental tracers are used to identify hydrogeological connections between deep coal seams and shallower aquifers, samples are ideally collected along transects that originate at shallow bores (<100 m deep) located within or near the outcrop beds of major aquifers such as the Pilliga Sandstone and extended toward the deeper part of the basin (Figure 2-31). Where upwards discharge from deeper into shallower aquifers occurs (e.g. along faults), this may result in older than expected ages along different flow path intervals.

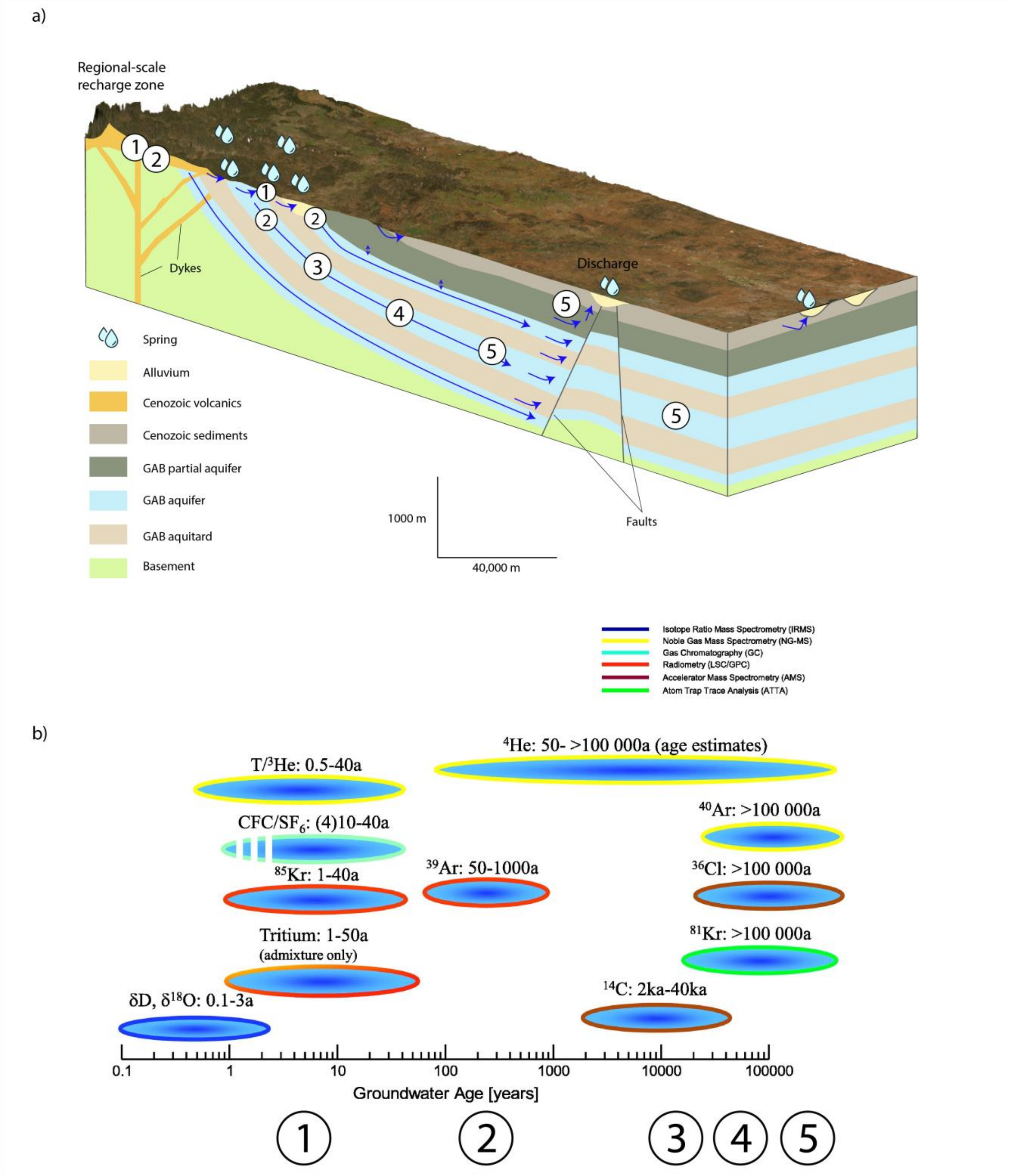

Figure 2-31 – a) Conceptual model of GAB aquifers and aquitards and spatial relationships with volcanic and alluvial aquifers and geological structures (modified from Raiber et al., 2022b) and b) examples of approximate age scales and tracer concentrations (Suckow, 2014) expected at different flow path intervals in a).

Short flow paths represent time scales from years to decades. Very long flow paths represent time scales from millennia to several hundred thousand or >1 million years. The length and density of flow lines is conceptual only, and does not represent relative flow velocities or volumetric flow rates. Flow path intervals 1a and 1b do not refer to the Cenozoic volcanics versus the outcrop of the GAB aquifers, and instead could both be present at both locations.

The initial conceptual model (Figure 2-31) provides some a priori information to understand which groundwater tracers are likely to be present in measurable concentrations at different parts of the groundwater flow paths (Suckow, 2014; Raiber et al., 2022b). In the same groundwater sample in shallow and unconfined aquifer systems, it is possible that young and old groundwater components are present simultaneously. Within the deeper parts of confined aquifer systems in sedimentary basins, presence of young groundwater components is less likely. To identify young and old groundwater components, it is necessary to analyse multiple groundwater age tracers with different age ranges (Figure 2-31 b) and consider the results of the different tracers sequentially or with multi-tracer models to determine mean residence time or an apparent groundwater age.

An apparent age of water can for example be determined using radioactive isotopes including ^{3}H, ^{14}C, ^{36}Cl and radioactive noble gas isotopes ^{85}Kr and ^{81}Kr. It is called an 'apparent age' as the tracer ages may not always directly correspond with actual water ages (Turnadge and Smerdon, 2014). For example, where groundwater interacts with stagnant zones (e.g. aquitard such as claystones) along a groundwater flow path, diffusive processes may result in tracer ages that are older than the actual water age (Turnadge and Smerdon, 2014). Likewise, the addition of dead carbon or dead chlorine leads to calculated groundwater radiocarbon or ^{36}Cl ages that are significantly older than the actual age. Incorporation of dead carbon or chlorine therefore requires careful correction.

When estimating an apparent groundwater age, it is useful to first determine whether there is a young groundwater component present. This can be achieved through the analysis of tracers such as ^{3}H or ^{85}Kr. If values of ^{3}H are significantly above the reported limit of quantification, then it is likely that a component of the groundwater is very young and was recharged within the last decades (<60 years). However, a value slightly above the limit of quantification in a groundwater sample collected from a very deep bore in a sedimentary basin may not necessarily mean that there is a young groundwater component present but can also result from contamination during sampling, transport and storage. This is especially the case in gas-rich and highly pressurised groundwater samples collected from deep bores in sedimentary basins where leakage of bottles due to the high pressure has been observed in other studies throughout the Great Artesian Basin. In the present study, to minimise compromising the sealing capacity of sampling bottles due to high gas contents and high pressure during transport and storage, we have used high-quality 1 L Nalgene bottles.

If the assessment of young tracer values indicates that there is no young groundwater component present, then an apparent groundwater age can be estimated from radiocarbon (^{14}C) by measuring the concentration of ^{14}C in dissolved inorganic carbon (DIC). Since ^{14}C decays with a known half-life of 5,730 years, the decrease in its activity compared to atmospheric levels provides an estimate of the time since the water sample was last in contact with atmosphere-derived CO2 in the soil and unsaturated zone. The measurements of ^{14}C can be used to determine an apparent groundwater age by applying the following decay equation:

$$t_{14_C} = \ln(14_A/14_{A0})\,/ -1.21 * \,10^{-4} = \,8267\ln\,(14_{A0}/14_A) \quad in\,(yr)$$

where ^{14}A is the activity of ^{14}C in Total Inorganic Carbon in the downgradient sample (% modern carbon – pMC) and ^{14}A0 is the activity in upstream sample (here considered as A0 = 100pMC).

However, corrections are needed to account for geochemical processes such as oxidation of organic matter and carbonate dissolution that can artificially alter the initial ^{14}C concentration (Cartwright et al., 2020). This can be achieved by using correction models (i.e., Vogel, 1967; Tamers, 1975; Pearson, 1965; Fontes and Garnier, 1979; IAEA, 1981; Evans, 1969; Eichinger, 1983) for more accurate age determinations. Based on the knowledge of the system, limitations and the uncertainty of each correction model, some assumptions have been made to provide corrected ages which then have been averaged and compared to ^{36}Cl ages.

The measurements of ^{36}Cl (with a half-life of approximately 301,000 years) can be used to determine an apparent ^{36}Cl groundwater age for very old groundwater (hundreds of thousands of years to > 1 million years) by applying the following decay equation (following the methodology described in Iverach et al. 2017):

$$\boldsymbol{t = -\frac{1}{\lambda}.\, ln(\frac{R_{sample} - R_{secular}}{R_{recharge} - R_{secular}})}$$

Where R_{sample} is the measured $^{36}Cl/Cl$ ratio in the water sample, $R_{recharge}$ is the initial ratio at the time of recharge. Three different assumptions for the $^{36}Cl/Cl$ of the recharge water were considered; the most representative was assumed to be 100×10^{-15} based on the youngest groundwaters in this area where we have analysed both ^{36}Cl and ^{81}Kr. As the input function of ^{81}Kr is more stable than that of ^{36}Cl, ^{81}Kr can be used to determine the likely initial ^{36}Cl ratio of recharge waters (discussed further in Section 3.8.7). $R_{secular}$ is the secular equilibrium ratio taken from Bentley et al. (1986). The decay constant λ is derived from the half-life of ^{36}Cl (approximately $\lambda^{36}Cl = \ln 2/T_{1/2} = 2.303 \cdot 10^{-6}\ yr^{-1}$). To characterise the secular equilibrium locally, further ^{36}Cl analysis of rock may be required.

Table 1 Secular equilibrium ^{36}Cl values used for calculation (Bentley et al., 1986).

Rock	Secular equilibrium ($^{36}Cl/Cl \times 10^{-15}$)	Assumptions
Granite	30.1	
Sandstone	4.68	For Purlawaugh Formation, Digby Formation, Orallo Formation as sandstone , Pilliga Sandstone and Orallo Formation
Shale	12.5	Coal seams
Limestone	10.9	

In addition to ^{3}H, ^{14}C and ^{36}Cl, stable noble gases (e.g. ^{4}He and ^{40}Ar) and radioactive noble gas isotopes such as ^{85}Kr and ^{81}Kr can also be used to determine the age of groundwater (Figure 2-31). Unlike ^{14}C and ^{36}Cl, noble gases are inert tracers that are less likely to be influenced by chemical and biological reactions (Gemeiner et al., 2025). Furthermore, the input function (the value of the tracer at the time of groundwater recharge) is better constrained for ^{81}Kr than for ^{36}Cl (Purtschert et al., 2023) where the initial value can vary significantly spatially and over time. However, compared to ^{36}Cl, radioactive noble gas isotopes such as ^{81}Kr are more sensitive to air contamination during sampling, and sample collection requires a completely air-tight connection. Furthermore, although the input function of ^{81}Kr is well constrained, the understanding of possible underground production of ^{81}Kr is still evolving, as reported in studies in old geological settings elsewhere (Purtschert et al., 2021).

No samples were collected for radioactive noble gas isotope tracers during the present study as all groundwater bores sampled during this study have low flow pumps installed with very low flow rates, and large water volumes are required for the analysis of radioactive noble gas isotope tracers. However, the results from previous studies (Suckow et al., 2019) for groundwater monitoring bores at Plumb Road (GW971623-2 screened within the Purlawaugh Formation and GW971623-3 screened within the Pilliga Sandstone) were considered when determining a representative age for the direct simulation of groundwater age.

The results of apparent groundwater age estimations, determined through the integration of multiple tracers and multiple lines of evidence, and associated uncertainties, are discussed in sections 3.8.8 and 4.

2.6 Multivariate statistical analysis

Hierarchical cluster analysis (HCA) is a multivariate statistical technique commonly adopted in groundwater hydrochemical studies to identify patterns within a dataset to enhance the understanding of physical and chemical processes that underpin groundwater evolution (e.g. Stetzenbach et al., 1999; Güler et al., 2002; Menció and Mas-Pla, 2008; Daughney et al., 2010; Raiber et al., 2012). Many variables should ideally be used in an HCA to enable an accurate depiction of groundwater chemistry and the processes that control it. In this study, ten variables were selected, namely, pH, Ca, Mg, Na, K, HCO_3, Cl, F, SO_4 and EC. The reason for selecting these parameters was that they are measured at most sites. Values below detection limit were replaced with the detection limit, as previously described and explained in other studies elsewhere (e.g. Farnham et al., 2002; Raiber et al., 2012).

Except for pH, all variables were log-transformed to ensure that they conform to a normal distribution before the multivariate statistical analysis was conducted. The HCA presented in this work was carried out using the StatGraphics Centurion software v19 (Manugistics Inc., USA). Two linkage rules were adopted, following the methodology described by Daughney et al. (2010) and Raiber et al. (2012): (1) the nearest neighbour rule, for identifying sites with significantly different hydrochemical signatures to recognise outliers that were placed as residuals in a separate group; and (2) Ward's rule, for generating distinct clusters based on an analysis of variance used to group all non-residuals into separate clusters. Similarities across all variables were assessed using the square of the Euclidean distance (E). The transformed input data along with linkage rules and the similarity measure are considered as the most appropriate techniques for classifying hydrochemical data (Güler et al., 2002; Daughney et al., 2010; Raiber et al., 2012). The outcome of this process is a dendrogram (Cloutier et al., 2008).

As it involves an element of judgment when determining the suitable number of clusters that are representative of a sample population, HCA is considered a semi-objective technique. In this study, the dendrogram was visually inspected, and then the centroid concentrations (represented by the median) for different input variables and clusters at different separation thresholds were compared (Cloutier et al., 2008; Raiber et al., 2012). The median was preferred as a better indicator of central tendency compared to the mean as it is less sensitive to extreme values (Helsel and Hirsch, 2002).

2.7 Integration of geological, geophysical, hydraulic and tracer data through numerical modelling

2.7.1 Overview

A suite of numerical modelling tools was employed to integrate and interpret the multitude of characterisation and monitoring data that were collected along a representative vertical transect (Section 2.7.2). This task involved the:

- selection of a suitable, data-rich and representative transect along the anticipated, general regional groundwater flow direction;
- definition of the geological model along this transect based on the available geophysical data (AEM and seismic) and stratigraphic logs;
- translation of the geological model into a high-resolution numerical flow and solute transport model to simulate groundwater flow and groundwater age patterns;
- history matching of the flow/solute transport model using observed hydraulic heads and estimated groundwater ages along the transect as model calibration constraints;
- definition of a wide range of geochemical inverse model variants that investigate and quantify the contributions of waters from both shallow and deeper geological sections along to the evolved groundwater hydrochemical compositions in the downgradient sections of the main aquifers;
- integration of the obtained flow/solute transport and inverse geochemical modelling results to assess the potential for a significant connectivity between coal seams and the shallow aquifers that could serve as environmental receptor of contaminants.

2.7.2 Development of transect

A high-resolution east-west vertical transect was developed through the central part of the Narrabri Gas Project area as a representative cross-section for the numerical modelling of groundwater flow and age patterns. The orientation of the transect was chosen due to the following reasons:

- availability of high-quality seismic data in the western part of the transect (Figure 2-4);
- availability of many high-quality exploration well stratigraphic logs at or within close distance of the transect;
- its approximate coincidence with the anticipated general east-west flow direction in the Pilliga Sandstone;

- the presence of multiple nested groundwater observation bore sites along the transect;
- the availability of high-quality hydrochemistry and environmental tracer data along the transect;
- the inferred presence of multiple potential hydrogeological connectivity pathways (e.g. intrusions, basement highs, faults and sub-cropping aquitards) along the transect.

The cross-section was developed in GoCAD/SKUA 3D geological modelling software through the integration of stratigraphic, seismic, AEM and digital elevation model data (1 second SRTM digital elevation model, Geoscience Australia, 2011) and interpretations. Seismic data and AEM data provide complementary insights into the subsurface: seismic data from geophysical surveys designed to identify hydrocarbon traps and gas or hydrocarbon reservoirs typically focus on depths below 400 m. In contrast, AEM focusses on the shallower parts of the subsurface to depths of approximately 200-400 m (depending on the system used for the survey and the specific subsurface characteristics of the investigated region).

2.7.3 Flow and solute transport model geometry and setup

The high-resolution vertical transect model was defined along a geological cross-section (Section 2.7.2 and 3.6) to simulate groundwater flow with the widely used tools MODFLOW (Harbaugh, 2005) and MT3DMS (Zheng and Wang, 1999). The lateral extent of the model was selected to be 46500 m and its vertical extent is 1200 m, ranging between -800 m Australian Height Datum (AHD) and +400 m AHD. Along this transect, spatially variable rainfall recharge was considered as the sole hydraulic driver of the simulated flow system, and the majority of the water exiting the model domain at the downgradient end through the Pilliga and Orallo aquifers, and a small fraction along selected drains that were set to prevent hydraulic heads exceeding the topographic elevation of the upper-most aquifer sections. Rainfall recharge for different formations was based on chloride-mass balance estimates for the Great Artesian Basin and adjacent coal basins by Crosbie et al. (2022).

The model discretisation was selected to be uniform with grid-dimensions of 250 m and 5 m in lateral and vertical direction, respectively. This relatively fine grid allowed to accurately discretise and represent the geological model. This approach was selected for numerical accuracy and stability over a discretisation approach lumping the entire thickness of geological formations into single numerical layers.

2.7.4 Groundwater flow

For pragmatic reasons, both groundwater flow and solute transport processes were assumed to be in a steady state, which resulted in highly efficient model run times compared to the alternative of transient simulations that would have needed to expand over millions of years.

A fixed head boundary was assumed for the Pilliga Sandstone and Orallo Formation aquifers at the model's downgradient boundary.

The initial estimates of the hydraulic conductivities of the considered geological layers were derived from various sources (Section 2.2.6). These initial estimates were successively revised during a trial-and-error calibration process, taking both groundwater head and age into account.

2.7.5 Groundwater age simulations

Groundwater age was in this study simulated as a direct groundwater age, following the approach proposed and discussed for example by Goode (1996). Potential limitations of the selected modelling approach, especially compared to the direct simulation of the fate of groundwater age tracers such as ^{14}C have been discussed for example by Turnadge and Smerdon (2014) and Salmon et al. (2015).

The simulations were implemented into MT3DMS by defining an "Age" solute species that enters the model domain within rainfall recharge at an age of zero, and a zero'th order reaction successively increasing the simulated age along the flowpaths. Extensive dispersive mixing might decrease groundwater age along a flow path. The simulated groundwater ages were constrained by comparison with the corresponding apparent groundwater ages estimated from the interpretation of measured age tracer concentrations. The age estimates used in the model calibration process are listed in Section and .

2.7.6 Joint inversion of Head and Age Observations

A manual trial-and-error model calibration was performed by using simulated hydraulic heads and groundwater ages with their corresponding observation. In this process, horizontal hydraulic conductivities of individual geological layers, a uniform vertical anisotropy ratio and spatially varying rainfall recharge estimates were successively varied until the general simulated hydraulic head and groundwater age distribution agreed reasonably well with observations.

The joint inversion was performed to reduce model uncertainties associated with the non-uniqueness of a head-only model calibration, where head observations may be matched by a wide range of combinations of highly correlated recharge rate and hydraulic conductivity estimates. Employing groundwater age estimates as additional calibration constraint can reduce this non-uniqueness and therefore model uncertainty (e.g. Schilling et al., 2019). Furthermore, compared to hydraulic head measurements, which can often be influenced by local and short processes and may not be representative for regional flow patterns, groundwater age tracer are good regional integrators which tend to be influenced less by local processes (e.g. groundwater extraction) and respond at different time-scales to changes than hydraulic heads.

2.7.7 Inverse geochemical modelling

In a previous study, Raiber et al. (2022a) have applied a simple end-member mixing analysis (EMMA) to investigate the relative contribution of three possible end-members to a mixed groundwater sample, which was based on a limited number of conservative tracers (e.g., Cl and F, or Cl and Sr). The mixing models were developed to test the likelihood of potential hydrogeological connectivity pathways between coal seams and the Pilliga Sandstone in the Narrabri Gas Project area. Although those earlier results were insightful, Raiber et al. (2022) highlighted the limitations and the remaining uncertainties due to the reliance on a small number of hydrochemical species, and the lack of considering rock–water interaction reactions along the flow paths; they recommended the application of inverse geochemical modelling.

In the present study, building up on the previous work, inverse geochemical modelling was applied to interrogate which water sources are likely to contribute to the hydrochemical mix of specific groundwater samples and to estimate their relative contribution to the mixed sample. As such, based on integration of many different hydrochemical and mineralogical data sets, this provides an alternative line of evidence for the likely existence or absence of specific groundwater flow patterns. In the present study, this involved development of a series of more complex and multivariate geochemical mixing models to provide a more comprehensive assessment of aquifer interactions, which, beyond the previous study, also considers (i) the potential hydrochemical evolution along flowpaths, especially reactions with the prevailing mineral assemblage, and (ii) concentrations of selected isotopes and isotope ratios, depending on data availability.

For this purpose, the inverse modelling capabilities of the geochemical model code PHREEQC (Parkhurst and Appelo, 2013) were used. This approach has previously been used to define and quantify the contributions of different source water compositions (or water qualities, WQs), to an "evolved" water composition (e.g., Cozzarelli et al., 2021). This "evolved" water composition is assumed to be:

- sampled at a location that is downgradient of all source water compositions;
- a mixture of the different source water compositions.

Figure 2-32 illustrates the general concept of the inverse geochemical modelling approach for a simple case, where three up-stream water compositions (WQ-Purl, a water composition sampled in the Purlawaugh Formation), WQ-Pil (a water composition sampled further upstream in the Pilliga Formation) and WQ-CS (a water composition sampled in the Maules Creek Formation) are assumed to have evolved into the water composition sampled downgradient in the Pilliga Formation (WQ-Mix). PHREEQC was tasked to define the fraction of each water type and to quantify the presence (or absence) of the user-defined geochemical reactions that could have occurred along the flow paths.

The inverse modelling calculation aims to define mixing proportion between groundwater from different aquifers. This calculation has been performed from geochemical data (mineralogy), physico-chemical parameters (i.e. temperature, pH, redox) and major and minor elements (e.g. alkalinity, Ca, F, and Br) measured in groundwater sampled in selected boreholes located along the cross sections where the aquifer is identified (for details of cross-sections, see Section 3.6). Unlike for the flow and solute transport model where a single transect was selected, two geological cross-sections (Section 3.6) were used as the framework for the inverse geochemical modelling. The two transects include areas where Raiber et al. (2022a) identified on-going uncertainties with regards to potential hydrogeological connectivity pathways.

In PHREEQC software, the inverse modelling function determines the molar transfers of phases for each solution that explain the changes observed in water chemistry in the downgradient solution (final solution – see abbreviation WQ-0) from several upstream solutions (WQ-A, B, C) and including solution from the same aquifer upstream – see abbreviation WQ-1).

The input file of the software includes physico-chemical parameters, major and minor elements and mineral phases considered in the equilibration. The results of XRD observations and some specific mineral phases (e.g. kaolinite, illite, chlorite(14a), analcime, dolomite, K-feldspar, barite and calcite) observed in core samples have also been considered in the mixing models.

Although PHREEQC's inverse modelling approach considers that user-defined water-sediment (or water-rock) interactions have modified the source water composition along the flowpaths, those reactions are assumed to occur as equilibrium reactions, i.e., are not controlled by (slow) reaction kinetics. However, given the slow groundwater flow and long residence times, this is not expected to be a severe limitation of the approach.

Here, the focus was on testing if contributions of water from deeper formations below the Pilliga Sandstone, in particular from the uppermost formations of the Gunnedah Basin (i.e., Digby and Napperby formations) and from the target coal seams (Hosksissons Coal seam and Maules Creek Formation), are likely to be found in the shallower aquifers and therefore suggesting aquifer connectivity. Each of the defined water compositions included major ions and selected trace elements (e.g. Ba, B, Li, Sr and F, when data was available), with measured isotopic ratios such as $^{87}Sr/^{86}Sr$ also considered in some of the models.

The potential mineral reactions that were included as "possible reactions" along each of the inferred flow paths towards the evolved water composition were selected based on the mineralogical composition of the considered geological formations that are assumed to be present along the flow paths.

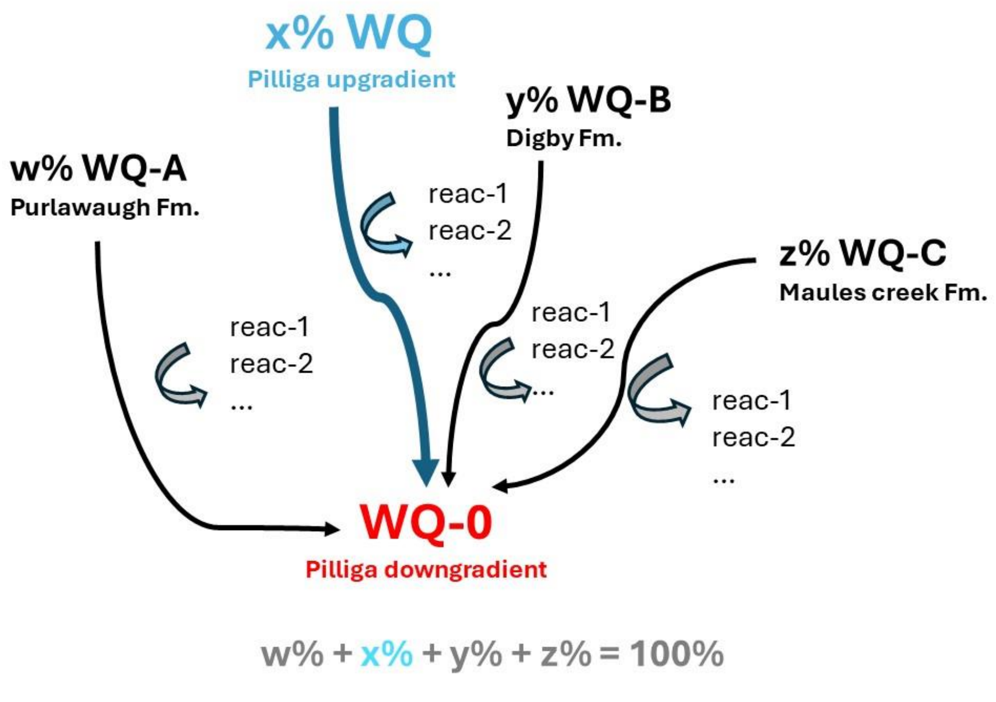

Figure 2-32 – Simplified explanation of the inverse geochemical modelling calculation.

WQ: water quality, WQ-0: aquifer downgradient ("receiving" aquifer), WQ-1: same aquifer but upgradient, reac-: geochemical reactions, while A, B and C are proportions of water from other geological formations (e.g. Purlawaugh Formation, Digby Formation and Maules Creek Formation- CSG target). This example is one of many geochemical model realisations tested in this study.

3 Results

Section 3 of this report presents the results of the multiple lines of evidence considered in this study sequentially according to the different levels of the integrated, multi-disciplinary workflow presented in Section 2.1.

The first sections (sections 3.1 to 3.6), corresponding to levels 1 and 2 of the "Hydrogeological Pyramid" in Figure 2-1, describe the characterisation of geometry and internal architecture of sedimentary and igneous rocks in the Narrabri Gas Project area and the geological framework of potential hydrogeological connectivity pathways.

Sections 3.7 to 3.8 demonstrate how hydrochemistry and environmental tracers were used to determine groundwater flow dynamics through the subsurface, and provide an indication of whether actual connectivity is likely to occur along potential hydrogeological connectivity pathways.

Sections 3.9 and 3.10 present the integration of all evidence from previous sections through numerical modelling of groundwater heads (pressure) and apparent groundwater ages and through geochemical mixing models to further assess potential connectivity and mixing processes.

3.1 Stratigraphic data

3.1.1 Spatial distribution of igneous intrusions

We have reviewed stratigraphic logs to identity which stratigraphic units were intersected by the igneous intrusions (Figure 3-1), and in some cases confirmed by visual inspection of the core samples we have collected from the Londonderry Drillcore Library, WB Clarke Geoscience Centre, NSW (Figure 2-23). The assessment showed that the intrusions mostly intersected the Digby Formation, Napperby Formation, and extended to the base of the Purlawaugh Formation. As shown using the example of the area where the Bohena anticline has been identified in previous studies, the assessment of stratigraphic logs shows that what is likely the same horizontal intrusion (sill) has intersected the subsurface at different stratigraphic intervals. For example, at the Water NSW Plumb Road groundwater monitoring site (GW971623), the sill has intersected the interface between the Napperby and Digby formations, whereas it has extended to the base of the Purlawaugh Formation at Bohena 2 and intersected multiple depth intervals within the Napperby Formation at Bohena 3. This suggests that the sill likely follows pre-defined zones of structural weakness, as discussed in Section 1.3. Only few intrusions were identified within the deeper parts of the Gunnedah Basin (including within the coal seams).

No intrusions are found in the Pilliga Sandstone in stratigraphic logs within the Narrabri Gas Project area, and the upper-most interval intersected is the base of the Purlawaugh Formation, although a thick and spatially extensive intrusion interfaces between the Pilliga Sandstone and Digby Formation at Nyora at a site where the Purlawaugh Formation and Napperby Formation appear to be absent. The sill or laccolith at Nyora, which is visible on the magnetic images (Section 2.2.5) and shown in geological cross-section 2 (Section 3.6.2), was dated as Early Jurassic. It therefore intruded prior to the deposition of the Pilliga Sandstone (deposited later during the Mid Jurassic) and there has therefore not been any heating or contact metamorphism of the Pilliga Sandstone strata.

It is important to note that although no intrusions were identified within the Pilliga Sandstone within the Narrabri Gas Project area, exploration wells are sparse in the eastern part of the Narrabri Gas Project area (Figure 3-1), and it cannot be ruled out that some intrusions extended into the Pilliga Sandstone that may have not been intersected by exploration wells. This will be discussed further in subsequent sections and in Section 4.

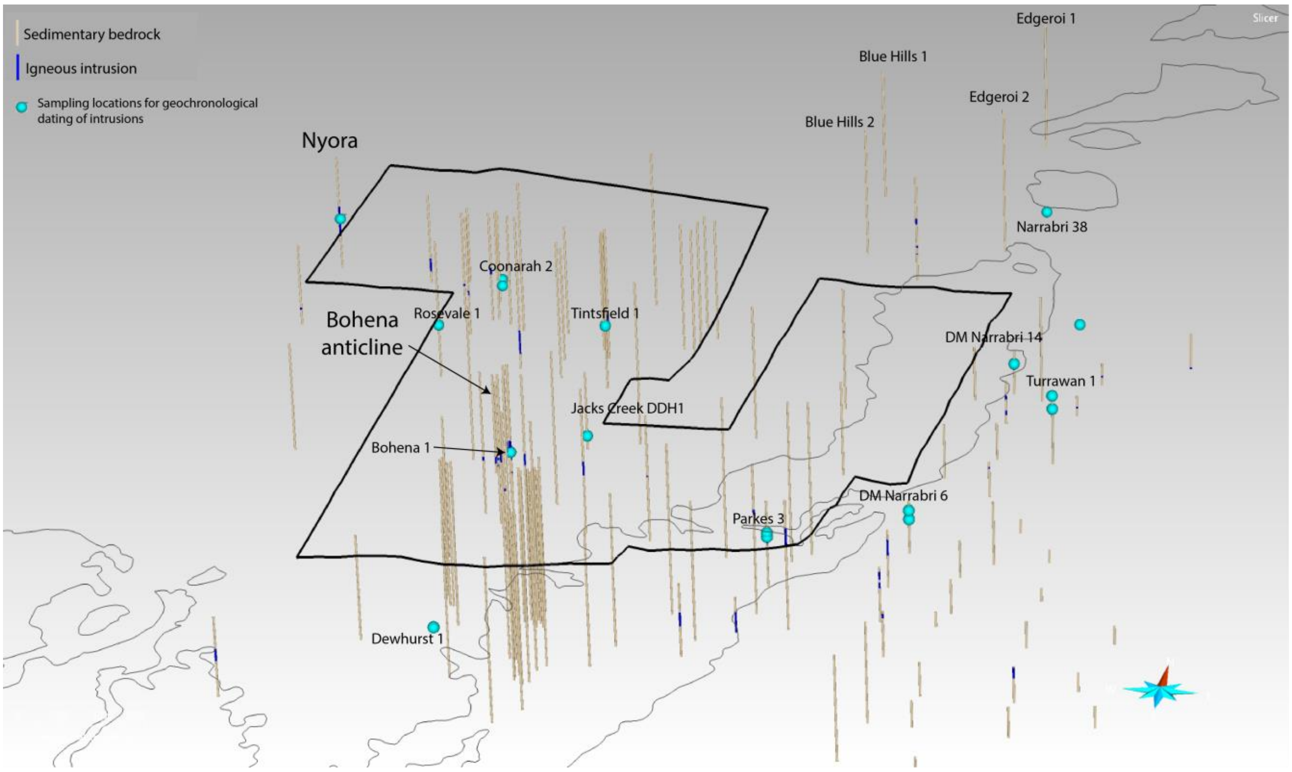

Figure 3-1 – Three-dimensional view of stratigraphic logs and intrusions (dark blue intervals) recorded within sedimentary bedrock (beige intervals) sequences along exploration well paths in the Narrabri Gas Project area.

The outline of the Narrabri Gas Project area is represented by the black line. Grey lines show the extent of the Pilliga Sandstone outcrops. Multiple igneous rocks samples from different depth intervals were collected at some sites (e.g. Coonarah 2 and Parkes 3). The 3D visualisation was created in SKUA (Aspentech™).

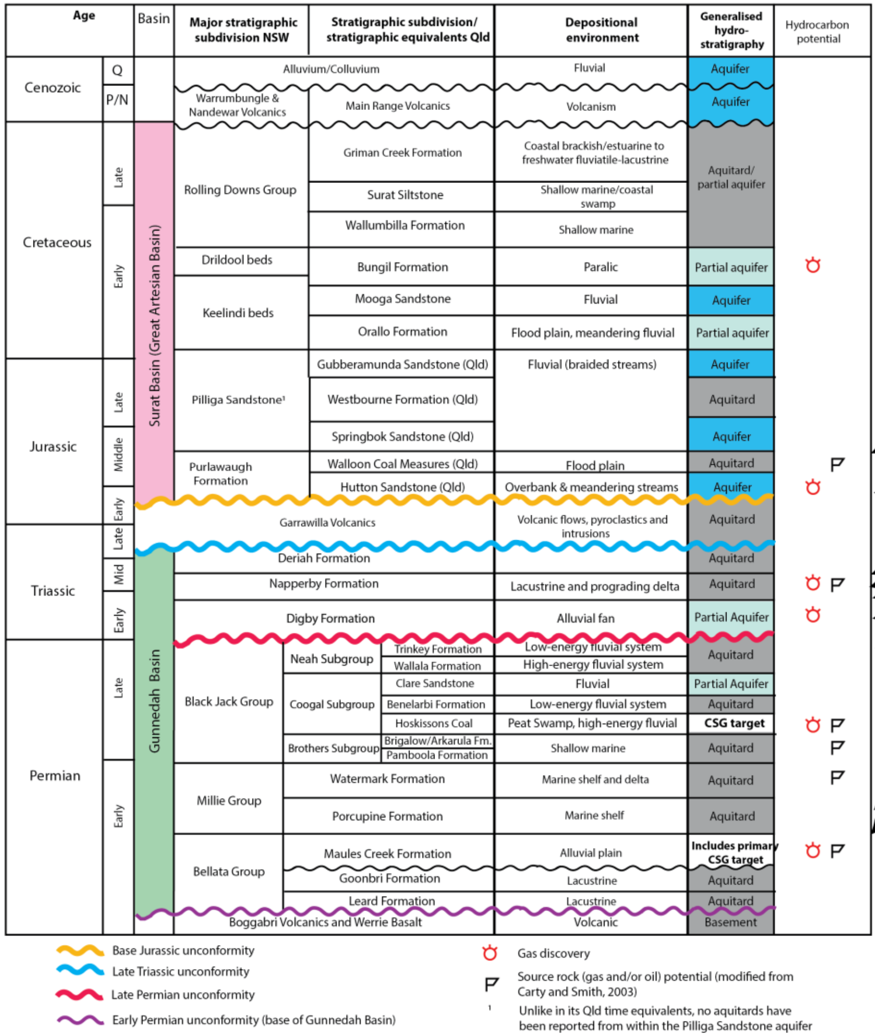

Intersections of intrusive rocks in stratigraphic logs

Stratigraphic formation intersected	Number of bores
Orallo Formation	N/A
Pilliga Sandstone	N/A
Interface Pilliga Sandstone - Digby Formation	1
Purlawaugh Formation	N/A
Garrawilla Volcanics	2
Deriah Formation	N/A
Interface Purlawaugh Formation - Napperby Formation	9
Interface Deriah Formation - Napperby Formation	1
Napperby Formation	12
Interface Napperby Formation - Digby Formation	7
Digby Formation	4
Black Jack Group	2
Porcupine Formation	2
Interface Porcupine Formation - Maules Creek Formation	1
Intrusions (unknown/uncertain stratigraphy)	17
Stratigraphic bores with no intrusions	83

Figure 3-2 - Observed occurrences of intrusive igneous rocks and corresponding stratigraphic units intersected in stratigraphic and exploration wells and groundwater monitoring bores.

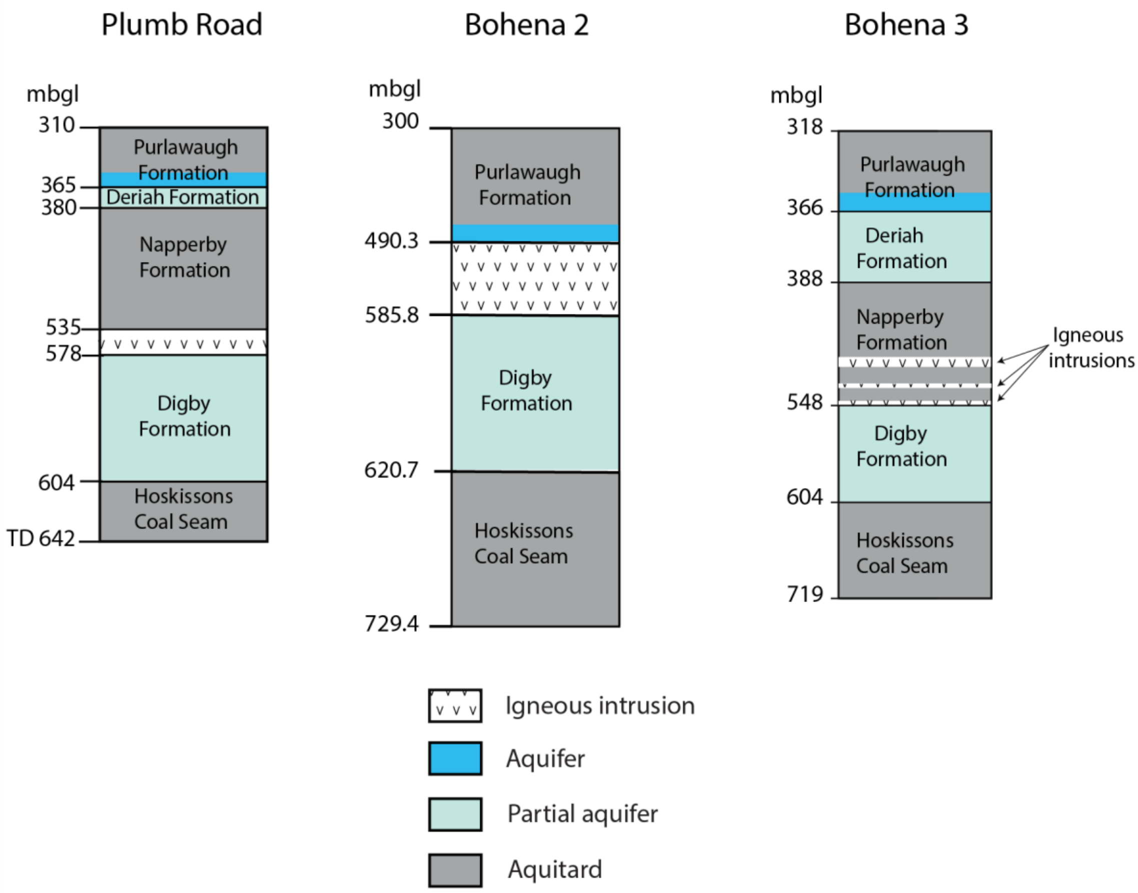

Figure 3-3 – Igneous intrusions at Bohena anticline, showing variability of thickness observed at different exploration wells and groundwater observation bores (Plumb Road – GW971623) (stratigraphic logs are sourced from NSW DIGS).

3.1.2 Variability of lithology in Surat and Gunnedah basins

Generalised sand/shale calculations developed by Geoscience Australia (Norton and Rollet, 2023) were considered in this study to determine spatial lithological variability within the Surat and Gunnedah basins strata (Figure 3-4).

Although the exploration wells where sand/shale calculations were available are located to the north of the Narrabri Gas Project area (their locations are shown in Figure 3-1), they provide useful insights for the present study. Previous studies suggested that the Pilliga Sandstone is generally a quartzose sandstone with limited clay and feldspar content (e.g. Arditto, 1982; Troedson and Bull, 2018); however, the sand/shale calculations especially at Edgeroi 1 and Blue Hills 2 show that there is likely more lithological variability with a higher presence of “shale” (or clay) than what was previously assumed within the Narrabri Gas Project area. Furthermore, the sand/shale calculations showed that there is no clearly identifiable interface between the Orallo Formation and Pilliga Sandstone in these logs, and that multiple fining upwards sequences exist in both formations and both units have interbedded mudstone and siltstone.

For the Purlawaugh Formation, the sand/shale calculations confirm that there is a low permeability upper part and likely aquitard (dominated by shale/claystone in this model) and a more permeable lower part (a likely aquifer, dominated by sand) at some locations. For the

Gunnedah Basin formations, the sand/shale calculations confirm the dominance of shale (or claystone, representing aquitards) over sand, although some minor sand intervals also appear to be present within the Napperby Formation, Digby Formation, Black Jack Group and Maules Creek Formation.

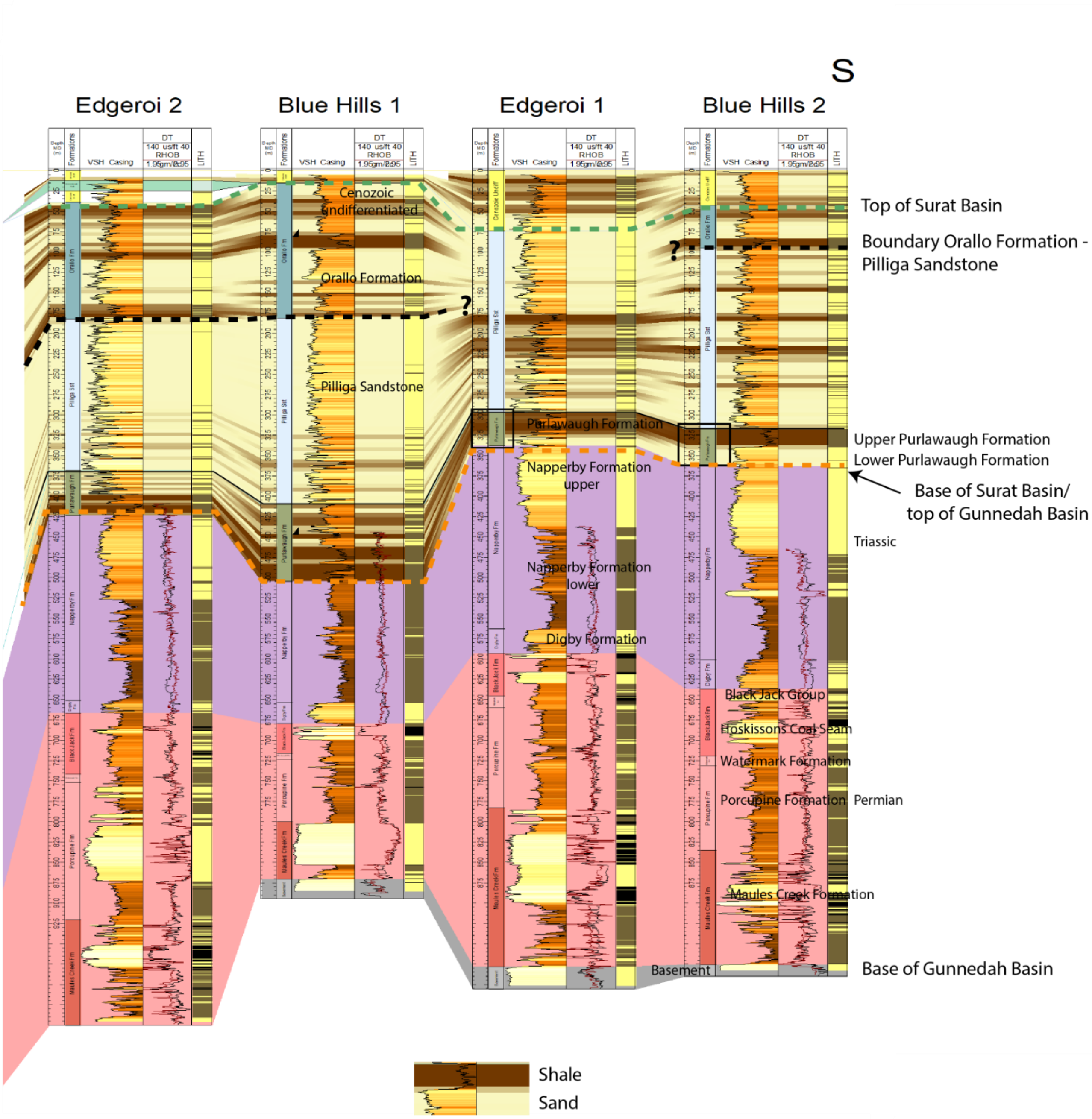

Figure 3-4 – Lithological variability within Surat Basin and Gunnedah Basin formations in NSW along selected exploration wells (modified from Norton and Rollet, 2023). The locations of wells are shown in Figure 2-8 and Figure 3-1.

The vertical and lateral variability in lithology within the Surat and Gunnedah Basin are expressed based on generalised sand/shale calculations (with sandy facies represented in yellow and shaley facies represented in brown).

In addition to the sand/shale calculations, the Palaeogeographic Atlas of Australia (Geoscience Australia, 2025a) was also used to provide a better understanding of the depositional environment at the time of the deposition of the Surat and Gunnedah basin strata, with the depositional environment together with burial history considered as primary controls of the spatial variability of lithological and petrophysical properties in sedimentary basins.

During the Early Jurassic (190 to 179 million years ago), when the deposition of the Purlawaugh Formation commenced, the depositional environment is described as fluvial in the Narrabri region (Figure 3-5 a). Fluvial depositional environments are high energy environments where coarser sediments such as sand and gravel (which after millions of years of exposure to overburden pressure are more likely form aquifers) are more likely to be deposited than finer-grained sediments such as clay and silt (which are more likely to form aquitards).

a) Depositional environment during the upper (younger) part of the Purlawaugh Formation

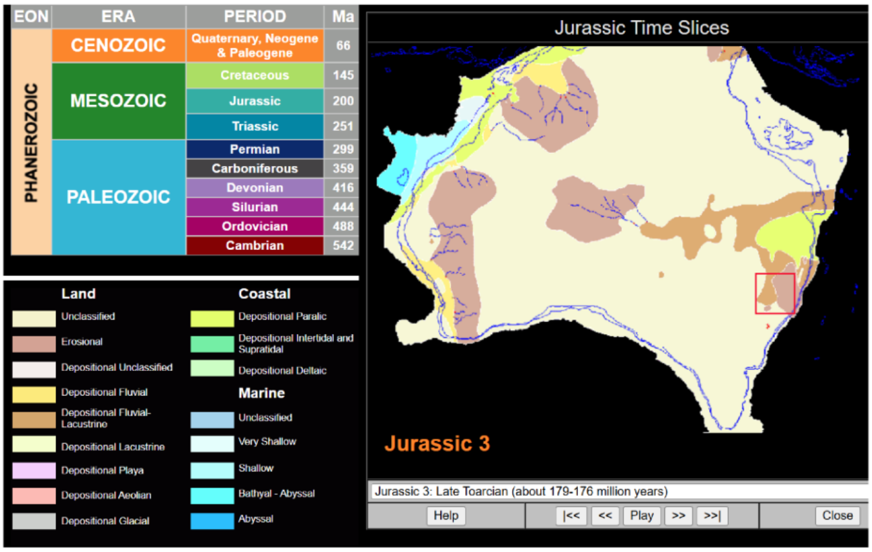

a) Depositional environment during the lower (older) part of the Purlawaugh Formation

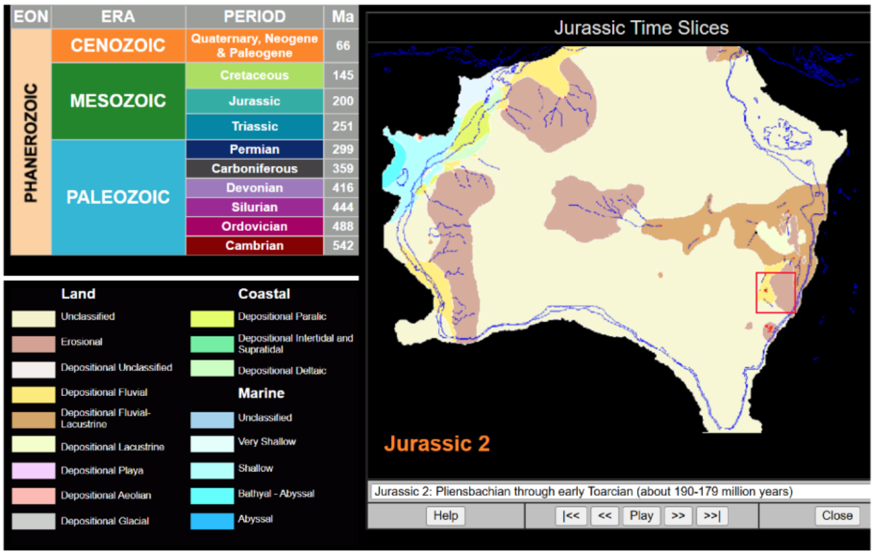

Figure 3-5 – Sedimentary environment at the time of the deposition of the a) upper and b) lower part of the Purlawaugh Formation (deposited between 190 to 165 million years ago; Australian Stratigraphic Unit Database) (Geoscience Australia, 2025a).

The red square indicates the approximate location of the Narrabri region.

When the upper part of the Purlawaugh Formation was deposited during the later part of the Early Jurassic between 179 to 160 million years ago, depositional fluvial and lacustrine environments dominated within the eastern part of the Coonamble Embayment (e.g. Figure 3-6 b). Lacustrine depositional environments are low-energy environments where sedimentary deposits are mainly composed of small particle sizes such as clay, silt or carbonates, which are more likely to form aquitards.

The observed patterns of depositional environment agree with the lithological variability of the Purlawaugh Formation described above from the sand/shale calculations for selected exploration wells near the Narrabri Gas Project area.

During the deposition of the Late Jurassic to Early Cretaceous Orallo Formation (approximately 140 to 149 million years ago; Geoscience Australia, 2025b), the depositional environment is described as fluvial (likely dominated by sand) in proximity to the erosional land surface (sediment source area) and fluvial to lacustrine (with higher clay contents) with increasing distance from the sediment source area (Figure 3-6).

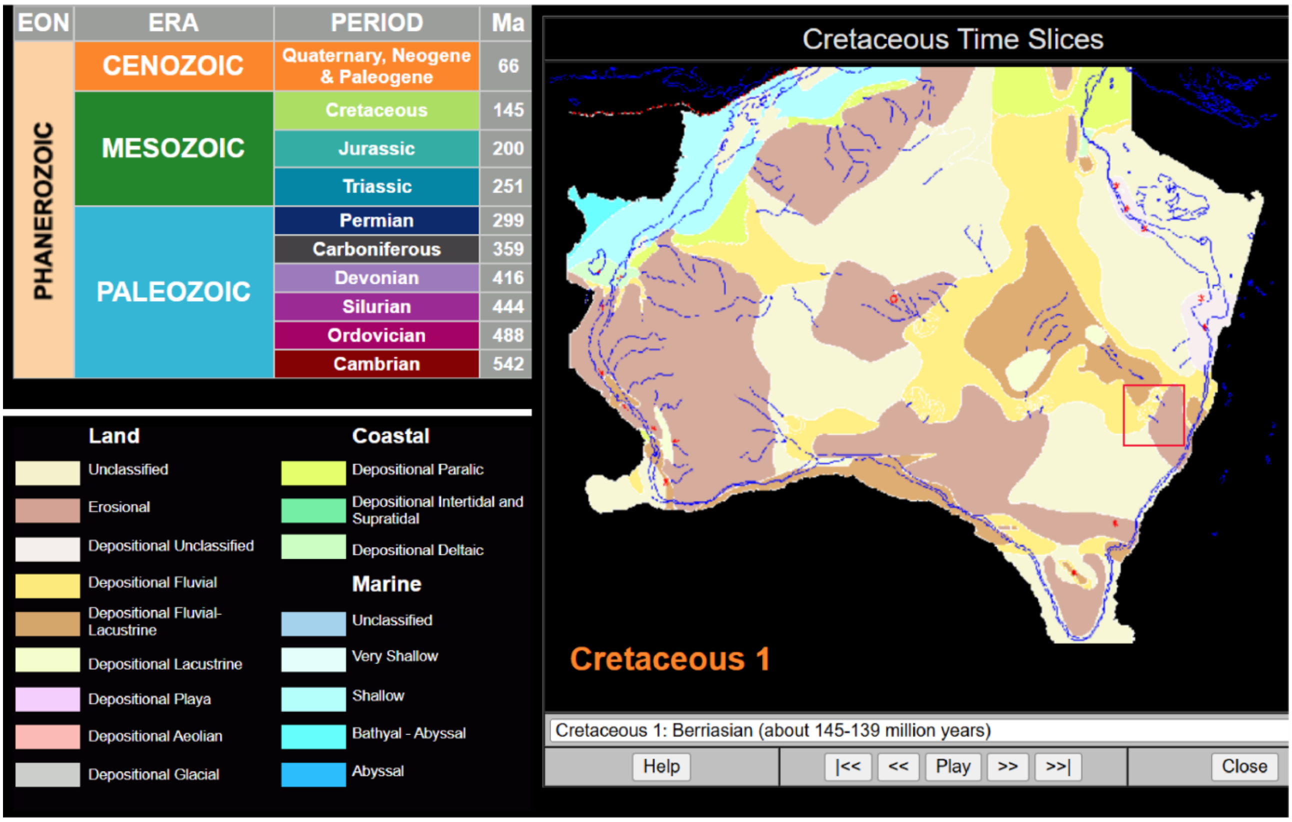

Figure 3-6 – Sedimentary environment at the time of the deposition of the Orallo Formation (deposited during the Cretaceous between 140 to 149 million years ago; Australian Stratigraphic Unit Database) (Geoscience Australia, 2025a).

The red square indicates the approximate location of the Narrabri region.

The exact time of deposition of the Pilliga Sandstone is not well constrained; however, it has been described as a chronological equivalent of the Springbok Sandstone, Westbourne Formation and Gubberamunda Sandstone of the Surat Basin in Qld and is likely to have been deposited between approximately 160 to 150 million years ago during the Late Jurassic (Geoscience Australia, 2025b). While fluvial-lacustrine deposition dominated between 164 to 160 million years ago in the Narrabri region, there was a change to fluvial deposition between 160 to 151 million years ago (Geoscience Australia, 2025b).

3.2 Hydraulic data

3.2.1 Petrophysical properties of Surat and Gunnedah basins formations

Petrophysical data were compiled from different sources to underpin the development of groundwater models, as described in Section 2.2.6. Summary statistics (minimum, maximum and out best estimate for horizontal hydraulic conductivity (Kh) and porosity for different formations are shown in Table 2.

Table 2 Petrophysical properties used in the groundwater flow modelling.

Formation	Kh (m/d): Best initial estimate	Kh (m/d): Min	Kh (m/d): Max	Porosity: Best initial estimate	Porosity: Min	Porosity: Max
Cenozoic Upstream	3.00×10^{-2}	1.45×10^{-2}	1	1.00×10^{-1}		
Cenozoic downgradient	3.00×10^{-2}	1.45×10^{-2}	1	1.00×10^{-1}		
Orallo Fm	1.00×10^{-2}	5.00×10^{-2}	5.66	1.00×10^{-2}		
Pilliga Sandstone	1.68×10^{-2}	5.00×10^{-2}	1.05	1.00×10^{-2}		
Purlawaugh Fm.	2.20×10^{-5}	2.00×10^{-6}	0.41	2.55×10^{-2}	1.18×10^{-2}	1.46×10^{-1}
Napperby Fm.	7.00×10^{-4}	1.66×10^{-7}	8.34×10^{-1}	5.80×10^{-3}	2.00×10^{-4}	9.15×10^{-2}
Intrusions	1.73×10^{-3}	3.61×10^{-5}	8.60×10^{-3}	5.00×10^{-3}	8.00×10^{-4}	3.00×10^{-2}
Digby Fm.	1.18×10^{-3}	7.78×10^{-7}	6.30×10^{-2}	1.00×10^{-3}		
Black Jack Group	3.00×10^{-4}	3.00×10^{-6}	0.14	1.00×10^{-1} [Nea subgroup]		
Hoskisssons Coal seam	1.12×10^{-2}	4.32×10^{-6}	4	5.00×10^{-4}	1.00×10^{-3}	2.00×10^{-1}
Watermark Fm.	1.61×10^{-5}	1.74×10^{-7}	7.67×10^{-2}	2.57×10^{-2}	9.00×10^{-4}	1.80×10^{-1}
Porcupine Fm.	5.00×10^{-6}	1.42×10^{-7}	2.00×10^{-3}	1.71×10^{-2}	2.20×10^{-3}	1.50×10^{-1}
Maules Creek Fm.	9.50×10^{-3}	1.66×10^{-6}	5.5	5.00×10^{-3}	1.00×10^{-3}	1.00×10^{-2}
Garrawilla Volcanics	1.10×10^{-1}	0.003	8.34×10^{-1}	2.00×10^{-3}		

Note: The data are compiled from the compilation of Bioregional Assessment Program (2016), OGIA (2019), Chris Turnadge et al (2018) and CDM Smith (2016). For hydraulic conductivities, i.e., Kh, the best initial estimates are taken as the median of all the measurements for most of the formations, except when there are only a couple of measurements available.

Previous studies in this region (e.g. Turnadge et al., 2018) suggested that all four inferred aquitards (Purlawaugh Formation from the Surat Basin, Napperby Formation, Porcupine Formation and Watermark Formation from the Gunnedah Basin) in the Gunnedah Basin area have low permeabilities which further decrease with depth. However, the authors also emphasised that more work is required to characterise the spatial continuity of these aquitards and determine if they are compromised by seal-bypass structures such as faults. As explained in previous sections of this report, the Purlawaugh Formation, which in previous studies was sometimes described as an aquitard or aquiclude, is composed of a higher permeability lower part (likely acting as an aquifer) and a lower permeabilty upper section dominated by claystone and other low permeability strata (likely acting as an aquitard).

3.2.2 Bore hydrographs

Representative hydrographs for groundwater bores used in the transect groundwater flow models are shown in Figure 3-7. The groundwater levels in the key formations in the Surat and Gunnedah basins, such as the Pilliga Sandstone, Purlawaugh Formation, Porcupine Formation, Hoskissons Coal seam, and Digby Formation, are relatively stable over the period where monitoring data are available.

Although head observations for most groundwater observations bores are only available for <10 years and there are some fluctuations observed in some hydrographs over time, these are relatively minor (i.e. cm’s of change) for most groundwater observation bores. This suggests that it is reasonable to assume a steady state in groundwater flow models developed in this study. Some of the limitations uncertainties with these assumptions are discussed in Section 3.9.3.

However, some groundwater bore hydrographs in the eastern part of the Narrabri Gas Project area are more variable. For example, at Tullamullen in a bore screened within the Napperby Formation, outside the eastern boundary of the Narrabri Gas Project area, the hydraulic head varied more than approximately 25 m with a continuous rise shown since 2014 (Santos Water Portal, 2025), possibly due to some groundwater extraction or changes in pressure loading in the area.

Observed hydraulic pressure gradients (e.g. at the Plumb Road nested groundwater monitoring sites) suggest that there is a general upwards hydraulic gradient from deeper hydrostratigraphic units towards the shallower formations (e.g. from the Digby Formation to the Purlawaugh Formation, which are both flowing artesian) and from the Purlawaugh Formation to the Pilliga Sandstone, where the water table is approximately 25 m below the ground surface. This suggests that there is a potential pressure differential to drive some fluid migration through any connectivity pathway, although the considerable pressure differences in adjacent units also suggests that there is a competent hydraulic barrier at this specific location. The relative pressure (head) gradients between different formations at nested bores sites along cross-section 1 are shown in Section 3.6.1.

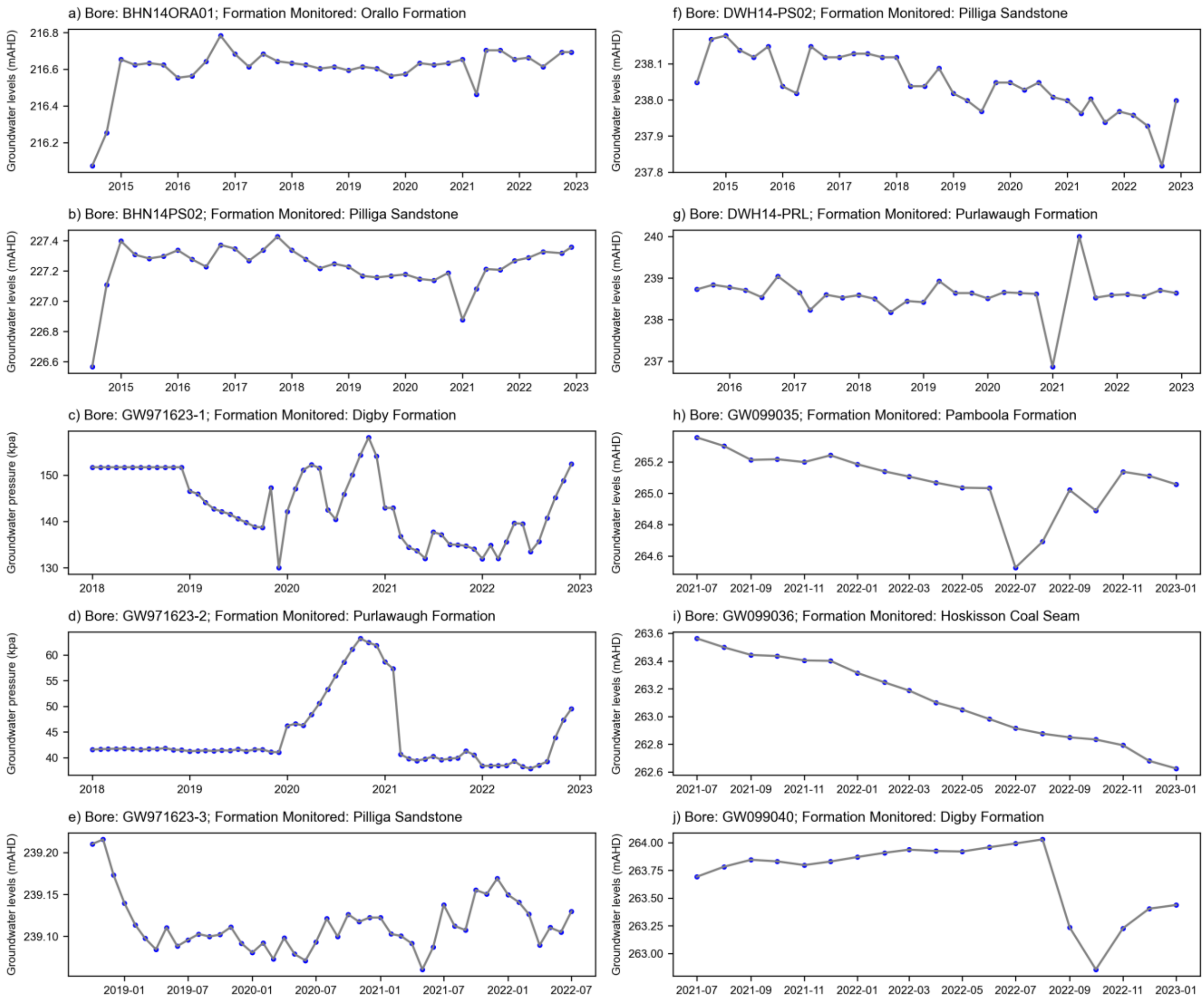

Figure 3-7 – Hydrographs for selected bores used in our cross-section groundwater flow models. Note that both GW971623-1 and GW971623.2 are artesian and measured in pressure.

3.2.3 Head observations used in flow and solute transport model

The head observations employed in the model calibration process are listed in Table 3, together with specific comments regarding the anticipated reliability of the head observation as calibration constraints. Heads in AHD are converted from meters below ground level (mbgl) using the 1second DEM (Geoscience Australia, 2011) to be consistent with the profile of the cross-section, the top of which is constructed using the 1s DEM.

Table 3 Hydraulic head median measurements used as history matching constraints for the groundwater flow and solute transport model. See Figure 3-45 for the location of the bores on the cross-section.

Monitoring Bore	Head (m AHD)	SWL (mbgl)	Aquifer/Aquitard	Comment
BHN14ORA	216.6	25.55	Orallo Fm.	
BHN14PS02	227.24	14.36	Pilliga Sst.	
GW971623-1	277.69	15.7	Digby Fm.	
GW971623-2	268.89	6.89	Purlawaugh Fm.	

GW971623-3	239.11	22.88	Pilliga Sst.	
DWH14-PS01	237.86	52.51	Pilliga Sst.	
DWH14-PS02	238.03	53.21	Pilliga Sst.	
DWH14-PRL	238.59	52.65	Purlawaugh Fm.	
GW099040	259.41	108.07	Digby Fm.	
GW099041	224.8	142	Purlawaugh Fm.	
GW099042	378.36	215	Watermark Fm.	Limited measurements with gas bubbles
GW098012	218.3	28.76	Pilliga Sst.	Projected from distance
GW099035	268.01	43.46	Pamboola Fm.	
GW099036	265.81	45.51	Hoskisson Coal seam	
GW099037	237	82.17	Pilliga Sst.	
TUL_NAP01	232.44	91.55	Napperby Fm.	
TUL_DGY02	253.91	70	Digby Fm.	Large variability of head measurements possibly showing impact of pumping or equilibration

3.3 Geochemical analysis of rocks

3.3.1 XRD and XRF

X-ray diffraction (XRD) and X-ray fluorescence (XRF) were conducted to understand the horizontal and vertical variability of mineralogy and petrology of rocks within the Narrabri Gas Project area. We integrated the results of XRD analyses for all the major formations/groups in the Surat (GAB) and Gunnedah basins (Figure 3-8 to Figure 3-10). The mineralogical composition of rocks is a primary control on hydraulic properties and on the hydrochemical evolution of water contained within the formations. Together with core descriptions and bore completion reports, this enables a quantitative understanding of the minerology and petrology of the major formations in the Surat Basin, such as Orallo Formation, Pilliga Sandstone, and Purlawaugh Formation, and in the Gunnedah Basin strata such as Maules Creek Formation, Black Jack Group, and Napperby and Digby formations.

Surat Basin

XRD and XRF results of Surat Basin rock samples were collected from two different exploration wells, with one well (Tunamallalee 1) located within the outcrop area of the Pilliga Sandstone, and the other well (Coonarah 2) located more than 40 km down-gradient from the Pilliga Sandstone outcrop (Figure 2-26).

Figure 3-8 shows the XRD results of rock samples from the Orallo Formation, Pilliga Sandstone, Purlawaugh Formation (all part of the Great Artesian Basin) at variable depth intervals. Generally, the results show a predominance of quartz, feldspar (plagioclase and K-feldspar) and kaolinite.

However, there are some very notable differences especially for the Pilliga Sandstone when comparing the results from the two exploration wells:

- samples collected from the Pilliga Sandstone within the outcrop beds at exploration well Tunamallalee 1 are chemically mature with very high quartz contents (ranging from 75 to 97%), with no or only very minor plagioclase and k-feldspar but significant kaolinite content, which formed from extensive feldspar and lithic leaching. Well-sorted, coarse-grained quartz sandstones typically have higher hydraulic conductivity because the grains are more uniform, creating larger and more connected pore spaces.
- samples collected from the Pilliga Sandstone in a down-gradient location at Coonarah 2 have a much more heterogeneous and immature mineralogy with significantly less quartz (60-70%) and higher overall content of detrital micas, feldspars (plagioclase and k-feldspar), kaolinite, smectite, and Ca–Mg carbonates. This is in agreement with generalised sand/shale calculations of Edgeroi 1 and Blue Hills 2 strata located to the north of the Narrabri Gas Project area (Figure 3-4 and Figure 2-26), which suggest that the Pilliga Sandstone is more heterogeneous away from the outcrop areas with sandy facies interbedded with clay, mudstone or siltstone.

A sample collected from the Orallo Formation at Connarah 2 has a similar composition as samples from the Pilliga Sandstone at the same site (although with a slightly smaller quartz content).

The Purlawaugh Formation, based on three samples from Coonarah 2 and Tunamallalee 1, exhibits a wide range of mineralogical compositions, including a sample with almost 60% quartz and thus only small contents of clay minerals and feldspars, and a sample with approximately 30% quartz and a dominance of illite and kaolinite.

The average mineralogical compositions for all samples for each formation for Surat Basin strata are shown in Figure 3-11.

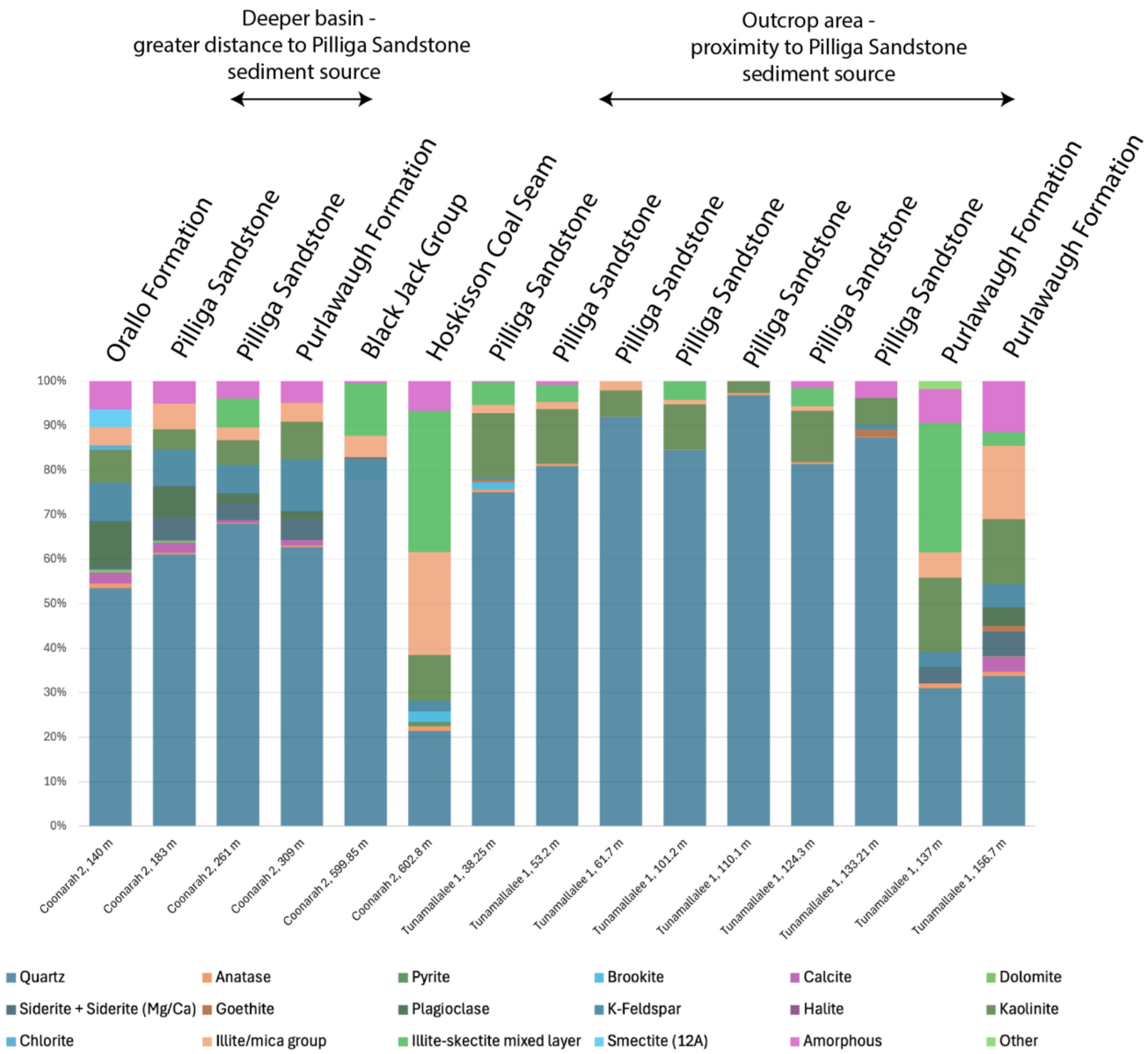

Figure 3-8 – XRD results from various intervals in the Coonarah 2 and Tunamallalee 1 exploration wells in the Narrabri Gas Project area. It shows that the mineralogy of most intervals is dominated by quartz and feldspar.

Depth intervals for each bore are rounded to the nearest 0.1 m for annotation purposes.

Gunnedah Basin

The sedimentary rocks of the Maules Creek Formation consist of lithic conglomerate, sandstone, siltstone, and claystone with coal seams up to 8 m thick. Within the Gunnedah Basin, multiple formations classified as aquitards (or seals) overlie the Hoskissons Coal seams and Maules Creek Formation. This includes the Napperby Formation, Neah Subgroup, Brothers Subgroup, Watermark Formation and Porcupine Formation, which were predominantly deposited in low-energy fluvial, lacustrine or marine shelf environments, favouring the formation of low-permeability rocks such as claystones, shale and mudstones (Figure 1-1).

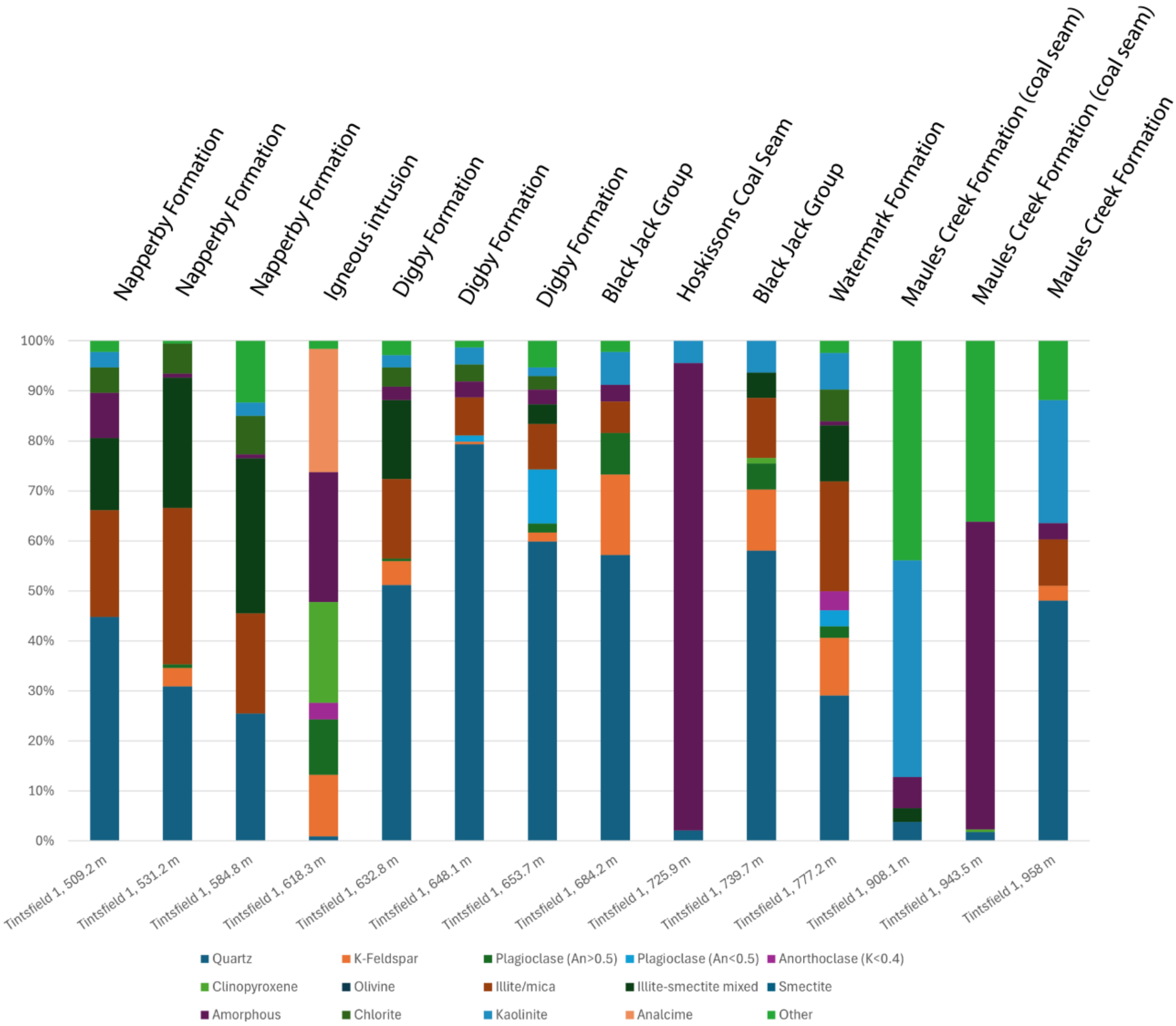

Figure 3-9 – XRD results of core samples from borehole Tintsfield 1 at various depth intervals, which are rounded to the nearest 0.1 m for annotation purposes.

XRD and XRF results of Gunnedah Basin samples were collected from exploration wells Coonarah 2 and Tintsfield 1. Figure 3-9 shows the XRD results of fine-grained core samples from the more densely sampled exploration well Tintsfield 1 from 500 m to 1000 m depth in the Gunnedah Basin. Additional samples from the Black Jack Group and Hoskissons Coal seam (which is also part of the Black Jack Group) are shown in Figure 3-8.

As expected, rock samples collected from the Hoskissons Coal seam and the coal seams of the Maules Creek Formation are dominated by coal. One of the Hoskissons Coal seam sample is almost exclusively composed of coal (indicated by the class “amorphous” at depth interval 752.9 m in Figure 3-9), whereas the samples collected from Parkes and Bohena coal seams of the Maules Creek Formation are more variable with significant contents of calcite (up to 13.7%), quartz, kaolinite and siderite. A small presence of halite (0.2%) was detected within the Black Jack Group, which also hosts the Hoskissons Coal seam. This agrees with the possible shallow marine or near coastal depositional environment proposed for some formations within the Black Jack Group

(Figure 1-1). However, no halite was detected in any other sample from the Surat and Gunnedah basin formations analysed during this study.

The data confirm that most of these formations are predominantly fluvial-lacustrine in origin and dominated by quartz, feldspar and clay minerals such as illite. At 618.3 m, the results show the presence of an igneous intrusion. These results are consistent with direct core description, estimated shale-sand ratios (e.g. Figure 3-4) and well completion reports.

Figure 3-11 and Figure 3-12 clearly show the contrast between sandstone dominated clay-poor aquifers, such as Pilliga Sandstone and Orallo Formation, and clay-rich aquitards, such as the Napperby Formation, Black Jack Group, Maules Creek and Watermark formations. Such detailed understanding of aquifer and aquitards is especially useful for the inverse geochemical modelling of groundwaters, both conceptually and quantitatively, and for the interpretation of hydrochemistry and environmental tracers.

Igneous intrusions

Figure 3-10 show the mineralogical composition of igneous intrusions from various exploration wells in the Narrabri Gas Project region. In these samples, quartz, plagioclase, olivine and pyroxene dominate the mineral compositions, although other minor minerals such as for example analcime, magnetite, hematite and fluorapatite are also present. Furthermore, in some samples, smectite, a product of weathering or hydrothermal alteration is also abundant. Chlorite, which forms at temperatures above 220^{o}C in veins as an alteration product of pyroxene or olivine (Fulignati, 2020) is also present in some samples.

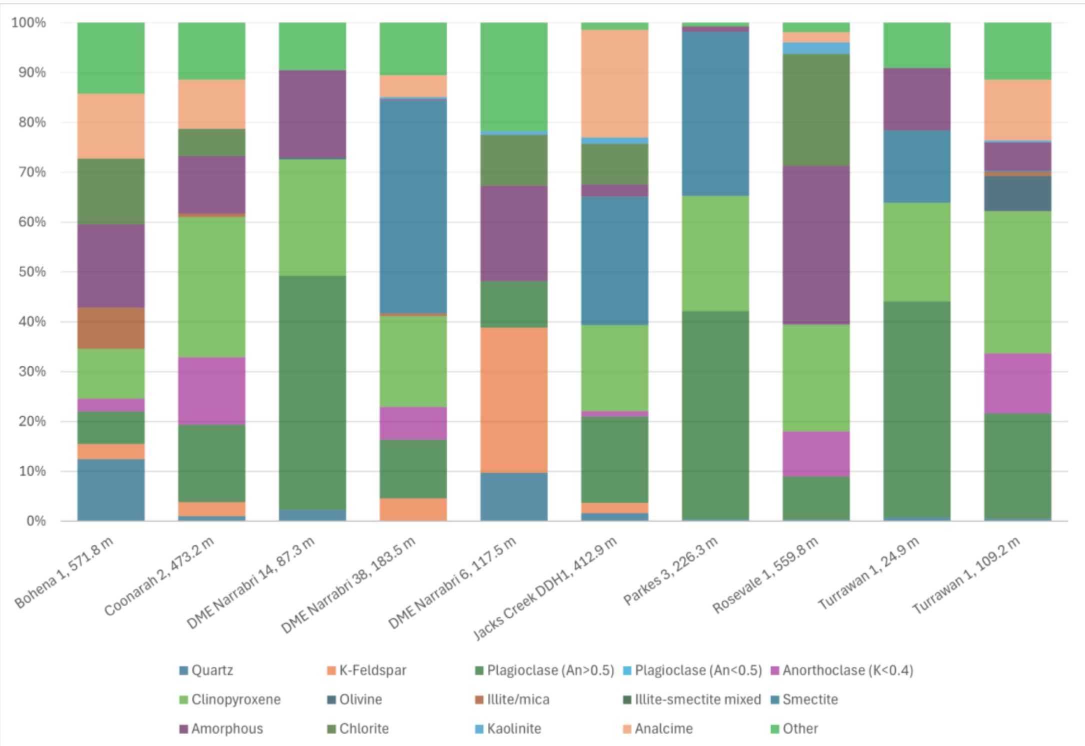

Figure 3-10 – XRD results of core samples of igneous intrusions from exploration wells in the Narrabrah Gas Project region, which show a dominant quartz, plagioclase and pyroxene compositions.
Depth intervals are rounded to the nearest 0.1 m for annotation purposes.

In addition, five samples dominated by clay in appearance were analysed at the CSIRO Diffraction Laboratory (Table 4). For all the five samples analysed, the grain size is principally larger than 2 µm, i.e., more than 80%, except for DME Parkes 3, where it is more than 60%. XRD analysis for each sub-division of sizes was completed separately for < 0.2 µm, 0.2-2 µm and > 2 µm. The combined results show that most of the samples are mainly composed of plagioclase, K-feldspar and different forms of smectite, such as dioctahedral smectite, trioctahedral smectite and interstratified chlorite-smectite.

The highly variable mineralogical composition of the intrusive rocks in the Narrabri region agrees with rock descriptions in well completion reports, where the intrusive rocks are commonly described as dolerites, teschenite (which are similar to dolerites) or basalts (which are extrusive rather than intrusive).

Table 4 Quantitative XRD analysis results (weight %) of the bulk, micronized and calcium saturated samples.

Sample	Pl	Or	Anl	Dioctahedral Sm	Aug	Trioctahedral Sm	Chl	Qtz	Interstratified Chl-Sm	Others
DM Dewhurst DDH1, 293.8 m	44				21	24	6	1		3
Tintsfield 1, 624 m	23	15	13	3	21	10	7	1		6
DME Narrabri 28, 116,4 m	33	12		2	17	18	9	<1		9
DME Narrabri 6, 62.4 m	47	3						11	32	6
DME Parkes 3, 200.4 m	13			43		7	3	15		17

Note: Pl-plagioclase, Or-K-feldspar, Anl-Analcite, Aug-Augite, Sm-smectite, Chl-chlorite, Qtz-quartz, Others-hematite, ilmentite, magnetite, linotilolite-Na, fluorapatite, rutile, anatase, calcite, most of which are less than 1%. Depth intervals are rounded to the nearest 0.1 m.

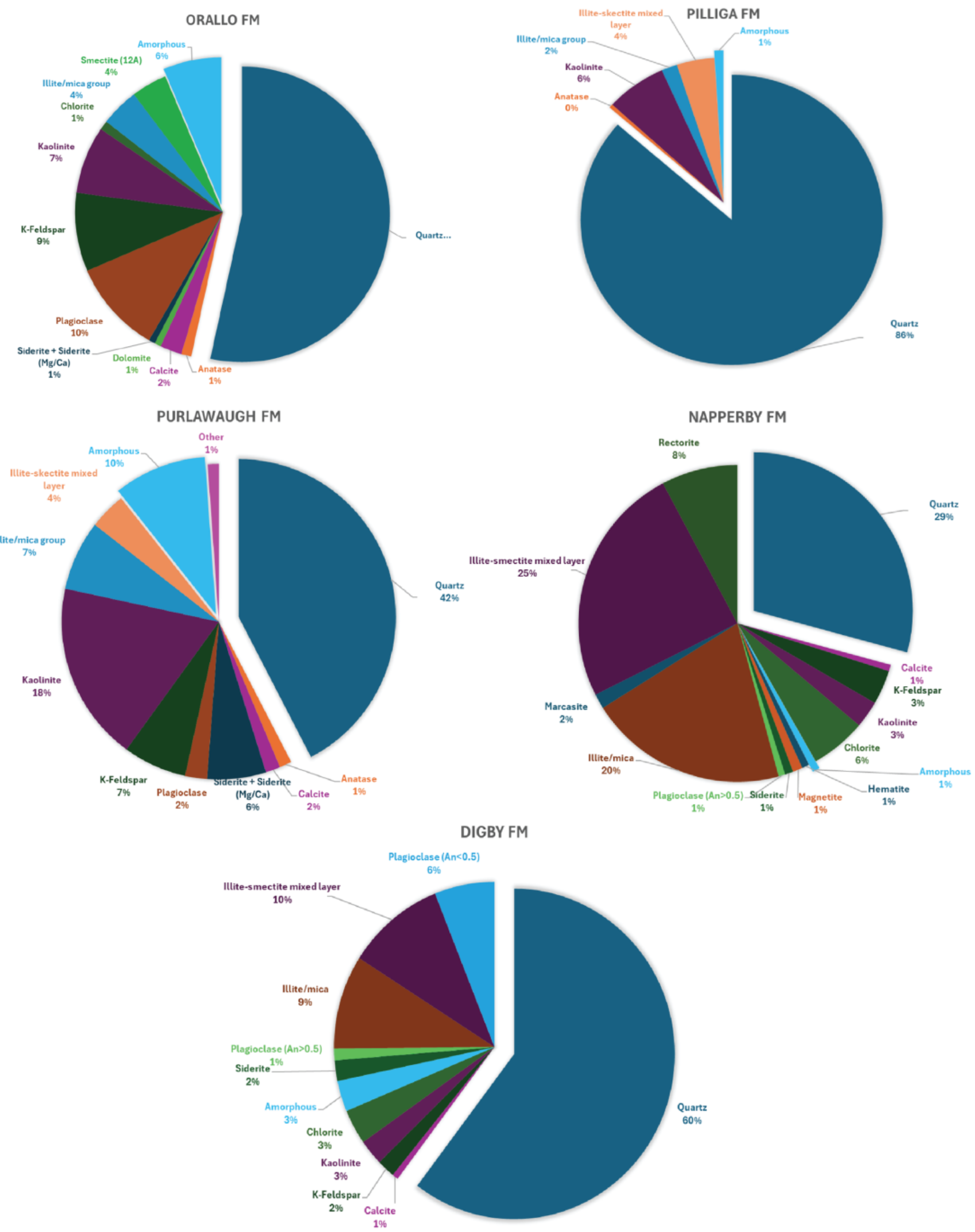

Silicate minerals	Quartz, Plagioclase, K-Feldspar
Clay minerals	Illite/mica, Kaolinite, Smectite, Illite-smectite mixed layer, chlorite
Carbonate minerals	Calcite, dolomite, siderite
Evaporite	Halite
Accessory minerals	Brookite, anatase
Sulfide mineral	Pyrite

Figure 3-11 – X-ray diffraction (XRD) showing mineralogical composition of Surat Basin and shallow Gunnedah Basin formations. Where multiple measurements were available for a formation, the median composition is presented.

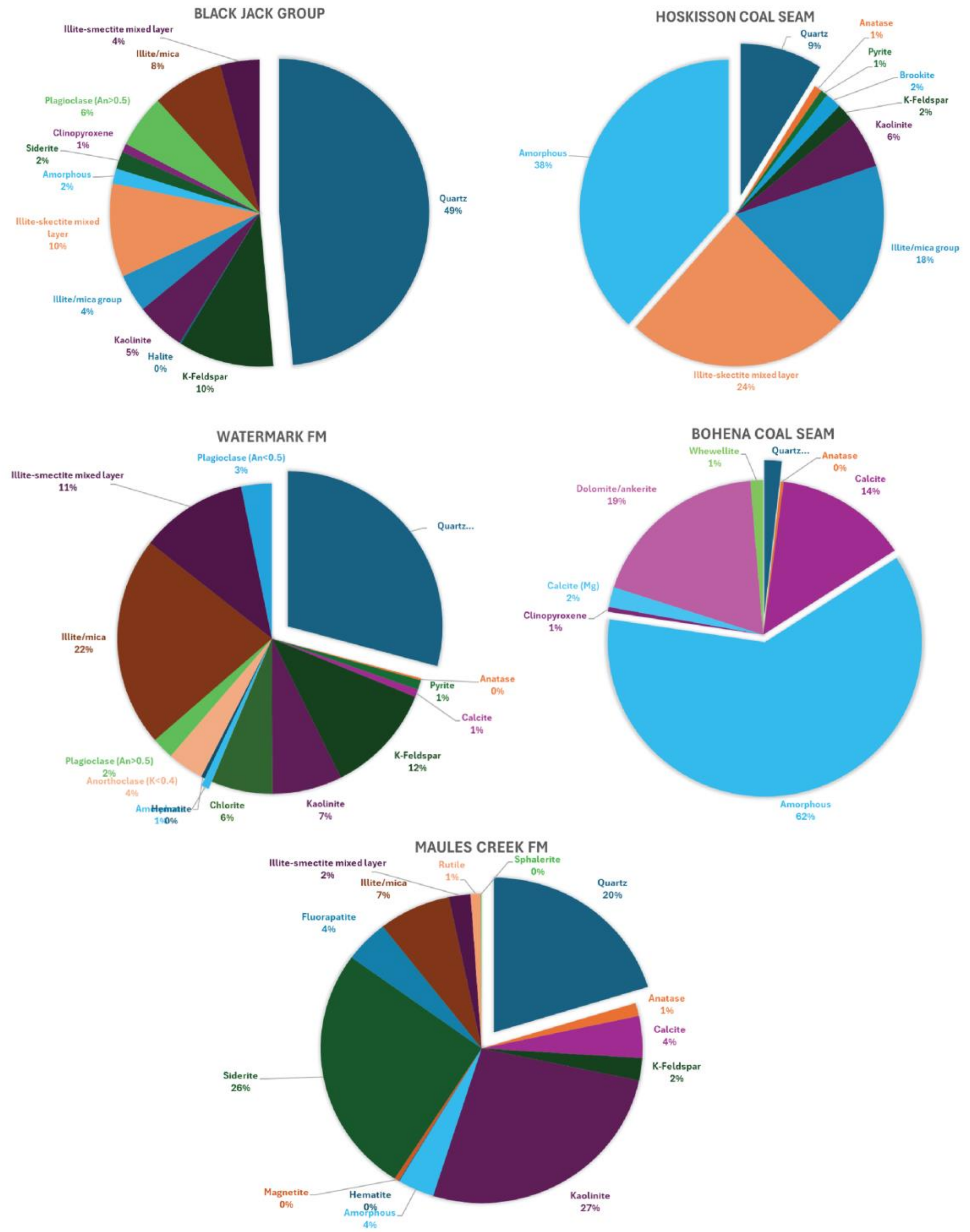

Silicate minerals	Quartz, Plagioclase, K-Feldspar
Clay minerals	Illite/mica, Kaolinite, Smectite, Illite-smectite mixed layer, chlorite
Carbonate minerals	Calcite, dolomite, siderite
Evaporite	Halite
Accessory minerals	Brookite, anatase
Sulfide mineral	Pyrite

Figure 3-12 – X-ray diffraction (XRD) showing mineralogical composition of deeper Gunnedah Basin formations. Where multiple measurements were available for a formation, the median composition is presented.

3.3.2 Strontium isotopes

The strontium isotope signature ($^{87}Sr/^{86}Sr$) measured in rock core samples, displayed by depth and according to the hydro-stratigraphic log of the following core samples (A) Coonarah 2, (B) Tintsfield 1, and (C) Tunmallallee, are shown in Table 5 and Figure 3-13. In the hydrostratigraphic column, each geological unit is represented by a colour corresponding to its hydrogeological characterisation as aquitard, partial aquifer or aquifer.

Strontium isotope values are shown in Table 5. The $^{87}Sr/^{86}Sr$ signature from the Surat Basin formations is relatively narrow, ranging from 0.71087 to 0.71987. Strontium signatures of rocks from the Gunnedah Basin formations are more variable (ranging from 0.70559 to 0.72424), with the lowest values observed within the Hoskissons Coal seam (hosted within the Black Jack Group) and Bohena Coal seam (hosted within the Maules Creek Formation) and the highest within the Napperby and Digby formations (Figure 3-13).

The $^{87}Sr/^{86}Sr$ of intrusive rocks (based on the analysis of 11 samples) are within a narrow range of 0.7038 to 0.7060. Their $^{87}Sr/^{86}Sr$ does not show any relationship with age of the intrusion. The range of $^{87}Sr/^{86}Sr$ of intrusive rocks is similar to the range (0.7031 to 0.7047) presented by Raiber et al. (2024) for igneous (extrusive) rocks in the Surat and Clarence-Moreton basins in Qld.

Table 5 Strontium isotope signatures of rocks (min, max and samples count (N)) displayed by stratigraphic unit and according to analytical method (i.e. whole rock or partial digestion by weaker acid)

	Rock Formation	$^{87}Sr/^{86}Sr$ whole rock			$^{87}Sr/^{86}Sr$ rocks (partial digestion)		
		Min	Max	N	Min	Max	N
Surat Basin	Orallo Fm.	0.71168	0.71168	1	0.70529	0.70529	1
	Pilliga Sandstone	0.71087	0.71807	10	0.71518	0.7192	3
	Purlawaugh Fm.	0.71276	0.71987	3	0.70931	0.70931	1
Igneous rocks	Igneous rocks	0.70381	0.70605	11			
Gunnedah Basin	Napperby Fm.	0.70588	0.72424	4			
	Digby Fm.	0.71541	0.72152	3			
	Black Jack Group	0.71278	0.71278	1			
	Hoskisson Coal Seam	0.70620	0.71808	4	0.70662	0.7067	2
	Watermark Fm.	0.71964	0.71964	1			
	Maules Creek Fm.	0.70806	0.70806	1			
	Bohena Coal Seam	0.70559	0.71756	2			

Selected rock samples were also analysed using partial digestion with a weaker acid (1M acetic acid) to represent the more reactive and soluble mineral phases of the rocks that are likely to interact with groundwater as described by Raiber et al. (2024) for the Surat Basin in Qld. In the study of the Surat Basin in Qld, the partially digested samples generally yielded lower $^{87}Sr/^{86}Sr$

values. In the present study, the partial digestion did not result in significantly lower $^{87}Sr/^{86}Sr$ for the Pilliga Sandstone samples, but resulted in a significant decrease of the $^{87}Sr/^{86}Sr$ ratio of an Orallo Formation sample (Figure 3-13).

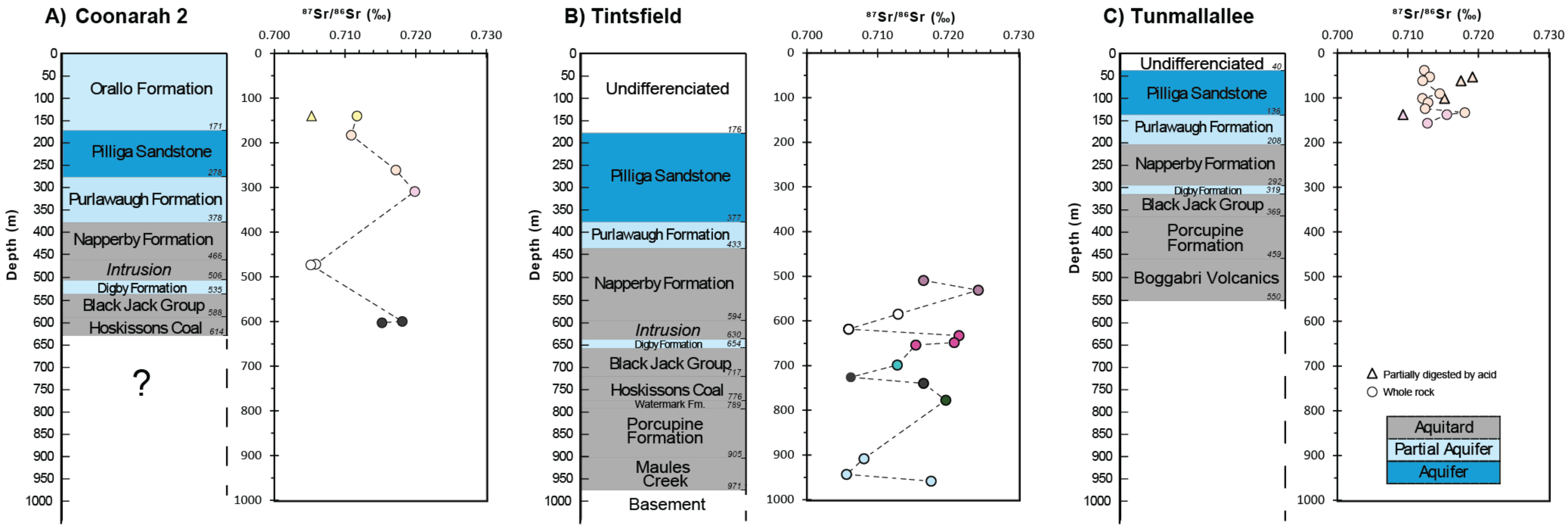

Figure 3-13 - Strontium isotope ($^{87}Sr/^{86}Sr$) signature in rock (core) samples.

Triangles refer to analyses made from partially digested rocks via treatment by acetate acid, whereas dots represent the whole rock strontium isotope signature (analysed via full digestion with hydrofluoric acid). Questions marks represent undifferentiated units between the last one displayed and the basement.

3.3.3 Thin sections of igneous intrusive rocks

A petrographic analysis of thin sections of igneous intrusive rock samples obtained from different exploration wells was conducted to support the interpretation of rock age dating results and the general understanding of the role of intrusions as potential connectivity pathways in the Narrabri region.

Petrography microscopy images and interpretations for selected thin sections are presented below. The mineralogical analysis confirmed that many of the igneous rock samples are dominated by quartz, plagioclase and pyroxene, although other minor minerals such as for example analcime, magnetite and fluorapatite were also detected. To complement the quantification of mineral composition, the assessment of thin sections focussed on the identification of fractures and mineral alteration, which will support the interpretation of the geochronological (age) assessment of the igneous rocks in the Narrabri region.

Parkes 3 (collected at 200.38 to 200.40 m depth below ground level)

The igneous rock at Parkes 3 (Figure 3-14 to Figure 3-16) is a sample of a substantially altered basalt. Some primary texture of the rock is preserved, including randomly oriented plagioclase laths and sparse coarser grained basalt/dolerite xenoliths (Figure 3-14). Xenoliths are fragments of older rock incorporated into the igneous rock. Plagioclase and minor magnetite are the only remaining primary minerals. The alteration assemblage includes clays (largely smectite/chlorite), hematite, limonite, calcite, zeolite, and microcrystalline quartz.

Figure 3-15 shows an area within the thin section where primary minerals have been replaced by opaques oxides, smectite, chlorite and calcite. Patches of silicifications as microcrystalline quartz occur in the right half. Hairline fractures radiate out from the altered zone, and these are mostly unfilled.

Figure 3-16 shows variation in groundmass grainsize, attributed to xenoliths with a prominent, medium-grained, brown, glassy xenolith shown near the centre of the image. The groundmass is mostly devitrified to brown clayey material, although isotropic areas remain. A ring of opaque oxides (likely magnetite) surrounds the xenolith, indicating a reaction rim when it was incorporated into the melt. Amygdales occur in the lower left and top of the image, both filled with patchy calcite, hematite, zeolite and orange smectite.

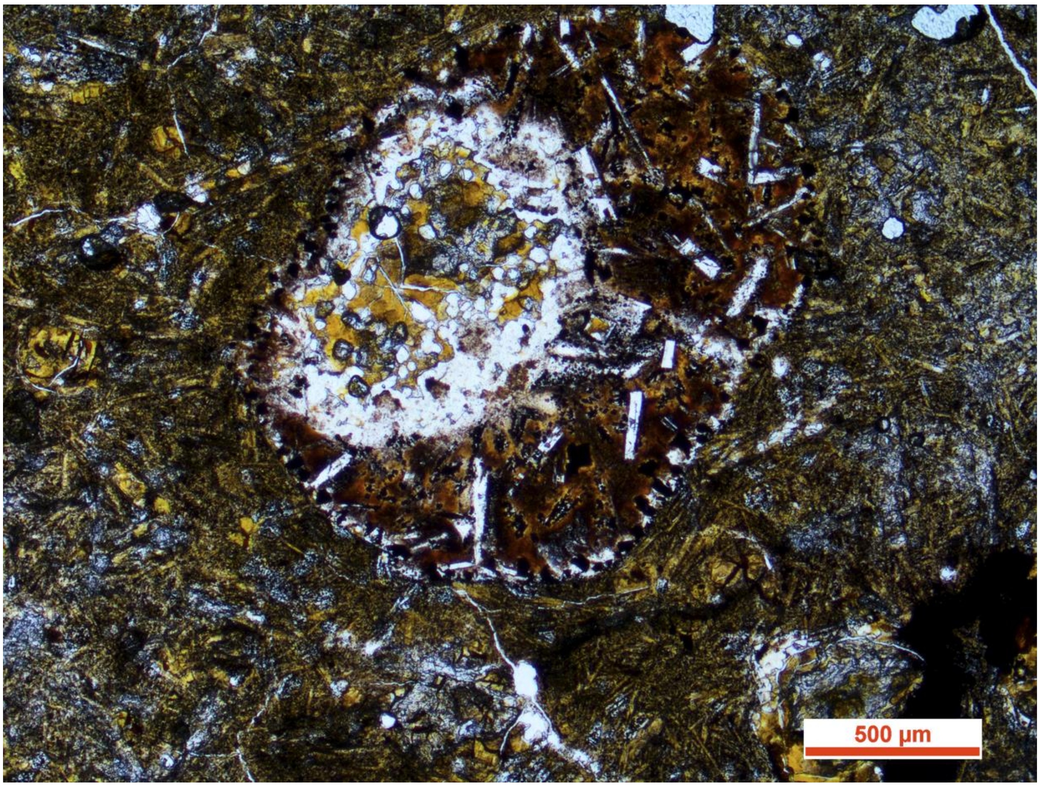

Figure 3-14 – Thin section of Parkes 3 (PPL)

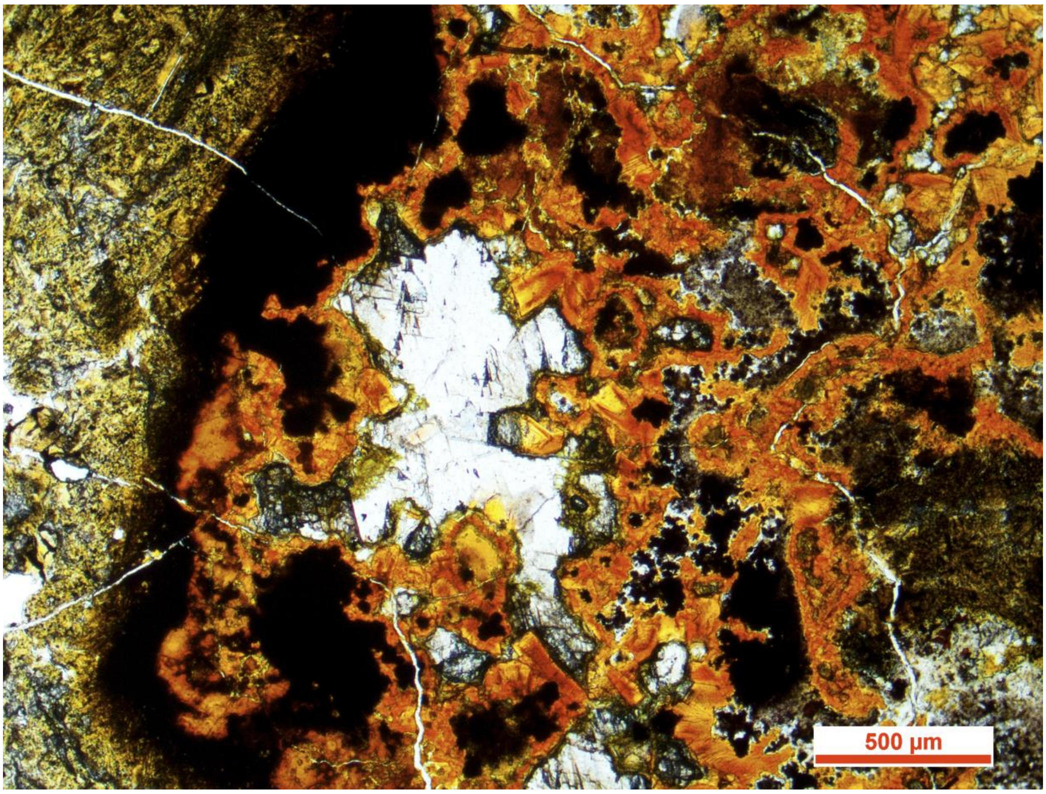

Figure 3-15 – Thin section of Parkes 3 (200.38-200.40 m depth)

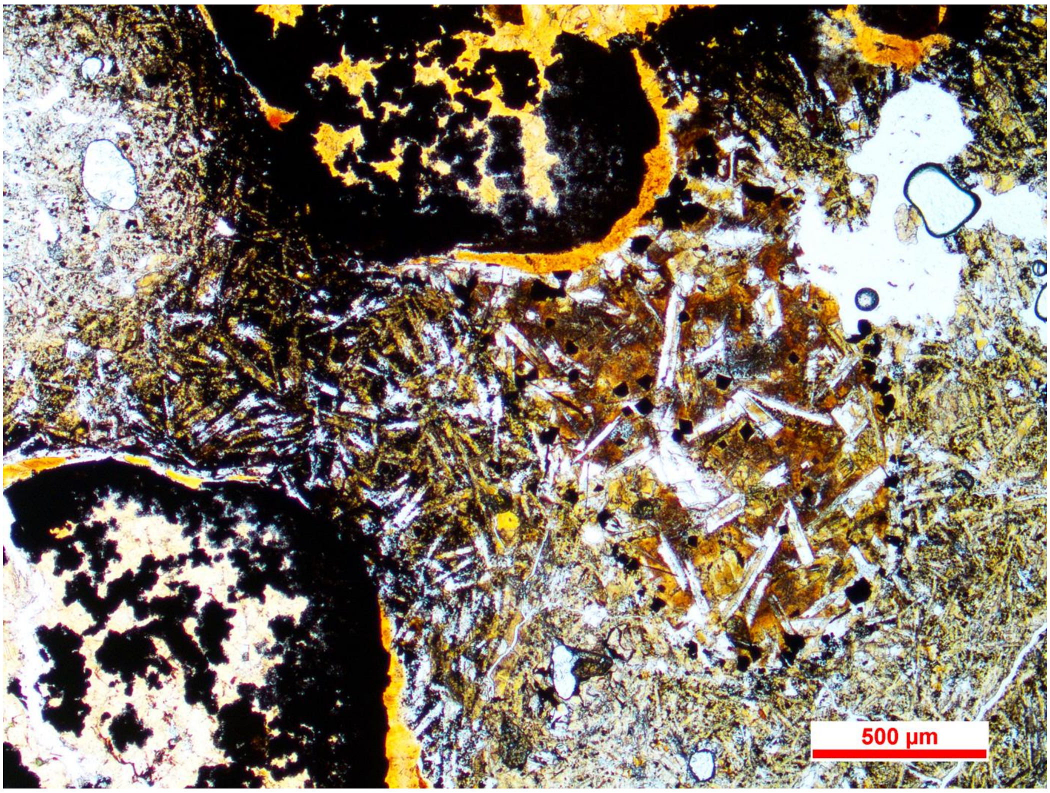

Figure 3-16 – Thin section of Parkes 3 (200.38-200.40 m depth)

Dewhurst DDH1 (collected at a depth of 293.80-293.87 m below ground level)

The sample collected from Dewhurst DDH1 is a sample of a mildly altered ophitic dolerite. Most primary textures and minerals are preserved, including coarse plagioclase laths, pyroxene (augite) oikocrysts and anhedral interstitial magnetite. Alteration includes total replacement of interstitial glass by pale brown smectite/chlorite, and replacement of olivine by orange-brown smectite/chlorite.

Figure 3-17 shows ophitic texture in the sample, with augite oikocrysts enclosing medium plagioclase laths. Interstitial magnetite is moderate in abundance as anhedral opaque crystals. In the centre of the image, former olivine is fully replaced by orange-brown smectite-chlorite. Pale brown areas are fully altered interstitial glass, also to smectite and chlorite.

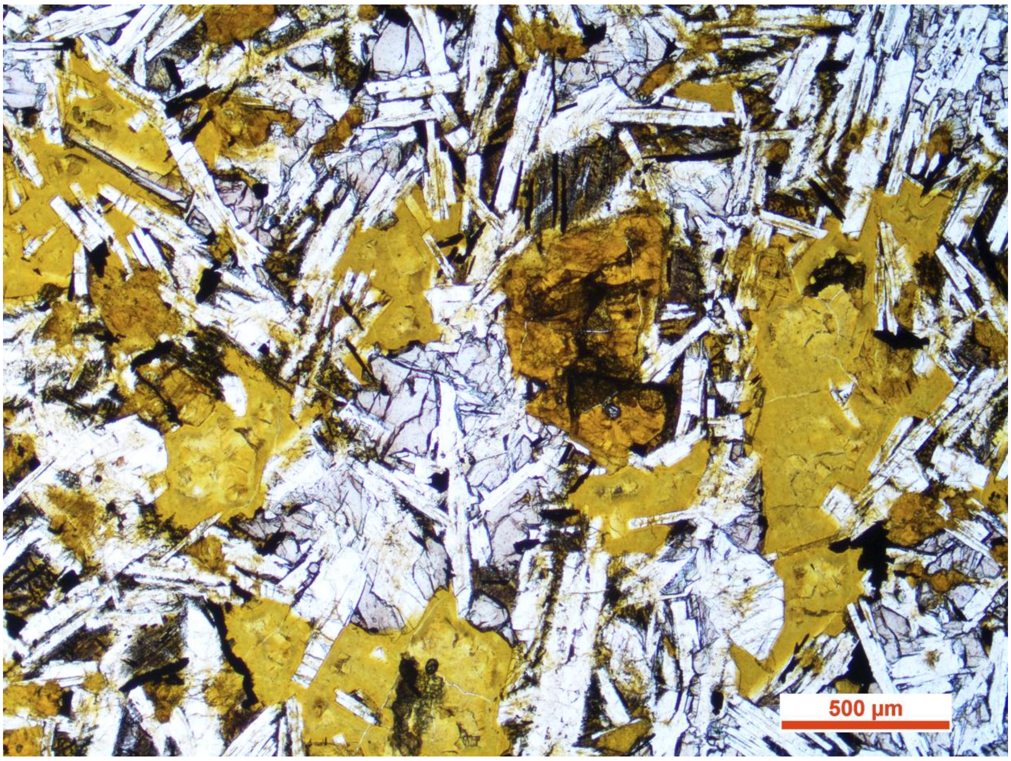

Figure 3-17 – Thin section of Dewhurst DDH1 (PPL) (293.80-293.87m).

Turrawan 1 (collected at 24.93 to 24.96 m below ground level)

The sample collected from Turrawan 1 (Figure 3-18) represents a mildly altered ophitic dolerite. The primary texture and mineralogy is similar to the Dewhurst DDH1 sample, but it differs slightly in alteration. In this image, much of the glass is altered to smectite/chlorite. A >1 mm long plagioclase crystal is visible in the centre.

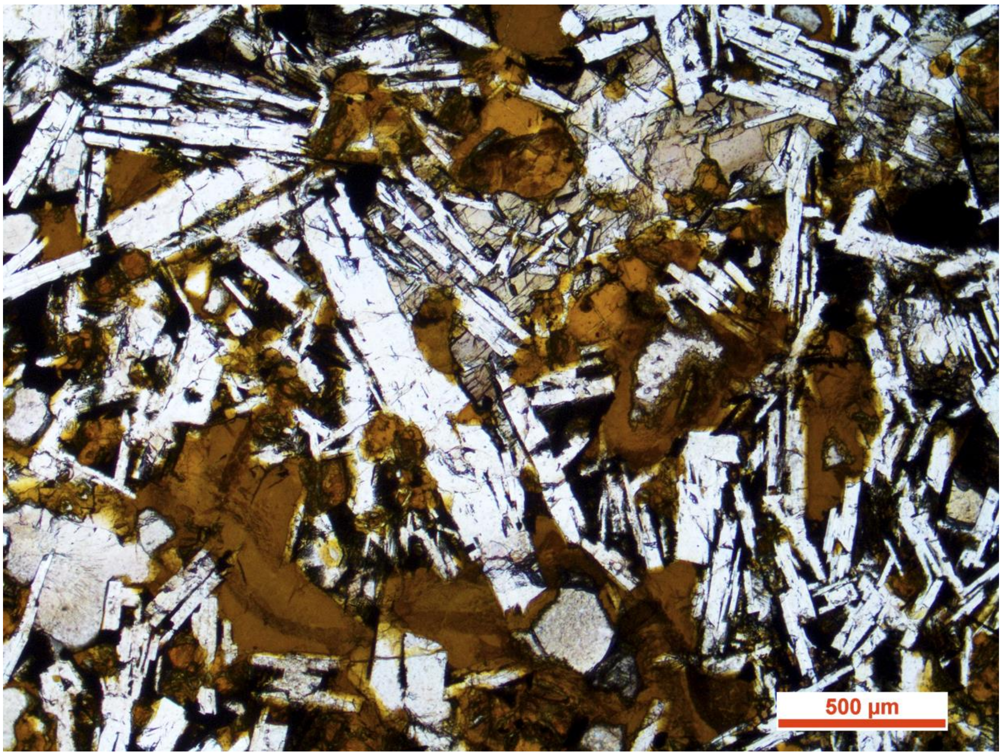

Figure 3-18 – Thin section of Turrawan 1 Set 3 PPL

Narrabri 6 (collected from 62.30-62.50 m below ground level)

The rock sample from Narrabri 6 is a substantially altered glassy basalt (Figure 3-19). The primary texture of the rock is preserved as randomly oriented, medium-sized plagioclase laths. Alteration is at a slightly higher grade than at the sample from the Parkes 3 exploration well and includes abundant silicification and spherical replacement structures in the glass.

Figure 3-20 shows a spherical structure appearing to replace an area of glass or an amygdule. It shows abundant silicification as microcrystalline quartz within the structure and along a cross-cutting vein. Strongly pleochroic green actinolite forms “wedges” within the structure. Minor alteration phases here include dusty clayey material and fine-grained calcite. Dark interstitial glass in the surrounding groundmass is variably replaced by smectite/chlorite.

Figure 3-21 shows the texture and mineralogy observed throughout most of the sample. Plagioclase laths retain their primary shape but contain mild albitization, sericitisation and patchy replacement by microcrystalline quartz. Interstitial space is filled with dark glass or fully altered to microcrystalline quartz, calcite, and/or smectite/chlorite.

Figure 3-22 shows a large vein passing through a corner of the thin section. The vein contains large areas of microcrystalline quartz with wispy staining by goethite, chlorite and clay. The left side of the image shows calcite partially replacing the quartz in the vein, resulting in it having a dusty colour due to abundant inclusions. A significant amount of calcite was also detected in XRD for the sample collected from another depth interval (117.55 to 117.59) of the Narrabri 6 exploration well. A sparry calcite vein cuts through the quartz in the upper centre. Wispy smectite and goethite occur in some areas.

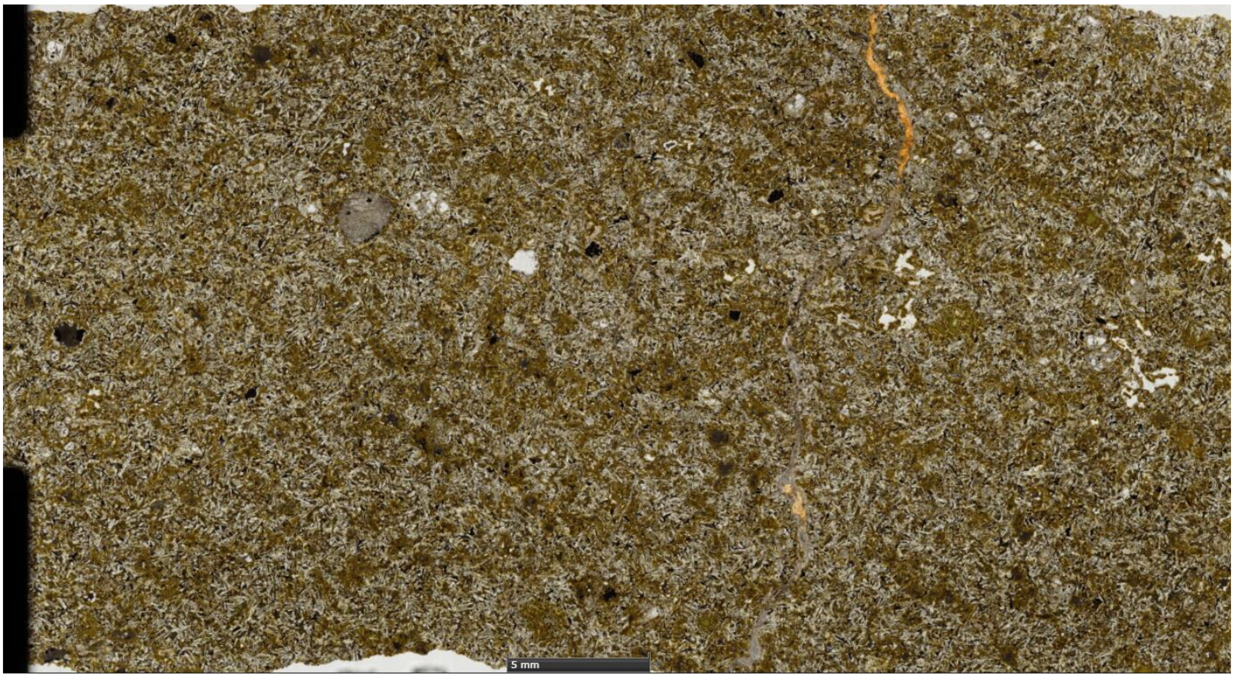

Figure 3-19 – Thin section of Narrabri 6 at 10x exaggeration.

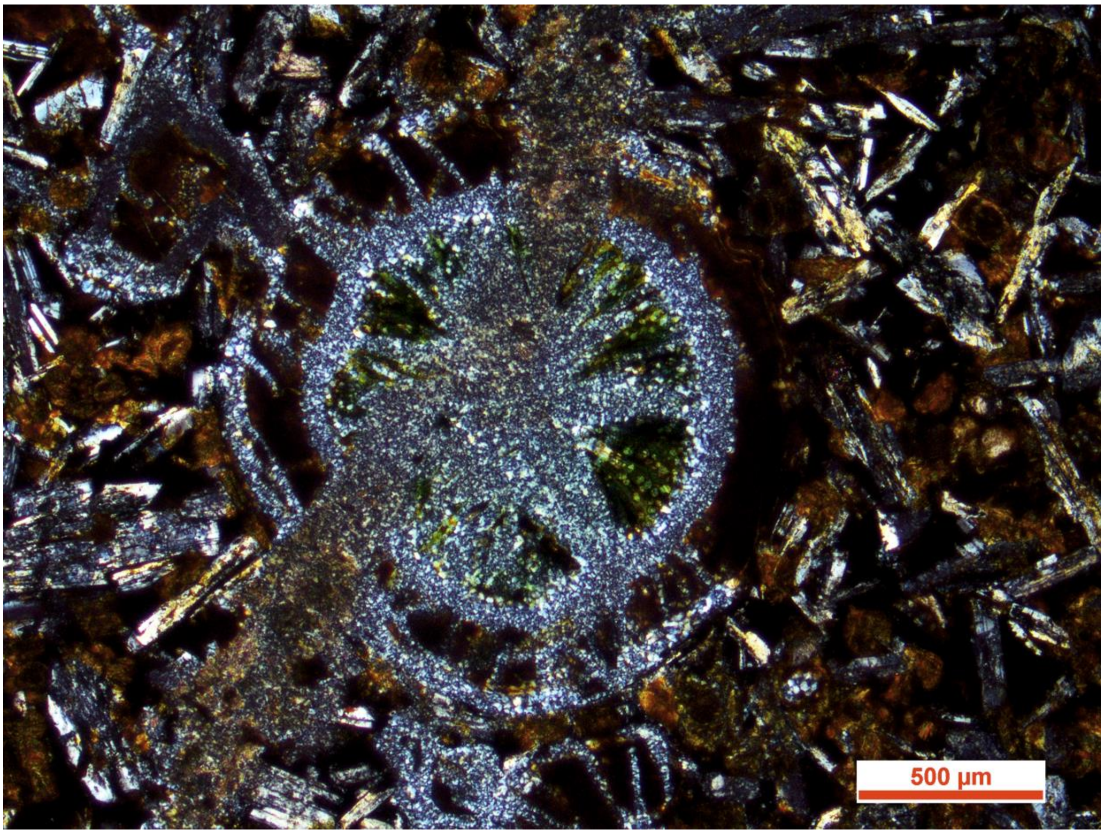

Figure 3-20 – Selected part of thin section of Narrabri 6 Set 1 XPL

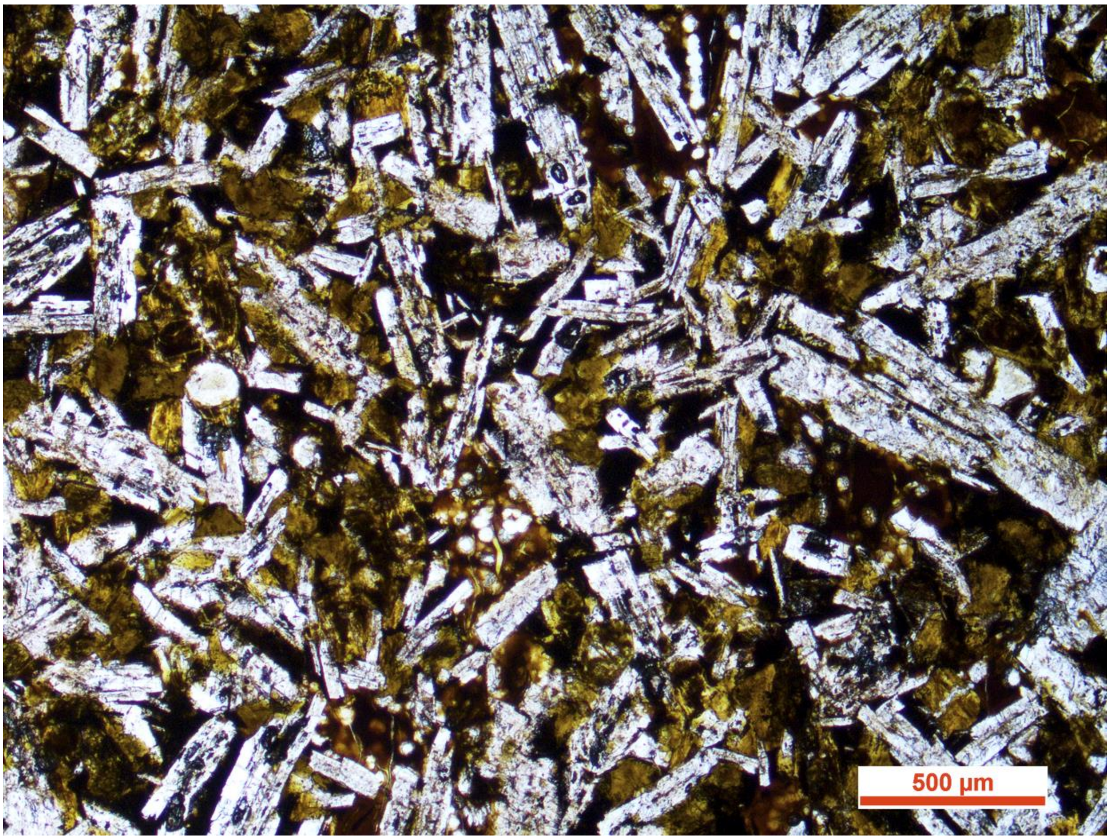

Figure 3-21 – Selected part of thin section of Narrabri 6 Set 1 XPL

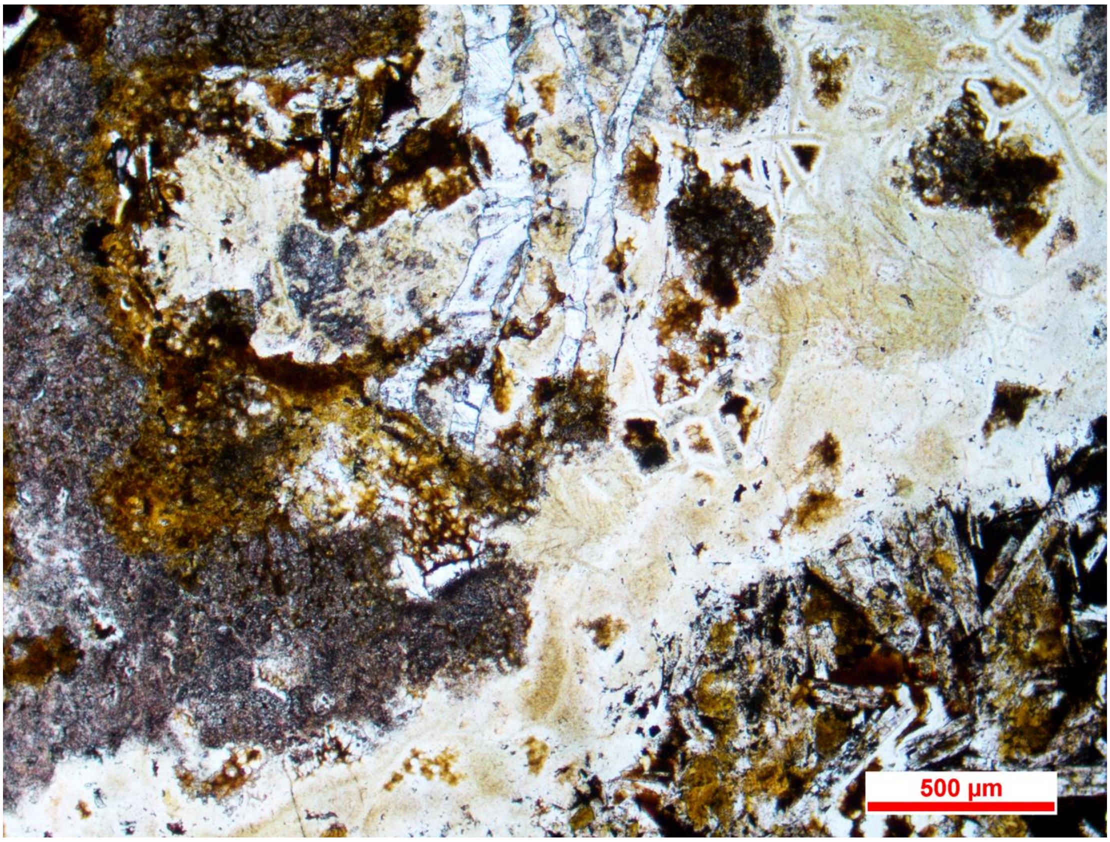

Figure 3-22 – Selected part of thin section of Narrabri 6 Set 5 XPL

Summary

Although the visual assessment of rock samples at the core library suggested that most samples are fresh without obvious alterations, the microscopic examination showed that some of the samples were significantly altered. The XRD showed presence of large amounts of smectite, chlorite and calcite in some samples, also suggesting that there are significant alterations in some of the rock samples.

In igneous rocks, smectite, which was identified both in thin section and in the XRD analyses for some samples, is often a product of weathering. Smectite minerals often form through the alteration of igneous rocks in environments with high rainfall. However, most igneous rock samples analysed in this study are intrusive rock samples that were likely not exposed to surface weathering, and smectite can also form in the subsurface through hydrothermal alteration processes, where hot, mineral-rich fluids interact with the rock, altering its mineral composition. In intrusive rocks, chlorite forms primarily through hydrothermal alteration or low-grade metamorphism in veins as an alteration product of mafic minerals (e.g. pyroxene and olivine) at temperatures above 220^{o}C (Fulignati, 2020). Minerals of the smectite group are also commonly found in hydrothermal alteration facies (Fulignati, 2020). There is no evidence for an increased geothermal gradient in the Narrabri Gas Project area at present, and the identification of chlorite and abundance of smectite in thin-sections and XRD suggests that hydrothermal processes have occurred here at the time of igneous activity.

For the results of the K/Ar dating technique to be valid, the system must have remained closed and cooling after the volcanic event must have occurred rapidly (New Mexico Geochronology

Research Laboratory, 2025). Alteration and high temperature can affect the rock and mineral lattice sufficiently to allow radiogenic ^{40}Ar to be released, which can result in a younger calculated K/Ar compared to the true age of the rocks.

Conversely, excess argon (^{40}Ar that is attributed to radiogenic ^{40}Ar and/or atmospheric ^{40}Ar) may be derived from the mantle (e.g. as bubbles trapped in a melt) or it could be a xenocryst/xenolith trapped in a magma/lava during emplacement of the intrusion (New Mexico Geochronology Research Laboratory, 2025). For example, xenoliths (Figure 3-14) can contain inherited argon, which was produced by the decay of potassium in the xenolith before it was incorporated by the host rock. When K/Ar dating is performed, this inherited argon can lead to an overestimation of the age of the rock (Phillips, 2015). The presence of calcite veins can also affect the results of the K/Ar dating.

The implication for the K/Ar dates will be discussed in the next section.

3.4 K-Ar age dating

The results of seventeen conventional K/Ar ages of igneous intrusive rocks (see Table 6 and Figure 3-23 for the detailed compilation of historic and our new age dating results) conducted during this study combined with historic K-Ar and $^{40}Ar/^{39}Ar$ data sourced from Gibson (2007) and NSW MinView (NSW Geological Survey, 2021) show that there were multiple phases of intrusive activity during the Mesozoic and Cenozoic in the Narrabri region, with the minimum and maximum ages obtained in this study ranging from 229 ± 5 million years to 50 ± 1 million years (Table 6).

Historic geochronological (K-Ar) dating of basalt samples from the Nandewar Range to the north-east and the Warrumbungle Volcanic Complex to the south of the Narrabri Gas Project area yielded Cenozoic ages indicating that the eruption of magmas has occurred here approximately 13 to 20 million years ago. Samples collected from the Garrawilla Volcanics to the east of the Narrabri Gas Project area yielded Late Triassic to Early Jurassic ages (~175 to 206 million years), stratigraphically placing this formation at the interface between the shallowest formation of the Gunnedah Basin (Napperby Formation) and the basal formation of the Surat Basin (Purlawaugh Formation).

Some exploration well completion reports in the Narrabri Gas Project area suggested a Tertiary (an outdated stratigraphic term now replaced by “Cenozoic”) age for intrusions in this region at Nyora (number 1 in Figure 3-23). However, the mafic intrusion intersected in well Nyora 1 at the north-western edge of the Narrabri Gas Project (Figure 3-23) area yielded a K–Ar isotopic age of 203 ± 2 Ma (corresponding to Early Jurassic) (Morrison and Harris, 1988; Totterdell et al., 2009).

Age determination of igneous rocks collected from within or near the Narrabri Gas Project area in the current study demonstrate that the timing of intrusive activity was more variable than what was previously captured by the historic geochronological data to the north and east, with main phases of igneous activity occurring during the Late Triassic, Early and Middle Jurassic and Cretaceous periods. In addition, a core sample from Coonarah 2 at ~ 471.75 m suggests that a more recent intrusive event has occurred in the Eocene (~50 million years ago) representing the only sample within the Narrabri Gas Project area yielding a Cenozoic age. The samples at Connarah

2 were collected from an area where the AEM survey and seismic data indicate the presence of a forced fold associated with a significant intrusion.

Table 6 K-Ar dating results of core samples from various intrusions within the Narrabri Gas Project region.

Exploration well	Sample depth (m)	Age (Ma)	Error (Ma)	Geological Time
Rosevale 1	559.74 - 559.94	229	5.3	Carnian, Upper Triassic
Dewhurst DDH1	293.80 - 293.87	172.5	4	Aalenian, Middle Jurassic
DME Narrabri 38	183.00 - 184.00	171.6	4	Aalenian, Middle Jurassic
Jacks Creek DDH1	412.88 - 413.03	202.1	4.7	Rhaetian, Upper Triassic
Tintsfield 1	618.24 - 618.39	173.5	4	Aalenian, Middle Jurassic
Tintsfield 1	623.48 - 624.58	187	4.4	Pliensbachian, Lower Jurassic
Bohena 1	571.80 - 571.85	177.6	5.3	Toarcian, Lower Jurassic
DME Narrabri 14	87.32 - 87.35	143.6	6.3	Berriasian, Lower Cretaceous
DME Narrabri 28	116.40 - 116.43	229.3	6.2	Carnian, Upper Triassic
DME Narrabri 6	62.50 - 62.30	90.3	3.4	Turonian, Upper Cretaceous
DME Narrabri 6	117.55 - 117.59	186.6	6.6	Pliensbachian, Lower Jurassic
Parkes 3	200.38 - 200.40	116.9	2.8	Aptian, Lower Cretaceous
Parkes 3	226.35 - 226.38	132.8	6.5	Hauterivian, Lower Cretaceous
Turrawan 1	24.93 - 24.96	171.9	19.1	Aalenian, Middle Jurassic
Turrawan 1	109.26 - 109.28	211.6	4.9	Norian, Upper Triassic
Coonarah 2	471.74 - 471.75	50.4	1.2	Ypresian , Eocene, Paleogene
Coonarah 2	473.23 - 473.25	71.4	1.7	Maastrichtian, Upper Cretaceous

This wide range of ages of intrusive and extrusive activity indicated by the geochronological data is likely related to large-scale tectonic processes in Eastern Australia at this time. The eastern margin of Australia has experienced complex deformation since the Triassic, principally controlled by the subduction of the Pacific plate beneath the Australian plate (e.g., Müller, et al, 2019). The igneous intrusions in the Mesozoic are most likely linked to collisional events due to the subduction of the Pacific plates beneath the Australian plate, whereas those after ~ 90 Ma are associated with the rifting and seafloor spreading in the Tasman Sea and Coral Sea (e.g, Müller, et al., 2016, Segev et al., 2012).

The most recent igneous activity (13-20 million years ago) during the Cenozoic generated the extrusive magmas of the Nandewar Volcanic Range and the Warrumbungles Volcanic Complex. Unlike for the Warrumbungle Volcanic Complex, no previous detailed geological study has been conducted for the Nandewar Volcanic Complex. However, given their similar age, common type (a central shield volcano) and common genesis in response to intraplate domains of high-heat flow, or 'hot-spot' magmatism (Bull et al., 2021), it is likely that the spatial patterns of intrusive features associated with these volcanoes are relatively similar at both volcanic centres. This suggests that the largest density of dykes occurs within the central volcano and that the dyke density decreases with increasing distance from the centre of the volcanic eruption, which is likely located near

Mount Lindesay and Mount Kaputar which are both visible as prominent features on the TMI map (Figure 2-5).

The presence of xenoliths and calcite veins identified in some thin sections that could lead to a loss of radiogenic Ar means that careful consideration of the results is required. The results need to be considered with some caution and assessed together with other lines of evidence. In future studies, other dating techniques could be employed to independently cross-check the results of the current study.

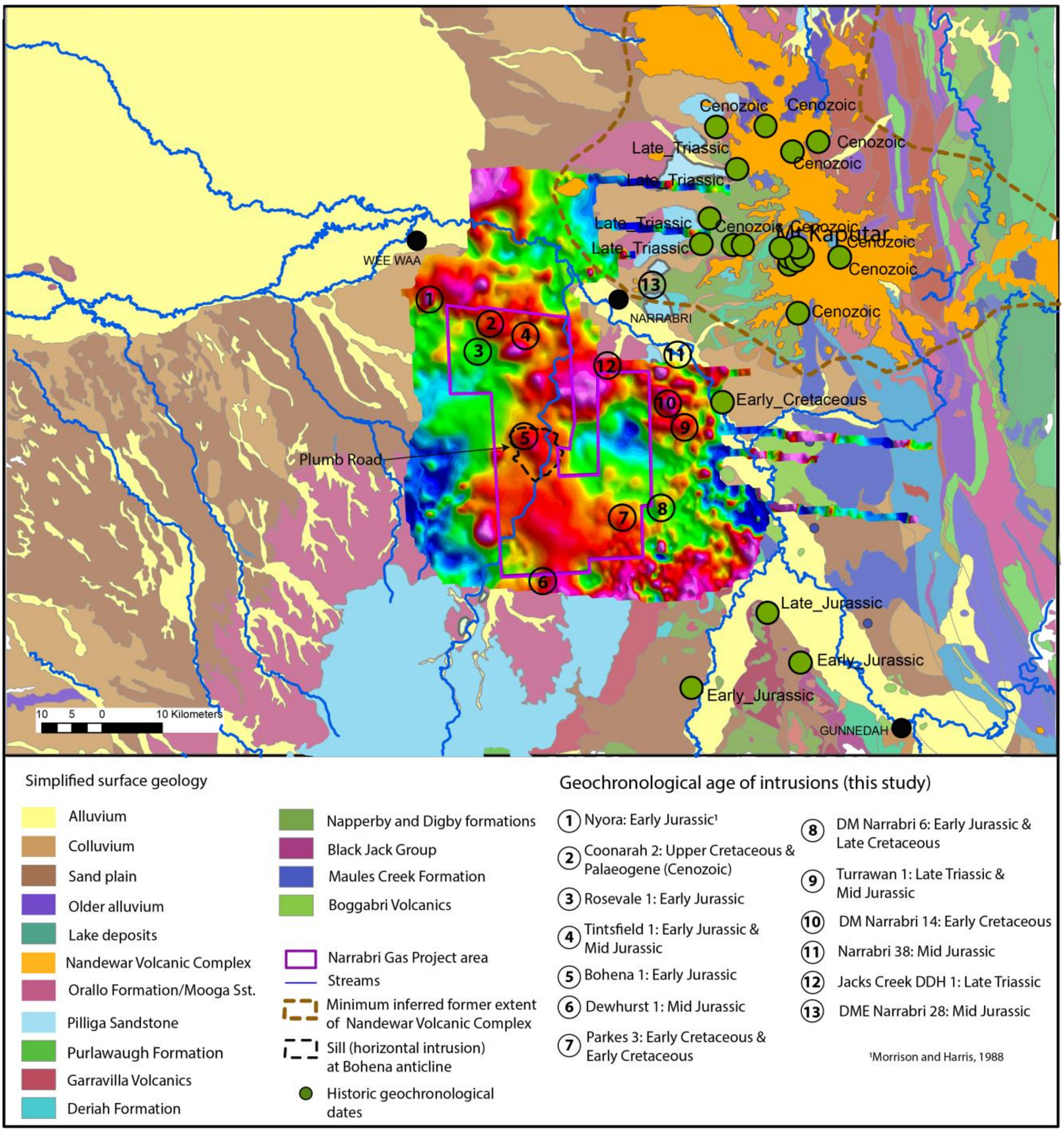

Figure 3-23 - Historic and new igneous (intrusive and extrusive) rock age analysis data and airborne magnetic survey overlain on simplified surface geology and total magnetic intensity. The scale for the total magnetic intensity survey data is shown in Figure 3-24.

Historic rock age data were sourced from NSW MinView.

Together with XRD analysis, AEM survey and tectonic history of the Namoi region, the geochronological dating results show that igneous intrusions, mainly sills (which are connected to a feeder dyke somewhere), were emplaced in the broader Narrabri Gas Project region during both the Mesozoic and Cenozoic. Igneous intrusions deform their intruded formations and cause fractures and often lead to dome-like structures in its vicinity (Section 1.3.3). These structures potentially enhance the hydraulic conductivity of the deformed formations that may connect formations at different depths and potentially act as pathways for deeper and usually older groundwaters in the Gunnedah Basin to migrate upwards into shallower aquifers, such as the Pilliga Sandstone and Orallo Formations. This will be discussed in following sections of this report.

3.5 Airborne geophysical survey

3.5.1 Total Magnetic Intensity

Total magnetic intensity maps display the intensity of the Earth's magnetic field, which is influenced by the magnetic properties of rocks (Section 2.2.5). A regional total magnetic intensity grid from Geoscience Australia (Figure 2-5; Minty and Poudjom Djomani, 2019) was used together with the newly developed AEM-based total magnetic intensity map (Figure 3-24) and its first derivative (Figure 3-25) to identify subsurface anomalies related to spatially extensive intrusions or other structural features in the Narrabri region. Intrusions can be often delineated as peaks in Total Magnetic Intensity maps due to their higher contents of magnetic minerals such as magnetite and hematite. The presence of magnetite or hematite has been identified by the XRD analysis and thin sections for many of the igneous samples analysed in this study, including for example at Coonarah (Figure 3-8) where the analysis yielded 4.1% of magnetite. Other prominent peaks can be identified on the Total Magnetic Intensity map and its first derivative at Nyora and Brigalo in the northern part of the Narrabri Gas Project area, at Bohena in the central part of the Narrabri Gas Project area and at the southern border of the area. These are locations where thicknesses of intrusive rocks larger than 100 m have been intersected in exploration wells.

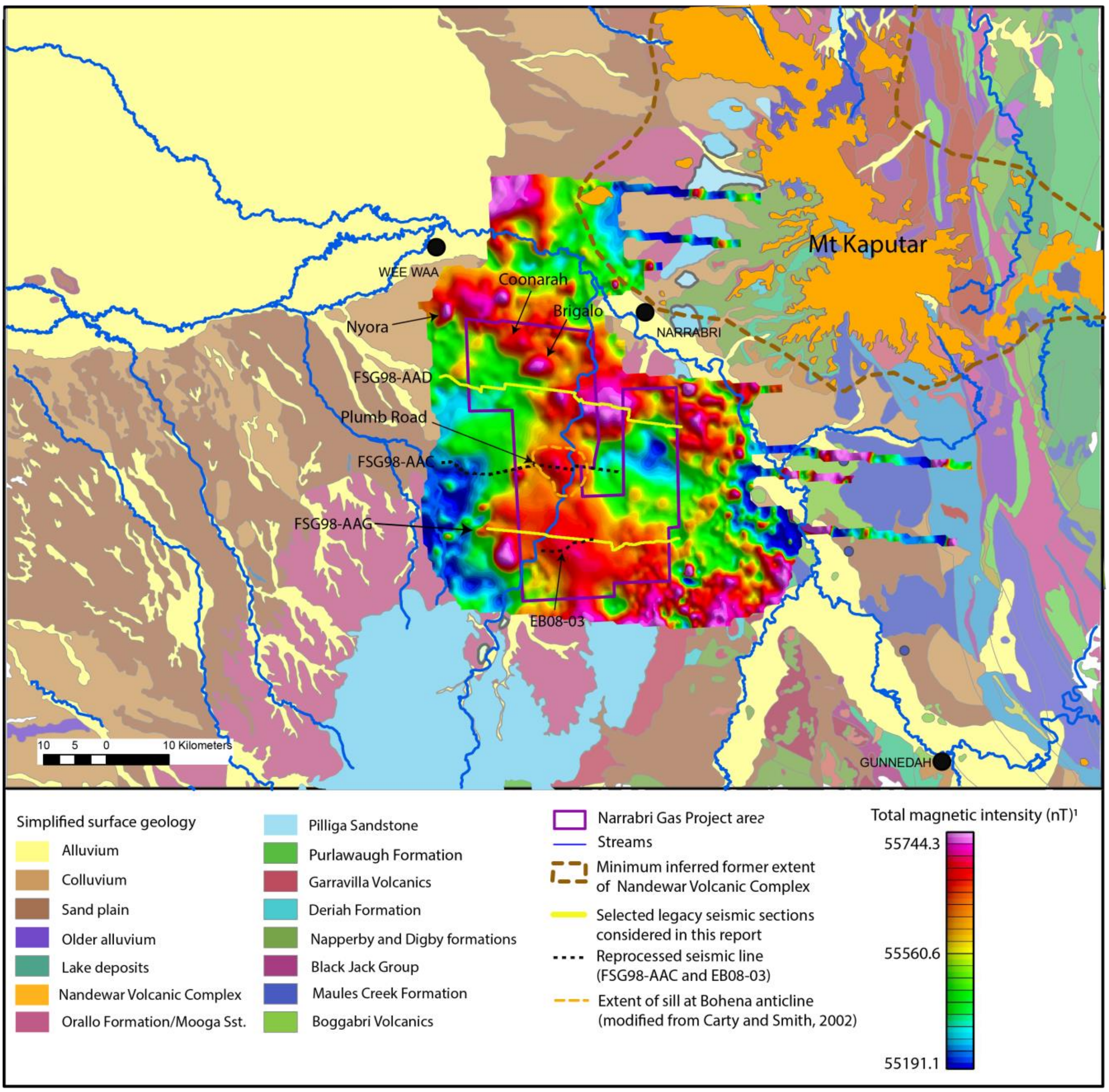

Figure 3-24 – Total Magnetic Intensity map in the Narrabri Gas Project area derived from SkyTEM airborne electromagnetic survey overlain on simplified surface geology.

Legacy and re-processed seismic lines, minimum inferred extent of former Nandewar Volcanic Complex and inferred extent of sill at Bohena anticline area also shown.

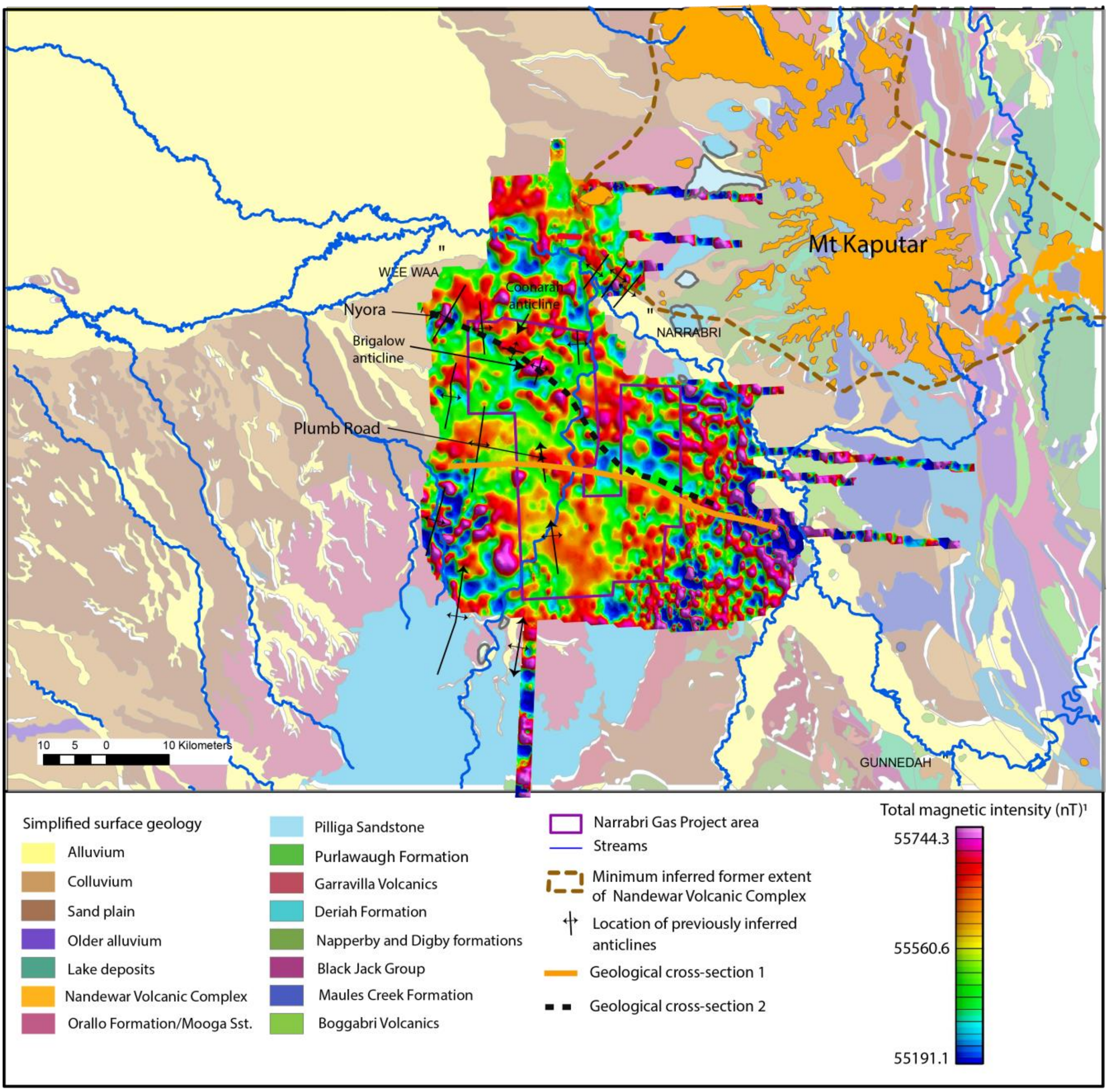

Figure 3-25 – First derivative of Total Magnetic Intensity map in the Narrabri Gas Project area derived from SkyTEM airborne electromagnetic survey overlain on simplified surface geology.

Inferred anticlines are based on Bretherton and Delbaere (1994), Tadros (1995), Eastern Star Gas (2004b) and Raiber et al. (2022a).

In a previous seismic survey at Coonarah and Brigalow, geological structures were identified in the Gunnedah Basin and extending to the base of the Purlawaugh Formation (Figure 3-27). These features were commonly described as anticlines or four-way closures and investigated as potential hydrocarbon traps (Section 1.3.2).

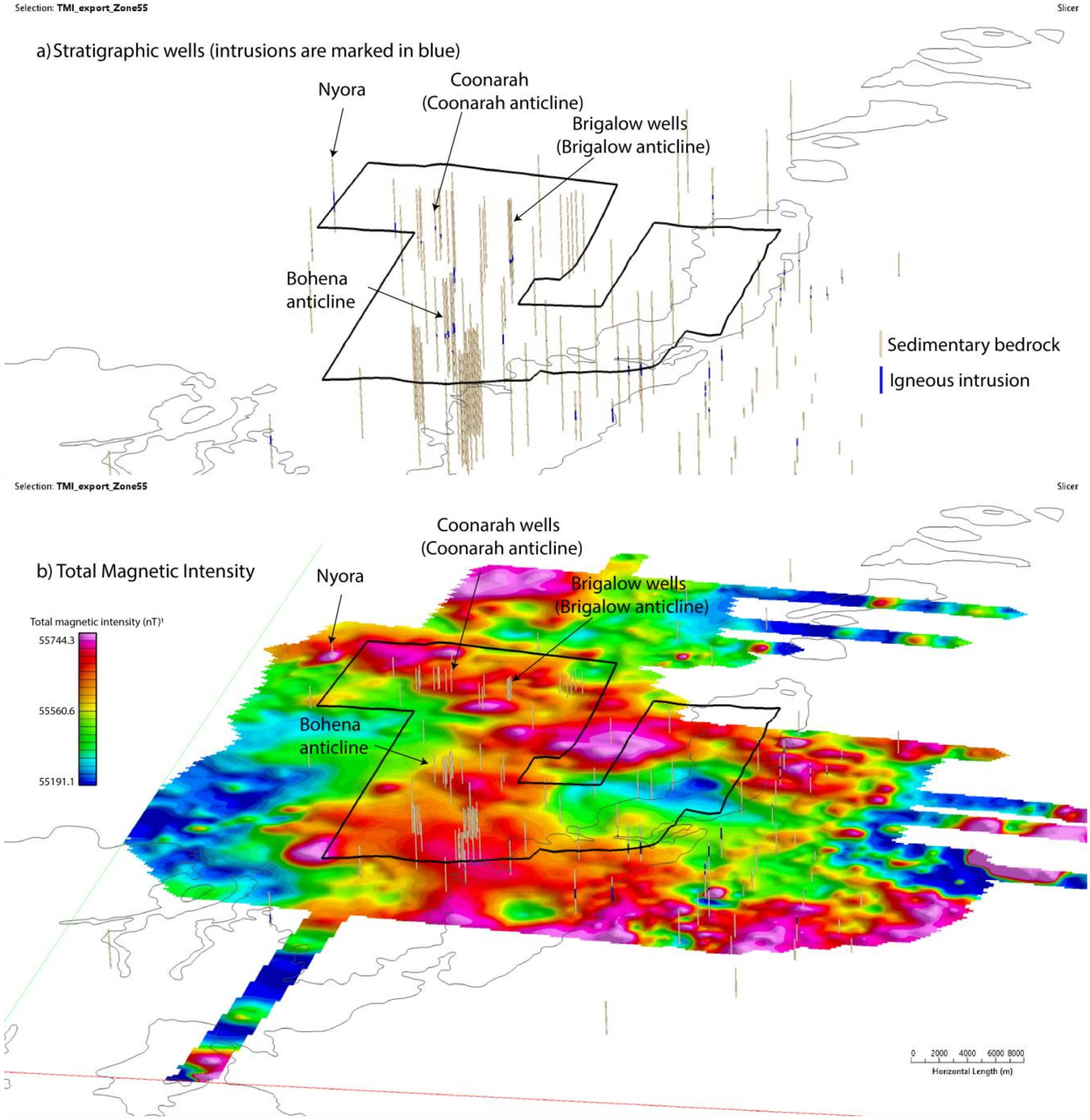

Figure 3-26 – Comparison of a) intersection of igneous rocks in stratigraphic wells with b) Total Magnetic Intensity map in the Narrabri Gas Project area derived from SkyTEM airborne electromagnetic survey.

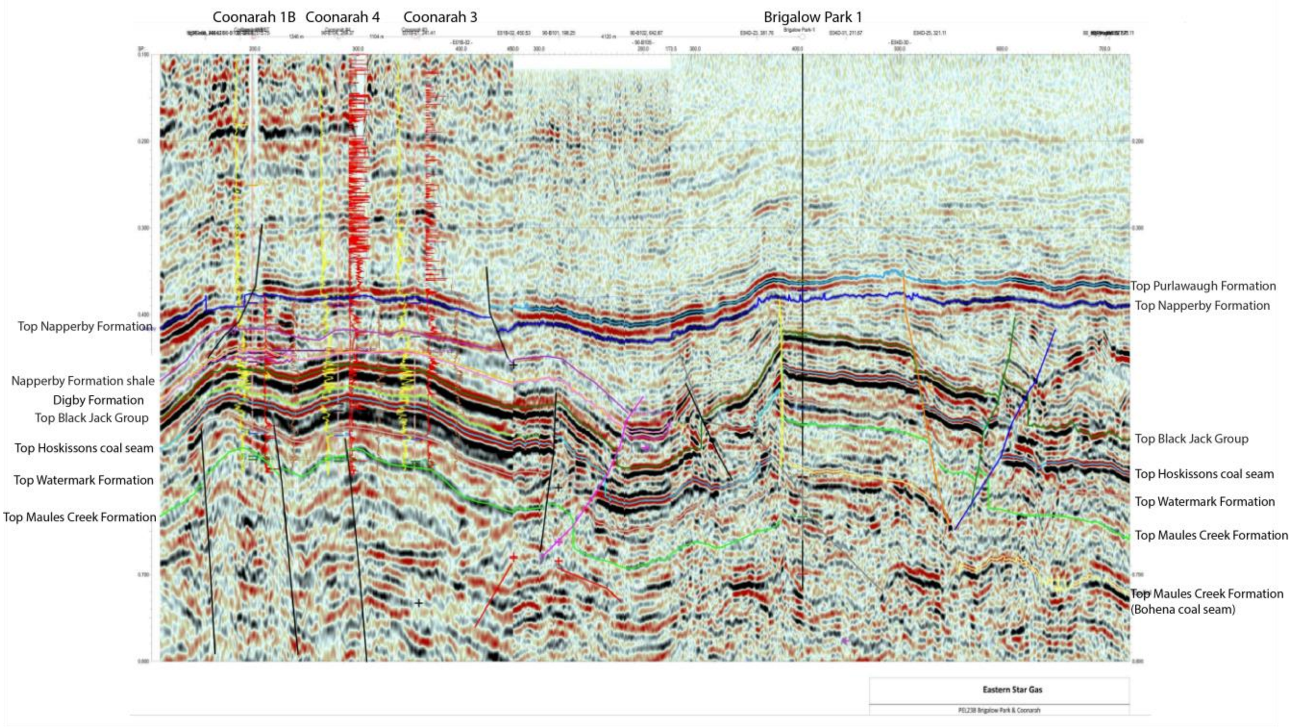

Figure 3-27 – Composite seismic section through the Brigalow Park and Coonarah anticlines (for locations, see Figure 3-25) with mapped horizons (Eastern Star Gas, 2004), modified by Raiber et al. (2022a).

3.5.2 Spatial patterns of conductivity-depth structure in the Narrabri region

The Narrabri airborne electromagnetic survey conducted during this study covered 2,765 km along more than 60 east-west and one north-south oriented flight lines. In the following section, the patterns of subsurface conductivity structure throughout the wider Narrabri Gas Project area are discussed for four different geographic zones from north to south and towards the east (the different geographic zones are displayed in Figure 3-28, Figure 3-29, Figure 3-30 and Figure 3-31).

Eight representative conductivity-depth sections and multiple three-dimensional representations (created in SKUA 3D geological modelling software, Aspentech™) were selected to explain noticeable subsurface stratigraphic and structural features and the geometry and internal architecture of different formations.

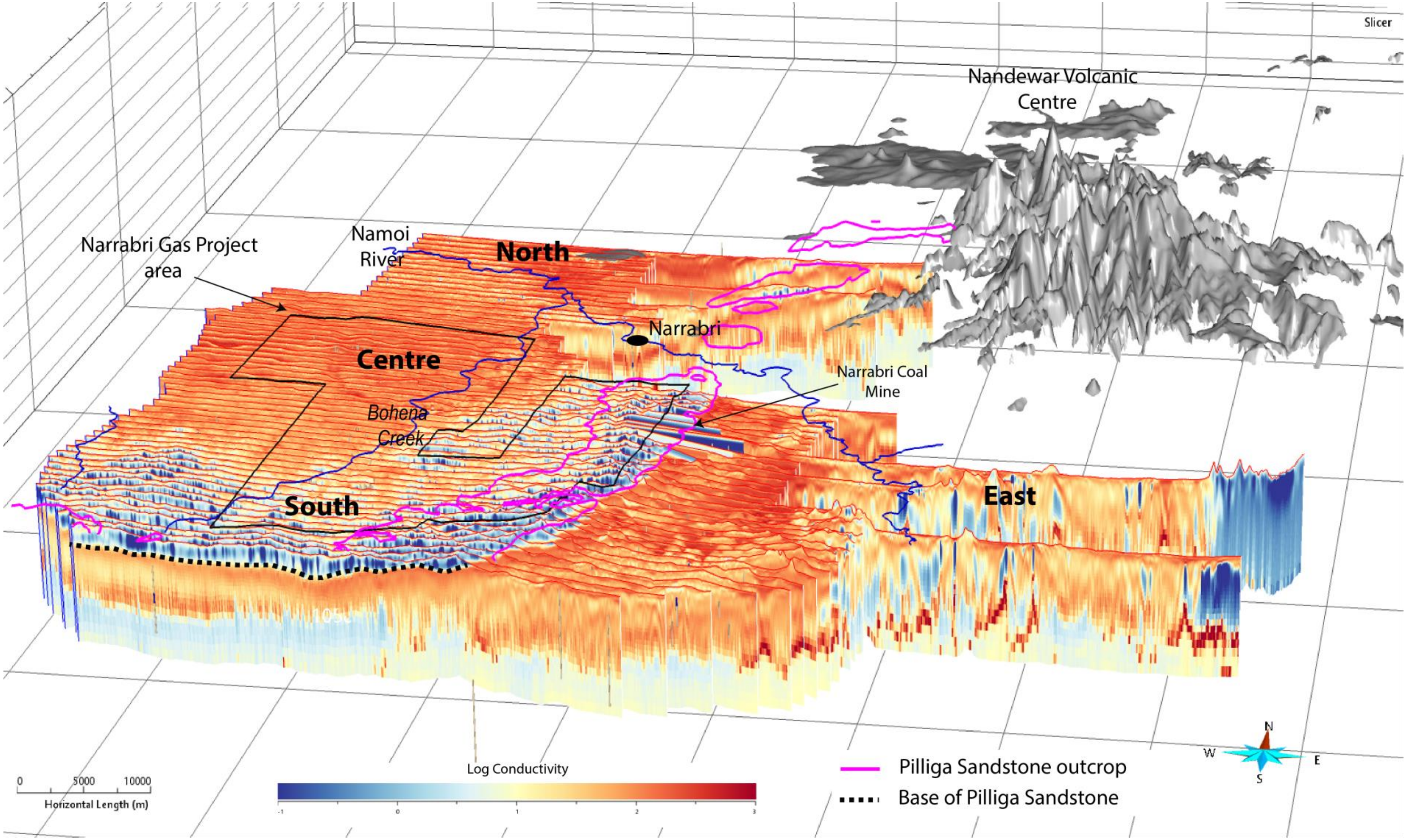

Figure 3-28 – Narrabri airborne electromagnetic (AEM) inversions, showing >60 AEM sections, major surface water courses and outcrop areas of the Pilliga Sandstone. Red colours correspond to conductive material (e.g. clay) and blue colours correspond to resistive material such as sand.

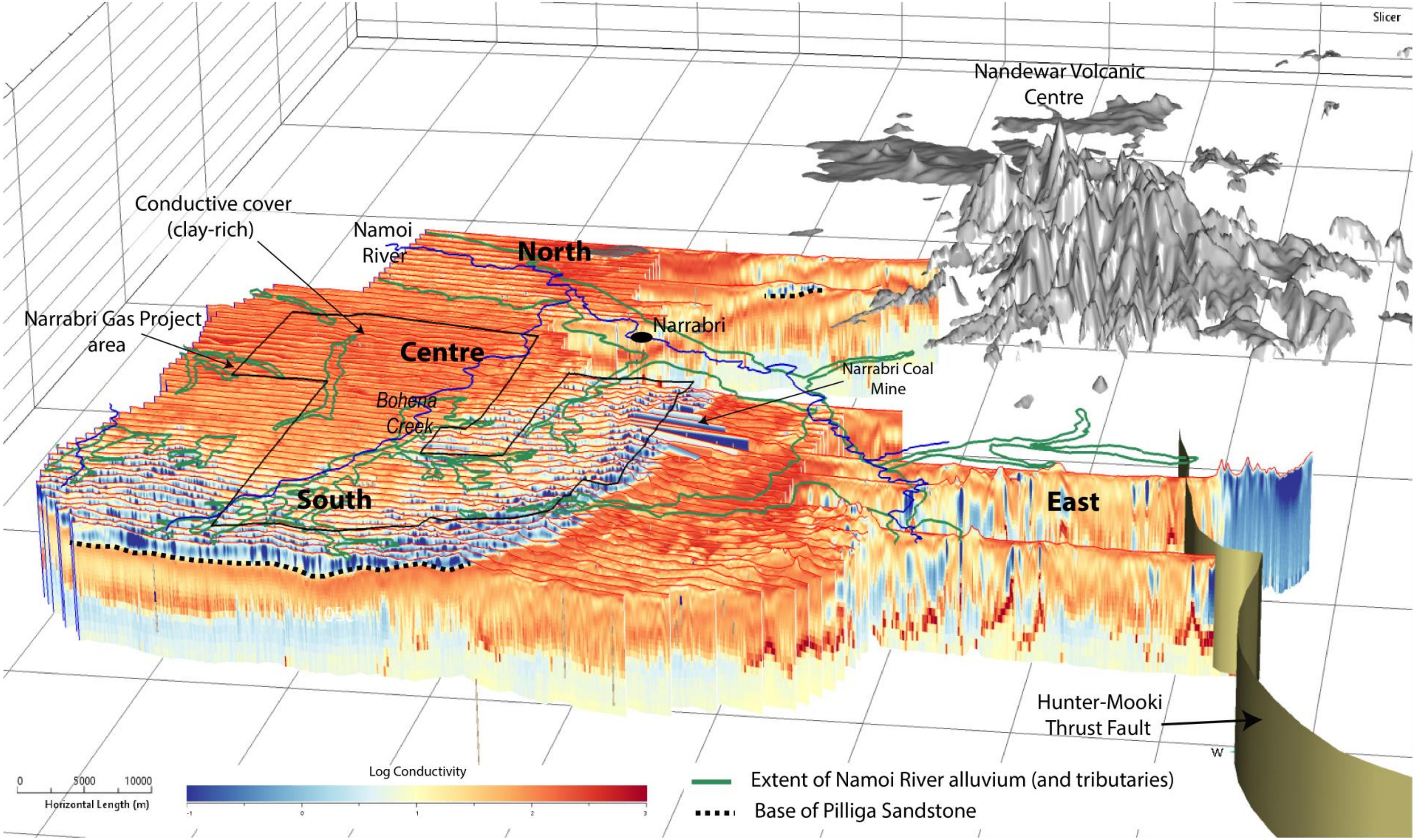

Figure 3-29 – Narrabri airborne electromagnetic (AEM) inversions, showing >60 AEM sections, surface water courses and selected geological features. The figure also shows the location of the Hunter-Mooki Thrust Fault.

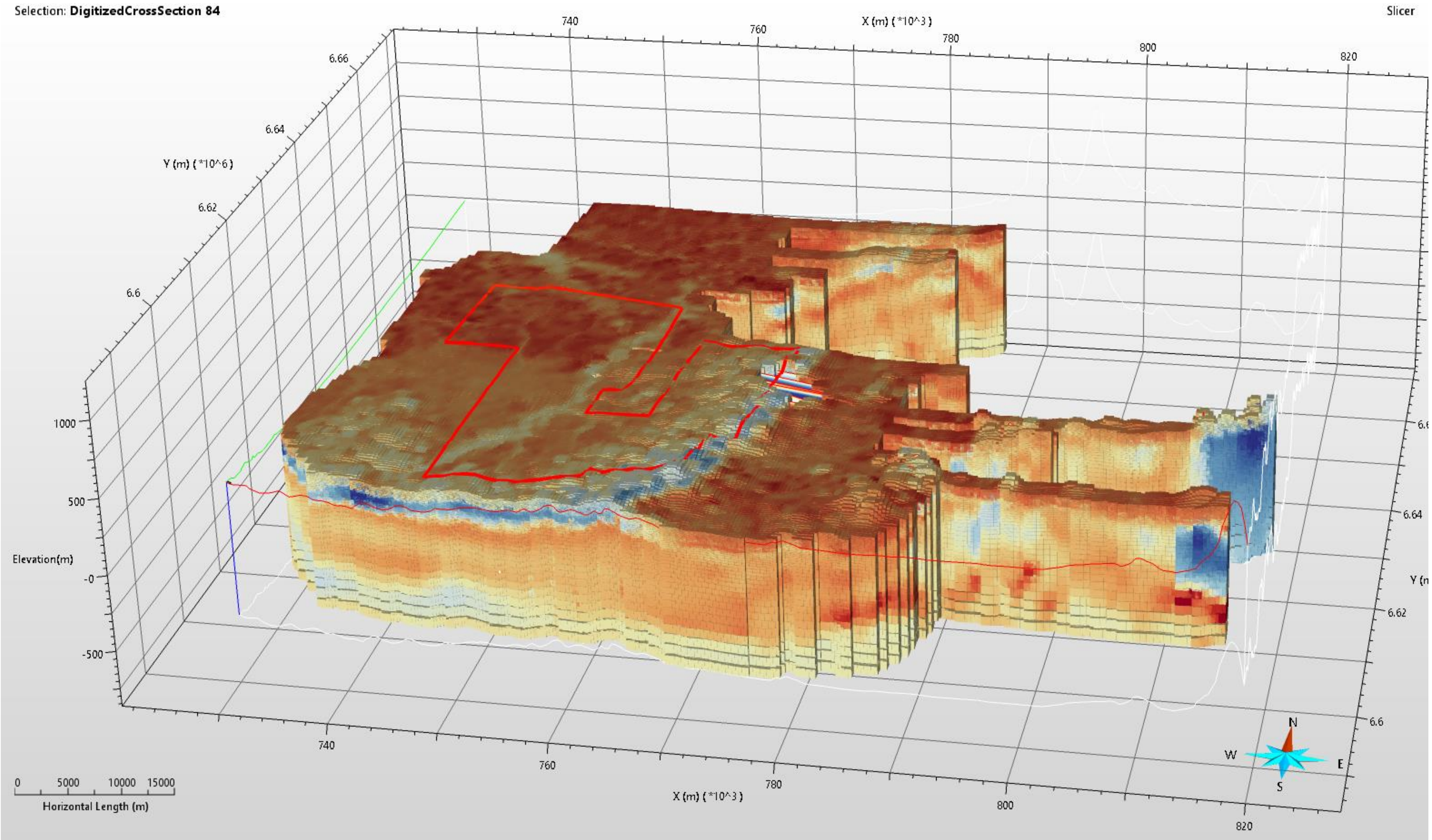

Figure 3-30 – Three-dimensional model of Narrabri airborne electromagnetic (AEM) inverted conductivity, surface water and selected geological features. Red colours correspond to conductive material (e.g. clay) and blue colours correspond to resistive material such as sand.

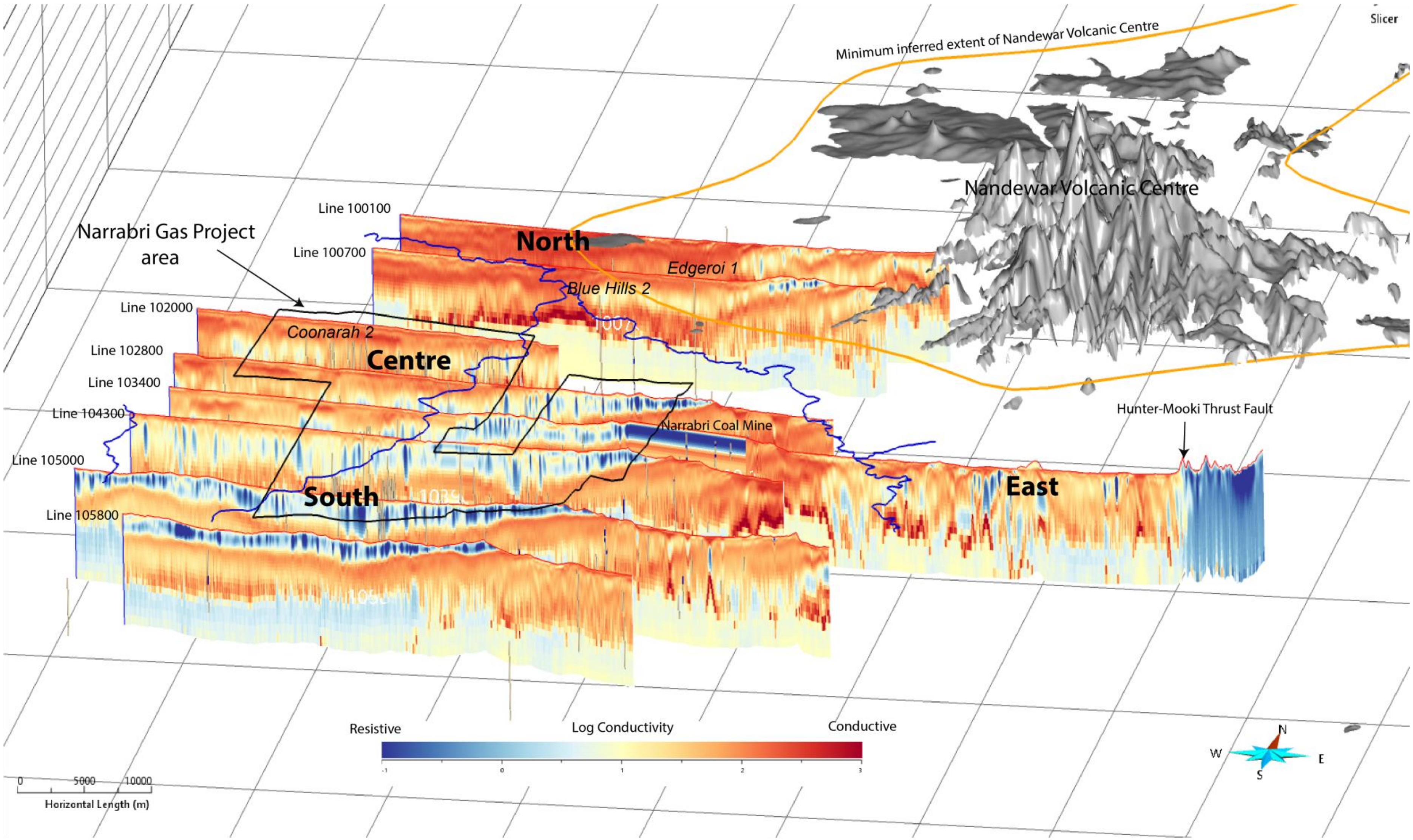

Figure 3-31 – Selected representative AEM depth conductivity sections discussed further in this report. The orange line represents the minimum inferred extent of the Cenozoic Nandewar Volcanic Centre. The approximate locations of selected exploration wells are shown in italic letters.

Northern survey area

In the northern-most line flown during this AEM survey (line 100100 in Figure 3-31 and Figure 3-33) and in other lines in the northern part of the Narrabri region, the conductivity-depth structure shows that thick surficial sequences of highly conductive cover sediments occur in the western part of AEM lines (e.g. lines 100100 and 100700 in Figure 3-33 and Figure 3-34). Clays can conduct electricity and produce strong electromagnetic responses because of their mineral composition and moisture content. Where thick conductive cover occurs in AEM surveys, this generally limits the resolution and depth of characterisation of underlying formations.

In comparison to the western part of these lines, the thickness of conductive cover is significantly smaller in the eastern part of this section, where sedimentary bedrock formations of the Surat Basin and Gunnedah Basin are exposed at the surface with relatively little cover.

At the surface, the spatial extent of the more recent Namoi River alluvium is distinguishable in the AEM by its lower bulk conductivity (orange-yellow colour in Figure 3-33) from adjacent, older sediments, which are marked by slightly higher conductivities (represented by orange-red colours). Within the Namoi River alluvium, two vertical zones of lower conductivity (represented by green colours, which indicates higher sand and less clay content) can be recognised in AEM survey lines 100100 and 100700 (Figure 3-33 and Figure 3-34). These lower and upper layers are separated by an apparent laterally extensive but thin conductive layer (represented by yellow colour in conductivity-depth sections). The pattern is also visible in other survey lines in this region, although the electromagnetic conductor does not seem to be laterally continuous everywhere. However, although the conductivity-depth lines show promise as a tool to support the characterisation of the internal heterogeneity of the Namoi River alluvium, it is important to note that the assessment of the Namoi River alluvium was not a primary purpose of this survey and that it covers only a relatively small part of the Namoi River alluvium. Alluvial aquifers are highly heterogeneous in composition, and this is likely reflected by complex conductivity and resistivity patterns. Other previous studies on the Lower Namoi catchment (e.g. Kelly et al., 2014) suggested that the internal complexity of the valley-filling sequence is very complicated, consisting of many isolated palaeovalley channel deposits, and the authors highlighted the limitations of simplifying the alluvial aquifer system into basic layers.

Two survey lines in the northern part of the Narrabri region were selected to extend further east, aiming to include the outcrop of the Pilliga Sandstone, adjacent sedimentary bedrock formations and remnants of Cenozoic volcanism. One of these lines, the northern-most line of the Namoi AEM survey (line 100100; Figure 3-33), extends far into the inferred former minimum extent of the Cenozoic Nandewar Volcanic Centre and close to its present-day remnants. At this line, located approximately 20-30 km north of the Narrabri Gas Project area, the outcrop of the Pilliga Sandstone is discernible by its low conductivity (represented by green and blue colours in Figure 3-33). In the eastern part of this AEM line near the Pilliga Sandstone outcrops, the displacement of electromagnetic conductors (represented by a yellow colour) below the Pilliga Sandstone suggests that significant subsurface structure is present in this area. These structures could be linked to faults or intrusions (e.g. dykes). Due to its proximity to the Nandewar Volcanic Centre, it is likely that dyke swarms may be present in this area, as previously described by Bull et al. (2021) for the central area of the Warrumbungle Volcanic Centre south of the Narrabri Gas Project area. In this previous study, Bull et al. (2021) suggested that the largest density of dykes occurs within the central volcano and that the dyke density decreases with increasing distance from the centre of the volcanic eruption. In the Nandewar Volcanic centre, this centre of volcanic eruption is located near Mount Lindesay and Mount Kaputar which are both visible as prominent features on the regional total magnetic intensity map (Figure 3-24).

With increasing distance towards the west, the subsurface conductivity structure becomes more dominated by higher conductivity. The geo-electrical response of a clean, sandy (quartz-rich) facies in a sandstone is expected to be a relatively resistive (blue-green) pattern, as quartz is not a good conductor of electric currents. In contrast, increasing proportions of fine-grained material provide a (relatively) more conductive response (green to yellow and orange). The observed patterns may be caused by the influence of the thick conductive cover which is present in these areas. A thick conductive cover in an AEM survey can have a significant impact on the resolution of underlying strata, as conductive materials tend to attenuate the electromagnetic signal more than resistive materials. This means that in areas with less and thinner conductive cover, the signals from deeper strata are clearer and the survey can potentially detect deeper features. As a result of the thick Cenozoic cover, formation boundaries such as the interface between Orallo Formation and Pilliga Sandstone are difficult to identify at depth and are subjected to higher uncertainties in the northern part of the AEM survey area. Furthermore, this could also be influenced by the variable lithology in the Pilliga Sandstone and Orallo Formation shown by the XRD from Coonarah 2 (south of this area in the central survey area) and the generalised sand/shale calculations at Edgeroi 1 and Blue Hills (Figure 3-4 and Figure 3-31) in this northern survey area. The generalised sand/shale calculations of exploration wells in this northern survey area suggest that there is a higher clay content and likely some mudstone and siltstone in the Orallo Formation and Pilliga Sandstone at these locations and depths.

Central survey area

In the centre of the AEM survey area (corresponding to the northern part of the Narrabri Gas Project area), the conductive cover thins compared to the northern region, although there is still a considerable thickness (e.g. lines 102000 and 102800; Figure 3-37 and Figure 3-38). The electromagnetic response of the Pilliga Sandstone here is characterised by a more resistive electromagnetic response in comparison to lines further north. This is likely influenced by the thinning of the conductive cover towards the south (Figure 3-35). In this central survey area, an east-west evolution of the geo-electrical response within the Pilliga Sandstone can be observed for example along lines 102000 and 102800. In the eastern part of the aquifer where the Pilliga Sandstone outcrops at the surface, the geo-electrical response (a resistive blue-green pattern) of the Pilliga Sandstone suggest that the aquifer is dominated by a clean, sandy facies. This agrees with XRD analysis of rock samples from exploration well Tunmallallee within the outcrop south of the Narrabri Gas Project area (Figure 3-8 and Figure 3-36), where the content of quartz was generally between 75 and 97% (with a median of 85%), suggesting a quartz sandstone facies with very little cementation. This also confirms previous descriptions of the Pilliga Sandstone as a clean quartzose sandstone with limited clay mineral and feldspar content (Arditto, 1982).

From east to west along the conductivity-depth sections (e.g. line 102800; Figure 3-38), the geo-electrical response of the Pilliga Sandstone in the northern part of the Narrabri Gas Project area becomes relatively more conductive, as seen by the green colours here. This is consistent with the presence of a higher proportion of finer-grained material 'smearing' the electrical response of the material. This change in sedimentary facies was also confirmed by XRD analysis of Pilliga Sandstone rock samples from the Coonarah 2 exploration well, where the analysis of rock samples confirmed a significantly lower quartz content (61 to 68%) and higher proportions of clay minerals, plagioclase, siderite and calcite compared to the mineralogical analysis of Pilliga Sandstone samples within the outcrop beds. This suggests an increasing degree of cementation and a reduction in hydraulic conductivity from east to west.

An important question this study aims to address is the degree and direction of potential connection between Orallo Formation and Pilliga Sandstone. The Pilliga Sandstone is generally classified as an aquifer and the Orallo Formation is often characterised as an aquitard or partial aquifer. However, Raiber et al. (2022a) suggested that there may be some connectivity between the two formations in some areas. Although the airborne electromagnetic response of the Pilliga Sandstone and the Orallo Formation are different within their respective outcrop areas (with the Pilliga Sandstone displaying a more resistive signature than the Orallo Formation), the difference towards the west becomes less and it is difficult to identify the interface between these two formations with high confidence. Similarly, in many stratigraphic logs of exploration wells within the Narrabri Gas Project area, the Orallo Formation and Pilliga Sandstone were not differentiated.

A main aim of the AEM survey was to complement seismic survey data and acquire a more continuous understanding on whether there is any evidence for deep-seated faults or dykes (near-vertical igneous intrusions) extending into the shallower subsurface (the upper approximately 400 m of the subsurface). Evidence from the AEM survey that could indicate such a vertical extension of structural features includes the presence of significant vertical displacements of conductors (i.e. aquitards such as claystones). The uppermost spatially extensive sedimentary bedrock conductor in this area is the top of the Purlawaugh Formation. This is confirmed along a cross-section that traverses multiple AEM lines over the locations of multiple high-quality stratigraphic logs from exploration wells (Figure 3-32). At this section, the depth of the first sedimentary bedrock conductor closely matches the stratigraphic picks representing the top of the Purlawaugh Formation at most exploration well locations.

The spatial assessment of the interface between the Pilliga Sandstone and the Purlawaugh Formation in the northern part of the Narrabri Gas Project area shows that there are likely some low amplitude folds present in this region, as also confirmed by the total magnetic intensity (Figure 3-24) and seismic images (Figure 3-27). When magma intrudes into the Earth's crust, it creates space by uplifting and bending the overlying rock layers. This process can result in the formation of folds, including low amplitude folds (also referred to as forced folds, as discussed in Section 1.3.3), especially where an intrusion is relatively shallow and where the deformation forces are not very intense. This is exhibited by the variations in the bedrock topography in this region. Forced folds are typically characterized by gentle undulations rather than by sharp or steep bends, often creating dome-like or flat-topped structures, which makes them ideal traps for fluids such as oil, gas, and groundwater. In the Narrabri Gas Project area, these structural features co-occur in areas previously identified as anticlines, which have been explored as hydrocarbon traps (Carty and Smith, 2004).

Dating of some of these intrusions in the present study showed that there were multiple phases of intrusive activity ranging from Late Triassic to Cenozoic. For example, intrusions at Coonarah 2 in the north-western part of the Narrabri Gas Project area were dated as Late Cretaceous and Eocene (approximately 50 to 70 million years ago), confirming that they have occurred after the deposition of the Purlawaugh Formation and Pilliga Sandstone. These age-dated and relatively thin intrusions at Coonarah 2 have intruded at the interface between the Napperby and Digby formations. However, based on the time of when the intrusion occurred, it is possible that folding may have also impacted the Purlawaugh Formation and Pilliga Sandstone. In comparison, at exploration well Connarah 9, an intrusion of more than 150 m thickness was intersected at the interface between the Porcupine and Maules Creek formations. This intrusion is considerably thicker than other intrusions intersected at Coonarah, and it is therefore uncertain whether this is a sill or dyke. No core was available for this intrusion, and it could therefore not be dated. Seismic imagery (Figure 3-27) in this area and at Brigalow Park to the east indicates that the Purlawaugh Formation has been subjected to some low amplitude folding. While the seismic images suggest that some displacements and deformation of the Gunnedah Basin strata has occurred in this area and some faults possibly extend to the base of the Purlawaugh Formation, there is no visible evidence for significant displacement of the Purlawaugh Formation.

Most other intrusions in this part of the Narrabri Gas Project area occurred during the Late Triassic or Early Jurassic, and thus, pre-dated the deposition of the Pilliga Sandstone.

Although seismic imagery, total magnetic intensity (and the first derivative), AEM sections and stratigraphic data show an overall good agreement on where forced folds are present, some of the apparent dome-like features in AEM lines may be influenced by thickness variations of the conductive cover and further processing will be conducted to refine the conductivity-depth structure in these areas. This may for example be the case in Line 102800 (Figure 3-38), where areas of thicker conductive surficial cover coincide with dome-like structures underneath and areas of thinner conductive surface cover coincide with troughs.

Southern survey area

In the southern part of the AEM survey and Narrabri Gas Project areas, the base of the Pilliga Sandstone and its interface with the underlying Purlawaugh Formation are clearly defined by a sharp contrast in the conductivity structure (Figure 3-36, Figure 3-41, Figure 3-42 and Figure 3-43). The Pilliga Sandstone displays the resistive (blue) geo-electric response of a clean, sandy facies, whereas the underlying Purlawaugh Formation is characterised by significantly higher proportions of fine-grained material and a more conductive geo-electric response (green to yellow). The more uniform geo-electric response of the Pilliga Sandstone here compared to the northern part of the survey area is due to the closer proximity to the sediment source area of the Pilliga Sandstone, whereas the pattern of the Purlawaugh Formation retains a similar electromagnetic response as observed further north. The sharper boundaries identified here compared to the northern part of the survey area are also influenced by the much thinner and less conductive cover, which has decreased further from the central area as shown in Figure 3-35. This agrees with the findings from Raiber et al. (2022a), who based on ground-based TEM and AgTEM surveys suggested that an AEM survey would likely be able to achieve great depths of penetration with good layer resolution.

The interface between the Pilliga Sandstone and Purlawaugh Formation in the south is generally smooth with no obvious vertical displacements, although some gentle undulations of conductors are visible (e.g. Figure 3-41 and Figure 3-42). The thickness of the first sedimentary bedrock conductor (inferred to correspond to the Purlawaugh Formation) across these structural features appears to be maintained, suggesting that no post-depositional juxtaposition (vertical displacement) or erosion of the Purlawaugh Formation has occurred. These structural features may represent low amplitude fold deformation or pre-existing bedrock or basement highs, which may have been already in place at the time of the deposition of the Surat Basin strata. The latter would mean that the Surat Basin strata have inherited the topography of the underlying Gunnedah Basin, whereas the deformation of low amplitude folds may have occurred prior to or following the deposition of the Surat Basin strata. The total magnetic intensity images show that magnetic anomalies exist in the southern area of the AEM survey, which could indicate presence of igneous intrusions (Figure 2-5 and Figure 3-24). Although available stratigraphic well logs in this region are sparse, an intrusion intersected at Dewhurst DDH1 was dated as Mid-Jurassic (Figure 3-23; Section 3.4) and has therefore occurred after the deposition of the Purlawaugh Formation and likely prior to, or at a similar time as, the deposition of the Pilliga Sandstone.

Eastern survey area

In the eastern part of the AEM survey area to the east of the Narrabri Gas Project area (Figure 3-31 and Figure 3-39), multiple longer lines were selected to extend over the Hunter-Mooki Thrust fault. The Hunter-Mooki Thrust fault is located approximately 50 km to the east of the Narrabri Gas Project area. It is one of the major tectonic boundaries in Eastern Australia and delineates the eastern edge of the Sydney-Gunnedah Basin and the western front of the New England Orogen. It was formed due to compressional forces during the Permian and mid-Triassic periods, which also influenced the deformation of the New England Fold Belt. The tectonic processes that created the Hunter-Mooki Thrust fault are part of the broader tectonic regime that shaped the New England Fold Belt. Compared to areas within the Narrabri Gas Project area where low amplitude folds have been identified, the eastern extension of AEM depth-conductivity lines suggest that there is likely higher amplitude folding in closer proximity of the Hunter-Mooki Thrust fault, indicating more significant deformation of the geological formations within the vicinity of the Hunter-Mooki Thrust fault which does not visibly extend very far into the west.

The resolution of Gunnedah Basin aquitards and coal seams to the east of the Pilliga Sandstone and Purlawaugh Formation outcrop areas and some formation interfaces (e.g. base of Cenozoic cover, base of Orallo Formation and the base of Purlawaugh Formation) within the central and northern part of the AEM survey area can likely be further improved with additional processing/inversions of the AEM data. This will be explored further and may be reported in an update to this publication at a later stage.

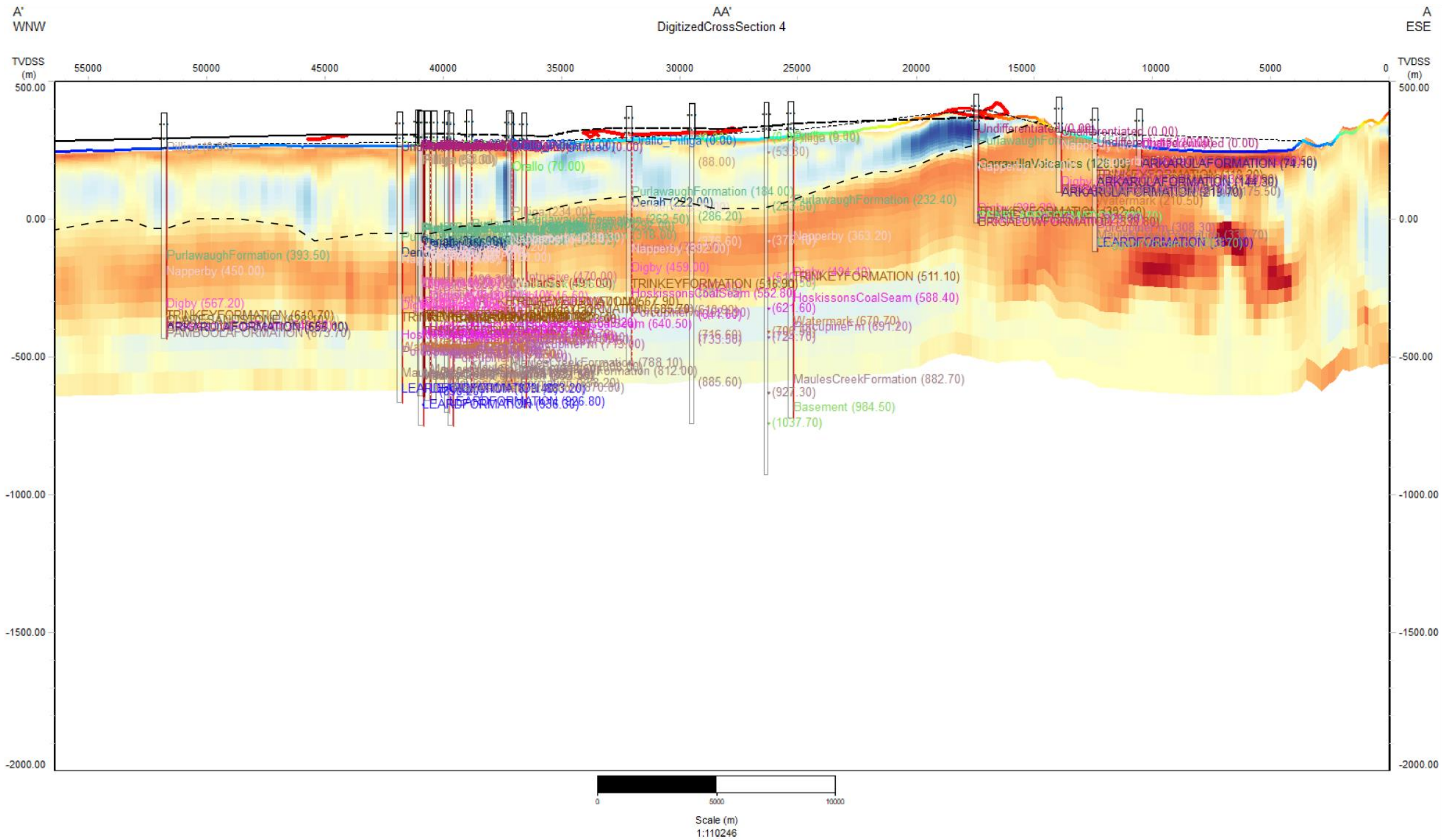

Figure 3-32 – Comparison of AEM patterns with stratigraphic well data. The dashed black line represents the inferred interface between the Pilliga Sandstone and the Purlawaugh Formation. Green labels on cross-section show where the formation top of the Purlawaugh Formation has been identified in stratigraphic logs.

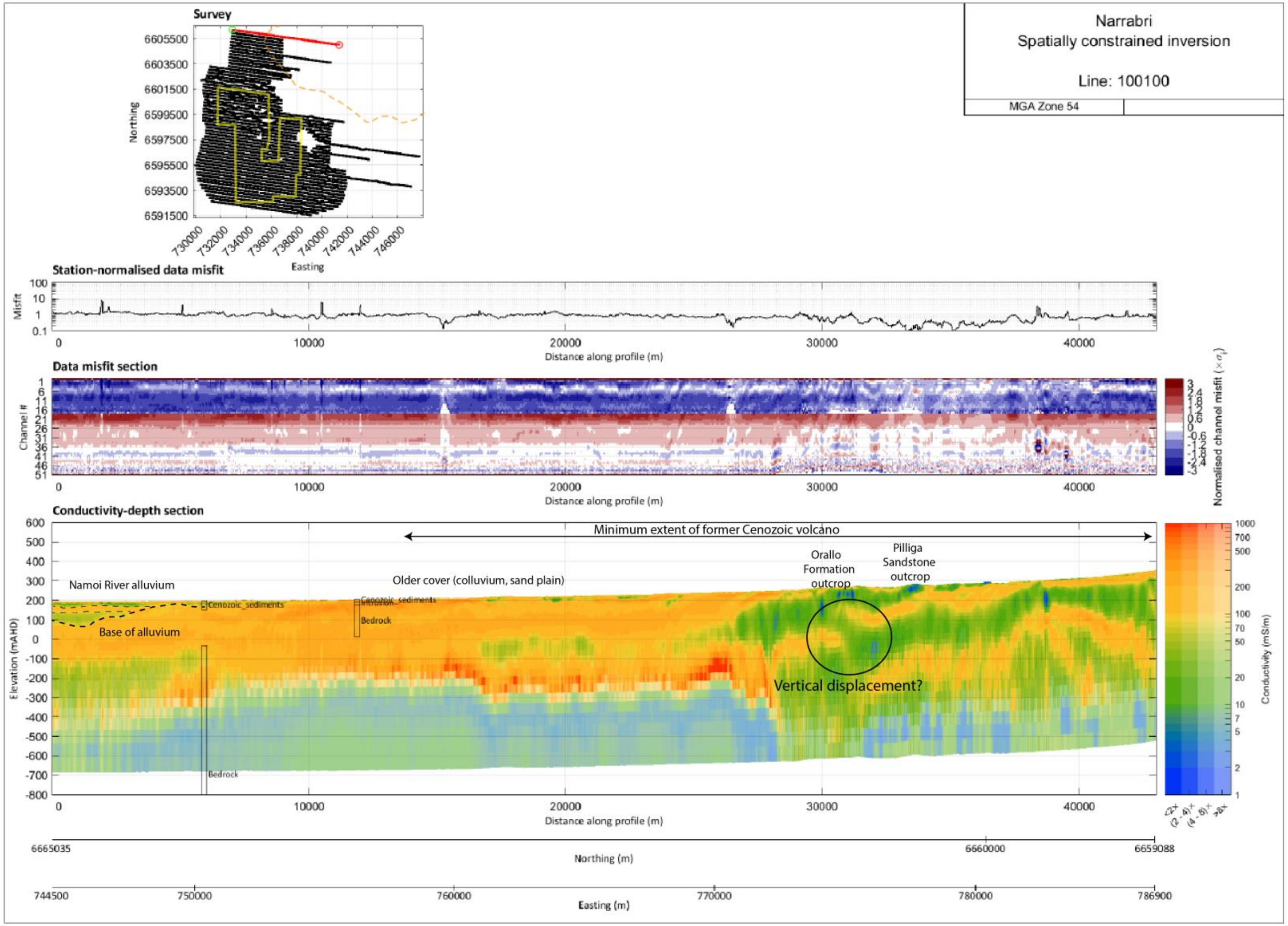

Figure 3-33 – Conductivity-depth structure along AEM line 100100. The orientation of the line is shown in the inset map.

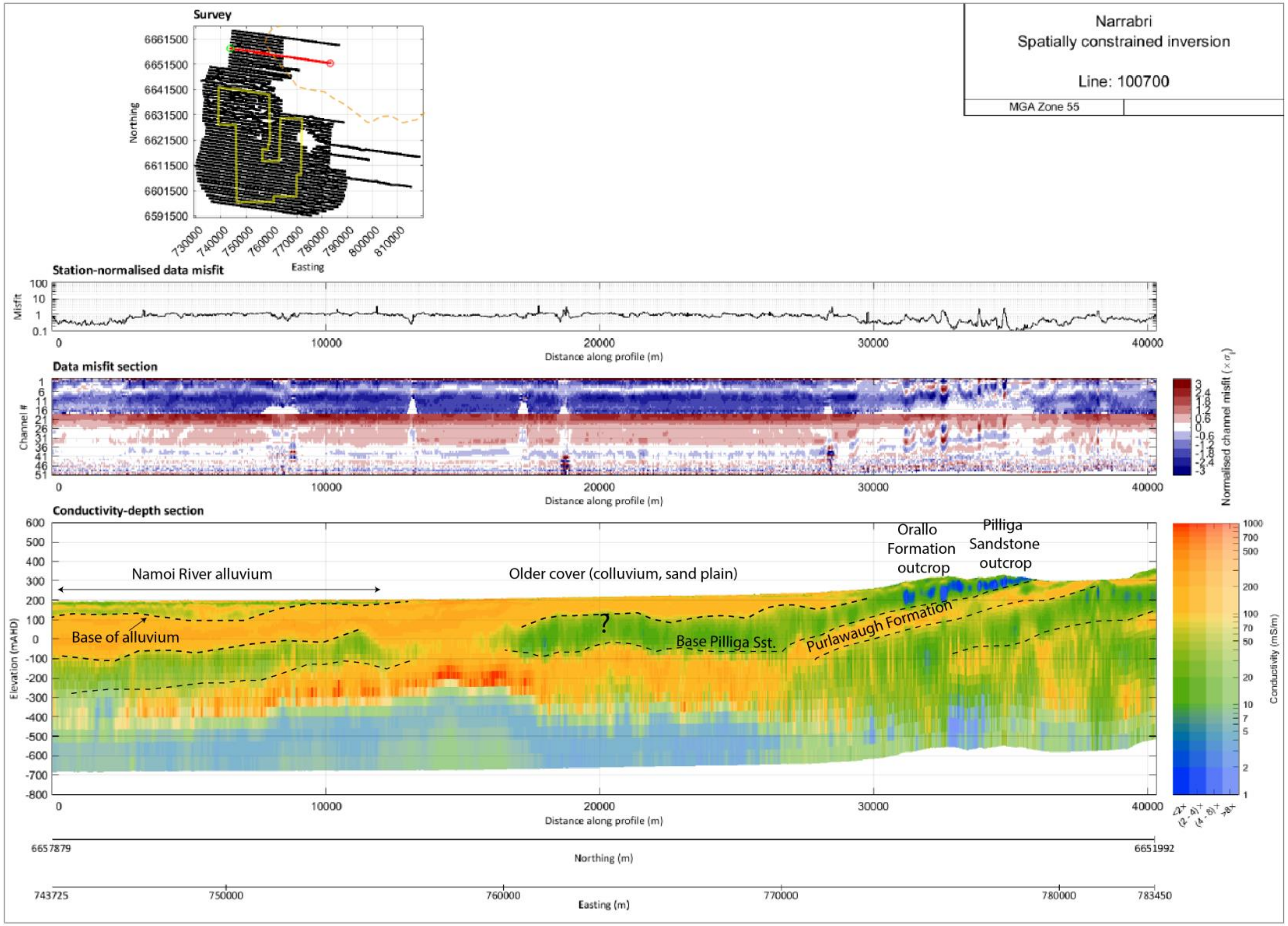

Figure 3-34 – Conductivity-depth structure along AEM line 100700. The orientation of the line is shown in the inset map.

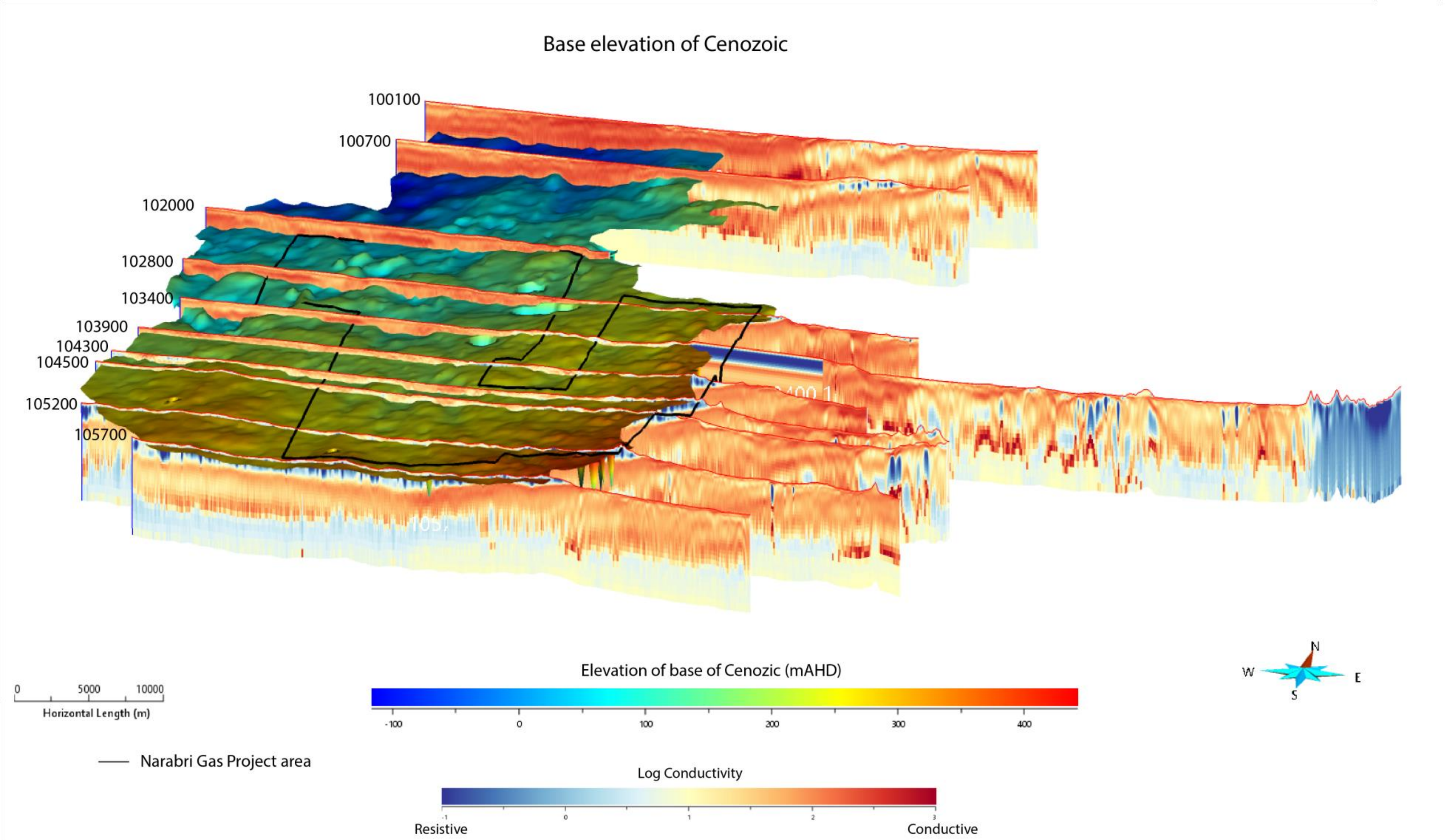

Figure 3-35 – Selected AEM lines and base of Cenozoic elevation showing increase of thickness of Cenozoic from south to north and east to west.

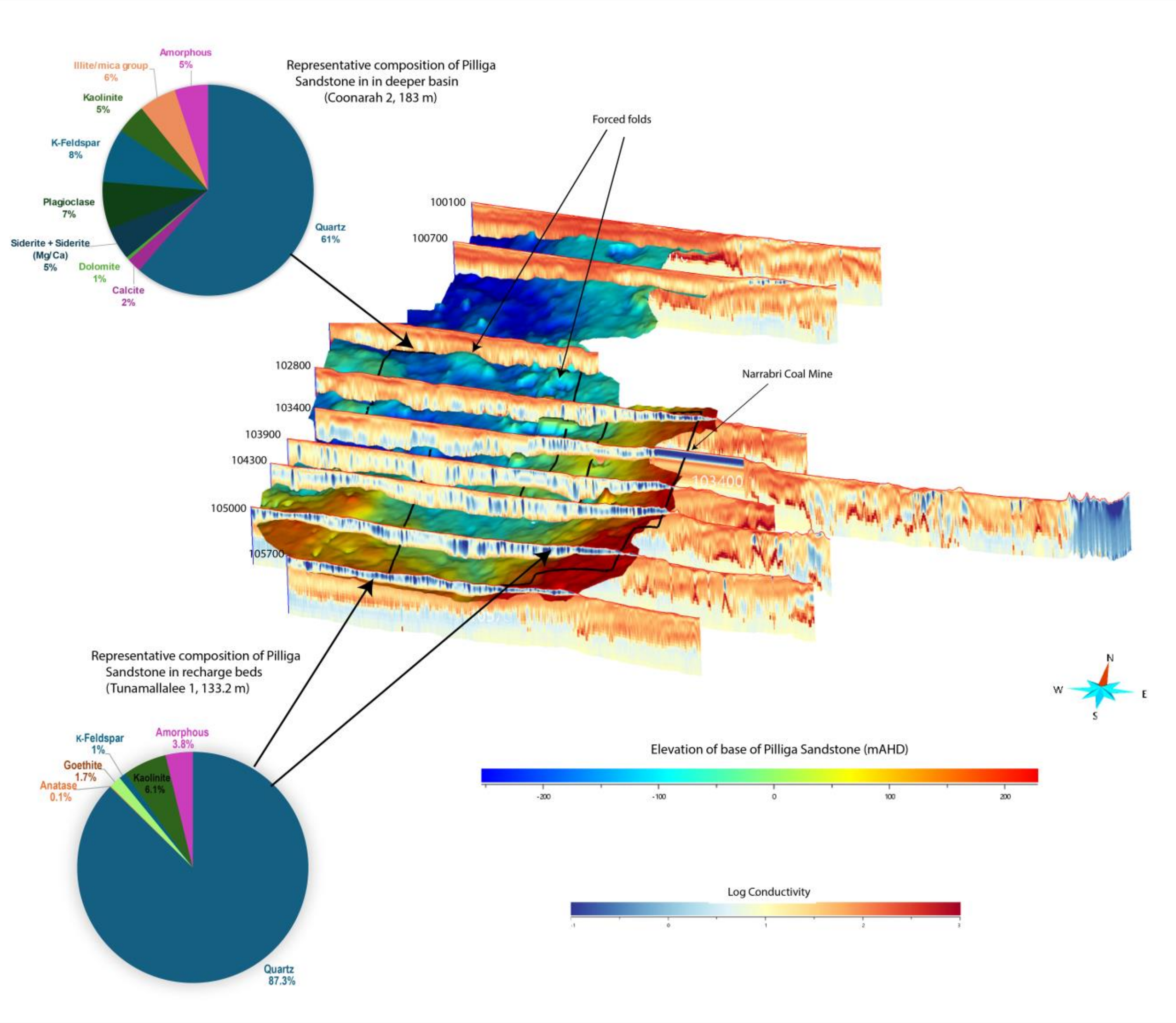

Figure 3-36 – Selected AEM lines, elevation of the base of Pilliga Sandstone and representative XRD patterns of the Pilliga Sandstone within the recharge beds and in deeper parts of the Surat Basin.

The mineralogical composition at Tunmallallee 1 (132.2 m) represents the sample with the median quartz content analysed at this location.

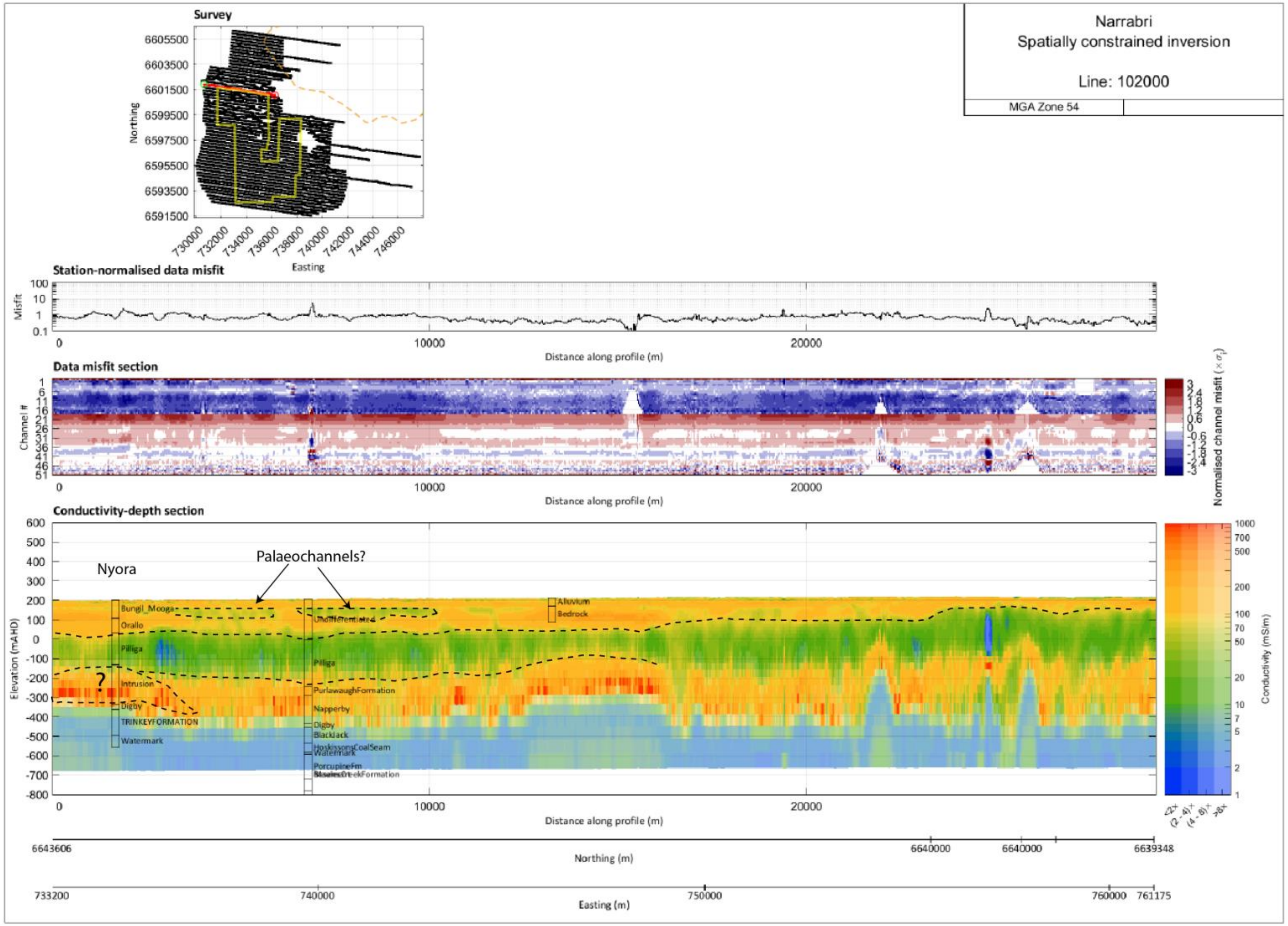

Figure 3-37 – Conductivity-depth structure along AEM line 102000. The orientation of the line is shown in the inset map. The question mark indicates the possible extent of a Jurassic intrusion at Nyora where the stratigraphic log at Nyora 1 exploration well suggests that both Purlawaugh Formation and Napperby Formations are absent.

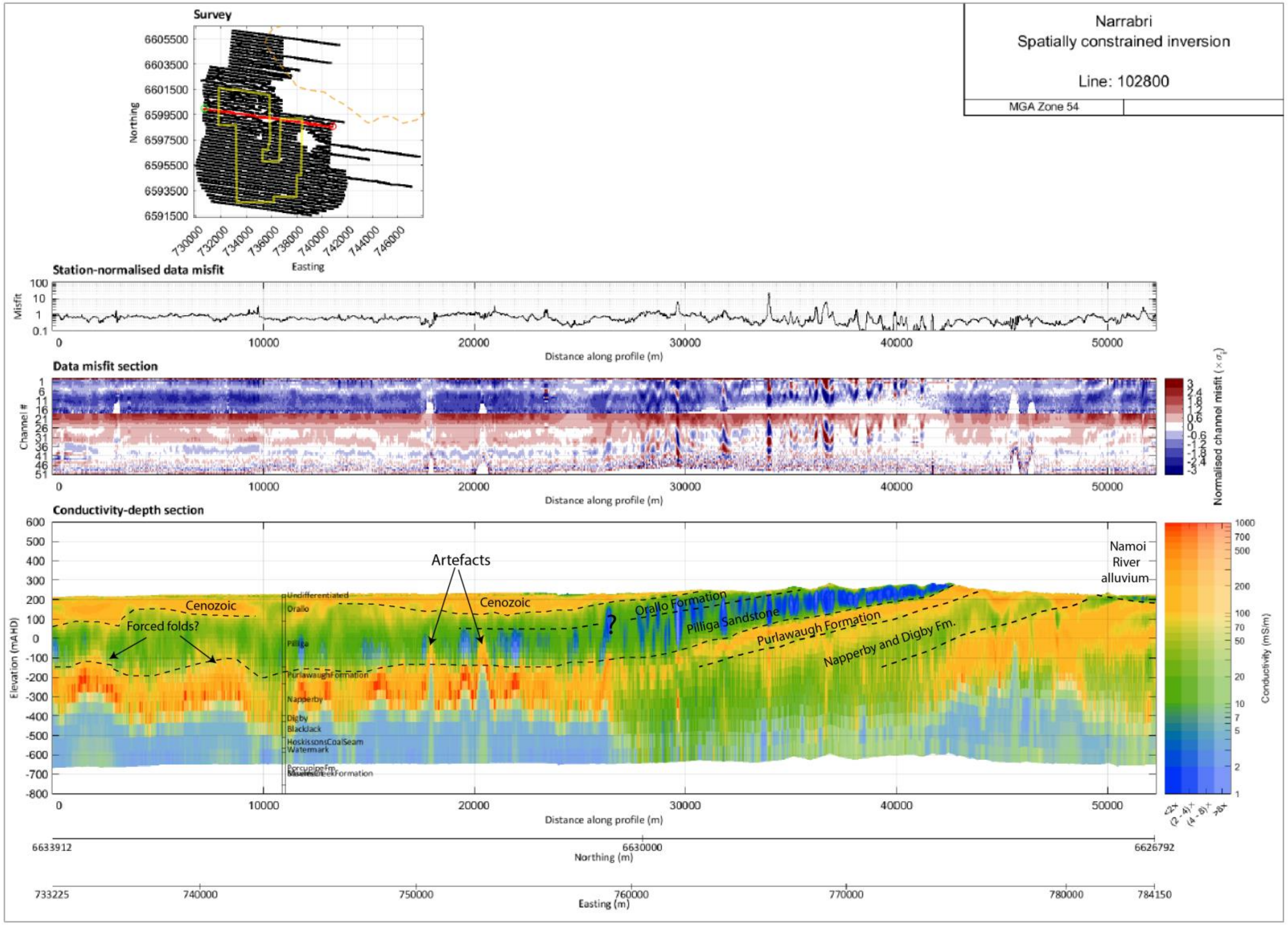

Figure 3-38 – Conductivity-depth structure along AEM line 102800. The orientation of the line is shown in the inset map. The question mark indicates an area where the interface between the Orallo Formation and Pilliga Sandstone cannot be differentiated with high confidence based on the electromagnetic signal.

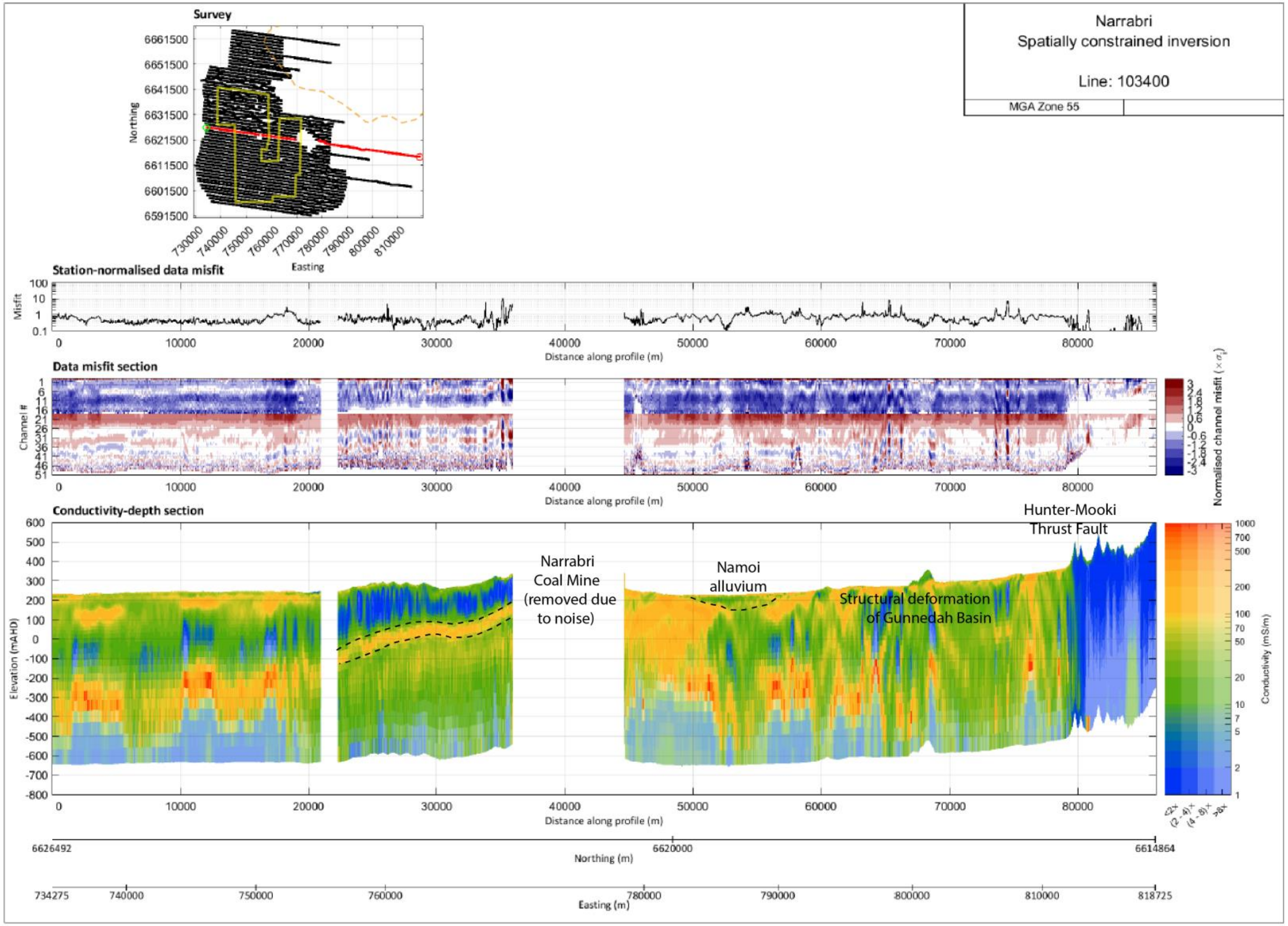

Figure 3-39 – Conductivity-depth structure along AEM line 103400. The orientation of the line is shown in the inset map.

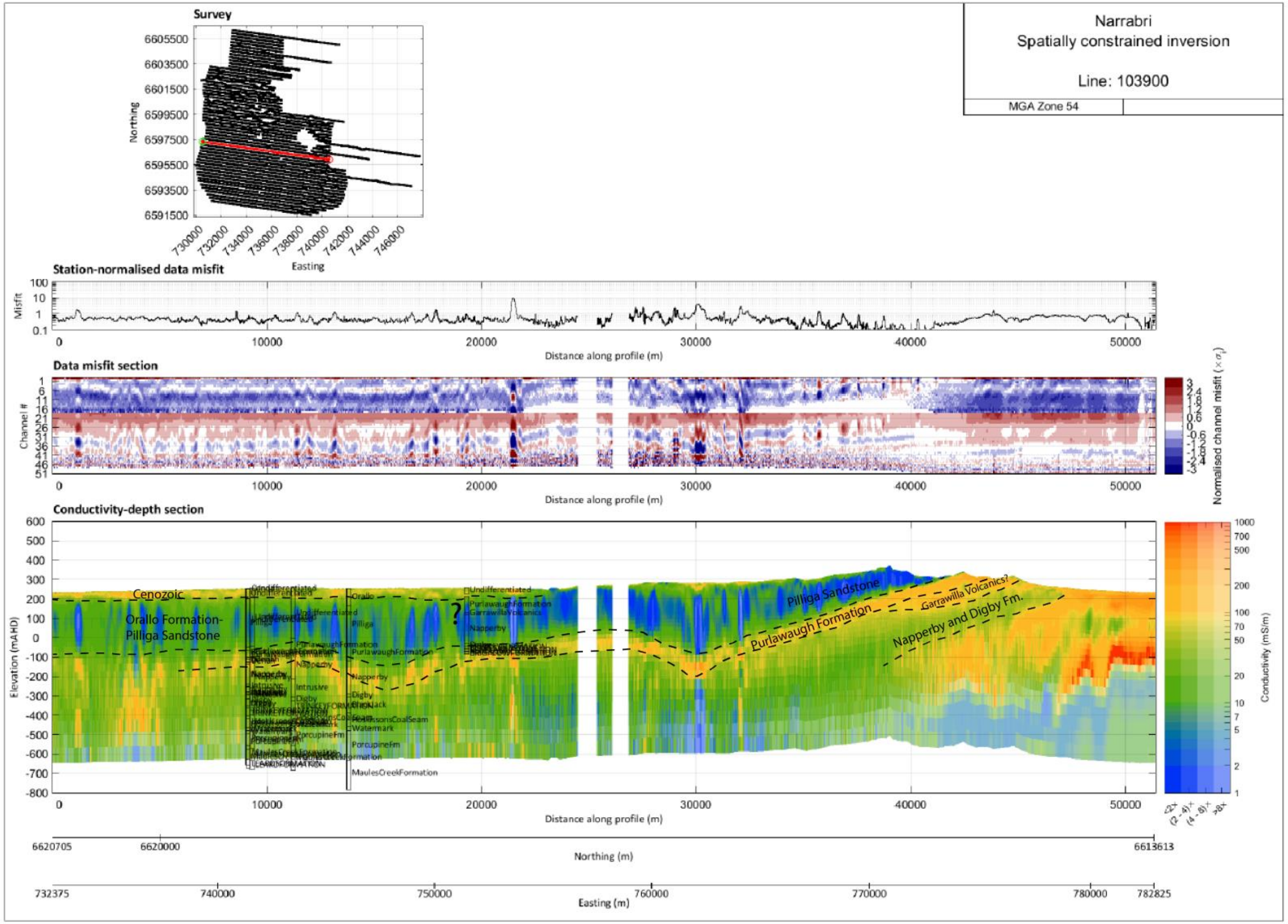

Figure 3-40 – Conductivity-depth structure along AEM line 103900. The orientation of the line is shown in the inset map. The question mark indicates an area where a miss-match between AEM interpretations and well log stratigraphic picks has been observed, likely due to an incorrect well location or stratigraphic records.

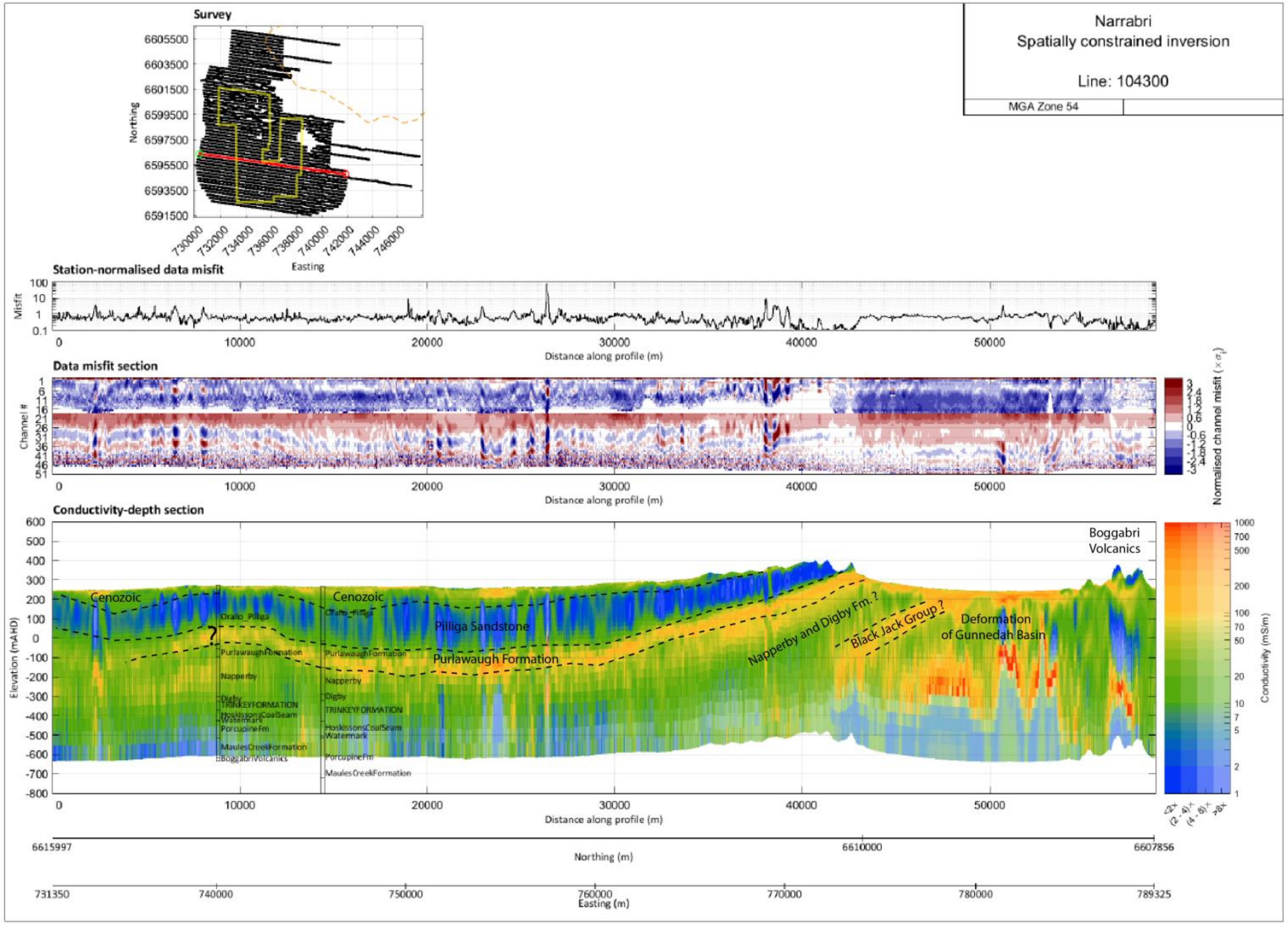

Figure 3-41 – Conductivity-depth structure along AEM line 104300. The orientation of the line is shown in the inset map. The question mark in the west indicates an area where a miss-match between AEM interpretations and well log stratigraphic picks has been observed, possibly due to an incorrect well location or stratigraphic records. Question marks in the east indicate uncertain formation attributions, which will be further explored in updated inversions.

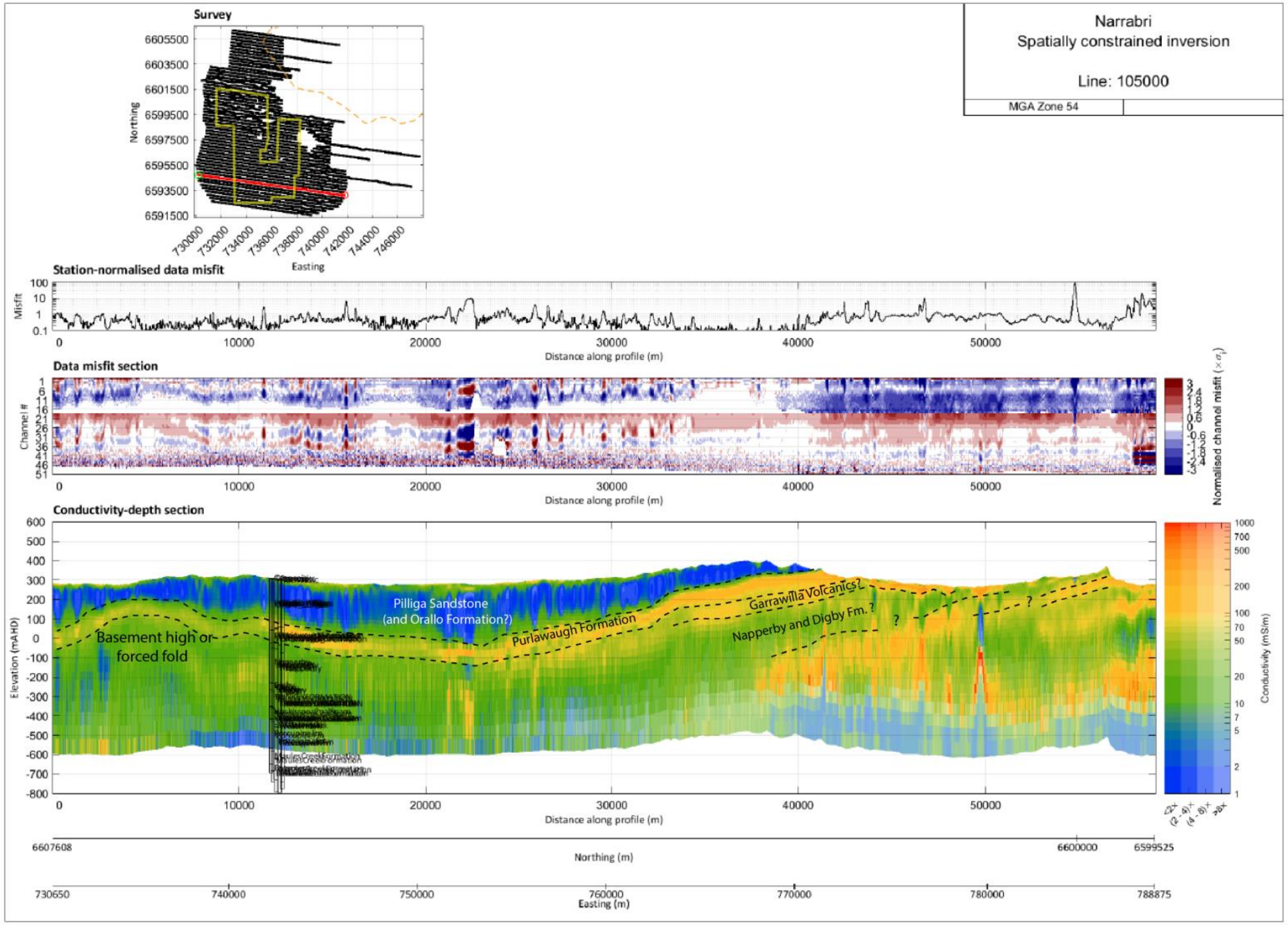

Figure 3-42 – Conductivity-depth structure along AEM line 105000. The orientation of the line is shown in the inset map. Question marks in the east indicate uncertain formation attributions and boundaries, which will be refined further in updated inversions.

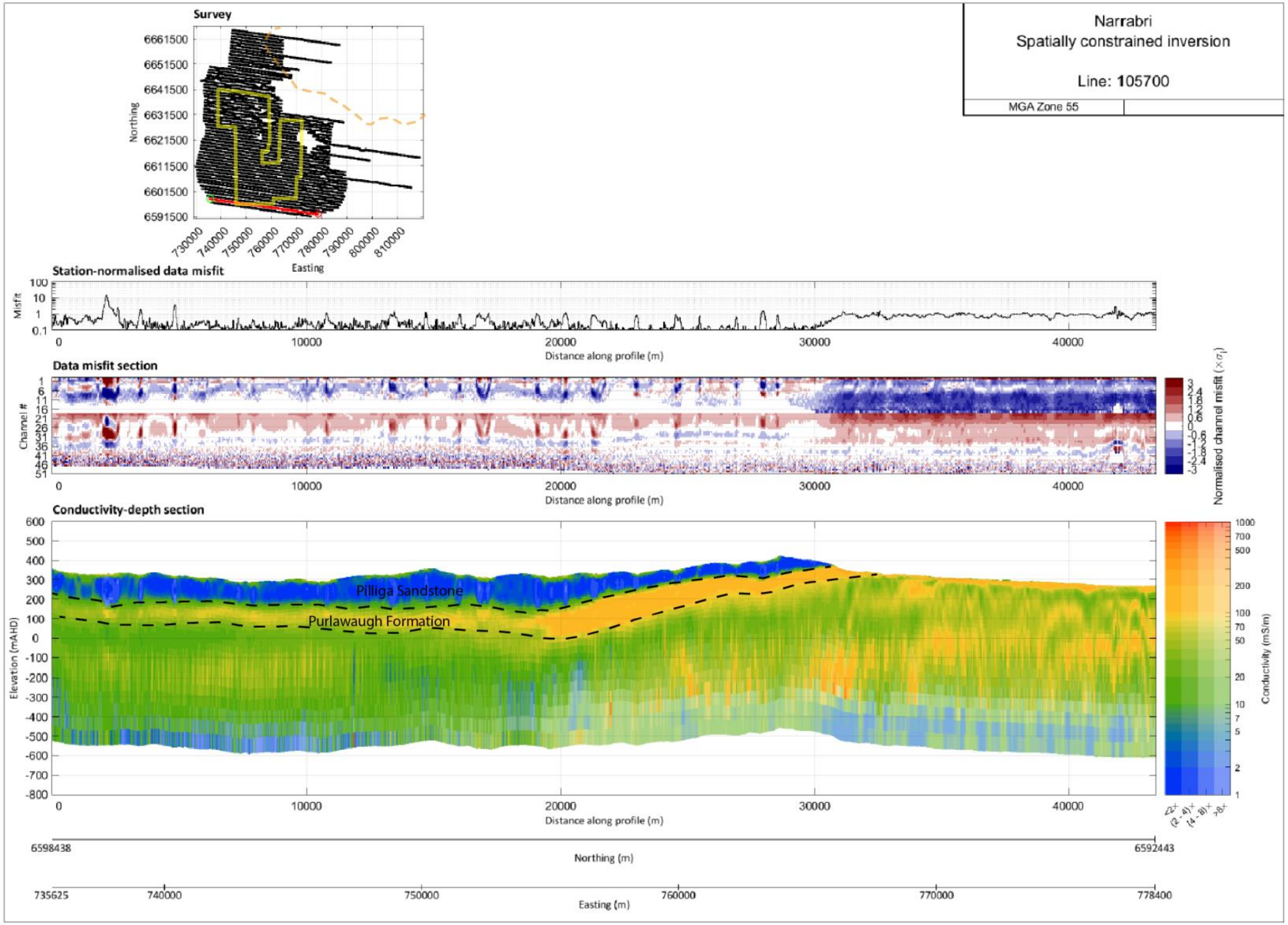

Figure 3-43 – Conductivity-depth structure along AEM line 105700. The orientation of the line is shown in the inset map.

Summary of AEM survey results and interpretation

The results of the AEM survey have enabled us to generate a continuous image of the subsurface to depths of about up to 400 m across the Narrabri region. Within the different zones of the AEM survey extent from north to south and from east to west, several observations and spatial patterns can be recognised with regards to geometry and internal architecture of stratigraphic units:

- The thickness of the Cenozoic cover significantly decreases from north to south and from east to west (Figure 3-35). In the northern part of the survey area, the thickness of this clay-rich cover is more than 100 m, whereas it is very thin at the southern and eastern boundary of the Narrabri Gas Project area. Thick conductive cover generally reduces the depth to which the AEM signal can penetrate the subsurface, and it can also affect the resolution of the survey as conductive clays can attenuate the electromagnetic signal, and thus obscure deeper, less conductive features. Consequently, the depth of penetration of the electromagnetic signal and resolution of subsurface stratigraphy is higher in the south and east than in the north.
- There is a significant variability in the geo-electrical response of the Pilliga Sandstone from north to south and east to west (Figure 3-36). In the east and south within and near the outcrop beds of the Pilliga Sandstone, its geo-electrical response indicates a clean, quartz-rich and sandy facies (blue pattern), whereas its more conductive response (green to yellow colours) in the west and north indicate an increasing proportion of fine-grained material; this was independently confirmed by XRD mineralogical analysis.
- Within the Narrabri Gas Project area, the geometry of conductive sedimentary bedrock layers (e.g. the Purlawaugh Formation) suggests that there are some low amplitude or forced folds. These are typically characterized by gentle undulations rather than by sharp or steep bends, often creating dome-like or flat-topped structures. In the south, where the depth resolution of the AEM is better than in the north due to the thinner conductive cover, the thickness of conductors (i.e. the Purlawaugh Formation) remains preserved with no obvious vertical displacements. In the north-western part of the Narrabri Gas Project area, where multiple forced folds have been identified from the Total Magnetic Intensity map and in seismic surveys by previous studies, the resolution of sedimentary bedrock conductors underneath thick conductive cover is relatively poor. No significant juxtaposition of the Pilliga Sandstone or Purlawaugh Formation is visible, although previous seismic surveys suggest that there may be some juxtaposition of the base of the Purlawaugh Formation.
- To the north of the Narrabri Gas Project area (close to the Nandewar Volcanic Centre) and to the east (close to the Hunter-Mooki Thrust fault), significantly more deformation of sedimentary bedrock conductors is visible in the AEM conductivity-depth sections.

Alternative inversions and model realisations of the conductivity-depth structures are possible. These will be explored further and may be reported in an update to this publication at a later stage.

3.6 Geological cross-sections

In a previous GISERA project, Raiber et al. (2022a) suggested that there is likely some minor degree of hydrogeological connection between the Pilliga Sandstone and the underlying Purlawaugh Formation and/or the late Gunnedah Basin strata (Digby Formation) in the northern and north-western parts of the Narrabri Gas Project area, starting near the Plumb Road groundwater monitoring site at the Bohena anticline. Two geological cross-sections were constructed in the current project based on geological and geophysical data presented in previous sections as representatives of areas where previous studies suggested that there may be some connectivity. The cross-sections form the basis for the numerical and geochemical modelling of groundwater flow and age patterns (Section 3.9) and support the interpretation of hydrochemistry and environmental tracer data (Sections 3.7 and 3.8).

3.6.1 Cross-section 1 (CS1)

An east-west oriented geological cross-section was constructed through the centre of the Narrabri Gas Project area and the Plumb Road groundwater monitoring site (GW971623) at the Bohena anticline to test conceptual models of potential hydrogeological connectivity pathways in this area.

The confidence in the geometry and sub-surface layer structure along the line is variable:

- Eastern part of the cross-section: there is lower confidence in this area due to a higher level of structural complexity in the Gunnedah Basin in proximity to the Hunter-Mooki thrust fault and the lack of high-quality stratigraphic data; multiple cross-section realisations are possible with the available data.
- Central-western part of the cross-section: there is higher confidence in this area due to the availability of many high-quality stratigraphic logs, a high-quality seismic line (Figure 2-4) in combination with distinct patterns shown on the AEM survey data.
- Western part of the cross-section: there is moderate confidence due to the coverage of the seismic line but there is a lack of stratigraphic logs.

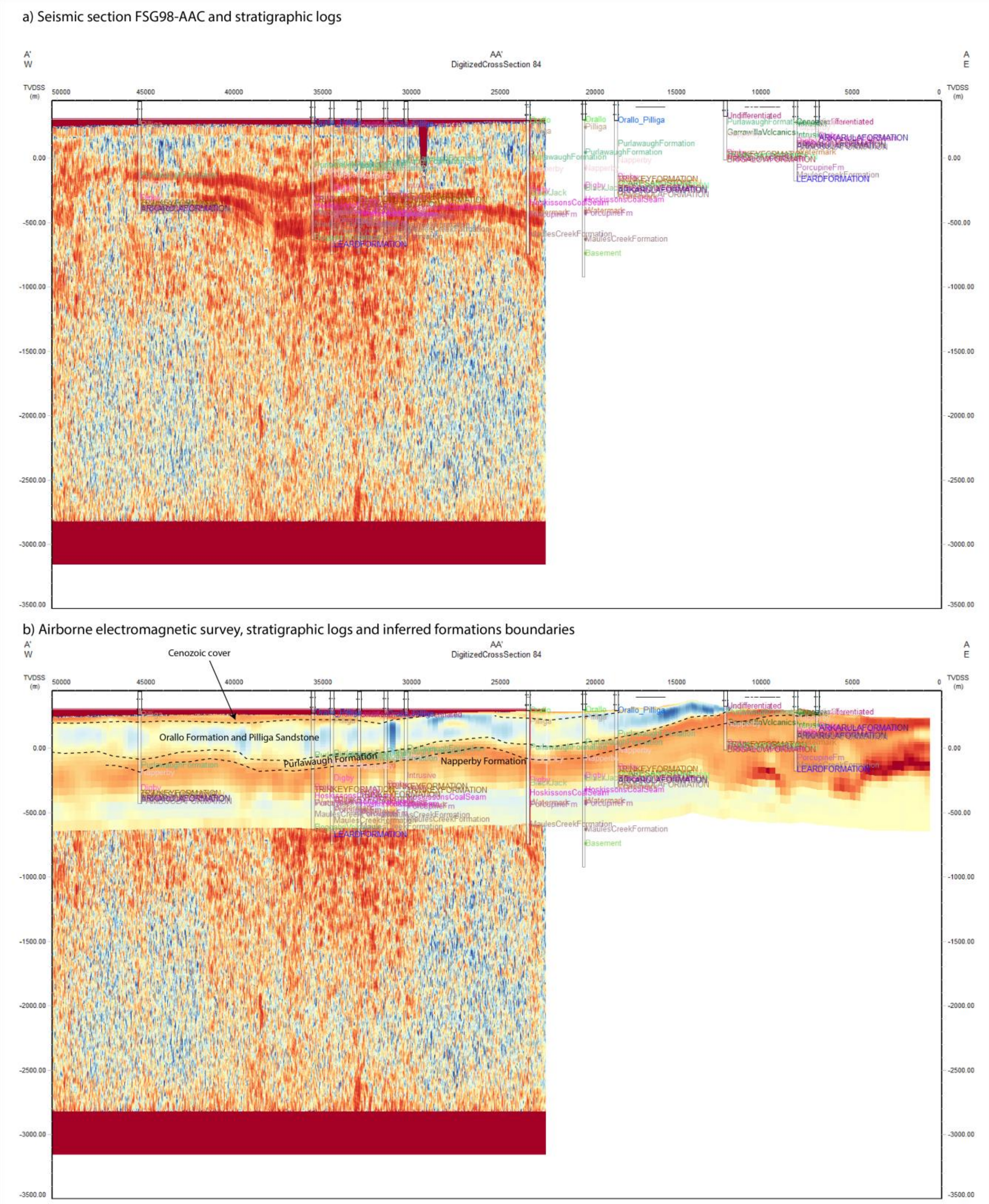

Figure 3-44 – a) Seismic line FSG98-AAC (see also Figure 2) and stratigraphic logs along transect for geochemical modelling (see also Figure 2-4) and b) AEM, stratigraphic logs and inferred shallow formation interfaces along transect CS1. For orientation, see Figure 3-25. The vertical exaggeration is approximately 25.

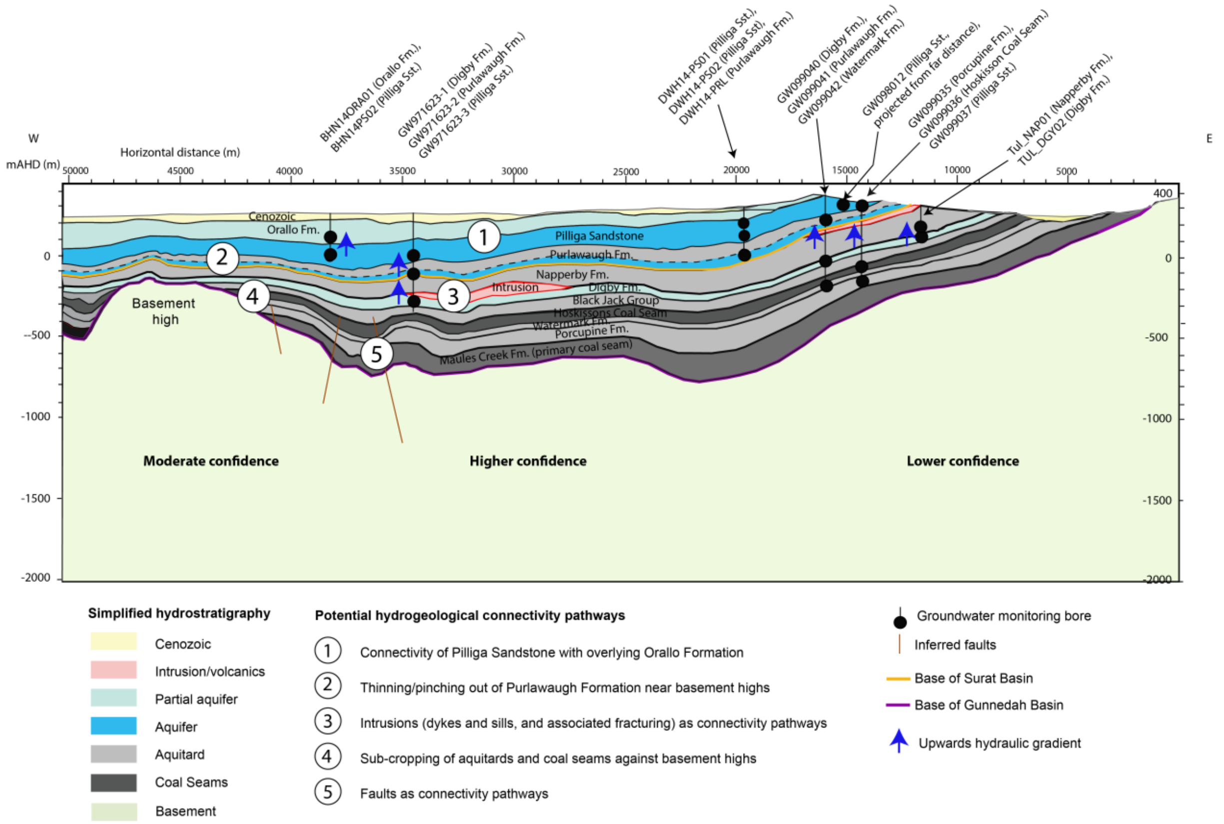

Figure 3-45 – Representative east-west oriented geological cross-section CS1 through the Narrabri Gas Project area (for orientation of cross-section, see Figure 3-25). The vertical exaggeration is approximately 25.

Noticeable geological features on geological cross-section 1 include:

- A thick igneous intrusion in the centre of the cross-section. This intrusion corresponds to the intrusion displayed at different stratigraphic intervals in Figure 3-3 (potential hydrogeological connectivity pathway 3); igneous rocks are also present at the eastern end of the cross-section (likely corresponding to the Garrawilla Volcanics).
- Thinning of Purlawaugh Formation from east to west (potential hydrogeological connectivity pathway 4);
- Sub-cropping of multiple Gunnedah Basin formations against basement high (potential hydrogeological connectivity pathway 4).

3.6.2 Cross-section 2 (CS2)

A second geological cross-section with an approximate east to north-west orientation (Figure 3-25) was developed to support the interpretation of hydrochemistry and environmental tracer data and assess the evolution of water chemistry from the eastern part of the Narrabri Gas Project area towards the Nyora groundwater monitoring site outside the north-western boundary of the Narrabri Gas Project area observed by Raiber et al. (2022a).

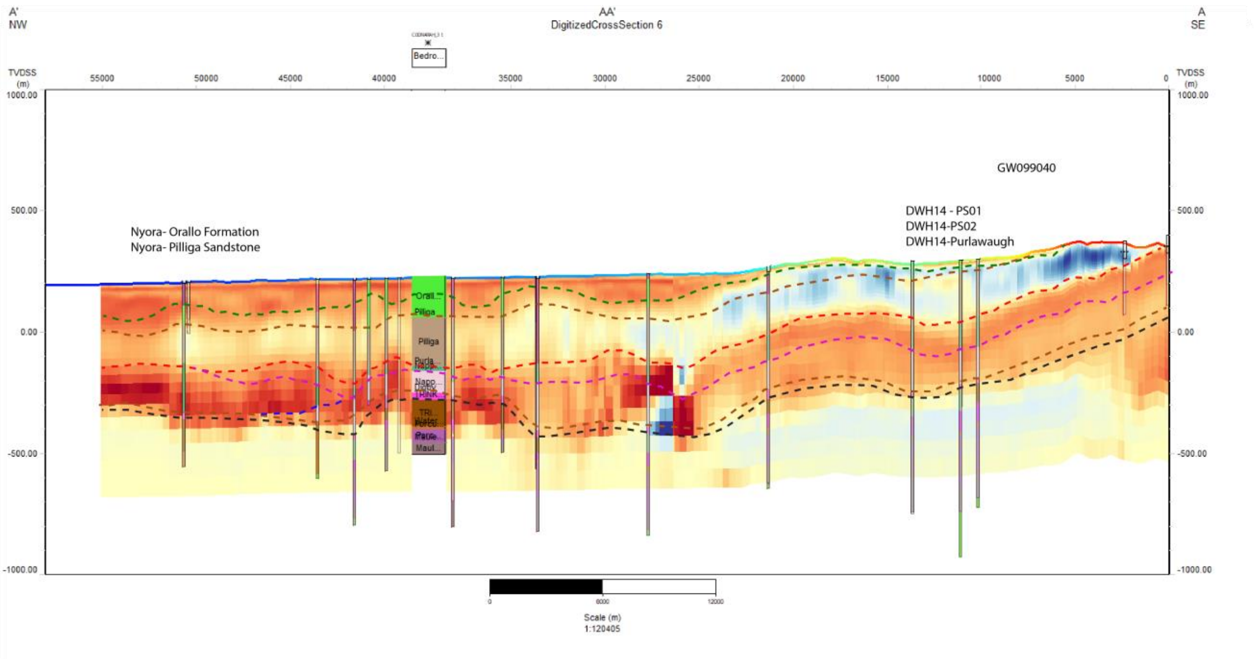

Figure 3-46 – Representative east-northwest oriented geological cross-section CS2 with stratigraphic logs, AEM and inferred layer boundaries through the Narrabri Gas Project area (for orientation, see Figure 3-25). The vertical exaggeration is approximately 30.

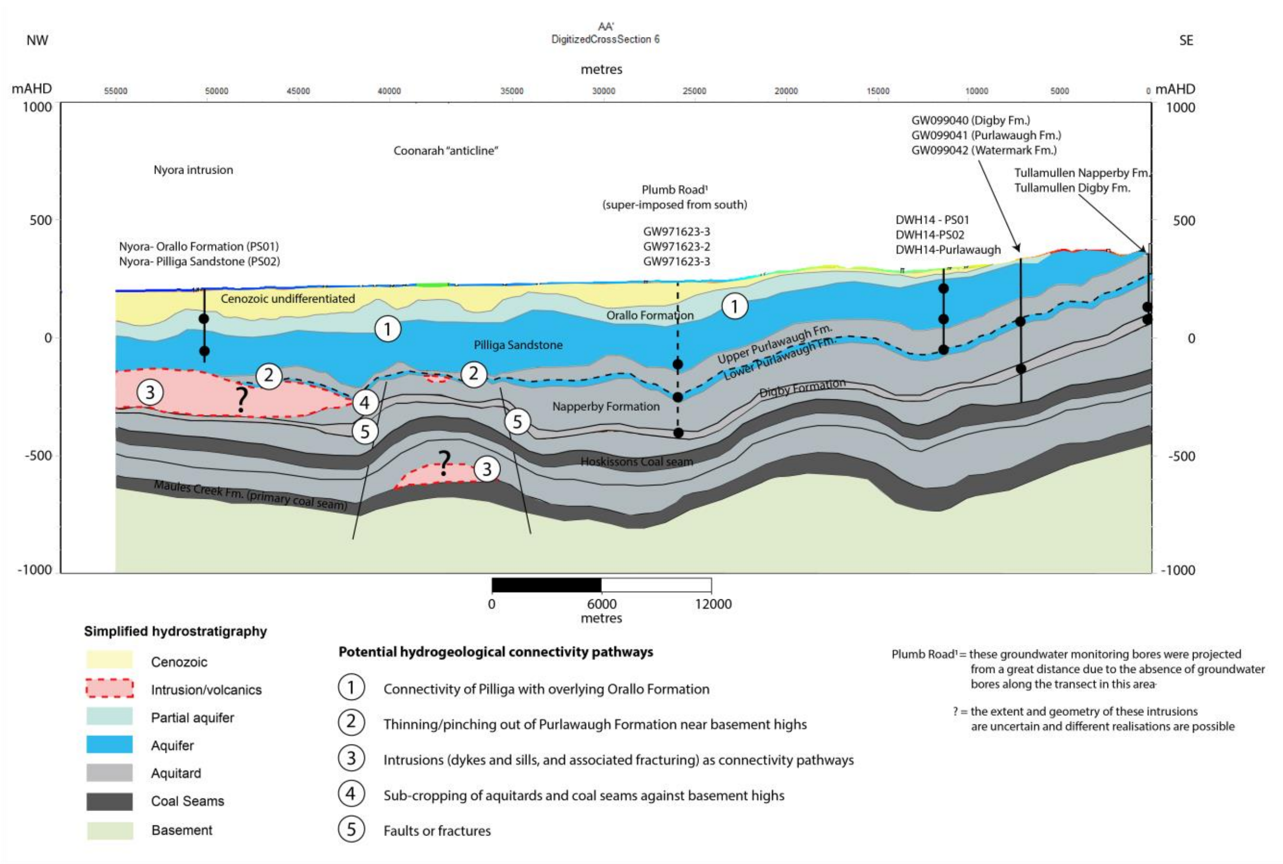

Figure 3-47 – Representative east-northwest oriented geological cross-section CS2 through the Narrabri Gas Project area (for orientation, see Figure 3-25). The vertical exaggeration is approximately 30.

Noticeable geological features on geological cross-section 2 include:

- Thinning of the Purlawaugh Formation from east to west (potential hydrogeological connectivity pathway 2 in Figure 3-47);
- A thick igneous intrusion at Nyora; at this site, the Purlawaugh Formation and Napperby Formation are absent according to stratigraphic logs of Nyora 1 exploration well (potential hydrogeological connectivity pathway 3);
- A thick igneous intrusion at Coonarah anticline; the intrusion appears to have resulted in doming (or forced folding) of overlying strata (potential hydrogeological connectivity pathway 3);
- Faulting within the Gunnedah Basin identified by a previous seismic survey (Figure 3-27; potential connectivity pathway 5).

3.7 Groundwater hydrochemistry

3.7.1 Spatial distribution of salinity

We have investigated the hydrochemical evolution within the Pilliga Sandstone, the major GAB aquifer in this region, by assessing the spatial patterns of salinity (represented by the proxy electrical conductivity -EC), aiming to better understand potential connectivity with or separation between adjacent hydrostratigraphic units. As rainfall water that recharges aquifers displays a low EC, this tracer is very useful for assessing aquifer connectivity or separation of aquifers in areas where distinct water chemistries are observed in different formations.

The spatial assessment showed that groundwater within the Pilliga Sandstone is very fresh within the south-eastern and central part of the proposed CSG development area (Figure 3-48). In this area, the EC of Pilliga Sandstone groundwater (with most bores screened at ~80 to 120 m depth) is typically below 150 µS/cm (for comparison, the upper limit for EC of drinking water is ~1000 µS/cm), except for Dewhurst 14 (DWH-PS02), where the EC measured for the deeper bore in the Pilliga Sandstone was minimally higher (~160 µS/cm, which is still very fresh for sedimentary bedrock groundwater in the GAB). In comparison, the shallower bore at the same location (DWH-PS01) is fresher (~107 µS/cm). Similarly, very fresh Pilliga Sandstone groundwater (92 and 112 µS/cm) was also observed at two bores screened at different depths within the Pilliga Sandstone at Dewhurst 3 (Figure 3-48). Furthermore, the spatial distribution of EC shows that Pilliga Sandstone groundwater in the north-western part of the proposed CSG development area has a higher salinity compared to groundwater in the south-eastern and central part of the proposed CSG development area.

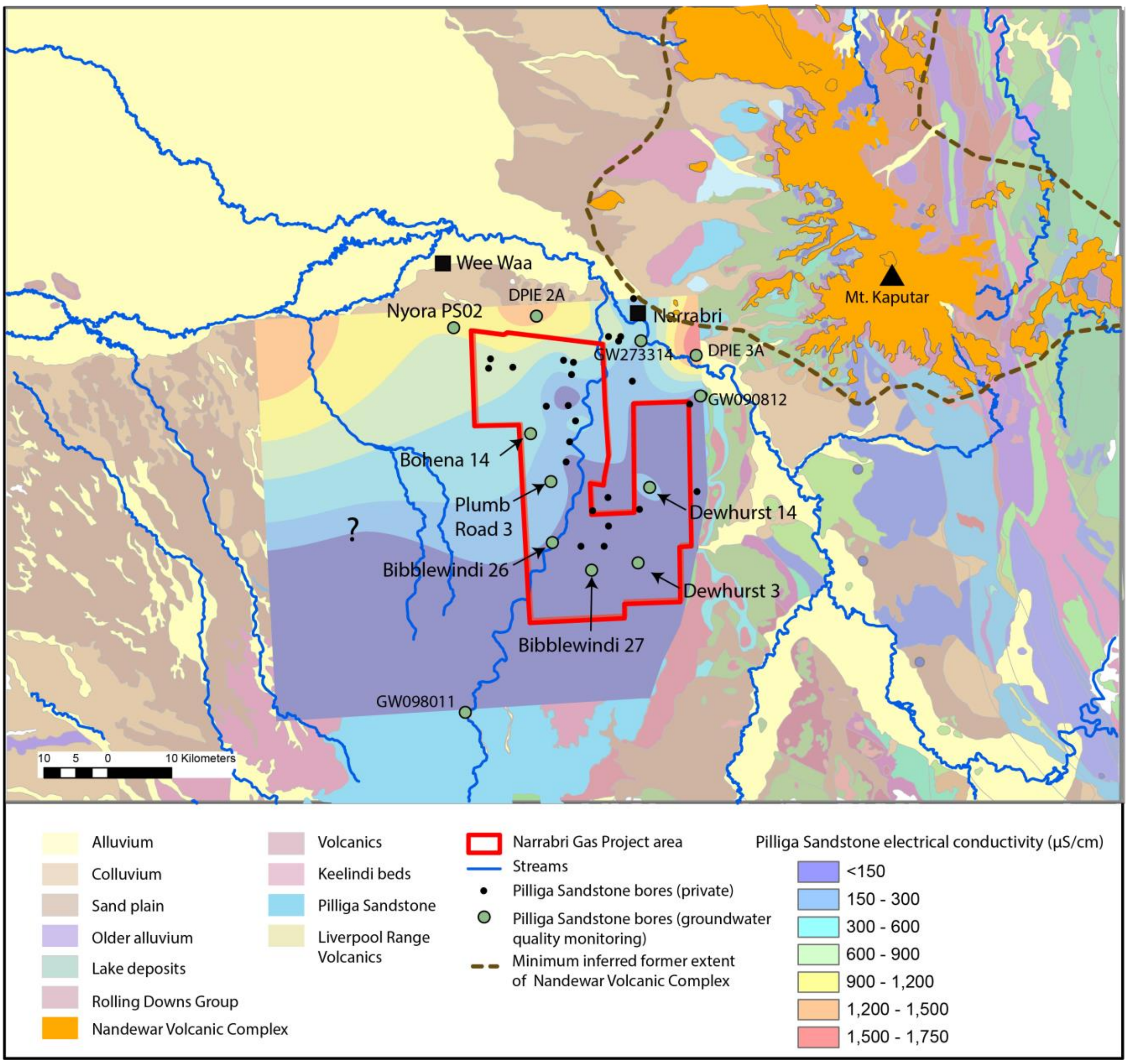

Figure 3-48 – Spatial distribution of groundwater salinity for Pilliga Sandstone in the Narrabri Gas Project area overlain on simplified surface geology (from Raiber et al., 2022a).

At the Plumb Road NSW DPIE monitoring site (Plumb Road 3/GW971623-3 on Figure 3-48), the EC of a bore screened in the Pilliga Sandstone is slightly higher than at groundwater bores further east (although with an EC of ~220 µS/cm, it is still very fresh compared to other GAB groundwaters). At the same site, the EC of Purlawaugh Formation (the aquifer below the Pilliga Sandstone, which is the basal unit of the Surat Basin in this area) groundwater is approximately 2100 µS/cm, while groundwater within the Digby Formation (a partial aquifer or leaky aquitard in the Gunnedah basin) is approximately 14,200 µS/cm (Figure 3-49). The EC of groundwater within the Maules Creek Formation at nearby sites (e.g. at Bohena 4, which is located only approximately 300 m away from this site; Figure 3-49) is generally much higher, ranging from approximately 7000 to almost 19,000 µS/cm.

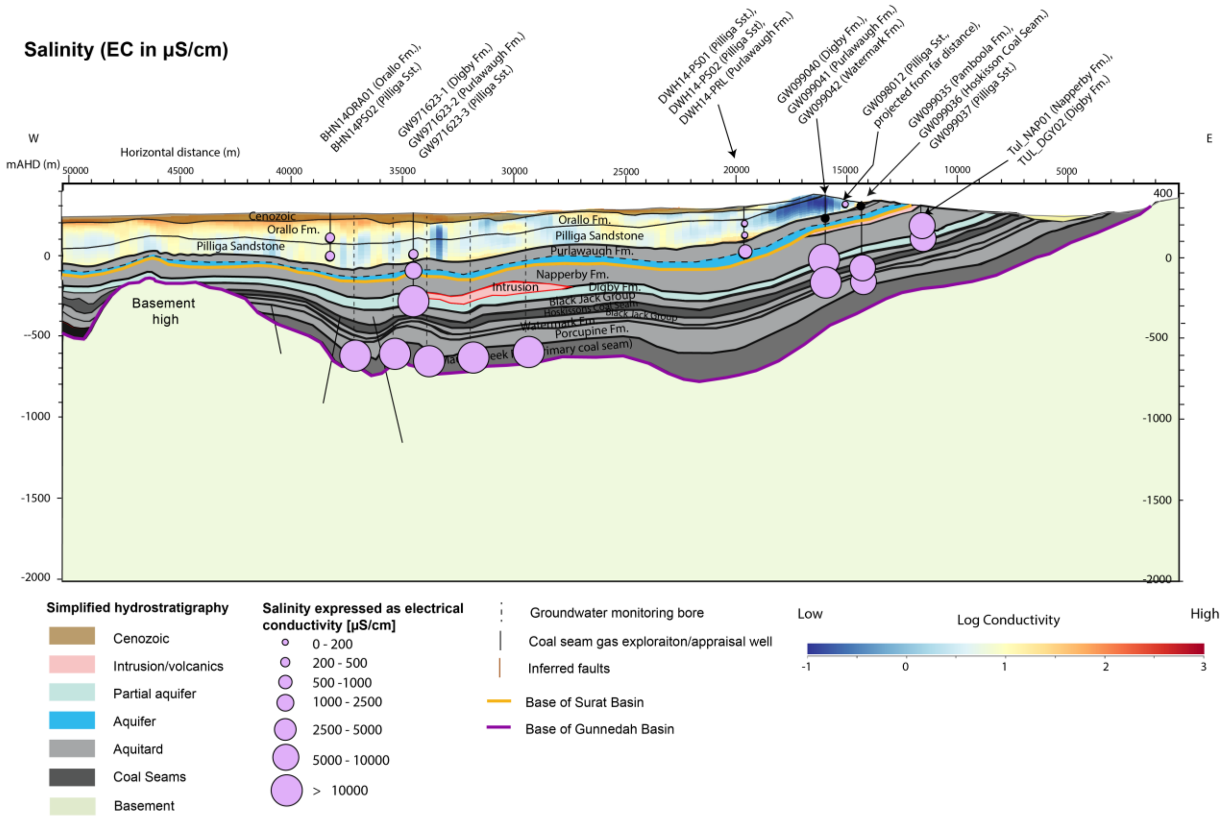

Figure 3-49 – Groundwater salinity for Surat and Gunnedah basins formation and electromagnetic depth-conductivity structure for the Orallo Formation and Pilliga Sandstone along east-west oriented geological cross-section CS1 through the Narrabri Gas Project area (for orientation, see Figure 3-25).

In this area, the assessment suggests that there is a clear depth-dependency of groundwater salinity, where groundwater is freshest the uppermost aquifers and brackish and saline in deeper underlying partial aquifers or aquitards (Figure 3-49 and Figure 3-50).

As shown in Figure 3-49, at Plumb Road, multiple aquitards (e.g. Watermark Formation, Porcupine Formation, Napperby Formation and the upper part of the Purlawaugh Formation) with a combined thickness of several hundred metres, creates a physical separation of the Maules Creek Formation (CSG target) from the Pilliga Sandstone. These observations highlight that shallow fresh Surat Basin aquifers here do not seems to be influenced significantly by interactions with the deeper formations which contain more mineralised groundwater. This provides an initial evidence of aquifer disconnection at this location, which will be discussed further in subsequent sections.

Towards the north-western part of the proposed Narrabri Gas Project area, a further increase in EC can be observed. At a monitoring bore at Nyora and at the DPIE 2A monitoring bore west of Narrabri (Figure 3-48 and Figure 3-50) the EC of the Pilliga Sandstone groundwater is above 1000 µS/cm (approximately 1100 µS/cm, respectively). At the same site (Nyora), the EC of groundwater sampled from the Orallo Formation, which overlies the Pilliga Sandstone, is almost identical to that of the Pilliga Sandstone. Likewise, at Bohena 14 (Figure 3-49), the EC of groundwater in the Pilliga Sandstone and the Orallo Formation are also almost identical (~410 and 420 µS/cm, respectively), suggesting that these aquifers are potentially connected. As indicated by the multivariate statistical analysis and as shown by Raiber and Suckow (2018) and Raiber et al. (2022a), there is no significant further increase of the EC in the Pilliga Sandstone towards the west.

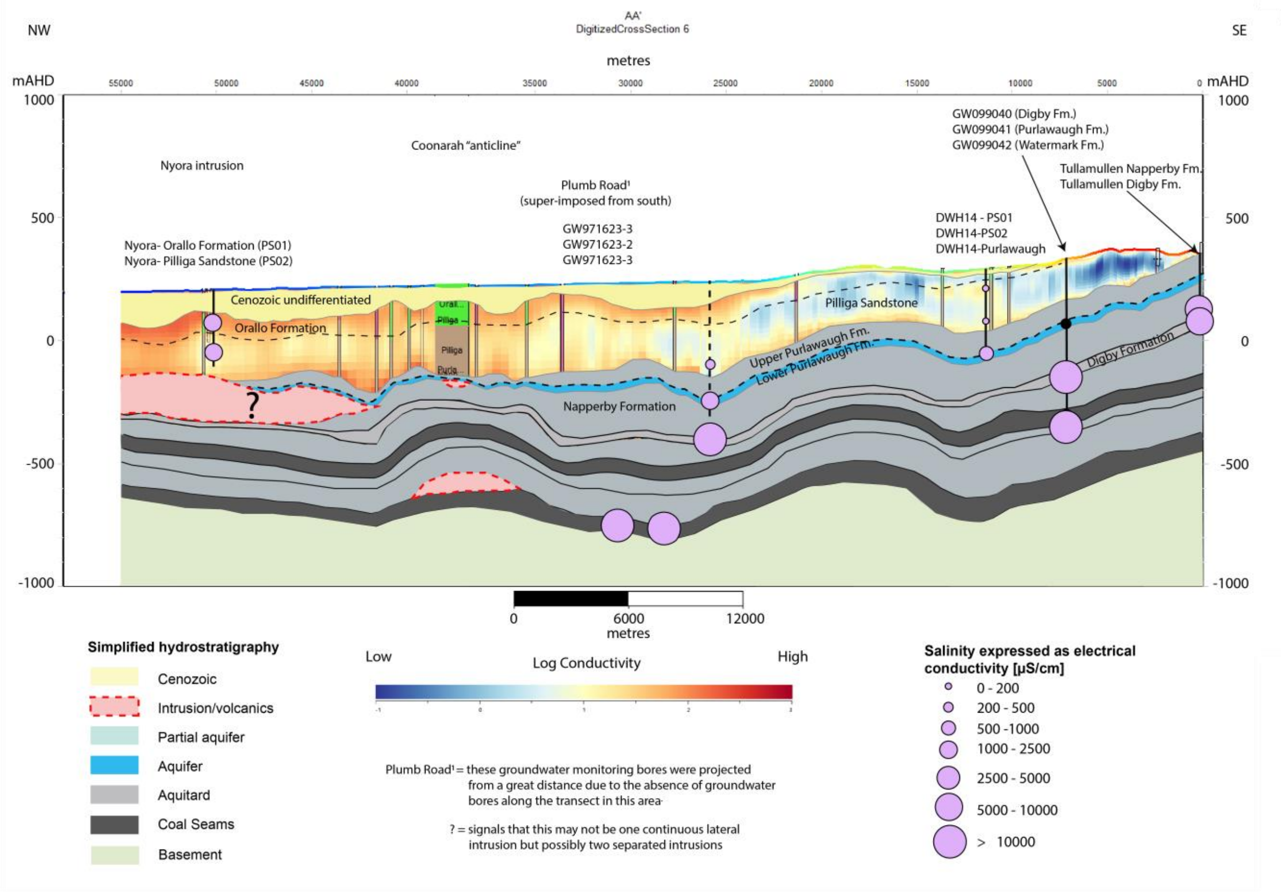

Figure 3-50 – Groundwater salinity for Surat and Gunnedah basins formation and Pilliga Sandstone along east-northwest oriented geological cross-section CS2 through the Narrabri Gas Project area (for orientation, see Figure 3-25).

3.7.2 Groundwater type

A Piper diagram of groundwater samples in the Narrabri Gas Project area was constructed to provide an overview on groundwater type (or hydrochemical facies) in this area.

The low left Triangle (cations) shows the relative concentrations of calcium (Ca^{2+}), magnesium (Mg^{2+}), sodium (Na^{+}), and potassium (K^{+}). whereas the low right Triangle (Anions) displays the relative concentrations of bicarbonate (HCO_3^{-}) + carbonate (CO_3^{2-}), sulphate (SO_4^{2-}), chloride (Cl^{-}), and nitrate (NO_3^{-}). The central diamond is formed by projecting points from the two triangles below; it indicates overall water type by combining both cation and anion compositions.

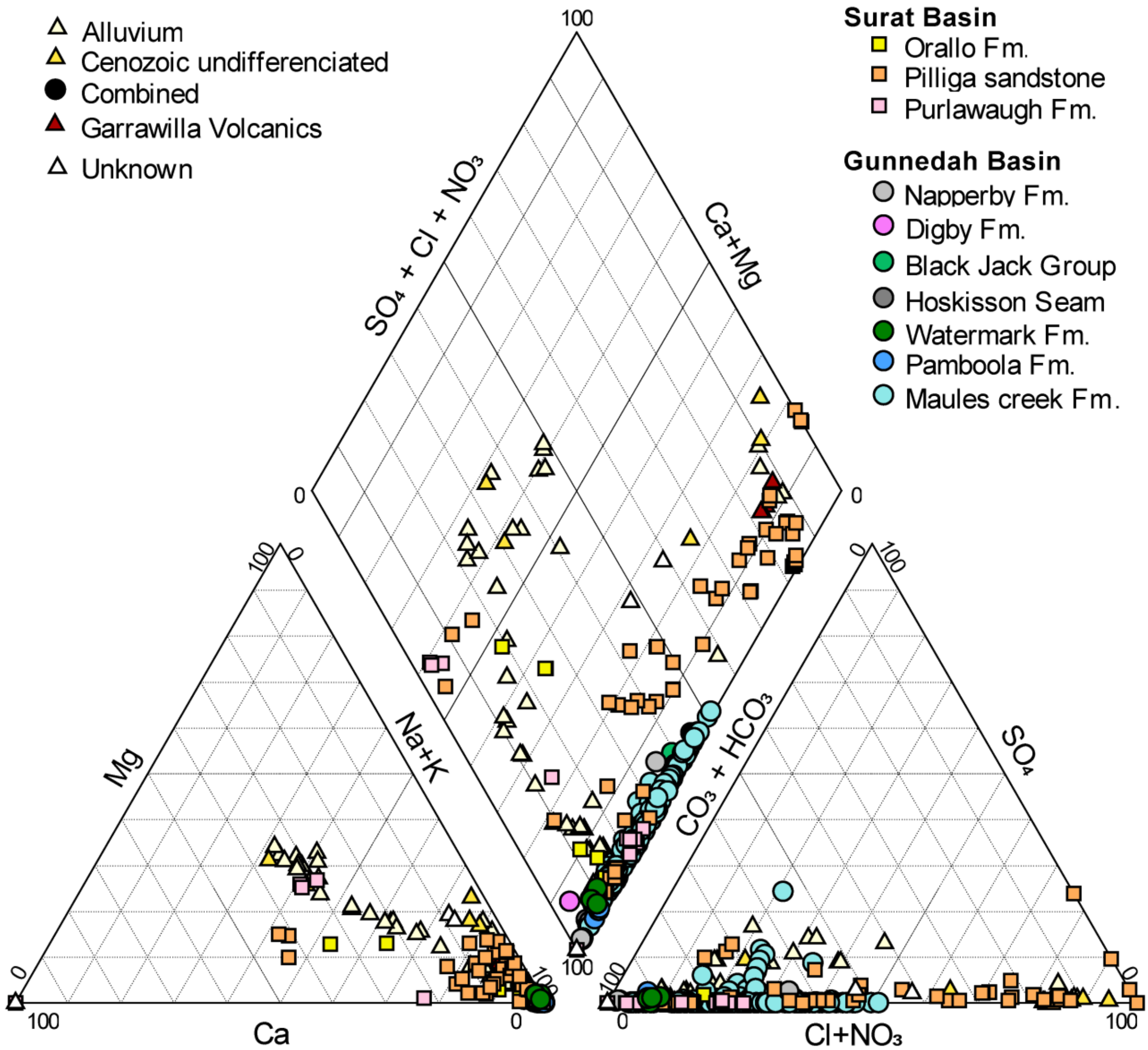

Figure 3-51 - Piper diagram that represent relative proportion of major ions in all groundwaters within the Narrabri Gas Project area. The data displayed in this figure present an ionic balance below 20%.

Groundwater samples collected from the deep Gunnedah Basin (represented as circles in Figure 3-51) are sodium-bicarbonate waters with a slight variation in HCO_3 content for the Maules Creek Formation (the primary CSG target). Groundwaters extracted from the Surat Basin (represented as squares in Figure 3-51) have various hydrochemical facies ranging from sodium-bicarbonates to sodium chlorite type. Groundwaters from the Pilliga Sandstone have the highest variability in chloride, calcium and sodium proportions. This is likely due to a complex pattern of groundwater evolution, with some groundwater samples near the outcrop beds characterised by very low pH (~5) and very low salinities, suggesting very rapid recharge and limited evapotranspiration prior to recharge.

3.7.3 Hierarchical cluster analysis (HCA) of groundwater chemistry in the Narrabri region

Building up on the work by Raiber et al. (2022a) and the assessment of spatial patterns of salinity and basic hydrochemistry presented in sections 3.7.1 and 3.7.2, a multivariate statistical analysis (hierarchical cluster analysis – HCA) was conducted with the hydrochemical records used by Raiber et al. (2022a) and additional data from samples collected from new NSW DPIE/Water NSW, Santos groundwater monitoring bores and groundwater monitoring bores from the NSW coal basin monitoring network during this study. This assessment focussed on samples from the wider Narrabri Gas Project area.

A multivariate statistical analysis was conducted in Statgraphics software on hydrochemical data from aquifers within the wider Narrabri Gas Project area to assess the variability within different aquifers and determine if there are similarities or characteristic differences between different aquifers, with a focus on understanding where potential hydrogeological connectivity between Gunnedah Basin strata (including coal seams) and overlying Surat Basin aquifers in the Narrabri region may occur.

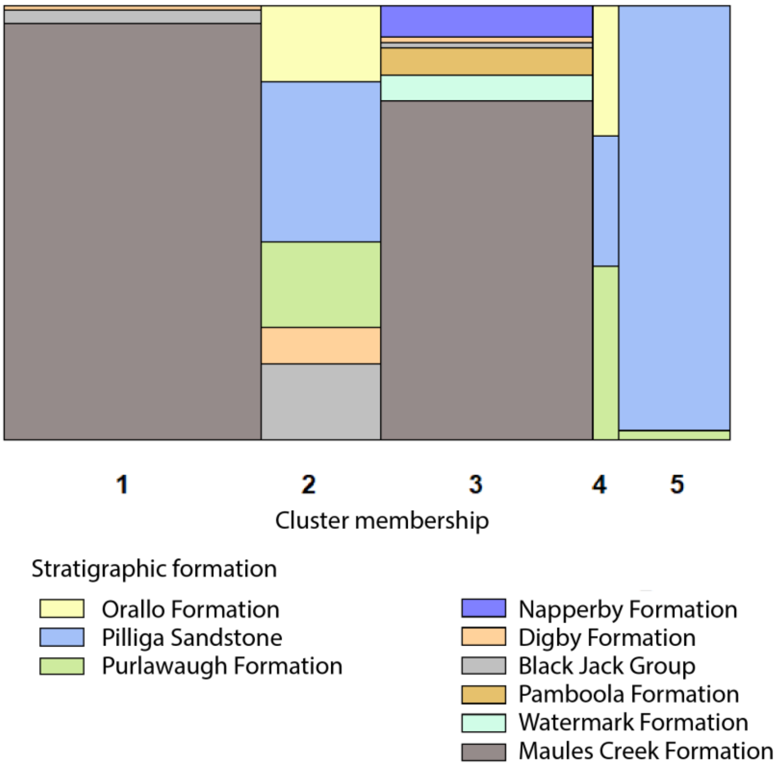

Figure 3-52 – Cluster-membership for groundwaters in the Pilliga region based on all available data (Cresswell (2014), WaterNSW (2024), Iverach et al. (2017, 2020a), Raiber and Suckow (2018), Suckow et al. (2019), NSW DPIE (2021), Raiber et al. (2022a) and the current study).

The thickness of each box corresponds to the number of samples and the width to the relative number of groundwaters assigned to different clusters, with numbers on the colour bars showing the number of samples for each aquifer. For example, in Cluster 2, 5 samples were assigned to the Orallo Formation and 33 samples to the Pilliga Sandstone.

A cross-tabulation was conducted to determine if there is a statistical relationship between aquifer membership and the HCA-derived cluster (Figure 3-52). A hypothesis test was conducted to determine whether to reject the hypothesis that the 'aquifer membership' and 'cluster membership' classifications are independent. This test showed that the P-value is less than 0.05, and the hypothesis that the observed value of 'aquifer membership' for a case is independent from its value for 'cluster membership' can therefore be rejected at the 95% confidence level. In other words, statistically 'aquifer membership' and 'cluster membership' are mutually dependent and the aquifers are characterised by their water chemistry.

Multivariate statistical analysis showed that there are five hydrochemical groups (clusters) within the dataset comprising all sedimentary bedrock groundwater hydrochemical records available for this study in the Narrabri region in NSW (a spatial sub-set of samples used by Raiber and Suckow (2018) for the entire Coonamble Embayment). The different clusters are marked by differences in pH, EC or ion ratios. The major characteristics (represented by median concentrations) for all parameters are presented in Table 1. Spatial and vertical aquifer relationships are shown along geological cross-section CS1 in Figure 3-52.

Table 7 – Median concentrations of hydrochemical parameters for the five groundwater chemistry clusters of data in the Narrabri region based on all data available for this study (Cresswell (2014), Raiber et al. (2018), Suckow et al. (2019), Raiber et al. (2022a), data provided by WaterNSW and the current study. The ratios are by mass. Median depths of each cluster are also shown.

Parameter	Cluster 1	Cluster 2	Cluster 3	Cluster 4	Cluster 5
N	99	46	85	14	43
Percentage of all records	34	16	30	5	15
EC (µS/cm)	15300	1900	13484	1164	181
Depth (mbgl)	987	260	903	167	201
pH	8.32	9.12	7.5	7.32	5.83
Na (mg/L)	4260	352	4180	212	26
Ca (mg/L)	8.1	2	18	38.5	1
Mg (mg/L)	4.36	0.5	15	11	1
K (mg/L)	65	14	120	5.5	6
Cl (mg/L)	1490	68.5	1131	41.5	33
HCO_3 (mg/L)	8080	540	8006	197	19.6
SO_4 (mg/L)	0.7	1	15	0.5	0.5
F (mg/L)	5.45	0.936	3.94	0.2	0.05
Ba (mg/L)	16	0.18	0.19	0.55	0.112
Ca/Na	0.002	0.006	0.004	0.182	0.038
Mg/Na	0.001	0.001	0.003	0.05	0.04
K/Na	0.015	0.039	0.029	0.026	0.231
HCO_3/Cl	5.42	7.88	7.08	4.75	0.59
SO_4/Cl	0.004	0.015	0.013	0.012	0.015
F/Cl	0.003	0.014	0.003	0.004	0.004

The multivariate statistical analysis of the hydrochemistry of all groundwaters with hydrochemical data available for this study within the wider Narrabri Gas Project area showed that hydrochemical records of all hydrostratigraphic units are assigned to multiple clusters, indicating that some hydrochemical variability occurs within all formations (Figure 3-52). The hydrochemical clusters each include groundwater hydrochemical records with similar characteristics. The HCA and cross-tabulation also show that the hydrochemistry of the Pilliga Sandstone and the major coal-bearing formations of the Gunnedah Basin are very distinct, as all of the Pilliga Sandstone hydrochemical records are assigned to clusters 2, 4 and 5, whereas all groundwaters from the Maules Creek Formation (the primary CSG target unit) are assigned to clusters 1 and 3. The vertical differences in cluster assignment for groundwaters hydrochemical records from different formations is highlighted in the geological cross-section CS1 in Figure 3-53.

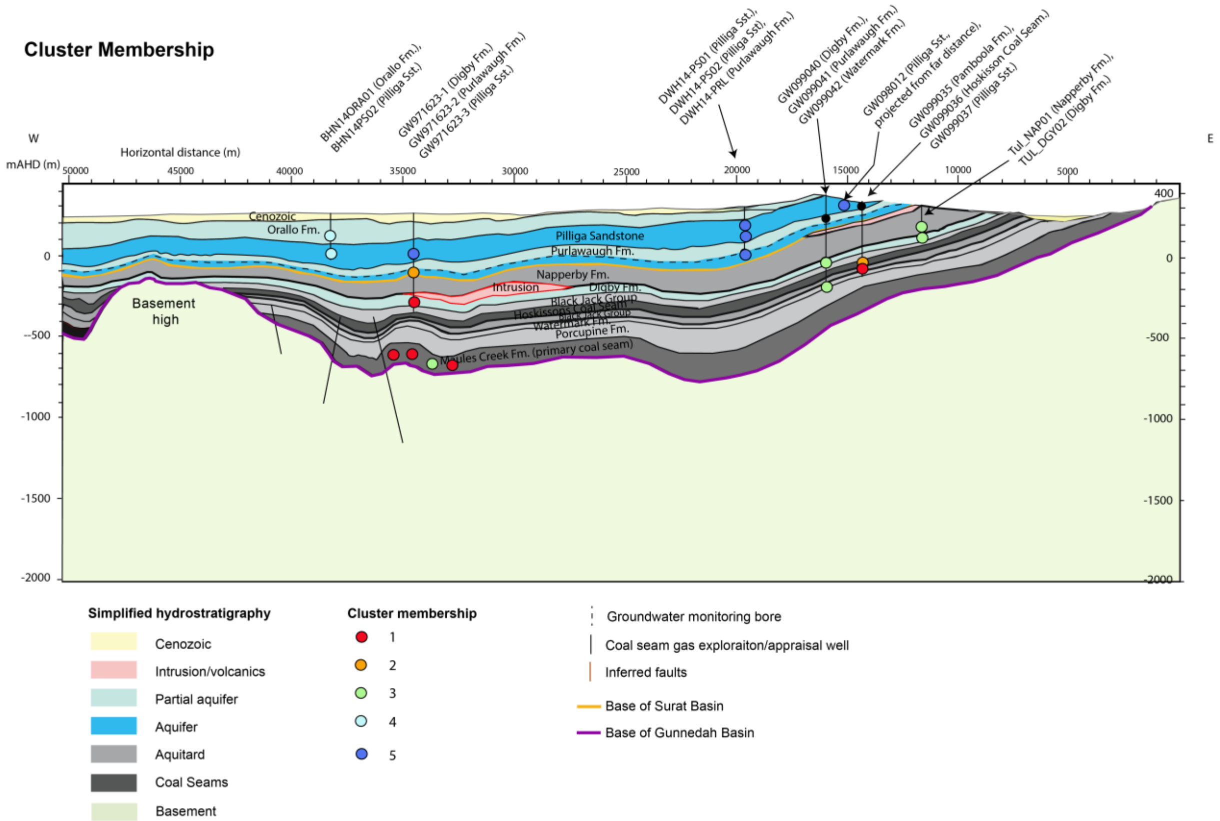

Figure 3-53 – Groundwater chemistry cluster membership for Surat and Gunnedah basins formation along east-northwest oriented geological cross-section through the Narrabri Gas Project area (for orientation, see Figure 3-25).

The major characteristics of different hydrochemical clusters are described below:

Cluster 1: Groundwaters assigned to Cluster 1 have a median EC of 15,300 µS/cm and are dominated by Na and HCO_3. This cluster contains groundwater hydrochemical records with a low median Ca and Mg, with most groundwaters assigned to this cluster showing ion/Cl ratios for these parameters below those of seawater. Median SO_4 concentration is 0.7 mg/L, with most samples having concentrations at or close to the detection limit. K concentrations are relatively high (median of 65 mg/L), and many samples have concentrations above the seawater K/Cl ratio.

Na and HCO_3 versus Cl ratios are high and mostly above the ratios of seawater. Furthermore, there is an increase of these ion/Cl ratios with increasing salinity. Fluoride concentrations are high (median concentration of 5.45 mg/L). Groundwaters assigned to this cluster are sourced mostly from deep wells within the Maules Creek Formation (median depth of 987), with only few samples from the Black Jack Group (which hosts the Hoskissons Coal seam) and the Digby Formation (e.g. GW971623-1 at Plumb Road; Figure 3-53).

Cluster 2: Groundwaters assigned to Cluster 1 have a median EC of 1,900 µS/cm and are dominated by Na and HCO_3 (HCO_3/Cl ratio of 7.88). These groundwaters have low Ca and Mg and relatively high K concentrations (median of 14 mg/L). Sulfate concentrations are low and mostly at the detection limit. Fluoride concentrations are high, with the F/Cl ratio one order of magnitude higher than for other clusters (based on the mass concentrations of the median). Groundwater chemistry records from this cluster are mostly collected from the deeper bores within the Surat Basin strata (median depth of 260 m), with a few samples also collected from the Digby Formation and Black Jack Group close to the eastern recharge bed (e.g. Figure 3-53).

Cluster 3: Groundwaters assigned to Cluster 3 are similar to those of Cluster 2. They have high ECs (median of 13,484 µS/cm), and are dominated by Na and HCO_3 with relatively lower Cl concentrations than Cluster 1. Groundwaters within this cluster have similar salinities as those in Cluster 1, but have higher median Ca, Mg and K concentrations. Sulfate concentrations are also higher than in Cluster 1 and above the detection limit. Samples in this cluster are all sourced from the deeper groundwater bores or exploration wells within the different Gunnedah Basin formations (median depth of 903 m), with most of them collected from the Maules Creek Formation.

Cluster 4: Groundwaters assigned to this cluster have a median EC of 1,164 µS/cm and are dominated by Na and HCO_3. Ca and Mg concentrations are high with Ca/Na and Mg/Na ratios clearly higher than those in clusters 1 and 2. SO_4 concentrations are low and mostly at the detection limit, and fluoride concentrations are also low (median of 0.2 mg/L). Groundwaters assigned to this cluster are sourced exclusively from the Surat Basin formations and the Garrawilla Volcanics (Figure 3-52), including samples within the Pilliga Sandstone and Orallo Formation in the western part of the proposed CSG development area at the deeper parts of the Surat Basin (further away from the outcrop beds) (e.g. Orallo Formation and Pilliga Sandstone groundwater at BHN14 on Figure 3-53). Here, the lithology of the Orallo Formation and Pilliga Sandstone is more variable with higher contents of clay, mudstone and siltstone and less quartz, as shown by the XRD (Section 3.3.1) and AEM survey results (Section 3.5.2). The median depth of groundwater bores assigned to this cluster is 167 m.

Cluster 5: Groundwaters assigned to Cluster 5 are very fresh (represented by a median EC of ~181 µS/cm) with a low pH (median of 5.8, and close to the pH of rainwater) and are relatively shallow compared to other clusters. These groundwaters are dominated by Na, Cl and HCO_3, but with the lowest HCO_3/Cl ratio of all clusters. Sulfate concentrations are low and mostly close to or below the detection limit. Ca and Mg concentrations are higher than those of hydrochemical records in Cluster 2. Fluoride concentrations are very low (median of 0.05 mg/L) and mostly at detection limit. Samples assigned to this cluster are almost exclusively collected from the Pilliga Sandstone, with the only samples from other formations assigned to this cluster collected from the Purlawaugh Formation at DWH14 (Figure 3-53). They were collected from bores located in the east, south-east or centre of the proposed CSG area and within or close to the recharge beds of the Pilliga Sandstone with a median bore depth of 201 m.

3.7.4 Stable isotopes of water

Oxygen-18 ($\delta^{18}O$) versus deuterium ($\delta^{2}H$) values measured in groundwater are displayed by aquifer in Figure 3-54. These data are plotted with the monthly amount-weighted mean of water-stable isotopes in rainfall measured at Cobar ($\delta^{18}O$ = –4.64‰ and $\delta^{2}H$ = –23.5‰) with its associate local meteoric water line as $\delta^{2}H = –7.67 \times \delta^{18}O + 12.09$ (LMWL - Cobar) and as $\delta^{2}H = –8.05 \times \delta^{18}O + 13.67$ (LMWL - Brisbane) from Hollins et al. (2018). The Australian-wide Local Meteoric Water Line has been defined as $\delta^{2}H = –7.1 \times \delta^{18}O + 8.21$ by Liu et al. (2010). Exported from the Global Network of Isotopes in Precipitation (GNIP), Cobar (the closest GNIP station to Narrabri) rainfall amount-weighted mean of water-stable isotopes signature is plotted according to amount of precipitation (below and above 50 mm/month). The global meteoric water line (GMWL) $\delta^{2}H = 8 \times \delta^{18}O + 10$ from Craig (1961) is also included in the plot.

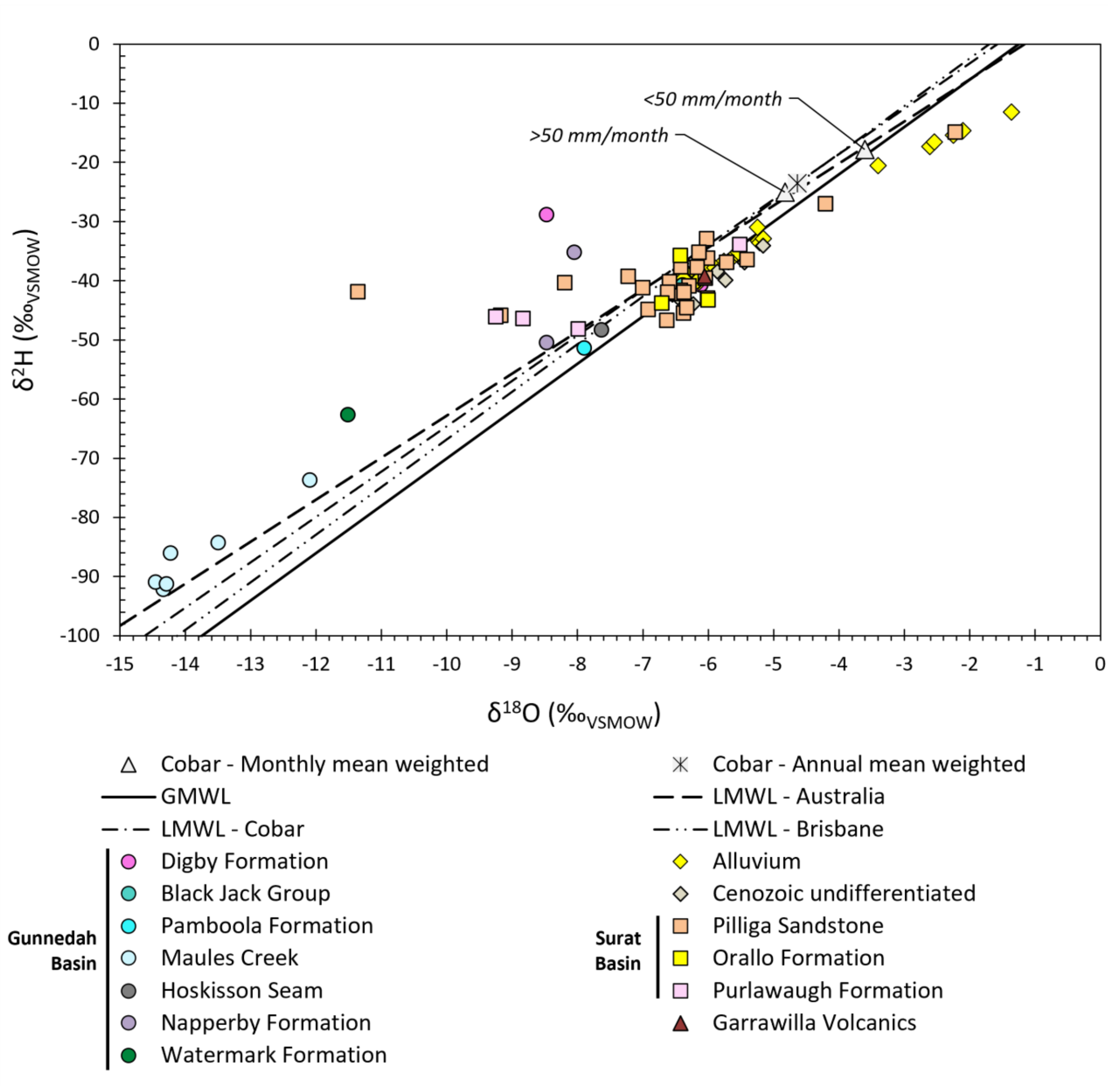

Figure 3-54 - Water stable isotopes (δ^2H vs $\delta^{18}O$) in groundwaters displayed by aquifer.

Rround shape = Gunnedah basin, square shape = Surat Basin), compared to rainfall signature at Cobar (NSW) and Brisbane (QLD). LMWL = local meteoric water line; GMWL = global meteoric water line, VSMOW = Vienna standard mean ocean water. Rainfall data source from Global Network of Isotopes in Precipitation (GNIP) and water lines from Hollins et al. (2018) and Liu et al. (2010). Alluvial groundwater samples are sourced from Iverach et al. (2017).

Groundwaters from alluvial aquifers (yellow diamond) displayed the most enriched signature and plot to the right of the LMWL and the GMWL, showing a clear evaporation signature, which indicates that evaporation occurred prior to a local recharge for this shallow aquifer. In addition, some of the groundwater samples plot close to rainfall levels below 50 mm/month, indicating that recharge to the alluvium also occurs at lower rainfall levels.

Groundwaters from the Surat Basin (square shape) show an intermediate signature (Figure 3-54) ranging from -11.36 to -2.22 for $\delta^{18}O$ (‰) and from -48.20 to -14.90 for δ^2H (‰) (Table 8). Pilliga Sandstone groundwater samples mostly displayed an intermediate signature, but some signatures show a slightly evaporated signature. This may indicate that a connectivity with the surface existed at some point, indicating that evaporation occurred prior to recharge.

Groundwater samples from the Gunnedah Basin (round shape) are mostly more depleted than Surat Basin groundwater, with values ranging from -14.45 to -6.11 for $\delta^{18}O$ (‰) and from -92.16 to -28.87 for $\delta^{2}H$ (‰). Moreover, samples from the Maules Creek Formation (primary CSG target unit) have highly depleted signatures with values of $\delta^{18}O$ and $\delta^{2}H$ reaching -14.49‰ and -92.16‰ respectively. These values represent some of the most depleted groundwaters measured in sedimentary basins in Australia so far. This is closely followed by a sample collected from the Watermark Formation.

The very depleted signatures of Maules Creek Formation groundwater samples and the significant gap compared to samples from the Surat Basin show that there is no evidence of connectivity between the Surat and the Gunnedah basins that can be observed within the water stable isotope data set.

Table 8 - Water stable isotope signature by aquifer. GB : Gunnedah Basin, SB : Surat Basin. Alluvial groundwater samples are mostly sourced from Iverach et al. (2017).

Aquifer	Basin name	$\delta^{18}O$ (‰)		$\delta^{2}H$ (‰)		N
		Min	Max	Min	Max	
Alluvium	-	-6.56	-1.36	-41.88	-11.52	43
Cenozoic undifferentiated	-	-6.55	-5.16	-43.95	-34.09	8
Orallo Formation	SB	-6.71	-6	-43.78	-35.75	3
Pilliga Sandstone	SB	-11.36	-2.22	-46.7	-14.9	28
Purlawaugh Formation	SB	-9.25	-5.52	-48.2	-33.94	4
Garrawilla Volcanics	-	-6.06	-6.06	-39.25	-39.25	1
Napperby Formation	GB	-8.47	-8.04	-50.48	-35.2	2
Digby Formation	GB	-8.47	-6.11	-40.73	-28.87	2
Black Jack Group	GB	-6.39	-6.39	-40.74	-40.74	1
Hoskisson Seam	GB	-7.63	-7.63	-48.32	-48.32	1
Pamboola Formation	GB	-7.9	-7.9	-51.41	-51.41	1
Watermark Formation	GB	-11.51	-11.51	-62.71	-62.71	1
Maules Creek Formation	GB	-14.45	-12.09	-92.16	-73.74	6

3.7.5 Methane concentrations as an indicator of aquifer connectivity

Background

Another parameter that can provide valuable insights into hydrogeochemical evolution and the connection between shallow sedimentary bedrock, alluvial aquifers and underlying coal seams are hydrocarbon gases such as the concentrations of methane concentrations in groundwater. In the

Pilliga region, methane is the major hydrocarbon gas measured in exploration wells and in groundwater bores.

Given the mobility of dissolved or gaseous methane in aquifers, methane (CH_4) is often considered as a precursor of other organic or even inorganic contaminants derived from coal. Hence, understanding methane dispersion is pivotal to understanding the occurrence of other chemicals. Prior experiences from the Surat and Clarence-Moreton basins in Queensland (e.g. Mallants et al., 2016) and unconventional gas projects in North America highlight the importance in obtaining pre-CSG development methane and other hydrocarbon baseline data to help understand exploitation-related risks and build community confidence. Methane observed in shallow alluvial or sedimentary bedrock aquifers can be produced in situ within these aquifers or be the result of migration from deeper coal-bearing formations. When there is no hydrogeological connection between the hydrocarbon source and a groundwater aquifer, methane detections in groundwater are most likely due to a shallow source (e.g. near-surface coal seams or other organic sediments) unrelated to the target coal seams. Therefore, to determine if methane in groundwater represents the natural background in an aquifer or is related to CSG activities, it is critical to obtain adequate baseline data and a thorough understanding of natural methane gas migration pathways, and to confirm the origin of methane, additional isotopic analysis (and other gas compounds) is needed (Jackson et al., 2013). These understandings can include methane migrating as gas and subsequent dissolution in different formation water with otherwise low concentrations or mixing between waters with different methane concentrations.

In the context of conventional and unconventional gas development, coal-bearing Hoskissons Coal seams (secondary CSG target) and deeper coal seams within the Maules Creek Formation (primary CSG target) are considered the primary source of CSG in the Pilliga region (whereas multiple formations are considered potential source rocks for hydrocarbon generation more broadly; Figure 1-1). In the context of CSG, the proposed gas development is targeting these coal seams directly, whereas earlier stages of conventional gas exploration targeted reservoir rocks above hydrocarbon source rocks (where gas is held in place by overlying seals such as the marine strata shown in Figure 1-1). Shallower formations including the coarser sediments at the base of the Purlawaugh Formation and sandy facies within the Digby Formation have been targeted for earlier conventional gas exploration; these rocks represent potential gas reservoir rocks to which gas has migrated from the underlying source rocks over very long geological time frames.

Morrison and Harris (1988) suggest that the Pilliga Sandstone has excellent reservoir properties, but that it lacks intraformational seals that stop gas from escaping upwards. Previous studies also suggested that the Pilliga Sandstone is a relatively clean, quartzose sandstone (Section 1.1), and it was therefore considered unlikely that there is significant methane generation within the formation. This will be discussed further below.

In contrast, the more variable lithological nature of the Purlawaugh Formation and presence of coal in the upper part of the Purlawaugh Formation (which is a chronological equivalent to the Walloon Coal Measures in Qld; Figure 1-1) means that some in situ methane generation may occur in this formation.

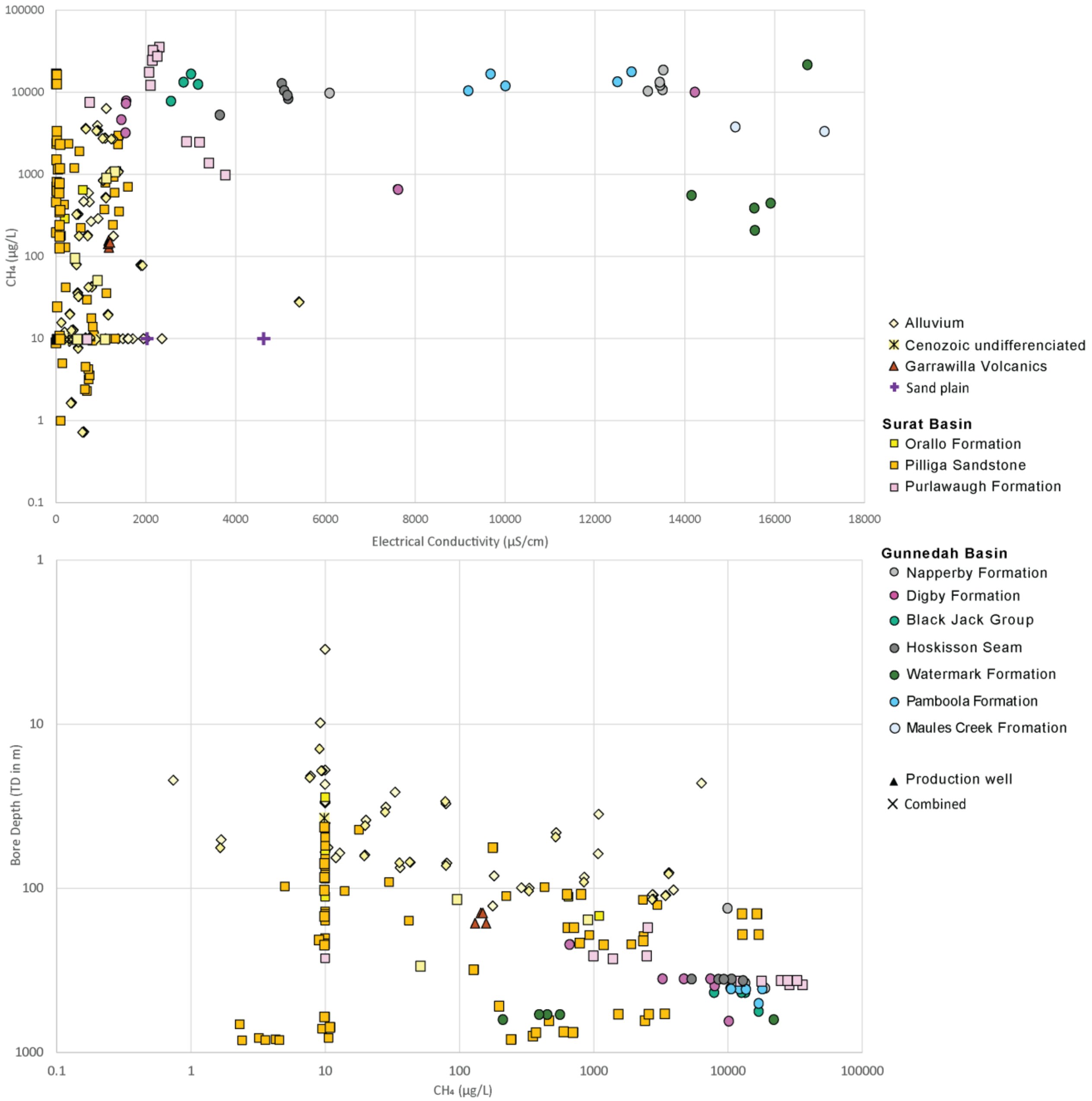

Figure 3-55 – Concentrations of methane versus a) electrical conductivity (EC); and b) bore depth.
Methane concentrations are based on Cresswell (2014), Iverach et al. (2020a), Suckow et al. (2019), Raiber et al. (2022a) and the current study.

No ethane (C_2H_6) was detected in Pilliga Sandstone groundwater samples, although a small concentration of ethane was measured at Tullamullen, east of the proposed Narrabri Gas Project area in the Napperby Formation. In exploration wells, the dominant component of the natural gas is also methane, although smaller amounts of ethane and propane were recorded in samples from some wells (reported in well completion reports published by Eastern Star Gas between 2008 and 2011).

Presence of dissolved methane in aquifers in the Narrabri Gas Project area

Methane concentration data available in this study (n = 137, including some bores with repeat measurements) from Cresswell (2014), Streamline Hydro (2018), Suckow et al. (2019), Iverach et al. (2020a), Raiber et al. (2022a) and the current study) show that the concentrations range from below or close to the detection limit (10 µg/L for most samples analysed at ALS laboratories and ~3 µg/L for samples analysed at UCDavis) and up to 36,000 µg/L measured in a groundwater sample collected from the Purlawaugh Formation (Figure 3-55). It is important to note that methane measured at groundwater bores within the productive shallow aquifers (e.g. Pilliga Sandstone and alluvial aquifers) at the observed concentrations does not pose a safety risk to water users.

Figure 3-55 show the methane concentration displayed by aquifer relative to bore depth (where known) and electrical conductivity (EC). This figure highlights mainly that groundwater samples collected from the Gunnedah Basin formations (circles) have typically both the higher EC and higher concentrations in methane than most Surat Basin groundwater samples. Furthermore, within the Gunnedah Basin, the deeper the bores are, the higher the methane concentrations tend to be, with a few exceptions for four samples from the Watermark Formation which have values that are significantly lower than boreholes at the same depth and in the same aquifer.

For the Surat Basin, although the EC values are all lower than 4000 µg/L, and boreholes have shallower depths, the methane concentrations have an overall higher variability (from below the detection limit to 36,000 µg/L).

The methane concentrations by aquifer will be discussed in more detail in the following paragraphs.

Gunnedah Basin (Maules Creek Formation and Hoskissons Coal seams)

Within the coal seams underneath the Surat Basin and the Digby and Napperby formations, methane concentrations are likely to be very high (as these rocks are both the source rocks for methane and targets for CSG development). Although no measurements of dissolved methane concentrations were available for groundwater extracted from exploration wells screened within these formations in this study, values from the Gloucester Basin and Surat Basin give an indication of the expected presence of very high methane concentrations within the deeper CSG target formations. For example, Banks et al. (2017) measured dissolved methane of up 215,000 µg/L within coal seams in the Gloucester Basin in NSW, and dissolved methane concentrations of up to 44000 µg/L were measured in the Walloon Coal Measures (water bores and some CSG wells) in Surat Basin in Qld (Julie Pearce, University of Queensland, personal communication; Pearce et al., 2021).

Within the Gunnedah Basin coal seams, methane gas concentrations collected using gas desorption and analysed using gas chromatography by Isotech of up to approximately 800,000 ppm (normalised to 1,000,000 ppm) have been reported in well completion reports by previous exploration lease holder Eastern Star Gas between 2008 to 2011 (compiled from a large number of well completion reports, as for example Eastern Star Gas, 2011b). Unlike the concentrations measured in groundwater, these values are not dissolved methane concentrations, and the concentrations are therefore not directly comparable.

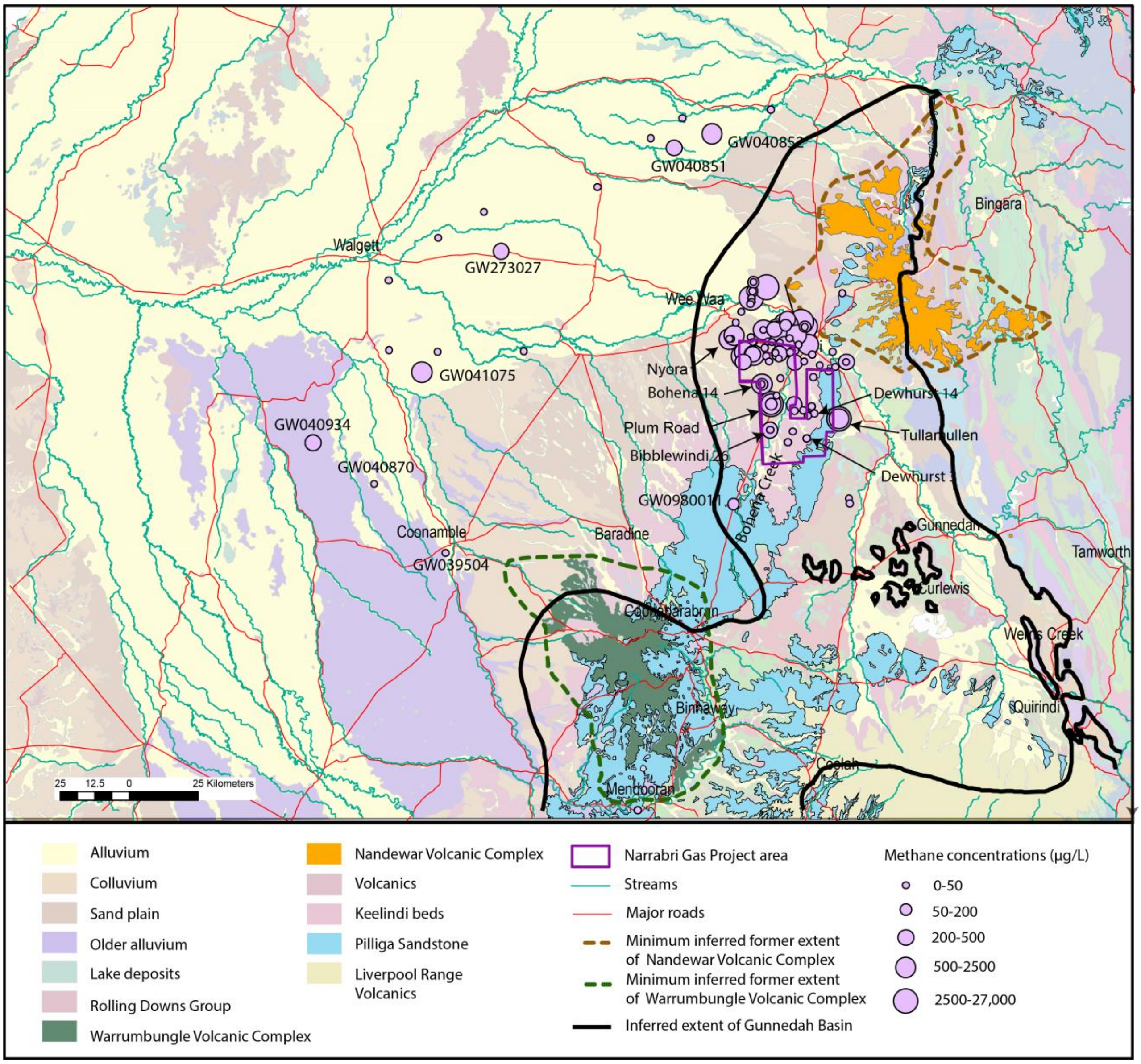

Figure 3-56 – Spatial distribution of dissolved methane concentrations without differentiation of hydrostratigraphic formations overlain on simplified surface geology. Methane concentrations are based on Cresswell (2014), Iverach et al. (2020a), Suckow et al. (2019), Raiber et al. (2022a) and the current study.

More detailed maps of the distribution of methane within the Pilliga Sandstone and alluvial aquifer are shown in Figure 3-59 and Figure 3-63.

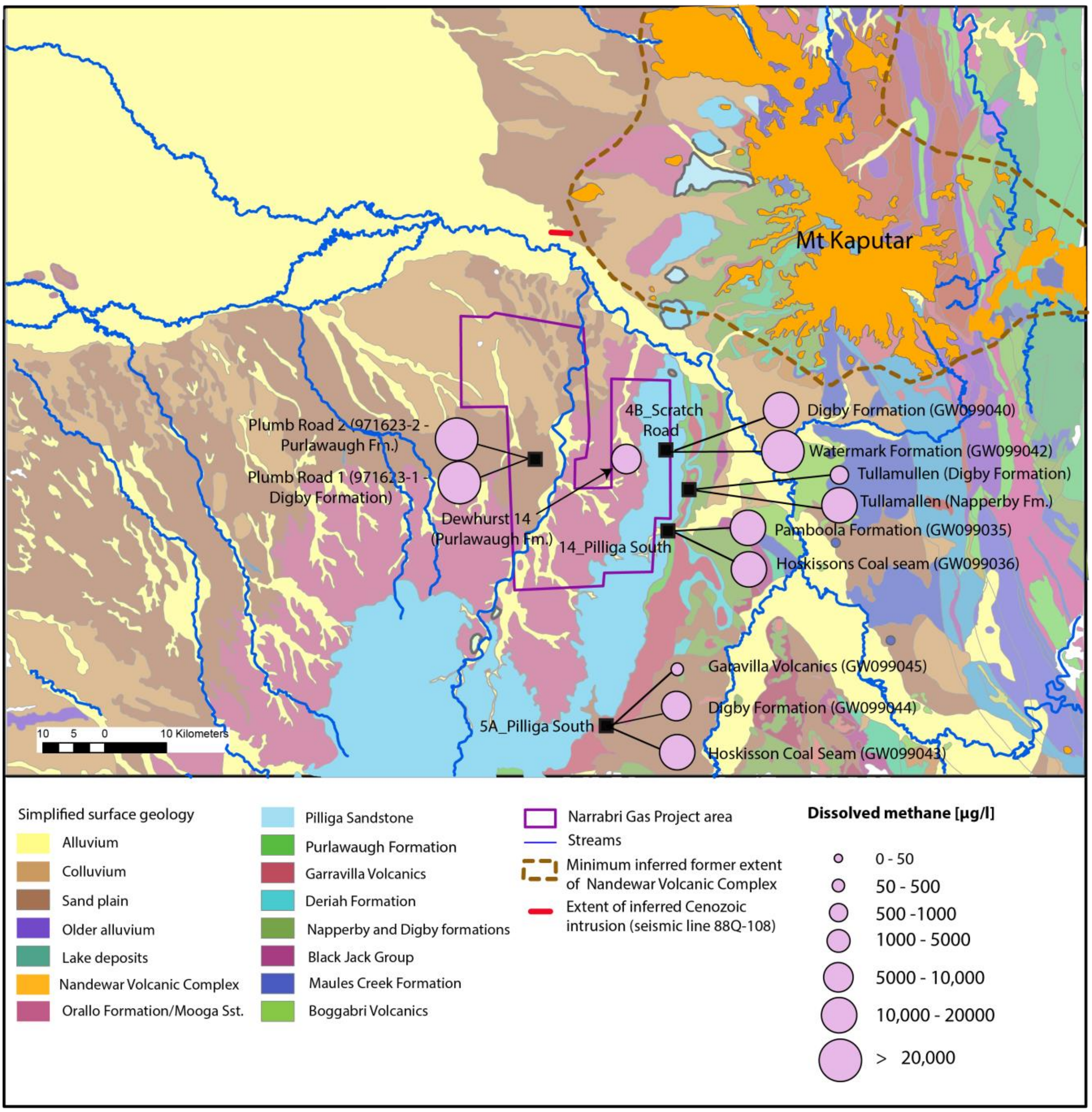

Figure 3-57 – Spatial distribution of methane concentrations in formations below the Pilliga Sandstone (i.e. Purlawaugh Formation and Gunnedah Basin strata) overlain on simplified surface geology.

Methane concentrations are based on Cresswell (2014), Iverach et al. (2020a), Suckow et al. (2019), Raiber et al. (2022a) and the current study

Gunnedah Basin (outside coal seams and formations hosting coal seams near the basin margins to the east of the Narrabri Gas Project area)

Complementing samples collected by Raiber et al. (2022a), additional samples have been analysed in the current study for dissolved methane concentrations of the Gunnedah Basin formation groundwater samples near the basin margin to the east of the Narrabri Gas Project area (Figure 3-56). The measurements showed that concentrations of dissolved methane within all Gunnedah Basin formations are relatively high (Figure 3-57), with concentrations ranging from approximately 1,000 to 22,000 µg/L. Small amounts of ethane (154 µg/L) were also observed in multiple groundwater samples from the Gunnedah Basin formations to the east of the Narrabri Gas Project area based on samples collected in isoflasks (Section 2.5.2), whereas most samples analysed in amber glass vials at ALS did not yield any ethane.

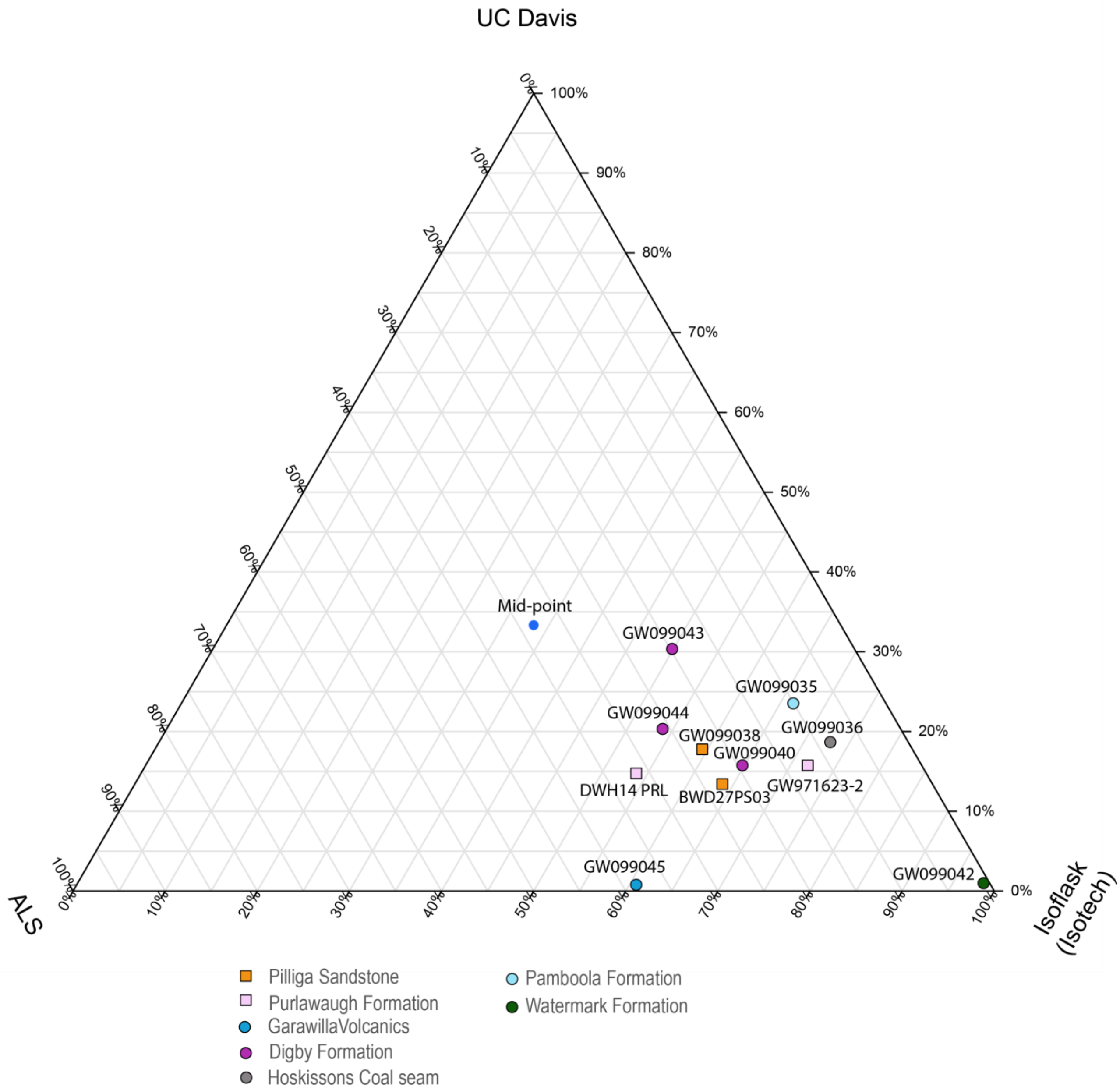

Figure 3-58 – Ternary diagram showing dissolved methane based on measurements at three different analytical laboratories. The mid-point indicates where a sample would be located if concentrations in all laboratories were equal.

Discrepancies between concentrations analysed via different sample collection and analytical techniques also exist for methane, as highlighted on Figure 3-57. The mid-point on this figure shows where a sample would be located if concentrations measured at all laboratories would be equal. The figure shows that there is a strong bias towards higher measured concentrations using isoflasks and analysis at Isotech laboratory.

For example, the methane concentration measured for GW099042 (for location, see Figure 3-57) ranges from approximately 200 to 22,000 µg/L depending on sampling and analytical technique. While at other sites discrepancies between different analytical techniques were also identified, these were generally smaller, and the analysis of other parameters suggested that this site is not representative for the Gunnedah Basin groundwater samples. Here, the headspace and dissolved gas analysis yielded extremely high CO_2 concentrations: the headspace analysis of gas in the isoflask at Isotech laboratories suggested that 92.5% of gas present is CO_2 and the analysis of dissolved CO_2 at the University of California suggested that the concentration is > 100,000 µg/L. In comparison, all other samples had less than approximately 10% of CO_2 in headspace and mostly less than 5,000 µg/L of dissolved CO_2, whereas they had higher head space methane percentages. This groundwater sample was also the only Gunnedah Basin sample where both He and H_2 were detected in headspace gas analysis. In the adjacent Sydney Basin, Faiz et al. (2007 a, b) suggested that high concentrations of CO_2 in coal seam gas are derived from igneous activity that occurred from the Permian to Cenozoic.

Purlawaugh Formation

During the 2018 GISERA sampling campaign, groundwater observation bore Plumb Road 2 (GW971623-2) screened within the Purlawaugh Formation between the depths of 359 and 365 mBGL) was sampled and methane concentrations were measured, revealing high concentrations of up to 17,900 µg/L within the screened basal sandstones. As discussed by Suckow et al. (2019), very high artesian flow (with flow rates of more than 12,000 L/hour according to the well completion report) and a high degree of exsolution could be visually observed at this monitoring site (Suckow et al., 2019). This bore was sampled again in 2018 by an environmental consultancy on behalf of NSW DPIE during the installation of groundwater monitoring equipment, yielding dissolved methane concentrations of 20,600 and 27,000 µg/L (Streamline Hydro, 2018). In 2023, we have collected a sample again from this groundwater bore using an installed low flow pump and an isoflask, where an air-tight connection is established, reducing the degree of exsolution (Section 2.5.2). This yielded a dissolved methane concentration of 36,000 µg/L. As explained in Section 2.5.2, methane concentrations were also analysed using 12 ml exetainer vials (analysed at the University of California, Davis) and amber glass exetainer vials (analysed at ALS).

The discrepancy of methane concentrations from multiple temporal measurements ranging from approximately 12,400 to 36,000 µg/L at Plumb Road 2 (GW971623-2) highlights the challenge in obtaining reliable methane baseline concentrations, which is critical to assess potential impacts of CSG activities in the future. In addition to the Plumb Road 2 (GW971623-2) groundwater monitoring bore, the concentration of dissolved methane in the Purlawaugh Formation was also measured at the Dewhurst 14 nested monitoring bore site (Figure 3-60) in the current study, yielding relatively consistent results of 3,020 µg/L (UC Davis), 6450 µg/L (ALS laboratories) and 7,700 µg/L (in a sample collected in an isoflask and analysed at Isotech laboratories).

Although the installation of dedicated groundwater monitoring and sampling infrastructure that sources samples from deeper parts of the groundwater bore at the screened interval means that the exsolution of methane will likely be reduced, challenges in obtaining accurate dissolved methane concentrations remain (as discussed for example by Banks et al., 2017 and Pearce et al., 2021) and the observed concentrations may often underestimate actual concentrations. This is also highlighted by a ternary diagram which compares the relative differences in measurements from different laboratories for the same sampling event (Figure 3-58). It shows that all measurements are biased towards higher concentrations for samples collected in isoflasks at

Isotech laboratories. For most samples, the measurements are in a similar range, whereas for some samples, and most notably GW099042), the discrepancies are very high.

Pilliga Sandstone and Orallo Formation

The spatial distribution of methane concentrations in the Pilliga Sandstone and Orallo Formation within the Narrabri Gas Project area is shown in Figure 3-59.

A histogram of dissolved methane concentrations within the Pilliga Sandstone (Figure 3-61) shows that concentrations in most groundwater samples are very low (median of 25 µg/L), with most of the samples at or below the quantification/reporting limit (Figure 3-61); of all Pilliga Sandstone groundwater samples (54 samples, including many duplicates), only five samples (all collected from GW099038 north-east of the Narrabri Gas Project area) (Figure 3-59) had methane concentrations >3500 µg/L (and up to about 17,000 µg/L). The reason for the elevated methane concentrations at this site is not clear. However, it could indicate (i) a higher content of dispersed organic matter in the Pilliga Sandstone; (ii) connectivity with underlying formations or (iii) bore construction issues (i.e. a bore screening both Pilliga Sandstone and the underlying Purlawaugh Formation).

Compared to the range of methane concentrations measured in the Pilliga Sandstone, Mallants et al. (2016) showed that maximum CH_4 concentrations in the Hutton Sandstone in the Surat Basin in Qld are ~20,000 µg/L, about 3500 µg/L within the Gubberamunda Sandstone (a partial stratigraphic equivalent of the Pilliga Sandstone), approximately 10,000 µg/L in the Springbok Sandstone and 5900 µg/L in the Condamine River alluvium. This suggests that the methane concentrations in the majority of the Pilliga Sandstone groundwaters appear to be relatively low compared to methane concentrations observed within other productive aquifers elsewhere within the GAB.

The spatial map of methane concentrations within the Pilliga Sandstone in the Pilliga region (Figure 3-59) and geological cross-section CS1 (Figure 3-60) show that Pilliga Sandstone groundwater methane concentrations at groundwater bores in the south and east of the proposed Narrabri Gas Project area were generally below the ALS reporting limit of 10 µg/L based on measurements from Cresswell (2014), Raiber et al. (2022a) and the current study; likewise, no methane peak was detected for groundwaters collected from groundwater monitoring bores at Dewhurst 3 and Dewhurst 14 during the analysis of δ^2H and $\delta^{13}C$ of methane at the University of California (UCDavis), which indicates that the concentration is below the limit of quantification (3 µg/L). The exception to this is a measurement at a bore screened in the lower part of the Pilliga Sandstone at Dewhurst 3, which confirmed the presence of a very small amount of dissolved methane (42 µg/L; Cresswell, 2014). No sample was collected from this bore during the current study or the study by Raiber et al. (2022a), although groundwater from the shallower Pilliga Sandstone bore at this nested bore site did not contain any measurable methane.

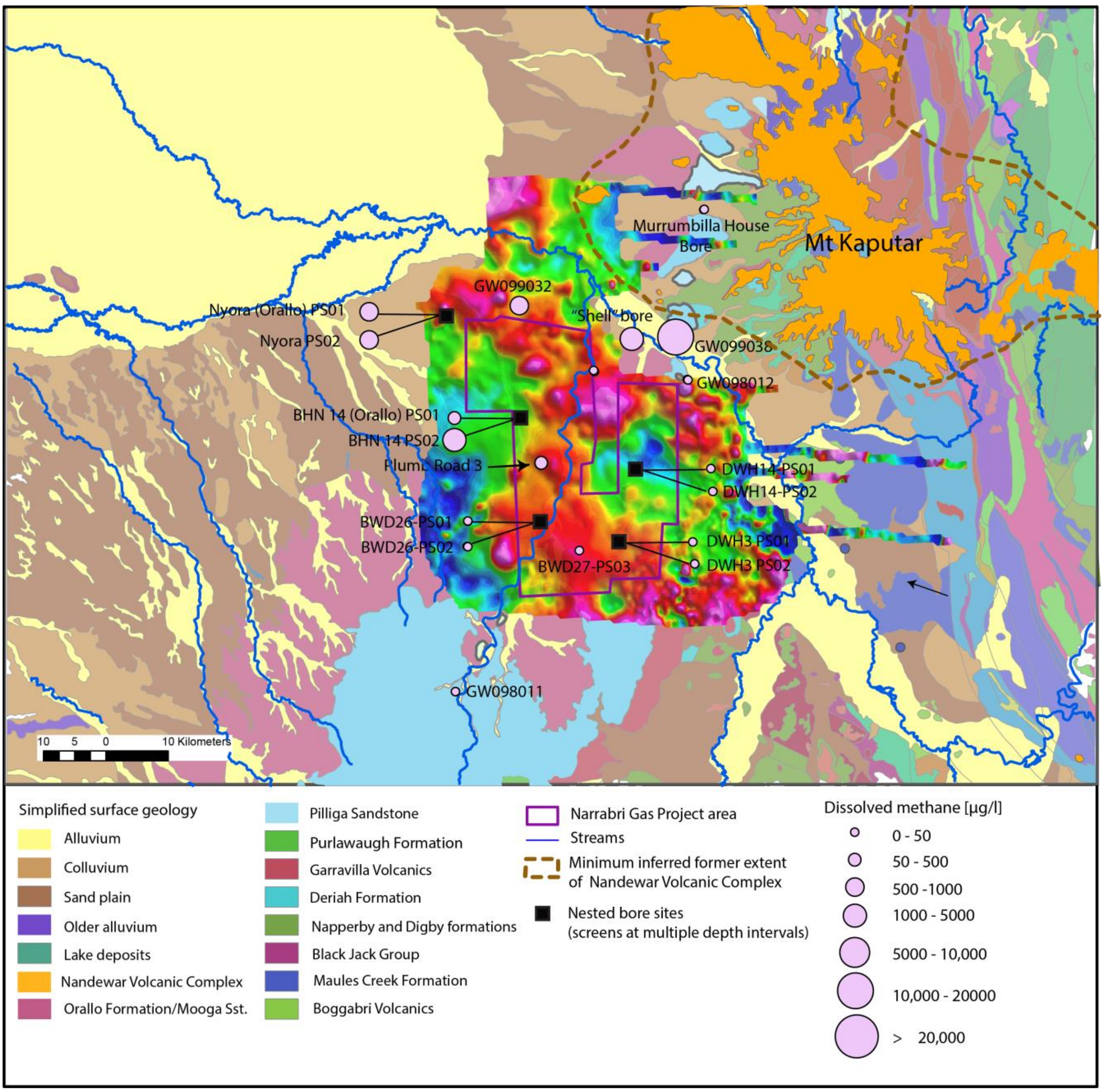

Figure 3-59 – Spatial distribution of methane (CH_4) concentrations within Pilliga Sandstone and Orallo Formation overlain on simplified surface geology and total magnetic intensity. For scale bar of total magnetic intensity, see Figure 3-24

Methane concentrations are based on Cresswell (2014), Iverach et al. (2020a), Suckow et al. (2019), Raiber et al. (2022a) and the current study.

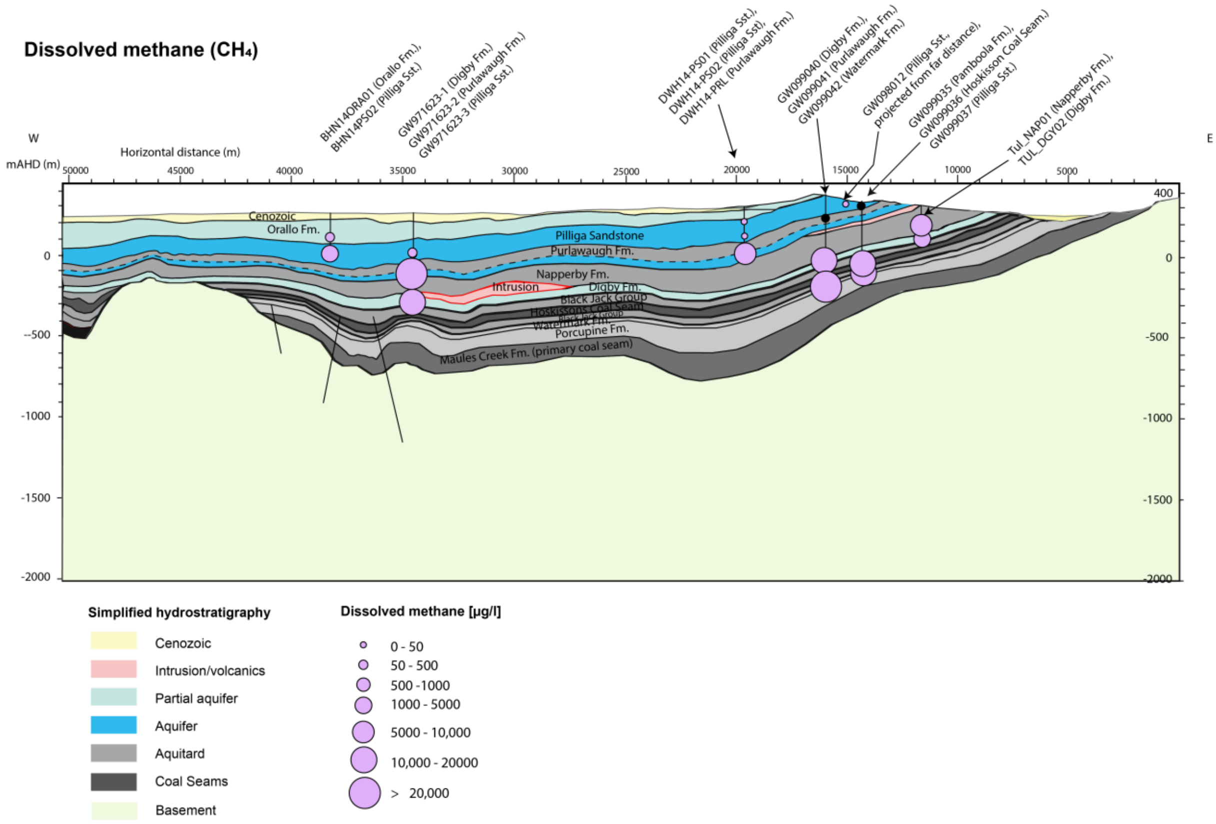

Figure 3-60 – Dissolved methane concentrations for Surat and Gunnedah basins formation along east-northwest oriented geological cross-section through the Narrabri Gas Project area (for orientation, see Figure 3-25).

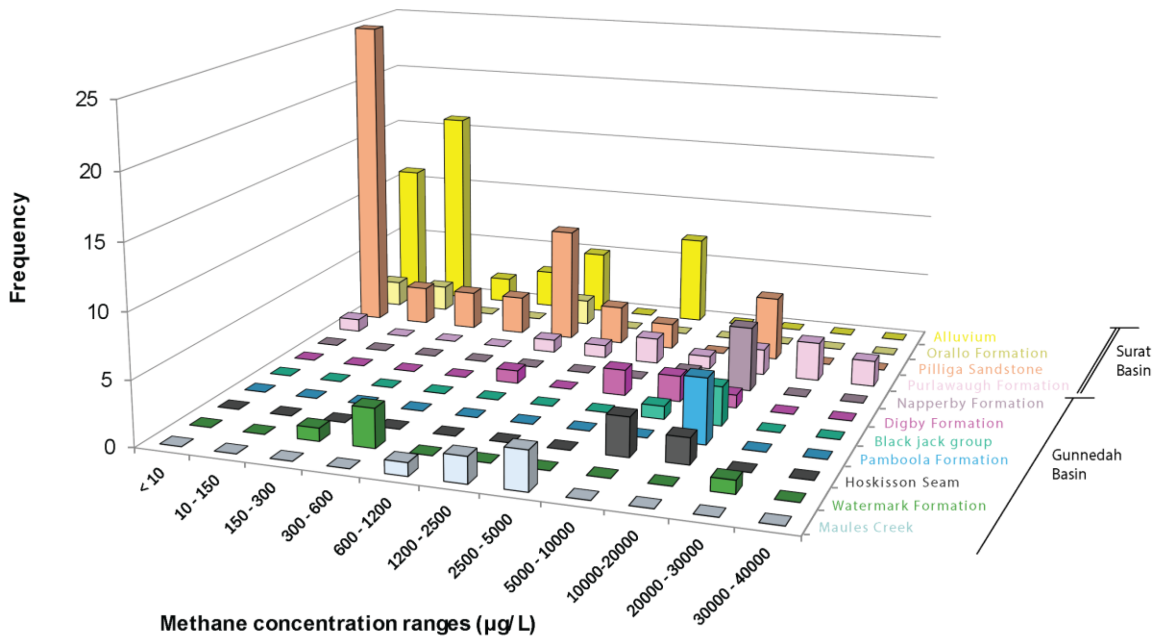

	< 10	10 - 150	150 - 300	300 - 600	600 - 1200	1200 - 2500	2500 - 5000	5000 - 10000	10000- 20000	20000 - 30000	30000 - 40000
Alluvium	11	16	2	3	5	0	7	0	0	0	0
Orallo Formation	2	2	0	0	2	0	0	0	0	0	0
Pilliga Sandstone	25	3	3	3	9	3	2	0	5*	0	0
Purlawaugh Formation	1	0	0	0	1	1	2	1	2	3	2
Napperby Formation	0	0	0	0	0	0	0	1	5	0	0
Digby Formation	0	0	0	0	1	0	2	2	1	0	0
Black Jack Group	0	0	0	0	0	0	0	1	3	0	0
Pamboola Formation	0	0	0	0	0	0	0	0	5	0	0
Hoskisson Seam	0	0	0	0	0	0	0	3	2	0	0
Watermark Formation	0	0	1	3	0	0	0	0	0	1	0
Maules Creek	0	0	0	0	1	2	3	0	0	0	0

Frequency

Figure 3-61 – Histogram of methane concentrations displayed by aquifers. The number of samples assigned to each interval are shown in table below the histogram. This includes multiple measurements at some sites. The *relates to measurements of dissolved methane at groundwater bore GW099038, the only groundwater bore screened within the Pilliga Sandstone where dissolved methane of >5000 µg/L was measured.

Methane concentrations (N: Number of samples, Average, Max, Min) displayed by bore ID and Aquifers. Concentrations are based on Cresswell (2014), Iverach et al. (2020a), Suckow et al. (2019), Raiber et al. (2022a), Water NSW and the current study.

In contrast to the absence of dissolved methane in the south and east, some groundwater samples collected from the Pilliga Sandstone further west and north-west have dissolved methane concentrations above the detection limit. For example, a groundwater sample collected after installation of headworks and a pump at the Plumb Road 3 NSW DPIE Plumb Road nested bore site (where the Pilliga Sandstone, Purlawaugh Formation and Digby Formation are screened) yielded a methane concentration of ~550 µg/L (Streamline Hydro, 2018). A previous water sample collected at the same bore prior to installation of the pump and headwork yielded a methane concentration of 129 µg/L (Suckow et al., 2019), and a sample collected during the current study using a permanently installed low flow pump had a concentration of 470 µg/L. The relatively small discrepancy is likely due to exsolution during sampling or analytical errors, with the lower concentration groundwater sample collected via placement of the pump at a shallower depth.

Groundwater samples collected from the Pilliga Sandstone at groundwater monitoring sites Bohena 14 and Nyora (Nyora PS02) further in the west and north-west (with the latter bore located slightly outside) of the Narrabri Gas Project area had higher dissolved methane concentrations, between approximately 800 and almost 1200 µg/L based on multiple measurements, whereas groundwater samples from the overlying Orallo Formation at the same locations yielded concentrations of 649 µg/L (Bohena 14) and 1100 µg/L (Nyora PS01), respectively.

Raiber et al. (2022a) suggested that there is no distinct relationship of methane concentration with either groundwater salinity or bore depth for the Pilliga Sandstone (Figure 3-55). However, they suggested that there is a noticeable relationship between methane concentrations and the redox potential (Figure 3-62). Redox potential (Eh) is a measurement of the tendency of an environment to oxidise or reduce substrates. Suthersan (2001) suggested that a redox potential of less than −100 mV indicates an anaerobic environment, whereas measurements greater than 100 mV indicate an aerobic environment. However, as Neumann (2012) explains, 'natural waters are often in a state of non-equilibrium and the redox conditions can therefore not be defined by a single well-defined redox potential'.

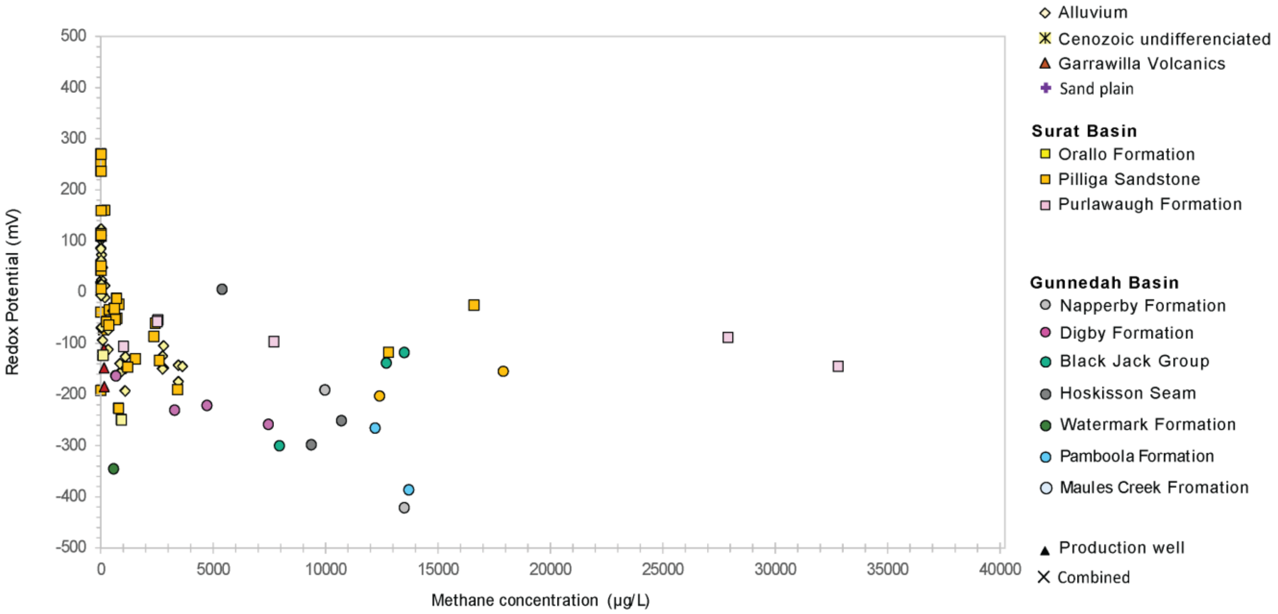

Figure 3-62 – Methane concentration versus redox potential of Pilliga Sandstone groundwater samples. Methane concentrations are based on Cresswell (2014), Iverach et al. (2020a), Suckow et al. (2019), Raiber et al. (2022a) and the current study.

[1] Alluvial groundwater measurements are from Iverach et al. (2017, 2020).

Within the Pilliga Sandstone aquifer, groundwater samples where a positive redox potential was measured contain no dissolved methane (except for GW098011), whereas many but not all samples with a negative redox potential contain measurable dissolved methane concentrations above the reporting limit. A discussion on the processes that can be observed when methane from a deeper source enters an oxygenated aquifer was presented by Wen et al. (2019). The authors suggested that as methane migrates upwards into an oxygenated aquifer, oxidation of methane consumes dissolved oxygen. If the migration of methane is a continuous long-term process, then over time oxygen will become depleted. Subsequently, once oxygen is depleted, a series of microbiological reactions takes place (e.g. anaerobic oxidation of methane coupled to iron reduction and anaerobic oxidation of methane coupled to sulfate reduction). Wen et al. (2019) suggest that after a lag period, concentrations of O_2, Fe, and SO_4 are then all low, whereas the concentrations of dissolved CH_4 are high. Furthermore, as for example discussed by VanVoast (2003), Taulis and Milke (2007) and Mallants et al. (2016), there are other reliable indicators of anaerobic conditions in sedimentary basin aquifers than just a redox potential measurement (which can be highly inaccurate), such as for example concentrations of SO_4 and Fe. These are typically low at all Pilliga Sandstone groundwater sampling sites, suggesting that there may be already an onset of reducing conditions at some of these the shallowest groundwaters within the outcrop beds of the Pilliga Sandstone.

Vertical patterns of methane in Gunnedah and Surat basins

As shown in Figure 3-57, Figure 3-59 and Figure 3-60, there is a significant vertical gradient in methane concentrations in Surat Basin and Gunnedah Basin formations, with concentrations in the Gunnedah Basin and Purlawaugh Formation typically significantly higher than those within the Pilliga Sandstone and Orallo Formation.

Raiber et al. (2022a) suggested that if methane had migrated along natural hydrogeological pathways from the coal seams of the Gunnedah Basin into the Pilliga Sandstone over many thousands of years, there would be measurable methane at Pilliga Sandstone groundwater monitoring bores in the south and east of the Narrabri Gas Project area. The absence of methane (combined with the very low groundwater salinities and pH) observed at these bores was therefore considered by the authors as an indicator that there is no or no significant hydrogeological connection between the Gunnedah Basin strata and the Pilliga Sandstone in the south and east of the Narrabri Gas Project area.

In contrast, Raiber et al. (2022a) suggested that the increase of dissolved methane concentrations in the Pilliga Sandstone towards the west and north-west may be primarily due to interaction with (i.e. groundwater flow or diffusion) underlying formations such as the Purlawaugh Formation or Digby Formation, which both contain high methane concentrations at Plumb Road and which were both considered conventional gas exploration targets in the past.

Multiple potential pathways for connectivity between the Pilliga Sandstone and underlying formations have been described in previous sections. These include the thinning and pinching of the Purlawaugh Formation towards the north-west (e.g. at the western edge of geological cross-section CS2) and structures (bounding faults, sills or dykes) at anticlines in the north-west. In contrast, the seismic assessment in Raiber et al. (2022a) and other studies suggested that other than at some of the major anticlines in the north, major faults with significant vertical displacements of both Gunnedah and Surat basins strata do not seem to be present, suggesting that this is unlikely to be a major hydrogeological connectivity pathway. This was also supported by the results of the AEM survey in the present study, which also did not show any significant vertical displacements within the Surat Basin formations in the Narrabri Gas Project area. Furthermore, it is also important to highlight that small concentrations of dissolved methane can be generated via other processes independent of hydrogeological connectivity with the Gunnedah Basin and that it can be transmitted across formations through diffusion where strong concentration gradients exist (although the rate of transmission is very low and this would involve long time scales). As shown on Figure 3-56, methane (~370 µg/L) is also present at groundwater bore GW040934 in a location where the Gunnedah Basin is absent and where groundwater samples from two bores (GW039504 and GW040870) closer to the basin margin (and closer to the area where the Gunnedah Basin is present; Figure 3-56) contain no measurable methane. This suggests that some methane may have been generated within the Pilliga Sandstone possibly due to the presence of small amounts of dispersed organic matter within the aquifer (Figure 3-4), as suggested by the generalised sand/shale calculations and possibly higher contents of mudstone and siltstone, indicating that small concentrations of methane are not necessarily due to connectivity with coal seams.

The increase of methane concentrations between the two bores screened within the Purlawaugh Formation (DWH14 and GW971623-2 at Plumb Road) can be related to many factors. As described in previous hydrogeological and hydrocarbon investigations (e.g. Webster and Woods, 1987; Terracorp, 1999), the Bohena anticline where the Plumb Road monitoring site is located has been a target for conventional gas exploration in the past. Seismic survey reports at most anticlines within the Narrabri Gas Project area suggested that they are closed (sealed off) on all sites and the AEM survey results do not show any obvious vertical displacements of major conductors. However, some fluids may escape from underlying strata (e.g. Digby Formation) to the Purlawaugh Formation via minor faults or fractures associated with the sill observed within the Digby Formation and at the interface between the Digby Formation and Purlawaugh Formation where the Napperby Formation appears to be absent (Figure 3-2). In contrast, at the Dewhurst 14 monitoring bore site, seismic sections and TMI show no structural disruption at this site, suggesting that there is no hydrogeological connectivity pathway at this site.

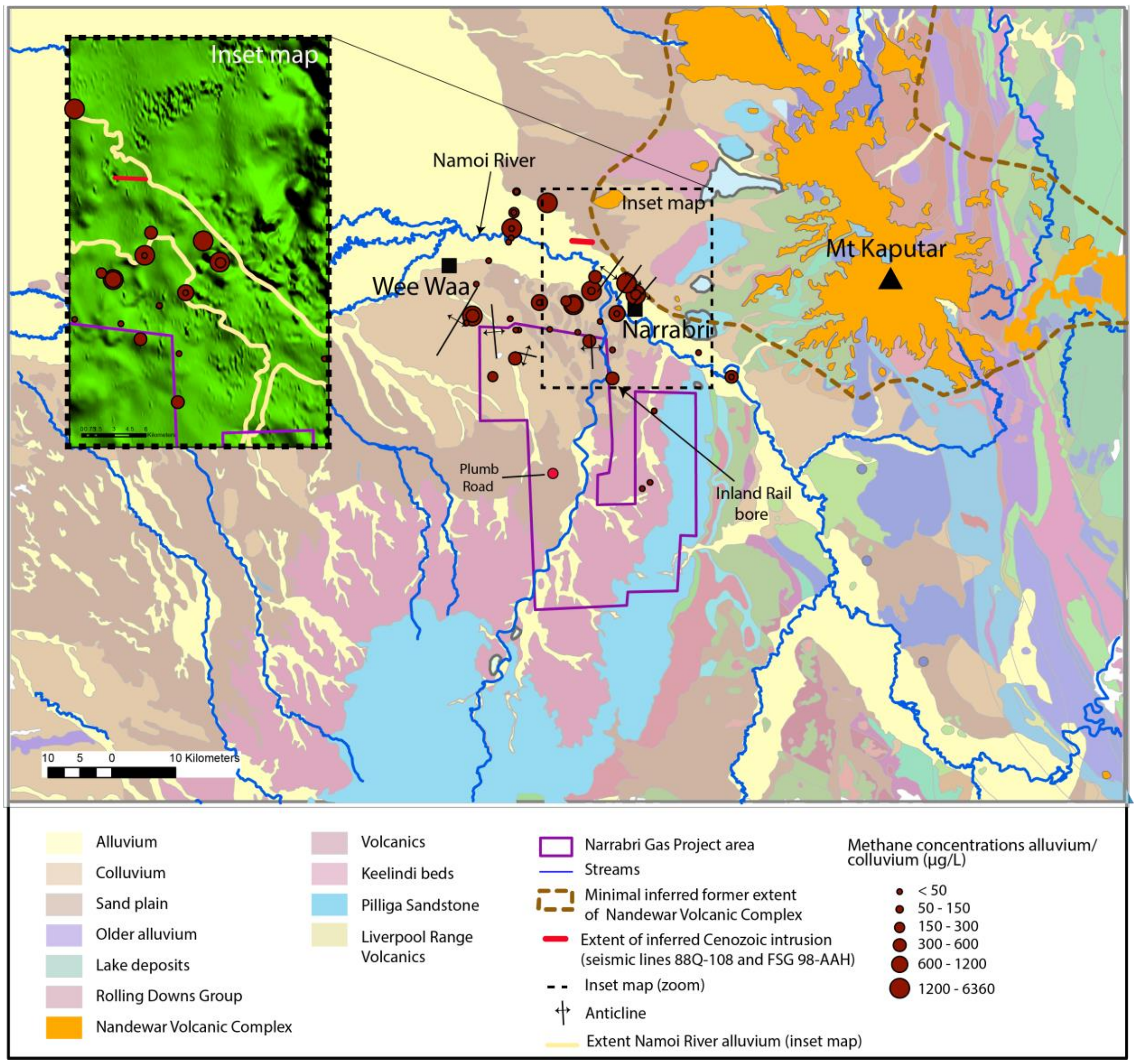

Figure 3-63 – Spatial distribution of CH_4 concentrations within alluvium/colluvium overlain on simplified surface geology (Cresswell (2014), Iverach et al. (2020a), Raiber et al., (2022a) and the current study).

The inset map shows the total magnetic intensity (TMI) grid (Poudjom Djomani, 2019). The beige outline in the inset map shows the extent of the Namoi River alluvium.

3.7.6 Methane isotopes (δ^2H and $\delta^{13}C$ of CH_4) and $\delta^{13}C$ of CO_2

Stable isotopes of methane (δ^2H and $\delta^{13}C$ of CH_4) have been used as tracers to differentiate between thermogenic and microbial methane in previous studies in Australia and overseas (e.g. Whiticar, 1986; Humez et al., 2016; Currell et al., 2017; Nicot et al., 2017; Thomas, 2018; Banks et al., 2019; Faiz et al., 2020; Iverach et al., 2020a); furthermore, the usefulness of these isotopes to determine the origin of methane in aquifers overlying coal seams or shale gas reservoirs was highlighted by many authors, particularly when combined with hydrogeochemical evidence and other tracers such as noble gas isotopes (Harkness et al., 2017; Banks et al., 2019; Iverach et al., 2020b). Golding et al. (2013) explained that conventional hydrocarbon reservoirs contain mostly thermogenic gas, whereas unconventional gas reservoirs (e.g. CSG) can be of thermogenic, microbial or mixed origin. Thermogenic gas typically contains considerable concentrations of higher-chain hydrocarbons (e.g. ethane and propane), while microbial activities produce predominantly methane with only minor volumes of ethane and propane (Bernard et al., 1978;

Thomas, 2018). Thomas (2018) suggests that partly because of isotope fractionation, methane originating from microbiological processes is isotopically lighter than thermogenic methane, and that this difference has been widely used as an indicator of methane origin. However, Thomas (2018) also suggests that there can be overlaps, which is also emphasised by McIntosh et al. (2019), who explain that with the increasing sensitivity of analytical instrumentation for the analysis of δ^2H and $\delta^{13}C$ of CH_4 and with the availability of larger global isotope datasets, there is now an overlap of different source regimes (i.e. microbial, thermogenic and abiotic) in graphical representations. The authors suggest that as a result, the application of single tracers such as hydrocarbon for source characterisation can be problematic and additional tracers may be required.

Samples from multiple aquifers (alluvium, Surat Basin formations and Gunnedah Basin formations) from the Pilliga region were analysed for their δ^2H and $\delta^{13}C$ of CH_4 and $\delta^{13}C$ of CO_2 during the current study and previous investigations (Iverach et al., 2020a; Suckow et al., 2019; Raiber et al., 2022a). In addition, the same isotopes were measured during exploration activities at some wells by Eastern Star Gas for the Gunnedah Basin CSG targets (Hoskissons Coal seam and Maules Creek Formation coal seams). These data are publicly available and were sourced from the NSW DIGS system. The assignment of the samples from the Gunnedah Basin CSG target units to different coal seams is based on sample depth information and stratigraphic tables provided in the well completion reports and associated documents.

Figure 3-64 a shows a plot of $\delta^{13}C$ of CH_4 versus $\delta^{13}C$ of CO_2 and Figure 3-64 b shows a plot of δ^2H of CH_4 versus $\delta^{13}C$ of CH_4 following the genetic isotope diagrams presented by Milkov and Etiope (2018). Only relatively few samples from the Pilliga Sandstone are represented on the graphs because of the low dissolved methane concentrations of many Pilliga Sandstone groundwaters, which were often below the detection limit or below the required minimum concentrations required for analysis of δ^2H of CH_4 and $\delta^{13}C$ of CH_4 at the analytical lab where the samples were analysed.

The graphs show that unlike in other Permian–Triassic sedimentary basins in Australia (e.g. Bowen and Cooper basins) none of the samples (including groundwaters collected from the current study and gas samples collected and analysed by Eastern Star Gas between 2008 to 2011) sit within the thermogenic part of the plot.

The comparison of $\delta^{13}C$ of CH_4 versus $\delta^{13}C$ of CO_2 (Figure 3-64 a) shows that there is a wide range of values for the Maules Creek Formation, with some samples characterised by more enriched $\delta^{13}C$ of CO_2 and $\delta^{13}C$ of CH_4. The group with the more depleted (more negative) isotope signatures is more similar to the signature of samples from the Hoskissons Coal seam, whereas the other samples evolve towards more positive/less negative isotope signatures as a result of carbonate reduction.

Alluvial samples are displaced from other samples, indicating oxidation of CH_4 as groundwater migrates upwards and is exposed to different biogeochemical conditions (Iverach et al., 2020a).

In the plot of δ^2H versus $\delta^{13}C$ of CH4 (Figure 3-64 b), two groundwater samples collected from the Purlawaugh Formation at Plumb Road plot in the 'Bacterial Carbonate Reduction' field together with samples from Digby and Napperby formations at Tullamullen and samples from Hoskissons Coal seam (Black Jack Group) and some samples from alluvium (Iverach et al., 2020a). In comparison, samples collected from groundwater bores screened within the Pilliga Sandstone (Nyora PS02) and the Orallo Formation at Nyora plot in the 'Mix & transition' field of the plot, together with samples of both the Maules Creek Formation and Black Jack Group.

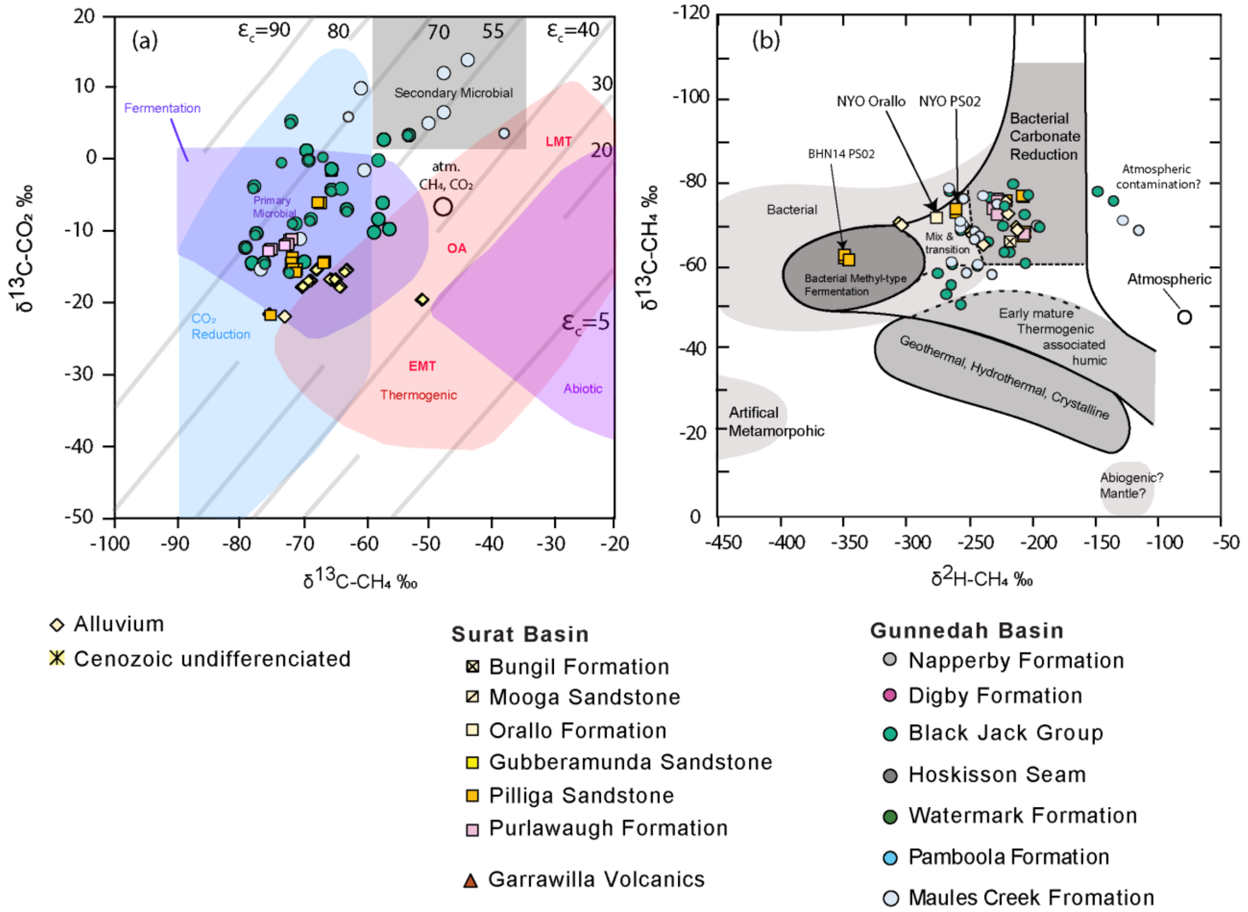

Figure 3-64 – Isotopes of a) $\delta^{13}C$ of CH_4 versus $\delta^{13}C$ of CO_2; and b) δ^2H of CH_4 versus $\delta^{13}C$ of CH_4.

Data from the Black Jack Group and the Maules Creek Formation are compiled from well completion reports published by Eastern Star Gas between 2008 and 2011. Data for alluvial aquifers are from Iverach et al. (2020a). The diagram follows the revised genetic isotope diagrams presented by Milkov and Etiope (2018).

Two samples from the same bore within the Pilliga Sandstone at the Bohena 14 groundwater monitoring site plot into the 'Bacterial Methyl-type Fermentation' field.

On a plot of $\delta^{13}C$-CH_4 versus depth (Figure 3-65), a pattern of an evolution towards less negative isotope signatures with shallower depth can be recognised, attributed to oxidation of CH_4 as groundwater migrates upwards and is exposed to different biogeochemical conditions (Iverach et al., 2020a). On the same plot, there is an apparent difference between the shallow Pilliga Sandstone groundwaters and samples from the Maules Creek Formation (samples from outside the Narrabri Gas Project area excluded), with many Maules Creek Formation samples marked by more enriched (less negative) values. In contrast, the signatures of samples from the Hoskissons Coal seam (Black Jack Group) overlap closer with those of shallow Pilliga Sandstone groundwater samples.

The deeper Pilliga Sandstone groundwater samples shown on this plot (corresponding to 'Pilliga Sandstone (outside the Narrabri Gas Project area)' in Figure 3-65) are all located further north, west, and south-west outside the Narrabri Gas Project area (the locations are shown on Figure

3-56). As described in Section 3.7.5, the presence of methane at GW040934 (Figure 3-56) cannot be attributed to a hydrogeological connection with the Gunnedah Basin due to the absence of the Gunnedah Basin in this area and the absence of methane in bores closer to the basin margin along the same inferred flow path (GW039504 and GW040870). This highlights the challenges in attributing methane to different sources: although the visual inspection of the patterns on Figure 3-65 could suggest that the methane $\delta^{13}C$ of CH_4 at bore location GW039504 originates from the coal seams of the Gunnedah Basin, there is no actual hydrogeological connectivity pathway that links the Pilliga Sandstone at this site to the Gunnedah Basin.

Overall, the patterns on the different isotopic plots suggest that there is considerable complexity in the evolution of methane with multiple overlaps. As explained, for example, by Whiticar (1999), the depth separation of formation and consumption of methane is often a transitional process that cannot always be separated into distinct zones. Furthermore, the complicated geological setting in the Narrabri region adds further complexities. For example, as explained in Section 3.3.1, some coal is also present within the Purlawaugh Formation, suggesting that methane may also be generated within the Purlawaugh Formation, and igneous intrusions contemporary to or after the deposition of the Purlwaugh Formation strata may have also influenced gas isotope signatures.

As a result of these complexities, the patterns of δ^2H and $\delta^{13}C$ of CH_4 and $\delta^{13}C$ of CO_2 alone without consideration of other lines of evidence are unlikely to be a clear and unambiguous indicator for distinguishing the sources of methane in formations such as the Purlawaugh Formation, Digby Formation and Pilliga Sandstone (where measurable methane is present) overlying the Early and Late Permian coal seams.

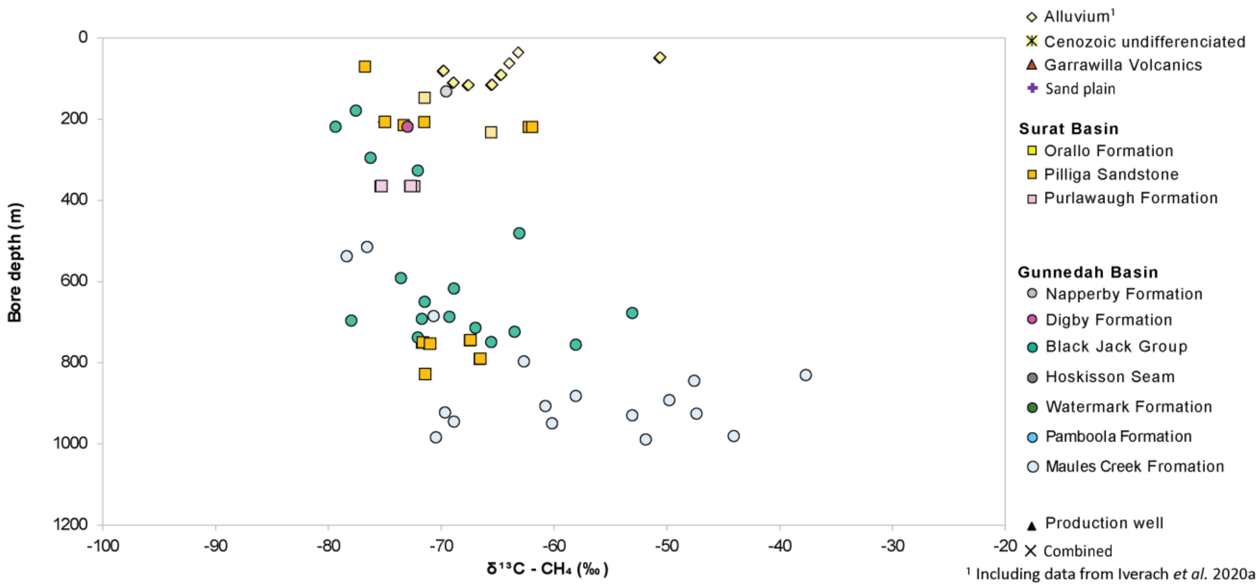

Figure 3-65 Comparison of δ13C of CH4 versus bore depth. Alluvial data are from Iverach et al. (2020a) and other data are from Eastern Star Gas (2008-2011), Suckow et al. (2019), Raiber et al. (2022a) and the current study.

'Pilliga Sandstone groundwater (outside Narrabri Gas Project area)' corresponds to groundwater bores GW040851, GW040852, GW040934 and GW041075 (for locations, see Figure 3-56). Exploration wells Strathmore 2 and Wialla 1 are located within another depositional centre of the Gunnedah Basin outside the Narrabri Gas Project area.

3.7.7 Strontium isotopes of groundwater

The Sr isotope ratio ($^{87}Sr/^{86}Sr$) of groundwater is primarily controlled by interactions of groundwater and the host rock and by water mass mixing (e.g. McNutt, 2000; Cartwright et al., 2004; Raiber et al., 2009; Raiber et al., 2024). As water flows through an aquifer, its strontium isotope ratio alters towards that of the rock. The major benefit of using Sr isotopes in groundwater or surface water studies therefore is the assessment of interactions between different aquifers or between groundwater and surface water (e.g. Cartwright et al., 2004; Raiber et al., 2009; Raiber et al., 2024). In older rocks such as the Permian to Cretaceous rocks in the Pilliga region, Sr derived from potassium-rich minerals (e.g. biotite and potassium-feldspar) will have higher $^{87}Sr/^{86}Sr$ ratios, whereas Sr derived from minerals with lower K/Ca ratios (e.g. plagioclase) will have moderate $^{87}Sr/^{86}Sr$ ratios (Cartwright et al., 2004). Strontium in Ca-rich minerals (e.g. calcite or gypsum) has low $^{87}Sr/^{86}Sr$. These remain unchanged over time, and unlike for other isotope systems, mineral dissolution and precipitation do not fractionate $^{87}Sr/^{86}Sr$ ratios (Cartwright et al., 2004).

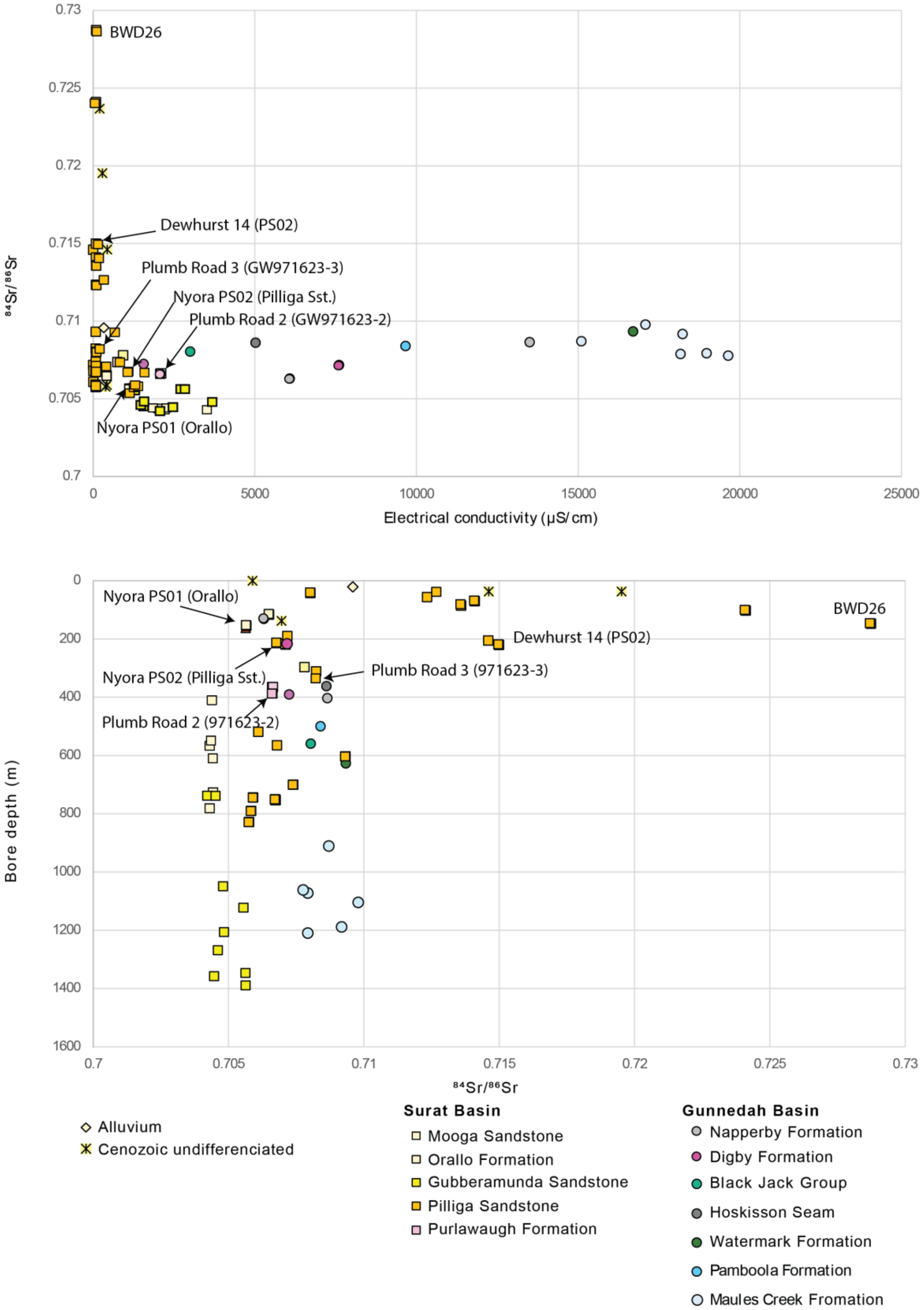

Figure 3-66 – Strontium isotope ratios versus a) electrical conductivity (EC); and b) depth in groundwaters collected from the Pilliga Sandstone and other formations within the Surat and Gunnedah basins.

Additional data from the Mooga and Gubberamunda sandstones in the Surat Basin in Qld based on Geoscience Australia (GA) (Feitz et al., 2014) are shown for comparison.

Strontium isotopes in the Gunnedah Basin

Building on the study by Raiber et al. (2022a), additional groundwater strontium isotope ratios were collected from groundwater bores in the Gunnedah Basin formations (e.g. Napperby Formation, Digby Formation and Maules Creek Formation). The $^{87}Sr/^{86}Sr$ ratios for these formations range from 0.7063 to 0.7071, with Sr concentrations ranging from 0.11 to 4.61 mg/L. Groundwaters collected from CSG appraisal or exploration wells within the primary CSG target formation (Maules Creek Formation) during the current study have $^{87}Sr/^{86}Sr$ ratios ranging from approximately 0.7078 to 0.7098 (based on measurements from six appraisal wells), with Sr^{2+} concentrations ranging from approximately 1 to 4.6 mg/L (median of 1.95 mg/L).

Strontium isotopes in the Surat Basin and Cenozoic

Previous studies in the Surat Basin in Qld showed that groundwaters sampled from most formations have a relatively narrow range of $^{87}Sr/^{86}Sr$ ratios (Raiber et al., 2024). This results primarily from the mineralogy of the sediment source material from which the aquifer is derived, and it appears to be controlled primarily by processes in the unsaturated zone during recharge, with no or minimal further changes occurring along the flow path unless there is connection with adjacent aquifers with a different $^{87}Sr/^{86}Sr$. For example, groundwater samples collected from the Mooga Sandstone and the Gubberamunda Sandstone (partly equivalent to the Pilliga Sandstone in NSW, Figure 1-1) within the Surat Basin in Queensland have $^{87}Sr/^{86}Sr$ ranges from 0.7043 to 0.7045 and 0.704 to 0.705, respectively (Figure 3-66) (Feitz et al., 2014; Raiber et al., 2024). The low radiogenic Sr isotope signature of these groundwater samples likely suggests a volcanogenic origin of the aquifer materials. Similar patterns were observed for other formations such as the Walloon Coal Measures within the Surat Basin in Queensland (Raiber et al., 2024).

In contrast to this narrow range of values observed for most hydrostratigraphic formations in the Surat Basin in Queensland, the $^{87}Sr/^{86}Sr$ ratios of the Pilliga Sandstone groundwaters analysed as part of previous GISERA studies (Suckow et al., 2019; Raiber et al., 2022a) and the current study vary considerably from approximately 0.705 to 0.728 (Figure 3-67). The lowest value from the Murrumbilla House bore (Figure 3-67) may reflect that this bore is likely partially screened in the alluvium or colluvium, which in this area may be composed of low radiogenic minerals resulting from the erosion of volcanic rocks of the Nandewar Volcanic Range.

The comparison of $^{87}Sr/^{86}Sr$ of the Pilliga Sandstone with groundwater salinity (represented by the EC) and depth (Figure 3-66) shows that the freshest Pilliga Sandstone groundwaters have considerably higher $^{87}Sr/^{86}Sr$ ratios than deeper groundwaters with higher salinities. This is also demonstrated by a map showing the spatial distribution of groundwaters $^{87}Sr/^{86}Sr$ measurements within the Pilliga Sandstone (Figure 3-67), where the freshest groundwaters within or near the recharge beds of the Pilliga Sandstone have the highest $^{87}Sr/^{86}Sr$ ratios. Concentrations of Sr^{2+} in Pilliga Sandstone groundwater range from 0.04 to 1.3 mg/L, with the freshest and shallowest groundwaters with high $^{87}Sr/^{86}Sr$ ratios generally having the lowest concentrations.

Previous petrographic studies of the Pilliga Sandstone in the southern Coonamble Embayment by Arditto (1982, 1983) confirmed the presence of clay minerals, and x-ray diffraction showed that this is almost exclusively authigenic kaolinite, which fills pores and fractures in between quartz grains; Arditto (1983) also indicated that the quartz grains of the Pilliga Sandstone are mostly derived from granitic rocks, with a smaller number of grains originating from metamorphic rocks, with microcline (a K-feldspar) as the dominant feldspar. If silicates with high $^{87}Sr/^{86}Sr$ ratios (e.g. biotite and K-feldspar) weather quickly, they can form clay-rich soils with higher $^{87}Sr/^{86}Sr$ ratios than the unweathered rock (McNutt, 2000), and can contribute strontium with a higher $^{87}Sr/^{86}Sr$ ratio to groundwater (Woods et al., 2000).

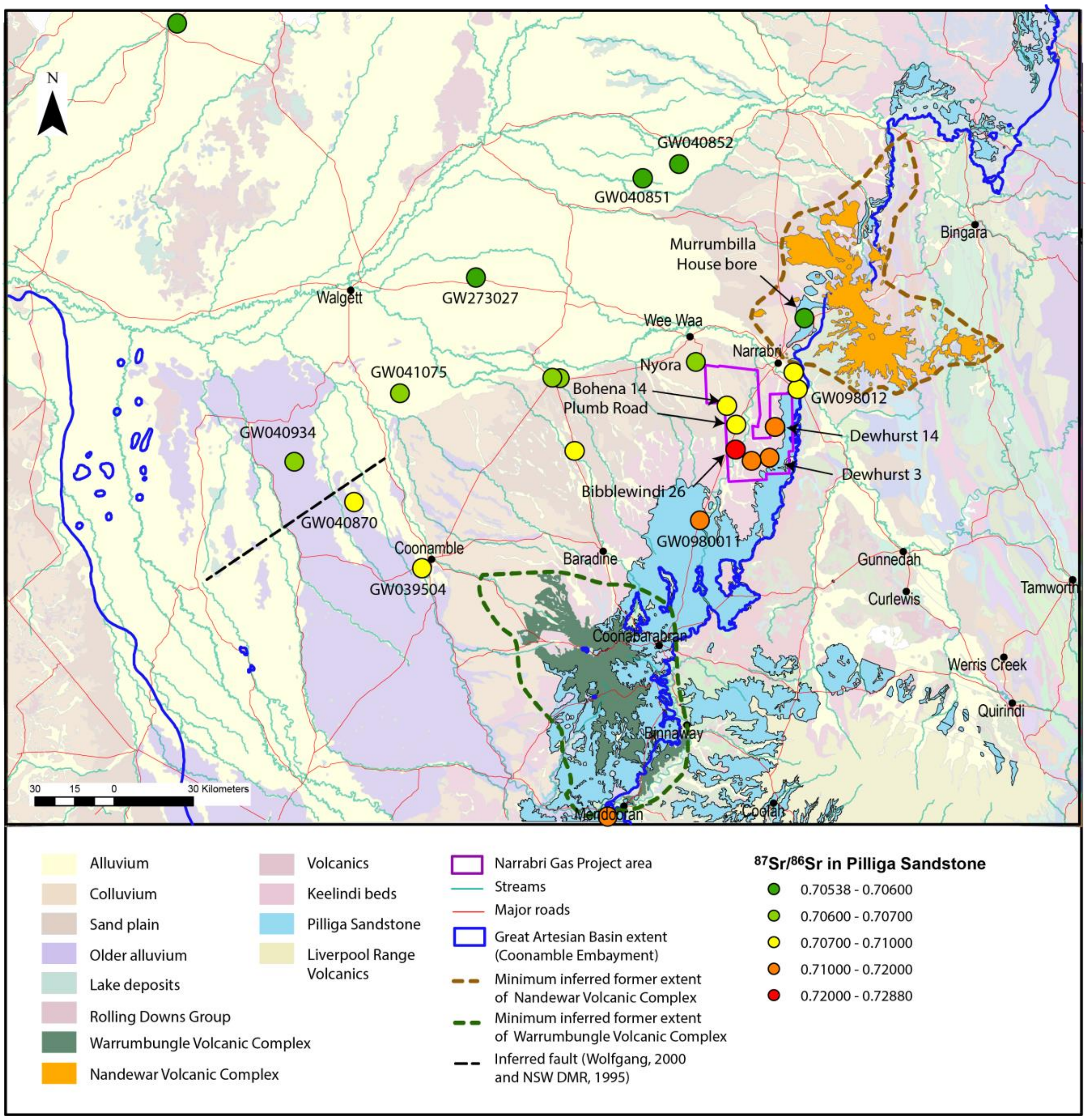

Figure 3-67 – Spatial distribution of $^{87}Sr/^{86}Sr$ ratios in Pilliga Sandstone groundwater overlain on simplified surface geology.

However, the mineralogical analysis (Section 3.3.1) and AEM survey (Section 3.5.2) in the present study demonstrated that there is a significant mineralogical change of the Pilliga Sandstone rock composition from the recharge outcrop beds (at Tunmallallee) and samples collected within the deeper part of the Pilliga Sandstone at Coonarah 2. As explained in Section 3.3.1, the Pilliga Sandstone in the recharge beds at Tunmallallee is chemically mature whereas it is more heterogeneous and immature in deeper parts of the aquifer where it contains more clay and likely some mudstone and siltstone (Section 3.7.7).

This suggests that the high $^{87}Sr/^{86}Sr$ ratios observed in the freshest Pilliga Sandstone groundwaters within or close to the recharge beds of the Pilliga Sandstone reflect the granitic source of the Pilliga Sandstone and subsequent weathering in the recharge area.

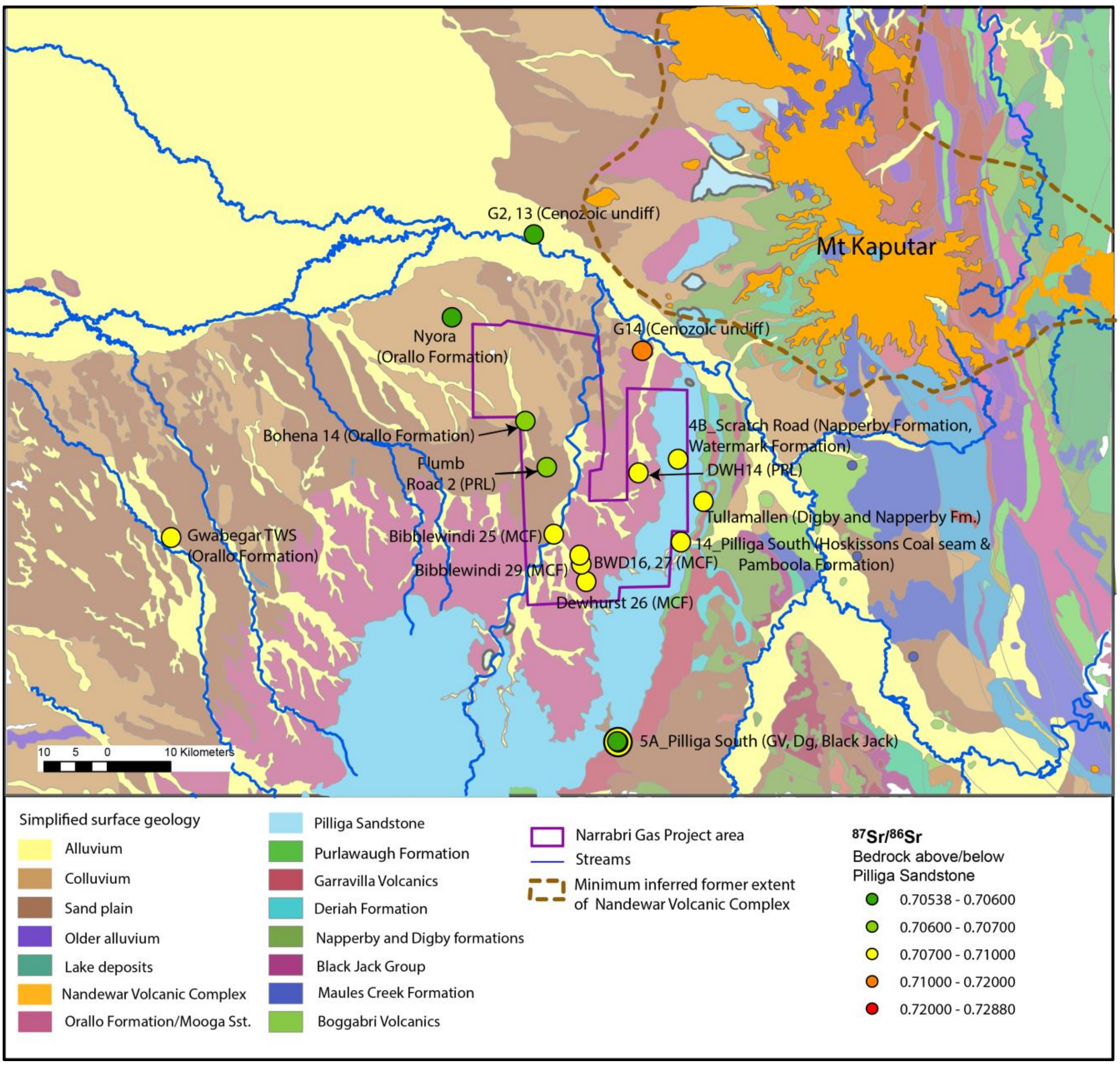

Figure 3-68 – Spatial distribution of $^{87}Sr/^{86}Sr$ ratios in groundwater (other than Pilliga Sandstone) in the Narrabri region overlain on simplified surface geology. Where only one circle is shown at nested bore sites, this means that the values of different formations are in the same $^{87}Sr/^{86}Sr$ interval.

Letters in brackets refer to screened aquifer: MC = Maules Creek Formation; PB = Pamboola Formation; HS = Hoskissons Coal seam; WM = Water Mark Formation; Dg = Digby Formation, Np = Napperby Formation; PRL = Purlawaugh Formation; O = Orallo Formation.

At the NSW DPIE groundwater monitoring site at Plumb Road, Pilliga Sandstone groundwater has a higher $^{87}Sr/^{86}Sr$ ratio than groundwater within the underlying Purlawaugh Formation (0.7082 versus 0.7066), whereas the Sr^{2+} concentration of the Pilliga Sandstone groundwater is much lower (0.07 versus 0.68 mg/L) (Figure 3-71).

At both nested groundwater bore sites (Bohena 14 and Nyora) where the Pilliga Sandstone and the overlying Orallo Formation are monitored, the $^{87}Sr/^{86}Sr$ of the Pilliga Sandstone is higher than that of the Orallo Formation (~0.707 versus 0.7064 at Bohena 14 and 0.7067 versus 0.7056 at Nyora). Cenozoic groundwater samples collected during the present study are variable, with some samples showing very low $^{87}Sr/^{86}Sr$ values (0.7058 to 0.7069) and others having significantly higher values (0.7146 to 0.7237).

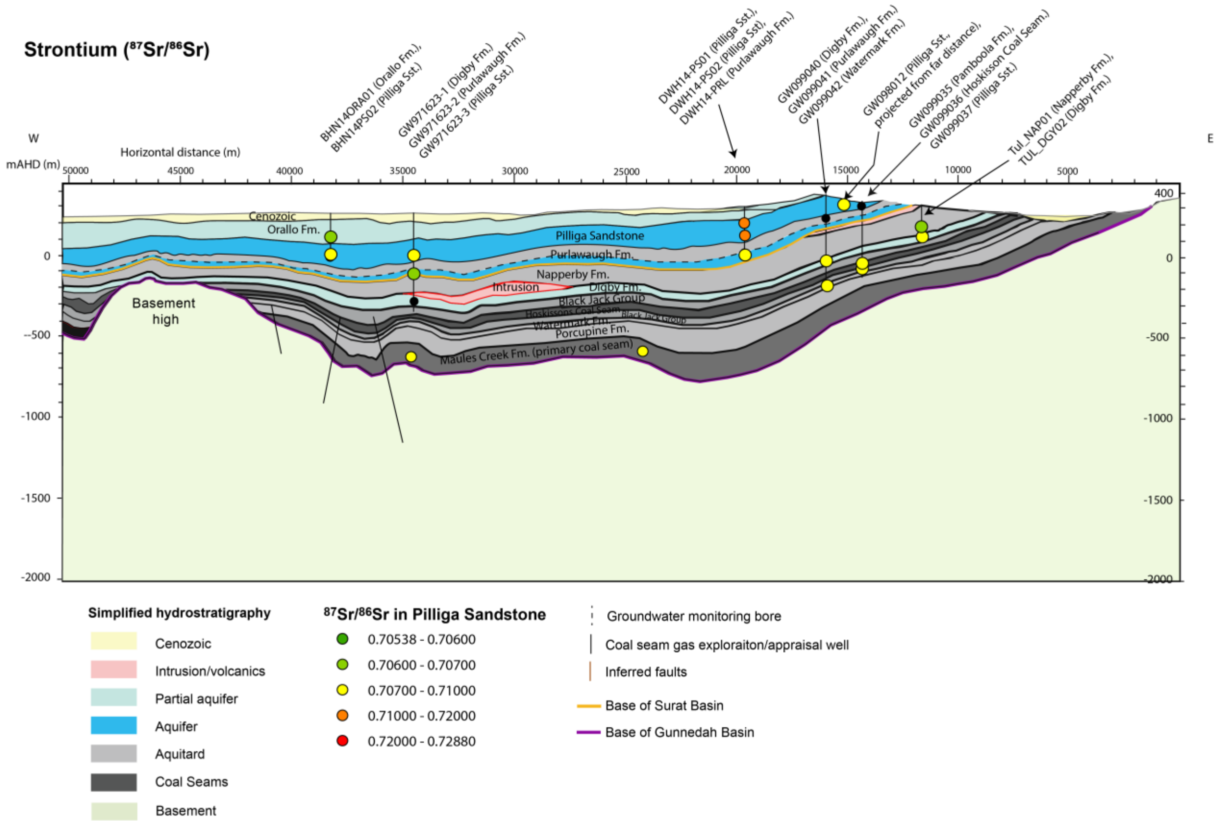

Figure 3-69 – Spatial distribution of $^{87}Sr/^{86}Sr$ ratios in groundwater along transect through central part of Narrabri Gas Project area (for orientation, see Figure 3-25).

The patterns of $^{87}Sr/^{86}Sr$ ratios for different aquifers in the Pilliga region allow for multiple conclusions:

1) The coal seams of the Maules Creek Formation do not likely contribute to the hydrochemical composition of the Pilliga Sandstone—the Sr concentrations of the Maules Creek coal seams are significantly higher than those of the Pilliga Sandstone (Figure 3-71), and the $^{87}Sr/^{86}Sr$ ratios of the coal seams are higher than those of Pilliga Sandstone groundwater downgradient of Plumb Road for example at Nyora PS02 (Figure 3-66). This means that even a small admixture of Sr from the coal seams to the Pilliga Sandstone along the flow path from the eastern part to the western margin of the Narrabri Gas Project area would result in higher than the observed $^{87}Sr/^{86}Sr$ at the Plumb Road, Bohena 14 and Nyora groundwater monitoring sites (Figure 3-68 and Figure 3-67).

2) Raiber et al. (2022a) suggested that the evolution of the $^{87}Sr/^{86}Sr$ ratio of Pilliga Sandstone groundwaters from higher ratios in the east to significantly lower $^{87}Sr/^{86}Sr$ in the west could be explained by an admixture of Sr with low $^{87}Sr/^{86}Sr$ ratios from the Purlawaugh Formation or from the shallow Gunnedah Basin formations to the Pilliga Sandstone. This was under the assumption that the Pilliga Sandstone has a homogeneous and mature chemical composition dominated by quartz. At the Plumb Road groundwater monitoring site, the ratios of Pilliga Sandstone groundwater are significantly different from the ratios in the underlying Purlawaugh Formation and Digby Formation. At Nyora, the $^{87}Sr/^{86}Sr$ of the Pilliga Sandstone groundwater is almost identical to that of the Purlawaugh Formation measured at Plumb Road, suggesting that discharge from the Purlawaugh Formation associated with the thinning and pinching out of this formation influences the $^{87}Sr/^{86}Sr$ of the Pilliga Sandstone.

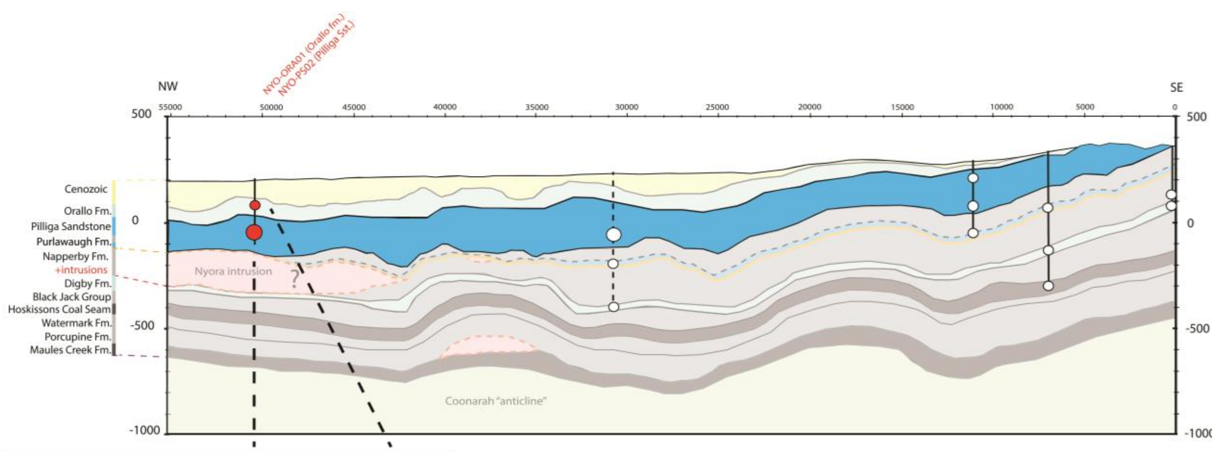

Unit	Parameters	NYO-ORA01	NYO-PS02
-	pH	8.4	8.45
µS/cm	EC	1120	1101
mg/L	TDS	717	704
	Bicarbonate Alkalinity as CaCO3	757	734
	Chloride	54	52
	Calcium	3.0	4.0
	Magnesium	1.0	1.0
	Sodium	344	317
	Potassium	2.0	2.0
	Barium	0.102	2.06
	Strontium	0.122	0.147
	Boron	0.24	0.21
	Fluoride	0.2	0.2
	Bromide	1.0	0.9
meq/L	Na/Cl	9.8	9.4
	Ca/Mg	1.8	2.4
	Ca+Mg/Na+K	0.015	0.020
	HCO3/Cl	9.93	10.00
	Ba/Cl	0.00098	0.02045
	F/Cl	0.03456	0.03230
(µg/L)	CH4	914	794
‰	87Sr/86Sr	0.70566	0.70677
‰ (x10-15)	36Cl/Cl	2.51E-14	3.06E-14
VSMOW‰	δ18O	-6.71	-6.63
	δ2H	-43.78	-46.70

Figure 3-70 Geochemical evidence of similarity in hydrochemical composition of the Pilliga Sandstone and Orallo Formation at Nyora in the north-western part of the Narrabri Gas Project area

The $^{87}Sr/^{86}Sr$ at Bohena 14 is very similar to that of the Digby Formation (based on the Digby Formation groundwater monitoring bore at Tullamullen, as no measurements are available from other Digby Formation bores at present). However, Raiber et al. (2022a) also indicated that the change within the Pilliga Sandstone could also be explained by leakage of groundwater with a lower $^{87}Sr/^{86}Sr$ from the overlying Orallo Formation.

Considering the new evidence collected during the present study from mineralogical analyses and the AEM survey including the potential connection between the Pilliga Sandstone and Orallo Formation and the change of mineralogy from east to west, it is more likely that the evolution of $^{87}Sr/^{86}Sr$ from east to west is due primarily to the change of mineralogical composition within the Pilliga Sandstone or connectivity with the overlying Orallo Formation (discussed further in subsequent sections). As noted above, the Orallo Formation has generally lower groundwater and rock $^{87}Sr/^{86}Sr$ than the Pilliga Sandstone as its source material is likely of volcanolithic rather than granitic origin.

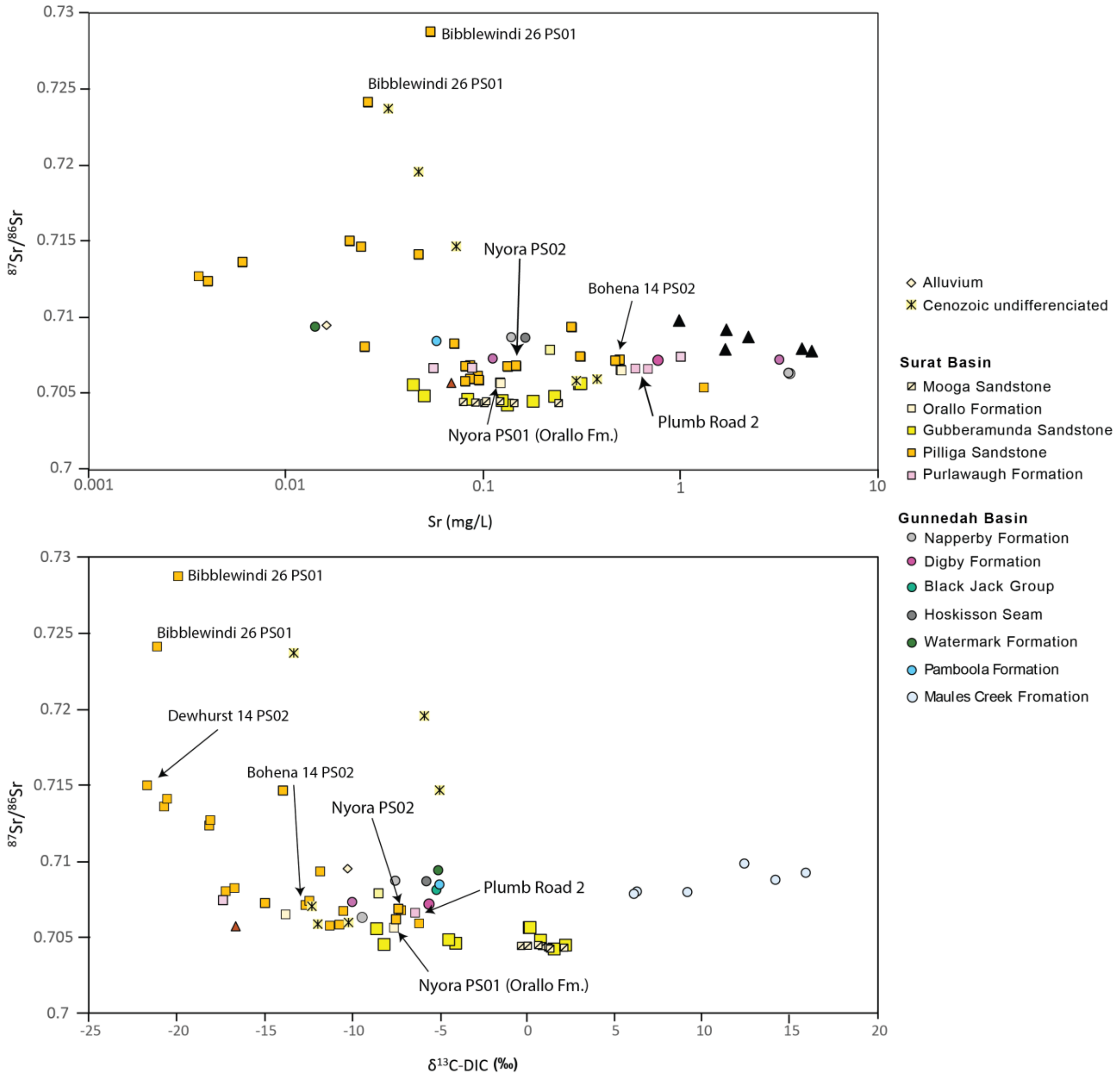

Figure 3-71 – Strontium isotope ratios versus a) Sr concentrations; and b) δ^{13}C-DIC in groundwaters collected from the Pilliga Sandstone and other formations within the Surat Basin in NSW.

Additional selected data from the Gubberamunda Sandstone (a chronological equivalent of the Pilliga Sandstone) in the Surat Basin in Queensland based on Raiber et al. (2024) are shown for comparison.

This is also supported by the observations along the southern flow path starting at the Warrumbungle Volcanic Complex, where there is a noticeable decrease of the $^{87}Sr/^{86}Sr$ ratio of Pilliga Sandstone groundwater between GW040870 and GW040934 (Figure 3-67). As shown by NSW DMR (1995) and Wolfgang (2000), a major fault is located in between these bores (Figure 3-67); this suggests that there is a possibility of an admixture of Sr with lower $^{87}Sr/^{86}Sr$ from over- or underlying formations affecting the $^{87}Sr/^{86}Sr$ ratio of the Pilliga Sandstone. At GW038504 along the southern flow path, the Gunnedah Basin is absent, and the Purlawaugh Formation also appears to be absent, indicating that the Pilliga Sandstone directly overlies basement. As basement is likely to have higher $^{87}Sr/^{86}Sr$ ratios, this indicates that there may be some leakage from the Orallo Formation into the Pilliga Sandstone in this area or that the change of $^{87}Sr/^{86}Sr$ is due to processes within the Pilliga Sandstone. Additional mineralogical analyses along the southern flow path could provide further insights.

3.7.8 Saturation indices

The calculation of saturation indices (SI) in groundwater investigations helps to assess whether an aqueous solution, here groundwater, is undersaturated, in equilibrium, or oversaturated with respect to a particular mineral (e.g., calcite ($CaCO_3$) or halite (NaCl)). Displaying SI values by aquifer can assist with identifying the likelihood of mineral dissolution or precipitation processes to occur along flow paths within different formations.

The SI is defined as SI = log $(\frac{IAP}{Ksp})$. where IAP is the ion activity product of the ionic species of the mineral and Ksp is the solubility constant of the mineral at a fixed temperature. The calculated saturation indices indicate the saturation state of each mineral. If the index is positive, the solution is oversaturated, and precipitation of the mineral can occur. Conversely, if the index is negative, the solution is undersaturated, suggesting that the mineral is likely to dissolve. According to the results, it can be interpreted as:

- SI < 0: the mineral may dissolve.
- SI = 0: thermodynamic equilibrium.
- SI > 0: the mineral may precipitate.

Saturation indices are calculated for a wide range of possibly prevailing or newly forming minerals, based on the measured hydrochemical composition of the analysed groundwaters (major and trace elements) and the mineralogical composition (XRD; Section 3.3.1). This comparison has highlighted some key mineral reactions that are likely to occur along the flow path or during groundwater mixing (e.g. quartz, kaolinite, illite, chlorite, analcime, halite, dolomite, baryte and calcite).

Figure 3-72 displays the saturation index (SI) values for various mineral phases across different aquifer formations encountered in the study area. Most minerals show negative SI values, indicating that they are undersaturated. This suggests that these minerals are more likely to dissolve rather than to precipitate under the current hydrochemical conditions. Carbonate minerals (e.g. calcite, dolomite and aragonite) tend to have SI values closer to 0, approaching equilibrium, especially in formations such as the Pilliga Sandstone and Watermark Formation. Some Mn-bearing phases (e.g. $MnCl_2 \cdot 4H_2O$) have extremely low SI values below < -50, indicating that they are highly undersaturated and not stable in the water chemistry of these aquifers. The extremely low SI value of $O_2(g)$ suggests that reducing conditions occur in these formations, and confirms that aquifers are under geological confinement.

Some mineral reactions (e.g. analcime, barite, calcite , chlorite(14a), dolomite, kaolinite, K-feldspar and illite) displaying a saturation index close to equilibrium were added to the inverse geochemical modelling to refine the flow model hypothesis (Section 3.9).

The saturation index (SI) for various mineral phases in groundwater bores located along the geological cross-sections studied are shown in Figure 3-73 (Section 3.6). The main patterns and observations previously identified remain applicable in this graph. However, to improve the readability of the diagram, the specific data of the cross-section is presented in a different plot. Calcite and dolomite minerals are undersaturated in the Pilliga Sandstone but over-saturated in other formations. Local boreholes still present a low SI value of $O_2(g)$ suggesting that geological confinement is also locally preserved.

·

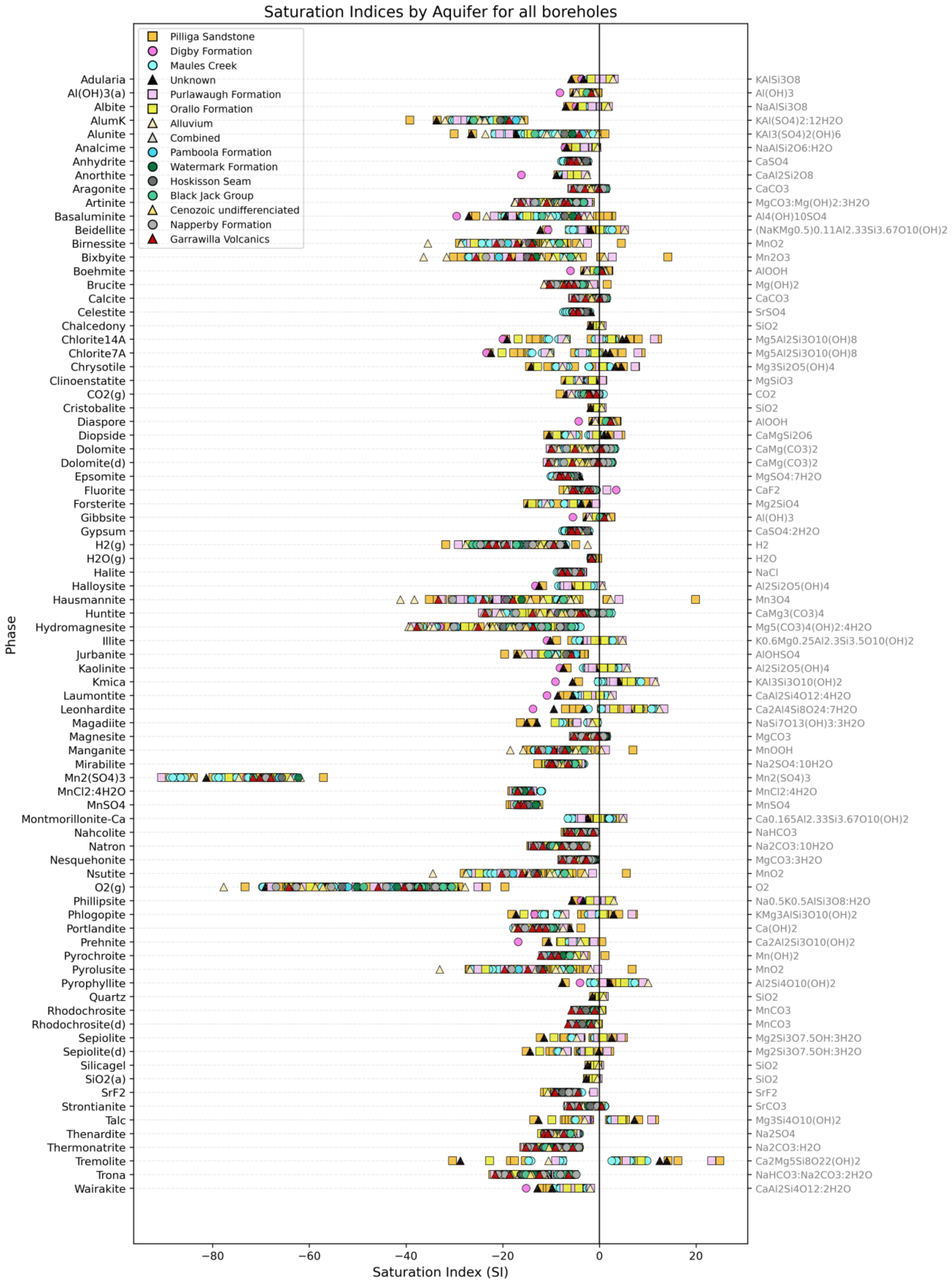

Figure 3-72 Saturation indexes displayed by aquifer for all bores sampled in the survey area.

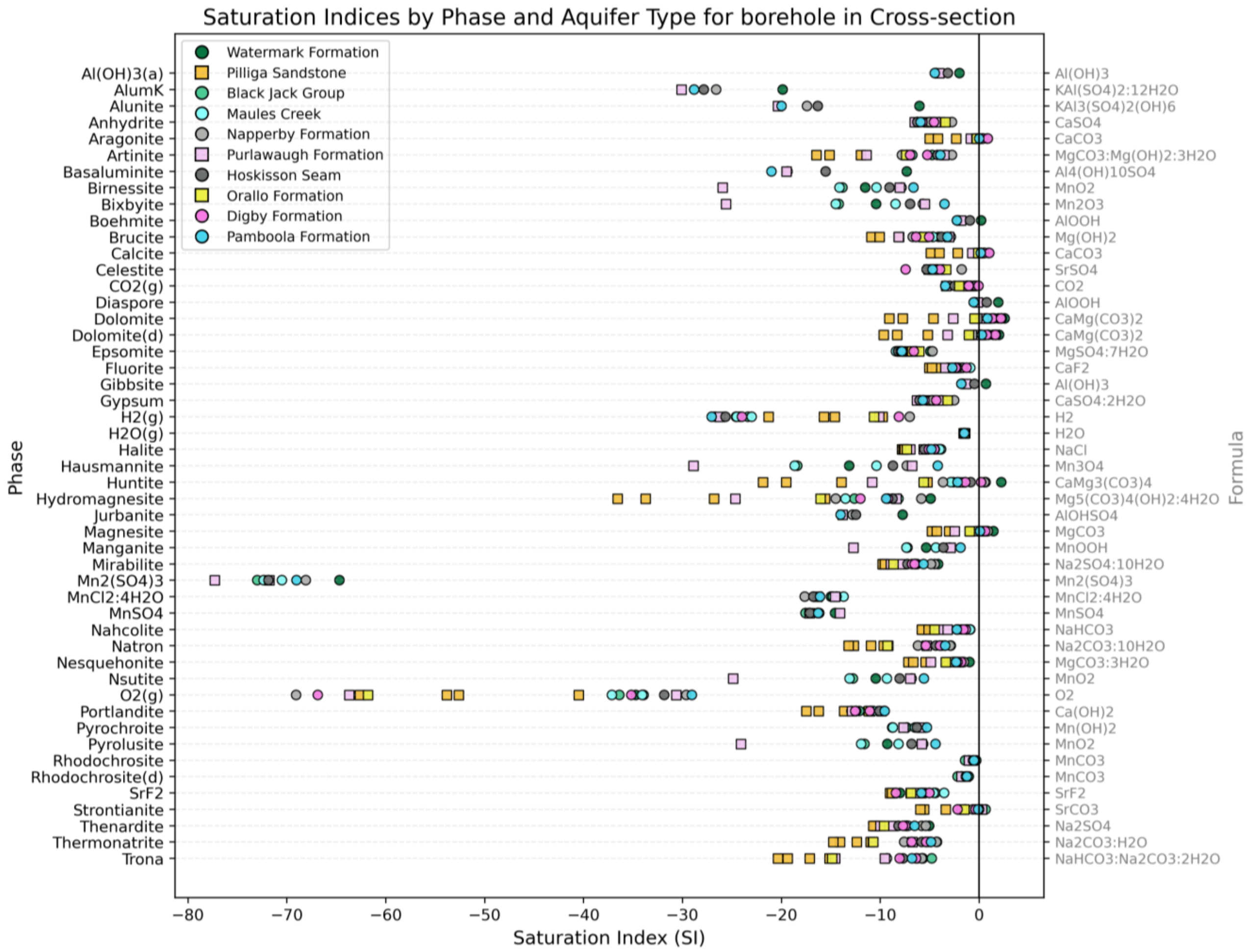

Figure 3-73 Saturation indexes displayed by aquifer for selected bores along the geochemical cross-section

3.8 Insights from new measurements of noble gases and 'age' tracers

Environmental tracers can provide an important line of evidence when examining hydrogeological connections between stacked aquifer-aquitard sequences in sedimentary basins.

In this section, we compare the results from multiple environmental tracers, including ^{3}H, ^{14}C, ^{36}Cl and stable noble gas concentrations and isotopes (e.g. $^{3}He/^{4}He$, ^{4}He and ^{40}Ar) and radioactive noble gas isotopes (^{85}Kr and ^{81}Kr), building upon the results and interpretations from previous studies (e.g. Radke et al., 2000; Cresswell, 2014; Iverach et al., 2017), from previous GISERA projects (Raiber and Suckow, 2018; Suckow et al., 2019 and Raiber et al., 2022a) and on previous sections of the current report.

The discussion of environmental tracer results in this section focusses on noble gas results, ^{3}H, ^{14}C and ^{36}Cl data from groundwater bores located close to the Narrabri Gas Project area.

A more detailed interpretation of the environment tracer results for the wider Coonamble Embayment has been previously described by Raiber and Suckow (2018), Suckow et al. (2019) and Raiber et al. (2022a).

3.8.1 Tritium (^3H)

Tritium is a radioactive isotope that occurs both naturally and due to nuclear testing in the 1950's and 1960's in the atmosphere. With a half-life of approximately 12.3 years, it can be used in dating modern groundwater of less than approximately 80 years primarily in shallow aquifer systems or in the outcrop beds of deeper aquifer systems. In deeper parts of sedimentary basin aquifer systems, it is generally assumed that there should be no ^3H present; however, analysing ^3H in such locations can help to identify any contamination during sampling, transport or storage.

Within the Narrabri Gas Project area and some samples from within the broader Coonamble Embayment, the activities of ^3H in groundwater samples collected from the Surat and Gunnedah basins are generally very low and below 0.18 tritium units (TU), including within or near the outcrop beds of the Pilliga Sandstone (e.g. GW098011 and GW098012). In contrast, some alluvial groundwaters in the Narrabri region have significantly higher activities of ^3H in a similar range as modern rainfall from 2 to 3 TU in Narrabri West. This was based on weighted values of precipitation from July 2005 to June 2011 extracted from Tadros et al. (2014), with current values of ^3H in precipitation likely to be slightly lower.

Although the ^3H measurements of some samples could indicate presence of a modern groundwater component, the comparison of ^3H and ^{14}C suggests that for most samples, this is unlikely to be the case. For example, for two samples collected from groundwater bores screened within the Napperby and Digby formations of the Gunnedah Basin at Tullamullen sampling site (Figure 3-68), the low values of ^{14}C and the sampling specifications (the bores are screened at depths of approximately 130 and 215 m depth in low permeability strata) suggests that these groundwater samples are unlikely to contain any modern groundwater component. However, high gas contents and exsolution of gas were observed during sampling at both groundwater bores and confirmed by the analytical results, suggesting that the ^3H above the limit of quantification is more likely due to minor contamination during sampling, transport or storage. Although the leakage due to high pressure and gas content is initially outwards, once a break of the seal of the bottle is established, this can lead to atmospheric contamination during transport and storage prior to analysis.

This is similar to observations in other parts of the Great Artesian Basin, where groundwaters collected from deep parts of the aquifers contained measurable ^3H above the limit of quantification, attributed to leakage from the seals of sampling bottles due to high gas content and pressure and observed contraction of sampling bottles.

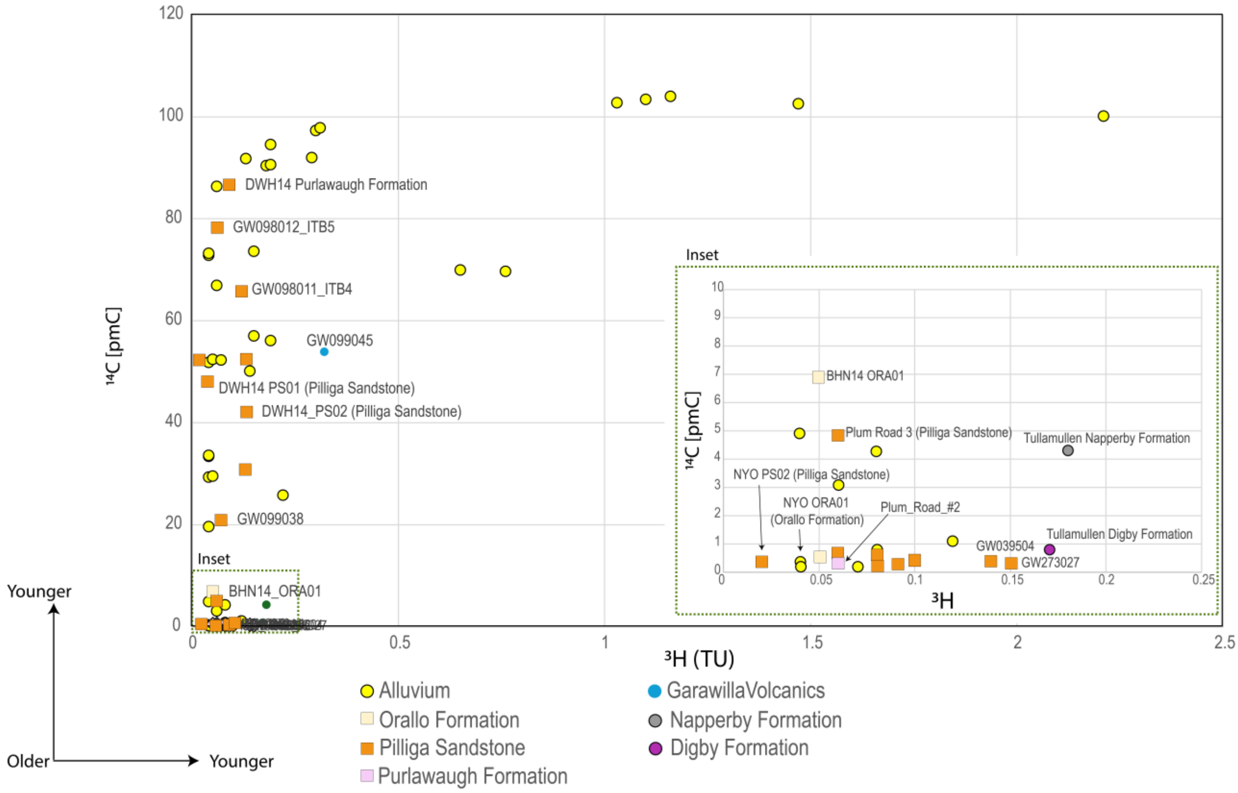

Figure 3-74 Comparison of ^{3}H and ^{14}C in groundwaters of the alluvium, Surat Basin, Gunnedah Basin and Garrawilla Volcanics.

Radiocarbon and ^{3}H values for the alluvium are from Iverach et al. (2017). All other values are from Suckow et al. (2019), Raiber et al. (2022a) and the current study. All sedimentary bedrock samples were collected and analysed for ^{3}H and ^{14}C between 2018 and 2024.

Most groundwater samples collected from the Orallo Formation, Pilliga Sandstone and Purlawaugh Formation also likely contain no modern groundwater based on the comparison of ^{3}H and ^{14}C. However, a few samples from within or close to the outcrop beds of these formations (e.g.GW098011, GW098012 and DWH14-Purlawaugh Formation) where both ^{3}H is above the limit of quantification and ^{14}C values are relatively high may contain a component of modern groundwater. However, some uncertainty exists at DWH14-Purlawaugh groundwater observation site, where the groundwater bore was temporarily decommissioned due to downhole equipment stuck in the casing, and the sample was collected relatively shortly after recommissioning of the groundwater bore.

3.8.2 Radiocarbon (^{14}C)

Radiocarbon is carried along in water as inorganic carbon (corresponding to the sum of dissolved CO_2, HCO_3^- and CO_3^{2-}, also called total dissolved inorganic carbon or TDIC, as discussed in Raiber et al., 2022). Radiocarbon is one of the routine tools used to determine hydrogeological connections between different aquifers (e.g. Raiber et al., 2015) and to determine flow velocities in groundwater, as described in Suckow et al. (2019).

The map of ^{14}C in Pilliga Sandstone groundwaters (Figure 3-75) shows multiple important patterns. Regionally within the Coonamble Embayment (a sub-basin of the Surat Basin in NSW), it highlights that higher values occur only within or in very close proximity to the recharge areas (where the

Pilliga Sandstone outcrops). At the time of groundwater recharge, ^{14}C activities of CO_2 in the unsaturated zone are typically assumed to be in equilibrium with the atmosphere (100 percent modern carbon, or pMC), although this can vary significantly under open system conditions. Outside the recharge area, values quickly drop and after a flow distance of approximately 40 km all values are generally below 4 pMC. There is, however, a very large scatter in the data, and even after a flow distance of 100 km some values still vary between 0.1% and 1.2 pMC.

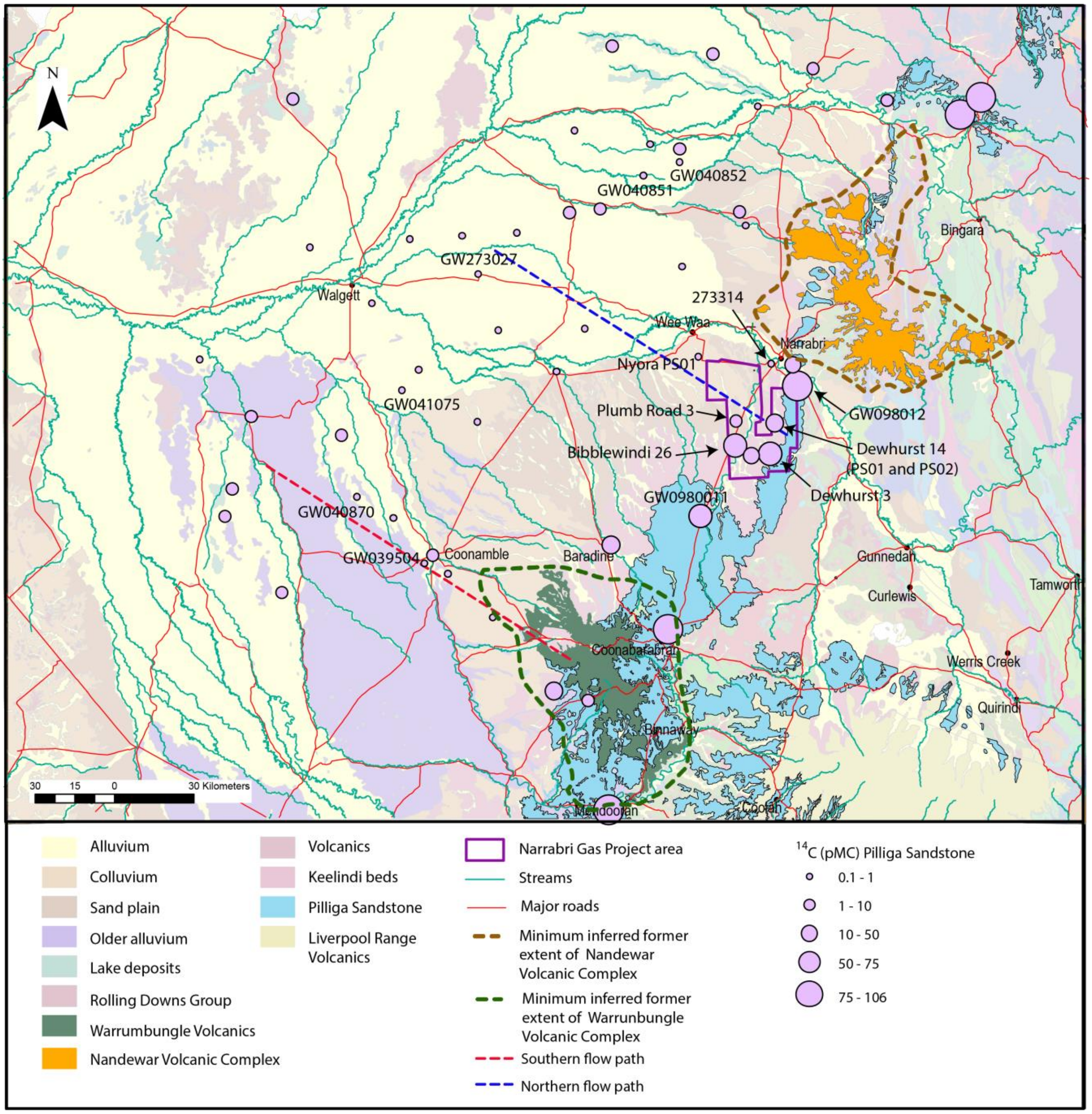

Figure 3-75 – Spatial distribution of radiocarbon activities of groundwater in the Pilliga Sandstone overlain on simplified surface geology.

Historical data are from Cresswell (2014) and Radke et al. (2000), combined with data from Iverach et al. (2017), Suckow et al. (2019), Raiber et al. (2022) and the current study.

A similar pattern can also be observed within or near the Narrabri Gas Project area. In the eastern part of this area, within or near the outcrop beds of the Pilliga Sandstone, groundwater ^{14}C is very high (e.g. 78 pMC at groundwater bore GW098012 and 67 pMC at Dewhurst 3 (Dewhurst 3-PS01, a bore screened in the upper part of the Pilliga Sandstone)), but both water samples have a value of ^3H at or close to the limit of quantification (Figure 3-74). Along the flow path and away from the recharge beds towards the west, radiocarbon remains relatively high at Bibblewindi 26 (in a bore screened within the lower part of the Pilliga Sandstone) with ~53 pMC. However, radiocarbon then rapidly decreases to 4.86 pMC within the Pilliga Sandstone at Plumb Road within a very short distance from Bibblewindi 26, and further decreases to 0.36 pMC at Nyora (bore Nyora-PS02). The ^{14}C measured in the overlying Orallo Formation at Nyora is similarly low (0.55 pMC). This is in good agreement with the AEM and XRD results, which indicate an increase of lithological variability and increase of clay content towards the west and north-west.

At the central-northern margin of the Narrabri Gas Project area, the radiocarbon measurement from the Pilliga Sandstone at NSW DPIE monitoring bore 273314 (Figure 3-75) located south of Narrabri and less than 10 km from the closest Pilliga Sandstone recharge beds yields 0.6 pMC (Iverach et al., 2017), which is much lower compared to the bores located further south at a similar or further distance from the Pilliga Sandstone recharge beds (e.g. Dewhurst 14 and Bibblewindi 26).

The spatial distribution of ^{14}C within or near the Narrabri Gas Project area shows similar patterns as other environmental tracers and hydrochemical parameters including chloride, bicarbonate, EC and CH_4, where a noticeable change occurs just east of the Plumb Road NSW DPIE monitoring site. In previous studies, the Pilliga Sandstone was generally characterised as a quartzose sandstone with limited clay and feldspar content (e.g. Arditto, 1982). Based on the same assumption, Raiber et al. (2022) suggested that that the rapid decline in ^{14}C observed within the Pilliga Sandstone between Bibblewindi and Plumb Road is unlikely to be a result of aging associated with a step change in distance velocity because of a change in petrophysical properties of the Pilliga Sandstone aquifer. Instead, the authors suggested that it is probably a reflection of hydrochemical reactions within the Pilliga Sandstone or indicates an admixture from underlying formations (e.g. Purlawaugh Formation or Gunnedah Basin strata). If fossil or “dead” (^{14}C-free) carbon (where all ^{14}C has already decayed), for example, derived from the oxidation of methane or from bicarbonate discharging into the Pilliga Sandstone from below (either from Gunnedah Basin formations or from the Purlawaugh Formation), is added to the TDIC pool of the Pilliga Sandstone, this would dilute the ^{14}C signal in a similar way as radioactive decay, resulting in an older apparent groundwater age. However, this would also suggest that Pilliga Sandstone groundwater samples would be over- or supersaturated with respect to calcite and dolomite, which does not appear to be the case (Section 3.7.8). Alternatively, this could also indicate diffusion of radiocarbon with low ^{14}C from the Purlawaugh Formation.

However, the newly collected mineralogical and AEM data (Figure 3-36) show that there is a significant change in petrophysical properties within the Pilliga Sandstone from east to northwest and south to north within the Narrabri Gas Project area. The implications will be discussed further in Section 4.

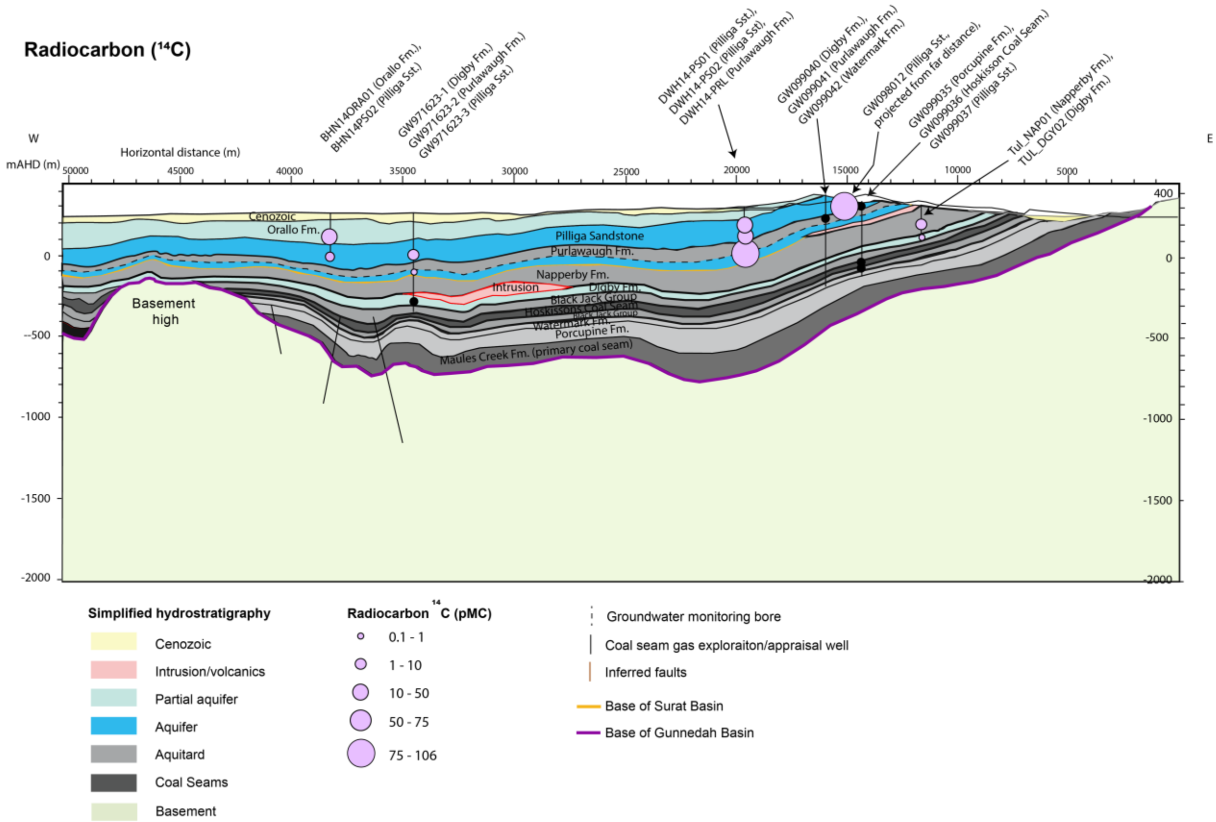

Figure 3-76 – Distribution of radiocarbon (^{14}C) in bores along cross-section 1 (for orientation of this cross-section, see Figure 3-25).

3.8.3 Chlorine-36 (^{36}Cl)

The principles of radiocarbon and ^{36}Cl applications in groundwater are identical. As for ^{14}C, ^{36}Cl also has a carrier (chloride). Chlorine-36 values are reported as $^{36}Cl/Cl$ ratios due to the ^{36}Cl concentration being many orders of magnitude lower than total Cl. The ^{36}Cl used for this purpose is produced in the upper atmosphere, then mixes with atmospheric chloride and this mixture is deposited on the land surface dissolved in rain or as dry aerosols, from where it infiltrates into the unsaturated zone. Details of the use of ^{36}Cl as groundwater tracer can be found in Raiber et al. (2022a).

Chloride has the advantage that it is more conservative in groundwater than TDIC, which is counterbalanced by the disadvantage that ^{36}Cl is in some cases produced in the ground (Phillips, 2013) or can be affected by dissolution of evaporites such as halite. The dissolution of halite can introduce additional chloride ions with “dead” ^{36}Cl (chloride that contains no measurable ^{36}Cl, typically because it has been isolated from cosmic ray exposure for a long period, allowing the Cl to decay completely) into the groundwater system. Determining whether evaporates are present and if dissolution of evaporates has likely occurred can be achieved through an assessment of the mineralogy and groundwater Cl/Br ratios, whereas mineralogical analysis of rocks and in particular analyses of Th and U concentrations can help to determine if subsurface production of ^{36}Cl is likely to occur.

Formations below the Pilliga Sandstone in the Narrabri region

The values of $^{36}Cl/Cl$ of groundwaters in the Gunnedah Basin formations and the Purlawaugh Formation at Plumb Road (GW971623-2) are generally very low (Figure 3-77). This indicates a very long residence time of groundwaters.

As shown in Figure 3-77, no groundwater samples with ^{36}Cl are available for Gunnedah Basin groundwaters within the central, western and northern part of the Narrabri Gas Project area. However, samples collected from the eastern part of the Narrabri Gas Project where these formations are within or relatively close to the outcrop beds have very low ^{36}Cl values, suggesting that groundwater further west within the Gunnedah Basin likely has even lower values than those measured due to radioactive decay along the inferred westerly flow paths. The low ^{36}Cl observed within or the near the recharge beds may indicate very low recharge rates for these formations, as previously suggested by chloride-mass balance estimation (Crosbie et al., 2022). Although most of the Gunnedah Basin formations are dominated by low permeability strata such as claystones, there is some variability and thin intervals of sand-dominated facies also exist (sections 3.1.2 and 3.3.1). This variability could lead to interaction with stagnant zones where diffusion may result in a loss of ^{36}Cl to low permeability intervals or aquitards along the flow path (Turnadge and Smerdon, 2014).

For the Purlawaugh Formation, there is a distinction between the values observed in groundwater at DWH14 and at Plumb Road (GW971623-2) (Figure 3-77). In the upgradient location at DWH14, the measured $^{36}Cl/Cl$ value is very high (157×10^{-15}). At Plumb Road, the ^{36}Cl value is the lowest of all samples analysed in the Coonamble Embayment (both within the Surat and Gunnedah basins) and one of the lowest values reported in the Great Artesian Basin, as further discussed in Section 3.8.7.

There are multiple uncertainties associated with these values: the groundwater bore screening the Purlawaugh Formation at DWH14 was temporarily decommissioned due to downhole equipment stuck in the bore casing. The sample for this study was collected relatively soon after recommissioning of the bore, and it is unknown if any water was added throughout the removal of downhole equipment and re-commissioning of the bore, and if so, whether the groundwater bore was purged. As for the Gunnedah Basin strata, the Purlawaugh Formation is characterised by some lithological heterogeneity, with a lower, thin (~10 m thick) and more permeable aquifer section dominated by sands and gravels, and an upper thicker low permeability zone dominated by claystone. This suggests that there may be a loss of ^{36}Cl to stagnant zones above or below (Napperby Formation) the aquifer. Furthermore, in a previous GISERA study, Raiber et al. (2022) suggested that there may be some upwards discharge of groundwater from the Napperby Formation or Digby Formation to the Purlawaugh Formation at Plumb Road. As described in previous sections (e.g. Section 3.1.1), a spatially extensive and thick sill has intruded into different formations of the shallow Gunnedah Basin and to the base of the Purlawaugh Formation at Bohena near the Plumb Road groundwater monitoring bore site. This sill and associated fractures represent a plausible connectivity pathway linking the Purlawaugh Formation and the Napperby and Digby formations. The observed uncertainty suggests that care must be taken if using groundwater age tracers to calculate a flow velocity between DWH14 and Plumb Road. This will be discussed further in subsequent sections of this report.

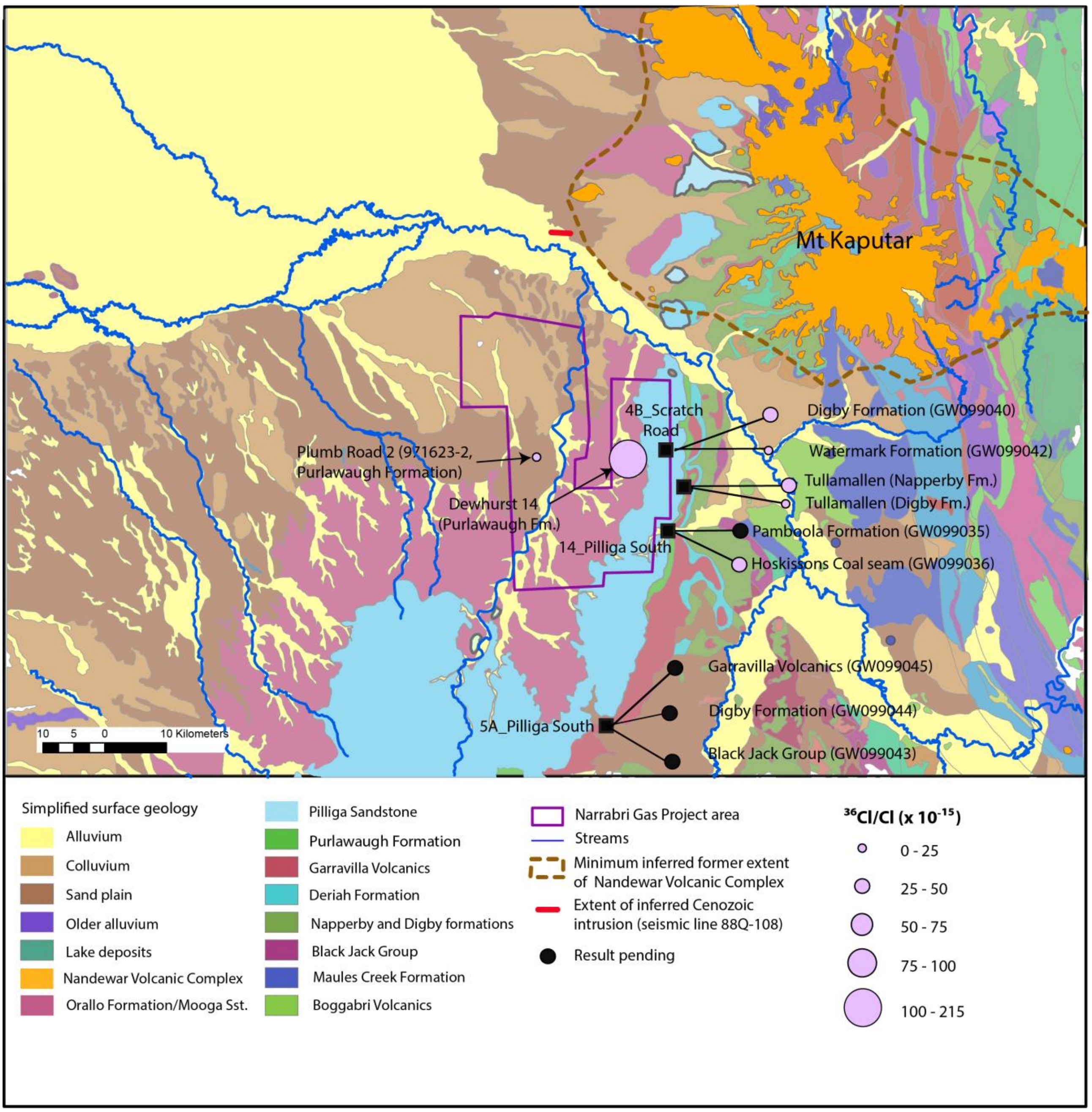

Figure 3-77 – Chlorine-36 in groundwaters of formations below the Pilliga Sandstone (Gunnedah Basin strata, Garrawilla Volcanics and Purlawaugh Formation) in the Narrabri Gas Project area)(some measurements are still pending) overlain on simplified surface geology.

Pilliga Sandstone and formations above in the Narrabri region

The map of $^{36}Cl/Cl$ ratios of Pilliga Sandstone groundwaters shows some distinct spatial patterns. In the southern part of the Coonamble Embayment (i.e. corresponding to the southern flow path described in previous sections and in Raiber and Suckow (2018), Suckow et al. (2019) and Raiber et al., 2022), a small area with a start of a flow line approximately south of Coonabarabran and the associated volcanic rocks of the Warrumbungle Volcanic Complex (Figure 3-79) shows much higher $^{36}Cl/Cl$ values along a flow line than within other parts of the Coonamble Embayment. The $^{36}Cl/Cl$ ratio at the start of the flow path is around $2x10^{-13}$, and only slightly decreases along the flow path. Since there is also considerable scatter on the data and as the initial ratio is not well defined, Suckow et al. (2019) estimated a distance velocity ranging from 0.2 m/year to 1.5 m/year for this inferred flow path, which was further narrowed down to 0.33m/y to 0.6 m/y with ^{81}Kr.

Further north within the Narrabri Gas Project area, measured ^{36}Cl/Cl ratios initially decrease only slightly with distance from the outcrop for samples within the Pilliga Sandstone (Figure 3-79 and Figure 3-80). For example, the ^{36}Cl/Cl ratios at Bohena 14 (groundwater bore Bohena 14-PS02), Bibblewindi 26 (BWD 26-PS01) and at Plumb Road 3 (screened in the Pilliga Sandstone) are all similar, ranging from $1.39\text{x}10^{-13}$ to $1.84\text{x}10^{-13}$. However, at Nyora 1, to the northwest of the Narrabri Gas Project area, the ^{36}Cl/Cl ratios at bores screened within the Pilliga Sandstone and Orallo Formation are an order of magnitude lower (30.64 and 25.1 x 10^{-15}, respectively).

This indicates that there is a significant decrease of the ^{36}Cl/Cl of groundwater within the Pilliga Sandstone aquifer by one order of magnitude over a relatively small flow distance between Plumb Road and Nyora. Raiber et al. (2022) in a previous GISERA study suggested that there is unlikely to be an increase of chloride along the flow path through within-formation processes in the Pilliga Sandstone once groundwater is below depths where evapotranspiration could occur due to the characterisation of the Pilliga Sandstone as a quartzose sandstone and the absence of any rock-forming minerals that could supply additional chloride (Section 3.4.2.2). This led Raiber et al. (2022a) to suggest that there is a likely admixture of chloride from adjacent formations that may be free of ^{36}Cl, or at least with a low ^{36}Cl/Cl in equilibrium with underground production, which is a reasonable assumption in deep sedimentary basin formations.

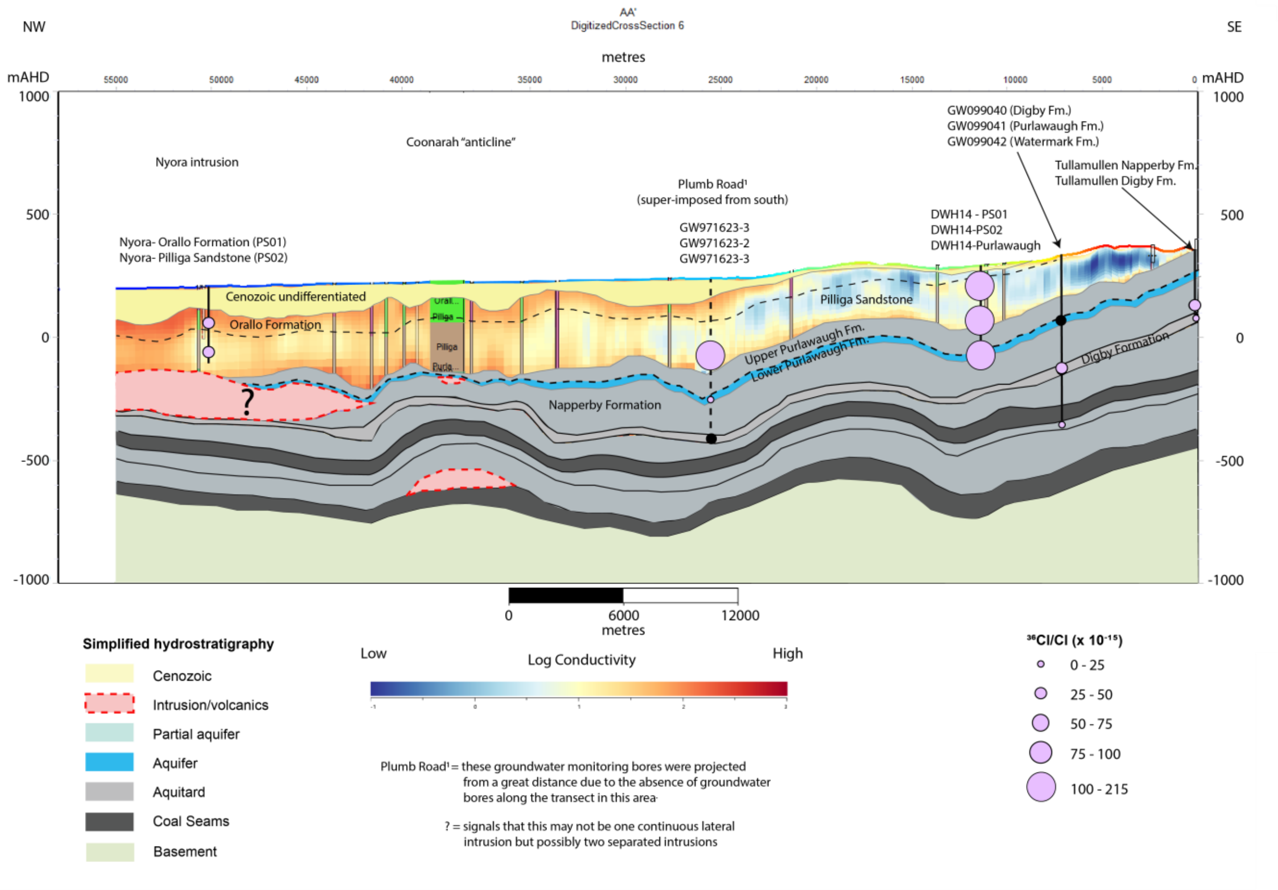

Figure 3-78 – Vertical distribution of ^{36}Cl in bores along cross-section 2 (for orientation of this cross-section, see Figure 3-25) and electromagnetic depth-conductivity structure for the Orallo Formation and Pilliga Sandstone.

As described by Raiber et al. (2022a), chloride concentrations increase significantly along the flow path within the Pilliga Sandstone from approximately 10–25 mg/L in the infiltration area to concentrations of more than 50 mg/L at Nyora and only a minor further increase to approximately 65 mg/L downgradient 100 km. Groundwaters in underlying formations have much higher chloride concentrations, as for example ~210 mg/L within the Purlawaugh Formation at Plumb Road, ~570 mg/L within the Digby Formation at Plumb Road and up to approximately 2000 mg/L within the primary CSG target Maules Creek coal seams.

However, as described for the observations of ^{14}C within the Narrabri Gas Project, the newly collected AEM data (Section 3.4) and new mineralogical data (Section 3.3.1) suggest that the composition of the Pilliga Sandstone likely changes from a quartzose sandstone within and near the outcrop beds to a sandstone with higher clay and plagioclase contents towards the deeper part of the Surat Basin. This is shown in Figure 3-78, where a distinct change in conductivity-depth structure within the Pilliga Sandstone indicates a facies change from east to west.

Furthermore, the new AEM survey data also show that there is no clear distinction in electromagnetic pattern between the Pilliga Sandstone and the overlying Orallo Formation in the western and north-western part of the Narrabri Gas Project area. This was also found during visual inspections of cores at the NSW core library. The difficulty in picking the interface between the Pilliga Sandstone and Orallo Formation may also be the reason why the two formations are lumped together in some stratigraphic logs in this area. The newly collected data therefore suggest that contrary to previous assumptions by Raiber et al. (2022), the rapid decline in ^{14}C and ^{36}Cl observed within the Pilliga Sandstone between Dewhurst 14-PS01 and PS02, Plumb Road 3 and Nyora PS01 indeed at least partially results from within-formation aging associated with a step change in distance velocity because of a sedimentary facies change within the Pilliga Sandstone aquifer along the flow path. Furthermore, at Nyora, the ^{36}Cl of the groundwater bore screening the Orallo Formation is very similar as the ^{36}Cl of the Pilliga Sandstone at the same site. The observed AEM subsurface structure in this area suggest that the observed tracer patterns are likely influenced by connectivity between the Orallo Formation and the Pilliga Sandstone, as also supported by the similarity in all hydrochemical and environmental tracer values at Nyora between bores screened in these formations. A possible contribution from formations underneath the Pilliga Sandstone will be discussed further in subsequent sections.

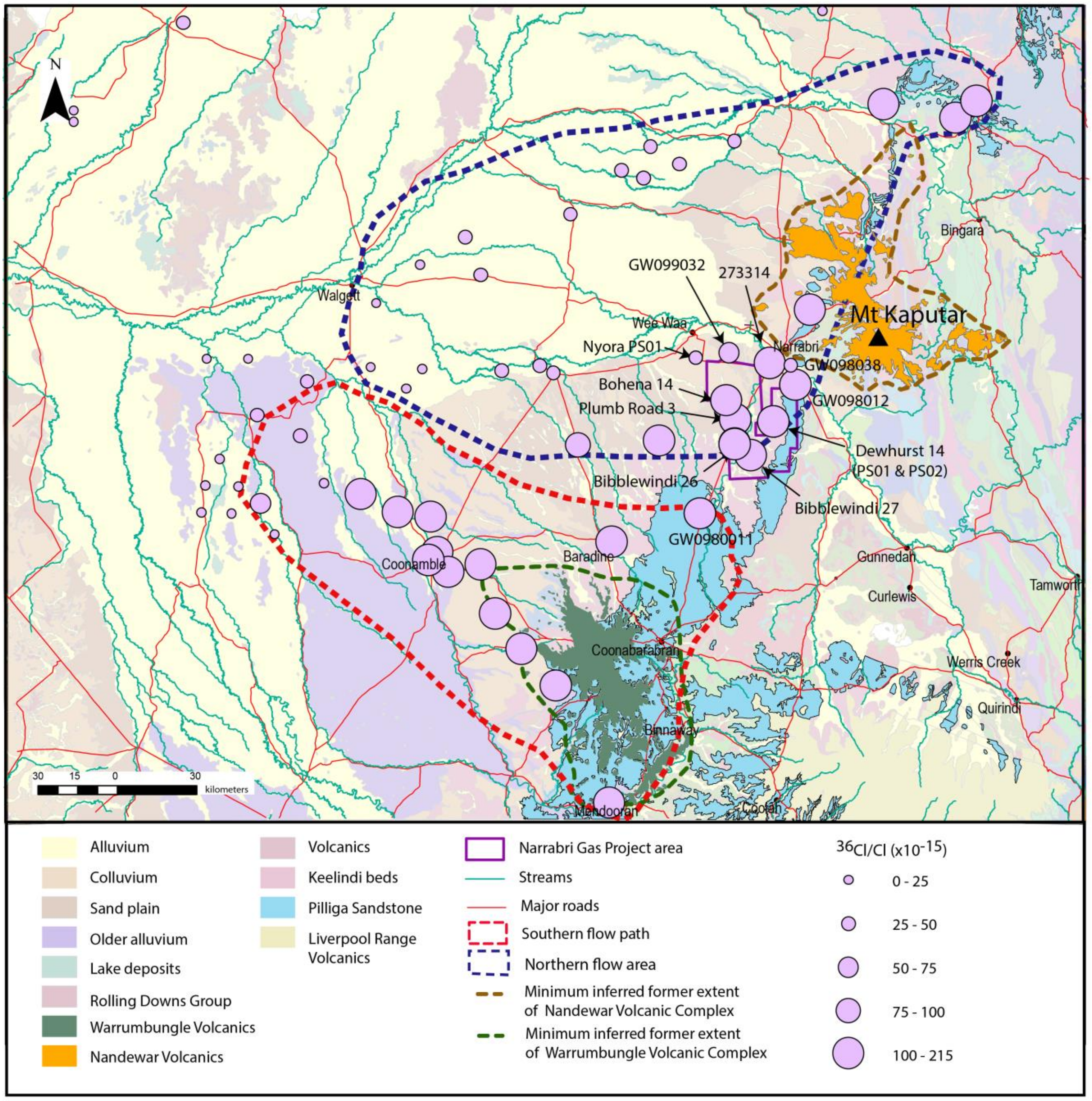

Figure 3-79 – Spatial distribution of $^{36}Cl/Cl$ of groundwater in the Pilliga Sandstone overlain on simplified surface geology.

The red area represents the southern flow path with higher $^{36}Cl/Cl$, the blue area the northern flow area (as described in the text). Historical data are from Radke et al. (2000), combined with the data from Iverach et al. (2017), Suckow et al. (2019), Raiber et al. (2022) and the current study.

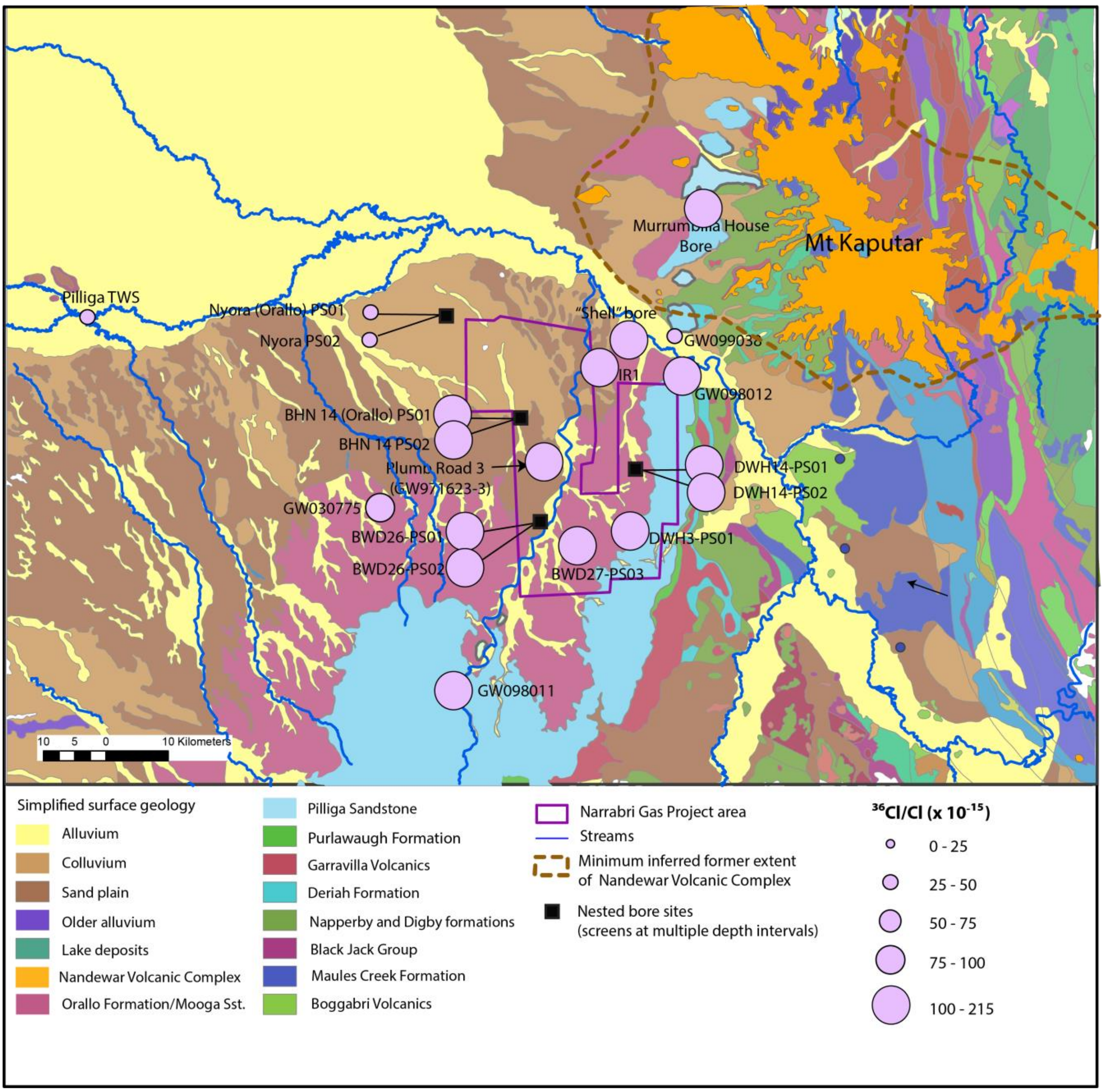

Figure 3-80 – Spatial distribution of $^{36}Cl/Cl$ of groundwater in the Pilliga Sandstone, Orallo Formation and a Cenozoic groundwater bore (IR1) in the Narrabri Gas Project area overlain on simplified surface geology.

Mixing is also likely to occur along the southern flow path (Figure 3-79). As discussed by Raiber et al. (2022a), chloride concentrations increase significantly from GW039504 to GW040870 and GW040934, attributed to a possible mixing with the overlying Orallo Formation as the Gunnedah Basin and Purlawaugh Formation appear to be absent underneath the Pilliga Sandstone along this flow path.

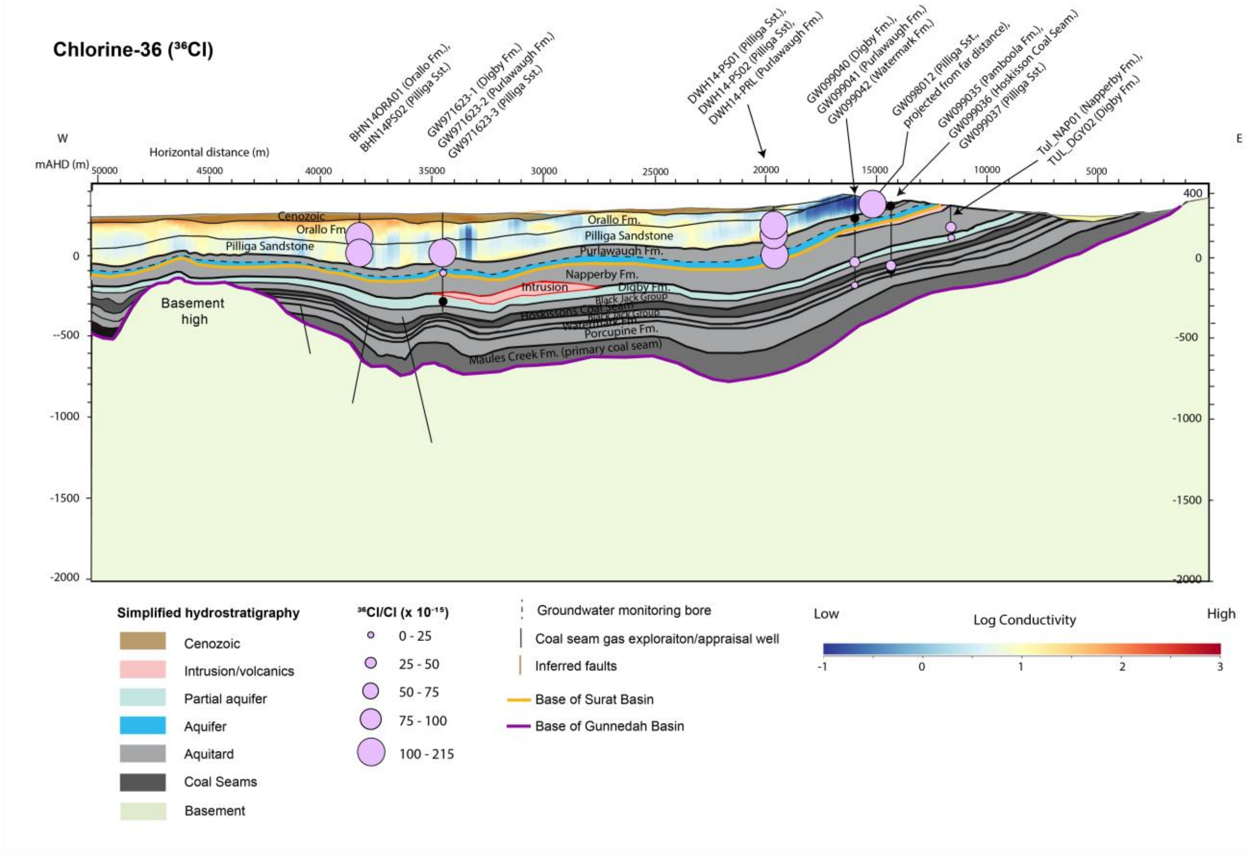

Figure 3-81 – Vertical distribution of chlorine-36 (^{36}Cl) in bores along cross-section 1 (for orientation of this cross-section, see Figure 3-25) and electromagnetic depth-conductivity structure for the Orallo Formation and Pilliga Sandstone.

3.8.4 Helium-4 (^{4}He)

Unlike most other environmental age tracers which decay over time, the concentration of ^{4}He in aquifers normally increases with flow direction and with the time the groundwater had to accumulate radiogenic helium from the radioactive decay of Uranium and Thorium isotopes (Mahara et al., 2009; Torgerson et al., 1987). Although ^{4}He is only considered as a semi-quantitative tool to determine groundwater ages, groundwater helium concentrations (^{4}He) are a useful indicator of connectivity between deep and shallower aquifers due to the high diffusion coefficient and mobility of helium (Torgerson et al., 1987; Torgerson and Stute, 2013; Turnadge and Smerdon, 2014).

Groundwater helium concentrations were analysed for 13 groundwater bores screened in the major formations of the Surat Basin and Gunnedah Basin within the wider Narrabri Gas Project area in this study. This complemented existing ^{4}He values presented by Suckow et al. (2019) for the wider Coonamble embayment and Raiber et al. (2022a) for the Narrabri Gas Project area.

Formations below the Pilliga Sandstone in the Narrabri region

In the Narrabri region, ^{4}He concentrations are generally very high within the Purlawaugh Formation, Garrawilla Volcanics and Gunnedah Basin strata, which are located beneath the Pilliga Sandstone. Helium-4 concentrations for these formations range from 92 x 10^{-7} cc(STP)/g to 1044 x

10^{-7} cc(STP)/g. As shown in Figure 3-82, most of these sampling sites are located at the eastern boundary of the Narrabri Gas Project area where they are at shallower depths than within the central and western part of the Narrabri Gas Project area. The only exception to this was a sample collected from the Purlawaugh Formation at Plumb Road 2 in a location where the Purlawaugh Formation, the hydrostratigraphic formation directly underlying the Pilliga Sandstone in the Narrabri Gas Project area, is at more than 500 m below ground level (Figure 3-82).

For the Purlawaugh Formation, measurements from two groundwater bores at Dewhurst 14 and Plumb Road 2 (Figure 3-82) yielded values ranging from 28 x 10^{-7} cc(STP)/g (at Dewhurst 14) to 310 x 10^{-7} cc(STP)/g (at Plumb Road 2). At Plumb Road 2 (GW971632-2), samples were collected and analysed during two sampling campaigns in 2019 and 2023; the concentrations for groundwater samples from this observation bore range from 117x 10^{-7} cc(STP)/g to 310 x 10^{-7} cc(STP)/g. The large discrepancy between these values is likely due to the use of different pumps: for the collection of the samples with the lower concentrations, samples were collected using a pump placed at a relatively shallow depth in an open borehole with artesian flow where significant exsolution was observed (Suckow et al., 2019). In contrast, the sample with the higher ^{4}He measurement was collected during the current study using a low flow pump permanently installed in the borehole, with the borehole capped by bore headworks.

Within the formations of the Gunnedah Basin, which are below the Purlawaugh Formation, ^{4}He values range from 102 x 10^{-7} cc(STP)/g to 1044 x 10^{-7} cc(STP)/g, with a median of 177 x 10^{-7} cc(STP)/g. The highest value (1044 x 10^{-7} cc(STP)/g) was measured in a sample collected from the Hoskissons Coal seam, the secondary CSG target, at groundwater observation bore GW099043 south-east of the Narrabri Gas Project area (Figure 3-82). This value represents one of the highest ^{4}He concentrations measured within the Great Artesian Basin and adjacent or underlying basins in Australia to date, confirming the findings from ^{36}Cl that this groundwater sample is very old.

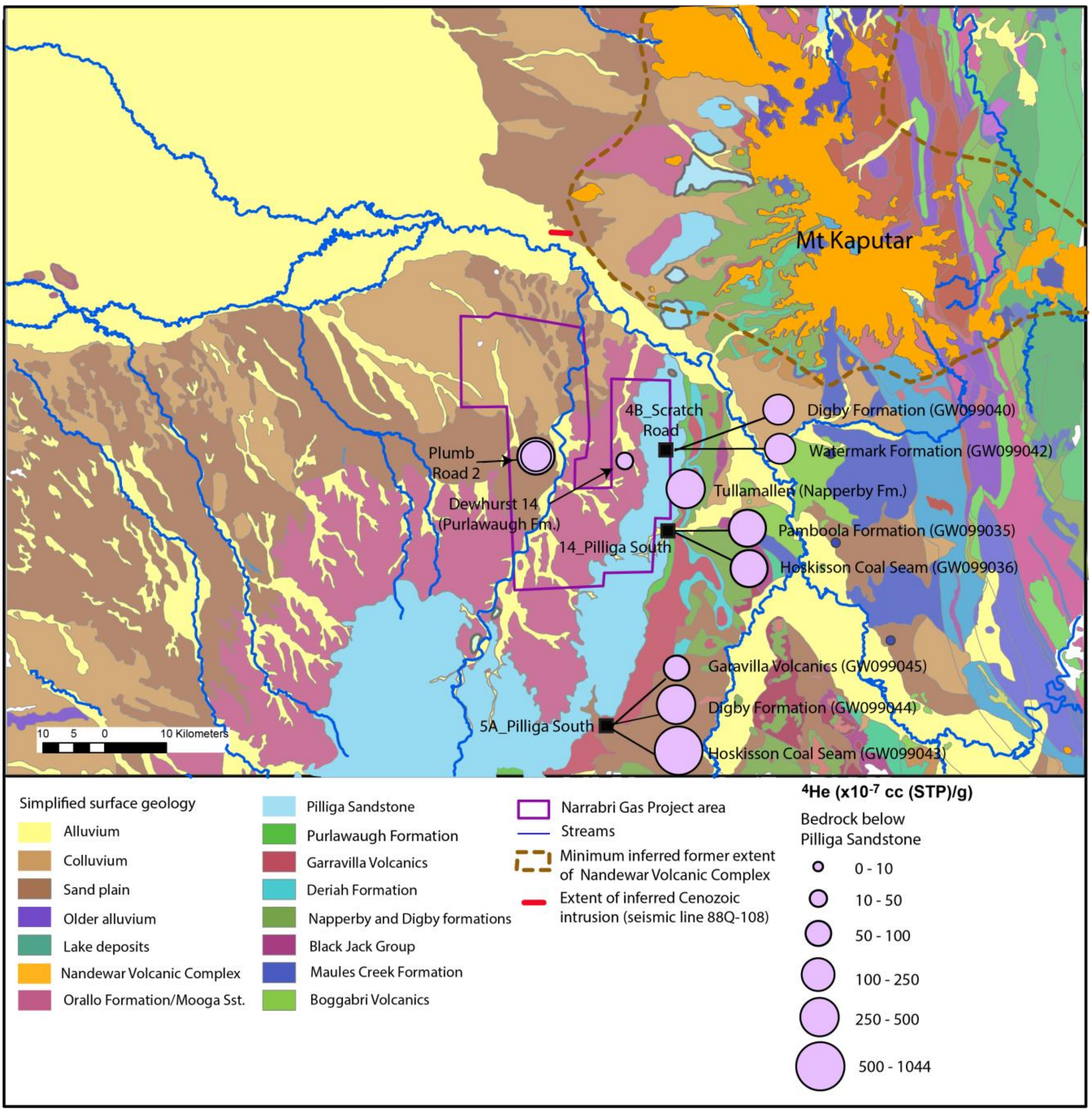

Figure 3-82 – Spatial distribution of ^{4}He in groundwaters below the Pilliga Sandstone (Gunnedah Basin strata and Purlawaugh Formation) in the Narrabri Gas Project area overlain on simplified surface geology.

Pilliga Sandstone and formations above in the Narrabri region

Groundwater helium concentrations (^{4}He) in the Pilliga Sandstone within the broader Coonamble Embayment ranged from the solubility equilibrium (4 x 10^{-7} cc(STP)/g) to multiple orders of magnitude above this value (Suckow et al., 2019; Raiber et al., 2022a). The lowest concentrations within the Pilliga Sandstone aquifer were recorded in groundwater samples collected from bores located within or close to the recharge area of the Pilliga Sandstone (e.g. GW0908011, Dewhurst 3-PS01 and Dewhurst 14-PS01 and PS02). High ^{4}He concentrations are generally observed in the west with a rapid increase along the flow path (Figure 3-83 and Figure 3-84). Some bores (e.g. a bore at the Nyora groundwater monitoring site screened in the Pilliga Sandstone) have very high ^{4}He concentrations despite being only approximately 40 km downgradient from the recharge beds along the inferred flow path (Figure 3-83). In contrast, along a southern inferred flow path originating from the Warrumbungle Volcanic Complex, lower ^4He concentrations are observed at distances located significantly further away from the Pilliga Sandstone recharge beds (e.g. GW040870; Figure 3-83).

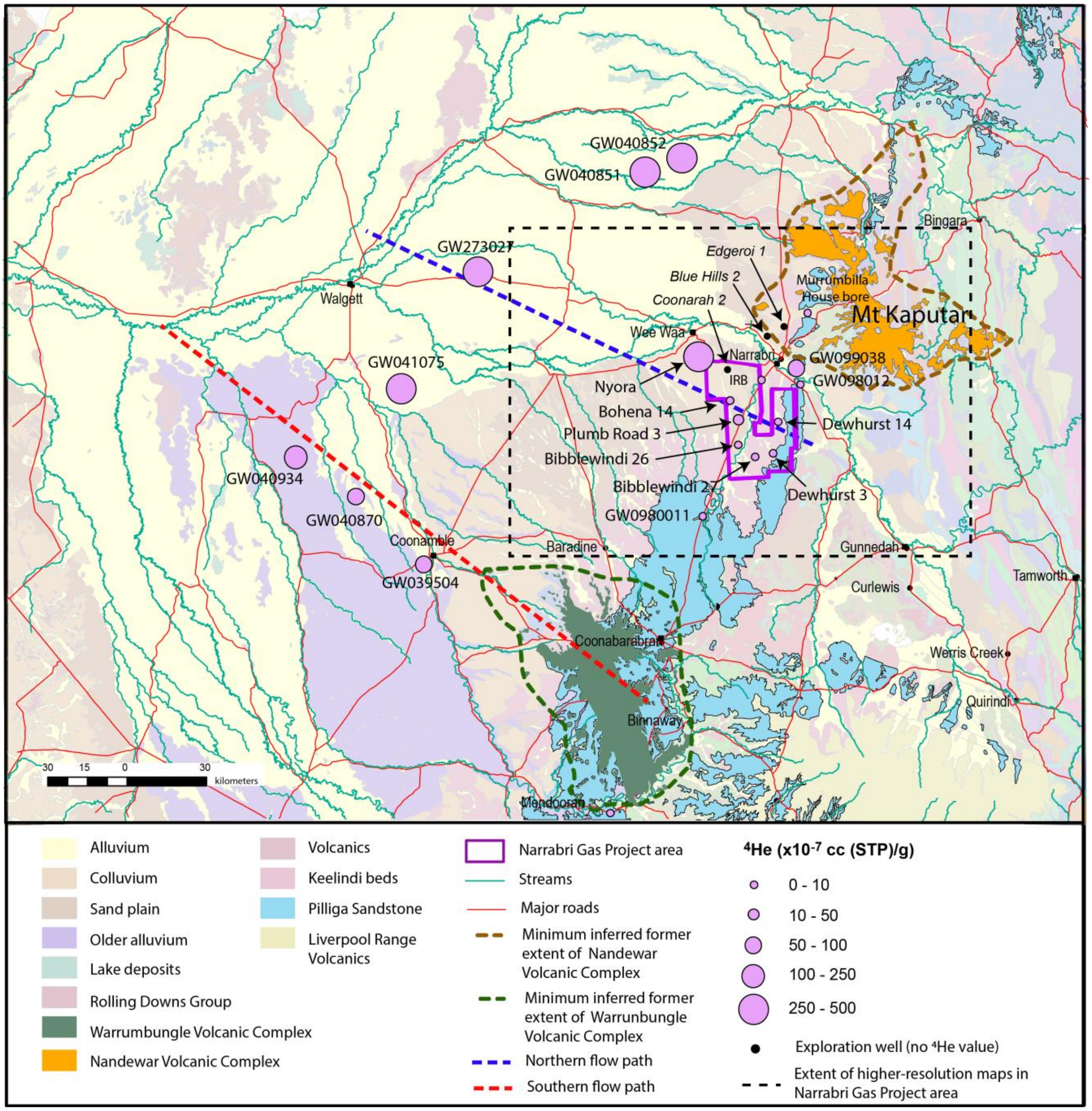

Figure 3-83 – Spatial distribution of ^4He in Pilliga Sandstone the wider Coonamble Embayment (a sub-basin of the Surat Basin) overlain on simplified surface geology.

Within the Narrabri Gas Project area, ^4He concentrations within the Pilliga Sandstone are mostly very low (typically less than 10 x 10^{-7} cc(STP)/g) and close to the atmospheric equilibrium, with no significant increase for example along an inferred flow path from DWH3 towards BWD 27-PS03 and BWD26 PS01 and PS02 (where ^4He remains at less than 10 x 10^{-7} cc(STP)/g; Figure 3-84). In contrast, a small increase of ^4He concentrations is observed in Pilliga Sandstone groundwaters between DWH14-PS01/PS02 (less than 10 x 10^{-7} cc(STP)/g) and Plumb Road 3 (ranging from 12 to 37 x 10^{-7} cc(STP)/g based on multiple measurements in 2019 and 2023) (Figure 3-85).

In addition to samples collected from the Pilliga Sandstone, Purlawaugh Formation and Gunnedah Basin formations, samples were also collected from the Orallo Formation at two nested bore sites and from a groundwater bore in the Bohena Creek alluvium (Inland Rail Bore/IRB). At the nested bore sites Nyora and BHN14 where individual bores are screened within the Pilliga Sandstone and Orallo Formation, the ^4He concentrations in the two formations are very similar. A very large increase of ^4He was observed from the eastern and central bores within the Narrabri Gas Project area towards Nyora PS01 (360 x 10^{-7} cc(STP)/g; screened within Orallo Formation) and Nyora PS02 (440 x 10^{-7} cc(STP)/g; screened within the Pilliga Sandstone). As shown in Section 3.3.1 and Section 3.8.3 (Figure 3-78), the AEM survey show that the Orallo Formation and Pilliga Sandstone are more conductive in the north-western part of the Narrabri Gas Project area (Figure 3-90), indicating a higher content of clay, siltstone or mudstone. Furthermore, they are overlain by more than 100 m of conductive cover, which likely acts as an aquitard.

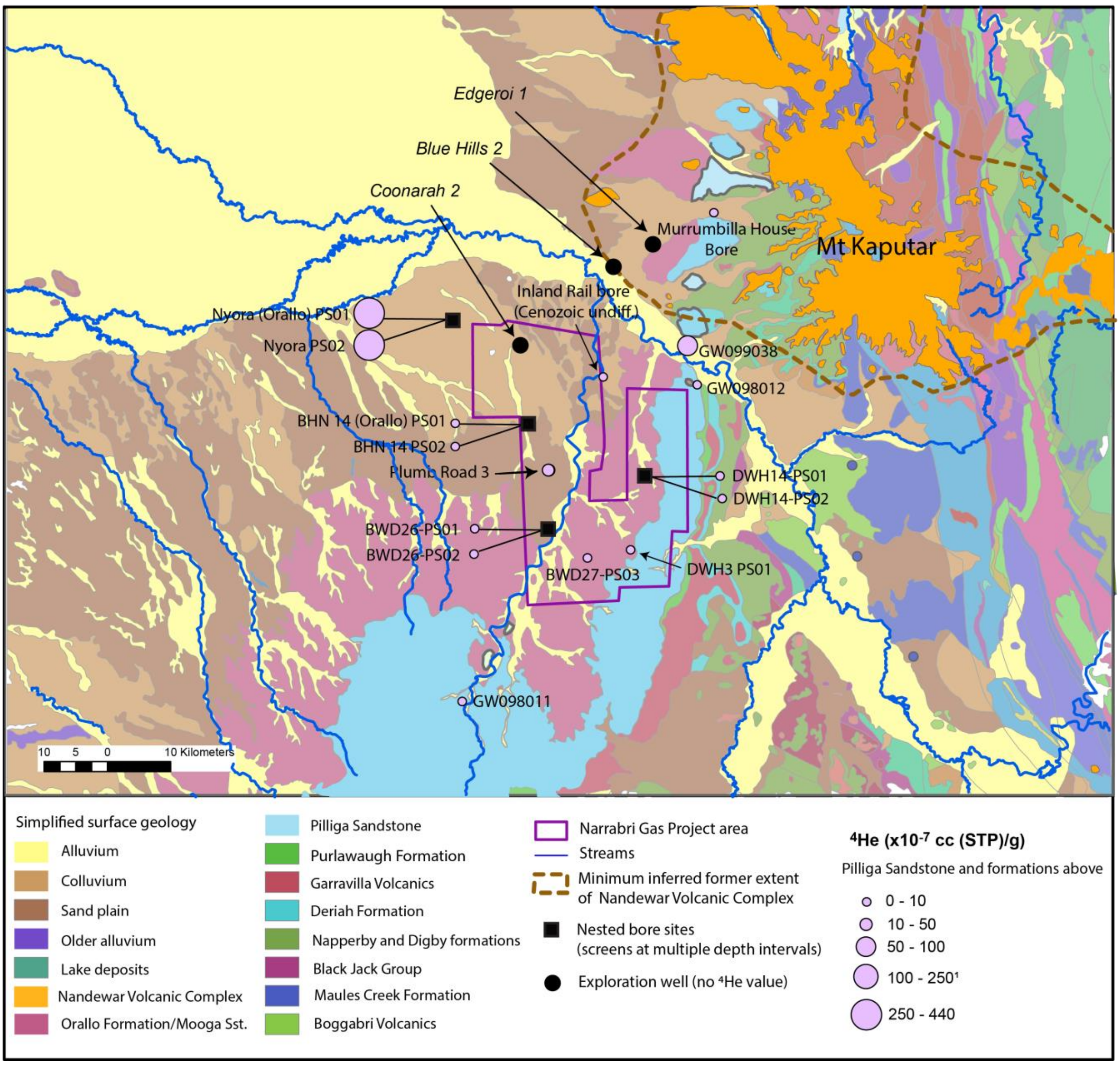

Figure 3-84 – Spatial distribution of ^{4}He in the Pilliga Sandstone, Orallo Formation and Bohena Creek alluvium (Inland Rail bore) in the Narrabri Gas Project area overlain on simplified surface geology. Selected exploration wells are shown for geological context.

Vertical variability of ^{4}He within the Narrabri Gas Project area

The comparison of the ^{4}He concentrations along a geological cross-section (Figure 3-85) shows that there is a very strong vertical contrast between the shallow formations (Pilliga Sandstone and Orallo Formation) and those in underlying formations (Purlawaugh Formation and Gunnedah Basin formations) in the Narrabri Gas Project area, with concentrations in the Pilliga Sandstone and Orallo Formation generally low (mostly below 10 x 10^{-7} cc(STP/g), with a median of 3.9 x 10^{-7}

cc(STP/g)) and concentrations in the Purlawaugh Formation and Gunnedah Basin formations generally high (all above 100 x 10^{-7} cc(STP/g), with a median of 177 x 10^{-7} cc(STP)/g)).

The east-west cross section and maps also highlight that there is a lack of ^{4}He data from formations below the Purlawaugh Formation in the centre, western and north-western part of the Narrabri Gas Project area. Unfortunately, a bore screened within the Digby Formation at Plumb Road NSW groundwater monitoring bore (GW971623-1 in Figure 3-85) could not be sampled during this study as the installed low-flow pump was not functional throughout the course of this project. Likewise, recently drilled Santos groundwater monitoring bores in the Napperby and Digby formations could not be sampled during this study. However, it is likely that ^{4}He concentrations in the central and western part of the Narrabri Gas Project area in the formations below the Purlawaugh Formations are also very high and probably considerably higher than those closer to the eastern outcrop and recharge beds as ^{4}He is generally expected to increase with flow direction and with the time the groundwater had to accumulate radiogenic helium.

This confirms findings from ^{14}C and ^{36}Cl that groundwaters in the Pilliga Sandstone and Orallo Formation within the Narrabri Gas Project area are generally young (except at Nyora) and groundwaters in the underlying formations are very old, making ^{4}He a very useful tracer to detect absence or presence of potential connectivity between deep and shallow groundwater systems. This will be discussed further in following sections.

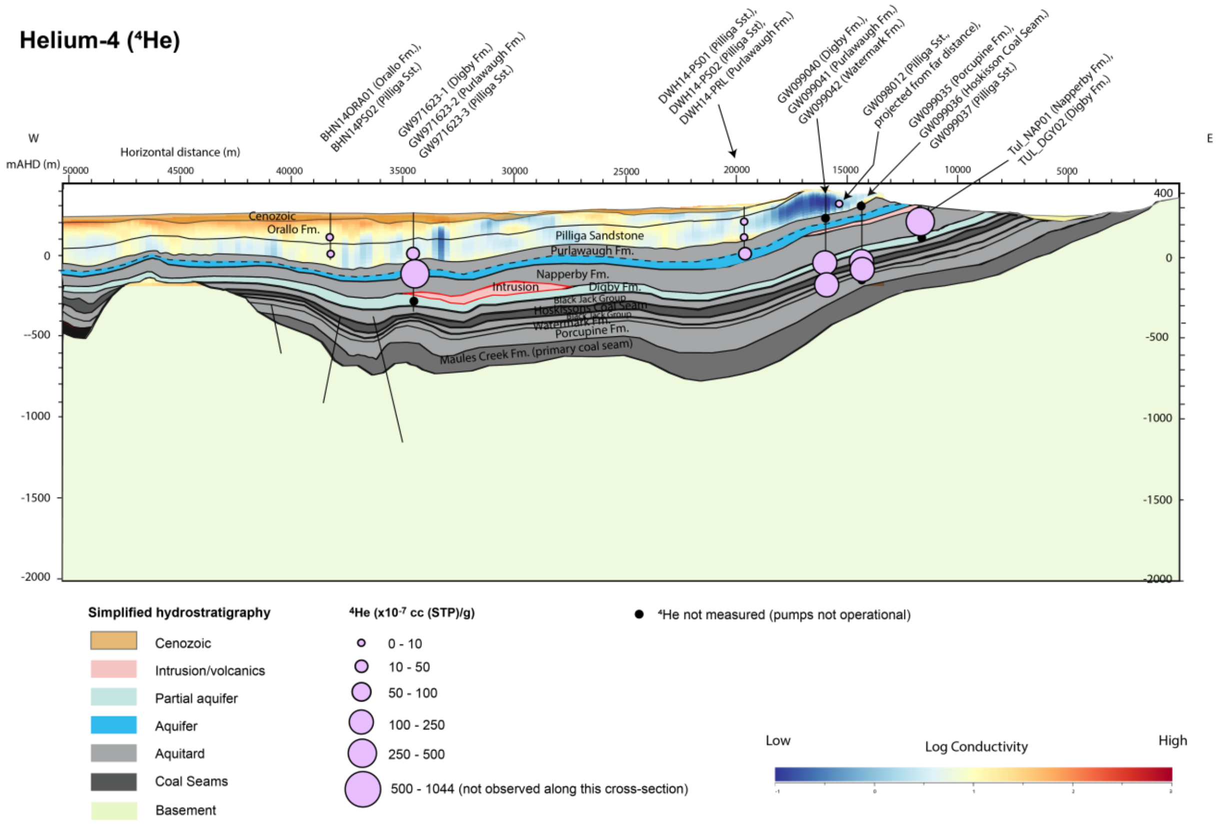

Figure 3-85 – ^{4}He distribution in bores along cross-section 1 (for orientation of this cross-section, see Figure 3-25).

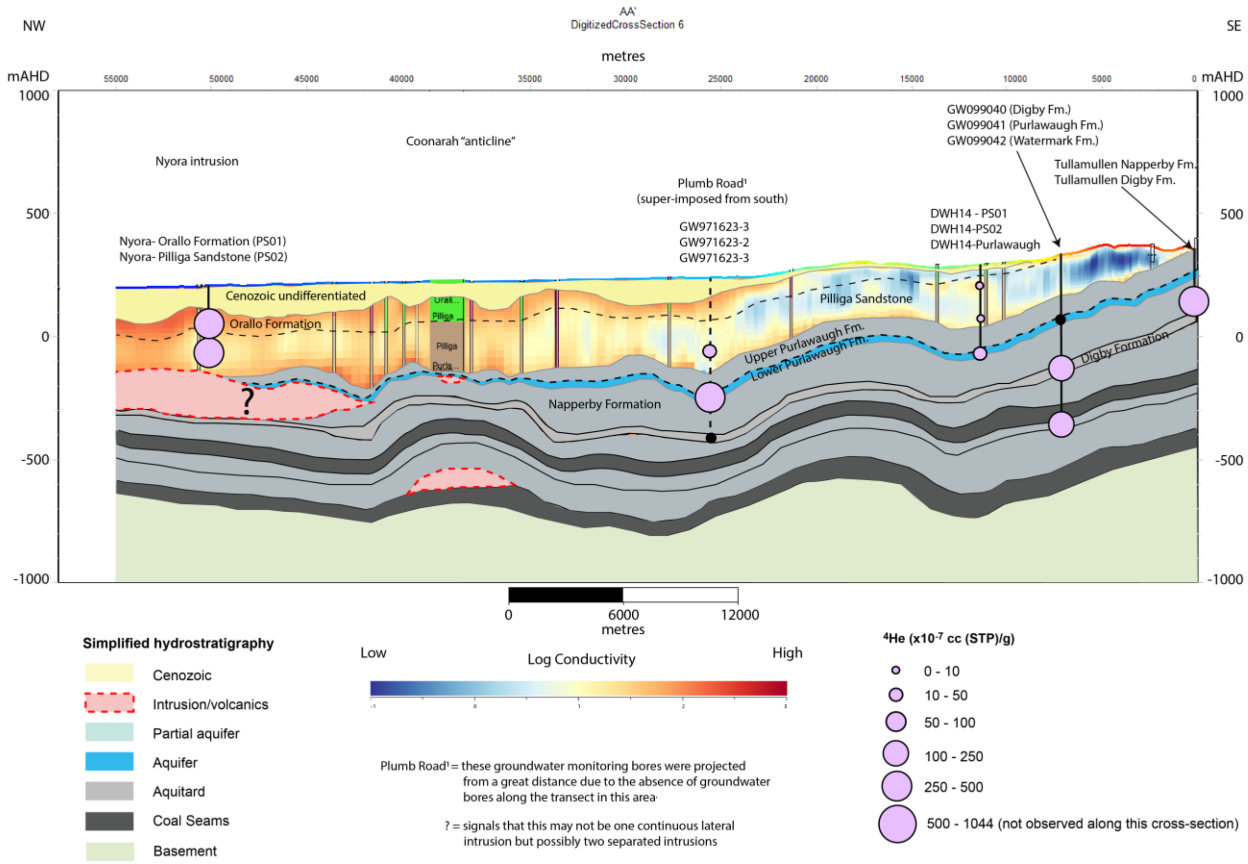

Figure 3-86 – ^{4}He distribution in bores along cross-section 2 (for orientation of this cross-section, see Figure 3-25).

3.8.5 ^{3}He/^{4}He versus Ne/He (mantle or "primordial" helium)

Mantle or "primordial" helium cannot be produced by radiogenic processes in rocks but is a remnant from when planet Earth formed from the solar cloud 4.5 billion years ago; it is stored in the Earth's deep interior (Jackson et al., 2017; Tyne et al., 2025).

In previous studies, Suckow et al. (2019) and Raiber et al. (2022a, b) demonstrated that there are groundwaters with significant amounts of mantle helium in the Coonamble Embayment, including in samples within the Narrabri Gas Project area. This included some of the highest estimates of mantle helium measured in groundwater samples throughout the Great Artesian Basin to date (Raiber et al., 2022b).

To identify different potential origins of helium, which supports the study on the provenance of groundwaters, measurements of the isotopic composition of helium from samples collected during the previous GISERA studies (Suckow et al., 2019 and Raiber et al., 2022) and new estimates from twelve groundwater samples collected during the current study are presented graphically by plotting the ^{3}He/^{4}He ratio versus the Ne/He ratio (Figure 3-87) and spatially on maps and cross-sections. In a previous study (Raiber et al., 2022a), mantle helium estimates could only be derived for one groundwater bore in the Gunnedah Basin strata (Napperby Formation). In the current study, mantle helium was estimated for an additional seven samples collected from Gunnedah Basin formations and an additional five bores from the Pilliga Sandstone and

Purlawaugh Formation, thus significantly improving the spatial coverage of baseline data in this multi-aquifer-aquitard system.

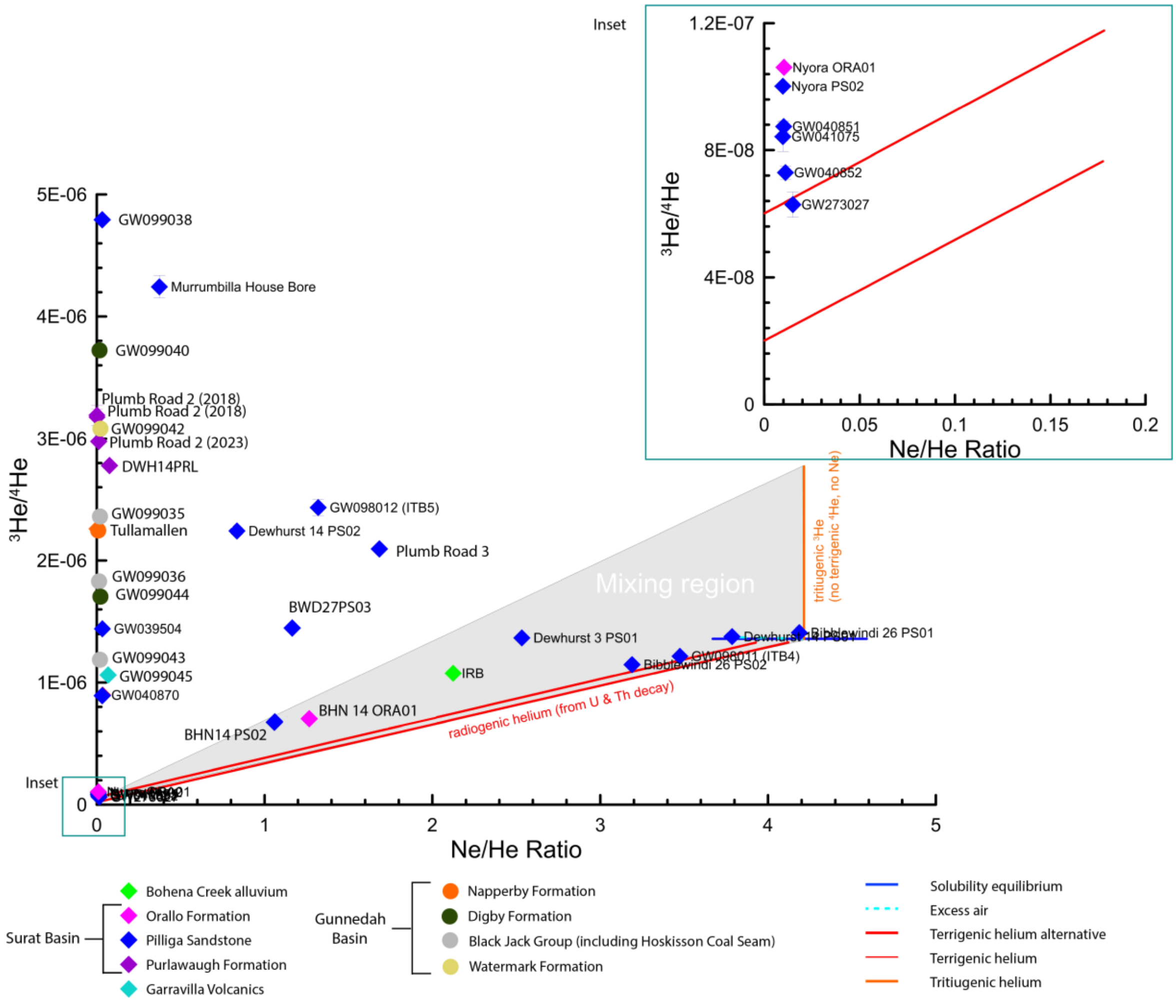

Figure 3-87 – Helium isotope ($^3He/^4He$) ratios versus the Ne/He elemental ratio in Surat Basin and Gunnedah Basin groundwaters and other selected samples.

The systematics of this plot (based on Suckow, 2013) are described in detail in Appendix 2 in Raiber et al. (2022 a). Terrigenic He is helium from mantle and crustal sources.

Mantle helium in formations below the Pilliga Sandstone in the Narrabri region

Mantle helium is discernible in Figure 3-87 by the higher $^3He/^4He$ isotope ratios above the grey shaded mixing region. These patterns cannot be explained by mixing with tritiogenic helium-3 (generated from the decay of tritium). The comparison of helium isotope ($^3He/^4He$) ratios versus the Ne/He elemental ratio shows that all groundwater samples collected from the Purlawaugh Formation and for multiple Gunnedah Basin formations have high primordial non-radiogenic $^3He/^4He$ ratios, suggesting that they contain significant mantle helium.

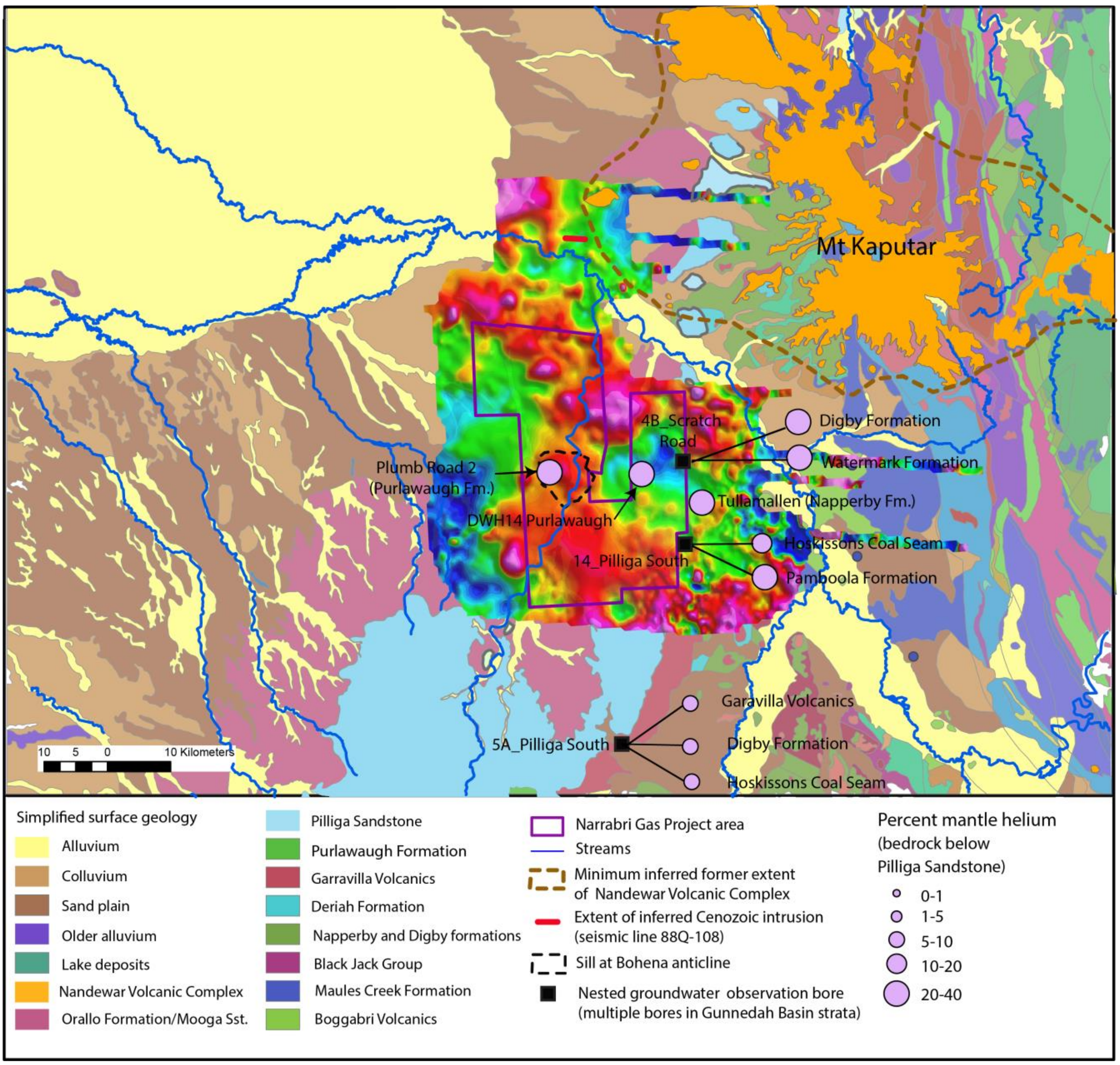

Figure 3-88 – Spatial distribution of estimated mantle (primordial) helium in the sedimentary bedrock below the Pilliga Sandstone in the wider Narrabri Gas Project area overlain on simplified surface geology and total magnetic intensity map.

The Total Magnetic Intensity map is also shown to highlight areas where magnetic anomalies suggest that igneous intrusions are likely to be present.

The estimated range of percentages of mantle helium for the Purlawaugh Formation and Gunnedah Basin strata is also shown spatially in Figure 3-88.

These elevated $^3He/^4He$ ratios can only be explained by the presence of ascending deep-mantle fluids, likely in the context of volcanic intrusions that have transported mantle helium with higher $^3He/^4He$ ratios than atmosphere to the aquifer during phases of igneous activity. As discussed in Section 3.4, intrusive activity occurred at multiple stages throughout the geological history of this area.

Raiber et al. (2022a) discussed key questions for the interpretation of these results:

- is there a need for a present-day (or very recent) helium connectivity down to the mantle to explain the observed values?
- is it also possible that a significant amount of helium was transported from the mantle into the intruded rock during the emplacement of the igneous intrusion into the surrounding sedimentary bedrock?
- could mantle helium associated with the emplacement of the igneous rocks (e.g. during the Cenozoic) be slowly released now from the intrusive rocks into the surrounding aquifer without an on-going replenishment from below?

This was also discussed by multiple authors in international studies. Luo et al. (2021) suggested that heat or partial (rock) melting preferentially releases ^3He stored in minerals and increase the $^3He/^4He$ ratios in the surrounding groundwater, although it is not clear if this is sufficient to create the observed signatures.

In the Karoo (sedimentary) Basin in South Africa, where dolerite intrusions into the sedimentary bedrock sequences have been identified, elevated $^3He/^4He$ were observed in sedimentary basin groundwaters (Eymold et al., 2018). As discussed by Eymold et al. (2018) and other authors for multiple international sedimentary basins (e.g. Ballentine and Sherwood Lollar, 2002, Darrah et al. 2015 and Moore et al., 2018), mantle-derived ^3He may be stored within sedimentary basins in structural or stratigraphic hydrocarbon traps for long periods of geological time after emplacement of igneous intrusions, and it can mix with or migrate into regions of locally produced fluids. However, similar to the questions above, Eymold et al. (2018) explained that it remains unclear if the mantle ^3He observed within the Karoo Basin is related to the dolerite intrusions or if it represents evidence for on-going fluid migration along preferential migration pathways.

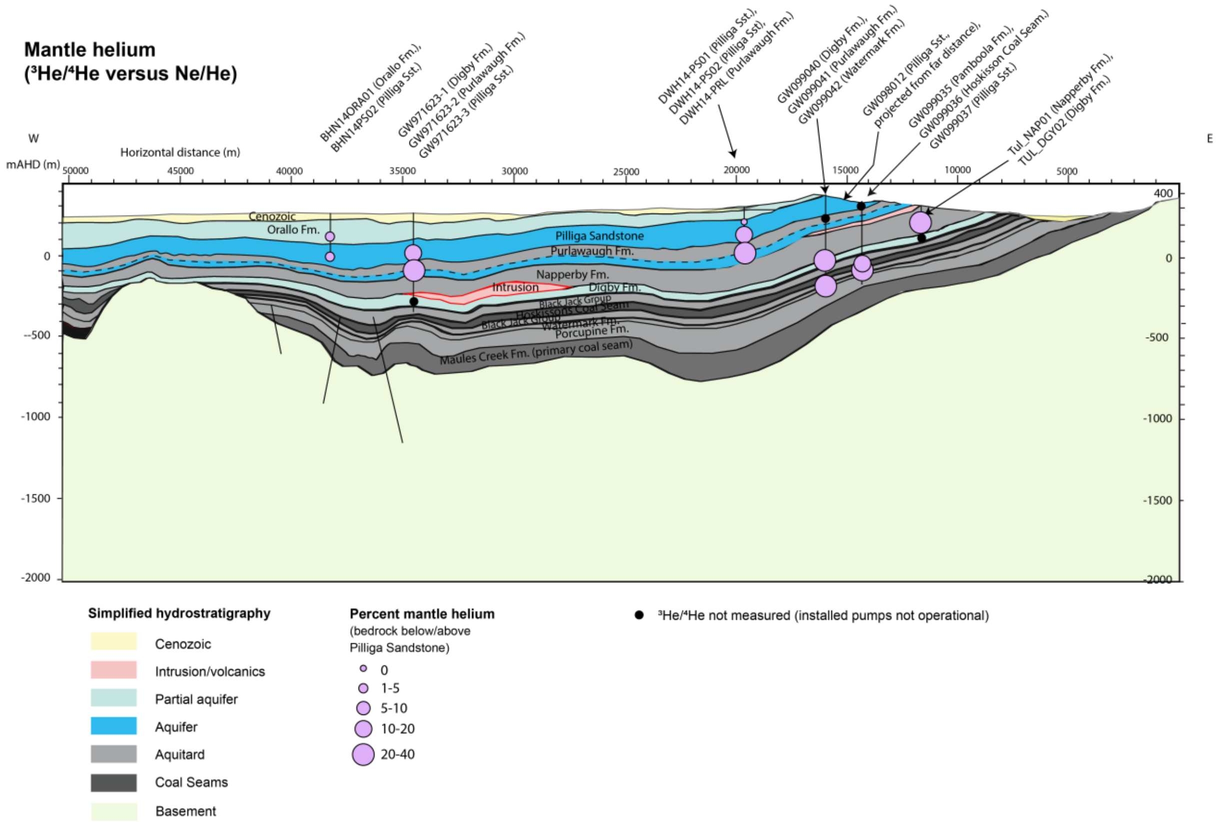

Figure 3-89 – Vertical distribution of mantle helium in bores along cross-section 1 (for orientation of this cross-section, see Figure 3-25).

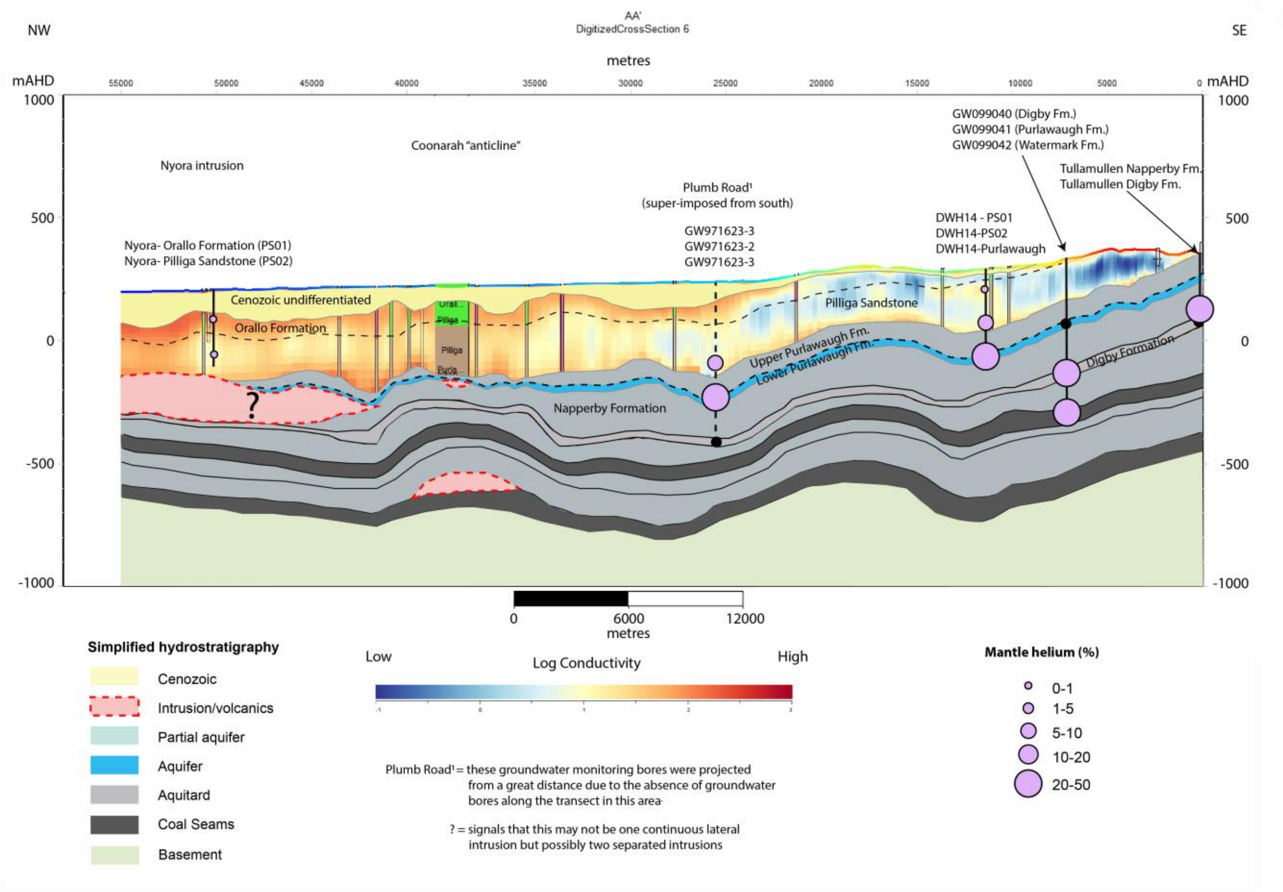

Figure 3-90 – Vertical distribution of mantle helium in groundwater and electromagnetic depth-conductivity structure for the Orallo Formation and Pilliga Sandstone along cross-section 2 (for orientation of this cross-section, see Figure 3-25).

To understand the significance of the measured $^3He/^4He$ values within the Narrabri Gas Project area, it is important to consider the spatial geological context and integrate $^3He/^4He$ versus Ne/He data with other lines of evidence. The spatial mapping of intrusions and the geochronological ages of intrusions provides valuable insights to support interpretation of the mantle helium estimations. As shown in Section 3.1.1, igneous intrusions composed of dolerites and other rock types are frequently observed in stratigraphic logs within the Gunnedah Basin strata within or near the Narrabri Gas Project area, where they were primarily recorded in the shallowest (youngest) Gunnedah Basin formations such as the Napperby Formation, the Digby Formation or at the contact between the Purlawaugh and Napperby formations. Intrusions are also visible as anomalies in total magnetic intensity maps (Figure 3-88; Section 3.5.1) including at or near some of the groundwater sampling sites. For example, at the Plumb Road groundwater monitoring site (observation bore GW971623-2 in Figure 3-88), a spatially extensive sill (a horizontal intrusion) dated in the current study as Early Jurassic is located at the interface between the Napperby and Digby formations (Section 3.1.1).

However, less than 5 km north of the Plumb Road groundwater observation bore at exploration well Bohena 2, a sill with a thickness of approximately 90 m appears to have completely replaced the Napperby Formation and forms the direct contact between the Digby and Purlawaugh formations (Figure 3-3). As this is likely the same intrusion dated at Bohena 1 using the K/Ar technique as Toarcian (the latest age of the Early Jurassic; Section 3.4), this intrusion occurred after the onset of the deposition of the lower part of the Purlawaugh Formation (which has commenced during the Pliensbachian, and earlier age of the Jurassic, according to the Geoscience Stratigraphic unit database; Geoscience Australia, 2025), suggesting that the Purlawaugh Formation strata may have been impacted by contact metamorphism during the emplacement of the sill (Section 1.3.3).

This suggests that the high mantle helium percentages estimated for the Purlawaugh Formation groundwater samples at Plumb Road are likely due to water-rock interaction with the spatially extensive sill at the base of the Purlawaugh Formation, although some contribution from the underlying Digby or Napperby formations may also occur (as discussed further in Section 4). Likewise, the high mantle helium percentages observed in Gunnedah Basin groundwater samples in the eastern part of the Narrabri Gas Project area are likely due to water-rock interactions within these formations.

Pilliga Sandstone and formations above in the Narrabri region

The spatial distribution of mantle helium in groundwaters within the Pilliga Sandstone, Orallo Formation and Bohena alluvium (Figure 3-87 and Figure 3-92) show that only three samples with primordial $^{3}He/^{4}He$ ratios are located within the Narrabri Gas Project area (Dewhurst 14-PS02, BWD27-PS03 and Plumb Road 3 (GW971623-3), the bore at Plumb Road NSW DPIE monitoring sites screened within the Pilliga Sandstone).

Within the Pilliga Sandstone and Orallo Formation within and near the Narrabri Gas Project area, some groundwater bores with primordial $^{3}He/^{4}He$ are located close to the areas where intrusions are expected. For example, the groundwater samples from the Murrumbilla House bore (likely screened partly in the colluvium and Pilliga Sandstone) and GW099038, located to the north-east of the Narrabri Gas Project area, have the highest $^{3}He/^{4}He$ ratio observed within the broader Narrabri Gas Project area and the highest estimates to date within Great Artesian Basin groundwaters. They are close to and downgradient of the Nandewar Range and within or near the area inferred as the original minimum extent of the Nandewar Volcanic Complex (Figure 3-92); they are also close to where Cenozoic dykes intrude into the Jurassic sedimentary rock sequences or where volcanic plugs associated with anticlines can be identified on seismic and TMI images (Section 3.5.1). Likewise, groundwater bore GW098012 is located relatively close to the inferred original minimum extent of the Nandewar Volcanic Complex and a positive relief magnetic feature (likely corresponding to a dyke or volcanic plug) is visible on the TMI map approximately 1 km south of the sampling site (Figure 3-92).

Groundwater monitoring bore Plumb Road 3 (GW971623-3 screened at the base of the Pilliga Sandstone; Figure 3-91) is located too far away from the Cenozoic Nandewar Volcanic Complex, and any influence of dykes associated with this Cenozoic volcanic complex can therefore be excluded. However, as discussed in Section 3.4, older igneous intrusions ranging in age from Late Triassic to Late Cretaceous, including a spatially extensive sill at the Bohena anticline dated as Early Jurassic in age, are present within the proposed Narrabri Gas Project area as well. As discussed in previous sections, the sill at Plumb Road likely intruded the rock sequences after the deposition of the lower part of the Purlawaugh Formation.

In contrast, some groundwater bores with primordial $^{3}He/^{4}He$ are in areas where no previously known igneous intrusive activity has occurred. For example, GW040870 is located more than 60 km away from any known intrusive activity (Warrumbungle Volcanic Complex). However, visual inspection of the TMI image for this area (inset map on Figure 3-91) shows presence of some magnetic anomalies, which suggests that there may be some plutons or volcanic plugs present. NSW DMR (1995) and Wolfgang (2000) also suggested that faults are likely to be present throughout the Coonamble Embayment. On the other hand, Sr isotopes of these groundwaters do not suggest any contribution from any more radiogenic igneous basement source (which would have significantly higher $^{87}Sr/^{86}Sr$). This indicates that if there is a pathway for ascending mantle helium at these sites, there is no groundwater flow associated with this pathway. Alternatively, admixture of mantle helium to the groundwater may have not occurred in situ at these sites but further upgradient (e.g. near the Warrumbungle Volcanic Complex, where dyke swarms have been reported by Bull et al. (2021)) (Section 3.1.1), and helium may have been transported with the groundwater to these locations, with some dilution occurring along the flow path.

This may also be the case at groundwater bore Dewhurst 14 (DWH14-PS02, the deeper bore screened within the Pilliga Sandstone at this site), where a mantle helium signature was measured (Figure 3-89). As explained in Raiber et al. (2022a), the visual inspection of seismic images (this bore is located close to multiple seismic legacy lines and the TMI grid (Figure 2-5) showed no evidence for the presence of intrusions or linear structural features in this area, with the closest noticeable intrusion (a possible igneous plug) inferred from the TMI grid located approximately 6 km north-east of this site. Furthermore, other hydrochemical indicators in DWH14-PS02 (e.g. electrical conductivity of ~160 µS/cm, pH of 5.46 and the absence of methane with no methane peaks detected during analysis) suggest that there is no groundwater flow connection at this site with the underlying Gunnedah Basin. This is because due to the very high electrical conductivities (and high concentrations of most major ions) and high methane concentrations of Gunnedah Basin groundwater, even a very small admixture (e.g. 0.3%) from Gunnedah Basin formations to the Pilliga Sandstone would result in significantly higher electrical conductivities, major ion and methane concentrations than those observed at DWH14-PS02. Furthermore, at the same site, the shallower bore (DWH14-PS01, also screened within the Pilliga Sandstone) shows no mantle-derived He contribution.

A possible pathway that could explain the mantle-derived helium measured at this site discussed by Raiber et al. (2022a) is mixing between the Pilliga Sandstone, Purlawaugh Formation and Garrawilla Volcanics (which are present in the north-eastern part of the Narrabri Gas Project area, as discussed in Section 3.1.1) upgradient (further east located closer to the basin margin). As shown in Figure 3-87, the Purlawaugh Formation at this groundwater monitoring site (DWH14-Purlawaugh) contains significant mantle helium. However, the Purlawaugh Formation groundwater sample at the same site contains approximately 6500 µg/L of methane. The absence of methane in the Pilliga Sandstone and relatively high concentrations of methane in the Purlawaugh Formation suggests that mixing between these formations could not likely explain the observed patterns for stable noble gases and other hydrochemical parameters. This suggest that although no intrusions into the Pilliga Sandstone have been identified in stratigraphic logs within the Narrabri Gas Project area, there may be some small and localised intrusions in the eastern part of this area where some geochronological (K-Ar) analyses suggest that there are some Cretaceous igneous intrusions here (Section 3.4). Although these rock samples were collected from deeper stratigraphic intervals below the Pilliga Sandstone, other Cretaceous intrusions may have intersected the Pilliga Sandstone. However, as explained above, the freshness of Pilliga Sandstone groundwater at DWH14-PS02 and the absence of methane suggests that there is unlikely to be any present-day groundwater flow connection with deeper formations.

The complexity of explaining the observed hydrochemical patterns highlights the need for the use of independent lines of evidence (e.g. geology, hydrogeology, geophysics, hydrochemistry and environmental tracers) when interpreting spatial hydrogeological processes to avoid misconceptions. Furthermore, it shows that even where a contribution from primordial helium is identified based on groundwater noble gas measurements, a potential connectivity pathway associated with igneous intrusions may not be necessarily located at or near the sampling site.

Most other groundwater samples within the Pilliga Sandstone and Orallo Formation within the Narrabri Gas Project area show little or no mantle helium contribution. As illustrated in Figure 3-87 (inset), some samples with very high radiogenic helium concentrations (low Ne/He ratio) may have slightly elevated $^{3}He/^{4}He$ ratios compared to pure radiogenic helium ($1\text{-}5x10^{-8}$, along the red lines in Figure 3-87). This is evident, for example, at bores at the Nyora groundwater monitoring site (screened in the Orallo Formation and Pilliga Sandstone). It indicates that there may be a very small addition of deep-mantle helium (likely less than 1% of the He) and that most of the helium is radiogenic (produced from U and Th decay in the Earth’s crust). As highlighted in Figure 3-78, at the Nyora site, the well completion report of Nyora 1 suggests that the Purlawaugh Formation is absent and that the Pilliga Sandstone directly overlies ~200 m of intrusive Jurassic igneous rocks (intruded prior to the deposition of the Pilliga Sandstone), which are also visible in the TMI image as a magnetic anomaly (Figure 2-5). This indicates that there is a plausible pathway to explain a very minor deep-mantle contribution.

Based on the assumption that the Pilliga Sandstone is a homogeneous porous quartzose sandstone and that this groundwater monitoring bore is located relatively close to the recharge beds of the Pilliga Sandstone, Raiber et al. (2022a) suggested that the measured high helium concentrations are therefore more likely to be due to mixing with older groundwater (e.g. the Purlawaugh Formation, which thins and pinches out at this area and which has recorded a primordial $^{3}He/^{4}He$ ratio at Plumb Road 2) from underlying formations rather than a result of in situ production (i.e. radiogenic) within the Pilliga Sandstone. However, as discussed in previous sections, the new mineralogical and AEM data collected during the current study suggest that the Pilliga Sandstone outside the recharge beds is more heterogeneous than previously assumed (with high clay mineral and feldspar content) and likely connected to the Orallo Formation, suggesting that the observed high helium concentrations at Nyora may indeed be the result of in situ production within the Pilliga Sandstone. This is illustrated in Figure 3-78 where the AEM confirms a gradual, but significant lateral facies change from a quartzose sandstone (represented by blue colours on the conductivity scale) at the eastern recharge beds to a clay- and feldspar-rich sandstone (represented by red colours in the western part of the cross-section) down-gradient at Nyora.

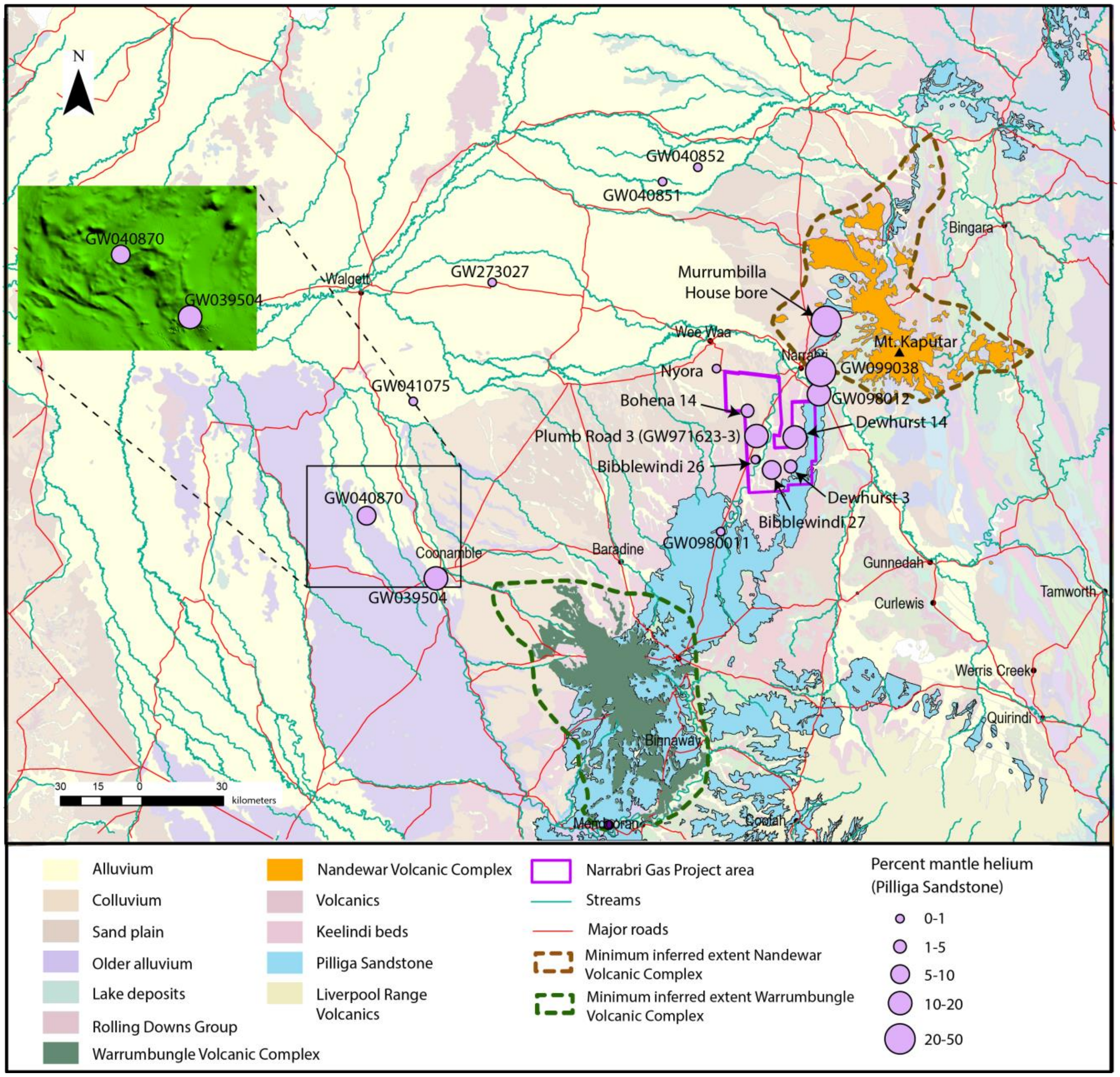

Figure 3-91 – Spatial distribution of $^3He/^4He$ ratios in the Pilliga Sandstone within the Coonamble Embayment area overlain on simplified surface geology.

The green inset map shows the Geoscience Australia total magnetic intensity (TMI) map for the area near GW039504 and GW04870 (Poudjom Djomani, 2019). The 'primordial' vs 'radiogenic' attribution does not correspond directly to the measured $^3He/^4He$ ratio, but rather to the ^3He excess as shown in Fig. 67.

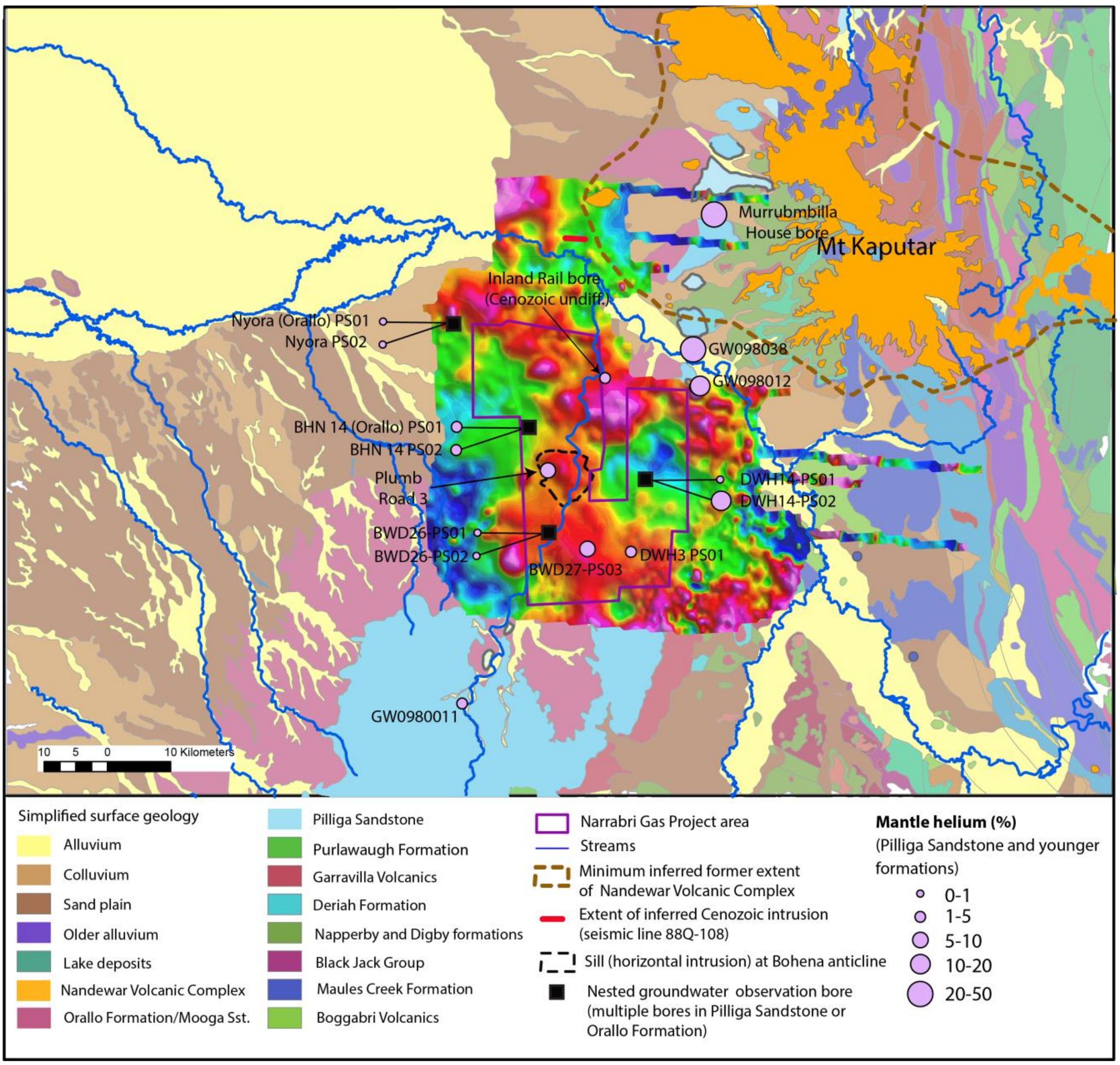

Figure 3-92 – Spatial distribution of estimated mantle (primordial) helium in the Pilliga Sandstone, Orallo Formation and alluvium (Inland Rail bore) in the wider Narrabri Gas Project area overlain on simplified surface geology and total magnetic intensity map.

The Total Magnetic Intensity map is also shown to highlight areas where magnetic anomalies suggest that igneous intrusions are likely to occur.

3.8.6 Argon-40 (^{40}Ar)

Argon-40 is the decay product of the naturally occurring ^{40}K (half-life 1.251×10^9 years). The two rare argon isotopes, ^{36}Ar and ^{38}Ar, are stable and have no radiogenic source and their ratio therefore can be used as a control signal for isotopic enrichment that might occur either during measurement (due to mass fractionation) or because of degassing during sampling (Severinghaus, 2021). The argon isotopes ^{40}Ar, ^{38}Ar and ^{36}Ar can be analysed with the new high-resolution mass spectrometer Helix MC at CSIRO since 2020 with high precision.

Formations below the Pilliga Sandstone in the Narrabri region

In a previous study by Raiber et al. (2022a), only three samples with ^{40}Ar measurements from two wells (from Tullamullen, the bore screened within the Napperby Formation and Plumb Road 2 (971623-2), where two samples were collected at different times from this Purlawaugh Formation bore on subsequent days) in formations below the Pilliga Sandstone were available.

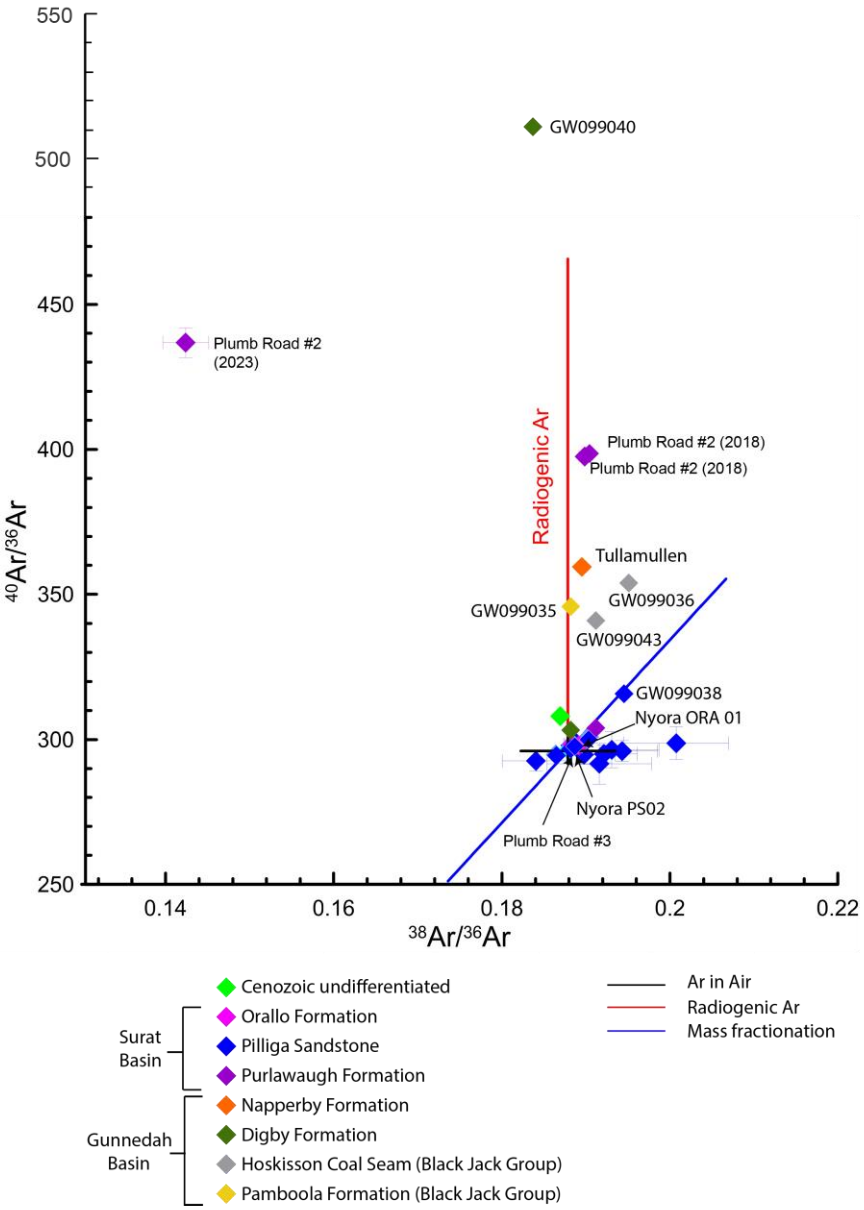

Figure 3-93 – Three-isotope plot of argon (based on data from Suckow et al., 2019, Raiber et al., 2022a and the current study).

In the current study, an additional six samples from the formations underneath the Pilliga Sandstone (Purlawaugh Formation, Garrawilla Volcanics and Gunnedah Basin formations) were collected and analysed for ^{40}Ar. Of all samples from these formations, only the sample from the Garrawilla Volcanics (GW099045) and the Purlawaugh Formation at DWH14 followed the mass fractionation line (Figure 3-93). In contrast, all other samples collected from these formations during the current study deviated vertically from the atmospheric $^{40}Ar/^{36}Ar$ ratio fractionation line.

This is demonstrated in Figure 3-93, where the blue line shows the isotopic enrichment expected from mass fractionation (e.g. due to degassing of a sample during the sampling or the measurement). Argon-40 is present only in the ratio on the y axis and therefore any radiogenic enrichment of ^{40}Ar results in a vertical upward deviation from the fractionation line.

None of the deviating samples follow the mass fractionation line, indicating that the deviation from the atmospheric $^{40}Ar/^{36}Ar$ ratio is due to an increase of ^{40}Ar from accumulation of radiogenic production in groundwater rather than due to degassing. Although some of the samples with elevated ^{40}Ar show significant degassing (inferred from lowered absolute concentrations of all noble gases, but particularly neon), this influences the radiogenic signature only to a minor extent and the radiogenic ^{40}Ar component is significant.

The values measured for ^{40}Ar measured for the Purlawaugh Formation at Plumb Road and some of the samples collected from the Gunnedah Basin formations are the highest values observed to date (to our knowledge) in groundwater samples in Australia. For example, the radiogenic Argon signatures at Plumb Road 2 (GW971623-2, screened within the Purlawaugh Formation) and samples collected from the Gunnedah Basin strata are higher than those observed in previous studies in Great Artesian Basin groundwaters, with the highest previous value being 326 in Torgersen et al. (1989). However, it is important to note that all of these deeper formations except for the Purlawaugh Formation in the current study are not part of the Great Artesian Basin and are collected mostly from strata with lower permeabilities than those within the Great Artesian Basin.

To explain higher than expected radiogenic ^{40}Ar signatures, an external flux of ^{40}Ar into the formations was discussed in Torgersen et al. (1989), while a selective release of argon due to mineral weathering processes in the formation was described in Arditto (1983) and Seltzer et al. (2021). As suggested by Raiber et al. (2022a), an enrichment of radiogenic ^{40}Ar as observed within groundwater samples collected from the Purlawaugh Formation and Gunnedah Basin formations would be visible only on timescales of several hundred thousand to millions of years (Torgersen and Stute, 2013). The two red model lines in Figure 3-94 B correspond to different radiogenic production rates of helium and assume that all ^{40}Ar produced from ^{40}K is released (rock density= 2.7g/cc, porosity=0.1, K concentration=100 mg/g and calculated using eq. 9.3 in Suckow (2013) and eq. 8.19 in Torgersen and Stute (2013). Several 100 ky are needed to produce the observed $^{40}Ar/^{36}Ar$ ratios under these assumptions. This agrees with the values of ^{4}He and ^{36}Cl measured for these groundwater samples (sections 3.8.3 and 3.8.4).

Furthermore, it is likely that the igneous intrusions (sill) at Plumb Road 2 groundwater monitoring bore (GW971623-2) and other sills and dykes within and near the Narrabri Gas Project area discussed in previous sections (e.g. Section 3.1.1) released sedimentary argon with the heat they implanted into the formation during the emplacement of the intrusions (as discussed in Section 1.3.3). If the ^{40}Ar originates from the magmatic intrusions observed at the base of the Purlawaugh Formation and within the Gunnedah Basin strata (Section 3.1.1), there should be a correlation with the $^{3}He/^{4}He$ ratio (since magmatic intrusions originate from the mantle, they exhibit a primordial helium isotopic signature). Such a correlation between the $^{3}He/^{4}He$ ratio and the $^{40}Ar/^{36}Ar$ ratio is indeed observed (Figure 3-94 A), as all samples with a higher $^{40}Ar/^{36}Ar$ ratios also all have elevated $^{3}He/^{4}He$. On the other hand, not all samples with elevated $^{3}He/^{4}He$ have higher $^{40}Ar/^{36}Ar$ ratios (e.g. DWH14 Purlawaugh).

Pilliga Sandstone and formations above in the Narrabri region

In addition to the samples collected from the formations underneath the Pilliga Sandstone, we have also collected and analysed three additional samples from the Pilliga Sandstone for ^{40}Ar in the present study, thus further enhancing the baseline data set within the Narrabri Gas Project area.

Unlike for the samples from the Purlawaugh Formation and Gunnedah Basin formations, only one groundwater sample (GW099038) collected from the Pilliga Sandstone (which forms part of the Great Artesian Basin) and Orallo Formation within the Narrabri Gas Project area during previous and the current studies showed any significant increase of ^{40}Ar, with all other samples having a radiogenic Argon signature within a similar range as those presented by Torgersen et al. (1989). At groundwater sampling site GW099038 (screened within the Pilliga Sandstone), a minor enrichment of radiogenic ^{40}Ar is observed; this site is located north-east and outside of the Narrabri Gas Project area near the Nandewar Volcanic Centre, where dyke swarms associated with the Cenozoic volcanic eruption are likely to be present. This groundwater sample is also the groundwater sample with the highest mantle helium observed in the Narrabri Gas Project area and has the highest methane concentration of all Pilliga Sandstone groundwater samples.

Although a relationship of ^{40}Ar with long residence times was suggested by other authors, the patterns observed for the Pilliga Sandstone suggest that a long residence time is not the only factor. In groundwater bores screened in the Orallo Formation and Pilliga Sandstone at Nyora (sections 3.8.3 and 3.8.4), long residence times were indicated by ^{4}He and ^{36}Cl, but no elevated ^{40}Ar signatures are observed at these sites. As described in Section 3.8.5 and shown in Figure 3-94A, there is no or no significant mantle helium in groundwaters at these sites. The absence of significant mantle helium at Nyora despite the presence of a thick and spatially extensive intrusion directly underneath the Pilliga Sandstone is likely because the intrusion occurred prior to the deposition of the Pilliga Sandstone during the Early Jurassic, and there has therefore not been any impact of contact-metamorphism during emplacement of the intrusion on the Pilliga Sandstone. The findings indicate that rather than resulting purely from very long residence times, elevated ^{40}Ar in the Narrabri Gas Project area are generally associated with igneous intrusions. This could also be part of the mantle signature, although the low ^{40}Ar despite high mantle helium at DWH14 Purlawaugh suggests that this may not be the case.

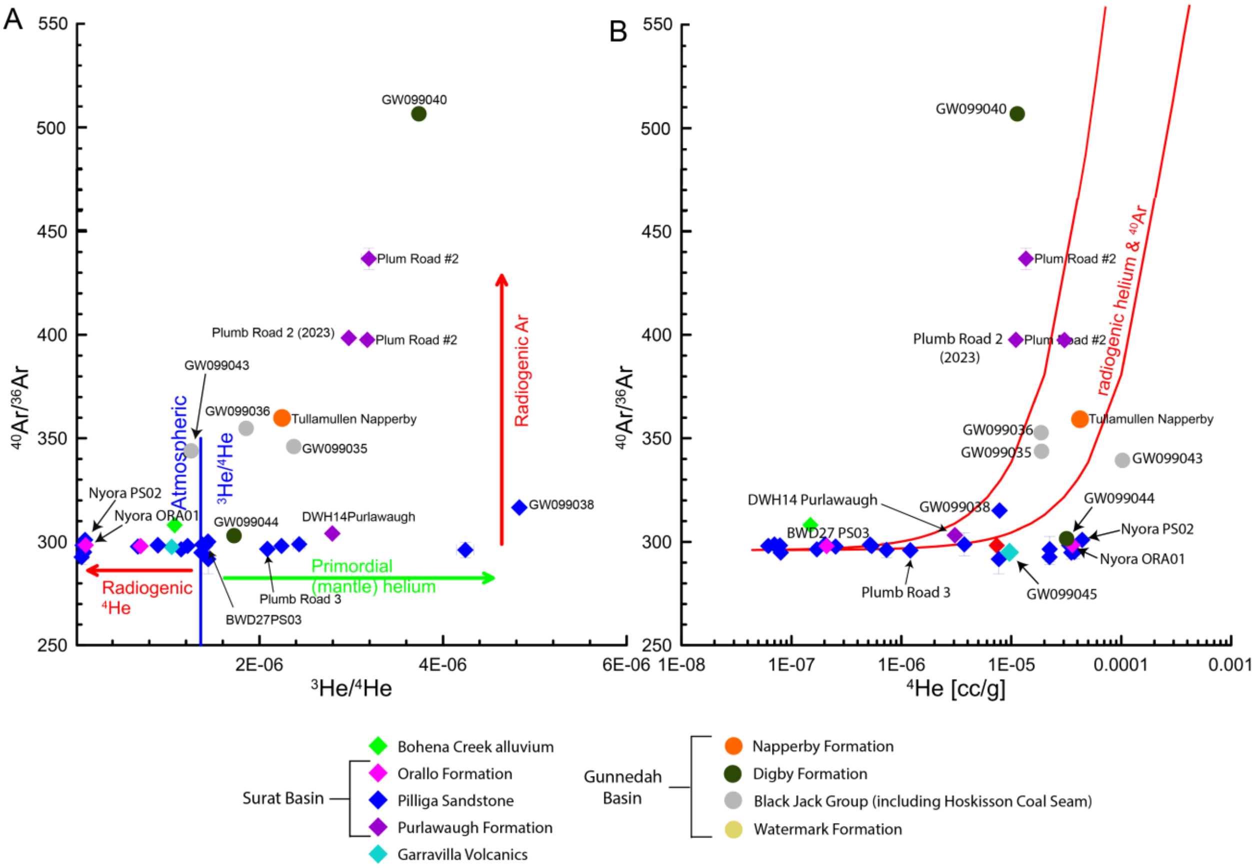

Figure 3-94 – A) $^{3}He/^{4}He$ versus $^{40}Ar/^{36}Ar$; and B) $^{40}Ar/^{36}Ar$ versus helium concentration.

3.8.7 Krypton-81 (^{81}Kr) and Krypton-85 (^{85}Kr)

In a previous GISERA study in the Narrabri region, samples were collected for analysis of radioactive noble gas isotopes ^{85}Kr and ^{81}Kr from groundwater bores screened within the Pilliga Sandstone and Purlawaugh Formation at the Plumb Road nested groundwater monitoring site (GW971623-2 and GW971623-3) and from other Pilliga Sandstone groundwater bores within the Coonamble Embayment (Suckow et al., 2019).

At groundwater bore GW971623-2 (Plumb Road 2) screened within the sand and gravels at the base of the Purlawaugh Formation, high artesian pressure with discharge (if uncapped) of approximately 12,000 L/hour and a value of 14% $^{81}Kr_{mod}$ of the radio-krypton noble gas isotope (krypton-81 has a half-life of about 229,000 years) were observed, corresponding to an apparent ^{81}Kr-based groundwater age of around 650 ky (1 ky = 1000 years). However, the value for $^{36}Cl/Cl$ for the same groundwater bore is the lowest values measured in this study and one of the lowest values measured within groundwaters of the Great Artesian Basin (e.g. Figure 3-95; Raiber et al., 2022b). The comparison of $^{36}Cl/Cl$ with ^{81}Kr shows that the value of ^{81}Kr is higher than expected compared to the value of $^{36}Cl/Cl$ based on the trend observed for other samples collected as part of the same study (Suckow et al., 2019). This indicates that either the value for $^{36}Cl/Cl$ may be too low or the value for ^{81}Kr too high or that significant mixing occurs. Krypton-81 is commonly considered as a more robust tracer than $^{36}Cl/Cl$ due to its inertness and constant input function

(Purtschert et al., 2023). This is shown in Figure 3-95 where the value of ^{36}Cl of young groundwater samples collected throughout different parts of the Great Artesian Basin is highly variable, whereas ^{81}Kr is relatively constant (close to 100% $^{81}Kr_{mod}$) across different sub-basins and geographic regions. However, during the sampling of groundwater bore GW971623-2, a significant degree of exsolution was observed (Figure 2-30). Noble gases isotopes such as ^{81}Kr are likely to be affected more significantly by atmospheric contamination than ^{36}Cl. At this site, a higher-than-expected value of ^{85}Kr (0.4 dpm/cc Kr; krypton-85 has a half-life of approximately 10.76 years) and at the same time a very low value of ^{3}H (<0.06 TU, indicating that no modern groundwater is present) suggest that ^{81}Kr may be influenced by a small degree of atmospheric contamination during sampling.

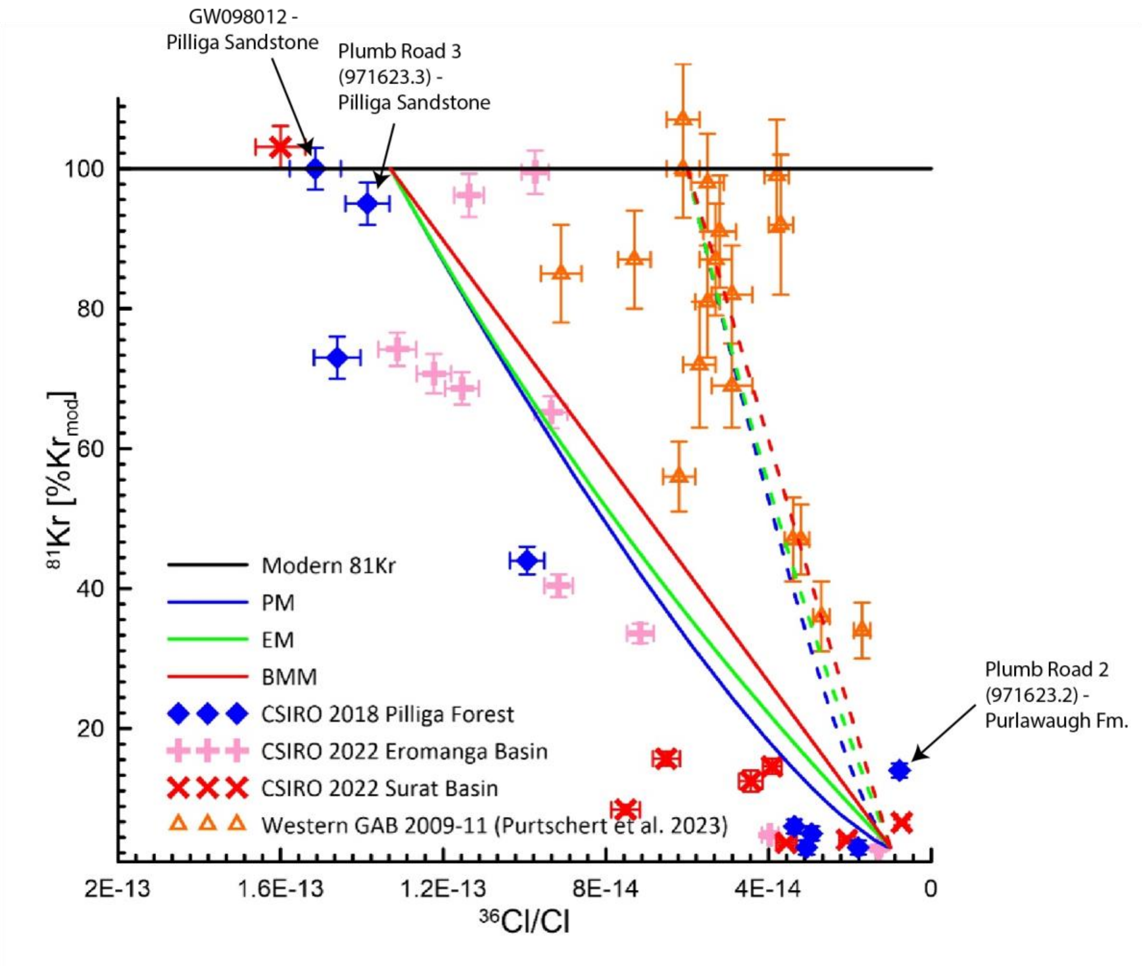

Figure 3-95 – Comparison of ^{36}Cl and ^{81}Kr in Great Artesian Basin groundwaters.

Data set "CSIRO 2018 Pilliga Forest" represents groundwater samples from the Pilliga Sandstone and Purlawaugh Formation in the broader Coonamble Embayment. Samples within or near the Narrabri Gas Project area are labelled.

Unlike for ^{81}Kr, the value of ^{36}Cl can be affected by biological and geochemical reactions. However, the XRD mineralogical analyses of the Purlawaugh Formation and over- and underlying formations confirmed that halite is absent in all samples except in one sample from the Black Jack Group which contained 0.2% of halite. The likely absence of any influence of halite dissolution is also supported by the assessment of groundwater Cl/Br ratios. This suggests that there is unlikely to be any fossil ^{36}Cl from halite dissolution which could affect the value of ^{36}Cl.

Considering that the Purlawaugh Formation aquifer is only approximately 10 m thick at Plumb Road and over- and underlain by thick sequences of claystone or other low-permeability strata (Figure 3-3), it is possible that ^{36}Cl is influenced by diffusion, leading to a lower ^{36}Cl value. However, regardless of the uncertainty on the absolute value of the apparent groundwater age, both ^{81}Kr and ^{36}Cl independently confirm that this groundwater is very old.

3.8.8 Determining representative groundwater ages

Determining an apparent groundwater age from environmental tracer values is subject to significant uncertainties, as groundwater sampled at a given location is a mixture of waters that have been transported via various flow paths (Suckow, 2014; Turnadge and Smerdon, 2014). The procedure of determining a representative groundwater age has been described in Section 2.5.3, and the patterns and spatial distribution of environmental tracer data were discussed in Section 3.8. Previous sections highlighted that when interpreting 'dating' tracers, all available geoscientific information need to be considered to avoid misinterpretations. Uncertainties exist and multiple age estimates are possible for individual groundwater samples depending on the selection of input parameters such as the $^{36}Cl/Cl$ values of recharge water and the use of different ^{14}C correction models. However, the use of multiple complementary tracers and lines of evidence ensures the relative robustness of the apparent groundwater age estimates. In the current study, the estimation of an apparent groundwater age involved consideration of interpretations from a very wide range of environmental age tracers including most tracers shown in Figure 2-31.

Regardless of the chosen input parameters and correction models, there are consistent patterns that can be observed:

- All groundwaters in the Pilliga Sandstone and Orallo Formation along transect CS1 are young (<20,000 years); this also applies to other Pilliga Sandstone groundwater samples within the Narrabri Gas Project area that are not represented in the cross-sections, except for groundwater at Nyora.
- Groundwaters ages in the Purlawaugh Formation are variable: groundwater samples collected at Plumb Road 2 (GW971623-2) are very old whereas an upstream sample collected at DWH14 is very young. The increase of groundwater age in the Purlawaugh Formation from DWH14 to GW971623-2 may not only be influenced by "natural ageing" through radioactive decay along the flow path but may also be affected by other processes. This could include for example diffusion into stagnant zones of the Purlawaugh Formation or underlying Napperby Formation, or a small degree of upwards discharge of fossil $^{36}Cl/Cl$ from the uppermost Gunnedah Basin formations, as discussed later in this report.
- All groundwaters in Gunnedah Basin strata along the transect (and at locations not represented on the transect) are very old. These samples are all collected from groundwater bores located within or close to the recharge area of the respective formations. Although no measurements are currently available from downgradient parts of

these aquifers, it is assumed that groundwater there will also be very old and likely close to, or outside, the maximum age range represented by $^{36}Cl/Cl$ and ^{81}Kr.

Table 9 Apparent groundwater age estimates based on ^{14}C and ^{36}Cl and complemented by evidence from ^{3}H, $^{3}He/^{4}He$, ^{4}He, ^{40}Ar, ^{81}Kr and ^{85}Kr used as history matching constraints for the groundwater flow and solute transport model. See Figure 3-96 for the locations of the bores on the cross-section.

BHN14ORA	12000	Orallo Formation	Low ^{3}H, low ^{4}He, moderate ^{14}C and high ^{36}Cl
BHN14PS02	Pending (waiting for lab result)	Pilliga Sandstone	Low ^{3}H, low ^{4}He, moderate ^{14}C and high ^{36}Cl
GW971623-1	N/A	Digby Formation	No tracer sample was collected due to faulty installed pump
GW971623-2	1,300,000 to 1,400,000 (multiple measurements)	Purlawaugh Formation	^{3}H below limit of quantification, very high ^{4}He, no ^{14}C, low ^{81}Kr, measurable ^{85}Kr, lowest ^{36}Cl measured in this study; ^{81}Kr value may be too high due to minor atmospheric contamination during sampling or the sample represents a mixture, or 36Cl is influenced by diffusion.
GW971623-3	20000	Pilliga Sandstone	Absence of ^{3}H, low ^{4}He, moderate ^{14}C, and high ^{36}Cl
DWH14-PS01	10000	Pilliga Sandstone	Low ^{3}H, low ^{4}He, moderate ^{14}C and high ^{36}Cl
DWH14-PS02	10000	Pilliga Sandstone	Low ^{3}H, low ^{4}He, moderate ^{14}C and high ^{36}Cl
DWH14-PRL	3000	Purlawaugh Formation	Low ^{3}H, low ^{4}He, high ^{14}C and high ^{36}Cl
GW099040	530000	Digby Formation	Very high ^{4}He, very low ^{14}C and very low ^{36}Cl
GW099041	N/A	Purlawaugh Formation	No tracer sample was collected due to faulty installed pump
GW099042	900000	Watermark Formation	Very high ^{4}He, very low ^{14}C and very low ^{36}Cl
GW098012	3500	Pilliga Sandstone	Very low ^{3}H, modern ^{81}Kr (100% $^{81}Kr_{mod}$), high ^{14}C, high ^{36}Cl
GW099035	Pending (waiting for lab result)	Porcupine Formation	
GW099036	700000	Hoskissons Coal seam	Very high ^{4}He, very low ^{14}C and very low ^{36}Cl
GW099037	N/A	Pilliga Sandstone	No sample was collected due to faulty installed pump
TUL_NAP01	600000	Napperby Formation	Very high ^{4}He, very low ^{14}C and very low ^{36}Cl
TUL_DGY02	730000	Digby Formation	Very low ^{36}Cl, very gas-rich groundwater, ^{3}H and ^{14}C may be affected by leakage.

3.9 Numerical modelling of groundwater flow and age patterns

3.9.1 Model calibration (history matching)

Starting with an initial parameter distribution that was populated with previously reported hydraulic conductivity, porosity (Table 2) and rainfall recharge estimates, sequential flow and solute transport simulations were undertaken to minimise the residuals between observed and measured hydraulic heads and groundwater age estimates. This process was mostly undertaken manually through a trial-and-error approach and partially supported by PEST.

After model calibration, simulated hydraulic heads and groundwater age patterns agree reasonably well in many parts of the model domain. However, at several wells in the eastern part of the investigated transect between 0 and 15,000 m, relatively large discrepancies persisted for hydraulic heads. Some of the discrepancies appear to suggest that measured values were biased by the presence of large fractions of gas or influenced by unresolved geological complexity in the Gunnedah Basin at the eastern part of the section (as discussed in Section 3.6).

3.9.2 Simulated groundwater flow and age

Groundwater flow in the investigated transect is induced by rainfall recharge as the only hydraulic driver. Most of the rainfall recharge in the model occurs at selected outcrop areas, with the highest rates assumed for the Orallo Formation and Pilliga Sandstone based on the recharge assessment by Crosbie et el. (2022). The distinctly higher hydraulic conductivities of these two formations (Table 2) imply that flow rates are accordingly higher without the generation of significant head gradients, while at the same time the groundwater remains relatively young, compared to all deeper sections of the investigated transect. The simulated head and age patterns reflect the corresponding field observations well, except for monitoring borehole BHN14 at the downgradient end, which is, however, not directly located on the simulated transect.

Below the Pilliga Sandstone, the upper section of the Purlawaugh Formation acts as an effective seal that causes significant head drops of >30 m over short vertical distances. This section of the Purlawaugh Formation acts as major groundwater barrier over the entire transect due to the dominance of claystone in the upper part of the Purlawaugh Formation. This is for example illustrated at Plumb Road (GW971623), where both the simulated and measured hydraulic head measurements in the Pilliga Sandstone (GW971623-3) are approximately 30 m lower than the head measured at the same nested bores site in the underlying Purlawaugh Formation (GW971623-2).

In contrast to the upper part of the Purlawaugh Formation, the lower section of the Purlawaugh Formation appears to have a significantly higher hydraulic conductivity, therefore acting as an effective lateral flow path from the Purlawaugh Formation outcrop area towards the west. Head and age observations below the Purlawaugh Formation are sparse, and therefore the simulated distribution of groundwater fluxes remains more uncertain. A key and non-intuitive result, however, is that groundwater flow and discharge in the deepest sections occur in the model towards the east. This simulated flow pattern allows to mimic the observed age distribution well, while the observed heads are deviating significantly at some locations, as discussed in the previous sections.

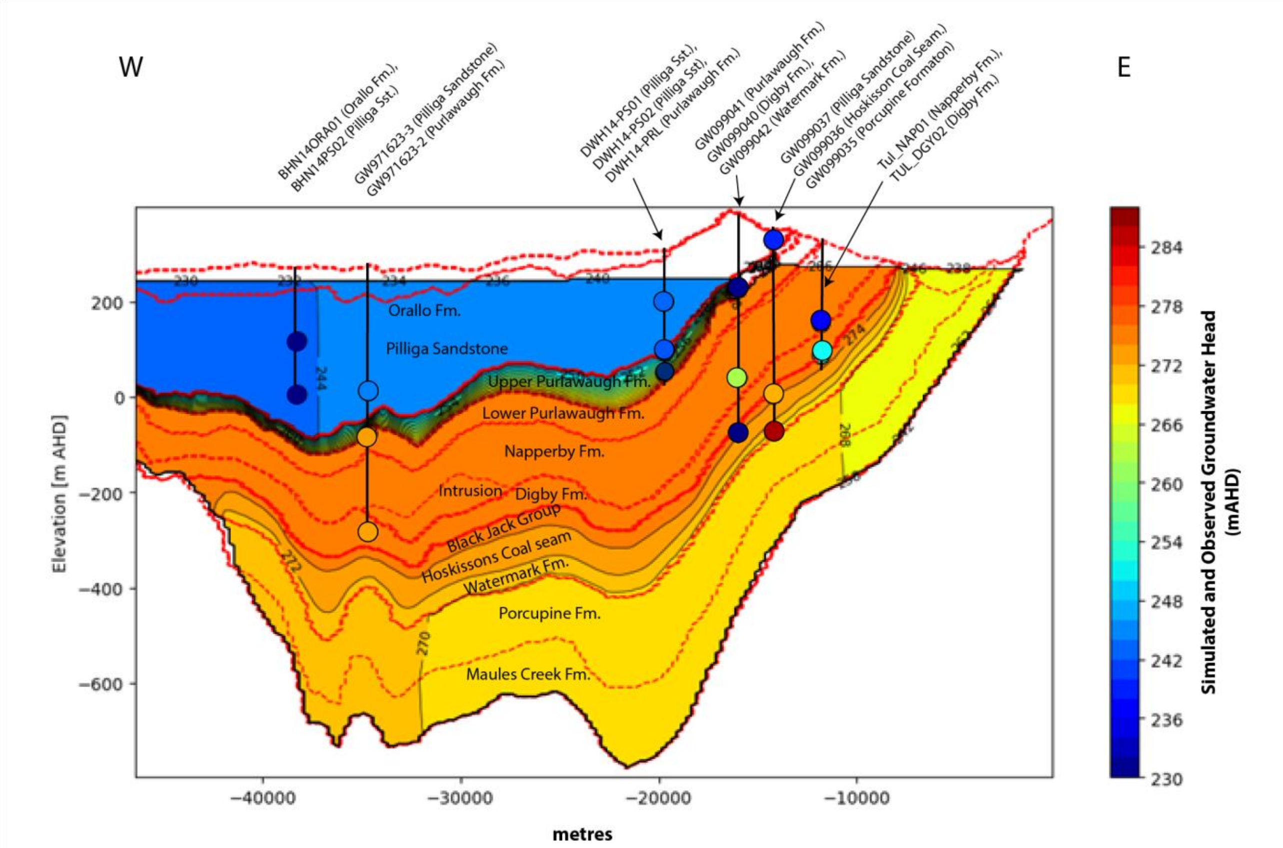

Figure 3-96 – Simulated and observed hydraulic heads in the investigated transect. Circles indicate observed heads at monitoring locations. The primary target coal seams are hosted within the Maules Creek Formation.

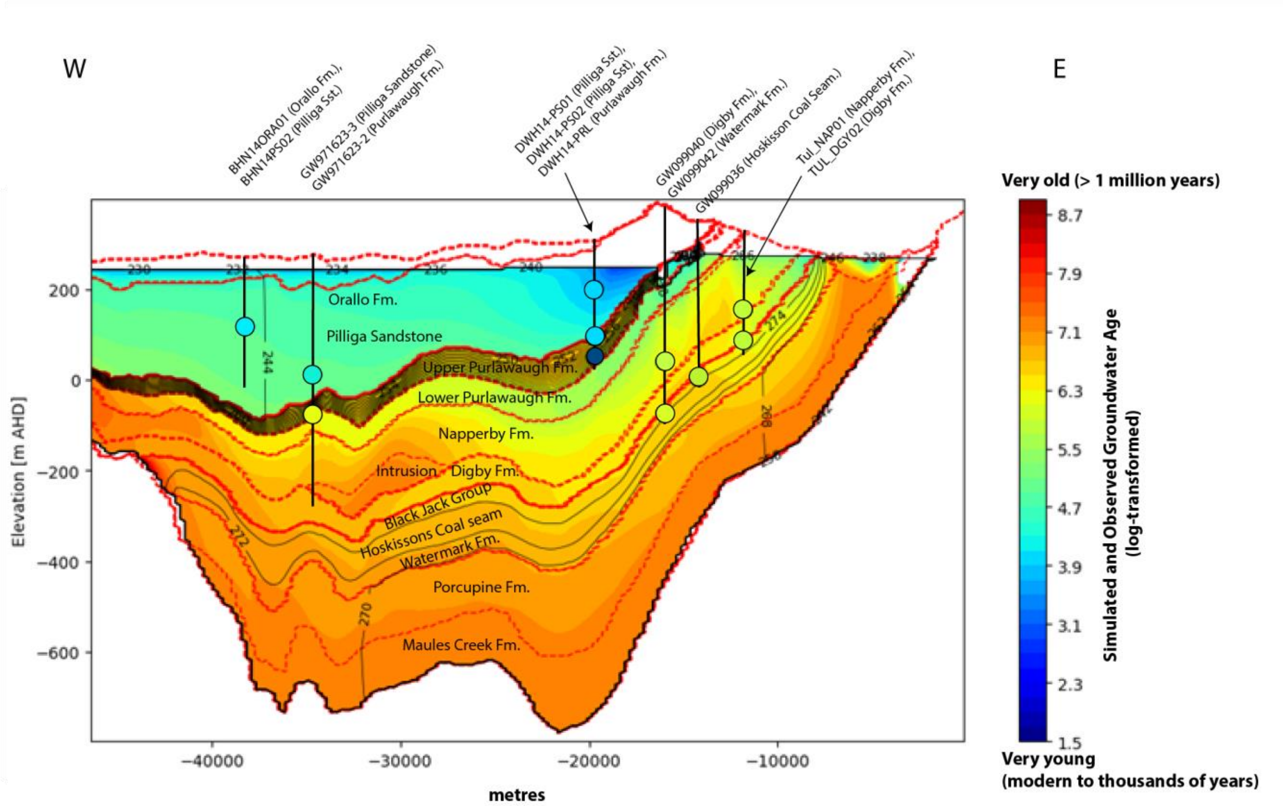

Figure 3-97 – Simulated and observed groundwater ages in the investigated transect. Circles indicate observed age estimates at monitoring locations. The primary target coal seams are hosted within the Maules Creek Formation.

3.9.3 Uncertainties and limitations

As illustrated in the previous section, a considerable difference between simulated and observed hydraulic heads has been identified in the eastern part of the investigated transect, whereas simulated and observed groundwater ages matched closely.

Some of the major uncertainties that could explain the persisting discrepancies for hydraulic heads are:

- Climate change and recharge variability across the long time periods represented by groundwater ages may affect hydraulic heads in some formations.
- While most considered groundwater bores are directly located on the transect (e.g., bores at Plumb Road and DWH14), data form some groundwater bores were superimposed from distances of several km away from the cross-section line, especially in the eastern part of the transect. Although the topographic relief is relatively minor within the extended Narrabri Gas Project area, there is some topographic relief in the south-east and east which may contribute to the discrepancy observed between simulated and observed heads where groundwater bores were superimposed on the cross-section from greater distances.
- As indicated in Section 3.6, the eastern part of transect 1 could only be constrained by a limited amount of reliable stratigraphic and seismic data. The uncertainty of the layer geometry here is therefore high, whereas it is considered low in the centre of the cross-section due to the availability of many high-quality stratigraphic logs, seismic data and AEM and less structural deformation (apart from the intrusion which is intersected by multiple wells). The AEM survey indicates that there is likely a high degree of structural deformation in the east, suggesting that multiple alternative geological realisations are possible.
- Some groundwater samples have high gas concentrations (both CO_2 and CH_4), which can significantly impact the accuracy of head measurements. For example, at groundwater bore GW099042 and at Tullamullen (within bores screened both within Napperby and Digby formations), very high concentrations of CO_2 and smaller concentrations of CH_4 were observed during sampling (with more than 100,000 µg of CO_2 measured at GW099042). Dual phase flow has not been considered by the numerical models developed in this study.
- Some groundwater samples in the eastern part of the transect have elevated salinities (up to approximately 19,000 µS/cm); density effects on head measurements have not been considered in this study. However, this alone cannot explain the observed discrepancies.
- More complex patterns of lithological heterogeneity than what is represented in the numerical models: as shown in some AEM lines and 3D visualisations and lithological descriptions in sections, there is considerably more internal heterogeneity within some formations than what is represented by the transect model.
- The proximity to the Narrabri Coal Mine in the eastern part of the transect could imply that some measurements along the simulated transect were affected by mine dewatering activities.

- Uncertainty on groundwater age estimates based on ^{14}C and ^{36}Cl: there are considerable uncertainties in estimating an apparent groundwater age, as discussed in Section 3.8.8. However, these uncertainties are unlikely to materially influence the interpretations of the direct age models or alter the overall conclusions, as the contrast between apparent groundwater ages in the Pilliga Sandstone compared to underlying formations is generally large regardless of input function of ^{36}Cl and correction models of ^{14}C. Efforts to use tracer concentration rather than apparent groundwater ages as calibration targets are currently underway in a joint effort with parallel project "Groundwater modelling and predictive analysis to inform CSG impact assessment, monitoring and management" and will be reported at a later stage.
- Uncertainties in aquifer attributions: although confidence in aquifer attributions for most groundwater bores along the transect is high, there are some ambiguities due to inconsistencies between well completion reports and screened aquifer assignments in the Water NSW database for some groundwater bores in the east.

3.10 Inverse geochemical modelling

3.10.1 Geochemical background of groundwater and aquifers at geological cross-sections

Hydrochemical changes observed within the Pilliga Sandstone in selected bores along geological cross-section CS2 (NW to SE oriented) are shown in Figure 3-98. Selected analytical results performed on groundwater samples from three boreholes (i.e. upstream at DWH14-PS02, mid-gradient at GW971623-3 (Plumb Road-3) and downgradient at NYO-PS02) are displayed in Figure 3-98. A colour gradient overlaying the table indicates solute concentrations, ranging from elevated (red) to lower (blue) value, highlighting zones of varying geochemical influences. Concentrations including the main parameters such as pH, electrical conductivity (EC), total dissolved solids (TDS), concentrations of major ions (e.g. alkalinity, chloride and calcium) and selected trace elements (barium, strontium, boron, fluoride and bromide) display the lowest values close to the eastern aquifer outcrop areas, with an increase of concentrations observed as the groundwater flows into the deepest part of the aquifer.

Several molar ratios (expressed in meq/L) are also included in the table to support the interpretation of ion concentrations and to help identify geochemical processes such as mineral dissolution, ion exchange, or mixing.

As previously observed in Figure 3-36, the Pilliga Sandstone aquifer near the outcrop beds has a higher content of quartz minerals, whereas in the deeper zones of the aquifer, alteration products such as siderite (Mg/Ca), minerals of the illite/mica group, K-feldspar, kaolinite, plagioclase, dolomite and calcite are commonly found.

Parameters such as pH tend to increase along the flow path, which agrees with the infiltration of acidic rainfall in the recharge beds of the aquifer; along the flow path, groundwater becomes progressively buffered through water-rock interactions. The variation in salinity within the aquifer, as indicated by changes in electrical conductivity (EC) and total dissolved solids (TDS), reflects water-rock interactions, residence time, and possibly differences in mixing with deeper, more mineralized groundwater or groundwaters from overlying formations. The following section (Section 3.10) aims to distinguish this potential mixing from other geochemical processes using inverse geochemical models.

As indicated in Section 3.7.7, Figure 3-98 shows the hydrogeochemical comparison at NYO-PS02 and NYO-ORA at Nyora in the western part of cross-section CS2, which are screened within the Pilliga Sandstone and the Orallo Formation. Although they are screened within different aquifers, groundwater hydrochemistry in these two boreholes exhibit remarkably similar values for parameters such as pH, salinity, concentrations of major elements (including conservative ions such as chloride), methane concentrations and strontium isotopes ($^{87}Sr/^{86}Sr$). The similarity of molar ratio of major elements suggests either a common hydrogeochemical influence or potential hydraulic connectivity between the aquifers. Given these hydrogeochemical similarities, the subsurface geometry of this area warrants further investigation to assess potential hydrogeological connectivity pathways that may facilitate inter-aquifer exchange.

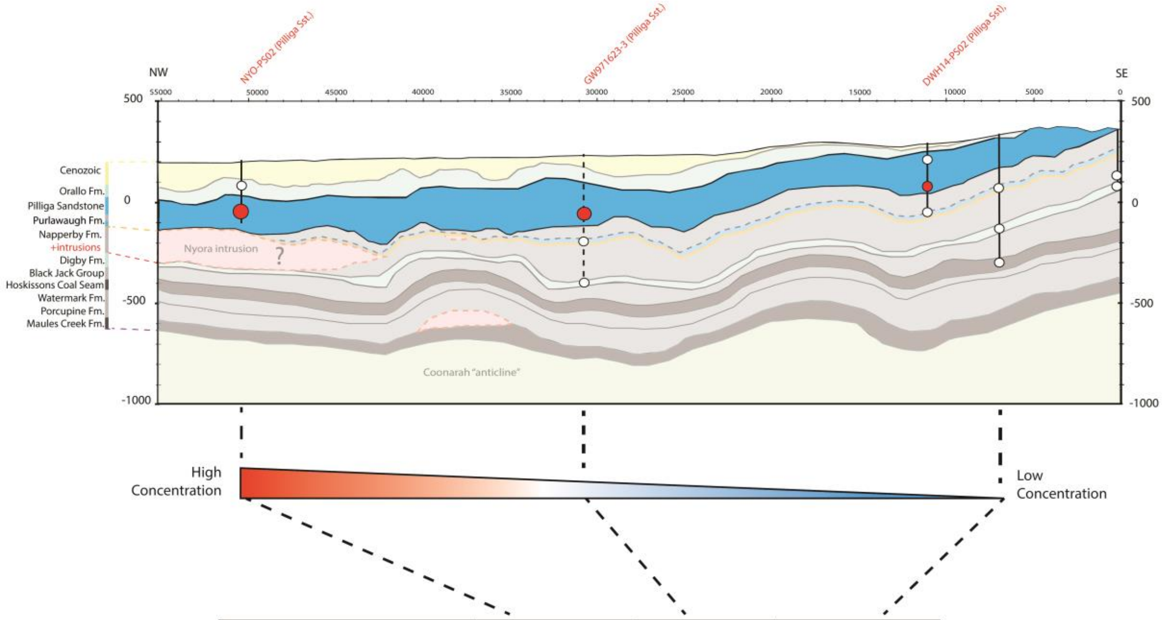

		NYO-PS02	GW971623-3	DWH14-PS02
-	pH	8	7	5
µS/cm	EC	1101	211	161
mg/L	TDS	704	135	102
	Bicarbonate Alkalinity as CaCO3	734	100	33
	Chloride	52	17	32
	Calcium	4	3	2
	Magnesium	1.0	0.8	2.0
	Sodium	317	32	29
	Potassium	2.0	10.9	4.0
	Barium	2.06		0.08
	Strontium	0.15	0.07	0.02
	Boron	0.21	0.05	0.05
	Fluoride	0.90	0.05	0.10
	Bromide	0.20	0.06	0.10
meq/L	Na/Cl	9.4	2.9	1.4
	Ca/Mg	2.4	2.5	0.6
	Ca+Mg/Na+K	0.02	0.14	0.19
	HCO3/Cl	10.0	4.1	0.7
	Ba/Cl	0.020		0.001
	F/Cl	0.032	0.005	0.006

Figure 3-98 - Geochemical evolution along inferred flow path in the Pilliga Sandstone at selected groundwater monitoring bores along the CS2

3.10.2 Inverse geochemical transect models

Several conceptual models of hypothesised flow and transport behaviour have been evaluated with respect to their ability to represent downgradient hydrochemical composition as a result of mixing of “upstream” groundwater compositions. Out of many investigated potentially plausible models, selected models which have resulted in at least two possible inverse models are reported here. For each of these reported inverse models, we define (i) the mixing proportion of the upstream groundwater compositions that were considered as a potential source contributing to the observed downgradient composition, and (ii) the range of mineral reactions that were deemed possible along the flow paths between the corresponding up- and downgradient locations. The selected models are summarised in Figure 3-99, Figure 3-100 and Table 11, respectively. The mixing proportions of the solutions were calculated during the modelling process and are summarized in the Table 11 and the cross section in Figure 3-100.

For each investigated model, the maximum uncertainties in elemental concentrations were successively reduced as much as possible in a trial-and-error process.

The results obtained by the inverse geochemical models (also called Inverse Model – i.e., IM) were used as a secondary line of evidence to confirm or reject the groundwater flow patterns that were obtained by the numerical groundwater flow and age simulations as well as the hydrochemical and environmental tracer interpretations. They were further compared to the results of environmental tracer analyses.

Table 10 Groundwater bores along cross-sections 1 and 2 used for geochemical mixing calculations

Bore ID	Aquifer intercepted	Position along flow path
DWH14PSO2	Pilliga Sandstone	Upgradient
TUL_DGY_02	Digby Formation	Upgradient
GW971623-1	Digby Formation	Downgradient
GW971623-2	Purlawaugh Formation	Downgradient
DWH14-Purlawaugh	Purlawaugh Formation	Upgradient
NYO_PS02	Pilliga Sandstone	Downgradient
DWH28 (CSG well)	Maules Creek Formation (primary CSG target)	Downgradient

Table 11 Interrogated inverse modelling variants (WQ: Water quality)

Inversion number	Number of models converging	WQ-0 (target - downgradient)		WQ-1 (same aquifer upgradient)			WQ-A			WQ-B			WQ-C		
		Aquifer (Bore ID)	Proportion in %	Aquifer (Bore ID)	Minimal Proportion in %	Maximal Proportion in %	Aquifer (bore ID)	Minimal Proportion in %	Maximal Proportion in %	Aquifer (bore ID)	Minimal Proportion in %	Maximal Proportion in %	Aquifer (bore ID)	Minimal Proportion in %	Maximal Proportion in %
IM2	4	Pilliga Sandstone (GW971623-3)	100	Pilliga sandstone (DWH14PSO2)	99.56	99.82	Digby Formation (TUL_DGY_02)	0	0	Purla-waugh Formation (DWH14PRL)	0	0.08	Purla-waugh Formation (GW971623-2)	0.07	4.36
IM4	11	Pilliga Sandstone (GW971623-3)	100	Pilliga Sandstone (DWH14PSO2)	98.04	100	Purlawaugh Formation (DWH14PRL)	0	0.02	Purla-waugh Formation (GW971623-2)	0	1.96			
IM5	5	Pilliga Sandstone (GW971623-3)	100	Pilliga Sandstone (DWH14PSO2)	96.93	99.49	Purlawaugh Formation (DWH14PRL)	0	0.03	Maules Creek Formation	0	0	Digby Formation (GW971623-1)	0.5	3.07
IM7	20	Pilliga Sandstone (NYO_PS02)	100	Pilliga Sandstone (DWH14PSO2)	36.37	50.53	Purlawaugh Formation (GW971623-2)	47.57	63.62	Digby Formation (GW971623-1)	0	2.99			
IM8	2	Pilliga Sandstone (NYO_PS02)	100	Pilliga Sandstone (DWH14PSO2)	92.29	92.35	Digby Formation (TUL_DGY_02)	7.64	7.64						
IM13	3	Purla-waugh Formation (GW971623-2)	100	Purlawaugh Formation (DWH14PRL)	70.94	100	Digby Formation (GW971623-1)	0	29.06						

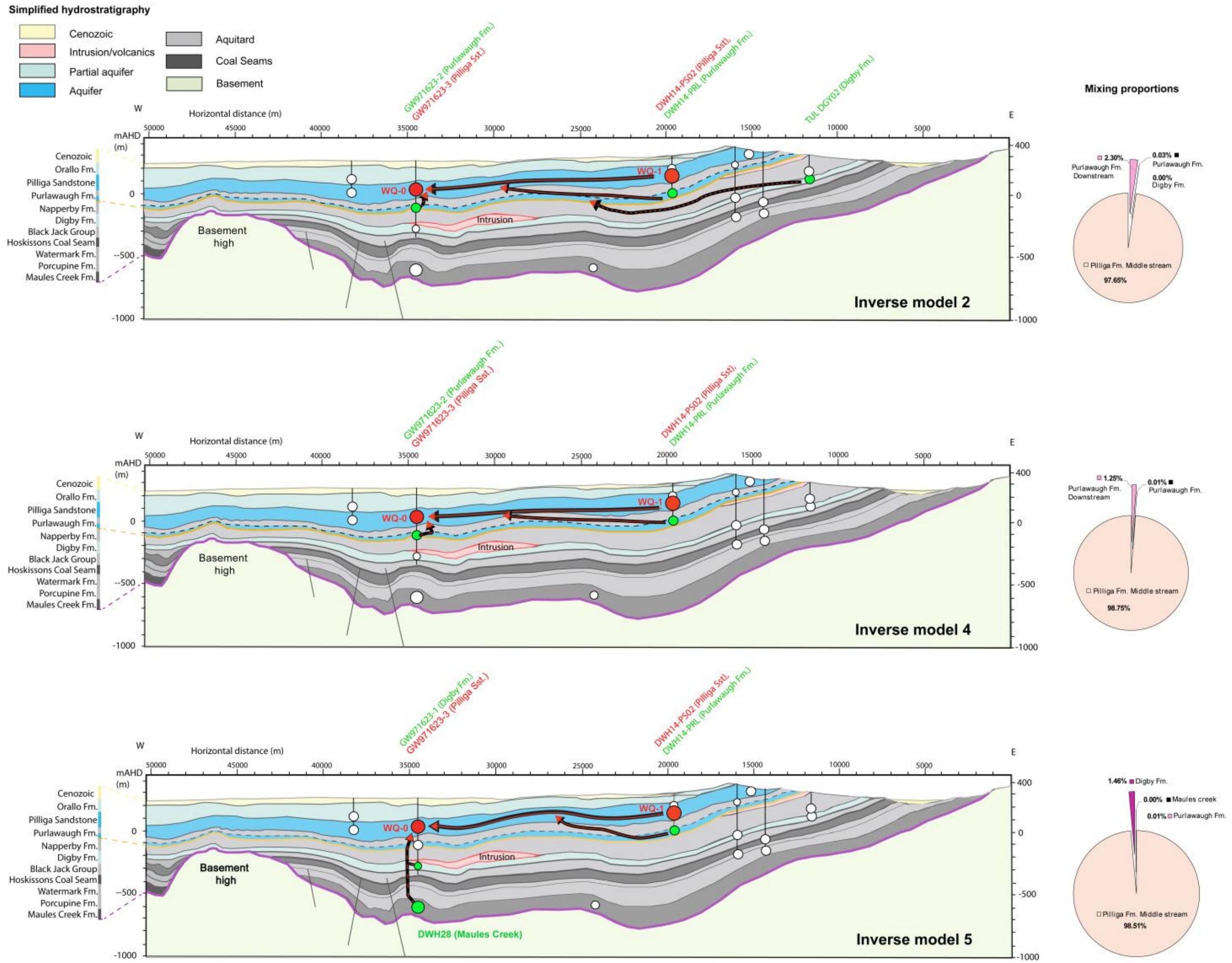

Figure 3-99 - Inverse model results represented with conceptual flows in cross-section 1 (CS1) (Part A)

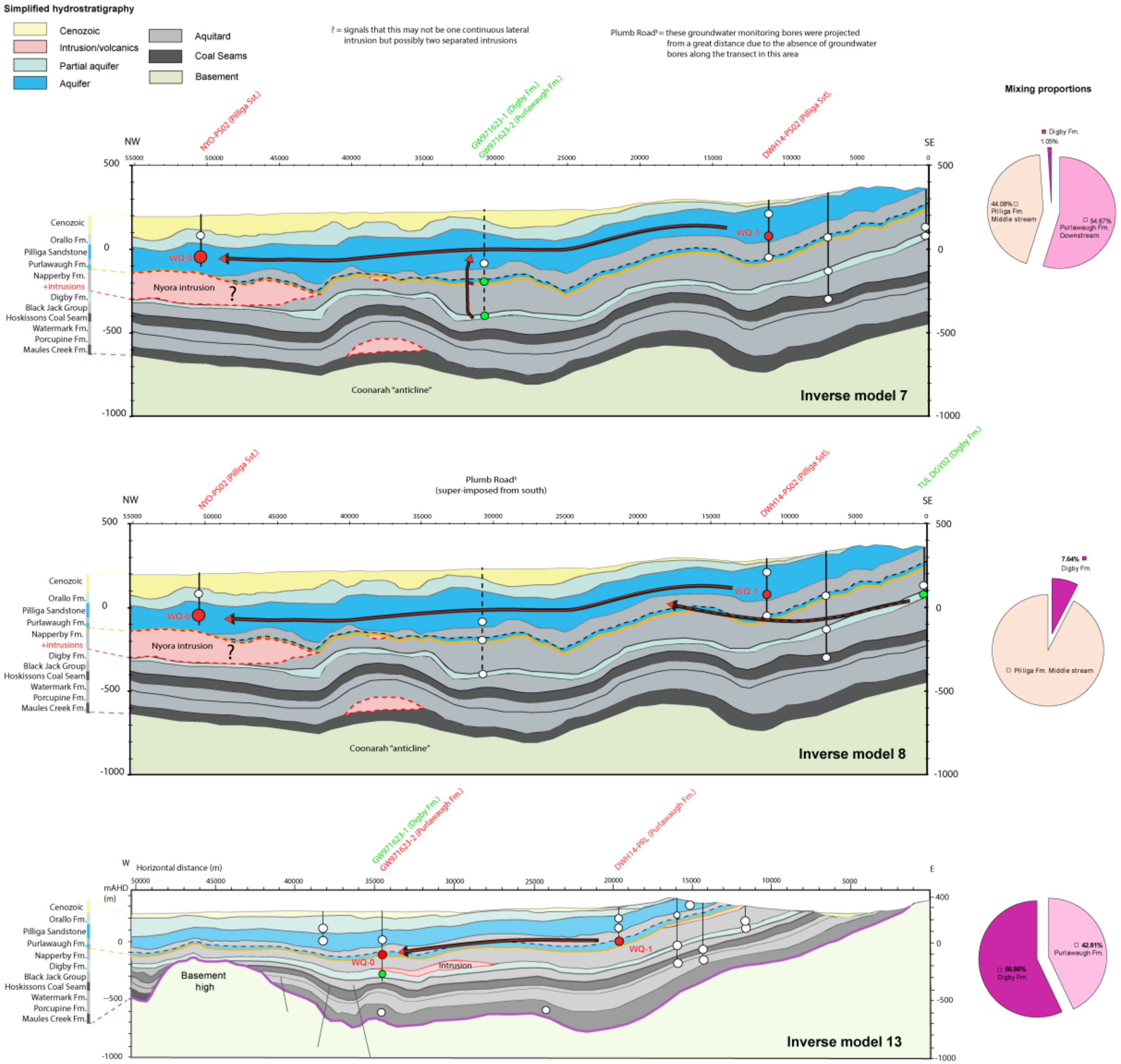

Figure 3-100 - Inverse model results represented with conceptual flows in cross-sections 2 (CS2) and cross-section 1 (CS1) (Part B)

The results of inverse geochemical modelling (IM) variants that were investigated are displayed in Table 11 summarised on cross-sections CS1 and CS2 (Figure 3-99 and Figure 3-100) and described below. As shown in Table 11, the mixing model results are non-unique, with multiple model realisations possible that match the input data.

Geochemical mixing along CS1

The results of IM2 provided one of the key results: it was aimed at reproducing the downgradient hydrochemical composition of the Pilliga Sandstone aquifer (GW971623-3) at the Plumb Road nested groundwater monitoring site because of inter-aquifer mixing and reactions of various fractions of upgradient groundwater compositions from the Purlawaugh Formation, Pilliga Sandstone, and Digby Formation, respectively. Importantly, the results suggest that there is unlikely to be any contribution and direct influence of the Digby Formation groundwater (WQ-A) on the downgradient Pilliga Sandstone hydrochemical composition (Table 11; Figure 3-99). Instead, the downgradient hydrochemical composition of the Pilliga Sandstone groundwater at Plumb Road (GW971623-3) can be largely explained by water originating from the upgradient interval of the Pilliga Sandstone aquifer, which accounts for an average of 97.65% of the downgradient Pilliga Sandstone groundwater composition (varying from 95.60% to 99.82% among different model realisations), a contribution ranging from 0.07% to 4.36% of the water sampled from the Purlawaugh Formation at Plumb Road (GW971623-2) and a small possible contribution from the upgradient Purlawaugh Formation at DWH14.

Building on IM2, IM4 is set up similar to IM2 but excludes the Digby Formation as a potential source water composition. IM2 aimed at deriving a refined assessment of the proportions computed by IM2. The results further reduce the contribution of the upgradient Purlawaugh Formation. The computed contribution to the Pilliga Sandstone downgradient composition (GW971623-3) shows still a minor contribution from the Purlawaugh Formation (up to 1.96% from GW971623-2 and up to 0.02% from DWH14PRL) with the Pilliga Sandstone from upgradient (DWH14PSO2) as the main contribution reaching at least 98.04% of the final composition.

Model variant IM5 aimed at explaining the downgradient composition of the Pilliga Sandstone at Plumb Road (GW971623-3) with potential contributions from the Purlawaugh Formation, the Digby Formation and a deep contribution of water from the Maules Creek Formation, which hosts the major coal seam and represents the primary CSG target formation. Importantly, the results indicate that there is no apparent influence from the Maules Creek Formation (yielding a value of 0%). Instead, the downgradient composition of the Pilliga Sandstone aquifer can be explained by minor contributions from the Digby Formation (GW971623-1, from 0.50 to 3.07%), minor contributions of the Purlawaugh Formation (DWH14PRL, up to 0.03%) and to a major extent by the water sampled further upstream in the Pilliga Sandstone (DWH14PSO2, ranging from 96.93 to 99.49%).

The model variant IM13 (Table 11) aimed at exploring the evolution of the downstream composition of the Purlawaugh Formation (GW971623-2). This model variant assumed potential contributions from the Purlawaugh Formation further upstream (DWH14PRL) and from the Digby Formation (GW971623-1). The results indicate that it is possible to explain the downgradient hydrochemical composition of Purlawaugh Formation groundwater as a mixture of the upgradient

Purlawaugh Formation composition (73.69%) and a contribution from the Digby Formation contribution (maximum of 26.31%).

Although many more model variants were investigated to investigate potential alternative hydrogeological connectivity pathways, they did not provide any significant additional insights.

Geochemical mixing along CS2

As described in section 3.6.2, there are multiple potential hydrogeological connectivity pathways identified previously near Nyora at the western edge of geological cross-section 2 (CS2).

IM7 and IM8 were set up to test whether upwards discharge from the Purlawaugh Formation or Digby Formation could potentially explain the patterns of hydrochemical evolution that were observed between the eastern section of the Narrabri Gas Project area towards the north-west. As already mentioned in section 3.6.2, the Pulawaugh and Napperby formations are absent at the Nyora 1 exploration well, with the Pilliga Sandstone separated from the Digby Formation by an approximately 200 m thick sill or laccolith. Due to the observed subsurface geometry and the increase in concentrations of key parameters such as salinity and methane and increase in groundwater age (represented by ^{14}C and ^{36}Cl) from the east towards Nyora, Raiber et al. (2022a) suggested that a small admixture of groundwater from underlying formations may contribute to the observed patterns.

IM7 was set up to explain the hydrochemical composition of Pilliga Sandstone groundwater downgradient (NYO_PS02) at Nyora in the north-western part of the Narrabri Gas Project area. Specifically, it was tested to determine if there is any evidence for mixing/contributions from the Purlawaugh and Digby formations. As no groundwater observation bores screened within the Purlawaugh and Digby formations exist further north in this area, the hydrochemical records of bore screened within these formations at Plumb Road were chosen. When the kaolinite mineral phase is considered, the results indicate that when the Purlawaugh Formation (GW971623-2) contributes between 47.57 to 63.62%, the contribution from the Digby Formation (TUL_DGY_02) is considered small, i.e., below 3%, while the composition of the Pilliga Sandstone upgradient remains the main source /contribution (36.37% to 50.53%). To maintain consistency between the presented models, the kaolinite phases were retained. However, additional mineral phases should be considered or removed specifically to refine the mixing proportions obtained and better account for potential geochemical mixing processes within the Pilliga Sandstone in future work opportunities. These estimated mixing calculations are discussed further in Section 4.1.

IM8 aimed at confirming the geochemical contribution of the Digby Formation to the (downgradient) hydrochemical composition of the Pilliga Sandstone (NYO_PS02) at Nyora by testing its maximum potential contribution in the absence of any Purlawaugh Formation input. This represents a scenario where the Purlawaugh Formation and Napperby Formation appear to be absent at the western edge of CS2. The results indicate that the potential contribution of the Digby Formation appears to be relatively low, reaching a maximum value of 7.64% towards the Pilliga Sandstone downgradient composition, while the remaining contributions increases to up to 92.29% for Pilliga Sandstone upgradient (DWH14PSO2). However, a significant limitation of the geochemical mixing models along CS2 is that no scenarios involving the Orallo Formation or Cenozoic sedimentary cover could be conducted. Multiple nested bore sites screen the Orallo

Formation at deeper (downgradient) intervals of the flow paths within the Surat Basin at Nyora and at Bohena 14 (BHN14), where hydrochemistry and environmental tracer values are very similar for the Orallo Formation and Pilliga Sandstone. However, no bores screened within the Orallo Formation further upgradient were available as representatives of a potential mid-gradient end-member that could explain the changes observed within the Pilliga Sandstone from upgradient to downgradient. This will be discussed further below in the text.

4 Discussions

In this section, we integrate and discuss the results of the multiple lines of evidence presented in previous sections of this report. This allows to examine and discuss the current understanding of potential connectivity pathways and other components of the iterative conceptual modelling workflow described in Section 2.1.

We discuss some of the key questions on hydrogeological connectivity pathways that remained open following the study by Raiber et al. (2022a) and update the conceptualisation and identify the further remaining uncertainties. A simple data worth analysis is presented to demonstrate how different techniques helped to answer the key questions.

On-going knowledge and data gaps are presented to highlight opportunities to further reduce uncertainties.

4.1 Hydrogeological connectivity pathways in the Narrabri region

When did intrusive activity occur in the Narrabri region?

Understanding the timing of intrusions is important as it determines whether an intrusion could potentially form a connectivity pathway between coal seams and the Pilliga Sandstone, the major GAB aquifer in this region (Section 1.3.2). Prior to the current study, no geochronological analysis of intrusions was completed within the Narrabri Gas Project area, although one rock sample of a sill (horizontal intrusion) at Nyora just to the northwest of this area was dated as Early Jurassic and igneous rocks further to the north at the Nandewar Volcanic Centre were dated as Cenozoic. The lack of information on the timing of intrusion was therefore identified as a key knowledge gap in a previous GISERA project (Raiber et al., 2022a).

The current investigation enabled a significantly improved understanding of the timing of intrusive activity within the Narrabri Gas Project area through the geochronological analysis of 17 intrusive rock samples (Section 3.4), supported by mineralogical analysis (Section 3.3.1) and the development of petrographic thin-sections (Section 3.3.3).

The K-Ar age dating of igneous rocks demonstrated that there were multiple phases of intrusive activity in the wider Narrabri Gas Project area between the Upper Triassic and early Cenozoic (229 to 50 million years ago). These different phases of igneous activity were associated with large-scale tectonic processes in Eastern Australia at this time. The eastern margin of Australia has experienced complex deformation since the Triassic, principally controlled by the subduction of the Pacific plate beneath the Australian plate (Section 3.4).

With the Pilliga Sandstone deposited approximately 150 million years ago, this means that some of the intrusions could form a potential connectivity pathway between deeper formations and the

Pilliga Sandstone, whereas others occurred prior to the deposition of the Pilliga Sandstone and can therefore be ruled out as direct connectivity pathways.

Some uncertainties remain on the results of the K-Ar dating due to the potential influence of weathering and hydrothermal alterations of rocks.

Do intrusions form potential hydrogeological connectivity pathways between coal seams and the Pilliga Sandstone?

The geochronological analyses indicate that some of the intrusions could have intersected the Pilliga Sandstone based on the time when they occurred relative to the deposition of the Pilliga Sandstone. However, the assessment of stratigraphic logs suggested that most of the sills (horizontal intrusions) intruded into the Late Triassic Digby and Napperby formations, the interfaces between them and/or at the interface between the uppermost Gunnedah Basin and the Early Jurassic Purlawaugh Formation. Although it cannot be ruled out that some formations intruded into the Pilliga Sandstone in the eastern or southern part of the Narrabri Gas Project area where reliable stratigraphic logs are relatively sparse (as discussed further below), there are two plausible explanations why no intrusions have been observed in formations above the Purlawaugh Formation in the Narrabri Gas Project area:

1) **absence of deep-seated faults extending into Surat Basin:** previous studies suggested that there are no faults with significant vertical displacements (juxtaposition) extending from the Gunnedah Basin into the Surat Basin, as also suggested by the AEM survey in the current study (discussed further in the next section). As lava often follows zones of structural weakness such as fault zones during its ascent from the mantle to the surface, the proposed lack of faults extending into the Surat Basin may explain the absence of intrusions within the Pilliga Sandstone.
2) **elevated thermal conductivity and higher convective heat loss of siliciclastic sandstones:** as described in Section 1.3.3, Mark et al. (2024) suggested that intrusions are much more likely observed within low permeability formations such as claystones due to the higher thermal conductivity and higher convective heat loss of siliciclastic sandstone. This was attributed to the higher permeabilities and presence of more pore fluids in sandstones. In the Narrabri Gas Project area, this could mean that when magma intruded into the basal sediments of the Purlawaugh Formation (which form an aquifer at some locations) or into the Pilliga Sandstone, the heat would have likely dissipated through the pores and fractures and rapid heat loss would have occurred as lava hit groundwater before it could form a significant intrusion.

Is there faulting and folding in the Narrabri region?

Geological structures that can form potential hydrogeological connectivity pathways are generally present in most sedimentary basins in Australia and globally. Apart from igneous intrusions such as dykes and sills, other types of subsurface geological structures that can be observed in sedimentary basins are faults, folds and forced folds.

Previous geological, hydrogeological and hydrocarbon investigations (e.g. Tadros, 1993; Carty and Smith, 2004; Raiber et al., 2022a) investigations suggested that several anticlines occur in the north and north-west of the Narrabri Gas Project area, and such geological structures appear to be linked to magmatic intrusive activity. Raiber et al. (2022a) revisited seismic imagery and suggested that it indicates that no significant reactivation of basement faults within the Surat Basin in the southern and eastern part of the Narrabri Gas Project area appears to have occurred, as suggested by the continuity of major seismic reflectors and the absence of significant major vertical displacement of stratigraphic horizons.

Building on the previous interpretations by Raiber et al. (2022a) and other studies (e.g. Carty and Smith, 2004), the assessment of AEM data combined with other lines of geoscientific evidence aimed to provide a more spatially continuous understanding of whether any geological structures are present within the upper approximately 400 m of the subsurface. The integrated evidence from the AEM survey, seismic survey data and stratigraphic data confirms that geological structures are present within some parts of the broader Narrabri region (including in regions outside the Narrabri Gas Project area) and absent elsewhere.

To the north of the Narrabri Gas Project area (approximately 20 km north of the northern boundary), apparent displacements of the shallowest sedimentary bedrock conductor (inferred to be the top of the Purlawaugh Formation) can be observed in some AEM lines (e.g. AEM line 100100 in Figure 3-33). These occur relatively close to the Nandewar Volcanic Centre, suggesting that these inferred structural features may be linked to the likely presence of dyke swarms in this area.

The presence of doming or forced folding (also often termed as four-way dip closures in previous studies; Carty and Smith, 2004) has been suggested by seismic surveys in previous studies in the north-western part of the Narrabri Gas Project area where they were investigated as potential hydrocarbon traps (Section 3.5). In this area, the geometry of the top of the first more conductive sedimentary bedrock layer observed in AEM lines representing the interface between the Pilliga Sandstone and Purlawaugh Formation also suggests that low amplitude folding or doming characterised by gently undulating surfaces is likely to have occurred here. This includes the Coonarah and Brigalow areas where anomalies can be identified on the Total Magnetic Intensity map (Figure 2-5 and Figure 3-24) and where up to approximately 100 m of intrusive igneous rocks have been intersected in some exploration wells. There are no visually apparent significant vertical displacements, although the relatively thick conductive cover and considerable depth means that the depth resolution of the AEM is limited in the north-western part of the Narrabri Gas Project area.

In the central part of the Narrabri Gas Project area at the Bohena anticline, stratigraphic data and total magnetic intensity imagery confirm the occurrence of spatially extensive intrusive rocks (a sill). These occur within the Napperby and Digby formations or at the interface of these formations with the Purlawaugh Formation (Section 3.1.1). The intrusions occur below a depth of 500 m, which is deeper than the maximum depth covered by the AEM survey, and the AEM survey can therefore not provide any new insights.

In the southern part of the Narrabri Gas Project area, the gently undulating nature of the top of the Purlawaugh Formation indicates that there is some low amplitude folding or doming of sedimentary strata over intrusive rocks or deposition over pre-existing basement highs. The thickness of the Purlawaugh Formation appears to be preserved across these features, and this conductive layer does not show any significant vertical displacements. Regional-scale magnetic anomalies are visible in the Total Magnetic Intensity imagery in these areas (Figure 3-24), suggesting that this may be linked to some igneous rocks. An intrusive rock in this area at exploration well Dewhurst DDH1 was dated as Mid Jurassic (Section 3.4), indicating that this event may have occurred after the deposition of the Purlawaugh Formation and at a similar time as the deposition of the Pilliga Sandstone.

Overall, the AEM does not show any significant vertical displacement of Surat Basin strata within the Narrabri Gas Project area that would indicate the continuation of basement faults from the Gunnedah Basin into the Surat Basin. Where minor displacements of the Purlawaugh Formation appear to occur in the north-western part of the Narrabri Gas Project area based on seismic images (Figure 3-27), these may be related to low amplitude folding over thick igneous intrusive rocks.

In contrast, more significant structural complexity can be observed in the AEM data to the east of the Narrabri Gas Project area closer to the Hunter-Mooki thrust fault, where deformation of Gunnedah Basin strata closer to this major eastern Australian tectonic boundary has occurred.

Are there any new insights into the lithological composition of the Surat Basin strata (Purlawaugh Formation, Pilliga Sandstone and Orallo Formation)?

The AEM survey combined with mineralogical analysis, stratigraphic and lithological data provided valuable new insights into the internal architecture of the Pilliga Sandstone, which was previously described as a homogeneous medium- to very coarse grained and well sorted, quartzose sandstone with minor pebble conglomerate and only rare to minor thin interbeds of mudstone, siltstone and fine-grained sandstone (e.g. Arditto, 1982 and Arditto, 1983). These previous characterisations likely focussed on the composition of the Pilliga Sandstone within the outcrop beds of the Pilliga Sandstone, whereas in the current study, the combined evidence from the AEM survey and mineralogical analysis of the Pilliga Sandstone enabled an assessment of the changes that occur from outcrop beds to deeper confined parts of the aquifer. This demonstrated that there are systematic changes of petrophysical, hydraulic and electromagnetic properties along the hydraulic gradient within the Pilliga Sandstone, with the Pilliga Sandstone composed primarily of quartz and limited clay minerals in the recharge beds and a much more variable composition with less quartz and higher clay mineral, carbonate and feldspar content further down-gradient.

The study also helped to better understand the heterogeneity within the Purlawaugh Formation and the relationships between Pilliga Sandstone, Purlawaugh Formation and Orallo Formation.

The assessment of selected stratigraphic logs showed that the Purlawaugh Formation is more complex than assumed in previous studies, where it was sometimes described as an aquitard or aquiclude. With drilling of more groundwater bores, the understanding has evolved, suggesting that the base of the Purlawaugh Formation forms at least locally a thin sandstone aquifer, whereas the top of the Purlawaugh Formation is an aquitard composed of claystone. A more systematic regional assessment, further mineralogical analysis or development of sedimentary facies models could help to further confirm the spatial variability of the Purlawaugh Formation.

The Orallo Formation, which overlies the Pilliga Sandstone, has been described as an aquitard in some previous studies. In AEM survey results, there is no clear distinction between the Pilliga Sandstone and Orallo Formation, and in most stratigraphic logs of exploration wells the two formations were not separated. The mineralogical analysis and AEM survey results indicate that towards the deeper part of the Surat Basin, the Pilliga Sandstone and Orallo Formation are likely to be connected, with the Orallo Formation more likely behaving as a partial aquifer.

The implications of these new insights on the hydrochemical evolution and hydrogeological connectivity will be discussed further below.

What evidence can hydrochemistry and environmental tracers provide on the understanding of the continuity (or otherwise) of aquitards throughout the Narrabri Gas Project area?

The assessment of hydrochemistry and environmental tracers in the current study confirmed the assessment by Raiber et al. (2022a) that in the south and east of the Narrabri Gas Project area, there is a high degree of separation between the Gunnedah Basin aquitards and coal seams and the Pilliga Sandstone. Complementing the data by Raiber et al. (2022a), additional stable noble gas data (mantle helium and ^{40}Ar) of Gunnedah Basin groundwaters collected during the present study further underpinned this assessment. In addition, the AEM survey demonstrated that the shallowest sedimentary bedrock conductive layer (likely the top of the Purlawaugh Formation) in the south and east of the Narrabri Gas Project area does not show any obvious displacements.

This indicates that the inferred aquitards that separate the CSG target units from the Pilliga Sandstone in the stratigraphic column (e.g. Gunnedah Basin aquitards Porcupine Formation, Watermark Formation and Napperby Formation and the upper low-permeability sequences of the Purlawaugh Formation in the Surat Basin) are more likely continuous with relatively minor structural disruption in the south and east.

Specific areas such as Plumb Road (Bohena anticline) and the north-western part of the Narrabri Gas Project area where Raiber et al. (2022a) suggested that there may be some hydrogeological connection between the Pilliga Sandstone and the underlying Purlawaugh Formation and/or the late Gunnedah Basin strata (Digby Formation) are discussed further below.

What are the reasons for the observed changes of hydrochemistry and environmental tracer patterns from east to the north-western part of the Narrabri Gas Project area?

In a previous GISERA study, Raiber et al. (2022a) observed that there is an increase of salinity, methane concentrations, groundwater age (represented by a change of environmental tracer compositions) and other parameters from the eastern outcrop beds of the Pilliga Sandstone towards the deeper parts of the aquifer in the north-west of the Narrabri Gas Project area. Based on these observations and simple mixing models, Raiber et al. (2022a) hypothesised that this change may be due to a small admixture of upwards discharge from the Purlawaugh, Digby or Napperby formations into the Pilliga Sandstone, possibly facilitated by thinning and localised absence of the Purlawaugh and Napperby formations near thick igneous intrusions. However, they identified the lack of environmental tracer data from the Napperby and Digby formations and other Gunnedah Basin formations as a key knowledge gap.

In the present study, a wide array of hydrochemical and environmental tracer connectivity indicators were analysed, including samples from the different Gunnedah Basin formations. Furthermore, geochemical mixing models using hydrochemistry, selected tracers and mineralogical rock analyses were developed to test different mixing scenarios. The results were considered within the geological and geophysical framework discussed above.

Hydrochemistry, geochemical mixing models and some isotopic age tracers such as ^{14}C, ^{36}Cl and ^{4}He suggests that it is plausible that a small admixture of groundwater from the Purlawaugh Formation or uppermost Gunnedah Basin formations could explain the spatial hydrochemical and environmental tracer patterns. In contrast, the geochemical mixing models confirmed the results from simple mixing models developed by Raiber et al. (2022a), which indicated that there is unlikely to be any contribution from the Maules Creek Formation (the primary CSG target unit) to the Pilliga Sandstone.

However, although the mixing models (which did not include stable noble gases) and other key parameters suggests that an admixture from the Purlawaugh Formation (up to 67%) or shallow Gunnedah Basin formations (up to 3% from Digby Formation) could explain the east-west observed groundwater evolution along geological cross-section CS2, stable noble gas isotopes ($^{3}He/^{4}He$ and ^{40}Ar) and strontium isotopes indicate that this is unlikely or that the admixture must be very minor (likely less than approximately 1%). For example, as explained in Section 3.8.5, mantle helium ($^{3}He/^{4}He$ versus Ne/He ratio) estimates of groundwater samples from the Pilliga Sandstone and Orallo Formation at Nyora are orders of magnitude lower than those in groundwater samples from the Purlawaugh Formation and Gunnedah Basin formations. Likewise, the values of ^{40}Ar of all groundwater samples collected from the Purlawaugh Formation and Gunnedah Basin formations are very high and (to our knowledge) the highest ever measured in Australia to date, whereas the groundwater samples from the Pilliga Sandstone and the Orallo Formation at Nyora show no evidence of elevated ^{40}Ar values (Figure 3-94).

Based on the newly collected AEM survey data and mineralogical and stable noble gas data, we propose an alternative explanation to the admixture from formations below the Pilliga Sandstone as the major control of the change of hydrochemical properties from east to west. The AEM data show that there is a significant change in lithological properties (and thus, a step change in hydraulic properties) from outcrop beds to deeper parts of the Pilliga Sandstone and that there is no distinct low permeability layer (aquitard) hydraulically separating the Pilliga Sandstone and Orallo Formation. Values of hydrochemical and isotopic parameters of the Pilliga Sandstone and Orallo Formation groundwaters at the Nyora groundwater monitoring bore site are nearly identical (Section 3.10). The lower permeability of the Pilliga Sandstone and Orallo Formation in this area can explain the older groundwater ages observed in these formations at Nyora, and the absence of a flow connection with underlying formations could explain the absence or very low values of mantle helium and ^{40}Ar. The presence of an overlying aquitard (the clay-rich conductive cover identified in the AEM survey data) limits recharge along the flow path outside the outcrop beds of the Pilliga Sandstone or Orallo Formation. Groundwater Sr isotopes in Surat Basin and Gunnedah Basin formations also indicate that if mixing with adjacent (over- or underlying) formations is assumed to be the primary process controlling the decrease of $^{87}Sr/^{86}Sr$ from east to west in Pilliga Sandstone groundwaters, then the Orallo Formation is the most likely mixing source. Unlike formations underlying the Pilliga Sandstone, the Orallo Formation has a lower $^{87}Sr/^{86}Sr$ than all Pilliga Sandstone groundwater samples. Furthermore, the hydrochemistry and environmental tracer values of Orallo Formation and Pilliga Sandstone groundwater samples at Nyora are very similar (Figure 3-98).

This suggests that the inferred connection between Orallo Formation and Pilliga Sandstone and the lithological and mineralogical variability within the Pilliga Sandstone are likely the major factors contributing to the east-west evolution of groundwater chemistry and rapid westwards increase of groundwater age within the Pilliga Sandstone in the Narrabri Gas Project area, although a very small admixture of upwards discharge from the formations immediately below the Pilliga Sandstone cannot be ruled out.

Is there hydrogeological connectivity at Plumb Road (Bohena anticline)?

In addition to the change of hydrochemistry and environmental tracer values observed in a previous GISERA study by Raiber et al. (2022a), the same authors also observed that there is a small increase of salinity, methane concentrations, groundwater age and other parameters from the eastern outcrop beds of the Pilliga Sandstone towards the central area of the Narrabri Gas Project area at Plumb Road and at the Bohena anticline. At the Plumb Road groundwater monitoring site, a significant upwards hydraulic gradient can be observed from the Digby Formation and Purlawaugh Formation (which are both artesian at this site) to the Pilliga Sandstone (where the depth of groundwater is >25 m below ground surface).

In this study, we have further combined multiple lines of evidence to refine the understanding of connectivity between Gunnedah Basin formations and the Purlawaugh Formation and between the Purlawaugh Formation and the Pilliga Sandstone at Plumb Road. As shown in earlier sections of this report (e.g. Section 3.6.1) and by Raiber et al. (2022a), there are multiple potential hydrogeological connectivity pathways in this area.

The assessment of exploration well log data in this area demonstrates that igneous intrusions have intersected multiple stratigraphic intervals within or at the interfaces between the Digby and Napperby formations and at the interface of these formations with the Purlawaugh Formation (Figure 3-2). The sill (a horizontal intrusion) at Bohena was dated as Early Jurassic (Table 6), with the K-Ar age suggesting that the intrusion was likely emplaced contemporary with the deposition of the Purlawaugh Formation (Section 3.4) and some contact metamorphism may have impacted the basal sequences of the Purlawaugh Formation.

Re-processing of seismic data presented by Raiber et al. (2022a) and seismic data investigated in other studies suggested that there is no evidence for major basement structures with significant juxtaposition (vertical displacements) extending from the Gunnedah Basin into the Surat Basin.

The assessment of hydrochemistry and environmental tracers confirmed that there is a very strong contrast in values for most parameters between groundwaters collected from the Pilliga Sandstone in comparison to groundwaters from the Purlawaugh Formation and deeper formations. A high degree of separation between the Pilliga Sandstone and underlying formations was also suggested by the integration of hydraulic head and groundwater age data through the simulation of groundwater flow and age along an east-west geological transect, which suggested that the upper section of the Purlawaugh Formation acts as an effective seal that causes significant head drops of >30 m over short vertical distances. Although there is likely a very high degree of separation, inverse geochemical models suggested that a very minor admixture of groundwater from the Purlawaugh Formation to the Pilliga Sandstone (0 to approximately 2%) somewhere along the flow paths from east to west along this transect is plausible. In contrast, the mixing models suggested that it is unlikely that there is any contribution from the primary coal seams hosted within the Maules Creek Formation. Similar to the observations at Nyora in the north-west of the Narrabri Gas Project area, most of the change of hydrochemistry within the Pilliga Sandstone is likely due to the variable mineralogy of the Pilliga Sandstone.

A significant change in hydrochemistry and environmental tracer values can be observed for the Purlawaugh Formation between DWH14 and Plumb Road. This change is visible for example by a significant increase of groundwater residence time tracers (e.g. ^{36}Cl and ^{4}He; Section 3.8), methane concentrations (Section 3.7.5) and salinity (Section 3.7.1) along this inferred flow path. Geochemical mixing models suggest that it is plausible that there is an admixture from the Digby Formation to the Purlawaugh Formation aquifer (Section 3.10). This might indicate that the emplacement of the sill and associated fracturing at various stratigraphic intervals within the uppermost Gunnedah Basin and Purlawaugh Formation in this area may have led to some connectivity between these formations. However, some geochemical mixing models were also able to explain the evolution without an admixture from the Digby Formation and alternative explanations such as internal processes occurring within the Purlawaugh Formation or interactions through diffusion with over- or underlying formations (i.e. the upper low permeability part of the Purlawaugh Formation and underlying Napperby and Digby formations) could also explain some of the observed patterns of environmental tracer evolution.

A significant limitation of the assessment of potential connectivity between the Purlawaugh Formation and the shallow Gunnedah Formations is that the Digby Formation groundwater monitoring bore at Plumb Road (GW971623-1) could not be sampled during the present study as the installed pump was not functional. Furthermore, there is at present a general lack of baseline hydrochemistry and environmental tracer data for the Napperby and Digby formations within the central part of the Narrabri Gas Project area.

What are the implications of this study for flow dynamics and the assessment of aquifer connectivity in the wider Great Artesian Basin?

Suckow et al. (2019) and Raiber et al. (2022 a, b) suggested that there are fast and slow groundwater flow paths in the Great Artesian Basin aquifers within the Coonamble Embayment, a sub-basin of the Surat Basin in NSW, and in other parts of the Great Artesian Basin in Queensland, based on the spatial assessment of groundwater age tracers ^{14}C and ^{36}Cl.

In other parts of the GAB, rapid changes of hydrochemistry or environmental tracer values along inferred flow paths are often attributed to connectivity of GAB aquifers with adjacent units. Although this may often be the case, the present study highlights the need to assess other possible factors such as the spatial variability of mineralogical, sedimentary and hydraulic properties within GAB aquifers and determine if step changes in lithological and petrophysical properties can explain changes in hydrochemistry and environmental tracer values along inferred flow paths. This study emphasises that although hydrochemistry is a critical tool to assess inter-basin or inter-aquifer connectivity, it needs to be complemented by different environmental tracers (e.g. stable noble gas isotopes) and placed within the geological and hydrogeological context to avoid misconceptions.

4.2 Revised stratigraphic table

The stratigraphic table representing the formations of the Surat and Gunnedah basins within the Narrabri Gas Project area has been updated with an improved understanding on when igneous (intrusive) activity took place in this region (Figure 4-1). The assessment also re-affirmed that the Purlawaugh Formation is not a complete aquitard or aquiclude as assumed in previous studies, but that it is likely comprised of a low-permeability upper part composed of claystone and other fine-grained sediments and a high-permeability lower part.

Most intrusive and extrusive activity occurred prior to deposition of the Pilliga Sandstone, but the K-Ar dates show that some post-depositional activity occurred during the Late Jurassic and Cretaceous. Similar to the observed patterns of $^{87}Sr/^{86}Sr$ in Qld, contemporary igneous activity as a sediment source during the deposition of the Cretaceous GAB formations also likely explains the lower $^{87}Sr/^{86}Sr$ of the Orallo Formation compared to the older GAB and Gunnedah Basin formations.

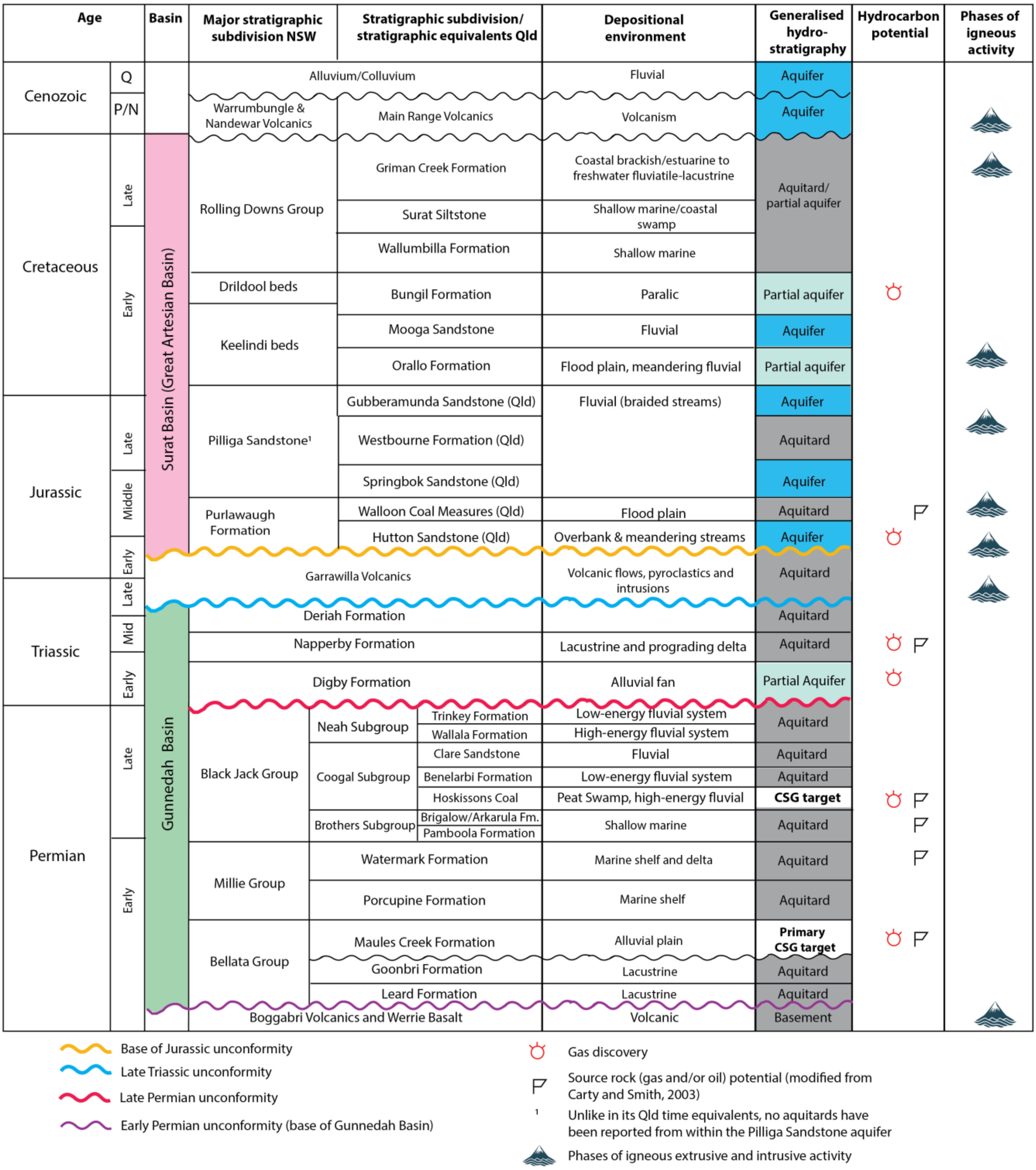

Figure 4-1 – Stratigraphy of the Surat and Gunnedah basins in NSW (compiled from Tadros (1993, 1995), Carty and Smith (2003), Korsch and Totterdell (2009), Totterdell et al. (2009), Geoscience Australia (2013), Ransley et al. (2015), Ruming (2015), Raiber et. al (2022a), Norton and Rollet (2023)) and the current study. Q and P/N in the Cenozoic era correspond to Quaternary and Palaeogene/Neogene.

4.3 Revised conceptual model of potential hydrogeological connectivity pathways in the Narrabri region

As described in Section 1.4, conceptual models of potential hydrogeological connectivity pathways can be refined over time as more field data or other information becomes available. As the understanding of pathways continues to mature, uncertainties may decrease and the degree of change between subsequent versions of conceptual models are likely to become smaller. The state of our knowledge on hydrogeological connectivity pathways prior to the start of this project was summarised in Section 1.4.3 and Figure 1-6.

With the acquisition of AEM survey data, collection of additional environmental tracer samples from Gunnedah Basin formations and geochronological and mineralogical analyses, the conceptual model of potential hydrogeological connectivity pathways has been further refined in this study. This means that the characterisation of some potential hydrogeological connectivity pathways has been updated, whereas for other potential pathways, the assessment confirmed the previous understanding with more confidence due to the acquisition of additional field data and enhanced data integration.

Overall, the assessment of hydrochemistry and integration of multiple data sources confirmed that there is likely a high degree of hydraulic separation between coal seams and the Pilliga Sandstone in the south and east of the Narrabri Gas Project area. The AEM survey provided a more spatially continuous picture of the upper approximately 400 m of the subsurface. This confirmed that there are no obvious significant juxtaposition of the Surat Basin strata within the Narrabri Gas Project area that would indicate a displacement of the shallowest aquitard (upper part of the Purlawaugh Formation), although some displacements are visible to the north of the Narrabri Gas Project area.

Previous projects suggested that the increase of salinity, methane concentrations and observed evolution of other parameters within the Pilliga Sandstone from the eastern part of the Narrabri Gas Project area towards Nyora may be due to a small admixture of groundwater from the formations underlying the Pilliga Sandstone (e.g. Purlawaugh Formation, Napperby Formation and Digby Formation). The AEM survey results supported the interpretations from previous hydrogeological and hydrocarbon investigation that there is some low amplitude folding in this area, likely associated with the emplacement of igneous intrusions in this area. However, the AEM survey and mineralogical analyses also confirmed that there is a significant change of the mineralogical and hydraulic properties of the Pilliga Sandstone from east to west and that there is no aquitard separating the Pilliga Sandstone and overlying Orallo Formation. The refined conceptualisation suggests that these observed changes of hydrochemistry and environmental tracers are more likely to be controlled primarily by the lithological heterogeneity within the Pilliga Sandstone and the potential connectivity of the Pilliga Sandstone with the Orallo Formation.

Previous studies also suggested that there may be some connectivity between the shallower formations of the Gunnedah Basin and the Purlawaugh Formation and between the Purlawaugh Formation and the Pilliga Sandstone. This was attributed to the emplacement of a spatially extensive sill that has intruded into the shallow formations of the Gunnedah Basin. Although the depth of this intrusion is too deep (>500 m) to be captured by the AEM survey, the assessment of stratigraphic logs confirmed that this sill has been emplaced at various stratigraphic intervals within the Digby and Napperby formations and up to the base of the Purlawaugh Formation. Although thick sills are often considered a barrier to groundwater flow rather than a conduit, it is possible that alteration of the host rock and fracturing associated with the emplacement of this sill may have generated some connectivity pathways between these formations. On the other hand, most hydrochemical and isotopic parameters and the numerical transect modelling suggest that the upper part of the Purlawaugh Formation acts as an aquitard that effectively separates the Pilliga Sandstone from underlying formations.

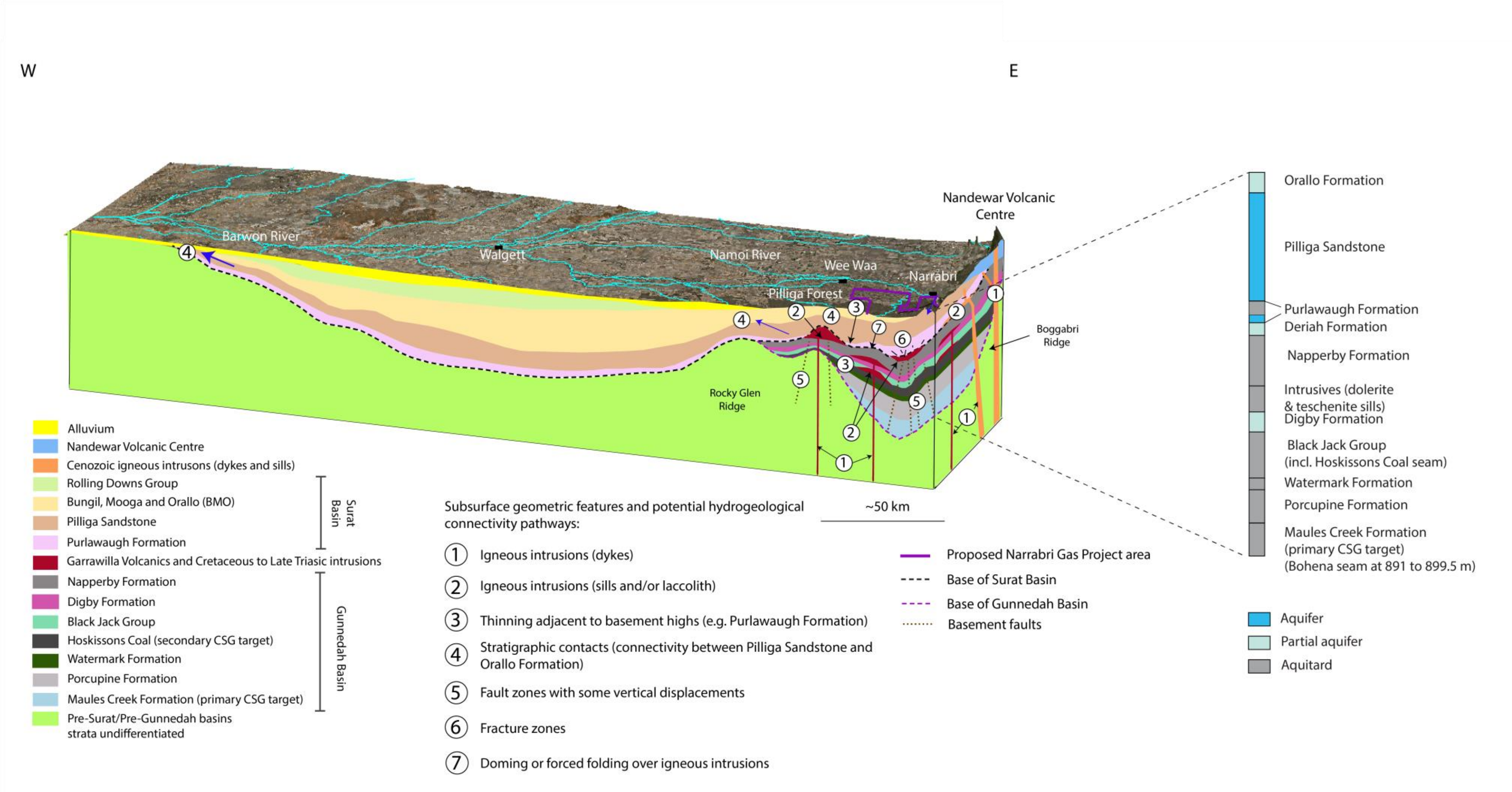

Figure 4-2 – Refined conceptual hydrogeological model and potential connectivity pathways in the wider Narrabri region.

4.4 Data worth analysis

As described in section 2.1 and 4.1 of this report, this study applied a wide array of different geoscientific techniques and they were integrated with existing data to enhance the understanding of aquifer geometry, potential connectivity between aquifers and the possible influence of structural controls on groundwater flow paths. With the project ending, we have conducted a retrospective assessment to determine which techniques were most effective in addressing region-specific key research questions answered in Section 4.1, reduce uncertainties and remove ambiguities identified in conceptual hydrogeological models in previous GISERA projects (e.g. Raiber et al., 2022a).

This assessment was carried out with a simple data worth analysis. Data worth analysis in hydrogeological and geoscientific investigations is traditionally used to assesses the potential impact of new data on improving the accuracy and reliability of geoscientific models (e.g. conceptual or numerical models), reducing the uncertainty of interpretations and optimising monitoring bore networks by analysing predictive uncertainty (e.g. Moore et al., 2011; Partington et al., 2020). This is important for decision-making in groundwater management, mineral or hydrocarbon exploration and development, and environmental monitoring, helping to determine whether investing in acquisition of new field or laboratory measurements or installing additional groundwater monitoring bores would likely result in a reduction of predictive uncertainties (Moore et al., 2011).

Data worth analysis can be quantitative or qualitative or a combination of both. Quantitative data worth analysis in hydrogeology involves numerical data to statistically evaluate and optimize model accuracy, focusing on measurable parameters such as groundwater levels and concentrations of hydrochemical parameters. It aims to reduce predictive uncertainty through statistical methods and model calibration.

Qualitative data worth analysis, on the other hand, uses descriptive information including both numerical or non-numerical information to understand contextual factors.

The reasons for conducting a qualitative data worth analysis rather than a quantitative data worth analysis in this study include:

- This study focussed on identifying and removing uncertainty in the conceptual hydrogeological models.
- The complexity of the geological setting (e.g. intrusions) is not represented by current groundwater numerical models.
- Although most data collected in this study are numerical, the wide array of different data types and techniques considered in this project (Table 12) would result in significant computational complexity.

For the data worth analysis, the ability of each technique to address key questions was assessed based on the following criteria:

- **N/A**: this technique did not address the key question

- ✓ = this technique provided limited information to address the key question
- ✓✓ = this technique provided valuable insights to address the key question and reduce uncertainty
- ✓✓✓ = this technique provided critical insights to address the key question, reduce uncertainty and resolve ambiguity

We also provide an indication of the relative cost of the different techniques based on the following criteria:

- **$** = requires limited operating investment (or in some cases can be achieved via sourcing of existing data) and time for planning, preparation, data processing and interpretation.
- **$$** = requires moderate operating investment and time for planning, preparation, data processing and interpretation.
- **$$$** = requires significant operating investment and time for planning, preparation, data processing and interpretation.

We provide a brief description of some of the key findings according to the different stages (column 2 in Table 12, corresponding to different stages/levels of the multi-disciplinary integrated workflow in the "hydrogeological pyramid" in Figure 2-1) below. It is important to note that all stages were iterative and that they were not necessarily conducted in sequential order.

Stage 1: geological and geophysical techniques applied in Stage 1 (Table 12) focussed on the characterisation of the geological framework in the wider Narrabri Gas Project area, including the geometry of the formations in the Surat and Gunnedah basins and the spatial distribution of igneous intrusive rocks. The outcomes of these techniques provided the foundation of the multi-disciplinary workflow (Figure 2-1), and they were essential in identifying where potential hydrogeological connectivity pathways within the Narrabri Gas Project area are likely to exist.

Evaluating existing geological and hydrogeological data and lithological and stratigraphic data does not incur significant operating costs, as it primarily relies on existing and publicly available data.

Airborne electromagnetic and seismic surveys are complementary geophysical techniques. Seismic surveys usually allow insights at depths below approximately 400 m depth, whereas AEM allows characterisation of the upper part of the subsurface (surface to a maximum of approximately 400 m below ground surface). Both techniques are relatively expensive, but they yield fundamentally important and spatially more continuous information than other techniques (which are mostly point information) and provided insights into many of the key questions of this study that no other technique could provide.

The AEM survey was rated higher in Table 12 as it directly addressed all key questions, whereas the seismic survey does not contribute to the understanding of some questions (e.g. the reasons for hydrochemical changes within the Pilliga Sandstone and broader implications for processes in the GAB).

Stage 2: techniques in this stage of the multi-disciplinary workflow focused on determining when intrusive activity occurred in the Narrabri Gas Project area and characterizing the internal heterogeneity within the Pilliga Sandstone and adjacent formations. K-Ar geochronological analysis, despite its low total rating, was crucial in understanding the timing of intrusive activity and potential hydrogeological connectivity pathways between coal seams and the Pilliga

Sandstone. Similarly, mineralogical analysis (XRD) was essential for understanding changes in hydrochemistry and environmental tracer patterns from east to northwest in the Narrabri Gas Project area and for providing valuable insights into hydrochemical evolution within the broader GAB.

Groundwater hydraulics, including petrophysical parameters and hydraulic heads, offered useful information for key questions and supported the numerical modelling of groundwater flow and age in Stage 5. However, point source information from groundwater monitoring bores in the Narrabri Gas Project area, including many nested bore sites, cannot fully eliminate ambiguity. Strontium isotopes are ideal tracers for assessing connectivity in other parts of the GAB (Raiber et al., 2024), but the mineralogical variability of the Pilliga Sandstone limits their effectiveness as connectivity indicators in this area.

Stage 3: hydrochemistry and environmental tracers were used to determine if plausible hydrogeological connectivity pathways identified in stages 1 and 2 of the multi-disciplinary workflow are likely to be actual connectivity pathways. While hydraulic data may sometimes be representative for smaller spatial areas, hydrochemistry and environmental tracers are effective regional integrators in sedimentary bedrock aquifers. Due to the strong contrast in values for many parameters between Pilliga Sandstone groundwaters and underlying formations, most hydrochemical and environmental tracer techniques provided useful information for some questions. However, few hydrochemical and environmental tracer parameters were able to remove ambiguity associated with some of the key questions such as whether the evolution of hydrochemistry from east to north-west is due to connectivity or processes within the Pilliga Sandstone. In this complex geological setting with widespread presence of igneous intrusions, stable noble gases (mantle helium estimated based on $^{3}He/^{4}He$ versus Ne/He ratios and ^{40}Ar) overall rated highest amongst the hydrochemical and environmental tracer parameters. This is due to their unique ability to detect the signature of intrusive activity in groundwaters within the Gunnedah Basin formations and the Purlawaugh Formation, and the absence of such a signal in most Pilliga Sandstone groundwaters.

Stage 4: during this stage of the workflow, existing conceptual models of potential connectivity pathways were further refined based on integration of all data from previous projects and data evaluated during stages 1 and 2. The integration of a wide array of data means that the development of conceptual hydrogeological model addresses all key questions and has the highest combined rating of all techniques applied in this study.

Stage 5: through integration of data from stages 1 to 3, numerical models of groundwater flow and age and inverse geochemical mixing models were developed to numerically test conceptual models of potential hydrogeological connectivity pathways (Stage 4). These models rated high on confirming the understanding of some of the key questions including those relating to the continuity of aquitards. However, the assessment also demonstrated that inverse geochemical mixing models, which are developed based on major and minor ion data and rock mineralogy but for example do not include stable noble gas results, can yield incorrect results when not all end members can be included in the mixing models due to a lack of suitable hydrochemical records.

Overall, the data worth analysis confirmed the benefits of integration of a wide array of different geoscientific data types, highlighting that all available information needs to be considered to avoid misinterpretations. Drilling new exploration wells to obtain rocks samples is very expensive, and the data worth analysis highlighted the benefits and cost-effectiveness of utilising samples in storage for further analyses. For example, the ability to collect existing core samples from the NSW core library at low cost and analyse their mineralogy and the age of intrusive rocks was invaluable for this project.

Additional data that may be collected to further reduce uncertainties on potential connectivity in the Narrabri Gas Project area are presented in the next section.

Table 12 Data worth analysis

Method	Stage/level in "Groundwater Pyramid" multi-disciplinary workflow (Figure 3-1)	Cost	Key tasks and questions: What is the spatial distribution of intrusions in the NGP?	When did intrusive activity occur in the Narrabri region?	Are intrusions hydrogeological connectivity pathways between Gunnedah and Surat basins?	Are faults connectivity pathways between Surat and Gunnedah basins in NGP area?	What are the reasons for observed changes of hydrochemistry and environmental tracers from east to the north-western part of the NGP area?	Is there hydrogeological connectivity at Plumb Road (Bohena anticline)?	Are there any implications of this study for flow dynamics and the assessment of aquifer connectivity in the wider Great Artesian Basin?	Are aquitards continuous and do they provide an effective seal?	Total count
Evaluating existing geological and hydrogeological data	1	$	✓✓	✓	✓	✓✓	✓	✓✓	✓	✓✓	12
Lithological and stratigraphic analysis	1	$	✓✓✓	✓✓	✓✓✓	✓	✓	✓✓✓	✓	✓	15
Airborne electromagnetic survey	1	$$$	✓✓	✓✓	✓✓✓	✓✓✓	✓✓✓	✓	✓✓✓	✓✓✓	21
Seismic surveys	1	$$$	✓✓	✓✓	✓✓	✓✓✓	✓	✓✓	N/A	✓✓✓	15
Total Magnetic Intensity	1	$ to $$$	✓✓✓	✓	✓	✓	✓	✓	N/A	N/A	8
K-Ar geochronological analysis	2	$	N/A	✓✓✓	✓✓	N/A	N/A	✓	✓	✓	8
Mineralogical analysis (XRD and thin sections)	2	$	N/A	N/A	✓	N/A	✓✓✓	✓	✓✓✓	✓	9
Groundwater hydraulics	2	$	N/A	N/A	✓	✓✓	✓	✓✓	✓	✓✓	9
Strontium isotopes rock and water	2	$	N/A	N/A	N/A	N/A	✓✓	✓	✓	✓✓	6
Groundwater salinity	3	$	N/A	N/A	✓✓	✓✓	✓	✓✓	✓✓	✓✓✓	12
Major and minor ion analysis	3	$	N/A	N/A	✓✓	✓✓	✓✓	✓✓	✓✓	✓✓✓	13

Method	Stage/level in "Groundwater Pyramid" multi-disciplinary workflow (Figure 3-1)	Cost	What is the spatial distribution of intrusions in the Narrabri Gas Project area?	When did intrusive activity occur in the Narrabri region?	Are intrusions hydrogeological connectivity pathways between Gunnedah and Surat basins?	Are faults connectivity pathways between Surat and Gunnedah basins in Narrabri GP area?	What are the reasons for observed changes of hydrochemistry and environmental tracer patterns from east to the north-western part of the Narrabri Gas Project area?	Is there hydrogeological connectivity at Plumb Road (Bohena anticline)?	Are there any implications of this study for flow dynamics and the assessment of aquifer connectivity in the wider Great Artesian Basin?	Are aquitards continuous and do they provide an effective seal?	Count
Methane concentrations	3	$	N/A	N/A	✓✓	✓✓	✓	✓✓	✓	✓✓✓	11
Methane isotopes	3	$	N/A	N/A	✓	✓	✓	✓✓	✓	✓✓	8
Multivariate statistical analysis	3	$	N/A	N/A	✓	✓✓	✓	✓	✓	✓✓	8
Young age tracers (e.g. ^{3}H and ^{85}Kr)	3	$$	N/A	N/A	✓	✓	✓✓	✓	✓✓	✓	8
Old age tracers (e.g. ^{14}C, ^{36}Cl, ^{81}Kr)	3	$$	N/A	N/A	✓✓✓	✓✓✓	✓	✓✓	✓✓✓	✓✓✓	15
Stable noble gas concentrations (^{4}He)	3	$$	N/A	N/A	✓✓✓	✓✓✓	✓	✓✓	✓✓✓	✓✓✓	15
Stable noble gas isotopes (Mantle helium $^{3}He/^{4}He$ and ^{40}Ar)	3	$$	✓	✓✓	✓✓✓	✓✓✓	✓✓✓	✓✓	✓✓✓	✓✓✓	20
Conceptual model development through integration of multiple lines of evidence	4	$ to $$$	✓✓	✓✓✓	✓✓✓	✓✓✓	✓✓✓	✓✓✓	✓✓✓	✓✓✓	23
Numerical modelling of groundwater flow and age	5	$$$	N/A	N/A	✓	✓✓✓	✓	✓✓✓	✓✓✓	✓✓✓	14
Geochemical mixing models	5	$ to $$	N/A	N/A	✓✓	✓✓	✓✓	✓✓✓	✓✓✓	✓✓	14

4.5 Limitations and opportunities for future work

The newly acquired data, compilation of existing data and knowledge and enhanced integration of multiple lines of evidence lead to an improved understanding of aquifer geometry, potential connectivity between aquifers and possible influence of structural controls on groundwater flow paths.

A suite of potential options for future work to further reduce uncertainties in the understanding of hydrogeological connectivity pathways include:

- At present, all baseline hydrochemistry data from the uppermost Gunnedah Basin formations are from the eastern part of the Narrabri Gas Project area. The collection of samples for hydrochemistry and environmental tracer suite from additional Water NSW Gunnedah Basin bores (e.g. Digby Formation at Plumb Road) that could not be sampled in this project due to issues with permanently installed pumps could help to further reduce uncertainties of geochemical mixing models.
- Sampling of new Santos bores (Napperby and Digby Formation) in the central part of the Narrabri Gas Project area and analyse them for a comprehensive suite of hydrochemistry and environmental tracers. This would provide valuable baseline data and reduce the uncertainty of mixing models.
- Further refinement of the AEM survey data: multiple realisations of AEM conductivity-depth sections are possible depending on criteria chosen during data processing and inversion. Further tests are currently undertaken, and the results will be reported in an updated version of this report.
- Use of tracer values for the direct simulation of the fate of groundwater age tracers: as a proof-of-concept for the joint simulation of groundwater flow and age, apparent groundwater ages were used in this study. Further efforts to use the actual tracer values of groundwater age tracers rather than apparent age tracers are currently underway and will be reported in parallel GISERA project “Groundwater modelling and predictive analysis to inform CSG impact assessment, monitoring and management” (GISERAW29).
- Including environmental tracers such as $^{87}Sr/^{86}Sr$ in geochemical mixing models.
- Expand on integration of seismic data with AEM survey data.
- Collect and analyse additional core data of Pilliga Sandstone in deeper parts of the Coonamble Embayment.
- Refine existing 3D geological models: the existing 3D geological models used for groundwater modelling in previous studies can be updated with new data to more accurately represent the subsurface structure in the Narrabri Gas Project area.
- Refine the lithological characterisation of the Purlawaugh Formation: the upper part of the Purlawaugh Formation is assumed to be an aquitard that limits connection between the Purlawaugh and shallow Gunnedah formations with the Pilliga Sandstone based on hydraulic and environmental tracer and numerical modelling. Development of a regional

sedimentary facies model of the Purlawaugh Formation could help to further confirm the characterisation of the Purlawaugh Formation as an aquifer (lower part) and aquitard (upper part).

- Close spatial data gaps: the study confirmed previous assessments that there is, at this stage, no evidence for significant connectivity in the south and east of the Narrabri Gas Project area based on baseline data from a relatively large number of groundwater observation bores (Figure 4-3). However, no groundwater observation bores are available in the central-western and north-western part of the Narrabri Gas Project area (Figure 4-3). Additional groundwater monitoring bore data in these areas could help to further reduce uncertainties of conceptual hydrogeological models.

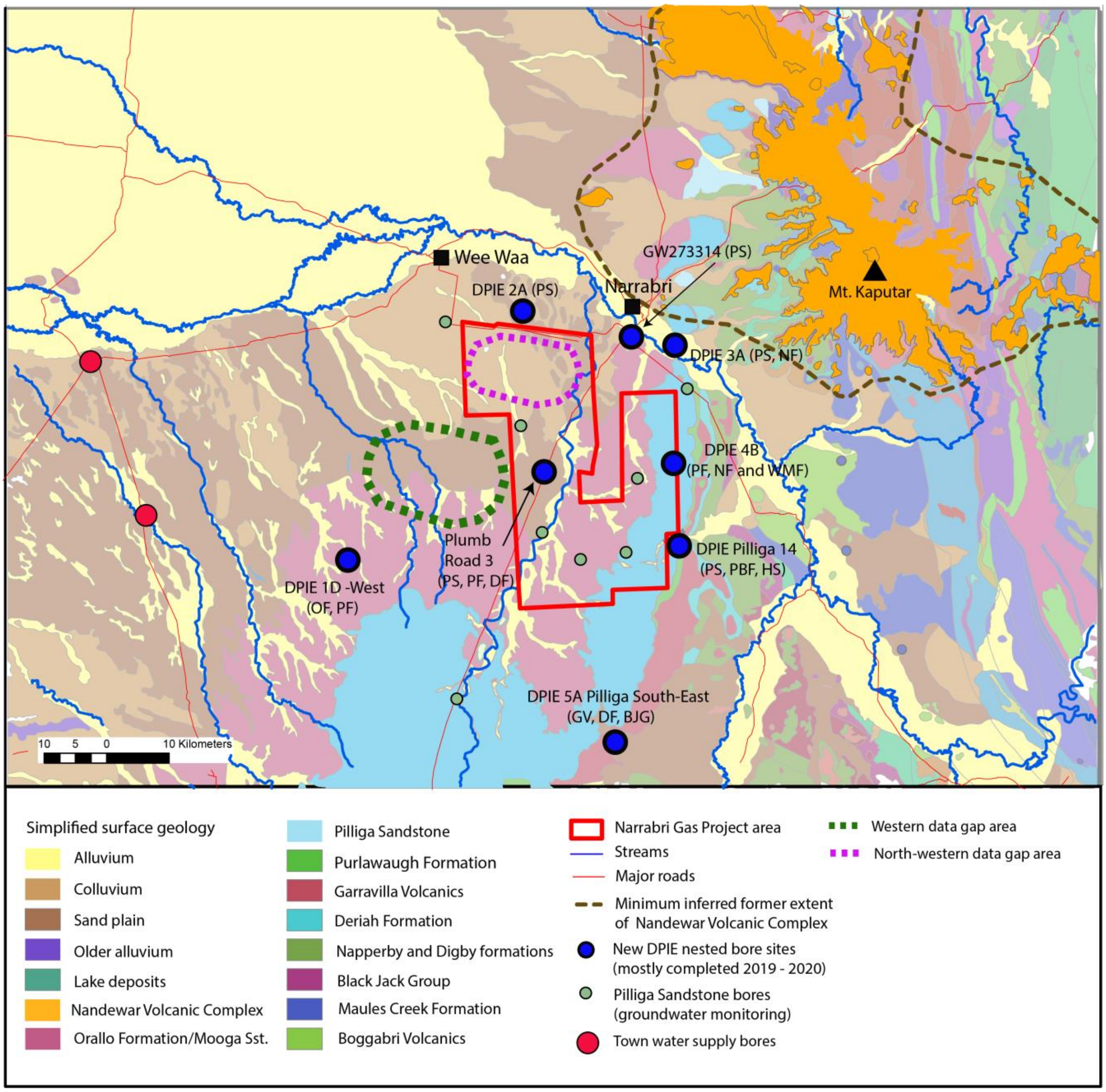

Figure 4-3 – Spatial data gaps within the Narrabri Gas Project area overlain on simplified surface geology.

5 Conclusions

The aim of this project was to address uncertainties and community concerns about the role of geological structures in aquifer inter-connectivity in the Narrabri region and to close on-going knowledge gaps on the role of faults and igneous intrusions (including their timing) as potential hydrogeological connectivity pathways.

The project applied a multi-disciplinary workflow including geochronological analysis, mineralogical and lithological assessments, an AEM survey, hydrochemistry and environmental tracer data collection, numerical modelling, and refinement of conceptual hydrogeological models through integration of all data to reduce uncertainties in the Narrabri Gas Project area.

Key findings include:

- **Geochronological assessment:** the geochronological (K-Ar) analyses in the Narrabri region aimed to determine the timing of intrusive activity within the Narrabri Gas Project area. The study identified multiple phases of intrusive activity during the Mesozoic and Cenozoic eras, with significant occurrences in the Late Triassic, Early and Middle Jurassic, and Cretaceous periods. A more recent Eocene intrusion (~50 million years ago) was also noted. These intrusions are linked to large-scale tectonic processes in eastern Australia, including subduction, rifting, and seafloor spreading.
- **Mineralogical and lithological assessment:** mineralogical and lithological assessments of the Surat and Gunnedah basins helped to refine the understanding of the spatial arrangement and connectivity of aquifer materials and aquitards. The study demonstrated that the Pilliga Sandstone has a more complex composition than previously thought, with significant mineralogical variations downgradient of the outcrop. Although some intrusions occurred after the deposition of the Pilliga Sandstone, none were identified in stratigraphic logs within the Pilliga Sandstone, possibly due to the absence of significant basement faults or the thermal properties of the sandstones which results in rapid heat loss and may prevent the emplacement of large intrusive bodies.
- **AEM survey:** the airborne electromagnetic (AEM) survey conducted by SkyTEM on behalf of CSIRO in November 2023 covered a large area with 2,765 km of survey lines and produced 60 east-west-oriented and one north-south-oriented conductivity-depth sections, with the longest east-west section approximately 80 km long. This survey aimed to map the subsurface structure to depths of approximately 400 m within the Narrabri Gas Project area. In the northern part of the survey area, a thick (>100 m) conductive cover composed of low permeability sediments limited the resolution of deeper formations. The eastern part showed thinner conductive cover with exposed bedrock formations and possible geological structures near the Nandewar Volcanic Centre to the north of the Narrabri Gas Project area. The Namoi River alluvium is distinguishable from surrounding older Cenozoic sediments by its lower conductivity. In the central part of the AEM survey

area, the conductive cover thinned, revealing a more resistive response from the Pilliga Sandstone. The survey confirmed significant variations in the Pilliga Sandstone's composition, with a resistive electromagnetic signature suggesting cleaner, sandy facies in the east and south and more conductive, finer-grained material in the west. No significant vertical displacements of conductive layers (Purlawaugh Formation) in the Surat Basin were observed, but low-amplitude folds likely related to large intrusions were identified in AEM, confirming seismic interpretations from previous studies. In the southern area, the conductive cover was minimal, enabling a clear identification of the interface between the Pilliga Sandstone and the Purlawaugh Formation. The survey indicated the presence of low-amplitude folds and possible igneous intrusions in this area. To the east of the Narrabri Gas Project area, the AEM survey suggests more significant deformation of Gunnedah Basin formations (which are outcropping or closer to the surface) near the Hunter-Mooki Thrust fault, a major tectonic boundary in eastern Australia.

- **Hydrochemistry and environmental tracers:** building on previous GISERA projects and other hydrogeological investigations, this project integrated existing and newly acquired hydrochemical and environmental tracer data. The collection of additional baseline data from the Gunnedah Basin formations in the eastern part of the Narrabri Gas Project area enhanced the understanding of inter-basin and inter-aquifer connectivity in the Narrabri Gas Project area. The study found a distinct contrast in connectivity indicators, such as salinity, methane concentrations, and groundwater age tracers, between the Gunnedah and Surat basins formations in most areas. The Pilliga Sandstone showed low salinity and young groundwater ages, while the Gunnedah Basin formations had higher values and contained generally very old groundwater marked low values of ^{36}Cl and high values of ^{4}He. High mantle helium ($^{3}He/^{4}He$) and ^{40}Ar levels in the Gunnedah Basin groundwater samples is attributed to widespread intrusions emplaced in these formations, contrasting with mostly low values in the Pilliga Sandstone, suggesting a high degree of hydrogeological separation between these systems.
- **Data integration through numerical modelling of groundwater flow and age patterns and geochemical mixing models:** Hydrochemistry and environmental tracers indicate a high degree of separation between the Pilliga Sandstone and underlying formations in the south and east of the Narrabri Gas Project area. However, a small degree of potential connectivity between the Pilliga Sandstone and underlying formations was hypothesized in previous studies at Plumb Road (Bohena anticline) and in the north-western part of the area. This study investigated these areas further using integration of geological, hydraulic, hydrogeological, hydrochemical, and geophysical data through numerical modelling and geochemical mixing models. At the Bohena anticline in the centre of the Narrabri Gas Project area, a thick sill intruded into the shallow Gunnedah Basin and Purlawaugh Formation, suggesting that some connectivity between these formations may be facilitated by the intrusion. Geochemical mixing models suggested that some mixing between the uppermost Gunnedah Basin formation and the Purlawaugh Formation can explain the patterns of hydrochemical evolution. The Pilliga Sandstone has a low salinity and a young groundwater age in this area, together with the numerical modelling indicating limited connectivity and suggesting that the upper part of the Purlawaugh Formation forms an effective aquitard in the area represented by the transect model. In the north-western part of the Narrabri Gas Project area, mineralogical analysis and AEM survey confirmed

significant changes in the Pilliga Sandstone's properties. Some hydrochemical parameters and geochemical mixing models suggested that an admixture from underlying formations to the Pilliga Sandstone is plausible, but mantle helium and ^{40}Ar data indicated limited mixing (<1%). The combined evidence from geophysics, mineralogical analyses and environmental tracers suggests that processes occurring within the Pilliga Sandstone and possibly connectivity with the overlying Orallo Formation may be the primary controls of the hydrochemical evolution observed from the eastern recharge beds towards the north-west.

- **Refined conceptual hydrogeological model:** the refined conceptual hydrogeological model confirmed that structural activity is more prevalent in the north and north-west of the Narrabri Gas Project area than in the south and east. Geochronological analyses showed that intrusions, although occurring from the Late Triassic to the Cenozoic, are mostly limited to the shallow Gunnedah Basin and up to the base of the Purlawaugh Formation. Seismic images and AEM conductivity-depth sections did not reveal significant faults in the Surat Basin strata within the Narrabri Gas Project area, whereas some shallow structures could be observed in conductivity-depth sections north and east of the Narrabri Gas Project area.
- **Data worth analysis:** a simple qualitative data worth analysis was conducted to determine which data types were most effective and cost-effective in answering the key research questions and provide lessons learned that are transferable to other regions.

This study represents one of the most comprehensive assessments of hydrogeological connectivity between aquifers of the Great Artesian Basin and underlying Permian-Triassic sedimentary basins such as the Gunnedah Basin. The results of this study provide new insights into the likelihood of presence or absence of different hydrogeological connectivity pathways within the Narrabri Gas Project area.

Although this research has resolved many knowledge gaps identified by previous GISERA projects and other hydrogeological investigations, some uncertainties remain. Future opportunities to reduce these uncertainties include collecting hydrochemistry and environmental tracer data from additional Gunnedah Basin bores in the central part of the Narrabri Gas Project area, sampling new Santos Gunnedah Basin bores for comprehensive analysis, and integrating seismic with AEM survey data. Refining the existing 3D geological models and lithological characterization of the Purlawaugh Formation could further confirm the role and spatial continuity of the upper part of the Purlawaugh Formation as an aquitard. Addressing spatial data gaps by adding groundwater monitoring bores in the central-western and north-western parts of the Narrabri Gas Project area could also reduce uncertainties in hydrogeological conceptual models.

6 References

Allen, D. (2019). Groundwater applications of towed TEM in diverse geology at farm scale. ASEG Extended Abstracts, 1, 1–4. DOI: 10.1080/22020586.2019.12073025

Arditto, P.A. (1982). Deposition and diagenesis of the Jurassic Pilliga Sandstone in the southeastern Surat Basin, New South Wales. Journal of the Geological Society of Australia, 29(1–2), 191–203.

Arditto, P.A. (1983). Mineral-groundwater interactions and the formation of authigenic kaolinite within the southeastern intake beds of the Great Australian (Artesian) Basin, New South Wales, Australia. Sedimentary Geology, 35(4), 249–261.

Auken, E., Christiansen, A.V., Jacobsen, B.H., Foged, N. and Sørensen, K.I. (2005). Piecewise 1D laterally constrained inversion of resistivity data. Geophysical Prospecting, 53: 497-506. https://doi.org/10.1111/j.1365-2478.2005.00486.x

Australian Museum (2018). Igneous intrusions. https://australian.museum/learn/minerals/shaping-earth/igneous-intrusions/

Ballentine, C.J., and Sherwood Lollar, B. (2002). Regional groundwater focusing of nitrogen and noble gases into the Hugoton-panhandle giant gas field, USA. Geochimica et Cosmochimica Acta66, no. 14: 2483–2497.

Banks, E., Smith, S., Hatch, M., Burk, L., Suckow, A. (2017). Sampling Dissolved Gases in Groundwater at in Situ Pressure: A Simple Method for Reducing Uncertainty in Hydrogeological Studies of Coal Seam Gas Exploration. Environmental Science & Technology Letters, Volume 4, 535-539

Banks, E.W., Hatch, M., Smith, S., Underschultz, J., Lamontagne, S., Suckow, A., Mallants, D. (2019). Multi-tracer and hydrogeophysical investigation of the hydraulic connectivity between coal seam gas formations, shallow groundwater and stream network in a faulted sedimentary basin, Journal of Hydrology, Volume 578, 124132, https://doi.org/10.1016/j.jhydrol.2019.124132.

Barnes, R.G., Dawson, M., Spiller, F.C.P. and McDonald, K.M. (2002). Interpreted and re-compiled geology of the Brigalow Belt South Bioregion – digital data set. NSW Department of Mineral Resources, for NSW Resource and Conservation Assessment Council.

Baxter-Crawford, H. (2018). Intrusions in the Sydney Basin with reference to the Greenacre Dyke. Australian Geomechanics Journal Volume 53, Number 2. 12 pages.

Bense, V.F., Gleeson, T., Loveless, S.E., Bour, O. and Scibek, J. (2013). Fault zone hydrogeology. Earth-Science Reviews, 127, 171–192. https://doi.org/10.1016/j.earscirev.2013.09.008

Bernard, B.B., Brooks, J.M. and Sackett, W.M. (1978). Light hydrocarbons in recent Texas continental shelf and slope sediments. Journal of Geophysical Research, 83(C8), 4053–4061.

Bioregional Assessment Programme (2016) Namoi hydraulic conductivity measurements. Bioregional Assessment Source Dataset. http://data.bioregionalassessments.gov.au/dataset/5f88517d-8154-411d-907f-4e2c2d12a912.

Bradley J. (1989). Laccolith. In: Petrology. Encyclopedia of Earth Science. Boston: Springer. https://doi.org/10.1007/0-387-30845-8_113

Bredehoeft, J. (2005) The conceptualization model problem – surprise. Hydrogeology Journal 13, 37-46.

Bretherton, T. and Delbaere, M. (1994). Coonarah-1 well completion report. Petroleum Securities PTY Limited, https://search.geoscience.nsw.gov.au/report/R00006641

Bull, K.F., Troedson, A.L., Bodorkos, S., Blevina, P.L., Bruce, M.C. and K. Waltenberg (2021). Warrumbungle Volcano: facies architecture and evolution of a complex shield volcano. Australian Journal of Earth Sciences, 68(2), 149–187. https://doi.org/10.1080/08120099.2020.1764622

Bunny, M.R. and Weber, C.R. (1996). Something old, something new. Recent coalbed methane exploration in the Gunnedah Basin. In: R.L Boyd and G.A MacKenzie (eds), Proceedings of the 30th Newcastle Symposium, Advances in the Study of the Sydney Basin, Newcastle: The University of Newcastle, 1–8.

Cartwright, I., Weaver, T.R., Fulton, S., Nichol, C., Reid, M. and Cheng, X. (2004). Hydrogeochemical and isotopic constraints on the origins of dryland salinity, Murray Basin, Victoria, Australia. Applied Geochemistry, 19(8), 1233–1254. DOI: 10.1016/j.apgeochem.2003.12.006

Cartwright, J., Huuse, M. and Aplin, A. (2007). Seal bypass systems. American Association of Petroleum Geologists Bulletin, 91(8), 1141–1166.

Cartwright, I., Currell, M.J., Cendón, D.I., Meredith, K.T., 2020. A review of the use of radiocarbon to estimate groundwater residence times in semi-arid and arid areas. Journal of Hydrology 580, 124247. doi.org/https://doi.org/10.1016/j.jhydrol.2019.124247.

Carty, C.J. and Smith, B.C. (2003). 2001 Bundock Creek seismic survey report. Survey report GS 2003/293. Eastern Star Gas. https://search.geoscience.nsw.gov.au/report/R00048232

Carty, C.J. and Smith, B.C. (2004). 2002 Pilliga East seismic survey report. Eastern Star Gas, survey report GS 2003/296. https://search.geoscience.nsw.gov.au/report/R00029410

CDM Smith (2016). Santos Narrabri Gas Project groundwater impact assessment. Subiaco, Western Australia: Santos.

Christiansen AV and Auken E (2012) ‘A global measure for depth of investigation’, Geophysics, 77(4):WB171–WB177.

Christophersen, N. and Hooper, R.P. (1992). Multivariate analysis of stream water chemical data: the use of principal components analysis for the end-member mixing problem. Water Resources Research, 28(1), 99–107.

Clark, I. and Fritz, P. (1997). Environmental isotopes in hydrogeology. New York: Lewis Publishers.

Cloutier, V., Lefebvre, R., Therrien, R. and Savard, M.M. (2008). Multivariate statistical analysis of geochemical data as indicative of the hydrogeochemical evolution of groundwater in a sedimentary rock aquifer system. Journal of Hydrology, 353, 294–313. DOI: 10.1016/j.jhydrol.2008.02.015

Cole, J.J. and Prairie, Y.T. (2014). Dissolved CO_2 in freshwater systems. Reference Module in Earth Systems and Environmental Sciences, Elsevier. https://doi.org/10.1016/B978-0-12-409548-9.09399-4

Cook, P.G. and Böhlke, J-K. (1999). Determining timescales for groundwater flow and solute transport. In: Cook, P.G. and Herczeg, A.L. (eds), Environmental tracers in subsurface hydrology, Boston: Kluwer Academic Press, 1–30.

Cozzarelli, I.M., Kent, D.B., Briggs, M., Engle, M.A., Benthem, A., Skalak, K.J., Mumford, A.C., Jaeschke, J., Farag, A., Lane, J.W., Akob, D.W. (2021). Geochemical and geophysical indicators of oil and gas wastewater can trace potential exposure pathways following releases to surface waters, Science of The Total Environment, Volume 755, Part 1, ISSN 0048-9697, https://doi.org/10.1016/j.scitotenv.2020.142909.

Cresswell, R.G. (2014), Groundwater geochemistry of the Narrabri Gas Project area. Sinclair Knight Merz Pty Ltd (Jacobs).

Crosbie, R.S., Morrow, D., Cresswell, R.G., Leaney, F.W., Lamontagne, S. and Lefournour, M. (2012). New insights into the chemical and isotopic composition of rainfall across Australia. Australia: CSIRO Water for a Healthy Country Flagship.

Crosbie, R., Raiber, M., Wilkins, A., Dawes, W., Louth-Robins, T., Gao, L. (2022). Quantifying diffuse recharge to groundwater systems of the Great Artesian Basin, the NSW coalfields and surrounds. Australia: CSIRO; CSIRO:EP2022-2355. https://doi.org/10.25919/fwyj-cp80

Currell, M., Banfield, D., Cartwright, I. and Cendón, D.I. (2017). Geochemical indicators of the origins and evolution of methane in groundwater: Gippsland Basin, Australia. Environ Sci Pollut Res 24, 13168–13183. https://doi.org/10.1007/s11356-016-7290-0

Darrah, T.H., Vengosh, A., Jackson, R.B., Warner, N.R., and Poreda, R.J. (2014). Noble gases identify the mechanisms of fugitive gas contamination in drinking-water wells overlying the Marcellus and Barnett Shales. PNAS, 111(39), 14076–14081.

Darrah, T.H., Jackson, R.B., Vengosh, A., Warner, N.R., Whyte, C.J., Walsh, T.B., Kondash, A.J. and Poreda, R.J. (2015). The evolution of Devonian hydrocarbon gases in shallow aquifers of the northern Appalachian Basin: Insights from integrating noble gas and hydrocarbon geochemistry. Geochimica et Cosmochimica Acta170: 321–355.

Daughney, C.J., Morgenstern, U., van der Raaij, R. and Reeves, R.R. (2010). Discriminant analysis for estimation of groundwater age from hydrochemistry and well construction: application to New Zealand aquifers. Hydrogeology Journal, 18(2), 417–428. DOI: 10.1007/s10040-009-0479-2

Dickin, A.P. (2005). K–Ar and Ar–Ar dating. In: Radiogenic Isotope Geology. Cambridge University Press, 254-290.

Donaldson, C.H., Reavy, R.J. and O'Mahony, M.J. (2003). Plutonic geology. In: Meyers, R.A. (ed.), Encyclopedia of physical science and technology (third edition), Academic Press, 491–508. https://doi.org/10.1016/B0-12-227410-5/00588-3

Drymoni, K., Browning, J. and Gudmundsson, A. (2021). Volcanotectonic interactions between inclined sheets, dykes, and faults at the Santorini Volcano, Greece, Journal of Volcanology and Geothermal Research, Volume 416, 107294, https://doi.org/10.1016/j.jvolgeores.2021.107294.

Eastern Star Gas (2004). 2004 Dampier seismic survey report, PEL 238, Gunnedah Basin, New South Wales. https://search.geoscience.nsw.gov.au/report/RE0001563

Eastern Star Gas (2009). Dewhurst 10 well completion report. https://search.geoscience.nsw.gov.au/report/RE0000664

Eastern Star Gas (2010). Baradine Creek 1 well completion report, PEL 234. https://search.geoscience.nsw.gov.au/api/download/b0f4a9813d9e3996df41358482389f70/Baradine_Creek_1_Well_Completion_Report.pdf

Eastern Star Gas (2011a). 2008 Dewhurst seismic survey overview report, PEL 238, PAL 2, Gunnedah Basin, New South Wales. https://search.geoscience.nsw.gov.au/api/download/d1d979bd641f83128c6ece0dafb3b184/2008_Dewhurst_Seismic_Survey_Overview_Report.pdf

Eastern Star Gas (2011b). Dewhurst 11, Well Completion Report. https://search.geoscience.nsw.gov.au/report/RE0000617

Eichinger, L. (1983). *A Contribution to the Interpretation of 14C Groundwater Ages Considering the Example of a Partially Confined Sandstone Aquifer*. Radiocarbon, 25(2), 347–356.

Emerson, D. and Wang, Y. (1997). 'Effects of water salinity and saturation on the electrical resistivity of clays', ASEG Preview, CSIRO Publishing 68, 19–24.

Enemark, T., Peeters, L., Mallants, D. and Batelaan, O. (2019). Hydrogeological conceptual model building and testing: A review. Journal of Hydrology, Volume 569, Pages 310-329, https://doi.org/10.1016/j.jhydrol.2018.12.007.

Evans, W.C. (1969). *Carbon-14 dating of groundwater in carbonate aquifers*. Journal of Hydrology, 9(1), 1–14.

Eymold, W.K., Swana, K., Moore, M.T., Whyte, C.J., Harkness, J.S., Talma, S., Murray, R., Moortgat, J.B., Miller, J., Vengosh, A. and Darrah, T.H. (2018). Hydrocarbon-Rich Groundwater above Shale-Gas Formations: A Karoo Basin Case Study. Groundwater, 56: 204-224. https://doi.org/10.1111/gwat.12637

Faiz, M.M., Saghafi, A., Barclay, S.A., Stalker, L., Sherwood, N.R., Whitford, D.J. (2007a). Evaluating geological sequestration of CO2 in bituminous coals: The southern Sydney Basin, Australia as a natural analogue. International Journal of Greenhouse Gas Control, Volume 1, Issue 2, 223-235, https://doi.org/10.1016/S1750-5836(07)00026-6.

Faiz, M.M., Saghafi, A., Sherwood, N. and Wang, I. (2007b). The influence of petrological properties and burial history on coal seam methane reservoir characterisation, Sydney Basin, Australia, International Journal of Coal Geology, Volume 70, Issues 1–3, 193-208, https://doi.org/10.1016/j.coal.2006.02.012.

Faiz, M., Zoitsas, A., Altmann, C., Baruch, E. and Close, D. (2020). Compositional variations and carbon isotope reversal in coal and shale gas reservoirs of the Bowen and Beetaloo basins, Australia. Geological Society, London, Special Publications 484(1), 51-70.

Farnham, I.M., Singh, A.S., Stetzenbach, K.J. and Johannesson, K.H. (2002). Treatment of nondetects in multivariate analysis of groundwater geochemistry data. Chemometrics and Intelligent Laboratory Systems, 60, 265–281. DOI: 10.1016/S0169-7439(01)00201-5

Feitz, A., Ransley, T., Hodgkinson, J., Preda, M., Dunsmore, D., McKillop, J., Spulak, R., Dixon, O., Kuske, T., Draper, J. (2014). GA-GSQ Hydrochemistry Dataset (2009–2011), GEOCAT No. 78549, Geoscience Australia, Canberra, Australia

Fifield, L. K., T. R. Ophel, J. R. Bird, G. E. Calf, G. B. Allison, and A. R. Chivas (1987). The chlorine-36 measurement program at the Australian National University, Nucl. Instrum. Methods Phys. Res., Sect B, 29, 114-119.

Fink, D., Hotchkis, M., Hua, Q., Jacobsen, G., Smith, A. M., Zoppi, U., Child, D., Mifsud, C., van der Gaast, H., Williams, A., and Williams, M. (2004). The ANTARES AMS facility at ANSTO, Nucl. Instrum. Meth. B, 223–224, 109–115, 2004.

Fontes, J. C., & Garnier, J. M. (1979). Determination of the initial 14C activity of the total dissolved carbon: A review of the existing models and a new approach. *Water resources research*, *15*(2), 399-413.

Frery, E., Byrne, C., Crosbie, R., Deslandes, A., Evans, T., Gerber, C., Huddlestone-Holmes, C., Markov, J., Martinez, J., Raiber, M., Turnadge, C., Suckow, A. and Wilske, C. (2022). Fault-Related Fluid Flow Implications for Unconventional Hydrocarbon Development, Beetaloo Sub-Basin (Northern Territory, Australia). Geosciences, 12(1):37. https://doi.org/10.3390/geosciences12010037

FrogTech (2013). OZ SEEBASE products. Viewed 27 November 2013, www.frogtech.com.au/products/oz-seebase

Fulignati, P. (2020). Clay Minerals in Hydrothermal Systems. Minerals, 10(10), 919. https://doi.org/10.3390/min10100919

Gemeiner, H., Teramoto, E.H., Veroslavsky, G., Chang, H.K. (2025). Using dissolved noble gases to characterize the groundwaters of the Southern Portion of the Guarani Aquifer System at the Brazil-Uruguay Border Region, Science of The Total Environment, Volume 966, 178690, https://doi.org/10.1016/j.scitotenv.2025.178690.

Geological Survey of New South Wales (2019). DIGS® (Digital Imaging Geological System). Viewed August 2019, https://search.geoscience.nsw.gov.au/

Geological Survey of New South Wales (2024). DIGS® (Digital Imaging Geological System). Viewed July 2024, https://search.geoscience.nsw.gov.au/

Geoscience Australia (2011). 1 second SRTM digital elevation model (DEM). Canberra: Geoscience Australia.

Geoscience Australia (2012). Surface geology of Australia 1:1 million scale dataset 2012 edition. Canberra: Geoscience Australia.

Geoscience Australia (2013). Geoscience Australia Stratigraphic Units Database. Canberra: Geoscience Australia.

Geoscience Australia (2021a). Stratigraphic unit database. Canberra: Geoscience Australia. Viewed 10 September 2021, https://asud.ga.gov.au/

Geoscience Australia (2025a). Palaeogeographic Atlas. Canberra, viewed April 2025. https://www.ga.gov.au/static/palaeo/palaeo.html

Geoscience Australia (2025b). Stratigraphic unit database. Canberra: Geoscience Australia. Viewed 10 January 2025, https://asud.ga.gov.au/

Gibson, D, 2007. Potassium-Argon Ages of Late Mesozoic and Cainozoic Igneous Rocks of Eastern Australia. CRC LEME Open File Report 193. pp 53.

Golding, S.D., Boreham, C.J. and Esterle, J.S. (2013). Stable isotope geochemistry of coal bed and shale gas and related production waters – a review. International Journal of Coal Geology, 120, 24–40.

Goode, D. J. (1996), Direct Simulation of Groundwater Age, *Water Resour. Res.*, 32(2), 289–296, doi:10.1029/95WR03401.

Green, A. and Lane, R. (2003) 'Estimating Noise Levels in AEM Data', ASEG Extended Abstracts, 2003(2):1, doi:10.1071/ASEG2003ab093.

Güler, C., Thyne, G.D., McCray, J.E. and Turner, K.A. (2002). Evaluation of graphical and multivariate statistical methods for classification of water chemistry data. Hydrogeology Journal, 10(4), 455–474. DOI: 10.1007/s10040-002-0196-6

Guggenmos, M.R., Daughney, C.J., Jackson, B.M. and Morgenstern, U. (2011). Regional-scale identification of groundwater–surface water interaction using hydrochemistry and multivariate statistical methods, Wairarapa Valley, New Zealand. Hydrology and Earth System Sciences, 15, 3383–3398. DOI:10.5194/hess-15-3383-2011

Gurba, L.W. and Weber, C.R. (2001). Effects of igneous intrusions on coalbed methane potential, Gunnedah Basin, Australia. International Journal of Coal Geology, 46(2–4), 113-131. https://doi.org/10.1016/S0166-5162(01)00020-9

Harbaugh, A.W. (2005). MODFLOW-2005, the U.S. Geological Survey modular ground water model – the Ground-Water Flow Process: U.S. Geological Survey Techniques and Methods 6-A16.

Harkness, J.S., Darrah, T.H., Warner, N.R., Whyte, C.J., Moore, M.T., Millot, R., Kloppmann, W., Jackson, R.B. and Vengosh, A. (2017). The geochemistry of naturally occurring methane and saline groundwater in an area of unconventional shale gas development, Geochimica et Cosmochimica Acta, Volume 208, Pages 302-334, https://doi.org/10.1016/j.gca.2017.03.039.

Helsel, D.R. and Hirsch, R.M. (2002). Statistical methods in water resources. Techniques of water-resources investigations of the U.S. Geological Survey. Book 4, Hydrologic analysis and interpretation, 524 pp.

Herr, A., Brandon, C., Beringen, H., Merrin, L.E., Post, D.A., Mitchell P, Crosbie R, Aryal SK, Janardhanan S, Schmidt RK and Henderson BL (2018) Assessing impacts of coal resource development on water resources in the Namoi subregion: key findings. Product 5: Outcome synthesis for the Namoi subregion from the Northern Inland Catchments Bioregional Assessment. Department of the Environment and Energy, Bureau of Meteorology, CSIRO and Geoscience Australia, Australia. http://data.bioregionalassessments.gov.au/product/NIC/NAM/5.

Hollins, S.E., Hughes, C.E., Crawford, J., Cendón, D.I., Meredith, K.T. (2018). Rainfall isotope variations over the Australian continent – Implications for hydrology and isoscape applications. Science of The Total Environment, Volume 645, Pages 630-645, https://doi.org/10.1016/j.scitotenv.2018.07.082

IAEA (1981). *Isotopic Discrimination and Correction Factors in Radiocarbon Dating*. In: Proceedings of the Symposium on Radiocarbon Dating, IAEA, Vienna, 241–295.

IESC (Independent Expert Scientific Committee on Coal Seam Gas and Large Coal Mining Development) (2017). Advice to decision maker on coal seam gas project – 2017-086: Narrabri Gas Project – EPBC 2014/7376. Australian Government and NSW, 20 pp.

InGauge (2017). Water Monitoring Bore Construction Plumb Road Narrabri. Well Completion Report Plumb Road 1, 2 & 3. 225 pages.

Isles, D.J and Rankin, L.R. (2013). Geological interpretation of aeromagnetic data. The Australian Society of Exploration Geophysicists, 365 pp.

Iverach, C.P., Cendón, D.I., Meredith, K.T., Wilcken, K.M., Hankin, S.I., Andersen, M.S. and Kelly, B.F.J. (2017). A multi-tracer approach to constraining artesian groundwater discharge into an alluvial aquifer. Hydrology and Earth System Sciences, 21(11), 5953–5969.

Iverach, C.P., Cendón, D.I., Beckmann, S., Hankin, S.I., Manefield, M. and Kelly, B.F.J. (2020a). Constraining source attribution of methane in an alluvial aquifer with multiple recharge pathways. Science of The Total Environment, 703, 134927. https://doi.org/10.1016/j.scitotenv.2019.134927

Iverach, C.P., Bold, T.A., O'Neill, C. and Hocking, M. (2020b). Geochemical interpretations of groundwater processes and methane origin, Onshore Otway Basin, Victoria. Victorian Gas Program Technical report 25. Geological Survey of Victoria, catalogue record 161773. Melbourne: Department of Jobs, Precincts and Regions, 72 pp.

Jackson, R.E., Gorody, A.W., Mayer, B., Ryan, M.C. and Van Stempvoort, D.R. (2013). Groundwater protection and unconventional gas extraction: the critical need for field-based hydrogeological research. Groundwater, 51 (4), 488–510.

Jackson, M., Konter, J. & Becker, T. (2017). Primordial helium entrained by the hottest mantle plumes. Nature 542, 340–343. https://doi.org/10.1038/nature21023

Janardhanan, S., Crosbie, R., Pickett, T., Cui, T., Peeters, L., Slatter, E., Northey, J., Merrin, L.E., Davies, P., Miotlinski, K., Schmid, W. and Herr, A. (2018). Groundwater numerical modelling for the Namoi subregion. Product 2.6.2 for the Namoi subregion from the Northern Inland Catchments Bioregional Assessment. Department of the Environment and Energy, Bureau of Meteorology, CSIRO and Geoscience Australia, Australia. http://data.bioregionalassessments.gov.au/product/NIC/NAM/2.6.2.

Kelley, S. (2002). K-Ar and Ar-Ar Dating. Reviews in Mineralogy and Geochemistry; 47 (1): 785–818. doi: https://doi.org/10.2138/rmg.2002.47.17

Kelly, B. F. J., W. Timms, T. J. Ralph, B. M. S. Giambastiani, A. Comunian, A. M. McCallum, M. S. Andersen, R. S. Blakers, R. I. Acworth, and A. Baker. (2014). A Reassessment of the Lower Namoi Catchment Aquifer Architecture and Hydraulic Connectivity with Reference to Climate Drivers. Australian Journal of Earth Sciences 61 (3): 501–11. doi:10.1080/08120099.2014.900647.

Korsch, R.J. and Totterdell, J.M. (2009). Subsidence history and basin phases of the Bowen, Gunnedah and Surat basins, eastern Australia. Australian Journal of Earth Sciences, 56(3), 335–353. DOI: 10.1080/08120090802698687

Lamontagne, S., Taylor, A.R., Batlle-Aguilar, J., Suckow, A., Cook, P.G., Smith, S.D., Morgenstern, U., Stewart, M.K. (2015). River infiltration to a subtropical alluvial aquifer inferred using multiple environmental tracers. Water Resources Research, 51, 4532-4549.

Lane, R. (2000). Conductive unit parameters: summarising complex conductivity distributions. 70th Meeting, SEG, Calgary, Expanded Abstracts, Volume 1, Section EM 4.2, p. 328-331.

Lane R. (2002). Ground and Airborne Electromagnetic methods. In Geophysical and Remote Sensing Methods for Regolith Exploration. (Ed É Papp) pp. 53-79. CRC LEME Open File Report 144. CRC LEME, Perth.

Lane, R and Pracilio, G, 2000. Visualisation of Sub-Surface Conductivity Derived From Airborne EM. SAGEEP 2000 Conference Proceedings

Levenberg, K. (1944). A method for the solution of certain non-linear problems in least squares. Quarterly of Applied Mathematics, 2(2), 164–168. http://www.jstor.org/stable/43633451

Liu, J., G. Fu, X. Song, S. P. Charles, Y. Zhang, D. Han, and S. Wang (2010). Stable isotopic compositions in Australian precipitation, J. Geophys. Res., 115, D23307, doi:10.1029/2010JD014403.

Luo, H., Karki, B.B, Ghosh, D.B. and Bao, H. (2021). Diffusional fractionation of helium isotopes in silicate melts. Geochemical Perspectives Letters, 19, 19–22.

Magee, C. (2024). Fractures and faults across intrusion-induced forced folds: a georesource perspective. Geological Society, London, Special Publications, Volume 547, Pages 109 – 129, https://doi.org/10.1144/SP547-2023-47

Mahara, Y., Habermehl, M.A., Hasegawa, T., Nakata, K., Ransley, T.R., Hatano, T., Mizuochi, Y., Kobayashi, H., Ninomiya, A., Senior, B.R., Yasuda, H. and Ohta, T. (2009), Groundwater dating by estimation of groundwater flow velocity and dissolved ^{4}He accumulation rate calibrated by ^{36}Cl in the Great Artesian Basin, Australia. Earth and Planetary Science Letters, 287(1–2), 43–56.

Mallants, D., Raiber, M. and Davis, P. (2016). Decision support system for investigating gas in water bores and links to coal seam gas development. Report prepared by CSIRO for the Queensland Department of Natural Resources and Mines. PDF available from http://bit.ly/2qV5deA

Mallants, D., Underschultz, J. and Simmons, C.T. (eds) (2018). Integrated analysis of hydrochemical, geophysical, hydraulic and structural geology data to improve characterisation and conceptualisation of faults for use in regional groundwater flow models. CSIRO in collaboration with University of Queensland and Flinders University of South Australia.

Mark, N. J., Schofield, N., Watson, D.A., Holford, S., Pugliese, S. and Muirhead, D. (2024). The Impact of Igneous Intrusions on Sedimentary Host Rocks: Insights From Field Outcrop and Subsurface Data. Petroleum Geoscience 30, no. 1: petgeo2022-086. https://doi.org/10.1144/petgeo2022-086

Marquardt, D. W. (1963). An Algorithm for Least-Squares Estimation of Nonlinear Parameters. Journal of the Society for Industrial and Applied Mathematics, 11(2), 431–441. http://www.jstor.org/stable/2098941

McDougall, I. (1990). Potassium—argon dating in archaeology. Science Progress (1933-), 74(1 (293)), 15–30. http://www.jstor.org/stable/43423874

McDougall, I., and Harrison, T.M. (1999). Geochronology and thermochronology by the $^{40}Ar/^{39}Ar$ method: New York, Oxford University Press, xii, 269 p.

McIntosh, J.C., Hendry, M.J., Ballentine, C., Haszeldine, R.S., Mayer, B., Etiope, G., Elsner, M., Darrah, T.H., Prinzhofer, A., Osborn, S., Stalker, L., Kuloyo, O., Lu, Z.T., Martini, A. and Sherwood Lollar, B. (2019). A Critical Review of State-of-the-Art and Emerging Approaches to Identify Fracking-Derived Gases and Associated Contaminants in Aquifers. Environmental Science & Technology 53 (3), 1063-1077. DOI: 10.1021/acs.est.8b05807

McNeill, J. D. (1980). Electromagnetic Terrain Conductivity Measurement at Low Induction Numbers. Geonics Ltd., Technical Note TN-6.

McNutt R.H. (2000). Strontium isotopes, in Environmental Tracers in Subsurface Geology, ed. by P.G. Cook & A.L. Herczeg, pp. 234-260. Environmental tracers in subsurface hydrology. Kluwer, Boston.

Menand, T., Daniels, K.A., and Benghiat, P. (2010). Dyke propagation and sill formation in a compressive tectonic environment, Journal of Geophysical Research, 115, B08201. DOI: 10.1029/2009JB006791

Menció, A. and Mas-Pla, J. (2008). Assessment by multivariate analysis of groundwater–surface water interactions in urbanized Mediterranean streams. Journal of Hydrology, 352, 355–366. DOI: 10.1016/j.jhydrol.2008.01.014

Milkov, A.V. and Etiope, G. (2018). Revised genetic diagrams for natural gases based on a global dataset of >20,000 samples. Organic Geochemistry, Volume 125, Pages 109-120, https://doi.org/10.1016/j.orggeochem.2018.09.002.

Minsley, B.J., Rigby, J.R., James, S.R. et al. (2021). Airborne geophysical surveys of the lower Mississippi Valley demonstrate system-scale mapping of subsurface architecture. Commun Earth Environ 2, 131. https://doi.org/10.1038/s43247-021-00200-z

Minty, B.R.S and Poudjom Djomani, Y. (2019). Total magnetic intensity (TMI) grid of Australia 2019 – seventh edition – 40 m cell size. Canberra: Geoscience Australia. https://ecat.ga.gov.au/geonetwork/srv/api/records/7c38a2b2-28e4-4c79-b0ce-517d9861e20d

Moore, C.R., Woehling, T. and Wolf, L. (2011). Optimisation of monitoring data for increased predictive reliability of regional water allocation models. 19th International Congress on Modelling and Simulation, Perth, Australia.

Moore, M.T., Vinson, D.S., Whyte, C.J., Eymold, W.K., Walsh, T.B. and Darrah, T.H. (2018). Differentiating between biogenic and thermogenic sources of natural gas in coal bed methane reservoirs from the Illinois Basin using noble gas and hydrocarbon geochemistry. In From Source to Seep: Geochemical Applications in Hydrocarbon Systems, ed. M. Lawson, M. J. Formolo, and J. M. Eiler. London, UK: Geological Society of London, Special Publication no. 468.

Morrison, W.K. and Harris, R.I. (1988). Nyora no. 1 well completion report. Consolidated Petroleum Australia N.L., Australian Gas Light Company, Peko Oil Limited. Geological Survey of New South Wales WCR226. https://search.geoscience.nsw.gov.au/report/R00017086

Müller, R. D., Seton, M., Zahirovic, S., Williams, S. E., Matthews, K. J., Wright, N. M., et al. (2016). Ocean basin evolution and global-scale plate reorganization events since Pangea breakup. Annual Review of Earth and Planetary Sciences, 44(1), 107–138. https://doi.org/10.1146/annurev-earth-060115-012211

Müller, R. D., Zahirovic, S., Williams, S. E., Cannon, J., Seton, M., Bower, D. J.& Gurnis, M. (2019). A global plate model including lithospheric deformation along major rifts and orogens since the Triassic. Tectonics, 38(6), 1884-1907.

Murray, T.A. and Power, W.L. (2021a). Information guidelines explanatory note: characterisation and modelling of geological fault zones. Report prepared for the Independent Expert Scientific Committee on Coal Seam Gas and Large Coal Mining Development through the Department of Agriculture, Water and the Environment, Commonwealth of Australia 2021.

Murray, T.A. and Power, W.L. (2021b). A framework for inclusion of faults in coal seam gas risk assessments. The APPEA Journal 61, 695-698.

Narrabri Courier (2023). CSIRO Narrabri airborne electromagnetic survey. Published on 7th of November 2023. https://narrabricourier.com.au/2023/11/07/csiro-narrabri-airborne-electromagnetic-survey/

Neumann, T. (2012). Fundamentals of aquatic chemistry relevant to radionuclide behaviour in the environment. In: Poinssot, C and Geckeis, H. (eds), Radionuclide behaviour in the natural environment, Woodhead Publishing Series in Energy, 13–43. https://doi.org/10.1533/9780857097194.1.13

Newman, G.A., Anderson, W.L., and Hohmann, G.W. (1987). Interpretation of transient electromagnetic soundings over three-dimensional structures for the central-loop configuration. Geophysical Journal of the Royal Astronomical Society, 89, 889–914.

New Mexico Geochronology Research Laboratory (2025). K/Ar and 40Ar/39Ar methods. Viewed on 28 May 2025. https://geoinfo.nmt.edu/labs/argon/methods/home.html

Nicot, J.P., Mickler, P., Larson, T., Clara Castro, M., Darvari, R., Uhlman, K. and Costley, R. (2017). Methane occurrences in aquifers overlying the Barnett Shale play with a focus on Parker County, Texas. Groundwater, 55(4), 469–481.

NSW DMR (1995). Basin Structure Interpretation, 1:500,000 Map Sheet, Surat Basin Geophysical Program, Geological Survey of NSW, Sydney.

NSW DPIE (2019). Water monitoring strategy for coal basins, factsheet. Sydney: NSW Department of Planning, Industry and Environment. Viewed 9 February 2022, https://www.industry.nsw.gov.au/__data/assets/pdf_file/0003/167070/expanding-the-water-monitoring-network.pdf.

NSW DPIE (2020). Narrabri Gas Project. State Significant Development. SSD 6367, June 2020. https://www.ipcn.nsw.gov.au/resources/pac/media/files/pac/projects/2020/03/narrabri-gas-project/referral-from-the-department-of-planning-industry-and-environment/dpie-final-assessment-report.pdf

NSW DPIE (2021). Well completion reports for new NSW DPIE groundwater monitoring bores. Supplied April 2021.

Northey, J., Pinetown, K. and Sander, R. (2014). Coal and coal seam gas resource assessment for the Namoi subregion. Product 1.2 for the Namoi subregion from the Northern Inland Catchments Bioregional Assessment. Australia: Department of the Environment, Bureau of Meteorology, CSIRO and Geoscience Australia. Available at https://www.bioregionalassessments.gov.au/sites/default/files/ba-nic-nam-120-resourceassessment-20141031.pdf

Norton, C.J. and Rollet, N. (2023). Regional stratigraphic correlation transects across the Great Artesian, Lake Eyre basins and Upper Darling Floodplain region (part 2): Infilling data and knowledge gaps. Record 2023/28. Geoscience Australia, Canberra. https://dx.doi.org/10.26186/147243

OGIA (2019). Groundwater Modelling Report – Surat Cumulative Management Area. OGIA, Brisbane.

OGIA (2020). Hydrogeological characterisation of faults in the Surat Basin: assessing fault-induced connectivity between the Walloon Coal Measures and adjacent aquifers. Brisbane: Office of Groundwater Impact Assessment.

Onajite, E. (2014). Chapter 1 Sedimentation and oil/gas formation In: Onajite, E. (ed.), Seismic data analysis techniques in hydrocarbon exploration, 3–16. https://doi.org/10.1016/B978-0-12-420023-4.00001-0

Othman, R., Arouri, K.R., Ward, C.R., McKirdy, D.M. (2001). Oil generation by igneous intrusions in the northern Gunnedah Basin, Australia. Organic Geochemistry, 32(10), 1219–1232. https://doi.org/10.1016/S0146-6380(01)00089-4

Palacky G.J. (1983). Tutorial: Research, applications and publications in electrical and electromagnetic methods. Geophysical Prospecting 31, 861–872.

Palacky, G. (1987) Resistivity Characteristics of Geological Targets. In: Nabighian, M., Ed., Electromagnetic Methods in Applied Geophysics-Theory, Society of Exploration Geophysicists Tulsa, OK, 53-129.

Parkhurst, D.L., and Appelo, C.A.J. (2013). Description of input and examples for PHREEQC version 3—A computer program for speciation, batch-reaction, one-dimensional transport, and inverse geochemical calculations: U.S. Geological Survey Techniques and Methods, book 6, chap. A43, 497 p.,

Partington, D., Knowling, M.J., Simmons, C.T., Cook, P.G., Xie, Y., Iwanaga, T. and Bouchez, C. (2020). Worth of hydraulic and water chemistry observation data in terms of the reliability of surface water-groundwater exchange flux predictions under varied flow conditions, Journal of Hydrology, Volume 590, 125441, https://doi.org/10.1016/j.jhydrol.2020.125441.

Paterson, R., Silic, J. and FitzGerald, D. (2016), AEM 2.5D inversion results for GSSA TEMPEST and VTEM data from the Quinyambie, Cariewerloo, Gawler south and western Craton Areas. Geological Survey of South Australia 2016. Geological Survey of South Australia Discovery Day 2016: presentation abstracts and posters, Report Book 2016/00032. Department of State Development, South Australia, Adelaide

Pearce, J. K., Golding, S. D., Hayes, P., Baublys, K. A., Hofmann, H., Herbert, S. J. and Gargiulo, G. (2021). Gas sources and concentrations in Surat Basin shallow aquifers: a field sampling method comparison, and isotopic study. The APPEA Journal, 61 (2), 707-713. https://doi: 10.1071/aj20061

Pearson, F.J. (1965). *Use of C-13/C-12 ratios to correct radiocarbon ages of material initially diluted by limestone*. In: Proceedings of the Symposium on Isotope Hydrology, IAEA, Vienna, 305–312.

Phillips, F.M. (2013). Chlorine-36 dating of old groundwater. In: Suckow, A., Aggarwal P.K. and Araguas-Araguas, L.J. (eds), Isotope methods for dating old groundwater, Vienna: International Atomic Energy Agency, 125–152.

Phillips, D. (2015), Kimberlites (K-Ar and Ar-Ar), in Rink, W.J., and Thompson, J.W., eds., Encyclopedia of Scientific Dating Methods: Dordrecht, Springer, p. 361–364, https://doi.org/10.1007/978-94-007-6304-3_20

Poudjom Djomani, Y. (2019). Total magnetic intensity grid of Australia 2019 – first vertical derivative (1VD). Canberra: Geoscience Australia. http://dx.doi.org/10.26186/5dd48b1368ece

Purtschert, R., R. Yokochi, W. Jiang, Z.-T. Lu, P. Mueller, J. Zappala, E. Van Heerden, E. Cason, M. Lau, T.L. Kieft, C. Gerber, M.S. Brennwald, T.C. Onstott (2021). Underground production of ^{81}Kr detected in subsurface fluids, Geochimica et Cosmochimica Acta, Volume 295, Pages 65-79, https://doi.org/10.1016/j.gca.2020.11.024.

Purtschert, R., Love, A.J., Jiang, W., Lu, Z.T., Yang, G.M., Fulton, S., Wohling, D., Shand, P., Aeschbach, W., Bröder, L., Müller, P. and Tosaki, Y. (2023). Residence times of groundwater along a flow path in the Great Artesian Basin determined by ^{81}Kr, ^{36}Cl and ^{4}He: Implications for palaeo hydrogeology, Science of The Total Environment, Volume 859, Part 1, 159886, https://doi.org/10.1016/j.scitotenv.2022.159886.

Radke, B., Ferguson, M.J., Cresswell, R.G., Ransley, T.R. and Habermehl, M.A. (2000). Hydrochemistry and implied hydrodynamics of the Cadna-owie-Hooray Aquifer Great Artesian Basin. Australia: Bureau of Rural Sciences.

Raiber, M., Webb, J.A. and Bennetts, D.A. (2009). Strontium isotopes as tracers to delineate aquifer interactions and the influence of rainfall in the Basalt Plains of southeastern Australia. Journal of Hydrology, 367 (3–4), 188–199.

Raiber, M., White, P.A., Daughney, C.J., Tschritter, C., Davidson, P. and Bainbridge, S.E. (2012). Three-dimensional geological modelling and multivariate statistical analysis of water chemistry data to analyse and visualise aquifer structure and groundwater composition in the Wairau Plain, Marlborough District, New Zealand. Journal of Hydrology, 436–437, 13–34.

Raiber, M., Webb, J.A., Céndon, D.I., White, P.A. and Jacobsen, G.E. (2015). Environmental isotopes meet 3D geological modelling: a study of recharge, aquifer connectivity and structurally-controlled groundwater flow in the basalt plains of south-western Victoria, Australia. Journal of Hydrology, 527, 262–280

Raiber, M. and Suckow, A. (2018). Hydrochemistry of the Pilliga Sandstone aquifer in NSW – data availability, preliminary assessment of spatial patterns and conceptual model uncertainties. Australia: CSIRO.

Raiber, M., Martinez, J., Suckow, A., Deslandes, A., Gerber, C. (2022a). Assessment of the influence of geological structures on aquifer connectivity in the Pilliga Forest area, NSW – an integrated hydrogeological, geophysical, hydrochemical and environmental tracer approach. Canberra: CSIRO; 2022. csiro:EP2022-1375. https://doi.org/10.25919/exee-za89

Raiber, M., Suckow, A., Deslandes, A., Gerber, C., Martinez, J., Crane, P. (2022b). Assessing recharge processes and flow dynamics using environmental tracers in the Great Artesian Basin. CSIRO, Australia: CSIRO; 2022. csiro:EP2022-5860. https://doi.org/10.25919/kb99-x235

Raiber, M., Feitz, A.J., Flook, S., Cendón, D.I., Suckow, A., Schöning, G., Hofmann, H., Martinez, J., Maas, R., Kelly, B.F.J. (2024). Strontium isotopes in the atmosphere, geosphere and hydrosphere: Developing a systematic "fingerprinting" framework of rocks and water in sedimentary basins in eastern Australia. Sci Total Environ. 2024 Nov 15;951:175522. doi: 10.1016/j.scitotenv.2024.175522. Epub 2024 Aug 14. PMID: 39151615.

Rajabi, M., Tingay, M. and Heidbach, O. (2016). The present-day stress field of New South Wales, Australia. Australian Journal of Earth Sciences, 63(1), 1–21. DOI: 10.1080/08120099.2016.1135821.

Ransley, T.R., Radke, B.M., Feitz, A.J., Kellett, J.R., Owens, R., Bell, J., Stewart, G. and Carey, H. (2015). Hydrogeological atlas of the Great Artesian Basin. Geoscience Australia, Canberra. http://dx.doi.org/10.11636/9781925124668

Reid, J.E., Pfaffling, A. and Vrbancich, J. (2006). Airborne electromagnetic footprints in 1D earths. GEOPHYSICS, 71(2):G63–G72, doi:10.1190/1.2187756.

Ruming, K. (2015). Exploration in the house 2015: high precision zircon dating of tuffs in the Sydney-Gunnedah Basin. Viewed 10 Feb 2018, https://www.slideshare.net/nswdre/05-eith2015ruming

Salmon, S.U., Prommer, H., Park, J., Meredith, K.T., Turner, J.V., McCallum, J.L. (2015). A general reactive transport modeling framework for simulating and interpreting groundwater ^{14}C age and δ^{13}C, Water Resources Research, 10.1002/2014WR015779, **51**, 1, (359-376).

Santos (2017a). EIS Chapter 6 Project description, 89 pp. Viewed July 2019, https://majorprojects.accelo.com/public/1e6475194c440a225a59dddcb004fd53/Chapter%2006%20Project%20description.pdf

Santos (2017b). EIS Chapter 11 Groundwater and geology, 74 pp. Viewed July 2019, https://majorprojects.accelo.com/public/2d334d5defe206318a77b57240ca92af/Chapter%2011%20Groundwater%20and%20geology.pdf

Santos (2020). Narrabri Gas Project (SSD 6456). Submission to IPC following public hearing, 10 August 2020. https://www.ipcn.nsw.gov.au/resources/pac/media/files/pac/projects/2020/03/narrabri-gas-project/correspondence/santos-submission/200810-santos-_final-submission-incl-attachments.pdf

Santos (2025). Santos water portal. Viewed February 2025. http://map.santoswaterportal.com.au/

Sattel, D, 1998. Conductivity information in three dimensions. Exploration Geophysics 29, 157-162.

Sattel, D, 2005. Inverting airborne electromagnetic (AEM) data with Zohdy's method,: Geophysics, 70 (4), G77-G85.

Schilling, O. S., Cook, P. G., &Brunner, P. (2019). Beyond classical observations in hydrogeology: The advantages of including exchange flux, temperature, tracer concentration, residence time, and soil moisture observations in groundwater model calibration. Reviews of Geophysics, 57,146–182.

Segev, A., Rybakov, M., & Mortimer, N. (2012). A crustal model for Zealandia and Fiji. Geophysical Journal International, 189(3), 1277–1292. https://doi.org/10.1111/j.1365-246X.2012.05436.x

Senger, K., Buckley, S.J., Chevallier, L., Fagereng, A., Galland, O., Kurz, T.H., Ogata, K., Planke, S., Tveranger, J. (2015). Fracturing of doleritic intrusions and associated contact zones: Implications for fluid flow in volcanic basins, Journal of African Earth Sciences, Volume 102, Pages 70-85, ISSN 1464-343X, https://doi.org/10.1016/j.jafrearsci.2014.10.019.

Sengpiel, K.P. and Siemon, B. (2000). Advanced inversion methods for airborne electromagnetic exploration: Geophysics, 65, 1983–1992.

Severinghaus, J.P. (2021). The triple argon isotope composition of groundwater on ten-thousand-year timescales. Chemical Geology 120458.

Smerdon, B.D. and Ransley, T.R. (2012). Water resource assessment for the Surat region. Australia: CSIRO Water for a Healthy Country Flagship.

Stetzenbach, K.J., Farnham I.M., Hodge, V.F. and Johannesson, K.H. (1999). Using multivariate statistical analysis of groundwater major cation and trace element concentrations to evaluate groundwater flow in a regional aquifer. Hydrological Processes, 13, 2655–2673.

Streamline Hydro (2018). Plumb Road groundwater monitoring equipment Installation. Report no. 2018072001-RPT-001. Commissioned by Crowns Lands and Water Division, NSW Department of Industry.

Suckow, A. and Dumke, I. (2001). A database system for geochemical, isotope hydrological, and geochronological laboratories. Radiocarbon, 43(2A), 325-337.

Suckow, A. (2013). System analysis using multi-tracer approaches. In: Suckow, A., Aggarwal P.K. and Araguas-Araguas, L.J. (eds), Isotope methods for dating old groundwater, Vienna: International Atomic Agency, 217–244.

Suckow, A. (2014). The age of groundwater – definitions, models and why we do not need this term. Applied Geochemistry, 50, 222–230.

Suckow, A., Raiber, M., Deslandes, A. and Gerber, C. (2019). Constraining groundwater recharge in the Pilliga Sandstone (Surat Basin, NSW) through environmental tracer data. Australia: CSIRO, 81 pp.

Suthersan, S.S. (2001). Natural and enhanced remediation systems. Washington, DC: Lewis Publishers.

Tadros, N.Z. (1993). The Gunnedah Basin, New South Wales, Memoir 12. Sydney: Geological Survey of New South Wales.

Tadros, N.Z. (1995). Structure and tectonics of the Gunnedah Basin, N.S.W: implications for stratigraphy, sedimentation and coal resources, with emphasis on the Upper Black Jack group. PhD thesis, Department of Geology, University of Wollongong. http://ro.uow.edu.au/theses/840

Tadros, C. V., Hughes, C. E., Crawford, J., Hollins, S. E., & Chisari, R. (2014). Tritium in Australian precipitation: A 50 year record. *Journal of hydrology*, *513*, 262-273. ISSN 0022-1694, https://doi.org/10.1016/j.jhydrol.2014.03.031.

Tamers, M.A. (1975). *Validity of Radiocarbon Dates on Ground Water*. Geophysical Surveys, 2, 217–239.

Taulis, M. and Milke, M. (2007). Coal seam gas water from Maramarua, New Zealand: characterisation and comparison to United States analogues. Journal of Hydrology: New Zealand, 46(1), 1–17.

Terracorp (1999). 1998 Bohena seismic survey, PEL 238, Gunnedah Basin, New South Wales. Field acquisition and operations report for First Sourcenergy Group Pty Ltd. https://search.geoscience.nsw.gov.au/report/R00031623

Thomas, M.A. (2018). Chemical and isotopic characterisation of methane in groundwater of Ohio, 2016. U.S. Geological Survey Scientific Investigations Report, 2018-5097.

Torgersen, T., Habermehl, M.A. and Clarke, W.B. (1987). Helium isotopic evidence for recent subcrustal volcanism in eastern Australia. Geophysical Research Letters, 14, 1215–1218.

Torgersen, T., Kennedy, B.M., Hiyagon, H., Chiou, K.Y., Reynolds, J.H. and Clarke, W.B. (1989). Argon accumulation and the crustal degassing flux of ^{40}Ar in the Great Artesian Basin, Australia. Earth and Planetary Science Letters, 92, 43–56.

Torgersen, T. and Stute, M. (2013). Helium (and other noble gases) as a tool for understanding long timescale groundwater transport. In: Suckow, A., Aggarwal P.K. and Araguas-Araguas, L.J. (eds), Isotope methods for dating old groundwater, Vienna: International Atomic Agency, 179-216.

Totterdell, J.M., Moloney, J., Korsch, R.J. and Krassay, A.A. (2009). Sequence stratigraphy of the Bowen–Gunnedah and Surat basins in New South Wales. Australian Journal of Earth Sciences, 56, 433–459.

Troedson, A. and Bull, K.F. (2018). Geological mapping of the Warrumbungle National Park and surrounds: final report, February 2018. Geological Survey of New South Wales, Report, GS2018/0575, 62p

Turnadge, C., Esteban, L., Emelyanova, I., Nguyen, D., Pervukhina, M., Han, T. and Mallants, D. (2018). Multiscale aquitard hydraulic conductivity characterisation and inclusion in groundwater flow models: application to the Gunnedah Basin, New South Wales. Canberra: CSIRO.

Turnadge, C. and Smerdon, B. D. (2014). A review of methods for modelling environmental tracers in groundwater: Advantages of tracer concentration simulation. Journal of Hydrology, 519, 3674–3689. https://doi.org/10.1016/j.jhydrol.2014.10.056

Tyne, R.L., Broadley, M.W., Bekaert, D.V. et al. (2025). Passive degassing of lithospheric volatiles recorded in shallow young groundwater. Nat. Geosci. 18, 542–547. https://doi.org/10.1038/s41561-025-01702-7

Underschultz, J., Esterle, J., Strand, J. and Hayes, S. (2018). Conceptual representation of fluid flow conditions associated with faults in sedimentary basins. Prepared for the Department of the Environment and Energy by The University of Queensland Centre for Coal Seam Gas, Queensland, 61 pp.

Upstream Petroleum Consulting Services (2000). Assessment of hydrocarbon potential: Southern Brigalow Bioregion, Pilliga, New South Wales. Prepared for New South Wales Department of Mineral Resources, March 2000.

Vogel, J.C. (1967). Investigation of groundwater flow with radiocarbon. Proceedings of the Symposium, Vienna, 14–18 November 1966, International Atomic Energy Agency (IAEA), pp. 355–369.

WaterNSW (2017). Groundwater chemistry data. Data supplied to CSIRO.

WaterNSW (2025). Continuous water monitoring network. Viewed March December 2025, https://realtimedata.waternsw.com.au/

Watkins, J.K. and Meakin, N.S. (1996). Nyngan and Walgett 1:250 000 geological sheets SH/55-15 & SH/55-11: explanatory notes. Sydney: Geological Survey of New South Wales.

Webster, S.S. and Woods, K.T. (1987). Orientation geophysical surveys over potential hydrocarbon reservoirs near Narrabri, NSW. Geological Survey Report GS 1987/225. https://search.geoscience.nsw.gov.au/report/R00008351

Weiss, R.F. (1968). Piggyback samplers for dissolved gas studies on sealed water samples. Deep Sea Research, 15, 659–699.

Wellman, P., McElhinny, M.W. and McDougall, I. (1969). On the polar-wander path for Australia during the Cenozoic. Geophysical Journal International, 18(4), 371–395. DOI: 10.1111/j.1365-246X.1969.tb03575.x

Wellman, P. and McDougall, I. (1974). Potassium-argon ages on the Cainozoic volcanic rocks of New South Wales. Journal of the Geological Society of Australia, 21, 247–272.

Wen, T., Woda, J., Marcon, V., Niu, X., Li, Z. and Brantley, S.L. (2019). Exploring how to use groundwater chemistry to identify migration of methane near shale gas wells in the Appalachian Basin. Environmental Science & Technology, 53(15), 9317–9327. DOI: 10.1021/acs.est.9b02290

Whiticar, M.J. (1999). Carbon and hydrogen isotope systematics of bacterial formation and oxidation of methane. Chemical Geology, 161(1–3), 291–314. https://doi.org/10.1016/S0009-2541(99)00092-3

Wilcken, K. M., Fink, D., Hotchkis, M. A. C., Garton, D., Button, D., Mann, M., Kitchen, R., Hauser, T., and O'Connor, A. (2017). Accelerator Mass Spectrometry on SIRIUS: New 6 MV spectrometer at ANSTO, Nucl. Instrum. Meth. B, 406, 278–282, https://doi.org/10.1016/j.nimb.2017.01.003.

Wilson, M.J. (2004). Weathering of the primary rock-forming minerals: processes, products and rates. Clay Minerals; 39(3):233-266. doi:10.1180/0009855043930133

Wolfgang, C. (2000). Hydrogeology of the Pilliga Sandstone, Coonamble Embayment and water resource management. PhD Thesis, Fenner School of Environment & Society, The Australian National University, Canberra.

Woods, T.L., P.D. Fullagar, R.K. Spruill, and L.C. Sutton (2000). Strontium isotopes and major elements as tracers of ground water evolution: Example from the Upper Castle Hayne Aquifer of North Carolina. Gound Water, 38 (5), 762-771.

Zheng, C., and Wang, P.P. (1999). MT3DMS: A modular three-dimensional multi-species transport model for simulation of advection, dispersion and chemical reactions of contaminants in groundwater systems; Documentation and user's guide: Contract report SERDP-99-1: U.S. Army Engineer Research and Development Center, Vicksburg, MS, 169 p.

Contact us

1300 363 400
+61 3 9545 2176
csiro.au

For further information

1300 363 400
gisera.csiro.au